SPOTLIGHT ON SOLANACEAE METABOLISM: BIOTECHNOLOGICAL APPLICATION

EDITED BY: Zsófia Bánfalvi, Amalia Barone and Glenn Bryan

PUBLISHED IN: Frontiers in Plant Science

frontiers Research Topics

ISSN 1664-8714
ISBN 978-2-88971-592-3
DOI 10.3389/978-2-88971-592-3

About Frontiers

Frontiers is more than just an open-access publisher of scholarly articles: it is a pioneering approach to the world of academia, radically improving the way scholarly research is managed. The grand vision of Frontiers is a world where all people have an equal opportunity to seek, share and generate knowledge. Frontiers provides immediate and permanent online open access to all its publications, but this alone is not enough to realize our grand goals.

Frontiers Journal Series

The Frontiers Journal Series is a multi-tier and interdisciplinary set of open-access, online journals, promising a paradigm shift from the current review, selection and dissemination processes in academic publishing. All Frontiers journals are driven by researchers for researchers; therefore, they constitute a service to the scholarly community. At the same time, the Frontiers Journal Series operates on a revolutionary invention, the tiered publishing system, initially addressing specific communities of scholars, and gradually climbing up to broader public understanding, thus serving the interests of the lay society, too.

Dedication to Quality

Each Frontiers article is a landmark of the highest quality, thanks to genuinely collaborative interactions between authors and review editors, who include some of the world's best academicians. Research must be certified by peers before entering a stream of knowledge that may eventually reach the public - and shape society; therefore, Frontiers only applies the most rigorous and unbiased reviews.
Frontiers revolutionizes research publishing by freely delivering the most outstanding research, evaluated with no bias from both the academic and social point of view. By applying the most advanced information technologies, Frontiers is catapulting scholarly publishing into a new generation.

What are Frontiers Research Topics?

Frontiers Research Topics are very popular trademarks of the Frontiers Journals Series: they are collections of at least ten articles, all centered on a particular subject. With their unique mix of varied contributions from Original Research to Review Articles, Frontiers Research Topics unify the most influential researchers, the latest key findings and historical advances in a hot research area! Find out more on how to host your own Frontiers Research Topic or contribute to one as an author by contacting the Frontiers Editorial Office: frontiersin.org/about/contact

SPOTLIGHT ON SOLANACEAE METABOLISM: BIOTECHNOLOGICAL APPLICATION

Topic Editors:
Zsófia Bánfalvi, National Agricultural Research and Innovation Centre, Hungary
Amalia Barone, University of Naples Federico II, Italy
Glenn Bryan, The James Hutton Institute, United Kingdom

Citation: Bánfalvi, Z., Barone, A., Bryan, G., eds. (2021). Spotlight on Solanaceae Metabolism: Biotechnological Application. Lausanne: Frontiers Media SA.
doi: 10.3389/978-2-88971-592-3

Table of Contents

05 ***Editorial: Spotlight on Solanaceae Metabolism: Biotechnological Application***
Zsófia Bánfalvi, Amalia Barone and Glenn J. Bryan

07 ***Root Exudates Metabolic Profiling Suggests Distinct Defense Mechanisms Between Resistant and Susceptible Tobacco Cultivars Against Black Shank Disease***
Chengsheng Zhang, Chao Feng, Yanfen Zheng, Jing Wang and Fenglong Wang

22 ***Effects of Nutrient and Water Supply During Fruit Development on Metabolite Composition in Tomato Fruits (*Solanum lycopersicum *L.) Grown in Magnesium Excess Soils***
Yangmin X. Kim, Min Cheol Kwon, Seulbi Lee, Eun Sung Jung, Choong Hwan Lee and Jwakyung Sung

30 ***Characterization of the DREBA4-Type Transcription Factor (SlDREBA4), Which Contributes to Heat Tolerance in Tomatoes***
Lianzhen Mao, Minghua Deng, Shurui Jiang, Haishan Zhu, Zhengan Yang, Yanling Yue and Kai Zhao

43 ***Simultaneous CRISPR/Cas9 Editing of Three PPO Genes Reduces Fruit Flesh Browning in* Solanum melongena *L.***
Alex Maioli, Silvia Gianoglio, Andrea Moglia, Alberto Acquadro, Danila Valentino, Anna Maria Milani, Jaime Prohens, Diego Orzaez, Antonio Granell, Sergio Lanteri and Cinzia Comino

56 ***Future-Proofing Potato for Drought and Heat Tolerance by Overexpression of Hexokinase and SP6A***
Günter G. Lehretz, Sophia Sonnewald, Nitsan Lugassi, David Granot and Uwe Sonnewald

65 ***Variation for Composition and Quality in a Collection of the Resilient Mediterranean 'de penjar' Long Shelf-Life Tomato Under High and Low N Fertilization Levels***
Elena Rosa-Martínez, Ana M. Adalid, Luis E. Alvarado, Resurrección Burguet, María D. García-Martínez, Leandro Pereira-Dias, Cristina Casanova, Elena Soler, María R. Figàs, Mariola Plazas, Jaime Prohens and Salvador Soler

84 ***An Eggplant Recombinant Inbred Population Allows the Discovery of Metabolic QTLs Controlling Fruit Nutritional Quality***
Maria Sulli, Lorenzo Barchi, Laura Toppino, Gianfranco Diretto, Tea Sala, Sergio Lanteri, Giuseppe Leonardo Rotino and Giovanni Giuliano

101 ***Natural Genetic Diversity in Tomato Flavor Genes***
Lara Pereira, Manoj Sapkota, Michael Alonge, Yi Zheng, Youjun Zhang, Hamid Razifard, Nathan K. Taitano, Michael C. Schatz, Alisdair R. Fernie, Ying Wang, Zhangjun Fei, Ana L. Caicedo, Denise M. Tieman and Esther van der Knaap

124 ***Screening and Interaction Analysis Identify Genes Related to Anther Dehiscence in* Solanum melongena *L.***
Zhimin Wang, Chao Yuan, Shaowei Zhang, Shibing Tian, Qinglin Tang, Dayong Wei and Yi Niu

136 ***Ascorbic Acid-Induced Photosynthetic Adaptability of Processing Tomatoes to Salt Stress Probed by Fast OJIP Fluorescence Rise***
Xianjun Chen, Yan Zhou, Yundan Cong, Pusheng Zhu, Jiayi Xing, Jinxia Cui, Wei Xu, Qinghua Shi, Ming Diao and Hui-ying Liu

frontiers in Plant Science

EDITORIAL
published: 17 September 2021
doi: 10.3389/fpls.2021.756948

Editorial: Spotlight on Solanaceae Metabolism: Biotechnological Application

Zsófia Bánfalvi[1]*, *Amalia Barone*[2] *and Glenn J. Bryan*[3]

[1] National Agricultural Research and Innovation Centre, Gödöllő, Hungary, [2] Department of Agricultural Sciences, University of Naples Federico II, Naples, Italy, [3] Cell and Molecular Sciences, The James Hutton Institute, Dundee, United Kingdom

Keywords: Solanaceae, transcriptomics, metabolomics, stress tolerance, nutritional quality, tomato flavor, eggplant browning, potato drought and heat tolerance

Editorial on the Research Topic

Spotlight on Solanaceae Metabolism: Biotechnological Application

The Solanaceae family consists of more than 90 genera and nearly 3,000 species distributed throughout the world with a great diversity, and contains many species with economic importance as food and medicinal plants, spices and ornamentals. Among the most important agricultural crops are potato, tomato, pepper, eggplant and tobacco, which serve also as model systems for the investigation of fundamental biological and agronomic questions. The recently developed "omics" technologies and their various combinations have started to shed light on flower, fruit and tuber development, as well as on abiotic and biotic stress responses of sensitive and stress-tolerant varieties, and provided molecular markers for breeders. In this Research Topic, we provided a platform for articles based on "omics" studies in Solanaceae plants to further advance our knowledge on the perturbation of metabolic pathways in different conditions, and their regulation for improved biosynthesis of molecules of interest.

Global climate change with rising temperatures and reduced water availability is challenging agricultural systems worldwide. Potato plants are very sensitive to drought and elevated temperatures. To improve water use efficiency as well as tuberization of potato plants under drought and heat stress Lehretz et al. co-expressed *HEXOKINASE 1* from *Arabidopsis thaliana* (*AtHXK1*) and *SELF-PRUNING 6A* (*SP6A*) from *Solanum tuberosum*, encoding a mobile tuberisation signal, in guard cells and shoots, respectively. Although the plants showed a bushy growth habit the yield and starch content of tubers were only slightly affected by the heat and drought stress combination. Dehydration-responsive element binding (DREB) transcription factors play crucial regulatory roles in stress responses. Mao et al. found that the only *DREB* that responded to heat was *SlDREBA4* in the model tomato cultivar Microtom. Overexpression of *SlDREBA4* enhanced tolerance of tomato plants to heat stress by regulating the expression of many heat shock- and calcium-binding protein genes, and by altering the content of osmolytes and stress hormones as well as the activities of antioxidant enzymes. It was also demonstrated that application of exogenous ascorbic acid counteracts the salt-induced photoinhibition in tomato (Chen et al.). Thus, these studies provided new genetic resources and rationales for abiotic stress-tolerance breeding of Solanaceae plants.

Plants are confronted not only with abiotic, but also with biotic stresses. *Phytophthora nicotianae* is a soil borne pathogen causing black shank disease in tobacco. Plants have evolved complex defense systems against pathogens including root exudates of some resistant varieties with an inhibitory effect on pathogen growth. Metabolic profiling performed by Zhang et al. depicted differing metabolic patterns of root exudates between a resistant and susceptible tobacco

OPEN ACCESS

Edited and reviewed by:
Zhi-Yan Du,
University of Hawaii at Manoa, United States

***Correspondence:**
Zsófia Bánfalvi
banfalvi.zsofia@abc.naik.hu

Specialty section:
This article was submitted to Plant Metabolism and Chemodiversity, a section of the journal Frontiers in Plant Science

Received: *11 August 2021*
Accepted: *23 August 2021*
Published: *17 September 2021*

Citation:
Bánfalvi Z, Barone A and Bryan GJ (2021) Editorial: Spotlight on Solanaceae Metabolism: Biotechnological Application. Front. Plant Sci. 12:756948. doi: 10.3389/fpls.2021.756948

cultivar. Some of the detected defense compounds (e.g., tartaric-, ferulic-, lauric acid, and phenylpropanoids) have potential for disease control application.

The greenhouse cultivation of tomatoes involves the application of a considerable amount of fertilizers and produces an accumulation of surplus salts in soil. Kim et al. demonstrated that minimal nutrient and water supplies improves tomato quality in soils with surplus salt. Rosa-Martínez et al. dealt with a similar problem and searched for tomato varieties with improved nitrogen use efficiency to reduce the need for fertilization in line with the sustainable agriculture policies. The "de penjar" tomatoes from the Spanish Mediterranean region were selected for the study because these tomatoes are cultivated under low-input conditions and carry the *alc* mutation, which provides long shelf-life for the fruit. A large amount of variation between the local varieties was observed especially in lycopene content that together with β-carotene presented a strongly significant genotype x nitrogen input interaction. These results revealed the potential of "de penjar" varieties as a genetic resource in breeding for low nitrogen inputs, while keeping the high organoleptic and nutritional quality of traditional tomato cultivars. Tomato flavor, which is determined by the right balance of sugars and organic acids, as well as a range of volatile organic compounds, is obviously a primary focus of tomato breeding. Using newly available high quality genome assemblies, Pereira et al. associated five flavor-controlling genes with trait variation and described the genetic diversity at these loci in a red-fruited tomato clade. The tomato collection used in this study would be an excellent set of material to discover new flavor genes through genetic mapping approaches.

Eggplant, cultivated for over 1,500 years, represents the third most important crop of the Solanaceae family after potato and tomato. Most of its nutritional properties are related to phenolic compounds. However, there is a correlation between the concentration of phenolics and browning of the fruit flesh. The polyphenol oxidases (PPOs) catalyze the oxidation of phenolic compounds leading to browning. Based on this knowledge Maioli et al. generated knock-out mutants in three *PPO* genes of an eggplant cultivar using the CRISPR/Cas9 technology. Upon cutting, edited eggplant fruits showed a reduction in browning. Through this approach it will be possible to develop non-, or reduced browning eggplant varieties that maintain their antioxidant and nutritional properties. Metabolic QTLs controlling fruit nutritional quality were discovered by Sulli et al., who analyzed a population of recombinant inbred lines (RILs), derived from two eggplant lines differing in several key agronomic traits using a combination of untargeted and targeted metabolomics approaches. As a result of this study, candidate genes underlying the nutritional quality traits were identified in eggplant.

Hybrid eggplant seed production needs a reliable male-sterile system. Functional genic male sterility (GMS) based on anther indehiscence, i.e., the anthers do not open to release pollen, exists in eggplant. In order to uncover differences in the anther dehiscence network Wang et al. performed transcriptome analysis to compare a fertile line and a male sterile eggplant line and detected major differences in jasmonic acid signal transduction.

We believe that this collection of publications represents well the current stage of Solanaceae "omics" research and thank the authors and reviewers for their valuable support.

AUTHOR CONTRIBUTIONS

ZB, AB, and GB: writing and editing. All authors contributed to the article and approved the submitted version.

Conflict of Interest: The authors declare that the research was conducted in the absence of any commercial or financial relationships that could be construed as a potential conflict of interest.

frontiers in Plant Science

ORIGINAL RESEARCH
published: 10 September 2020
doi: 10.3389/fpls.2020.559775

Root Exudates Metabolic Profiling Suggests Distinct Defense Mechanisms Between Resistant and Susceptible Tobacco Cultivars Against Black Shank Disease

Chengsheng Zhang[1,2,3*†], *Chao Feng*[1,3†], *Yanfen Zheng*[1], *Jing Wang*[1,2] *and Fenglong Wang*[1,3*]

[1] Marine Agriculture Research Center, Tobacco Research Institute of Chinese Academy of Agricultural Sciences, Qingdao, China, [2] Qingdao Special Crops Research Center of Chinese Academy of Agricultural Sciences, Qingdao, China, [3] Pest Integrated Management Key Laboratory of China Tobacco, Qingdao, China

There is increasing evidence that root exudates play important roles in plant disease resistance. Black shank, caused by *Phytophthora nicotianae*, is a destructive soil-borne disease in tobacco (*Nicotiana tabacum* L.). The aim of the present study was to investigate the activity and composition of the root exudates from resistant and susceptible tobacco cultivars. The root exudates of the resistant cultivar Gexin 3 showed inhibitory activity against *P. nicotianae*, while the exudates of susceptible cultivar Xiaohuangjin 1025 stimulated the colony growth but had no effect on spore germination. Metabolic profiling using liquid chromatography/electrospray ionization-quadrupole-time-of-flight mass spectrometry depicted differing metabolic patterns of root exudates between Gexin 3 and Xiaohuangjin 1025. The activity and composition of root exudates was altered by *P. nicotianae* inoculation. Multivariate analysis showed that root exudates (including organic acids, alkaloids, fatty acids, and esters) were different between the two varieties. The defense substances in root exudates, such as tartaric acid, ferulic acid, and lauric acid, may represent a pre-infection prevention strategy for tobacco. Phenylpropanoids as well as inducers of salicylic acid, fatty acids, 6-hydroxyhexanoic acid, and hydrojasmonate may be involved in tobacco defense responses. Compared to the susceptible cultivar, the roots of the resistant cultivar exhibited high enzyme activities of phenylalanine ammonia-lyase, cinnamate-4-hydroxylase and 4-coumarate-CoA ligase, which may prompt the synthesis and secretion of phenylpropanoids. Our results indicated that the root exudates not only provide a pre-infection prevention strategy by exuding antimicrobial substances, but also increase tobacco disease resistance by eliciting plant defense responses. In addition, some defense compounds as well as compounds that

OPEN ACCESS

Edited by:
Zsófia Bánfalvi, National Agricultural Research and Innovation Centre, Hungary

Reviewed by:
Rachel Leisso, Montana State University, United States
Katja Witzel, Leibniz Institute of Vegetable and Ornamental Crops, Germany

***Correspondence:**
Fenglong Wang
wangfenglong@caas.cn
Chengsheng Zhang
zhangchengsheng@caas.cn

†These authors have contributed equally to this work

Specialty section:
This article was submitted to Plant Metabolism and Chemodiversity, a section of the journal Frontiers in Plant Science

Received: *07 May 2020*
Accepted: *17 August 2020*
Published: *10 September 2020*

Citation:
Zhang C, Feng C, Zheng Y, Wang J and Wang F (2020) Root Exudates Metabolic Profiling Suggests Distinct Defense Mechanisms Between Resistant and Susceptible Tobacco Cultivars Against Black Shank Disease. Front. Plant Sci. 11:559775. doi: 10.3389/fpls.2020.559775

play a role in inducing plant defense responses, showed potential for disease control application. This study provides an insight into possible disease resistance mechanisms of root exudates, and attempts the beneficial utilization of these secondary metabolites of plants.

Keywords: *Phytophthora nicotianae*, metabolic profiling, tobacco, *Nicotiana*, disease resistance, defense mechanisms

INTRODUCTION

Phytophthora nicotianae Breda de Haan (syn. *P. parasitica* Dastur) is a typical soil borne pathogen with great economic significance and academic research value (Panabières et al., 2016). It can infect 255 species of plants in 90 families, and cause serious disease in a variety of crops, such as tobacco (*Nicotiana* spp.), tomato (*Lycopersicum esculentum*), and citrus (*Citrus* spp.) (Cline et al., 2008). Because of long surviving resting structures (oospores and chlamydospores), coupled with hidden initial infection sites, it is very difficult to prevent. The use of host resistance has proved to be the most economical, effective, and environmentally-friendly strategy for the control of disease; knowledge about these mechanisms can benefit the development of approaches to disease control and prevention (Wang et al., 2018).

Plants have evolved complex defense systems during long-term interactions with pathogens (Dodds and Rathjen, 2010). Recently, there is increasing evidence that root exudates play important roles in plant resistance against biotic and abiotic stress (reviewed by Coninck et al., 2015; Tsunoda and van Dam, 2017; Canarini et al., 2019). However, the significance of root exudates associated with plant disease resistance has long been underestimated. Previous studies have indicated that root exudates of resistant and susceptible crop cultivars had different effects on pathogens (Whalley and Taylor, 1973; Stevenson et al., 1995). Root exudates of some resistant varieties had an inhibitory effect on pathogen growth, whereas those of some susceptible varieties exhibited a stimulatory effect (Wu et al., 2008; Schalchli et al., 2012), indicating a relationship between the activity of root exudates and plant disease resistance.

There are distinct differences between cultivars with respect to the effect of root exudate composition on pathogen activity. Therefore, deciphering the chemical profiles in exudates is important to understanding plant–pathogen interactions belowground. However, it is very difficult to collect and identify the components of plant root exudates because of their low content and complex composition, and their metabolism being affected by many factors. Thus, the lack of comprehensive knowledge on exudate chemistry represents a major bottleneck in the understanding of "plant–pathogen interactions" in the rhizosphere (Vives-Peris et al., 2019). Benefiting from the recent advances in metabolomics and multivariate analysis, liquid and gas chromatography platforms have successfully been used for profiling of root exudates (van Dam and Bouwmeester, 2016; Tsunoda and van Dam, 2017; Gfeller et al., 2018). In this study, tobacco-*P. nicotianae* interaction was selected as the host-pathogen research system. We systematically investigate the activity and composition of root exudates from a resistant and a susceptible cultivar. The associations between the presence of particular root exudates and disease resistance are analyzed. Moreover, some components with potential application in disease control are evaluated. The results provide an insight into the plant defense strategies mediated by root exudates.

MATERIAL AND METHODS

Materials

The highly susceptible tobacco cultivar "Xiaohuangjin 1025" (S) and the highly resistant cultivar "Gexin 3" (R) were obtained from the National Medium-term Genebank of Tobacco Germplasm Resource of China. *P. nicotianae* race 0 strain JM01 with high pathogenicity was obtained from the Integrated Pest Management Key Laboratory of China Tobacco, Qingdao, China. All reagents used in this study were purchased from Sigma Chemical Co. (St. Louis, MO, USA).

Preparation of Swimming Spores of *P. nicotianae*

The zoospores of *P. nicotianae* were prepared according to the method described by Zhang et al. (2017). Briefly, *P. nicotianae* were cultured for 21 days on oatmeal agar (OA) in a Petri dish. Then, 0.1% KNO_3 solution was added (10 ml per dish), followed by culturing at 26°C for 72 h, and immediately chilled to 4°C for 0.5 h. Spore suspension was carefully drawn, adjusted to 10^6 colony-forming units (cfu) ml^{-1}, and stored at -4°C.

P. nicotianae for field inoculation were prepared by culturing on a medium prepared from millet. The millet seed was boiled until half of the seed coat ruptured. The seed was then filtered through gauze, placed in a conical flask, and sterilized for 20 min at 121°C. After cooling, a cake of *P. nicotianae* was transferred to the millet medium, cultured at 26°C for 15 d, and used within 24 h.

Identification of Disease-Resistant Tobacco Varieties

The tobacco black shank resistance of the S and R cultivars was evaluated with disease nursery artificial induction in the field and the greenhouse. Tobacco plants (R and S) with five true leaves cultured in sterilized potting soil (10 cm × 10 cm) were used for the greenhouse experiment. Each plant was irrigated with 10 ml of *P. nicotianae* spore suspensions (10^6 cfu ml^{-1}). After incubating at 28°C for 7 days (relative humidity 70%, light

intensity 300 μmol m^{-2} s^{-1}, 12 h light/12 h dark), the disease severity was recorded, and the disease index was calculated based on the method described by Zhang et al. (2017). In the control treatment, plants were irrigated with 10 ml of distilled water. Each treatment repeated three times, and every replicate had 15 seedlings for each cultivar.

Field experiments were conducted in 2017 in a disease nursery of tobacco black shank located at Jimo Tobacco Resources and Environmental Field Experiment Station of the Chinese Academy of Agricultural Sciences (36°27′N, 120°35′E). Tobacco seedlings were planted in early-June, and inoculated with millet containing *P. nicotianae* in early-July. The disease severity and the disease index were assessed in early-August using the method described by Han et al. (2016), when the tobacco plants had reached a mature stage. Each treatment was repeated 3 times with each replicate containing about 45 tobacco plants (three rows, 15 plants per row).

Root Exudate Collection

Tobacco plants were treated according to the greenhouse experiment method described above, and root exudates were collected when the plants had eight true leaves. The treatments included: resistant variety (R), susceptible variety (S), resistant variety inoculated with *P. nicotianae* (Ri), and susceptible variety inoculated with *P. nicotianae* (Si). Inoculated plants were sampled at the third day after inoculation. The seedlings were carefully dug up, the soil attached to the root surface was washed away with tap water, and the roots were washed three times with distilled water. Three seedlings were put in a conical flask (500 ml), and the roots immersed in 300 ml of distilled water. After incubating for 6 h under aeration conditions, the culture solution was freeze-dried, weighed, and transferred to a test tube with 10 ml of precooled methanol, and stored at -80°C. The yield of root exudates was defined as the ratio of root exudates to root dry weight. Each treatment was repeated six times.

Effect of Root Exudates on Mycelium Growth and Zoospore Germination of *P. nicotianae*

The mycelial growth and zoospore germination assays of root exudates obtained from R, S, Ri, and Si were performed according to the method described by Zhang et al. (2017). Root exudates were dissolved in dimethyl sulfoxide (DMSO), filtered with microporous membrane (0.22 μm), and added to OA plates (Φ=9 cm) at a final concentration of 0.05 g ml^{-1}. Then, each dish was inoculated with a *P. nicotianae* mycelium cake (with diameter of 5 cm), and incubated at 26°C in the dark. The diameter of mycelium was determined on the third day. An equal volume of sterilized distilled water served as a control. Each treatment had five replicates.

Then, 100 μl of spore suspension (diluted to 10^3 cfu ml^{-1}) was placed on a concave slide, blended with an equal volume of root exudate with a final concentration of 0.05 g ml^{-1}, and incubated for 10 h at 26°C in the dark with relative humidity of 80%. Spore germination was recorded as a percentage of the total zoospores by using a light microscope and a hemocytometer. An equal volume of sterilized distilled water served as a control. The relative inhibitory rate (RIR) was calculated according to the following equation.

$$\mathrm{RIR} = \frac{(\text{Germination rate of control} - \text{Germination rate of treatment})}{\text{Germination rate of control}} \times 100$$

Liquid Chromatography-Mass Spectrometry Analysis of Root Exudates

Freeze-dried root exudates (200 mg) were suspended in 5 ml of 0.1% HCOOH in 80% methanol, filtered through a 0.22-μm cellulose membrane and transferred to an amber vial for analysis. Samples (4 μl) were analyzed using ultra-high-performance liquid chromatography coupled with electrospray ionization quadrupole-time-of-flight mass spectrometry (UHPLC/ESI-Q-TOF-MS) (Ultimate 3000 LC, Orbitrap Elite, Thermo Fisher, America). The chromatographic separation was performed on a Hypergod C_{18} (length × internal diameter × Silica gel: 100 mm × 4.6 mm × 3 μm) column. The mobile phase was 0.1% formic acid-water (A) and acetonitrile with 0.1% formic acid (B). The gradient conditions of the mobile phase were as follows: 0–1 min, 95% A; 1–6 min, 95–80% A; 6–9 min, 80–50% A; 9–13 min, 50–5% A; 13–15 min, 5% A.

Each sample (4 μl) was injected in random order at 4°C, and the analysis was performed in both positive and negative ion modes. In positive ion mode, the dissolution gas temperature was 350°C and the flow rates of sheath gas, aux gas, and sweep gas were 45, 15, and 1 arb, respectively. The mass spectra were acquired using electrospray ionization (ESI) in negative and positive ionization modes. The mass scanning range was 50–1,000 m/z. The scan time of 0.03 s was used throughout the experiment, with interval scan time of 0.02 s. The spray voltage was 3.0 kV and the S-Lens RF Level was 30% in positive ion mode. In negative ion mode, the spray voltage was 3.2 kV and the S-Lens RF Level was 60%. To ensure accuracy and reproducibility, leucine–enkephalin was used as the lock mass for positive $[M+H]^+$ (m/z 556.2771) and negative $[M-H]^-$ (m/z 554.2615) ion modes.

To assess the reproducibility and reliability of the LC/ESI-Q-TOF-MS system, quality control (QC) samples were also prepared by mixing equal volumes (10 μl from each sample of root exudate. The pooled QC sample was injected six times at the beginning of the run to ensure system equilibrium and then after every 6 samples to further monitor the stability of the analysis (Luan et al., 2014; Zhou et al., 2016).

UHPLC/ESI-Q-TOF-MS Data Processing and Analysis

The original data collected by mass spectrometry were processed using sievev2.1 software (Thermo Fisher, MA, USA), including noise filtering, overlapping peak analysis, peak alignment, peak matching, standardization, and normalization. The peak table output from positive and negative ion were saved as Excel tables. Thereafter, features consistently detectable in at least 75% of the replicate exudate samples were screened. Post-acquisition processing included compound filtering by abundance (area > 5,000 counts), normalization at the 75th percentile, and

baselining to the median of the control. Unsupervised hierarchical cluster analysis was then carried out on the basis of fold-change-based heatmaps, setting the similarity measure as "Euclidean" and using "Wards" as the linkage rule.

Then, the resulting three-dimensional data matrix containing m/z-retention time pairs, sample names, and their normalized chromatographic peak areas (variables) were exported into SIMCA-P 11.0 (Umetrics, Sweden) for supervised orthogonal partial least squares discriminant analysis (OPLS-DA). OPLS-DA score plots were used to evaluate the quality of the model by the relevant parameters R^2 and Q^2. The differential metabolites were selected when the statistically significant threshold of variable importance in projection (VIP) values obtained from the OPLS-DA model was > 1.0. Furthermore, the *p* values from a two-tailed Student's t-test on the normalized peak areas were < 0.05. Log_2-fold-change was used to show how these selected differential metabolites varied between groups.

The screened discriminant compounds were tentatively annotated by comparing the measured relative molecular mas with the theoretical value (http://metlin.scripps.edu/). For better visualization of the metabolic signature among the four groups, the top 22 representative candidates (VIP > 1.5) were screened according to ANOVA for clearer thermographic visualization. The heatmap was generated using TB Tools software (Chen et al., 2020).

Key Enzyme Activities in Phenylpropanoid Metabolism

On days 0, 1, 2, 3, 4, and 5 after inoculation, fresh roots were sampled and used to determine activity of three enzymes involved in phenylpropanoid metabolism according to Fan et al. (2012): phenylalanine ammonia-lyase (PAL), cinnamate-4-hydroxylase (C4H), and 4-coumarate-CoA ligase (4CL).

A sample of 3 g of roots was ground with 3 ml of 0.1 mol l^{-1} boracic acid buffer [pH 8.8, containing 10% (w/v) PVPP, 1 mmol l^{-1} EDTA, and 50 mmol l^{-1} β-mercaptoethanol], followed by centrifugation for 30 min (15,000 g) at 4°C. The supernatant was collected as crude enzyme and used to determine PAL activity. The reaction system included 2 ml of 0.02 mmol l^{-1} L-phenylalanine (prepared with boracic acid buffer) and 200 μl of crude enzyme of PAL. The mixture was incubated for 30 min at 30°C, and 200 μl of 6 mol l^{-1} HCL was added to terminate the reaction. Optical density (OD) values were measured at a wavelength of 290 nm.

Crude C4H was extracted by grinding 3 g of tobacco root with 5 ml of extraction solution containing 50 mmol l^{-1} Tris-HCl, 15 mmol l^{-1} (pH 8.9), β-mercaptoethanol, 4 mmol l^{-1} $MgCl_2$, 5 mmol l^{-1} Vc, 10 μmol l^{-1} leupeptin, 1 mmol l^{-1} PMSF, 0.15% (w/v), and 10% glycerol, and centrifuged for 20 min (12,000 g). The supernatant was collected as crude C4H. The enzyme activity was assayed with the following steps: 0.8 ml of crude enzyme mixed with 2.2 ml of buffer (2 μmol l^{-1} trans-cinnamic acid, 50 mmol l^{-1} Tris-HCl (pH 8.9), 2 μmol l^{-1} $NADPNa_2$, 5 μmol l^{-1} G-6-pNa). OD values were measured at a wavelength of 620 nm.

For the crude 4CL extraction, 3 g of tobacco root were ground with 3 ml of 0.2 mol l^{-1} Tris-HCl (containing 25% glycerol and 0.1 mol l^{-1} DTT, pH 8.0) and a small amount of quartz sand and centrifuged for 20 min (15,000 g). The supernatant was collected. The reaction system for 4CL activity determination included: 0.45 ml of 15 μmol l^{-1} Mg^{2+}, 0.15 ml of 5 μmol l^{-1} p-coumaric acid, 0.15 ml of 5 μmol l^{-1} ATP, 0.15 ml of 1 μmol l^{-1} CoA, and 0.5 ml of crude enzyme. After 10 min of reaction at 40°C, the OD values were measured at a wavelength of 330 nm.

One enzyme activity unit (U) of PAL was defined as 0.01 of OD_{290} value change per hour, which was indicated as 1 U·h^{-1} g^{-1}·FW. One U of C4H and 4CL was defined as 0.01 of OD_{340} and OD_{333} per minute, respectively, and was indicated as 1 U·min^{-1} g^{-1}·FW.

The whole process of crude enzyme extraction was carried out at 4°C. Distilled water (equal volumes to the enzyme mixture) served as a control. Each treatment was repeated three times.

Effects of Compounds on Mycelium Growth of *P. nicotianae*

Twelve compounds were selected from the representative candidates for further study on *P. nicotianae* mycelial growth, including three organic acids (SA, tartaric acid, and ferulic acid), two esters (glycerol tripropanoate, isoamyl cinnamate), three fatty acids (linolenic acid, oleic acid, and lauric acid), and one alcohol (abietinol), ketone (prohydrojasmon), and terpenoid (casbene). These compounds are known as potential allelochemicals. The compounds tested were dissolved by DMSO, diluted to the required concentration as follows with ultrapure water, and filtered with 0.22 μm millipore filtration membrane. The prepared compound solutions were added to OA medium plate to ensure the final concentration as 5, 50, and 500 μg ml^{-1}, respectively. Then, a cake of *P. nicotianae* (0.6 cm diameter) was placed in the center of the plate, and incubated in dark at 26°C for 5 days. The colony diameter was measured by the cross method, and the inhibition rate of mycelium growth were calculated (Zhang et al., 2017). The DMSO served as the control. Each treatment had three replicates, and each replicate had three plates.

Pot Experiment of Tobacco Black Shank Control

To evaluate the potential of compounds for control of *P. nicotianae*, a pot experiment was carried out according to the method described in section 2.3. Seedlings of Xiaohuangjin 1025 (with five true leaves) were transplanted to pots (one plant per pot), and the seedlings were irrigated with 10 ml of ferulic acid (500 μg ml^{-1}), 10 ml of lauric acid (500 μg ml^{-1}), and 10 ml of salicylic acid (SA, 100 μg ml^{-1}). Our preliminary experimental results showed that a high concentration of SA (> 150 μg ml^{-1}) is harmful to tobacco seedlings. Therefore, the test concentration of SA was set at 100 μg ml^{-1}. After treatment for 24 h, plants were inoculated with *P. nicotianae* by irrigating each plant with 10 ml of zoospores (10^6 cfu ml^{-1}). Thereafter, the seedlings were incubated at 28°C and 70% relative humidity. The disease severity was assessed on the fifth day and tenth day after inoculation using the method described by Han et al. (2016). Each compound was diluted with 2% DMSO. For the

control, each compound was diluted with the same amount of distilled water. Each treatment consisted of 15 seedlings with three replicates.

Data Statistics

Excel 2013 and DPS 7.05 software were used for data analysis. Differences between groups were tested using one-way ANOVA, followed by Tukey's multiple comparison test. $P < 0.05$ indicates that the differences are statistically significant.

RESULTS

Disease Resistance of Two Tobacco Varieties

Xiaohuangjin 1025 (S) had a disease index of 73.33 in the pot experiment (**Figure S1A**) and 93.58 in the field experiment; Gexin 3 (R) showed a slight occurrence of black shank with a disease index of 1.25 in the pot experiment (**Figure S1B**) and 2.39 in the field experiment (**Figure 1**). These results verified that Gexin 3 is highly resistant to tobacco black shank both at the seedling stage and at the adult stage, while Xiaohuangjin 1025 is highly susceptible.

Root Dry Weight and Exudate Yield of Different Varieties

A significant difference was observed in the secretion of root exudates between the two varieties (**Figure 2**). The root exudate yield of cultivar S (31.32%) was significantly higher than that of cultivar R (21.12%) ($P < 0.05$). However, the root dry weight of R (0.17 g per plant) was significantly higher than that of S (0.13 g per plant) ($P < 0.05$), which led to no significant difference in the amount of root exudate per plant between the two varieties. The inoculation of *P. nicotianae* caused a decrease in root exudate yield of both S and R, but the difference was not significant.

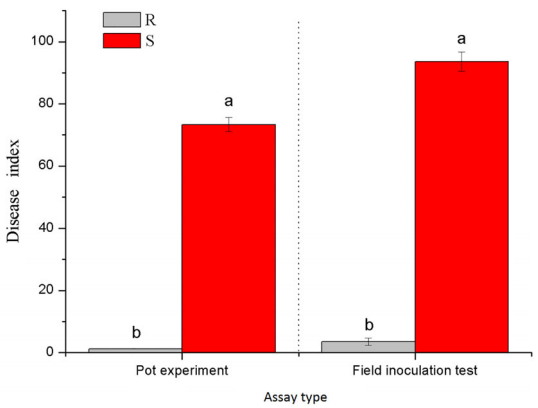

FIGURE 1 | Resistance identification of tobacco cultivars against black shank under pot (a) and field (b) conditions. R and S represent resistant and susceptible cultivars, respectively; different lowercase letters indicate statistical differences between groups at $P < 0.05$; the error bars represent standard error of the mean for n = 3.

Effects of Root Exudates on *P. nicotianae*

As shown in **Figure 3**, the effects of root exudates on mycelial growth and spore germination were distinct between cultivar R and cultivar S. Root exudates from healthy or infected plants of R displayed a strong inhibitory effect on both mycelial growth (30–46%) and spore germination (25–40%). The effect of root exudates from S differed significantly between healthy and infected plants, i.e., there was a significant stimulatory effect (7–14%) from exudates of healthy plants ($P < 0.05$), while the exudates of infected plants showed a slight inhibitory effect (< 5%). These results indicated that *P. nicotianae* infection led to changes in the root exudates of S plants, thus producing different effects on *P. nicotianae*.

Profiling of Root Exudates With UHPLC/ESI-Q-TOF-MS

To evaluate the repeatability of the metabolite extractions and detections, namely their technical repeatability, an overlay analysis was performed to the TIC plots of different QC samples. **Figure S2A** shows an overlay of the TIC plots between QC samples (six samples at the beginning, one QC after the first six samples, and one QC after the last six samples) under ESI positive mode, while **Figure S2B** exhibits that between QC samples (the first and last QC samples) under ESI negative mode. The retention time and peak area of all QC samples had a high degree of overlap, indicating good QC-sample repeatability and instrumental stability. Therefore, the data recorded in this study showed good repeatability and reliability.

The results of UHPLC/ESI-Q-TOF-MS analysis showed that the chemical diversity of the root exudates was wide. In total, 685 peaks of positive ions and 873 peaks of negative ions were observed in UHPLC, and were used for further statistical analysis. The hierarchical clustering showed different clustering results between the two ESI ion modes. In both positive (**Figure 4A**) and negative (**Figure 4B**) ion mode, 24 samples from different treatments were clustered into 4 different groups, and each cluster contained all repeats within a treatment. In the positive ion mode of ESI, the clustering relationship of Xiaohuangjin 1025 inoculated (Si) and non-inoculated (S) with *P. nicotianae* was closer, while that of the non-inoculated treatment of Gexin 3 (Ri) was relatively independent of the other three treatments. In ESI negative ion mode, samples from the same cultivar (including inoculated and non-inoculated plants) showed higher similarity, indicating that root exudate metabolites were more affected by plant genotypes than pathogen infection. Hierarchical cluster analysis (HCA) revealed significant differences in root exudate patterns between R and S.

The parameters of OPLS-DA models based on UHPLC/ESI-Q-TOF-MS are listed in **Table 1**. The cumulative (cum) values of R^2Y and Q^2 indicate the fitness and the prediction ability of the models, respectively. The closer the values are to 1, the more stable and reliable the model. The ranges of R^2X (cum) and R^2Y (cum) were 0.41–0.87 and 0.972–0.999, respectively, indicating that the variable differences between the two groups could be reflected by more than 41% of UHPLC/ESI-Q-TOF-MS data. Q^2

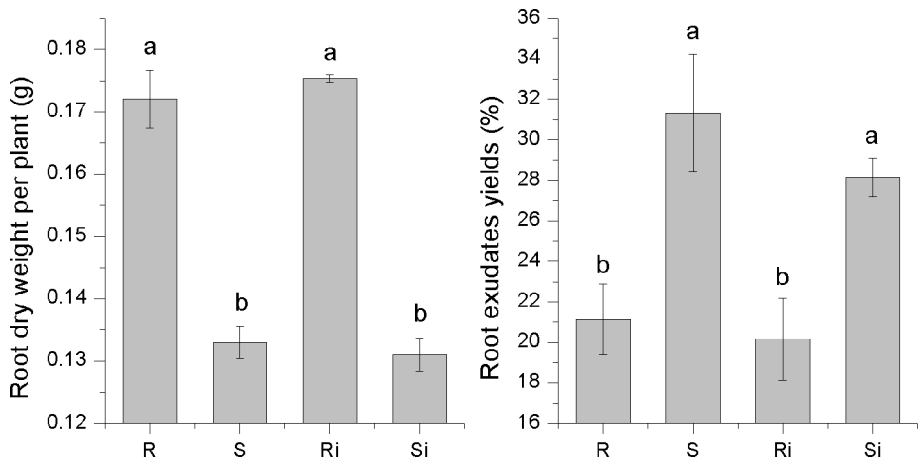

FIGURE 2 | The dry root weight and exudate yields of tobacco cultivars. Ri and R represent inoculated and non-inoculated plants of the resistant cultivar, respectively; Si and S represent inoculated and non-inoculated plants of the susceptible cultivar, respectively; different lowercase letters indicate statistical differences between groups at $P < 0.05$; the error bars represent standard error of the mean for n = 6.

(cum) was higher than 0.8, indicating that the model had better prediction. **Figure 5** shows that the OPLS model could clearly distinguish the samples in different groups, indicating that the root exudate patterns varied between the susceptible and resistant cultivars as well as between inoculated and non-inoculated plants.

Screening of Potential Biomarkers in Exudates

Table 1 shows the potential biomarkers in positive and negative ion revealed by variable importance in projection (VIP) analysis. Seventy-five, 52, and 72 discriminant compounds were screened in R vs S, R vs Ri and S vs Si, respectively, of which 45, 9, and 29 were found in ESI positive ion mode and 30, 43, and 43 in ESI negative ion mode. The 22 compounds with the highest discrimination potential (with a VIP score > 1.5 in at least one model) are listed in **Table 2**; the list includes four organic acids, three esters, seven alkaloids, four fatty acids, one alcohol, one ketone, one alkene, and one phenol. The negative ion mode revealed 15 compounds (mainly organic acids, alkaloids, and fatty acids), while the positive ion mode revealed seven compounds (mainly alkaloids, esters, and alcohols). Fold-change analysis was used to evaluate the regulation of these compounds, where log-fold changes > 1 and ≤ 1 were conceived as upregulation and downregulation, respectively. Log-fold changes of between -1 and 1 were not considered to represent changes in regulation. There are 12 compounds listed in **Table 3** with an R/S > 1; 7 compounds with an R/S ≤ -1; and 3 compounds with an R/S of between -1 and 1. The accumulation of SA, esculetin, oleic acid, isoamyl

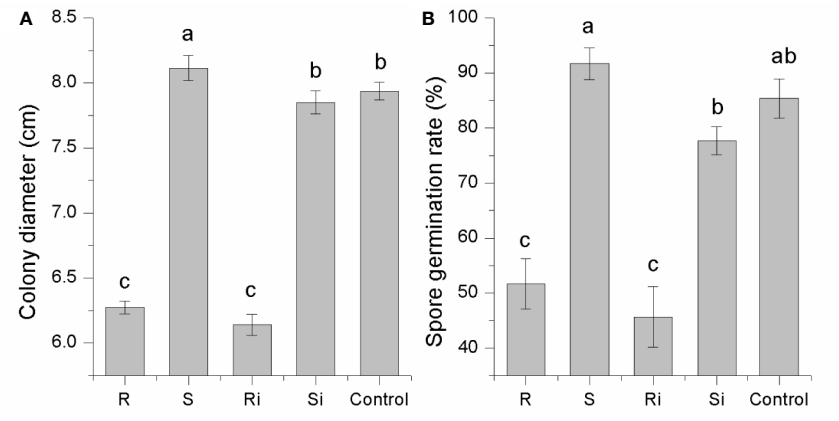

FIGURE 3 | Inhibitory effects of root exudates on mycelial growth **(A)** and spore germination **(B)** of *P. nicotianae*. Ri and R represent inoculated and non-inoculated plants of the resistant cultivar, respectively; Si and S represent inoculated and non-inoculated plants of the susceptible cultivar, respectively; different lowercase letters indicate statistical differences between groups at $P < 0.05$; the error bars represent standard error of the mean for n = 3.

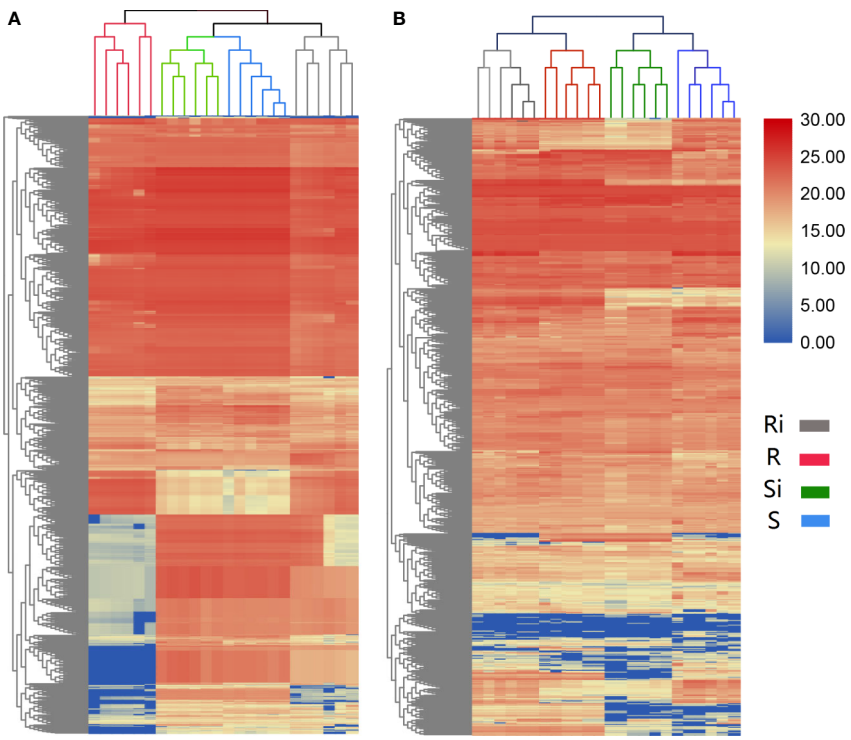

FIGURE 4 | Unsupervised hierarchical cluster analysis (with Euclidean distance and Ward's linkage rule) performed from root exudate chemical profile under positive **(A)** and negative **(B)** ion mode. R, non-inoculated Gexin 3; S, non-inoculated Xiaohuangjin 1025; Ri, inoculated Gexin 3; Si, inoculated Xiaohuangjin 1025. The numerical values for the blue-to-red gradient bar represent $\log_2$ peak area.

cinnamate, casbene, and 6-gingerol was enhanced by *P. nicotianae* inoculation in both the resistant cultivar (Ri) and the susceptible cultivar (Si), while the accumulation of methyl 5-hydroxyferulate was suppressed, indicating that these compounds may be related to the response of tobacco to *P. nicotianae* infection. Protoanemonin and linolenic acid exhibited opposite regulation between Si and Ri. These compounds with distinct regulation as well as level of change may be associated with differences in disease resistance between Gexin 3 and Xiaohuangjin 1025.

Analysis combined with hierarchical Pearson clustering was used to visualize the differences of metabolites in the four treatments. The top 22 representative candidates were screened according to ANOVA for clearer thermographic visualization. As shown in **Figure S3**, samples from the same treatment clustered together indicating that the differentially regulated compounds obtained have similar characteristics. This also illustrated that the metabolites of pathogen infected of plants (Ri and Si) varied from those of healthy plants (R and S). In particular, Si was separated from the other three groups. This may be related to the higher disease severity of Si compared to non-inoculated groups (R and S) and Ri (no obvious disease symptoms). R was richer in SA, ferulic acid, esculetin, prohydrojasmon, glycerol tripropanoate, lycaconitine, olitorin, nudicauline, linolenic acid, rishitin, and lauric acid compared to S, while S had higher contents of tartaric acid, protoanemonin, isomyl cinnamate, abietinol, and

TABLE 1 | Parameters of OPLS-DA models based on UHPLC/ESI-Q-TOF-MS.

Sample comparison group	Ion mode	Number of principal components (principal + orthogonal)	R^2X (cum *)	R^2Y (cum)	Q^2 (cum)	VIP value > 1 variables no.
R vs. S	+	2 + 1	0.752	0.999	0.982	46
R vs. S	–	1 + 1	0.473	0.965	0.847	30
S vs. Si	+	4 + 1	0.869	0.994	0.917	29
S vs. Si	–	1 + 1	0.411	0.994	0.882	45
R vs. Ri	+	3 + 1	0.819	0.974	0.824	10
R vs. Ri	–	1 + 1	0.585	0.972	0.904	43

**cum, cumulative.*

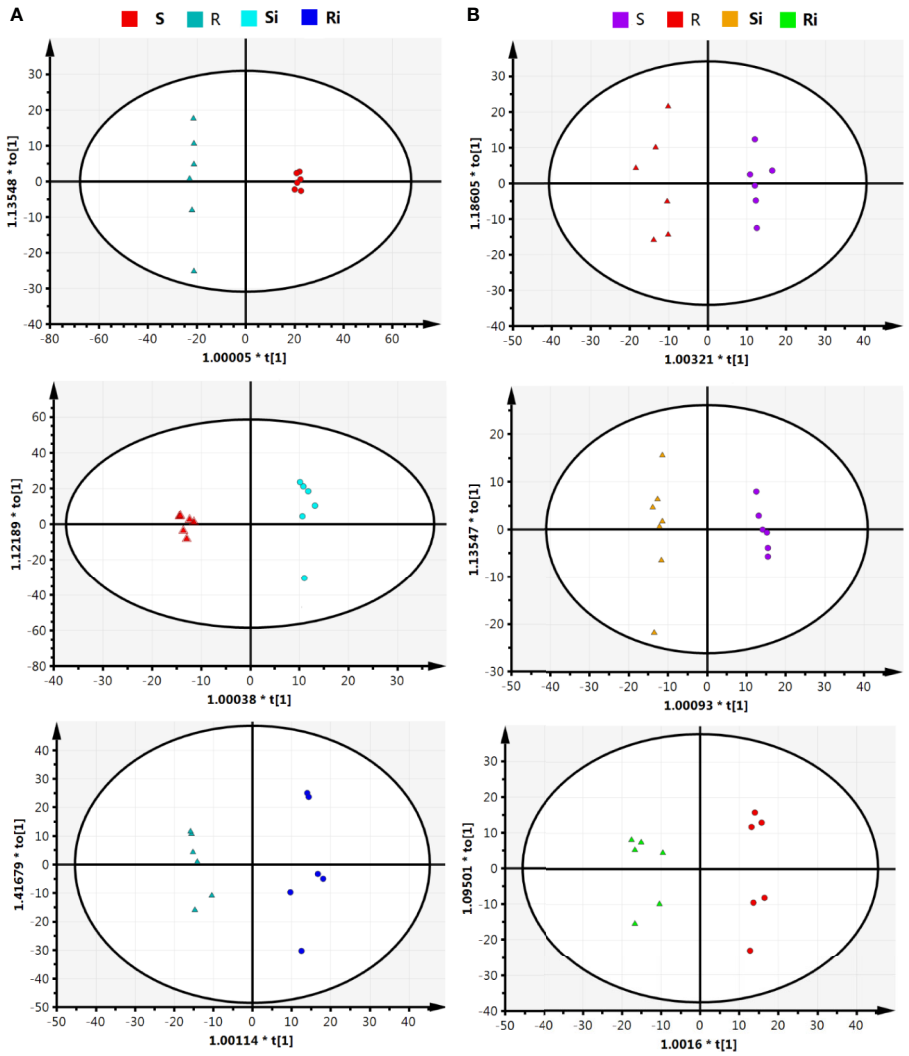

FIGURE 5 | Orthogonal partial least squares discriminant analysis (OPLS-DA) score plot on root exudate profiles gained through UHPLC-ESI/QTOF-MS analysis under condition of positive **(A)** and negative **(B)** ion mode. R, non-inoculated Gexin 3; S, non-inoculated Xiaohuangjin 1025; Ri, inoculated Gexin 3; Si, inoculated Xiaohuangjin 1025.

6-gingerol. Isoamyl cinnamate, oleic acid, 6-gingerol, SA and esculetin were upregulated both in Ri and Si.

Key Enzyme Activity in Phenylpropanoid Metabolism

As shown in **Figure 6**, activities of PAL, C4H, and 4CL were higher in the roots of Gexin 3 than in those of Xiaohuangjin 1025. The enzyme activities were significantly affected by *P. nicotianae* inoculation ($P < 0.05$). The activities of PAL, C4H and 4CL increased significantly after inoculation, and peaked at the second or third day, followed by a quick descent. All three enzymes of Gexin 3 returned to a level close to the non-inoculated plants by the fifth day, and PAL activity of Xiaohuangjin 1025 also showed a similar trend. However, C4H and 4CL activities of Xiaohuangjin 1025 finally dropped to a level significantly lower than that of the non-inoculated plants ($P < 0.05$).

Effect of Representative Compounds on *P. nicotianae* Mycelial Growth

As shown in **Table 4**, most of the compounds did not inhibit the growth of mycelium at a concentration of 5 μg ml^{-1}. Three concentrations of glycerol tripropanoate, isoamyl cinnamate, linolenic acid, and oleic acid had no inhibitory effect, and there was even a stimulatory effect on the growth of *P. nicotianae*. Octadecanoic acid, abietinol, prohydrojasmon, and casbene showed low inhibitory activity with <50% inhibition rate after treatment with 500 μg ml^{-1}. Tartaric acid, ferulic acid, and lauric

TABLE 2 | Annotation of discriminant metabolites in tobacco exudates between resistant (R) and susceptible (S) cultivars through UHPLC/ESI-Q-TOF-MS analysis, including inoculation with *P. nicotianae* (Ri and Si).

Compound	Ion mode	Retention time	Measured mass	Calculated mass	Formula	Mass error (ppm)
Tartaric acid	ESI-	12.0130	150.0171	150.0164	$C_4H_6O_6$	4.67
Salicylic acid	ESI-	7.2374	138.0322	138.0317	$C_7H_6O_3$	3.62
Ferulic acid	ESI-	6.5892	194.0584	194.0579	$C_{10}H_{10}O_4$	2.58
Dehydrochorismic acid	ESI-	9.3485	224.0331	224.0321	$C_{10}H_8O_6$	4.46
Glycerol tripropanoate	ESI+	11.1400	260.1259	260.126	$C_{12}H_{20}O_6$	-0.38
Isoamyl cinnamate	ESI+	8.1833	218.1306	218.1307	$C_{14}H_{18}O_2$	-0.46
Methyl 5-hydroxyferulate	ESI-	6.2199	210.0533	210.0528	$C_{10}H_{10}O_5$	2.38
Rishitin	ESI-	9.7571	222.1624	222.162	$C_{14}H_{22}O_2$	1.80
Protoanemonin	ESI+	11.5827	96.0207	96.0211	$C_5H_4O_2$	-4.17
Horhammericine	ESI+	11.1696	368.1729	368.1736	$C_{21}H_{24}N_2O_4$	-1.90
Esculetin	ESI-	5.5484	178.0272	178.0266	$C_9H_6O_4$	3.37
Lycaconitine	ESI-	10.5605	668.3271	668.3309	$C_{36}H_{48}N_2O_{10}$	-5.69
Olitorin	ESI-	10.0616	696.3339	696.3357	$C_{35}H_{52}O_{14}$	-2.58
Nudicauline	ESI-	10.8287	710.3388	710.3415	$C_{38}H_{50}N_2O_{11}$	-3.80
Linolenic acid	ESI-	11.3836	278.2251	278.2246	$C_{18}H_{30}O_2$	1.80
Lauric acid	ESI-	5.6513	200.1766	200.1776	$C_{12}H_{24}O_2$	-5.00
6-Hydroxyhexanoic acid	ESI-	5.0280	132.0791	132.0786	$C_6H_{12}O_3$	3.79
Oleic acid	ESI-	14.0680	282.2565	282.2559	$C_{18}H_{34}O_2$	2.13
Abietinol	ESI+	12.8227	308.2709	308.2715	$C_{20}H_{36}O_2$	-1.95
Prohydrojasmon	ESI-	9.9044	254.1887	254.1882	$C_{15}H_{26}O_3$	1.97
Casbene	ESI+	13.5474	272.2499	272.2504	$C_{20}H_{32}$	-1.84
6-Gingerol	ESI+	10.6734	294.1829	294.1831	$C_{17}H_{26}O_4$	-0.68

The annotation of metabolites was based on comparison of accurate mass to the Scripps database (with 5 PPM of tolerance). Mass error = (measured mass – calculated mass)/calculated mass × 1,000,000.

TABLE 3 | Discriminant metabolites in tobacco root exudates were selected through OPLS-DA supervised multivariate statistics and thereafter subjected to fold-change analysis.

Compound	Non-inoculated plants			Inoculated with *P. nicotianae*					
	Log_2 R/S	Change	*P* value	Log_2 R/Ri	Change	*P* value	Log_2 S/Si	Change	*P* value
Tartaric acid	-1.55	down	0.0007	-0.88	–	0.0359	0.21	down	0.4129
Salicylic acid	1.88	up	0.0003	-1.05	down	0.0001	-1.52	down	0.0023
Ferulic acid	1.65	up	0.0024	-0.64	–	0.0766	-2.37	down	<0.0001
Dehydrochorismic acid	0.44	–	0.0368	-0.76	–	0.0005	-1.14	down	0.0008
Glycerol tripropanoate	9.76	up	0.0001	-0.01	–	0.9701	-2.78	–	0.1148
Isoamyl cinnamate	-6.27	down	0.0007	-4.92	down	0.0007	-5.08	down	0.0073
Methyl 5-hydroxyferulate	-0.18	–	0.0404	2.45	up	<0.0001	1.86	up	<0.0001
Rishitin	3.29	up	0.0055	-0.76	–	0.0199	-3.69	down	<0.0001
Protoanemonin	-3.37	down	0.0003	-3.09	down	0.0002	1.78	up	0.0001
Horhammericine	-1.32	down	0.3167	-0.09	–	0.1542	1.81	up	0.0025
Esculetin	1.41	up	0.0057	-2.09	down	0.0004	-4.17	down	0.0026
Lycaconitine	6.85	up	<0.0001	0.49	–	0.0279	0.73	–	0.0844
Olitorin	5.29	up	<0.0001	0.28	–	0.0796	0.61	–	0.2540
Nudicauline	4.28	up	0.0002	0.50	–	0.0092	-1.13	–	0.0178
Linolenic acid	3.35	up	0.0002	2.12	up	<0.0001	-1.76	down	0.0002
Lauric acid	2.53	up	0.0172	-0.80	–	0.0012	-0.91	–	0.0193
6-Hydroxyhexanoic acid	2.08	up	0.0005	-0.62	–	0.0207	-1.14	down	0.0291
Oleic acid	0.45	–	0.0875	-2.03	down	<0.0001	-1.99	down	<0.0001
Abietinol	-5.69	down	0.0005	-0.47	–	0.3150	3.51	up	<0.0001
Prohydrojasmon	8.11	up	0.0002	0.73	–	0.0004	1.75	up	0.0497
Casbene	-1.33	down	0.0058	-0.09	down	0.7916	1.81	down	0.0025
6-Gingerol	-5.42	down	0.0049	-6.14	down	<0.0001	-4.66	down	0.0404

The annotation of metabolites was based on comparison of accurate mass to the Scripps database (with 5 PPM of tolerance). The significance of differences between two groups compared was determined with the Student's t-test (n = 6). Results were considered significant at a 2-tailed P value of 0.05.

acid showed strong inhibitory activity with inhibition rates of 87, 87, and 85% at 500 μg ml^{-1}, respectively. SA also showed good inhibitory activity at 500 μg ml^{-1} (50%). Overall, organic acids and fatty acids showed a relatively higher inhibitory effect on *P. nicotianae* mycelial growth compared to esters, suggesting that these compounds are associated with the allelopathy of root exudates.

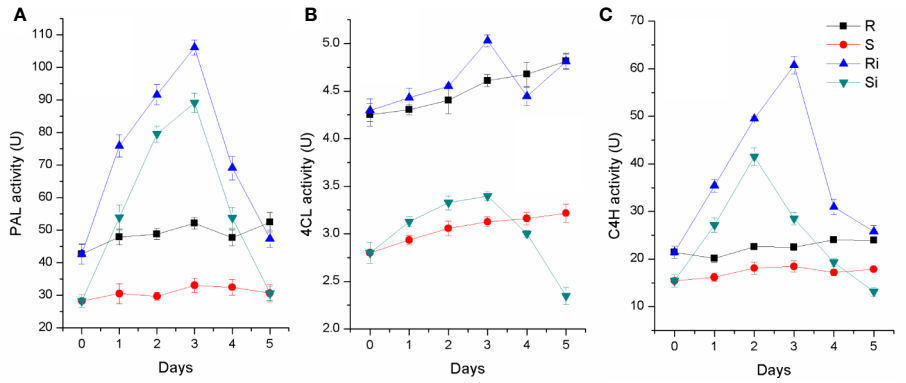

FIGURE 6 | The activities of PAL **(A)**, 4CL **(B)** and C4H **(C)** in tobacco root of Gexin 3 and Xiaohuangjin 1025 inoculated with *P. nicotianae*. R, non-inoculated Gexin 3; S, non-inoculated Xiaohuangjin 1025; Ri, inoculated Gexin 3; Si, inoculated Xiaohuangjin 1025. The values are mean ± SE of three replicates for each treatment. Bars indicate SEs.

Pot Experiment of Tobacco Black Shank Control

Ferulic acid and lauric acid were chosen for the disease control test because of their strong inhibitory activity. SA, the important disease resistance inducer, was also selected. The results of the pot experiment showed that all the compounds tested had a disease suppression effect (**Figure 7**). Compared with the control, the disease index of treatment with the three compounds was reduced by 63–70% and 27–58% at the fifth and tenth days after inoculation, respectively. The application of 500 μg ml^{-1} of ferulic acid and lauric acid showed better control efficacy than that of 100 μg ml^{-1} of SA.

DISCUSSION

Effect of Root Exudates on *P. nicotianae*

Increasing evidence suggests that plant-pathogen interaction can be mediated by root exudates. Several studies have compared the allelopathic effects of root exudates on pathogens between disease-resistant and susceptible cultivars. Stevenson et al. (1995) reported that the root exudates of two wilt-resistant chickpea (*Cicer arietinum*) cultivars significantly inhibited the spore germination of *Fusarium oxysporum* f. sp. *ciceri* as well as the hyphal growth of the germinated spores, while another two susceptible cultivars showed no antifungal activity. Schalchli et al. (2012) found that there was a positive correlation between the root exudate activity on *Gaeumannomyces grainis* var. *tritici* and disease-resistance level of wheat (*Triticum aestivum*) varieties. Similar results have also been observed in other plant–pathogen interactions, including: eggplant (*Solanum melongena*)-*Verticillium dahliae* (Zhou et al., 2011), faba bean (*Vicia faba*)-*Fusarium oxysporum* f. sp. *fabae* (Dong et al., 2014), pepper (*Capsicum annuum*)-*Phytophthora capsici* (Wang et al., 2014), cotton (*Gossypium hirsutum*)-*F. oxysporum* f. sp. *vasinfactum* (Ren and Gai, 2016), and cotton-*V. dahliae* (Wu et al., 2007). In accordance with the previous studies, our results showed that root exudates of black shank-resistant tobacco cultivar Gexin 3 significantly inhibited the zoospore germination and mycelial growth of *P. nicotianae* compared to the control, whereas the root exudates of the susceptible cultivar Xiaohuangjin 1025 stimulated the colony growth but had no effect on spore germination.

However, there was no perfect correlation between root exudate activity and the overall level of disease resistance of crops, since the defense response after root infection is another important resistance mechanism. Bani et al. (2018) found that root exudates from three *Fusarium* wilt-resistant cultivars of pea (*Pisum sativum*) inhibited spore germination of *Fusarium oxysporum* f. sp. *pisi*, but the other seven resistant cultivars, as well as two susceptible cultivars, stimulated germination. However, there is no doubt that the inhibition effect of root exudates may limit the survival and infection of soil-borne pathogens in the rhizosphere. Therefore, root exudates constitute a pre-infection defense mechanism in many crops, and can be a potential indicator for predicting crop resistance to soil-borne diseases.

Discriminant Compounds in Root Exudates

Organic acids were the most represented class of compounds in our findings. Several studies have reported that disease-resistant genotypes of crops are rich in phenolic acids (Sztejnberg et al., 1983; Bily et al., 2003; He, 2018). Jadhav et al. (2013) reported higher concentrations of ferulic acid in infected and non-infected resistant genotypes of castor (*Ricinus communis*), suggesting a critical role of phenols in castor disease resistance. Zhang et al. (2007) and Dong et al. (2014) found that the organic acid concentrations in pea root exudates showed a positive relation with disease resistance. In accordance with previous studies, higher concentrations of phenolic acids were also observed in

TABLE 4 | Effect of tested compounds on mycelial growth of *P. nicotianae*.

Compound	Mycelial growth inhibition (%)		
	Treatment with 5 μg ml^{-1}	Treatment with 50 μg ml^{-1}	Treatment with 500 μg ml^{-1}
Salicylic acid	0.16 ± 0.49 c	5.85 ± 0.76 d	50.36 ± 0.63 b
Tartaric acid	5.25 ± 0.72 a	22.12 ± 0.60 a	86.97 ± 0.91 a
Ferulic acid	5.73 ± 0.72 a	22.75 ± 0.47 a	87.05 ± 1.10 a
Glycerol tripropanoate	0.55 ± 0.72 c	1.26 ± 0.99 g	-1.12 ± 0.84 g
Isoamyl cinnamate	-0.16 ± 0.83 c	-0.95 ± 1.09g	-3.04 ± 0.73 g
Linolenic acid	-0.71 ± 0.47 c	-0.55 ± 0.49 g	3.04 ± 0.84 h
Oleic acid	0.31 ± 0.76 c	0.71 ± 0.85 g	0.08 ± 0.50 g
Lauric acid	0.24 ± 1.25 c	15.44 ± 1.31 b	85.37 ± 0.63 a
Octadecanoic acid	-0.95 ± 1.08 c	7.14 ± 0.36 c	19.05 ± 0.92 d
Abietinol	-1.88 ± 0.94 c	3.55 ± 0.63 f	21.10 ± 0.63 d
Prohydrojasmon	2.12 ± 0.85 b	4.34 ± 0.49 e	43.25 ± 0.50 c
Casbene	0.55 ± 0.49 c	1.42 ± 0.24 g	11.35 ± 0.60 e

The annotation of metabolites was based on comparison of accurate mass to the Scripps database (with 5 PPM of tolerance). Values are the means of three replicates ± SE; significance of difference was determined by one-way ANOVA followed by Tukey multiple comparisons test; the different letters within one column indicate statistically significant differences between the treatments ($P < 0.05$)

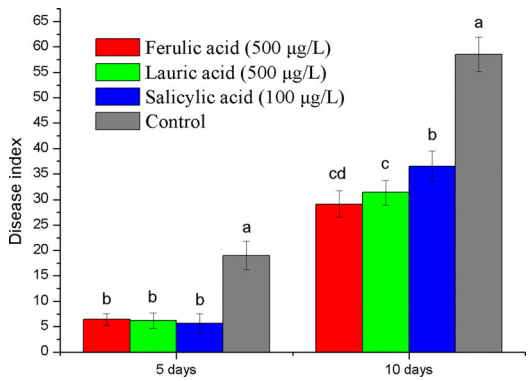

FIGURE 7 | Disease control effect evaluation of the three compounds selected by pot experiment. Lower case letters indicate statistical differences ($P < 0.05$); the values are mean ± SE of three replicates for each treatment. Bars indicate SEs.

root exudates of the resistant tobacco cultivar (R) than in those of the susceptible cultivar (S), suggesting important roles in disease resistance. SA is known as an important signal molecule for eliciting plant defenses, and especially systemic acquired resistance. Its up-regulation in root exudates of both Gexin 3 and Xiaohuangjin 1025 after *P. nicotianae* inoculation indicated that SA was involved in the plant defense response. Ferulic acid has also been reported to enhance plant disease resistance (Bily et al., 2003; He, 2018). Broad spectrum antifungal activity of organic acids (including ferulic acid and 6-hydroxyhexanoic acid) has been reported in previous studies (Ferrochio et al., 2013; Aranega-Bou et al., 2014; Ferruz et al., 2016). We also observed inhibitory effects of ferulic acid and tartaric acid against *P. nicotianae*. These results suggested that these organic acids in root exudates act not only to elicit defense responses in tobacco, but also directly inhibit *P. nicotianae* growth. Moreover, these functions may be more effective in the resistant cultivar Gexin 3 than in the susceptible cultivar Xiaohuangjin 1025.

There is increasing evidence that fatty acids are important in plant defense systems (Jiang et al., 2009; Kachroo and Kachroo, 2009). Linolenic and linoleic acid metabolites, such as oxylipins and jasmine acid, are known as signal molecules for systemic acquired resistance (SAR) (Blée, 2002). The unsaturated fatty acids, linolenic acid, linoleic acid, and oleic acid, have been reported to induce systemic resistance against *Phytophthora infestans* (Cohen et al., 1991). Increased levels of unsaturated fatty acids have been reported to enhance the resistance of tomato (*Lycopersicon esculentum*) against powdery mildew (*Erysiphe polygoni*) (Wang et al., 1998) and the resistance of eggplant against *V. dahliae* (Xing and Chin, 2000). In accordance with these observations, higher concentrations of linolenic acids in Gexin 3 root exudates indicated a possible correlation between linolenic acids and disease resistance. 6-hydroxyhexanoic acid is a derivative of hexanoic acid. This type of compound has been reported as a broad-spectrum inducer, acting mainly by enhancing the jasmonate signaling pathway (Vicedo et al., 2009; Llorens et al., 2013). 6-hydroxyhexanoic acid may play a similar role in Gexin 3, since higher content of 6-hydroxyhexanoic acid accumulated in root exudates of Gexin 3. Antifungal activity has also been reported for other fatty acids. For example, lauric acid exerts an inhibitory effect against *Aspergillus*, *Penicillium*, and *Fusarium* spp. (Altieri et al., 2009). The strong inhibitory activity of lauric acid was also observed in our study. These results indicated that fatty acids in root exudates may play a role in the plant defense response, not only by eliciting systemic resistance, but also by directly inhibiting the growth of pathogens.

Glycerol tripropanoate and isoamyl cinnamate were the main differential esters screened. Glycerol tripropanoate is mainly used in the manufacture of food, soaps, and candles, while the distribution and function of triglycerides in plants are not clear. Cinnamate and its derivative were ubiquitous in plant, but there are few studies of their roles in plant growth regulation (Shuab et al., 2016). In the current study, isoamyl cinnamate was extremely rich in root exudates of Xiaohuangjin 1025 compared to those of Gexin 3. Considering that it also showed no

significant inhibitory (500 μg ml^{-1}) or stimulatory effects on *P. nicotianae* (< 50 μg ml^{-1}), isoamyl cinnamate may be involved in the susceptibility of Xiaohuangjin 1025. However, this proposition needs further experimental verification.

Alkaloids are a kind of secondary metabolites produced by plants and are believed to serve as defense compounds (Zhang et al., 2014). Most of the alkaloids annotated in the current study are reported to exist in tobacco and other plants (Saidkhodzhaeva and Bessonova, 1996; Xie and Kúc, 1997; Bessonova and Saidkhodzhaeva, 1998; Zhong et al., 2010), but were first found in tobacco root exudates. Rishitin is a terpenoid phytoalexin, and esculetin is a coumarin phytoalexin. The accumulation of these compounds is an important resistance mechanism against pathogen infection (Gutierrez et al., 1995; Komaraiah et al., 2003). In the current study, the accumulation of esculetin was enhanced by pathogen infection for both Gexin 3 and Xiaohuangjin 1025, while rishitin was only significantly increased in Xiaohuangjin 1025. The function of horhammericine, lycaconitine, olirotin, and nudicauline in plant has been little reported, and the accumulation of these compounds was not significantly affected (except for horhammericine in Gexin 3) by *P. nicotianae* infection. Overall, the higher base level of alkaloids in root exudates of Gexin 3 is not only genetically determined, but also closely related to disease resistance.

Plant endogenous hormones have significant effects on plant growth as well as disease resistance. Jasmonate is an important inducer of the plant defense system. As a derivative of jasmonate, prohydrojasmon has the same bioactivity (Koshiyama et al., 2006). Prohydrojasmon was detected in root exudates of Gexin 3, while it was minimal in root exudates of Xiaohuangjin 1025. These results indicated that the jasmonate signal pathway was efficient in Gexin 3, but may be blocked in Xiaohuangjin 1025.

Possible Disease Resistance Signal Pathway Associated With Root Exudates

The phenylpropanoid metabolism pathway plays an important role in plant disease resistance and defense responses (Hammerschmidt, 1999), and the main defensive compounds, such as phenolics, phytoalexin, lignin, and flavonoids, need to be synthesized through this pathway (Jadhav et al., 2013). Pathogen infection usually activates phenylpropane metabolism in plants to enhance host resistance (Gong et al., 1995; Slatnar et al., 2010). There is considerable evidence to indicate that the phenylpropanoid metabolic activity of resistant varieties is significantly higher than that of susceptible varieties (Long et al., 2004; Wang et al., 2009; Bao et al., 2015). Several discriminant compounds are associated with the phenylpropanoid metabolism pathway, including SA, ferulic acid, esculetin and methyl 5-hydroxyferulate. The higher expression of these phenylpropanoid compounds in root exudates of both infected and uninfected plants indicated a higher basal and induced activity of phenylpropanoid metabolism pathway in the resistant cultivar Gexin 3 compared to the susceptible cultivar Xiaohuangjin 1025 (**Figure 8**). These suggestions were partially confirmed by key enzyme activity assays associated with the phenylpropanoid metabolism pathway. PAL is the key and rate limiting enzyme in phenylpropanoid metabolism, which is usually used to evaluate the resistance of plants (Stadnik and Buchenauer, 2000). C4H is associated with the synthesis of coumaric acid, the precursor for caffeic and ferulic acid synthesis, which can directly inhibit the growth of pathogens. 4CL catalyzes the formation of phenols, flavonoids, lignin, and other metabolites, which are believed to be important defense substances in plants. The higher activities of PAL, C4H, and 4CL in Gexin 3 may improve the synthesis and accumulation of inhibitory substances such as ferulic acid, which were in line with the root exudate profiling results. In accordance with previous studies (Gong et al., 1995; Slatnar et al., 2010), the higher activities of PAL, C4H, and 4CL were also observed in the roots of Gexin 3. These results indicated the higher phenylpropanoid metabolic activity in Gexin 3 may be associated with the secretion of antifungal substances to the rhizosphere.

Inhibitory Activity of the Discriminant Compounds on *P. nicotianae* In Vitro and In Vivo

Some discriminant compounds in tobacco root exudates showed a strong inhibitory effect against *P. nicotianae* mycelial growth, which supports the suggestion that root exudates can mediate plant disease resistance by direct inhibition of pathogens. Among them, tartaric acid and ferulic acid showed strong inhibition effect on *P. nicotianae* growth as well as disease suppression. The disease control effect has been reported in previous studies including tobacco black shank (Zhang and Wang, 2006; Fu et al., 2013; Feng et al., 2018). He (2018) reported that ferulic acid can induce resistance to gray mold (*Botrytis cinerea*) in apples. Our results also showed that SA significantly suppressed tobacco black shank by induced resistance, since it showed no inhibitory effect on *P. nicotianae* at test concentrations. Our previous study has proved that hydrojasmon has certain disease prevention effects on tobacco black shank (Feng et al., 2018). The above evidence indicated root exudates can be a source of disease resistant substances, and tartaric acid, ferulic acid, lauric acid, SA, and hydrojasmon have potential for use in tobacco black shank control.

CONCLUSIONS

The current study revealed differing metabolic patterns and functions between root exudates of a disease-resistant tobacco cultivar and a susceptible tobacco cultivar. Root exudates not only provide a pre-infection prevention strategy for tobacco by exuding antimicrobial substances to directly inhibit *P. nicotianae* growth, but also increase tobacco disease resistance by eliciting plant defense responses. Compared to the susceptible cultivar Xiaohuangjin 1025, the resistant cultivar Gexin 3 has higher richness of defensive compounds in root exudates. Our results provide useful insights into possible disease resistance mechanisms of root exudates, and attempt a beneficial utilization of these secondary metabolites of plants.

It should be noted that some inferences in this study need further experimental verification (i.e., the signal pathway related

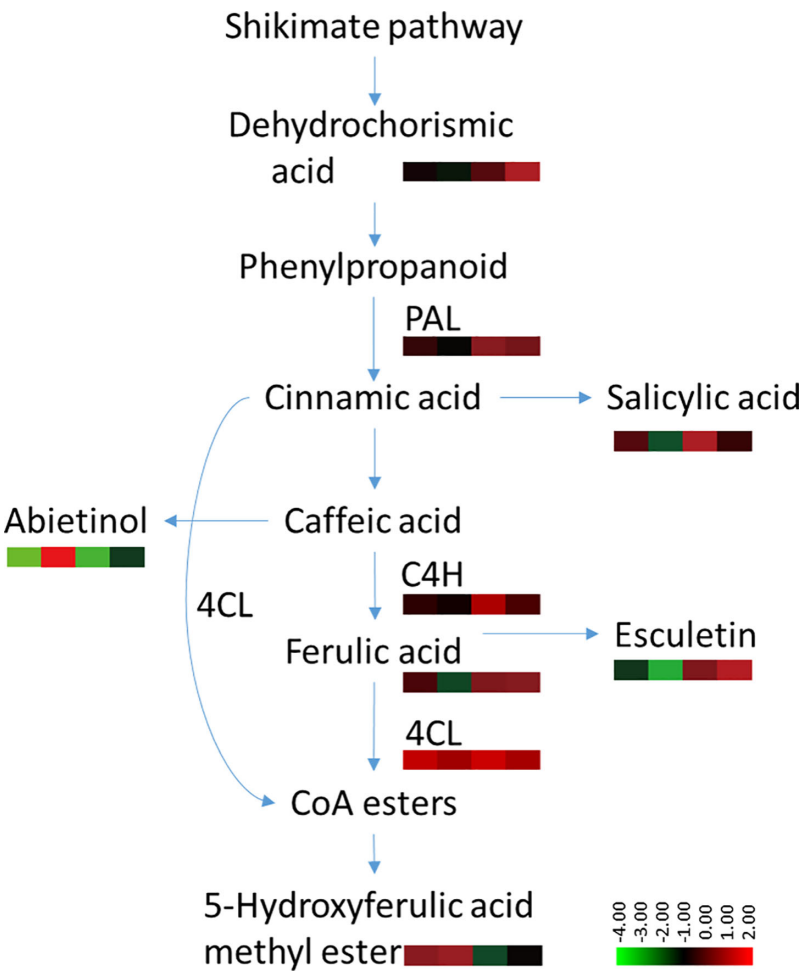

FIGURE 8 | Variable content and enzyme activities associated with the phenylpropanoid metabolism pathway in tobacco-*P. nicotianae* interaction. The annotation of metabolites was based on comparison of accurate mass to the Scripps database (with 5 PPM of tolerance). The color scale represents the relative compound abundance and enzyme activities; columns represent the four treatments from left to right: non-inoculated Gexin 3 (R), non-inoculated Xiaohuangjin 1025 (S), inoculated Gexin 3 (Ri), and inoculated Xiaohuangjin 1025 (Si). PAL, phenylalanine ammonia-lyase; C4H, cinnamate-4-hydroxylase; 4CL, 4-coumarate-CoA ligase; CoA, coenzyme A. The enzyme activity data were obtained after 3 days of pathogen inoculation.

to defense responses). In addition, root exudates can also affect the microbial community in the rhizosphere, which is worthy of further study.

DATA AVAILABILITY STATEMENT

The original contributions presented in the study are included in the article/**Supplementary Material**; further inquiries can be directed to the corresponding authors.

AUTHOR CONTRIBUTIONS

CZ and FW contributed to the conception and design of the study. CZ wrote the first draft of the manuscript. CF and JW performed the investigation. YZ performed the statistical analysis.

ACKNOWLEDGMENTS

This work was supported by Major Agricultural Technological Innovation Projects of Shandong Province: SD2019ZZ002.

SUPPLEMENTARY MATERIAL

The Supplementary Material for this article can be found online at: https://www.frontiersin.org/articles/10.3389/fpls.2020.559775/full#supplementary-material

REFERENCES

Altieri, C., Bevilacqua, A., Cardillo, D., and Sinigaglia, M. (2009). Antifungal activity of fatty acids and their monoglycerides against *Fusarium* spp. in a laboratory medium. *Int. J. Food Sci. Technol.* 44, 242–245. doi: 10.1111/j.1365-2621.2007.01639.x

Aranega-Bou, P., de la O Leyva, M., Finiti, I., García-Agustín, P., and González-Bosch, C. (2014). Priming of plant resistance by natural compounds. Hexanoic acid as a model. *Front. Plant Sci.* 5, 488. doi: 10.3389/fpls.2014.00488

Bani, M., Cimmino, A., Evidente, A., Rubiales, D., and Rispail, N. (2018). Pisatin involvement in the variation of inhibition of *Fusarium oxysporum* f. sp. *pisi* spore germination by root exudates of *Pisum* spp. germplasm. *Plant Pathol.* 67, 1046–1054. doi: 10.1111/ppa.12813

Bao, G., Bi, Y., Li, Y., Wang, Y., Wang, T., Tang, Y., et al. (2015). Comparison of phenylpropanoid pathway metabolism in slices of susceptible and resistant potato cultivars inoculated with *Fusarium sulphureum*. *Food Tech.* 36 (06), 251–256. doi: 10.7506/spkx1002-6630-201506048

Bessonova, I. A., and Saidkhodzhaeva, S. A. (1998). Alkaloids of the cultivated plant *Delphinium elatum*. *Chem. Nat. Compd.* 34, 198–199. doi: 10.1007/BF02249147

Bily, A. C., Reid, L. M., and Taylor, J. H. (2003). Dehydrodimers of ferulic acid in maize grain pericarp and aleurone: resistance factors to *Fusarium graminearum*. *Phytopathol* 93, 712–719. doi: 10.1094/PHYTO.2003.93.6.712

Blée, E. (2002). Impact of phyto-oxylipins in plant defense. *Trends Plant Sci.* 7, 315–321. doi: 10.1016/S1360-1385(02)02290-2

Canarini, A., Kaiser, C., Merchant, A., Richter, A., and Wanek, W. (2019). Root exudation of primary metabolites: mechanisms and their roles in plant responses to environmental stimuli. *Front. Plant Sci.* 10, 157. doi: 10.3389/fpls.2019.00157

Chen, C., Chen, H., Zhang, Y., Thomas, H. R., Frank, M. H., He, Y., et al. (2020). TBtools - an integrative toolkit developed for interactive analyses of big biological data. *Mol. Plant*. doi: 10.1016/j.molp.2020.06.009

Cline, E. T., Farr, D. F., and Rossman, A. Y. (2008). Synopsis of *Phytophthora* with accurate scientific names, host range, and geographic distribution. *Plant Health Prog.* 9 (1), 32. doi: 10.1094/PHP-2008-0318-01-RS

Cohen, Y., Gisi, U., and Mosinger, E. (1991). Systemic resistance of potato plant against *Phytophthora infestans* induced by unsaturated fatty acids. *Physiol. Mol. Plant Pathol.* 38, 255–263. doi: 10.1016/S0885-5765(05)80117-1

Coninck, B. D., Timmermans, P., Vos, C., Cammue, B. P. A., and Kazan, K. (2015). What lies beneath: belowground defense strategies in plants. *Trends Plant Sci.* 20, 91–101. doi: 10.1016/j.tplants.2014.09.007

Dodds, P. N., and Rathjen, J. P. (2010). Plant immunity: towards an integrated view of plant-pathogen interactions. *Nat. Rev. Genet.* 11, 539–548. doi: 10.1038/nrg2812

Dong, Y., Dong, K., Zheng, Y., Yang, Z., Tang, L., and Xiao, J. (2014). Allelopathic effects and components analysis of root exudates of faba bean cultivars with different degrees of resistance to *Fusarium oxysporum*. *Chin. J. Eco-Agri.* 22 (03), 292–299. doi: 10.3724/SP.J.1011.2014.31020

Fan, C., Bi, Y., Wang, Y., Ren, Y., Yang, Z., and Wang, Y. (2012). Effect of salicylic acid dipping on postharvest diseases and phenylpropanoid pathway in muskmelon fruits. *Scientia Agric. Sin.* 45 (03), 584–589. doi: 10.3864/j.issn.0578-1752.2012.03.022

Feng, C., Zhan, H., Cui, M., Xu, C., Wang, J., Wang, X., et al. (2018). Inhibition effect of root exudates on *Phytophthora parasitica* var *nicotianae*. *Tobacco Sci. Tech.* 51 (09), 7–13. doi: 10.16135/j.issn1002-0861.2017.0096

Ferrochio, L., Cendoya, E., Farnochi, M. C., Massad, W., and Ramírez, M. L. (2013). Evaluation of ability of ferulic acid to control growth and fumonisin production of *Fusarium verticillioides* and *Fusarium proliferatum* on maize based media. *Int. J. Food Microbiol.* 167, 215–220. doi: 10.1016/j.ijfoodmicro.2013.09.005

Ferruz, E., Atanasova-Pénichon, V., Bonnin-Verdal, M., Marchegay, G., Pinson-Gadais, L., Ducos, C., et al. (2016). Effects of Phenolic Acids on the Growth and Production of T-2 and HT-2 Toxins by *Fusarium langsethiae* and *F. sporotrichioides*. *Molecules* 21 (4), 449. doi: 10.3390/molecules21040449

Fu, R., Chen, Z., Zhou, B., and Ma, L. (2013). Effects of lauric acid to tomato leaf mildew and resistance physiology indexes of tomato. *J. Shenyang Agric. Univ.* 44 (04), 418–422. doi: 10.3969/j.issn.1000-1700.2013.04.007

Gfeller, A., Glauser, G., Etter, C., Signarbieux, C., and Wirth, J. (2018). *Fagopyrum esculentum* alters its root exudation after *Amaranthus retroflexus* recognition and suppresses weed growth. *Front. Plant Sci.* 9, 50. doi: 10.3389/fpls.2018.00050

Gong, D., Chen, R., and Lin, Y. (1995). Relation between phenylpropanoid metabolism in sugarcane and resistance to smut. *J. Fujian. Agric. Uni.* 24 (4), 394–398. doi: 10.13323/j.cnki.j.fafu(nat.sci.).1995.04.004

Gutierrez, M.-C., Parry, A., Tena, M., Jorrin, J., and Edwards, R. (1995). Abiotic elicitation ofcoumarin phytoalexins in sunflower. *Phytochem.* 38, 1185–1191. doi: 10.1016/0031-9422(94)00808-7

Hammerschmidt, R. (1999). Induced disease resistance: how do induced plants stop pathogens? *Physiol. Mol. Plant Pathol.* 55, 77–84. doi: 10.1006/pmpp.1999.0215

Han, T., You, C., Zhang, L., Feng, C., Zhang, C., Wang, J., et al. (2016). Biocontrol potential of antagonist *Bacillus subtilis* Tpb55 against tobacco black shank. *BioControl* 61, 195–205. doi: 10.1007/s10526-015-9705-0

He, J. (2018). Phlorizin and ferulic acid treatment reinforce the resistance system in postharvest apple fruit during gray mold infection. *Northwest A&F Univ. 2018.*

Jadhav, P. R., Mahatma, M. K., Mahatma, L., Jha, S., Parekh, V. B., and Khandelwal, V. (2013). Expression analysis of key genes of phenylpropanoid pathway andphenol profiling during *Ricinus communis–Fusarium oxysporum* f. sp.*ricini* interaction. *Indus. Crops Prod.* 50, 456– 461. doi: 10.1016/j.indcrop.2013.08.022

Jiang, C., Shimono, M., Maeda, S., Inoue, H., Mori, M., Hasegawa, M., et al. (2009). Suppression of the rice fatty-acid desaturase gene *OsSSI2* enhances resistance to blast and leaf blight diseases in rice. *Mol. Plant-Microbe Interact.* 22, 820–829. doi: 10.1094/MPMI-22-7-0820

Kachroo, A., and Kachroo, P. (2009). Fatty Acid–Derived Signals in Plant Defense. *Annu. Rev. Phytopathol.* 47, 153–176. doi: 10.1146/annurev-phyto-080508-081820

Komaraiah, P., Reddy, G. V., Srinivas Reddy, P., Raghavendra, A. S., Ramakrishna, S. V., and Reddanna, P. (2003). Enhanced production of antimicrobial sesquiterpenes and lipoxygenase metabolites in elicitor-treated hairy root cultures of *Solanum tuberosum*. *Biotech. Lett.* 25, 593–597. doi: 10.1023/A:1023038804556

Koshiyama, M., Seto, H., Kamuro, Y., and Kateora, M. (2006). A jasmonic acid analog, PDJ, comes into practical use as a plant growth regulator. *Plant Growth Regul.* 38, 35–47.

Llorens, E., Fernández-Crespo, E., Vicedo, B., Lapeña, L., and García-Agustín, P. (2013). Enhancement of the citrus immune system provides effective resistance against *Alternaria* brown spot disease. *J. Plant Physiol.* 170, 146–154. doi: 10.1016/j.jplph.2012.09.018

Long, S., Li, Y., Duan, S., Zhang, Y., Li, Q., Wang, W., et al. (2004). Relationship between metabolites of phenylpropanoid metablism and resistance of corn to stalk rot. *J. N.W. SCI-TECH Uni. Agri.and Fore.* 32 (09), 93–96. doi: 10.13207/j.cnki.jnwafu.2004.09.022

Luan, H., Meng, N., Liu, P., Feng, Q., Lin, S., Fu, J., et al. (2014). Pregnancy-induced metabolic phenotype variations in maternal plasma. *J. Proteome Res.* 13, 1527–1536. doi: 10.1021/acs.jproteome.5b00430

Panabières, F., Ali, G. S., Allagui, M. B., Dalio, R. J. D., Gudmestad, N. C., Kuhn, M. L., et al. (2016). *Phytophthora nicotianae* diseases worldwide: new knowledge of a long-recognised pathogen. *Phytopathol. Mediterr.* 55, 20–40. doi: 10.14601/Phytopathol-Mediterr-16423

Ren, Z., and Gai, Q. (2016). Root exudates of resistant and susceptible cotton cultivars and its effects on *Fusarium oxysporum* f. sp. *Vasinfectum*. *Acta Agric. Boreali-Occident. Sin.* 25 (05), 702–706. doi: 10.7606/j.issn.1004-1389.2016.05.009

Saidkhodzhaeva, S. A., and Bessonova, I. A. (1996). Alkaloids of *Delphinium retropilosum*. *Chem. Nat. Compd.* 32 (5), 720–722. doi: 10.1007/BF01375123

Schalchli, H., Pardo, F., Hormazabal, E., Palma, R., Guerrero, J., and Bensch, E. (2012). Antifungal activity of wheat root exudate extracts on *Gaeumannomyces graminis* var. *tritici* growth. *J. Soil Sci. Plant Nutr.* 12, 329–337. doi: 10.4067/S0718-95162012000200012

Shuab, R., Lone, R., and Koul, K. K. (2016). Cinnamate and cinnamate derivatives in plants. *Acta Physiol. Plant* 38, 64. doi: 10.1007/s11738-016-2076-z

Slatnar, A., Mikulic, P. M., Halbwirt, H., Stampar, F., Stich, K., and Veberic, R. (2010). Enzyme activity of the phenylpropanoid pathway as a response to apple scab infection. *Ann. Appl. Biol.* 156 (3), 449–456. doi: 10.1111/j.1744-7348.2010.00402.x

Stadnik, M. J., and Buchenauer, H. (2000). Inhibition of phenylalanine ammonia-lyase suppresses the resistance induced by benzothiadiazole in wheat to *Blumeria graminis* f. sp. *tritici*. *Physiol. Mol. Plant Pathol.* 57 (1), 25–34. doi: 10.1006/pmpp.2000.0276

Stevenson, P. C., Padgham, D. E., and Haware, M. P. (1995). Root exudates associated with the resistance of four chickpea cultivars (*Cicer arietinum*) to two races of *Fusarium oxysporum* f.sp. *cicero*. *Plant Pathol.* 44, 686–694. doi: 10.1111/j.1365-3059.1995.tb01692.x

Sztejnberg, A., Azaizia, H., and Chet, I. (1983). The possible role of phenolic compounds in resistance of horticultural crops to *Dematophora nexatrix* Hartig. *J. Phytopathol.* 107, 318–322. doi: 10.1111/j.1439-0434.1983.tb00551.x

Tsunoda, T., and van Dam, N. (2017). Root chemical traits and their roles in belowground biotic interactions. *Pedobiologia - J. Soil Eco.* 65, 58–67. doi: 10.1016/j.pedobi.2017.05.007

van Dam, N. M., and Bouwmeester, H. J. (2016). Metabolomics in the rhizosphere: tapping into belowground chemical communication. *Trends Plant Sci.* 21, 256–265. doi: 10.1016/j.tplants.2016.01.008

Vicedo, B., Flors, V., de la O Leyva, M., Finiti, I., Kravchuk, Z., Real, M. D., et al. (2009). Hexanoic acid-induced resistance against *Botrytis cinerea* in tomato plants. *Mol. Plant Microbe Interact.* 22 (11), 1455–1465. doi: 10.1094/MPMI-22-11-1455

Vives-Peris, V., de Ollas, C., Gómez-Cadena, A., and Pérez-Clemente, R. M. (2019). Root exudates: from plant to rhizosphere and beyond. *Plant Cell Rep.* 39 (11), 3–17. doi: 10.1007/s00299-019-02447-5

Wang, C., Chin, C. K., and Chen, A. (1998). Expression of the yeast D-9 desaturase gene in tomato enhances its resistance to powdery mildew. *Physiol. Mol. Plant Pathol.* 52, 371–383. doi: 10.1006/pmpp.1998.0158

Wang, W., Ruan, M., Qiu, Y., Wang, W., Ke, Y., and Pan, T. (2009). Phenylaprapanoid metabolism of sweet potato against *Pseudomonas solanacearum*. *Chin. J. Eco-Agri.* 17 (05), 944–948. doi: 10.3724/SP.J.1011.2009.00944

Wang, J., Lyu, Y., Yu, D., Zhang, W., Piao, F., and Shen, S. (2014). Effects of root exudates from different resistant pepper varieties on *Phytaphthara capsici*. *China Veget.* 1, 13–16.

Wang, Y., Xu, Y., Sun, Y., Wang, H., Qi, J., Wan, B., et al. (2018). Leucine-rich repeat receptor-like gene screen reveals that *Nicotiana* RXEG1 regulates glycoside hydrolase 12 MAMP detection. *Nat. Commun.* 9, 594. doi: 10.1038/s41467-018-03010-8

Whalley, W. M., and Taylor, G. S. (1973). Influence of pea-root exudates on germination of conidia and chlamydospores of physiologic races of *Fusarium oxysporum* f. *pisi*. *Ann. Appl. Biol.* 73, 269–276. doi: 10.1111/j.1744-7348.1973.tb00933.x

Wu, Y. X., Shen, X. J., and Fang, W. P. (2007). The effects of cotton root exudates on growth and development of *Verticillium dahliae*. *Cotton Sci.* 19, 286–290. doi: 10.1007/s11703-008-0079-2

Wu, H., Liu, D., Ling, N., Bao, W., Ying, R., and Shen, Q. (2008). Influence of root exudates of watermelon on *Fusarium oxysporum* f. sp. *niveum*. *Soil. Sci. Soc Am. J.* 73, 1150–1156. doi: 10.2136/sssaj2008.0266

Xie, C., and Kúc, J. (1997). Induction of resistance to *Peronospora tabacina* in tobacco leaf disks by leaf disks with induced resistance. *Physiol. Mol. Plant Pathol.* 51, 279–286. doi: 10.1006/pmpp.1997.0104

Xing, J., and Chin, C. (2000). Modification of fatty acids in eggplant affects its resistance to *Verticillium dahlia*. *Physiol. Mol. Plant Pathol.* 56, 217–225. doi: 10.1006/pmpp.2000.0268

Zhang, Y., and Wang, X. (2006). Effects of ferulic acid and oxalic acid to cowpea *Fusarium* wilt. *J. Anhui Agri.Sci.* 34 (13), 3113–3114. doi: 10.13989/j.cnki.0517-6611.2006.13.088

Zhang, J., Wang, J., and Xu, Y. (2007). Comparative study on organic acids and phenolic acids in root exudates of soybean cultivars. *J. Anhui Agric. Sci.* 35 (23), 7127–7129. doi: 10.13989/j.cnki.0517-6611.2007.23.052

Zhang, Y., Liu, H., Zhang, Z., Ma, C., Zhang, Z., Chen, Y., et al. (2014). The eco-physiological function of alkaloid and factors influencing the alkaloid formation. *Chin. Agric. Sci. Bull.* 30 (28), 251–254. doi: 10.11924/j.issn.1000-6850.2014-1584

Zhang, C., Gao, J., Han, T., Tian, X., and Wang, F. (2017). Integrated control of tobacco black shank by combined use of riboflavin and *Bacillus subtilis* strain Tpb55. *BioControl* 62, 835–845. doi: 10.1007/s10526-017-9849-1

Zhong, X., Wang, G., Wang, Y., Zhang, Q., and Ye, W. (2010). Monomeric indole alkaloids from the aerial parts of *Catharanthus roseus*. *Acta Pharma. Sin.* 45 (04), 471–474. doi: 10.16438/j.0513-4870.2010.04.005

Zhou, B., Chen, Z., Du, L., Xie, Y., and Ye, X. (2011). Allelopathy of the root exudates from different resistant eggplants to *Verticillium* wilt (*Verticillium dahliae* Kleb.). *Acta Ecol. Sin.* 31 (14), 3964–3972. doi: 10.1186/1471-2164-12-399

Zhou, C. X., Zhou, D. H., Elsheikha, H. M., Zhao, Y., Suo, X., and Zhu, X. Q. (2016). Metabolomic profiling of mice serum during toxoplasmosis progression using liquid chromatography–mass spectrometry. *Sci. Rep.* 6, 19557. doi: 10.1038/srep19557

Conflict of Interest: The authors declare that the research was conducted in the absence of any commercial or financial relationships that could be construed as a potential conflict of interest.

frontiers in Plant Science

ORIGINAL RESEARCH
published: 25 September 2020
doi: 10.3389/fpls.2020.562399

Effects of Nutrient and Water Supply During Fruit Development on Metabolite Composition in Tomato Fruits (*Solanum lycopersicum* L.) Grown in Magnesium Excess Soils

Yangmin X. Kim[1†], *Min Cheol Kwon*[2†], *Seulbi Lee*[1], *Eun Sung Jung*[3], *Choong Hwan Lee*[2,3,4*] and *Jwakyung Sung*[5*]

[1] National Institute of Agricultural Sciences, Rural Development Administration, Wanju, South Korea, [2] Department of Bioscience and Biotechnology, Konkuk University, Seoul, South Korea, [3] Department of Systems Biotechnology, Konkuk University, Seoul, South Korea, [4] Research Institute for Bioactive-Metabolome Network, Konkuk University, Seoul, South Korea, [5] Department of Crop Science, College of Agriculture, Life and Environment Sciences, Chungbuk National University, Cheongju, South Korea

OPEN ACCESS

Edited by:
Zsófia Bánfalvi,
National Agricultural Research and Innovation Centre, Hungary

Reviewed by:
Nina Kacjan Marsic,
University of Ljubljana, Slovenia
Radu Liviu Sumalan,
Banat University of Agricultural Sciences and Veterinary Medicine, Romania

***Correspondence:**
Choong Hwan Lee
chlee123@konkuk.ac.kr
Jwakyung Sung
jksung73@chungbuk.ac.kr

[†]These authors have contributed equally to this work

Specialty section:
This article was submitted to Plant Metabolism and Chemodiversity, a section of the journal Frontiers in Plant Science

Received: 03 June 2020
Accepted: 04 September 2020
Published: 25 September 2020

Citation:
Kim YX, Kwon MC, Lee S, Jung ES, Lee CH and Sung J (2020) Effects of Nutrient and Water Supply During Fruit Development on Metabolite Composition in Tomato Fruits (Solanum lycopersicum L.) Grown in Magnesium Excess Soils. Front. Plant Sci. 11:562399. doi: 10.3389/fpls.2020.562399

Tomato cultivation in the greenhouse or field may experience high surplus salts, including magnesium (Mg^{2+}), which may result in differences in the growth and metabolite composition of fruits. This study hypothesized that decreasing the supply of nutrients and/or water would enhance tomato fruit quality in soils with excess Mg^{2+} that are frequently encountered in the field and aimed to find better supply conditions. For tomato plants cultivated in plastic pots using a plastic film house soil, the fertilizer supply varied in either the nitrogen (N) or potassium (K) concentration, which were either 0.1 (lowest) or 0.75 times (lower) than the standard fertilizer concentrations. Water was supplied either at 30 (sufficient) or 80 kPa (limited) of the soil water potential. Lycopene content on a dry-weight basis (mg/kg) was enhanced by the combination of lowest N supply and sufficient water supply. However, this enhancement was not occurred by the combination of the lowest N supply and limited water supply. Sugars and organic acids were decreased by limiting the water supply. Therefore, we carefully suggest that an adjustment of nitrogen with sufficient watering could be one of strategies to enhance fruit quality in excess Mg^{2+} soils.

Keywords: water, tomato fruit quality, mineral nutrient, metabolite profiling, lycopene

INTRODUCTION

There is worldwide concern about soil salinization reaching 20% of irrigated land, which would cause a reduction in crop growth (Adams et al., 2019). The greenhouse cultivation of tomatoes (*Solanum lycopersicum* L.), including in plastic film houses, involves the application of an extensive amount of fertilizers and produces an accumulation of surplus salts in soil (e.g., Mg^{2+}, Ca^{2+}, Na^{+}, SO_4^{2-}, and Cl^{-}). Those surplus salts hinder water transport from soil to roots by producing negative osmotic potential in the soil and by changing root anatomy and root hydraulic conductivity

(Adams et al., 2019). Saline drainage water containing not only high Na^+ but also high Mg^{2+} has been used to cultivate tomatoes in the field (Mitchell et al., 1991). Recently, the effects of Mg oversupply on the metabolite content of tomato plants and fruits were extensively investigated by Kwon et al. and they reported poor fruit quality under excess Mg conditions (Kwon et al., 2019).

To improve fruit quality with enhanced nutrients and functional metabolites, many studies have applied minimal nutrients and irrigation to horticultural plants (Stefanelli et al., 2010). Developing a strategy to apply minimal nutrients and water in agriculture is appropriate considering the current context, e.g., increasing demand for an environmentally friendly strategy and the negative attitude toward genetically modified food (Liu et al., 2015; Carillo et al., 2020). Especially for tomato fruits, optimal nitrogen (N) and potassium (K) supplies in hydroponic tomato cultures were reported to be needed for the best lycopene content that is an antioxidant and a representative functional metabolite of tomato (Simonne et al., 2007; Almeselmani et al., 2010). Either the lowest or the medium level of N supply among the varying applications of N produced best lycopene content in tomato studies both in hydroponics and field studies (Aziz, 1968; Simonne et al., 2007; Kuscu et al., 2014). For K supply, there was a study showing that a medium level of K supply among the varying applications of K produced the best lycopene content of tomatoes in hydroponic cultures (Simonne et al., 2007), although the general trend of K was that increasing K concentration increased lycopene production (Dumas et al., 2003). Deficit irrigation improved the tomato fruit quality by increasing fruit soluble solid levels and concentrations of hexoses, citric acid, and potassium (Mitchell et al., 1991). The enhancement of the lycopene content of tomatoes has been reported under restricted irrigation conditions (Stefanelli et al., 2010; Wang and Xing, 2017). The combination of reduced water supply and high NPK fertilizer concentrations enhanced tomato fruit quality by increasing lycopene, organic acid, and soluble sugar content (Wang and Xing, 2017). The combined effects of nitrogen fertilization and water have been investigated for soluble sugar, vitamin C, and free amino acid contents, not only in tomato fruits but also in cucumber, and it was demonstrated that fruit quality increased under low irrigation conditions and a medium level of N application (Zhang et al., 2011). Therefore, controlling the nutrient and water supply is applicable for the purpose of enhancing fruit quality.

We postulated that minimal nutrient and water supplies may improve tomato quality in soils with surplus salt, which are frequently encountered in the field. Our aim in this study was to provide guidelines to improve tomato fruit quality by nutrient and water regulation in the case of excess Mg^{2+} soils. We hypothesized that minimal nutrient and water use may work in excess Mg^{2+} soil. In order to achieve our goal, the effects of a low nutrient level (N or K) compared to the standard level and/or a reduction in the water supply compared to sufficient water supply were analyzed in the case of excess Mg^{2+} soils. The scope of our study did not include comparing the case of Mg^{2+} excess soils and that of Mg^{2+} non-excess soils. The standard condition was the recommended nutrient supply for tomato cultivation in greenhouses (NIAS, 2017). The lower nutrient level was 0.75 times of the standard (N0.75, K0.75) and the lowest nutrient level was 0.1 times of the standard (N0.1, K0.1). We investigated the resulting fruits' lycopene content and primary metabolites, including sugars and organic acids, which affect tomato taste. The primary metabolites were measured using a non-targeted metabolomics using a comprehensive approach to evaluate different metabolomes under a specific set of conditions (Son et al., 2016). We have previously applied the method to investigate metabolic changes in various crops, including tomato plants, in response to varying environmental factors, such as light or mineral nutrient supply (Jung et al., 2013; Sung et al., 2015; Kim et al., 2018; Sung et al., 2018).

MATERIALS AND METHODS

Plant Materials, Soil Chemical Properties, and Variations in Nutrient and Water Supply

Three-month-old tomato seedlings (*Solanum lycopersicum* L., 'Super Dotaerang') were transplanted into plastic pots (15 L) containing 11 kg of soil on April 5, 2018 and were grown for 16 weeks at daily temperatures between 15–35°C in a greenhouse in the National Institute of Agricultural Sciences, Rural Development Administration, in Jeonju, Korea. Even though the temperature in the greenhouse fluctuated throughout the experimental period, the heating and ventilating systems were operated to avoid extreme temperature conditions (critical lowest and highest temperatures for tomato cultivation). The relative humidity in the greenhouse was not controlled, and natural light penetrating into the greenhouse was the only source of light. The fertilizer supply was in accordance with the recommendations for tomato cultivation in greenhouse soil (NIAS, 2017). For experimental group receiving the standard nutrient supply, the initial fertilizer containing N, P, K, and livestock manure-based compost was supplied at the recommended concentration and the initial fertilizer containing Mg was oversupplied to produce a high level of soil exchangeable Mg^{2+} (over the optimal level, 2.0 cmol kg^{-1} (**Table S1**). Two split applications of N, K, and Mg fertilizer were conducted by top-dressing (**Table S2**). To see the effects of low nitrogen and potassium supplies, the initial and additional fertilizer supplies varied either the N or K concentration by either 0.1 or 0.75 times the standard (N0.1, N0.75, K0.1, K0.75). The soils contained a high concentration of exchangeable Mg^{2+} (3.3–9.0 cmol kg^{-1}) after the final harvest. The soil pH was monitored during cultivation and the lowered pH of the soil was amended by applying saturated $Ca(OH)_2$ solution. To analyze water supply effects, variations in water supply started from fruit setting; water was supplied either at 30 kPa for the sufficient supply or 80 kPa of soil water potential for the limited supply by reading tensiometers (Soilmoisture Equipment Corp., Santa Babara, USA). The tensiometer's gypsum block, which senses the water potential, was placed at depth of the 0.07–0.13 m below the soil surface. There were 10 nutrient x water supply conditions. To improve the fruit setting, fully expanded flowers were treated

with hormones (gibberellin and 4-chlorophenoxyacetic acid). Ripened fruits from 40 plants were harvested at similar ripening stages at 10:00 to avoid the diurnal changes in metabolites (four plants for each nutrient x water supply condition). One to seven ripened tomato fruits from each plant were harvested from 28 June to 24 July.

Measurement of Physiological Parameters

Chlorophyll content was measured at the final harvest that was 16 weeks after the mineral nutrient treatments. A chlorophyll meter (SPAD-502Plus, Konica Minolta Sensing, Osaka, Japan) measured the SPAD values for the leaves closest to the tomato fruits (9^{th}–10^{th} nodes from the bottom), which were used as an indicator of plant performance rather than as a highly accurate measure of chlorophyll content.

Sample Preparation and Gas Chromatography-Time of Flight-Mass Spectrometry (GC-TOF-MS) Analysis

Lyophilized fruit samples were ground to powder using a mortar and pestle and were stored at −80°C. For primary metabolite extraction, 100 mg of sample was mixed with 1 ml of 80% (v/v) methanol and sonicated for 10 min. After the samples were homogenized for 10 min at 30 Hz/s by a mixer mill (Retsch GmbH & Co., Haan, Germany), the sample was centrifuged for 10 min at 27,237 × g and 4°C. The supernatants were filtered *via* a 0.2-μm polytetrafluoroethylene filter and were concentrated using a speed vacuum (Modulspin 31, Biotron, Seoul, Korea).

The dried extracts were derivatized through oximation and silylation reactions prior to GC-TOF-MS analysis. The oximation was performed by adding 50 μl of methoxyamine hydrochloride in pyridine (20 mg/ml) to the dried samples and the mixture was incubated for 90 min at 30°C. Subsequent silylation was performed by adding 50 μl of N-methyl-N-(trimethylsilyl)-trifluoroacetamide (MSTFA) to the mixture and incubating the mixture for 30 min at 37°C. A GC-TOF-MS analysis was performed using an Agilent 7890A GC system (Palo Alto, CA, USA) coupled with an Agilent 7693 auto-sampler and a TOF Pegasus III mass spectrometer (LECO, St. Joseph, MI, USA). The derivatized samples were injected with 1 μl with a split ratio of 1:5. For separation, an Rtx-5MS column (i.d. 30 m × 0.25 mm; 0.25 μm particle size; Restek Corp., Bellefonte, PA, USA) was used alongside a helium carrier gas with a flow rate of 1.5 ml/min. The injector and transfer line temperatures were 250 and 240°C, respectively. The oven temperature of the GC was programmed as follows: 75°C for 2 min, increased to 300°C at a rate of 15°C/min, and kept at 300°C for 3 min. Electron ionization was in EI mode at −70 eV, with a scan range of 45–1,000 mass to charge ratio (m/z).

Lycopene Analysis

For lycopene extraction, each powdered sample (200 mg) was extracted with 3 ml of chloroform/DCM (2:1, v/v) using a twist shaker (Biofree, Seoul, Korea) at 60 rpm for 20 min and then 1 ml of 1M sodium chloride solution was added. Subsequently, the extracts were centrifuged at 5,000 rpm for 10 min at 4°C, and the organic phases were filtered using Millex® GP 0.22 μm filters. The filtered organic phase was completely dried using a speed-vacuum concentrator (Biotron, Seoul, Korea). The dried samples were reconstituted with MeOH/MTBE (tert-Butyl methyl ether) (3:2, v/v) to a final concentration of 10 mg/ml. Lycopene content was analyzed by a UHPLC-DAD system. The UHPLC-DAD system consisted of a Dionex UltiMate 3000 RS Pump, a RS Autosampler, a RS Column Compartment, and a RS Diode Array Detector (Dionex Corporation, Sunnyvale, USA). Chromatographic separation was performed on a YMC carotenoid C30 column (250mm x 4.6mm x 5 μm particle size; YMC, Wilmington, NC) and the injection volume was 10 μl. The flow rate was 0.3 ml/min. The mobile phase consisted of 95% aqueous methanol (A) and MTBE (B). The gradient parameters were set as follows: 20% solvent B was maintained initially for 3 min, followed by a linear increase to 100% solvent B over 25 min and solvent B was then sustained at 100% for 3 min, with a gradual decrease to 20% solvent B over 6 min. The total run time was 37 min and sample absorbance was measured at 200–600 nm. Lycopene was identified based on its retention time and absorbance spectra, which were compared to the retention times of the lycopene standards.

Data Processing and Multivariate Statistical Analysis

Analyses were conducted of at least 4 biological replicates. The GC-TOF-MS raw data were converted to NetCDF (*.cdf) using the LECO Chroma TOF software (version 4.44). Converted CDF data were preprocessed with the MetAlign software package (http://www.metalign.nl) for peak detection, retention time correction, and alignment. The resulting data were exported to an Excel file. The multivariate statistical analyses, including partial least square-discriminant analysis (PLS-DA) score plot and loading plot, were performed by SIMCA-P+ 12.0 software. Variable importance in the projection (VIP) value was applied to select the discriminant variables among experimental groups. Selected metabolites were tentatively identified by comparisons with various data, including mass fragment patterns, retention times, and mass spectrums of data for standard compounds under the same conditions from published papers and commercial databases, such as the National Institutes of Standards and Technology (NIST) Library (version 2.0, 2011, FairCom, Gaithersburg, MD, USA), and Wiley 8, BioCyc Database Collection (https://biocyc.org/). Significant differences ($p < 0.05$) were tested by a one-way ANOVA using Statistica (version 7.0, StatSoft Inc., Tulsa, OK, USA).

RESULTS

Tomato Plant and Fruit Productions

The leaf chlorophyll content (SPAD value) and fruit yield were measured to compare the effects of mineral nutrient and water supply on shoot growth and fruit production of tomato plants (**Table 1**). Leaf SPAD values generally decreased, although not statistically significantly, as N or K supply was decreased under

sufficient water supply. The nutrient supply of N0.75 and N0.1 induced symptoms of yellowish leaves, and the K0.75 and K0.1 supply caused brown dots in the leaves (data not shown). Leaf SPAD values were higher under limited water supply conditions than under sufficient irrigation, and it is speculated that plant growth was slowed by the water limitation, resulting in higher SPAD values. The symptoms in the leaves under N0.75, N0.1, K0.75, and K0.1 supplies were suppressed under limited water supply conditions compared to sufficient water, and this indicates that leaves experienced less nutrient deficiency under limited water than sufficient water condition (see *Discussion*). The leaf SPAD values of N0.1-SW were significantly lower than those of SN-LW and K0.1-LW. The fruit yields under N0.75 and N0.1 applications were similar to the plants receiving the standard nutrient supply; however, plants receiving K0.75 and K0.1 treatments had improved fruit yields compared to the standard. Under all nutrient conditions, the limited water supply reduced fruit production. Nevertheless, none of the detected differences in fruit yield were significant.

TABLE 1 | Leaf chlorophyll content (SPAD) and fruit yield per plant cultivated under varied nutrient and water conditions.

Nutrient Supply	Water supply	Abbreviated name	Leaf SPAD at the final harvest	Fruit yield (g/plant)
Standard	Sufficient	SN-SW	$42.5 \pm 4.7^{ab*}$	261^{ns}
	Limited	SN-LW	44.1 ± 6.8^{a}	131
N0.75	Sufficient	N0.75-SW	34.8 ± 12.4^{ab}	221
	Limited	N0.75-LW	42.7 ± 6.8^{ab}	194
N0.1	Sufficient	N0.1-SW	25.1 ± 6.1^{b}	249
	Limited	N0.1-LW	29.5 ± 7.0^{ab}	149
K0.75	Sufficient	K0.75-SW	44.8 ± 1.2^{a}	272
	Limited	K0.75-LW	39.4 ± 13.1^{ab}	146
K0.1	Sufficient	K0.1-SW	33.5 ± 11.6^{ab}	415
	Limited	K0.1-LW	45.3 ± 1.3^{a}	382

Mean values ± SD of four biological replicates.
**Different alphabetical letters in a column indicate significant differences, as determined by ANOVA followed by Tukey's test ($p < 0.05$). Ns: no significant differences in a column without letters. SN, standard nutrient; SW, sufficient water; LW, limited water.*

Lycopene Content of Tomato Fruits Cultivated Under Different Mineral Nutrient and Water Supplies

We investigated the effect of mineral nutrient and water supply on lycopene content as a representative metabolite for tomato fruit quality (**Figure 1**). In N0.1-SW, lycopene content was significantly enhanced compared to the SN-SW, although the standard deviations were rather high (see *Discussion*). In N0.1-LW, the lycopene-increasing effects of N0.1 disappeared under a limited water supply. There was no significant difference in the effects of varying concentrations of K.

Non-Targeted Metabolite Profiling of Tomato Fruits Cultivated Under Different Mineral Nutrient and Water Supplies

We investigated the effects of nutrient and water supply on tomato primary metabolites, including sugars and organic acids (**Table S3**). To investigate the effect of the nutrient and water supply conditions on primary metabolites in tomato fruits, we performed a partial least square discriminant analysis (PLS-DA) for each of the two nutrient levels applied to plants, 0.75 and 0.1 (**Figures 2A** and **3A**, respectively). The clustering patterns of the two PLS-DA results were similar. In **Figures 2**, **3**, the SN and varying the N or K supply (N 0.75, N0.1, K0.75, and K0.1) groups were clearly separated from each other, with PLS1 (16.3%) and PLS1 (15.9%), respectively. In addition, the SW and LW groups were clearly separated from each other, with PLS2 (8.0%) and PLS2 (6.5%), respectively. The limited water groups with mineral applications of N0.75 and K0.75 were not clearly discriminated from the sufficient water supply groups. However, the limited water groups with mineral applications of N0.1 and K0.1 were clearly discriminated from the groups with sufficient water supply. These results indicate that the amount of nutrients supplied to plants affects the primary metabolites of tomato fruits more than irrigation conditions.

Based on the PLS-DA models, we selected significantly discriminant metabolites using variable importance in projection (VIP) values of >0.7. The same VIP values were selected by Azam et al. (2020) and Ibrahim et al. (2020) in metabolomic studies. A

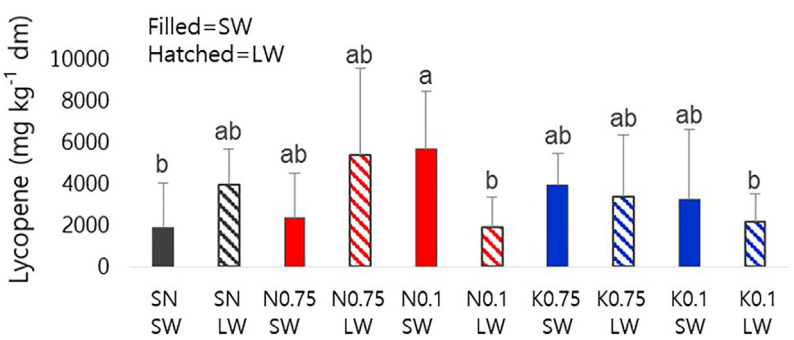

FIGURE 1 | Lycopene contents of tomato fruits on a dry-weight basis influenced by nutrient supply and water supply. The closed bars represent sufficient water and the hatched bars represent limited water. The different alphabetical letters above the bars indicate significant differences, as determined by ANOVA followed by Duncan's multiple-range test ($p < 0.05$). SN, standard nutrient; SW, sufficient water; LW, limited water.

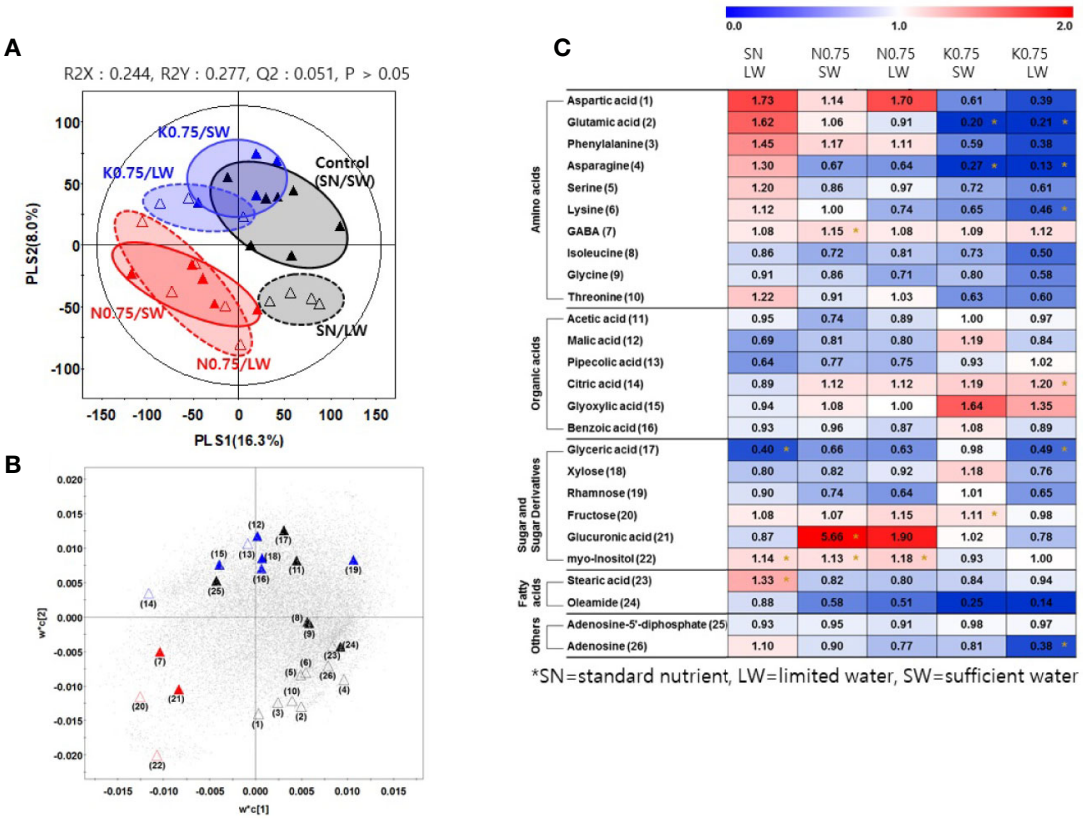

FIGURE 2 | Partial least square discriminant analysis (PLS-DA) score plot **(A)** and a loading plot **(B)** from gas chromatography-time of flight-mass spectrometry (GC-TOF-MS) analysis of tomato fruits grown under the lower nutrient supply (x0.75 of the standard nutrient, SN) and/or limited water (LW) supply compared to the control (SN-SW). ▲: standard nutrient and sufficient water (control, SN-SW), △: standard nutrient and limited water, ▲: x0.75 N and sufficient water, △: x0.75 N and limited water, C▲: x0.75 K and sufficient water, △: x0.75 K and limited water. A heat map **(C)** representing discriminate metabolites among experimental groups with relative metabolite levels. The relative content in the heat map represents fold-changes normalized to the average value of each compound in the control group (SN-SW). The content of each compound is on a dry-weight basis. The number of each metabolite shown in **(B)** is identical to the number in heatmap **(C)**. *: Significantly discriminant metabolites from the control (SN-SW) evaluated by t-test ($p < 0.05$). SN, standard nutrient; SW, sufficient water; LW, limited water.

total of 26 and 25 significantly discriminant metabolites were selected and identified for the two nutrient levels of 0.75 and 0.1 times the standard application concentrations, respectively (**Figures 2B**, **3B**). The relative primary metabolite levels of tomato fruits compared to the control, SN-SW, are shown in heat map (**Figures 2C**, **3C**). The effect of water limitation under standard nutrient conditions was analyzed by comparing SN-LW to SN-SW. Water limitation under standard nutrient conditions increased the amount of some amino acids but decreased the levels of most of the carbohydrates and organic acids present in the fruit (**Figures 2C**, **3C**). The effect of water limitation under lower nutrient supply was also analyzed in pairs, namely N0.75-SW/N0.75-LW, K0.75-SW/K0.75-LW, N0.1-SW/N0.1-LW, and K0.1-SW/K0.1-LW. Water limitation under the lowest N condition resulted in a drastic decrease in the amount of amino acids (**Figure 3C**). A similar effect of water limitation was detectable with K0.75-LW but not K0.1-LW (**Figure 2C**). Interestingly, changes in metabolite content compared to the control, SN-SW, were greater under the x0.75 nutrient condition than under the x0.1 nutrient condition. The amounts of most of the compounds were lowered by reduction of the N and K supply compared to SN-SW. However, there were some exceptions. For example, the level of aspartic acid, phenylalanine, and glucuronic acid were highly increased in N0.75 samples, while in N0.1 samples, only aspartic acid and phenylalanine were present in higher amounts than in the control. Lowering the K supply had a negative effect, mainly on amino acid content, and especially on asparagine levels, which were lowered in both K0.75 and K0.1 samples. In contrast, the glyoxylic acid concentration was highly elevated in K0.75, but not in K0.1 fruits.

DISCUSSION

Lycopene is one of the most potent antioxidants produced in tomato fruits. Although there were considerable fluctuations of

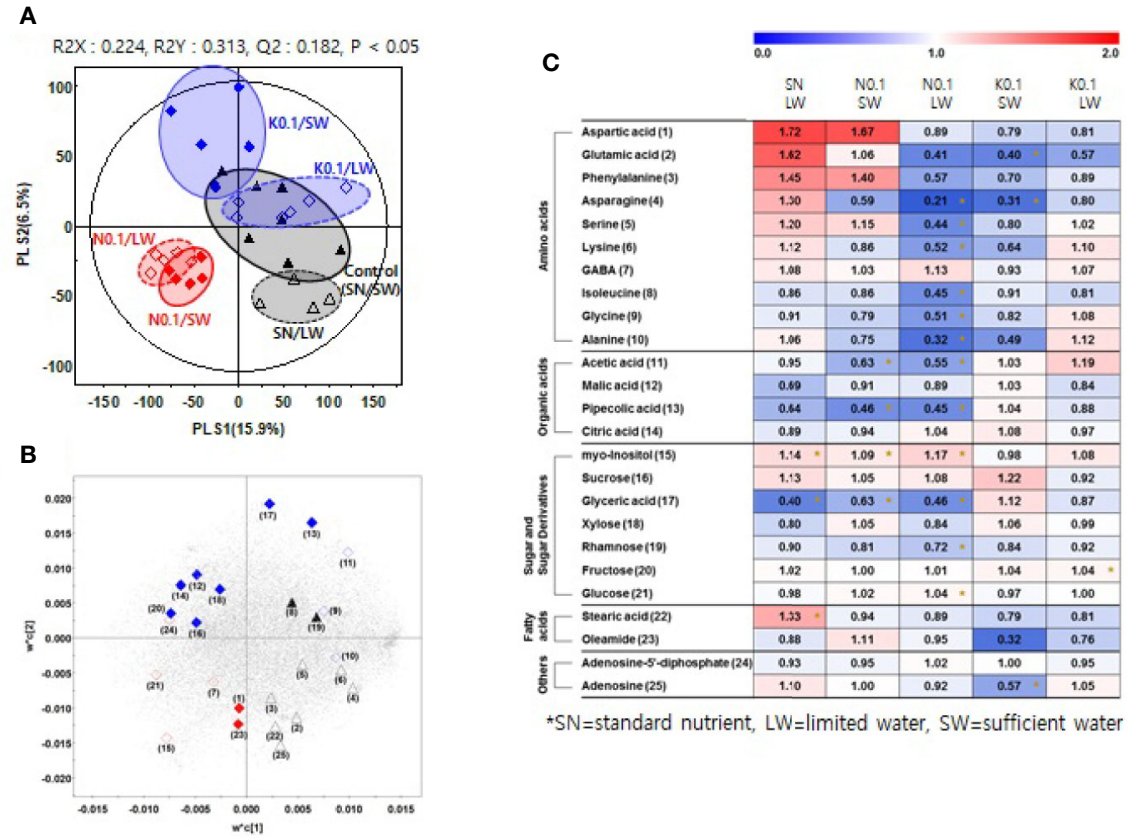

FIGURE 3 | Partial least square discriminant analysis (PLS-DA) score plot **(A)** and loading plot **(B)** from GC-TOF-MS data for tomato fruits grown under the lowest nutrient supply (x0.1 of the standard nutrient, SN) and/or the limited water (LW) supply compared to the control (SN-SW). ▲: standard nutrient and sufficient water (control, SN-SW), △: standard nutrient and limited water, ♦: x0.1 N and sufficient water, ◊: x0.1 N and limited water, ♦: x0.1 K and sufficient water, ◊: x0.1 K and limited water. A heat map **(C)** representing discriminate metabolites among experimental groups with relative metabolite levels. The relative content in the heat map represents fold-changes normalized to the average value of each compound in the control group (SN-SW). The content of each compound is on a dry-weight basis. The number of each metabolite shown in **(B)** is identical number in heatmap **(C)**. *Significantly discriminant metabolites from the control (SN-SW) evaluated by t- test ($p < 0.05$). SN, standard nutrient; SW, sufficient water; LW: limited water.

lycopene content due to the extreme environmental conditions in the growing season, we found a significant increase in lycopene content of tomato fruits grown under the lowest N supply with standard irrigation. Simonne et al. (2007) showed that optimal N supply is needed to reach high lycopene concentrations in tomato grown in hydroponic culture. Our results suggest that in soil with excess Mg^{2+}, the optimal N supply for lycopene production is x0.1 of the standard amount used.

The analysis of primary metabolites of tomato fruits by non-targeted metabolomics approaches revealed the changes caused by a limited water supply. The limited water supply decreased most of the carbohydrates and organic acids on a dry-weight basis. Therefore, limiting water was not recommended to improve tomato fruit quality in Mg^{2+} excess soil. There were reports that water deficit increased the acidity of tomato fruits (Rudich et al., 1977; 1985 experiment of Mitchell et al., 1991), however, acid levels stayed similar in the experiment of 1986 of Mitchell et al. (1991). In the latter study, hexose increased on a fresh-weight basis in 1985 but hexose stayed similar in 1986 when fruit water content was not changed (Mitchell et al., 1991). They concluded that the production of solutes such as hexoses and organic acids was not up-regulated but that fruit water content decreased, resulting in the increase in metabolite concentration on a fresh-weight basis.

Lower nutrient supply caused a reduction in most of the primary metabolite content of fruits. The observation of reduced concentrations of organic acids under the lower and lowest N conditions in this study is in line with the literature in which low N was found to decrease organic acid concentrations (Bénard et al., 2009; Kuscu et al., 2014; De Pascale et al., 2016; Wang and Xing, 2017). No significant changes in carbohydrates in tomato fruits under the lower and lowest K supplies were detected, which seems to contrast common knowledge about the effects of K on fruits. K is known to be important to high sink activity, as K deficiency causes sugar accumulation in the source, such as shoots, and reduces sugar transport to sinks, such as roots or fruits (Cakmak et al., 1994; Kanai et al., 2011; Hafsi et al., 2014; Kim et al., 2018). The K deficiency

effect may not be significant in the current study, and this could be related to the fact that high concentrations of Mg^{2+} in soil are not known to reduce K^+ uptake by plants (Gransee and Führs, 2013). In contrast to Mg stress, for tomatoes under salt stress from NaCl the uptake and translocation of K was highly hindered when K supply was low (Al-Karaki, 2000).

This study demonstrates that minimizing N supply helped enhance lycopene content in soil with excess Mg^{2+}, which was a strategy known to work in soils without Mg^{2+} surplus, so long as irrigation was sufficient. However, combining the lowest N conditions and limited water worsened the lycopene content in excess Mg^{2+} soil. For the best quality of tomato fruits in terms of sugars and organic acids, limiting water was not appropriate in excess Mg^{2+} soil, which was contrary to the conventional strategy for managing fruit production in soils without Mg^{2+} surplus.

CONCLUSION

In summary, we examined the effects of nutrient and water supply on metabolic changes in tomato fruits cultivated in soil with excess Mg^{2+} under greenhouse conditions. As the growth, metabolites, and fruit quality of tomato plants under excess Mg^{2+} soil were affected differently than plants in soils without excess Mg^{2+} in Kwon et al. (2019), the effects of nutrient and water were contrary to previous results. Our results suggest that the lowest nitrogen coupled with sufficient water supply condition enhanced the lycopene content of tomato fruits on a dry-weight basis, and that limiting water supply in any nutrient supply condition was not appropriate to enhance sugars and organic acids under greenhouse cultivation when soil had excess Mg^{2+}. The current pot experiments in the greenhouse demonstrated the possibility that supplying low levels of nitrogen without limiting water may work in tomato cultivation in the field with overuse of chemical fertilizer, and that this type of strategy needs to be further investigated in the field to set up guidelines for fertilizer supply recommendations.

DATA AVAILABILITY STATEMENT

All datasets presented in this study are included in the article/ **Supplementary Material**.

AUTHOR CONTRIBUTIONS

Conceptualization: SL and JS. Validation: SL, EJ, and JS. Investigation: SL, YK, and MK. Resources: SL and JS. Writing—original draft preparation: YK and MK. Writing—review and editing: YK, SL, EJ, CL, and JS. Supervision, CL. Project administration: SL and YK. Funding acquisition: SL.

FUNDING

This research was funded by the "Cooperative Research Program for Agriculture Science & Technology Development (Project No. PJ012523, PJ014977)" and by 2020 RDA Fellowship Program of Rural Development Administration, Republic of Korea.

ACKNOWLEDGMENTS

We are grateful to the staff of the Plant Nutrition Lab. of the National Institute of Agricultural Sciences for the technical support in tomato cultivation and measuring tomato physiological properties and soil chemical properties.

SUPPLEMENTARY MATERIAL

The Supplementary Material for this article can be found online at: https://www.frontiersin.org/articles/10.3389/fpls.2020.562399/full#supplementary-material

REFERENCES

Adams, S. N., Ac-Pangan, W. O., and Rossi, L. (2019). Effects of soil salinity on citrus rootstock 'US-942' physiology and anatomy. *HortScience* 54, 787–792. doi: 10.21273/HORTSCI13868-19

Al-Karaki, G. N. (2000). Growth, sodium, and potassium uptake and translocation in salt stressed tomato. *J. Plant Nutr.* 23, 369–379. doi: 10.1080/01904160009382023

Almeselmani, M., Pant, R. C., and Singh, B. (2010). Potassium level and physiological response and fruit quality in hydroponically grown tomato. *Int. J. Veg. Sci.* 16, 85–99. doi: 10.1080/19315260903271526

Azam, A. B. A., Ismail, I. S., Vidyadaran, S., Abas, F., and Shaari, K. (2020). ^{1}H NMR-based metabolomics of *Clinacanthus nutans* leaves extracts in correlation with their anti-neuroinflammation towards LPS-induced BV2 cells. *Rec. Nat. Prod.* 14, 231–247. doi: 10.25135/rnp.159.19.08.1384

Aziz, A. A. (1968). Seasonal changes in the physical and chemical composition of tomato fruits as affected by nitrogen levels. *Mededelingen Landbouwhogeschool Wageningen.* 68, 1–6. Available at: https://edepot.wur.nl/286347.

Bénard, C., Gautier, H., Bourgaud, F., Grasselly, D., Navez, B., and Caris-Veyrat, C. (2009). Effects of low nitrogen supply on tomato (*Solanum lycopersicum*) fruit yield and quality with special emphasis on sugars, acids, ascorbate, carotenoids, and phenolic compounds. *J. Agric. Food Chem.* 57, 4112–4123. doi: 10.1021/jf8036374

Cakmak, I., Hengeler, C., and Marschner, H. (1994). Partitioning of shoot and root dry matter and carbohydrates in bean plants suffering from phosphorus, potassium and magnesium deficiency. *J. Exp. Bot.* 45, 1245–1250. doi: 10.1093/jxb/45.9.1245

Carillo, P., Kyratzis, A., Kyriacou, M. C., Dell'Aversana, E., Fusco, G. M., Corrado, G., et al. (2020). Biostimulatory Action of Arbuscular Mycorrhizal Fungi Enhances Productivity, Functional and Sensory Quality in 'Piennolo del Vesuvio' Cherry Tomato Landraces. *Agronomy* 10, 911. doi: 10.3390/agronomy10060911

De Pascale, S., Maggio, A., Orsini, F., and Barbieri, G. (2016). Cultivar, soil type, nitrogen source and irrigation regime as quality determinants of organically grown tomatoes. *Sci. Hortic.* 199, 88–94. doi: 10.1016/j.scienta.2015.12.037

Dumas, Y., Dadomo, M., Di Lucca, G., and Grolier, P. (2003). Effects of environmental factors and agricultural techniques on antioxidant content of tomatoes. *J. Sci. Food Agric.* 83, 369–382. doi: 10.1002/jsfa.1370

Gransee, A., and Führs, H. (2013). Magnesium mobility in soils as a challenge for soil and plant analysis, magnesium fertilization and root uptake under adverse growth conditions. *Plant Soil* 368, 5–21. doi: 10.1007/s11104-012-1567-y

Hafsi, C., Debez, A., and Abdelly, C. (2014). Potassium deficiency in plants: effects and signaling cascades. *Acta Physiol. Plant* 36, 1055–1070. doi: 10.1007/s11738-014-1491-2

Ibrahim, A., Tanney, J. B., Fei, F., Seifert, K. A., Cutler, G. C., Capretta, A., et al. (2020). Metabolomic-guided discovery of cyclic nonribosomal peptides from *Xylaria ellisii* sp. nov., a leaf and stem endophyte of *Vaccinium angustifolium*. *Sci. Rep.* 10, 1–17. doi: 10.1038/s41598-020-61088-x

Jung, E. S., Lee, S., Lim, S. H., Ha, S. H., Liu, K. H., and Lee, C. H. (2013). Metabolite profiling of the short-term responses of rice leaves (*Oryza sativa* cv. Ilmi) cultivated under different LED lights and its correlations with antioxidant activities. *Plant Sci.* 210, 61–69. doi: 10.1016/j.plantsci.2013.05.004

Kanai, S., Moghaieb, R. E., El-Shemy, H. A., Panigrahi, R., Mohapatra, P. K., Ito, J., et al. (2011). Potassium deficiency affects water status and photosynthetic rate of the vegetative sink in green house tomato prior to its effects on source activity. *Plant Sci.* 180, 368–374. doi: 10.1016/j.plantsci.2010.10.011

Kim, Y. X., Kim, T. J., Lee, Y., Lee, S., Lee, D., Oh, T.-K., et al. (2018). Metabolite profiling and mineral nutrient analysis from the leaves and roots of bell pepper (*Capsicum annuum* L. var. *angulosum*) grown under macronutrient mineral deficiency. *Appl. Biol. Chem.* 61, 661–671. doi: 10.1007/s13765-018-0395-z

Kuscu, H., Turhan, A., Ozmen, N., Aydinol, P., and Demir, A. O. (2014). Optimizing levels of water and nitrogen applied through drip irrigation for yield, quality, and water productivity of processing tomato (*Lycopersicon esculentum* Mill.). *Hortic. Environ. Biotechnol.* 55, 103–114. doi: 10.1007/s13580-014-0180-9

Kwon, M. C., Kim, Y. X., Lee, S., Jung, E. S., Singh, D., Sung, J., et al. (2019). Comparative metabolomics unravel the effect of magnesium oversupply on tomato fruit quality and associated plant metabolism. *Metabolites* 9, 231. doi: 10.3390/metabo9100231

Liu, L., Shao, Z., Zhang, M., and Wang, Q. (2015). Regulation of carotenoid metabolism in tomato. *Mol. Plant* 8, 28–39. doi: 10.1016/j.molp.2014.11.006

Mitchell, J. P., Shennan, C., Grattan, S. R., and May, D. M. (1991). Tomato fruit yields and quality under water deficit and salinity. *J. Amer. Soc. Hortic. Sci.* 116, 215–221. doi: 10.21273/JASHS.116.2.215

National Institute of Agricultural Sciences (NIAS) (2017). *Fertilizer Recommendation for Crop Production. 3rd ed. NIAS* (Jeonju, Korea: Rural Development Administration), 66–67.

Rudich, J., Kalmar, D., Geizenberg, C., and Harel, S. (1977). Low water tensions in defined growth stages of processing tomato plants and their effects on yield and quality. *J. Hortic. Sci.* 52, 391–399. doi: 10.1080/00221589.1977.11514768

Simonne, A. H., Fuzere, J. M., Simonne, E., Hochmuth, R. C., and Marshall, M. R. (2007). Effects of nitrogen rates on chemical composition of yellow grape tomato grown in a subtropical climate. *J. Plant Nutr.* 30, 927–935. doi: 10.1080/15226510701375465

Son, S. Y., Kim, N. K., Lee, S., Singh, D., Kim, G. R., Lee, J. S., et al. (2016). Metabolite fingerprinting, pathway analyses, and bioactivity correlations for plant species belonging to the Cornaceae, Fabaceae, and Rosaceae families. *Plant Cell Rep.* 35, 1917–1931. doi: 10.1007/s00299-016-2006-y

Stefanelli, D., Goodwin, I., and Jones, R. (2010). Minimal nitrogen and water use in horticulture: Effects on quality and content of selected nutrients. *Food Res. Int.* 43, 1833–1843. doi: 10.1016/j.foodres.2010.04.022

Sung, J., Lee, S., Lee, Y., Ha, S., Song, B., Kim, T., et al. (2015). Metabolomic profiling from leaves and roots of tomato (*Solanum lycopersicum* L.) plants grown under nitrogen, phosphorus or potassium-deficient condition. *Plant Sci.* 241, 55–64. doi: 10.1016/j.plantsci.2015.09.027

Sung, J., Yun, H., Back, S., Fernie, A. R., Kim, Y. X., Lee, Y., et al. (2018). Changes in mineral nutrient concentrations and C-N metabolism in cabbage shoots and roots following macronutrient deficiency. *J. Plant Nutr. Soil Sci.* 181, 777–786. doi: 10.1002/jpln.201800001

Wang, X., and Xing, Y. (2017). Evaluation of the effects of irrigation and fertilization on tomato fruit yield and quality: a principal component analysis. *Sci. Rep.* 7, 1–13. doi: 10.1038/s41598-017-00373-8

Zhang, H.-X., Chi, D.-C., Wang, Q., Fang, J., and Fang, X.-Y. (2011). Yield and quality response of cucumber to irrigation and nitrogen fertilization under subsurface drip irrigation in solar greenhouse. *Agric. Sci. China* 10, 921–930. doi: 10.1016/S1671-2927(11)60077-1

Conflict of Interest: The authors declare that the research was conducted in the absence of any commercial or financial relationships that could be construed as a potential conflict of interest.

frontiers in Plant Science

ORIGINAL RESEARCH
published: 30 September 2020
doi: 10.3389/fpls.2020.554520

Characterization of the DREBA4-Type Transcription Factor (SlDREBA4), Which Contributes to Heat Tolerance in Tomatoes

*Lianzhen Mao†, Minghua Deng†, Shurui Jiang†, Haishan Zhu, Zhengan Yang, Yanling Yue and Kai Zhao**

College of Horticulture and Landscape, Yunnan Agricultural University, Kunming, China

Dehydration-responsive element binding (DREB) transcription factors play crucial regulatory roles in abiotic stress. The only DREB transcription factor in tomato (*Solanum lycopersicum*), SlDREBA4 (Accession No. MN197531), which was determined to be a DREBA4 subfamily member, was isolated from cv. Microtom using high-temperature-induced digital gene expression (DGE) profiling technology. The constitutive expression of *SlDREBA4* was detected in different tissues of Microtom plants. In addition to responding to high temperature, *SlDREBA4* was up-regulated after exposure to abscisic acid (ABA), cold, drought and high-salt conditions. Transgenic overexpression and silencing systems revealed that *SlDREBA4* could alter the resistance of transgenic Microtom plants to heat stress by altering the content of osmolytes and stress hormones, and the activities of antioxidant enzymes at the physiologic level. Moreover, *SlDREBA4* regulated the downstream gene expression of many heat shock proteins (Hsp), as well as calcium-binding protein enriched in the pathways of protein processing in endoplasmic reticulum (ko04141) and plant-pathogen interaction (ko04626) at the molecular level. SlDREBA4 also induces the expression of biosynthesis genes in jasmonic acid (JA), salicylic acid (SA), and ethylene (ETH), and specifically binds to the DRE elements (core sequence, A/GCCGAC) of the *Hsp* genes downstream from SlDREBA4. This study provides new genetic resources and rationales for tomato heat-tolerance breeding and the heat-related regulatory mechanisms of DREBs.

Keywords: Microtom, dehydration-responsive element binding transcription factor, abiotic stress, transgenic plants, gene function, heat tolerance

OPEN ACCESS

Edited by:
Amalia Barone,
University of Naples Federico II, Italy

Reviewed by:
Qingyu Wu,
Chinese Academy of Agricultural Sciences (CAAS), China
Julien Pirrello,
École Nationale Supérieure Agronomique de Toulouse, France

***Correspondence:**
Kai Zhao
kailixian1023@aliyun.com

†These authors have contributed equally to this work

Specialty section:
This article was submitted to Plant Biotechnology, a section of the journal Frontiers in Plant Science

Received: *30 April 2020*
Accepted: *11 September 2020*
Published: *30 September 2020*

Citation:
Mao L, Deng M, Jiang S, Zhu H, Yang Z, Yue Y and Zhao K (2020) Characterization of the DREBA4-Type Transcription Factor (SlDREBA4), Which Contributes to Heat Tolerance in Tomatoes. Front. Plant Sci. 11:554520. doi: 10.3389/fpls.2020.554520

HIGHLIGHTS

SlDREBA4 alters the resistance of transgenic Microtom plants to heat stress by altering the content of osmolytes and stress hormones, the activities of antioxidant enzymes at the physiologic level, and the downstream gene expression of many heat shock proteins, as well as calcium-binding protein at the molecular level.

INTRODUCTION

Dehydration-responsive element binding (DREB) proteins belong to the plant-specific APETALA2/ethylene-responsive element binding factor (AP2/ERF) family of transcription factors. DREBs can be induced by abiotic stresses, including drought, heat, cold, and high salt levels, and their overexpression in transgenic plants increases resistance to these stresses (Wu et al., 2017; Hu et al., 2018; Huang et al., 2018). Abiotic heavy-metal stress, like those induced by cadmium (Cd) and molybdenum (Mo) exposure, can also increase the transcription levels of DREBs, and DREB overexpression results in increased resistance levels against these metal elements (Charfeddine et al., 2017; Akbudak et al., 2018; Nasir and Fazal, 2018). Most previous DREB studies focused on abiotic stresses and a few studies have shown that DREBs play important roles in biotic stress responses. Salicylic acid (SA), jasmonic acid (JA), ethylene (ETH), and other hormones or pathogens induce the up-regulation of DREBs, which then change the resistance levels to these pathogens by altering the content of SA, JA, and ETH, and the expression of pathogenesis-related (PR) genes (Zhao et al., 2015; Wu et al., 2017; Xiong et al., 2018).

DREB transcription factors in the model plant *Arabidopsis thaliana* are divided into six subfamilies (A1 to A6) based on homology (Sakuma et al., 2002). Subsequent studies have classified DREBs from different plants into these six subfamilies. Each subfamily has similar response patterns and functions. After the first isolation of a DREB transcription factor using the single-hybrid yeast method (Liu et al., 1998), the focus of DREB research has mainly involved subfamilies A1, A2, A5, and A6. The response patterns of DREBA1 subfamilies are mainly correlated with responses to abiotic stresses, such as cold, high salt, drought and heavy metals, and biotic stresses, such as pathogenic bacteria. DREBA1 plays positive regulatory roles in responses to these abiotic and biotic stresses (Liu et al., 1998; Kitashiba et al., 2004; Yang et al., 2011; Wei et al., 2017; Wu et al., 2017). The responses and functions of the DREBA2 subfamily to stress are more diverse than those of the DREBA1 subfamily (Sakuma et al., 2006; Zhao et al., 2013; Wu et al., 2018). DREBA2 subfamily transcription factors require post-translational modifications to activate the downstream functional genes and increase resistance to heat and other stresses (Sakuma et al., 2006; Wu et al., 2018). Recent studies on the DREBA2 subfamily mainly focused on heat stress, and they conferred heat resistance to transgenic plants (Zhao et al., 2013; Qin et al., 2018; Wu et al., 2018). The stress-response mechanisms and functions of most transcription factors in the two subfamilies, DREBA5 and DREBA6, are similar to those of the DREBA1 subfamily (Huang and Liu, 2006; Tsutsui et al., 2009; Hu et al., 2018).

To date, only a few DREBA3 and DREBA4 subfamily genes have been isolated, and their regulatory mechanisms and functions under stress conditions are not yet clear. AtABI4 from *Arabidopsis thaliana*, belonging to the DREBA3 subfamily, is induced by ABA (Finkelstein et al., 1998). Another DREBA3-type transcription factor ZmABI4 from maize has an unknown induction mechanism (Niu et al., 2002). For the DREBA4 subfamily of transcription factors, some progress has been made. The transcription of ZmDBF2 is induced by ABA, drought, and high-salt conditions, and it increases the drought resistance of transgenic plants (Wang et al., 2010). The expression of AtTINY under stress conditions has not been explored (Wilson et al., 1996). DaCBF4 from *Deschampsia antarctica* has been isolated recently. Its transcriptional level increases during cold and drought stress, and it increases the cold resistance of transgenic plants (Byun et al., 2018). ZmDREB4.1 could not be induced by high salt, drought, ABA, auxin, cytokinins, gibberellic acid, or ETH, and it inhibited the growth of transgenic tobacco leaves, hypocotyls, and callus. However, its functions under stress conditions have not been explored (Li et al., 2018).

After the discovery of DRE element and DREB transcription factors (Yamaguchi-Shinozaki and Shinozaki, 1994; Liu et al., 1998), subsequent studies revealed that DREB plays important roles in both abiotic and biotic stress responses. In this study, the only tomato (*Solanum lycopersicum*) DREB transcription factor that responded to heat, SlDREBA4, was discovered in the cultivar Microtom, using DGE profiling technology. SlDREBA4 was determined to belong to the DREBA4 subfamily. The function of SlDREBA4 under high-temperature conditions was verified through transgenic overexpression and silencing systems. The resistance changes caused by SlDREBA4 under heat-stress conditions were explained at physiological and molecular levels.

MATERIALS AND METHODS

Materials and Heat Induction

The seeds of *S. lycopersicum* L. (var. Microtom) were first soaked in water at 55°C for 20 min, then in water at 30°C for 5 h. The treated seeds of *S. lycopersicum* L. (var. Microtom) were sown in a mixed matrix of 6:3:1 (v/v) peat, vermiculite and perlite. For heat treatment, Microtom plants with seven to eight leaves were treated at 37°C for 30 min. Both the control and heat-treated groups contained 30 plants. The 4th leaves from the base of each plant were removed. The 30 leaves of the control (Microtom-CK) and heat-treated (Microtom-HS) groups were mixed to form two independent materials for DGE profiling, which was performed by the Beijing Genomics Institution (BGI).

Screening of Differentially Expressed *DREB* Genes Induced by Heat

Based on Poisson distribution analysis (Audic and Claverie, 1997), a strict algorithm was used to identify differentially-expressed genes (DEGs) between two samples. The number of unambiguous clean tags from gene A was denoted by an x, given that the expression of every gene occupies only a small part of the library; x yields to the Poisson distribution:

$$p(x) = \frac{e^{-\lambda}\lambda^{x}}{x!}\ (\lambda \text{ is the real transcripts of the gene})$$

The total clean tag number of sample 1 is designated N1 and the total clean tag number of sample 2 is designated as N2. Gene

A holds x tags in sample 1 and y tags in sample 2. The probability of gene A expressed equally between two samples can be calculated as follows:

$$2\sum_{i=0}^{i=y} p(i|x)$$

$$or\ 2 \times \left(1 - \sum_{i=0}^{i=y} p(i|x)\right) \left(if \sum_{i=0}^{i=y} p(i|x) > 0.5\right)$$

$$p(y|x) = \left(\frac{N_2}{N_1}\right)^y \frac{(x+y)!}{x!\,y!\left(1+\frac{N_2}{N_1}\right)^{(x+y+1)}}$$

The P-value corresponds to the DGE test. The false discovery rate (FDR) was used to determine the threshold of the P-value in multiple tests (Benjamini and Yekutieli, 2001). DEGs between two samples (control and heat-treated) were screened, and the genes with FDR ≤ 0.001 and fold-change differences > 2 were selected as the candidate genes. A hypergeometric test was used to find the pathways significantly enriched (Q-value ≤ 0.05) with DEGs. The conserved AP2 sequence of the DREB transcription factor was download from PFAM (http://pfam.sanger.ac.uk/). A local BLAST program was used to compare AP2 sequences with the differentially expressed protein sequences to screen for the DREB transcription factor possessing only one AP2 domain (Yuan et al., 2013).

SlDREBA4 Cloning and Phylogenetic Tree Construction

The specific primer pSlDREBA4 (**Table S1**) was designed based on the *SlDREBA4* gene sequence. *SlDREBA4* was cloned and sequenced using Microtom cDNA as the template. A phylogenetic tree was established by the Neighbor-Joining algorithm with 1,000 bootstrap replications using MEGA5 version 5.05 software (Sakuma et al., 2002).

Identification of Tissue-Specific Expression and Stress-Response Patterns of *SlDREBA4* Using Real-Time Quantitative PCR (RT-qPCR)

Microtom seeds were germinated and sown in vermiculite. After growing two true leaves, the plants were transplanted into Hoagland's nutrient solution. After seven to eight leaves were grown, plants were exposed to stresses. For the dehydration stress, hydroponic seedlings fixed in planting baskets were transferred from nutrient solution along with the basket to the filter paper. For heat and cold stresses, hydroponic seedlings were exposed to 37°C and 4°C, respectively, in a growth chamber. For salt stress, hydroponic seedlings were transferred into Hoagland's nutrient solution containing 200 mM NaCl. For the ABA treatment, leaves of hydroponic seedlings were sprayed with 200 mM ABA solution. For all the treatments, the fourth leaves from the base were harvested at the designated time intervals (0, 0.5, 1, 3, 6, and 12 h). When the Microtom plants had red fruit approximately 60 days after sowing, tissue-specific expression was identified in the root, stem, leaf, flower, green fruit, and red fruit. The relative quantification value for the *SlDREBA4* (pSlDREBA4-q) gene was calculated using the $2^{-\Delta\Delta Ct}$ method (Zhao et al., 2013) with the tomato housekeeping gene ribosomal protein L2 (*RPL2*) (pRPL2-q) (Løvdal and Lillo, 2009) as an internal control. Primer sequences are provided in **Table S1**. All the above RT-qPCR analyses were performed in biological and technical triplicate.

Generation of Transgenic Microtom Lines

To generate overexpressed transgenic Microtom plants, full-length *SlDREBA4* cDNA was amplified using the specific primer, pSlDREBA4-o. The PCR product was fused into the reconstructed vector pBI121 (harboring *Xba*I and *Kpn*I sites) under the control of the constitutive CaMV 35S promoter. The pBI121-35S-*SlDREBA4* fusion plasmid was introduced into *Agrobacterium tumefaciens* strain GV3101. Positive GV3101 was transformed into Microtom cotyledons (Sun et al., 2015), and the rooting plants were screened by kanamycin and transferred to Hoagland's nutrient solution. The level of *SlDREBA4* transcription was assessed using RT-qPCR with the primer, pSlDREBA4-q. To generate virus-induced gene silencing (VIGS) transgenic Microtom plants, a specific primer, pSlDREBA4-v, was designed based on a sequence specificity analysis of *SlDREBA4* with other *DREBs* in tomatoes. The gene fragment was then cloned and inserted into the pTRV2 plasmid. The plasmids, pTRV2-*SlDREBA4* segment, pTRV2-PDS (phytoene desaturase), and pTRV1, were transformed into GV3101. Positive GV3101 containing pTRV2, pTRV2-*SlDREBA4* segment, or pTRV2-PDS were co-injected with positive GV3101 containing pTRV1 into cotyledons and leaves of Microtom (Shen et al., 2014). Plant phenotypes were observed 21 days after injection, and positive transgenic plants were identified using RT-qPCR with the primer, pSlDREBA4-q. Primers are provided in **Table S1**. All the above RT-qPCR analyses were performed in biological and technical triplicate.

The Heat-Stress Treatment and Determination of Physiologic and Molecular Indices

To achieve the rapid wilting effect and avoid the influence of plant phenotypic difference on high temperature treatment, the heat-treated groups were placed at 55°C in a plant growth chamber until whole wilted plant was observed. Heat-treated samples were immediately divided into two batches: one batch had its physiological indexes measured and underwent transcriptome sequencing. Another batch was transferred to normal conditions for 3 d, followed by phenotypic observation. According to the specific phenotypic changes under high-temperature stress treatment, the heat injury index (HII) grading criteria was established as follows: level 0, no leave curling; level 1, 0% to 50% leave curling with partial leave wilting; level 2, 50% to 100% leave curling with partial leave wilting; and level 3, the entire plant wilted or withered.

$$\mathrm{HII}(\%) = \Sigma\ (\text{plant numbers at each level} \times \text{level rank}) \times 100/(\text{highest level rank} \times \text{the total number of plants})$$

The concentrations of indole-3-acetic acid (IAA), ABA, JA, SA, and 1-aminocyclopropane-1-carboxylic acid (ACC) were measured by HPLC-MS/MS using Agilent 1290 HPLC (Agilent Technologies Inc., USA) and SCIEX-6500 Qtrap mass spectrometer (AB Sciex, USA) (Pan et al., 2010). Proline, malondialdehyde, soluble total sugar, soluble starch, peroxidase (POD), superoxide dismutase (SOD) and catalase (CAT) were detected using an ELISA kit (Shanghai Enzyme-linked Biotechnology Co., Ltd). Plasma membrane permeability was measured in terms of electrolyte leakage rate (Kumar et al., 1985). All the physiologic indices were measured in biological and technical triplicate.

Biosynthetic genes in the JA, SA, and ETH pathways were searched against the DEGs data in the *SlDREBA4*-overexpressed and -silenced lines, and the expression profiles of these genes were validated using RT-qPCR by the $2^{-\Delta\Delta Ct}$ method (Zhao et al., 2013). All the primers are provided in **Table S1**.

The *SlDREBA4*-overexpressed and -silenced, and empty vector-transformed plants were selected to carry out transcriptome sequencing. Readcount for each gene was normalized to reads per kilobase per million mapped reads (RPKM). Prior to differential gene expression analysis for each sequenced library, the readcounts were adjusted using the edgeR program package through one scaling normalized factor (Robinson et al., 2010). Analyses of significant differences in gene expression were performed using DESeq2 and the R package (Anders and Huber, 2010). Genes with a $p_{adj} < 0.05$ and $|\log_2(\text{foldchange})| > 1$ were selected as candidate genes. Based on the principles of hypergeometric distribution, clusterProfiler was used to perform a Kyoto Encyclopedia of Genes and Genomes (KEGG) pathway enrichment analysis of DEGs [$p_{adj} < 0.05$] (Mortazavi et al., 2008).

DRE-Binding Activities of SlDREBA4 Using the Yeast One-Hybrid (Y1H) System

Three potentially DREs (DRE1 [GACCGACGA], DRE2 [AGCCGACAC], and DRE3 [CGCCGACTT]) identified from the *Hsp* genes downstream from SlDREBA4 or one mutant DRE (mDRE [TATTTTCAT]) were inserted into the pHis2.1 vector with three tandemly repeats using *Eco*RI and *Spe*I to generate pHis2.1-3DRE or pHis2.1-3mDRE. The coding sequence of *SlDREBA4* was amplified by the primer, pSlDREBA4-y, harboring *Bam*HI and *Xho*I sites (**Table S1**). The product was inserted into the pGADT7 vector to generate pGADT7-*SlDREBA4*. The yeast strain, Y187, co-transformed by the corresponding vectors, was streaked on the selective SD medium to investigate the DRE-binding activities of SlDREBA4 (Wu et al., 2018).

RESULTS

Selection of DREB Transcription Factors Responding to Heat Using DGE Profiling

DGE profiling successfully selected 2,820 DEGs responding to heat, including 1,107 up-regulated genes and 1,713 down-regulated genes, which were listed in an excel. Only one DREB subfamily gene (Gene ID: Solyc06g066540) was up-regulated with a log2 ratio=4.28. The coding region contained 579 bp bases and encoded 192 amino acids with one typical AP2 domain. The phylogenetic tree was established, and the gene was found to be a member of the DREBA4 subfamily. Thus, it was named SlDREBA4 (Accession No. MN197531; **Figure 1**).

Expression Patterns of *SlDREBA4* in Different Tissues and Response to Various Stresses

The expression pattern of *SlDREBA4* in different tissues of Microtom plants was examined under normal conditions (**Figure 2A**). *SlDREBA4* was constitutively expressed in almost all tissues examined, including root, stem, leaf, flower, green fruit, and red fruit. The expression level of *SlDREBA4* was highest in flower, followed by green fruit, leaf, root and stem, and was lowest in red fruit.

We also tested the expression pattern of *SlDREBA4* in the leaves under various stress conditions. RT-qPCR revealed that *SlDREBA4* expression was induced by heat, exogenous ABA, cold, drought and salt (**Figure 2B**). Under different stress conditions, *SlDREBA4* showed different expression patterns. *SlDREBA4* expression was rapidly and transiently induced by the heat treatment and peaked at 12 h. ABA and drought resulted in the increased, followed by decreased expression of *SlDREBA4*. The transcription level of *SlDREBA4* peaked at 3 h after the ABA treatment and then declined, but the expression level at 12 h was still higher than that of the controls. Drought stress resulted in the expression level of *SlDREBA4* peaking at 1 h, followed by a decline, and then it maintained at the same level as the controls. Cold led to the expression level of *SlDREBA4* peaking at 0.5 h, and then, it maintained this expression level until 12 h. Salinity caused an increase in the expression of *SlDREBA4*, followed by a decrease and another increase, with an eventual peak at 12 h.

Functional Verification of *SlDREBA4* Transgenic Microtom Plants Under Heat Stress Conditions

Expression of the transgenic three *SlDREBA4*-overexpression lines (L-3, L-8, and L-12) were obtained using RT-qPCR (**Figure 3A**). Compared with the wild-type and empty vector-transformed plants, *SlDREBA4*-overexpression lines were significantly dwarfed, with slow growth and delayed flowering (**Figure 3B**). Heat stress led to wilted wild-type and empty vector-transformed tomato plants with HIIs of 100%. However, only a small portion of leaves on the three transgenic lines were slightly wilted, with HIIs ranging from 53% to 67% (**Figure 3C**).

The function of *SlDREBA4* under heat-stress conditions was determined using the VIGS system. Positive transgenic plants were obtained through the phenotypic analysis of PDS silencing and the expression level of SlDREBA4, and shown under normal conditions (**Figures 4A, B**). After the heat-stress treatment, leaves of *SlDREBA4*-silenced lines were more

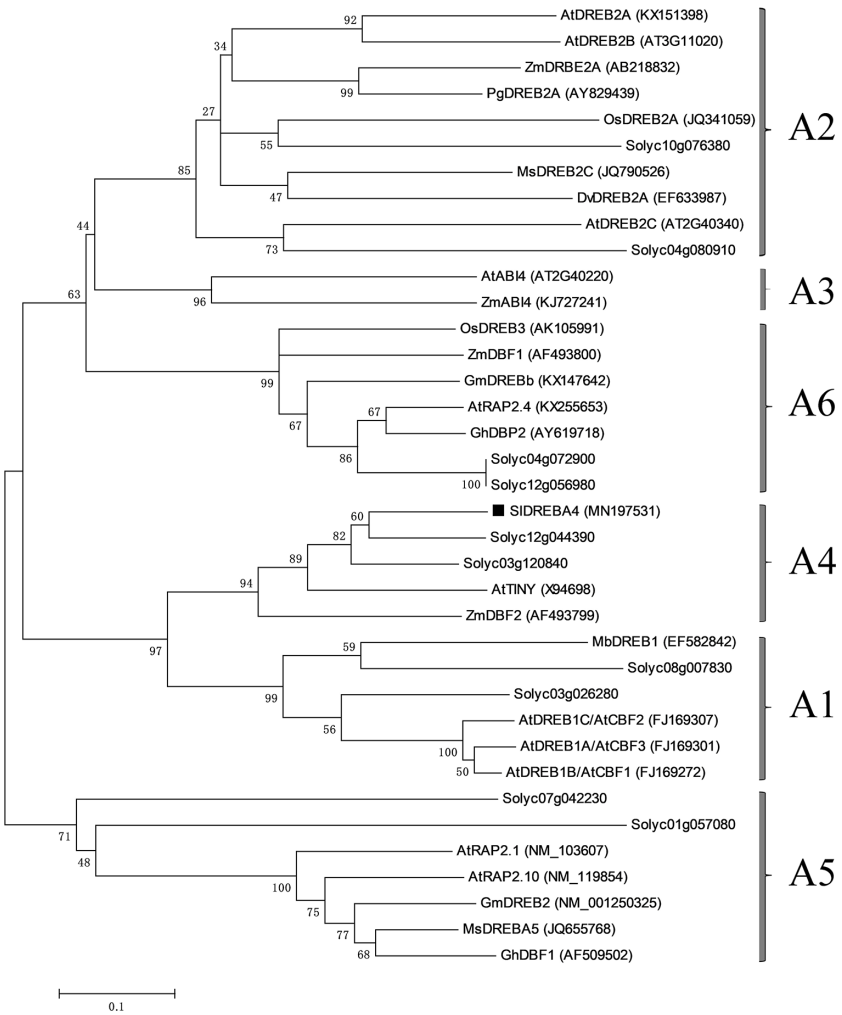

FIGURE 1 | Phylogenetic tree of SlDREBA4 and DREB proteins of other plants. SlDREBA4 is marked with black squares and the accession numbers are indicated in parentheses. The DREB proteins without accession numbers are discovered from tomatoes.

seriously damaged compared with empty vectors-transformed plants. The HII of empty vectors-transformed plants was 75%, while the HIIs of *SlDREBA4*-silenced lines ranged from 95% to 100% (**Figure 4C**).

The Causes for the Heat Tolerance Changes of *SlDREBA4*-Transgenic Lines

The causes of changes in the heat tolerance of transgenic lines were investigated at the physiological and molecular levels. The hormone content, enzyme activity, metabolite level, and gene expression level were measured, also. The contents of JA, SA, ACC, soluble total sugar, soluble starch, and proline, and the activities of POD, SOD and CAT in overexpressed lines under normal conditions were found to be higher than those of empty vector-transformed lines. Increased contents and activities of the above substances were measured under heat-stress conditions and were higher in overexpressed lines than in empty vector-transformed lines. Heat induction led to an increase in the ABA level, but no significant difference was observed between the level in empty vector-transformed and overexpressed lines under normal and heat-stress conditions. Under normal growth conditions, there were no significant differences in malondialdehyde level and electrolyte leakage rate between empty vector-transformed and overexpressed lines. Both indexes increased under heat-stress conditions, and increases in the indexes of overexpressed plants were significantly lower than those of empty vector-transformed lines. Heat decreased the IAA level, and under both normal and heat-stress conditions, the IAA level in overexpressed lines was extremely significantly lower than in empty vector-transformed lines (**Table 1**).

The contents of proline, malondialdehyde, soluble total sugar, soluble starch, ABA, JA, SA, and ACC, and the values of electrolyte leakage rate, and the activities of POD, SOD, and

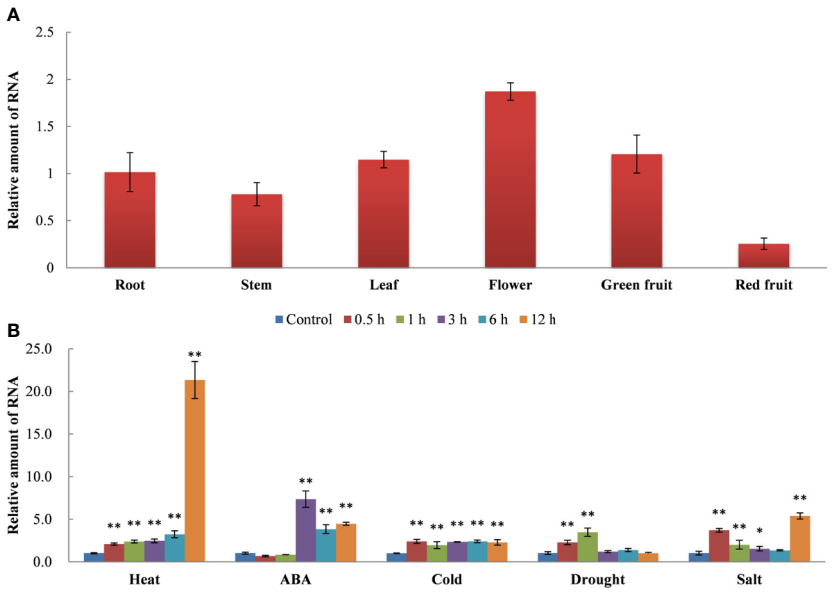

FIGURE 2 | Tissue-specific expression **(A)** and stress-response patterns **(B)** of *SlDREBA4*. The unstressed expression level (Control) was assigned a value of 1. The error bar on each column represents the standard deviation (SD) of the three biological replicates (Student's *t*-test, $^{*}P < 0.05$, $^{**}P < 0.01$).

CAT were induced and the content of IAA was suppressed under heat-stress conditions in both empty vector-transformed and *SlDREBA4*-silenced plants. Under both normal growth and heat conditions, physiologic indicators, including proline, POD, SOD, JA, SA, and ACC, were lower in the silenced plants than in the empty vector-transformed plants, whereas the other indicators, including malondialdehyde, soluble total sugar, soluble starch, CAT, ABA, and IAA, showed no significant difference in both silenced and empty vector-transformed plants. Under normal growth conditions, there was no significant difference in the electrolyte leakage rate between empty vector-transformed and silenced plants; however, the electrolyte leakage rate was higher in silenced plants than in empty vector-transformed plants under heat-stress conditions (**Table 2**).

We continued to dig for the target DEGs in the JA, SA, and ETH biosynthesis pathways against the DEGs data in the transcriptome of *SlDREBA4*-overexpressed and -silenced lines. The results showed that the target DEGs were distributed in each hormone biosynthesis pathway. Three, four, and two DEGs were found in JA, SA, and ETH biosynthesis, respectively. All the DEGs were induced in the *SlDREBA4*-overexpressed lines. However, one (JA), three (SA), and two (ETH) DEGs were inhibited and the remaining genes were not detected in the silenced plants (**Table 3**). RT-qPCR was employed to confirm the differential expression patterns of these biosynthesis genes in the leaves. The expression trends of the lipoxygenase and 12-oxophytodienoate reductase-like protein genes in JA biosynthesis, isochorismatase, and phenylalanine ammonia-lyase genes in SA biosynthesis, and 1-aminocyclopropane-1-carboxylate synthase gene in ETH biosynthesis were in agreement with the transcript abundance changes (**Figure 5**).

We compared the transcriptome results of *SlDREBA4*-overexpressed and -silenced lines with those of the empty vector-transformed plants to explain the changes in the tolerance of *SlDREBA4* transgenic plants to heat stress. There were 6333 (3978) DEGs in overexpressed (silenced) lines, including 2082 (1916) up- and 4251 (2062) down-regulated genes. An analysis of the KEGG enrichment pathways showed that 10 of the 20 pathways most enriched with up-regulated DEGs in *SlDREBA4*-overexpression lines were the same as those most enriched with down-regulated DEGs in VIGS lines (**Figures 6A, B**). Furthermore, three of the 20 most enriched pathways in the high-temperature-induced Microtom plants were shared by the above 10 common pathways (**Figure 6C**). One pathway was related to the circadian rhythms of plant (ko04712: circadian rhythms-plant) and the other two pathways were related to response to biotic stress and protein processing (ko04626: plant-pathogen interaction and ko04141: protein processing in endoplasmic reticulum). The common DEGs in the pathways of plant-pathogen interaction and protein processing in endoplasmic reticulum were discovered in the high-temperature-induced Microtom plants (up-regulated), *SlDREBA4*-overexpressed (up-regulated) and -silenced (down-regulated) lines. Two target genes which were described as heat shock proteins (Hsps) and calcium-binding protein were found in the pathway of plant-pathogen interaction. Seven target genes were found in the pathway of protein processing in endoplasmic reticulum, among which six were Hsps and one was skp1-like protein (**Table 4**). Further analysis of the DREs in the promoter sequences of the above 8 candidate genes found

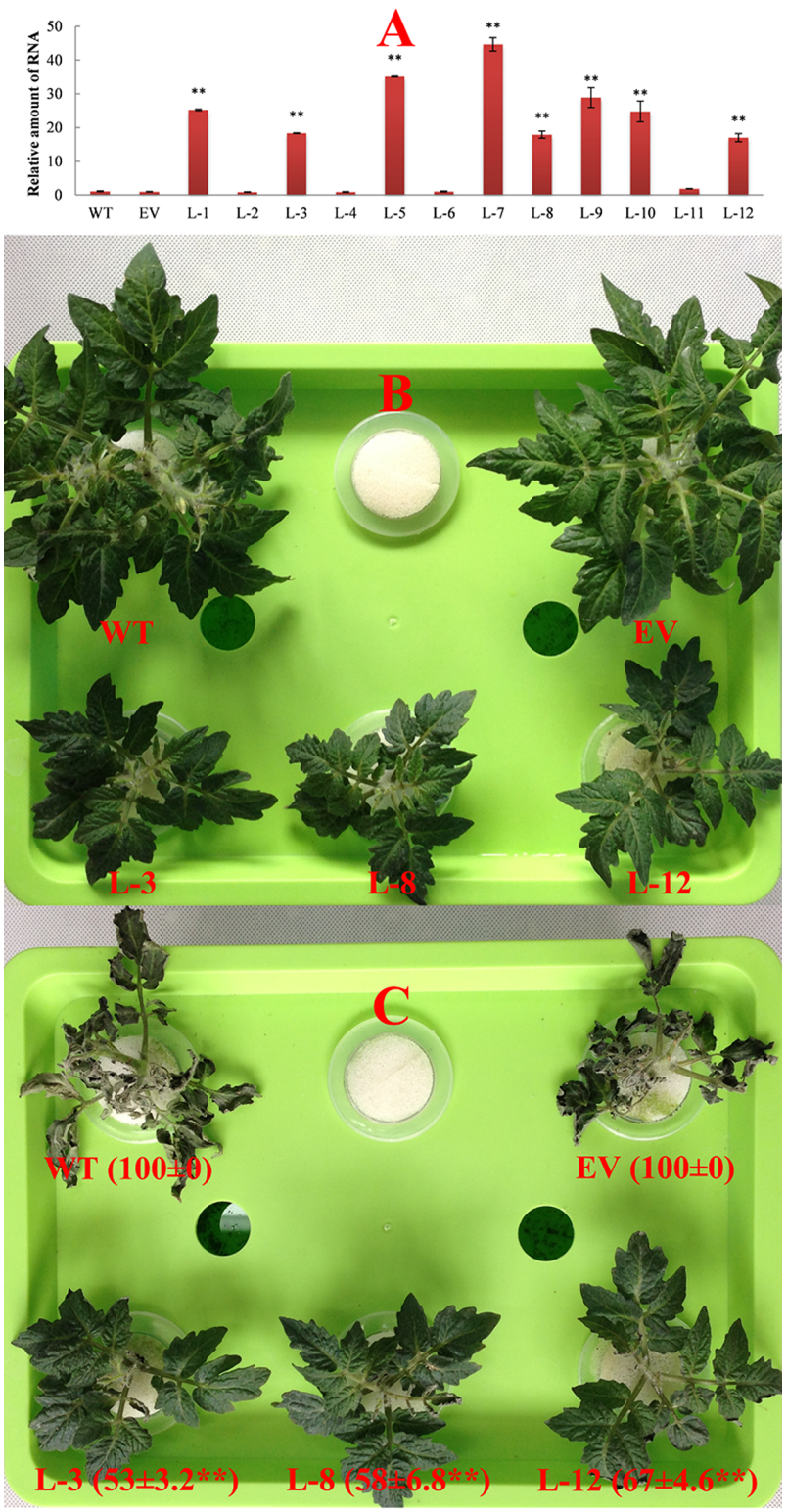

FIGURE 3 | Functional identification of *SlDREBA4*-overexpressing lines under heat-stress conditions. WT, wild-type plants; EV, empty vector-transformed plants; L-1 to L-12: *SlDREBA4*-overexpression lines. **(A)** RT-qPCR was used to identify *SlDREBA4* expression. The level of WT was assigned a value of 1. The error bar on each column represents the SD of the three biological replicates (Student's *t*-test, $^{**}P < 0.01$). Plants under normal **(B)** and heat-stress **(C)** conditions were grown in nutrient solution. The numbers in brackets indicate the HII values (%), which are shown as the means of the three biological replicates ± SDs (Student's *t*-test, $^{**}P < 0.01$).

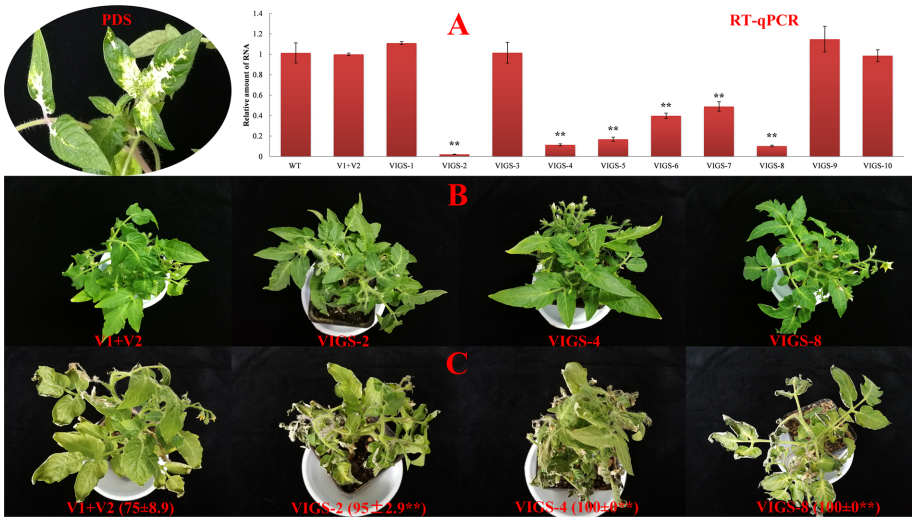

FIGURE 4 | Functional identification of *SlDREBA4*-silenced plants under heat-stress conditions. WT, wild-type plants; V1+V2: plants co-transformed by empty vectors pTRV1 and pTRV2; VIGS-1 to -10: *SlDREBA4*-silenced plants. **(A)** Identification of *SlDREBA4*-silenced plants, PDS, phenotypes of the plants with silenced *PDS*, RT-qPCR: transcription level of *SlDREBA4* using RT-qPCR in which the level of WT was assigned a value of 1. Error bar on each column represents the SD of the three biological replicates (Student's *t*-test, $^{**}P < 0.01$). Silenced plants under normal **(B)** and heat-stress **(C)** conditions were grown in nutrient solution. The numbers in brackets indicate the HII values (%), which are shown as the means of the three biological replicates ± SDs (Student's *t*-test, $^{**}P < 0.01$).

TABLE 1 | Physiologic indicators in *SlDREBA4*-overexpression and empty vector-transformed lines.

	Control				Heat stress			
	EV	**L-3**	**L-8**	**L-12**	**EV**	**L-3**	**L-8**	**L-12**
Proline (ng/g·FW)	85.2 ± 6.2	132.8 ± 11.9**	142.3 ± 13.9**	156.6 ± 15.8**	178.8 ± 10.5	458.6 ± 40.5**	487.8 ± 25.9**	603.6 ± 36.8**
Malondialdehyde (nmol/g·FW)	83.9 ± 7.2	76.9 ± 6.4	80.5 ± 7.8	75.9 ± 8.6	344.9 ± 23.6	189.3 ± 15.3**	145.9 ± 16.9**	159.8 ± 18.9**
Soluble total sugar (mg/g·FW)	21.4 ± 1.5	39.6 ± 2.1**	30.9 ± 1.8**	38.81 ± 1.0**	42.8 ± 5.2	78.9 ± 6.3**	91.6 ± 4.6**	82.3 ± 3.6**
Soluble starch (mg/g·FW)	21.7 ± 1.3	26.3 ± 2.3*	29.6 ± 3.1*	28.7 ± 1.5*	45.6 ± 1.2	82.6 ± 5.3**	75.1 ± 3.6**	91.2 ± 2.9**
Electrolyte leakage rate (%)	16.8 ± 0.9	15.6 ± 1.6	16.7 ± 0.8	15.4 ± 1.2	82.8 ± 9.6	36.1 ± 4.3**	35.4 ± 4.1**	38.9 ± 1.6**
POD (U/g·FW)	1.8 ± 0.1	5.7 ± 0.1**	6.6 ± 0.2**	4.6 ± 0.1**	5.4 ± 0.1	20.1 ± 0.5**	25.8 ± 0.3**	30.8 ± 0.4**
SOD (U/g·FW)	1654.6 ± 78.9	3335.8 ± 121.8**	3708.6 ± 198.6**	3658.3 ± 154.6**	2269.6 ± 45.5	6366.5 ± 69.5**	6432.5 ± 157.6**	8239.6 ± 110.6**
CAT (U/g·FW)	504.4 ± 56.4	935.1 ± 35.9**	919.2 ± 23.6**	990.9 ± 32.5**	909.8 ± 90.6	2023.9 ± 58.6**	2056.8 ± 115.6**	2123.8 ± 69.3**
ABA (ng/g·FW)	44.7 ± 1.5	49.2 ± 5.8	48.9 ± 6.7	48.1 ± 5.2	127.9 ± 5.9	123.8 ± 9.1	117.7 ± 6.8	122.8 ± 8.3
JA (ng/g·FW)	17.2 ± 2.1	81.3 ± 7.1**	91.6 ± 3.9**	87.5 ± 9.5**	38.8 ± 2.3	245.6 ± 22.6**	278.6 ± 30.2**	215.9 ± 11.9**
SA (ng/g·FW)	5.5 ± 0.2	39.7 ± 3.6**	45.3 ± 6.4**	36.8 ± 1.5**	10.6 ± 0.9	156.8 ± 14.5**	145.6 ± 12.6**	158.5 ± 10.3**
ACC (ng/g·FW)	756.6 ± 56.9	2063.8 ± 235.6**	2653.8 ± 214.6**	2145.8 ± 98.6**	1231.5 ± 156.3	3684.1 ± 312.5**	4123.8 ± 396.5**	3569.8 ± 212.3**
IAA (ng/g·FW)	0.79 ± 0.06	0.2 ± 0.01**	0.16 ± 0.01**	0.18 ± 0.01**	0.46 ± 0.05	0.1 ± 0.01**	0.13 ± 0.01**	0.15 ± 0.01**

EV, empty vector-transformed lines; L-3, L-8, and L-12, SlDREBA4-overexpression lines. The results are indicated as the means of the three biological replicates ± SDs (Student's t-test, $^{*}P < 0.05$, $^{**}P < 0.01$).

three potentially DREs (DRE1 [GACCGACGA], DRE2 [AGCCGACAC], DRE3 [CGCCGACTT]) which were located in the promoters of two *Hsp* genes (Solyc06g076570 and Solyc09g015020). The construction of the required vectors for the Y1H assay was shown in **Figure 7A**. Y1H experiment showed that yeast cells co-transformed with pGADT7-*SlDREBA4* and pHis2.1-3DRE grew well on the SD-LWH plates and even with 20 mM 3-amino-1,2,4-triazole (3-AT). However, the transformant yeast cells harboring the pGADT7-*SlDREBA4* and pHis2.1-3mDRE could not grow on SD-LWH plates (**Figure 7B**). The result indicated that SlDREBA4 possessed the ability to bind DRE as a general AP2 transcription factor.

DISCUSSION

DREB transcription factors are often differentially expressed in most high-temperature-induced transcriptomes (Wang et al., 2018; Xu and Huang, 2018). The DREBA4 subfamily genes, *AtTINY* (Wilson et al., 1996), *ZmDBF2* (Wang et al., 2010), *DaCBF4* (Byun et al., 2018), and *ZmDREB4.1* (Li et al., 2018)

TABLE 2 | Physiological indicators in *SlDREBA4*-silenced plants.

	Control				Heat stress			
	V1+V2	**VIGS-2**	**VIGS-4**	**VIGS-8**	**V1+V2**	**VIGS-2**	**VIGS-4**	**VIGS-8**
Proline (ng/g·FW)	79.8 ± 3.3	69.3 ± 5.0*	64.2 ± 7.5*	65.4 ± 5.6*	167.5 ± 13.8	120.8 ± 8.9**	113.7 ± 9.0**	119.8 ± 8.8**
Malondialdehyde (nmol/g·FW)	78.7 ± 6.9	76.0 ± 5.6	81.6 ± 6.3	79.0 ± 6.9	289.8 ± 12.9	303.3 ± 23.8	295.8 ± 20.1	318.3 ± 30.8
Soluble total sugar (mg/g·FW)	19.0 ± 0.9	19.4 ± 1.2	20.6 ± 2.0	18.9 ± 1.6	36.9 ± 4.1	37.0 ± 4.2	32.9 ± 1.4	31.9 ± 2.7
Soluble starch (mg/g·FW)	32.1 ± 2.9	35.8 ± 2.0	31.5 ± 2.9	36.0 ± 4.4	59.3 ± 4.3	55.9 ± 4.6	56.0 ± 6.5	50.9 ± 5.8
Electrolyte leakage rate (%)	23.9 ± 1.8	24.5 ± 0.9	21.8 ± 2.1	24.5 ± 3.9	68.0 ± 3.1	81.0 ± 6.6*	79.0 ± 9.2*	76.8 ± 7.9*
POD (U/g·FW)	2.3 ± 1.2	1.6 ± 0.1*	1.6 ± 0.1*	1.8 ± 0.02*	7.8 ± 4.5	5.2 ± 0.4**	4.8 ± 0.1**	5.1 ± 0.5**
SOD (U/g·FW)	1465.6 ± 67.8	1254.8 ± 89.7*	1189.7 ± 123.7*	1134.7 ± 134.7*	3078.9 ± 445.8	2078.4 ± 312.7**	2134.5 ± 178.9**	2218.5 ± 221.7**
CAT (U/g·FW)	476.8 ± 34.5	465.7 ± 34.6	509.4 ± 56.7	489.7 ± 34.6	789.9 ± 87.3	800.3 ± 39.7	768.7 ± 56.7	813.8 ± 70.4
ABA (ng/g·FW)	35.8 ± 4.3	38.6 ± 2.9	40.1 ± 4.2	36.8 ± 4.1	81.4 ± 4.0	76.5 ± 4.3	83.6 ± 7.9	74.5 ± 6.9
JA (ng/g·FW)	21.9 ± 1.5	8.8 ± 0.5**	7.3 ± 0.9**	8.3 ± 0.6**	58.9 ± 4.9	25.3 ± 1.3**	25.6 ± 1.6**	24.6 ± 1.9**
SA (ng/g·FW)	9.7 ± 0.2	6.6 ± 0.6**	5.9 ± 0.6**	4.9 ± 0.3**	28.9 ± 1.3	10.6 ± 1.3**	11.8 ± 1.2**	8.4 ± 0.7**
ACC (ng/g·FW)	1091.0 ± 114.3	265.2 ± 23.2**	273.6 ± 25.6**	337.5 ± 28.3**	2584.2 ± 22.3	568.2 ± 33.6**	568.5 ± 69.6**	756.3 ± 53.6**
IAA (ng/g·FW)	0.69 ± 0.05	0.73 ± 0.04	0.71 ± 0.07	0.71 ± 0.04	0.47 ± 0.03	0.51 ± 0.05	0.53 ± 0.0	0.48 ± 0.04

*V1+V2: plants co-transformed by empty vectors pTRV1 and pTRV2, VIGS-2, VIGS-4, and VIGS-8: SlDREBA4-silenced plants. The results are indicated as the means of the three biological replicates ± SDs (Student's t-test, *P < 0.05, **P < 0.01).*

TABLE 3 | DEGs in the JA, SA, and ETH biosynthesis pathways in the *SlDREBA4*-overexpressed and silenced plants.

Gene ID	Readcount (OE/EV)	Readcount [VIGS/(V1+V2)]	log_2FoldChange [(OE/EV)/(VIGS/V1+V2)]	Definition	Hormone biosynthetic pathway
Solyc01g009680	259.96/121.66	209.90/458.45	1.10/–1.12	Lipoxygenase	JA
Solyc08g029000	199.00/130.26	—	0.60	Lipoxygenase	JA
Solyc04g039930	8.18/1.67	—	2.32	12-oxophytodienoate reductase-like protein	JA
Solyc01g007920	383.01/252.28	223.35/332.24	0.60/–0.57	Isochorismatase	SA
Solyc03g042560	157.66/74.40	73.37/108.51	1.08/–0.56	Phenylalanine ammonia-lyase	SA
Solyc05g026500	192.30/133.32	9.40/117.59	0.52/–3.64	Phenylalanine ammonia-lyase	SA
Solyc03g036470	151.84/103.25	—	0.55	Phenylalanine ammonia-lyase	SA
Solyc03g007070	1039.70/546.89	86.91/231.66	0.93/–1.41	1-aminocyclopropane-1-carboxylate synthase	ETH
Solyc08g079750	4118.98/3204.55	713.15/1285.27	0.36/–0.85	1-aminocyclopropane-1-carboxylate synthase	ETH

OE, SlDREBA4-overexpressed plants; EV, empty vector-transformed plants; VIGS: SlDREBA4-silenced plants; V1+V2, plants co-transformed by empty vectors pTRV1 and pTRV2; "—", not detected.

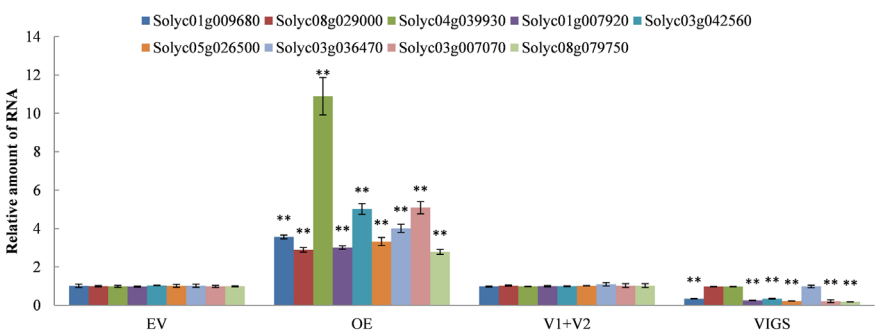

FIGURE 5 | Expression patterns of the DEGs in the JA, SA, and ETH biosynthesis pathways. The expression of the EV and V1+V2 plants were assigned a value of 1. The error bar on each column represents the SD of the three biological replicates (Student's *t*-test, $^{**}P < 0.01$).

have been isolated. However, the response patterns and functions of these transcription factors under heat-stress conditions have not been well investigated. SlDREBA4 was the only DREBA4 subfamily transcription factor in the high-temperature-induced DGE profile of Microtom, and the transcription of *SlDREBA4* was induced by ABA, heat, drought, cold, and high salt. In addition to improving the resistance of transgenic plants to heat stress, SlDREBA4 could

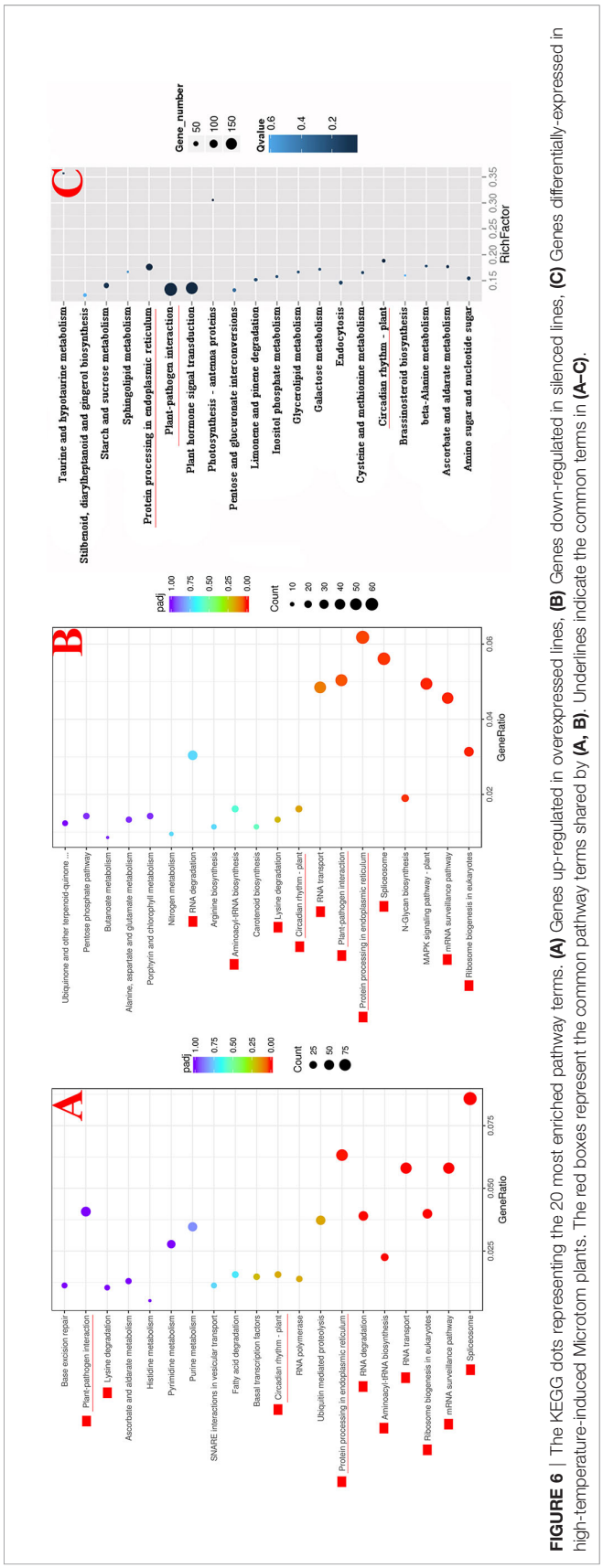

FIGURE 6 | The KEGG dots representing the 20 most enriched pathway terms. **(A)** Genes up-regulated in overexpressed lines, **(B)** Genes down-regulated in silenced lines, **(C)** Genes differentially-expressed in high-temperature-induced Microtom plants. The red boxes represent the common pathway terms shared by **(A, B)**. Underlines indicate the common terms in **(A–C)**.

also increase resistance to high salt, drought, and cold (data not shown). The diversified stress responses and functions of SlDREBA4 provide new data and regulatory gene resources for future studies on molecular mechanisms of stress useful for tomato breeding.

Physiological systems in plants respond appropriately to avoid heat injury. Under heat-stress conditions, the levels of osmotic substances, including proline (Xu and Huang, 2018), soluble sugar and starch (Wang et al., 2018) increased, as did the contents of SA and ETH (Biddington and Robinson, 1993), JA (Xu and Huang, 2018) and other stress-related hormones. The antioxidant enzyme activities, including POD, SOD and CAT increased (Wang et al., 2018). AtDREB1C enhanced resistance to heat by increasing the activities of POD, SOD and CAT in transgenic lines (Wei et al., 2017). Under normal conditions, the contents of osmolytes and stress hormones, and the activities of antioxidant enzymes in *SlDREBA4*-overexpressed plants were greater than those in the empty vector-transformed lines. These results indicated that *SlDREBA4* regulated the thermotolerance through comprehensively altering the content of osmolytes and stress hormones, and the activities of antioxidant enzymes at the physiologic level.

A large number of protective proteins, such as Hsps, were synthesized under heat-stress conditions (Muthusamyab et al., 2017; Wang et al., 2018). Ca^{2+}, as a central regulator of physiological responses to stress, plays an important role in regulating resistance to various stresses (Gong et al., 1998; Dodd et al., 2010; Wang et al., 2018). AtDREB2C and MsDREB2C increased the heat tolerance of overexpressed *Arabidopsis* by increasing the expression of *AtHsfA3* (Chen et al., 2010; Zhao et al., 2013). Six Hsps enriched in the protein processing in endoplasmic reticulum pathway and one calcium-binding protein enriched in the plant-pathogen interaction pathway were up-regulated in high-temperature-induced Microtom plants and *SlDREBA4*-overexpression lines, and were down-regulated in *SlDREBA4*-silenced lines. Here, three potentially DREs were identified in the promoters of two *Hsp* genes included in the above six *Hsps*, and bound with SlDREBA4, which demonstrated that SlDREBA4 transcription factor enhanced resistance to heat stress mainly through interactions with the *Hsps*.

Phytohormones are involved in plant growth and development, especially in adverse conditions. ABA plays a key role in plant acclimation to abiotic stress, including drought, heat, salt, and cold stress (Xiong et al., 2002; Suzuki et al., 2016; Zandalinas et al., 2016), and SA, JA, and ETH play regulatory roles in biotic stress (Dong et al., 1998). DREB transcription factors enhanced the resistance of transgenic plants to abiotic and biotic stress by increasing ABA, SA, JA, and ETH levels (Tsutsui et al., 2009; Zhao et al., 2013; Wu et al., 2017; Xiong et al., 2018). In our study, there was no significant difference in the ABA content in the empty vector-transformed with *SlDREBA4*-silenced and -overexpressed plants under normal growth and heat conditions. However, the SA, JA, and ACC contents in the empty vector-transformed plants were significantly higher than those in the *SlDREBA4*-silenced

TABLE 4 | Common DEGs in the high-temperature-induced Microtom plants (up-regulated), *SlDREBA4*-overexpressed (up-regulated), and -silenced (down-regulated) lines.

Gene ID	Pathway	log2FoldChange	Definition
Solyc06g036290	Plant-pathogen interaction	8.47/1.82/−0.20	Hsp90 protein
Solyc10g079420	Plant-pathogen interaction	1.16/0.20/−0.39	Calcium-binding protein
Solyc08g062450	Protein processing in endoplasmic reticulum	9.74/3.25/−0.43	Class II small heat shock protein
Solyc06g076570	Protein processing in endoplasmic reticulum	7.41/1.09/−0.26	Class I small heat shock protein
Solyc09g015020	Protein processing in endoplasmic reticulum	7.38/1.16/−0.39	Class I heat shock protein
Solyc09g015000	Protein processing in endoplasmic reticulum	7.19/1.56/−0.45	Class I heat shock protein
Solyc04g014480	Protein processing in endoplasmic reticulum	6.78/2.12/−0.59	Heat-shock protein
Solyc11g008420	Protein processing in endoplasmic reticulum	3.98/0.74/−0.59	SKP1-like protein

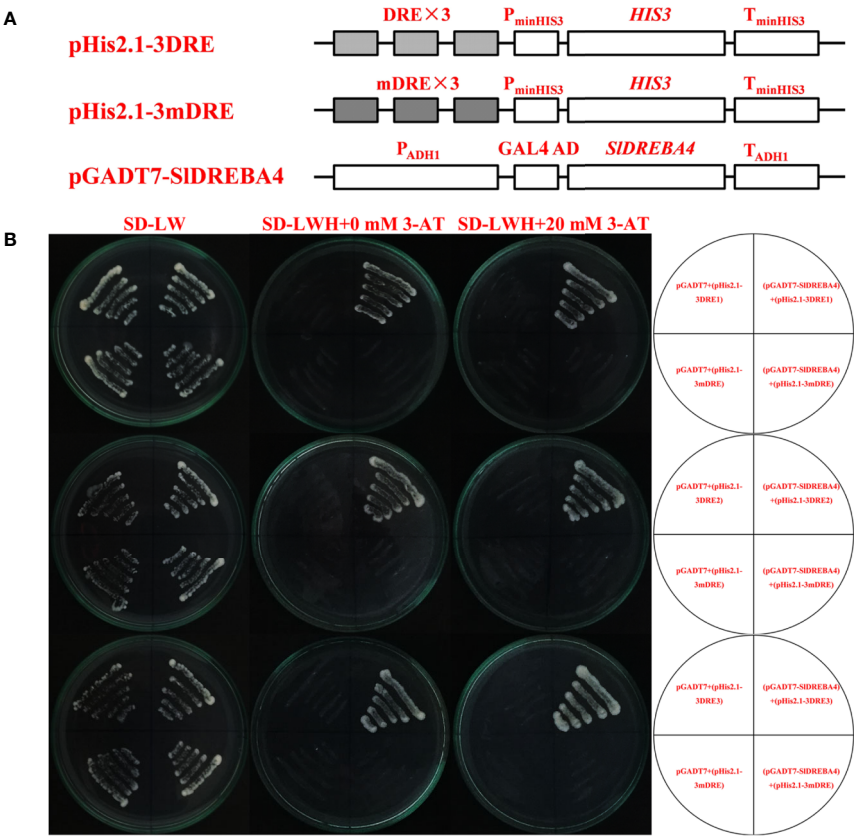

FIGURE 7 | Analysis of DRE binding specificity of SlDREBA4. **(A)** Construction of the required vectors for the Y1H assay. The bait plasmid pHis2.1 contained three tandem repeat DREs or mDREs and the HIS reporter gene. The coding sequence of *SlDREBA4* was cloned into the activation domain GAL4 of the prey plasmid pGADT7. **(B)** Yeast strain Y187 was co-transformed with bait (pHis2.1-3DRE or pHis2.1-3mDRE) and prey (pGADT7 or pGADT7-*SlDREBA4*) construct. Interaction between the bait and prey was examined by cell growth on SD medium lacking Trp, Leu, and His (SD-WLH) containing 3-AT.

plants and lower than those in *SlDREBA4*-overexpressed lines. The KEGG pathway of plant-pathogen interaction (ko04626) included in the 20 most enriched pathway terms was obtained in the high-temperature-induced plants and *SlDREBA4*-overexpressed and -silenced lines. The above research result also indicates that SlDREBA4 plays a potential role in biotic stress responses, but the specific biotic stress in which SlDREBA4 functioned remains to be further explored.

CONCLUSION

SlDREBA4 was determined to be a transcription factor of the DREBA4 family in tomato and plays an important regulatory role under heat-stress conditions. SlDREBA4 transcription factor enhances resistance to heat stress through interactions with the contents of osmolytes and stress hormones, and the activities of antioxidant enzymes at the physiological

level and the expression of Hsps and calcium-binding protein at the molecular level.

DATA AVAILABILITY STATEMENT

All of the RNA-Seq datasets generated in this study are available from the SRA-Archive (http://www.ncbi.nlm.nih.gov/sra) under the study accession numbers: PRJNA554738, PRJNA579195, and PRJNA579731.

AUTHOR CONTRIBUTIONS

KZ designed the experiments and wrote the manuscript. LM, MD, and SJ generated the transgenic materials and performed the experiments. HZ analyzed the RNA-Seq data and provided assistance on vector construction. ZY measured the physiologic index. YY conducted the heat phenotyping experiment. All authors contributed to the article and approved the submitted version.

FUNDING

This research was supported by the National Natural Science Foundation of China (31660576, 31760583), the Joint Project of Basic Agricultural Research in Yunnan Province (2018FG001-004), and the General Project of Yunnan Science and Technology plan (2016FB064).

SUPPLEMENTARY MATERIAL

The Supplementary Material for this article can be found online at: https://www.frontiersin.org/articles/10.3389/fpls.2020.554520/full#supplementary-material

REFERENCES

Akbudak, M. A., Filiz, E., and Kontbay, K. (2018). DREB2 (dehydration-responsive element-binding protein 2) type transcription factor in sorghum (*Sorghum bicolor*): genome-wide identification, characterization and expression profiles under cadmium and salt stresses. *3 Biotech.* 8, 426. doi: 10.1007/s13205-018-1454-1

Anders, S., and Huber, W. (2010). Differential expression analysis for sequence count data. *Genome Biol.* 11, R106. doi: 10.1186/gb-2010-11-10-r106

Audic, S., and Claverie, J. M. (1997). The significance of digital gene expression profiles. *Genome Res.* 10, 986–995. doi: 10.1101/gr.7.10.986

Benjamini, Y., and Yekutieli, D. (2001). The control of the false discovery rate in multiple testing under dependency. *Ann. Stat.* 29, 1165–1188. doi: 10.2307/2674075

Biddington, N. L., and Robinson, H. T. (1993). Heat enhances ethylene promotion of anther filament growth in Brussels sprouts (*Brassica oleracea* var. *gemmifera*). *Plant Growth Regul.* 12, 29–35. doi: 10.1007/BF00144579

Byun, M. Y., Cui, L. H., Lee, J., Park, H., Lee, A., Kim, W. T., et al. (2018). Identification of rice genes associated with enhanced cold tolerance by comparative transcriptome analysis with two transgenic rice plants overexpressing *DaCBF4* or DaCBF7, isolated from antarctic flowering plant *Deschampsia Antarctica*. *Front. Plant Sci.* 9601, 601. doi: 10.3389/fpls.2018.00601

Charfeddine, M., Charfeddine, S., Bouaziz, D., Messaoud, R. B., and Bouzid, R. G. (2017). The effect of cadmium on transgenic potato (*Solanum tuberosum*) plants overexpressing the StDREB transcription factors. *Plant Cell Tiss. Org.* 128, 521–541. doi: 10.1007/s11240-016-1130-2

Chen, H., Hwang, J. E., Lim, C. J., Kim, D. Y., Lee, S. Y., and Lim, C. O. (2010). *Arabidopsis* DREB2C functions as a transcriptional activator of HsfA3 during the heat stress response.Biochem. *Biophys. Res. Commun.* 401, 238–244. doi: 10.1016/j.bbrc.2010.09.038

Dodd, A. N., Kudla, J., and Sanders, D. (2010). The language of calcium signaling. *Annu. Rev. Plant Biol.* 61, 593–620. doi: 10.1146/annurev-arplant-070109-104628

Dong, X. N. (1998). SA, JA, ethylene, and disease resistance in plants. *Curr. Opin. Plant Biol.* 1, 316–323. doi: 10.1016/1369-5266(88)80053-0

Finkelstein, R., Wang, M. L., Lynch, T., Rao, S., and Goodman, H. M. (1998). The *Arabidopsis* abscisic acid response locus ABI4 encodes an APETALA2 domain protein. *Plant Cell* 10, 1043–1054. doi: 10.2307/3870689

Gong, M., van der Luit, A. H., Knight, M. R., and Trewavas, A. J. (1998). Heat-shock-induced changes in intracellular Ca^{2+} level in tobacco seedlings in relation to thermotolerance. *Plant Physiol.* 116, 429–437. doi: 10.1104/pp.116.1.429

Hu, X. Q., Xue, X. M., and Li, C. H. (2018). Ectopic expression of the LoERF017 transcription factor from *Larix olgensis* Henry enhances salt and osmotic-stress tolerance in *Arabidopsis thaliana*. *Plant Biotechnol. Rep.* 12, 93–104. doi: 10.1007/s11816-018-0473-z

Huang, B., and Liu, J. Y. (2006). A cotton dehydration responsive element binding protein functions as a transcriptional repressor of DRE-mediated gene expression. *Biochem. Bioph. Res. Co.* 343, 1023–1031. doi: 10.1016/j.bbrc.2006.03.016

Huang, L. Y., Wang, Y. X., Wang, W. S., Zhao, X. Q., Qin, Q., Sun, F., et al. (2018). Characterization of transcription factor gene *OsDRAP1* conferring drought tolerance in rice. *Front. Plant Sci.* 9, 94. doi: 10.3389/fpls.2018.00094

Kitashiba, H., Ishizaka, T., Isuzugawa, K., Nishimura, K., and Suzuki, T. (2004). Expression of a sweet cherry DREB1/CBF ortholog in *Arabidopsis* confers salt and freezing tolerance. *J. Plant Physiol.* 161, 171–1176. doi: 10.1016/j.jplph.2004.04.008

Kumar, R. K. E. C., Reddy, R. B., and Rao, K. R. (1985). Activity of isoproturon on leaf cell membrane permeability. *Plant Sci.* 95, 405–407. doi: 10.1007/bf03053678

Li, S. X., Zhao, Q., Zhu, D. Y., and Yu, J. J. (2018). A DREB-Like transcription factor from maize (*Zea mays*), ZmDREB4.1, plays a negative role in plant growth and development. *Front. Plant Sci.* 9, 395. doi: 10.3389/fpls.2018.00395

Liu, Q., Kasuga, M., Sakuma, Y., Abe, H., Miura, S., Yamaguchi-Shinozaki, K., et al. (1998). Two transcription factors, DREB1 and DREB2, with an EREBP/AP2 DNA binding domain, separate two cellular signal transduction pathways in drought- and cold-responsive gene expression, respectively, in *Arabidopsis*. *Plant Cell* 10, 1391–1406. doi: 10.1105/tpc.10.8.1391

Løvdal, T., and Lillo, C. (2009). Reference gene selection for quantitative real-time PCR normalization in tomato subjected to nitrogen, cold, and light stress. *Anal. Biochem.* 387, 238–242. doi: 10.1016/j.ab.2009.01.024

Mortazavi, A., Williams, B. A., McCue, K., Schaeffer, L., and Wold, B. (2008). Mapping and quantifying mammalian transcriptomes by RNA-Seq. *Nat. Methods* 5, 621–628. doi: 10.1038/nmeth.1226

Muthusamyab, S. K., Dalala, M., Chinnusamy, V., and Bansala, K. C. (2017). Genome-wide identification and analysis of biotic and abiotic stress regulation of small heat shock protein (*HSP20*) family genes in bread wheat. *J. Plant Physiol.* 211, 100–113. doi: 10.1016/j.jplph.2017.01.004

Nasir, A., and Fazal, H. (2018). CBF/DREB transcription factor genes play role in cadmium tolerance and phytoaccumulation in *Ricinus communis* under molybdenum treatments. *Chemosphere* 208, 425–432. doi: 10.1016/j.chemosphere.2018.05.165

Niu, X., Helentjaris, T., and Bate, N. J. (2002). Maize ABI4 binds coupling element in abscisic acid and sugar response genes. *Plant Cell* 14, 2565–2575. doi: 10.1105/tpc.003400

Pan, X. Q., Welti, R., and Wang, X. M. (2010). Quantitative analysis of major plant hormones in crude plant extracts by high-performance liquid chromatography-mass spectrometry. *Nat. Protoc.* 5, 986–992. doi: 10.1038/nprot.2010.37

Qin, F., Kakimotoet, M., Sakuma, Y., Maruyama, K., Osakabe, Y., Tran, L. P., et al. (2018). Regulation and functional analysis of *ZmDREB2A* in response to drought and heat stresses in *Zea mays* L. *Plant J.* 50, 243. doi: 10.3389/fpls.2018.00243

Robinson, M. D., McCarthy, D. J., and Smyth, G. K. (2010). edgeR: a Bioconductor package for differential expression analysis of digital gene expression data. *Bioinformatics* 26, 139–140. doi: 10.1093/bioinformatics/btp616

Sakuma, Y., Liu, Q., Dubouzet, J. G., Abe, H., Shinozaki, K., and Yamaguchi-Shinozaki, K. (2002). DNA-binding specificity of the ERF/AP2 domain of *Arabidopsis* DREBs transcription factors involved in dehydration- and cold-inducible gene expression. *Biochem. Bioph. Res. Co.* 290, 998–1009. doi: 10.1006/bbrc.2001.6299

Sakuma, Y., Maruyama, K., Osakabe, Y., Qin, F., Seki, M., Shinozaki, K., et al. (2006). Functional analysis of an *Arabidopsis* transcription factor, DREB2A, involved in drought-responsive gene expression. *Plant Cell* 18, 1292–1309. doi: 10.1105/tpc.105.035881

Shen, X. J., Zhao, K., Liu, L. L., Zhang, K. C., Yuan, H. Z., Liao, X., et al. (2014). A role for *PacMYBA* in ABA-regulated anthocyanin biosynthesis in red-colored sweet cherry cv. Hong Deng (*Prunus avium* L.). *Plant Cell Physiol.* 55, 862–880. doi: 10.1093/pcp/pcu013

Sun, S., Kang, X. P., Xing, X. J., Xu, X. Y., Cheng, J., Zheng, S. W., et al. (2015). *Agrobacterium*-mediated transformation of tomato (*Lycopersicon esculentum* L. cv. Hezuo 908) with improved efficiency. *Biotechnol. Biotec. Eq.* 29, 861–868. doi: 10.1080/13102818.2015.1056753

Suzuki, N., Bassil, E., Hamilton, J. S., Inupakutika, M. A., Zandalinas, S.II, Tripathy, D., et al. (2016). ABA is required for plant acclimation to a combination of salt and heat stress. *PloS One* 11, e0147625. doi: 10.1371/journal.pone.0147625

Tsutsui, T., Kato, W., Asada, Y., Sako, K., Sato, T., Sonoda, Y., et al. (2009). DEAR1, a transcriptional repressor of DREB protein that mediates plant defense and freezing stress responses in *Arabidopsis*. *J. Plant Res.* 122, 633–643. doi: 10.1007/s10265-009-0252-6

Wang, C. T., Yang, Q., and Wang, C. T. (2010). Isolation and functional characterization of ZmDBP2 encoding a dehydration-responsive element-binding protein in *Zea mays*. *Plant Mol. Biol. Rep.* 29, 60–68. doi: 10.1105/tpc.003400

Wang, R., Mei, Y., Xu, L., Zhu, X., Wang, Y., Guo, J., et al. (2018). Genome-wide characterization of differentially expressed genes provides insights into regulatory network of heat stress response in radish (*Raphanus sativus* L.). *Funct. Integr. Genomic.* 18, 225–239. doi: 10.1007/s10142-017-0587-3

Wei, T., Deng, K., Zhang, Q., Gao, Y., Liu, Y., Yang, M., et al. (2017). Modulating *AtDREB1C* expression improves drought tolerance in *Salvia miltiorrhiza*. *Front. Plant Sci.* 8, 52. doi: 10.3389/fpls.2017.00052

Wilson, K., Long, D., Swinburne, J., and Coupland, G. (1996). A dissociation insertion causes a semidominant mutation that increases expression of TINY, an *Arabidopsis* gene related to APETALA2. *Plant Cell* 8, 659–671. doi: 10.1105/tpc.8.4.659

Wu, J., Folta, K. M., Xie, Y. F., Jiang, W. M., Lu, J., and Zhang, Y. L. (2017). Overexpression of *Muscadinia rotundifolia* CBF2 gene enhances biotic and abiotic stress tolerance in *Arabidopsis*. *Protoplasma* 254, 239–251. doi: 10.1007/s00709-015-0939-6

Wu, Z., Liang, J. H., Zhang, S., Zhang, B., Zhao, Q. C., Li, G. Q., et al. (2018). A canonical DREB2-type transcription factor in lily is post-translationally regulated and mediates heat stress response. *Front. Plant Sci.* 9, 243. doi: 10.3389/fpls.2018.00243

Xiong, L. M., Schumaker, K. S., and Zhu, J. K. (2002). Cell signaling during cold, drought, and salt stress. *Plant Cell* 14, S165–S183. doi: 10.1105/tpc.000596

Xiong, C. M., Zhao, X. H., Jia, H. M., An, X., and Mao, H. Y. (2018). Cloning and expression analysis of *CmDREBa-2*, a resistance-related gene to chrysanthemum white rust. *Acta Hortic. Sin.* 45, 977–987.

Xu, Y., and Huang, B. R. (2018). Transcriptomic analysis reveals unique molecular factors for lipid hydrolysis, secondary cell-walls and oxidative protection associated with thermotolerance in perennial grass. *BMC Genomics* 19, 70. doi: 10.1186/s12864-018-4437-z

Yamaguchi-Shinozaki, K., and Shinozaki, K. (1994). A novel *cis*-acting element in an *Arabidopsis* gene is involved in responsiveness to drought, low-temperature, or high-salt stress. *Plant Cell* 6, 251–264. doi: 10.1105/tpc.6.2.251

Yang, W., Liu, X. D., Chi, X. J., Wu, C. A., and Li, Y. Z. (2011). Dwarf apple MbDREB1 enhances plant tolerance to cold, drought, and salt stress via both ABA-dependent and ABA-independent pathways. *Planta* 233, 219–229. doi: 10.1007/s00425-010-1279-6

Yuan, H. Z., Zhao, K., Lei, H. J., Shen, X. J., Liu, Y., Liao, X., et al. (2013). Genome-wide analysis of the GH3 family in apple (Malus x domestica). *BMC Genomics* 14, 297. doi: 10.1186/1471-2164-14-297

Zandalinas, S.II, Balfagón, D., Arbona, V., Gómez-Cadenas, A., Inupakutika, M. A., and Mittler, R. (2016). ABA is required for the accumulation of APX1 and MBF1c during a combination of water deficit and heat stress. *J. Exp. Bot.* 67, 5381–5390. doi: 10.1093/jxb/erw299

Zhao, K., Shen, X. J., Yuan, H. Z., Liu, Y., Liao, X., Wang, Q., et al. (2013). Isolation and characterization of dehydration-responsive element-binding factor 2C (MsDREB2C) from *Malus sieversii* Roem. *Plant Cell Physiol.* 54, 1415–1430. doi: 10.1093/pcp/pct087

Zhao, K., Guo, X. W., Liao, X., Wang, Q., Liu, D., and Li, T. H. (2015). *Arabidopsis* plants overexpressing the MsDREB2C exhibit increased susceptibility to *Alternaria mali* infection. *J. Plant Growth Regul.* 34, 78–87. doi: 10.1007/s00344-014-9444-y

Conflict of Interest: The authors declare that the research was conducted in the absence of any commercial or financial relationships that could be construed as a potential conflict of interest.

frontiers in Plant Science

ORIGINAL RESEARCH
published: 03 December 2020
doi: 10.3389/fpls.2020.607161

Simultaneous CRISPR/Cas9 Editing of Three PPO Genes Reduces Fruit Flesh Browning in *Solanum melongena* L.

Alex Maioli[1†], *Silvia Gianoglio*[2†], *Andrea Moglia*[1*], *Alberto Acquadro*[1], *Danila Valentino*[1], *Anna Maria Milani*[1], *Jaime Prohens*[3], *Diego Orzaez*[2], *Antonio Granell*[2], *Sergio Lanteri*[1] *and Cinzia Comino*[1]

[1] *DISAFA, Plant Genetics and Breeding, University of Torino, Grugliasco, Italy,* [2] *Crop Biotechnology Department, Instituto de Biología Molecular y Celular de Plantas (IBMCP), CSIC-UPV, Valencia, Spain,* [3] *Instituto de Conservación y Mejora de la Agrodiversidad Valenciana, Universitat Politècnica de València, Valencia, Spain*

OPEN ACCESS

Edited by:
Amalia Barone,
University of Naples Federico II, Italy

Reviewed by:
Yoshihito Shinozaki,
Tokyo University of Agriculture and Technology, Japan
Abdelali Hannoufa,
Agriculture and Agri-Food Canada (AAFC), Canada
Marina Tucci,
National Research Council (CNR), Italy

***Correspondence:**
Andrea Moglia
andrea.moglia@unito.it

[†] *These authors have contributed equally to this work*

Specialty section:
This article was submitted to Plant Metabolism and Chemodiversity, a section of the journal Frontiers in Plant Science

Received: *16 September 2020*
Accepted: *06 November 2020*
Published: *03 December 2020*

Citation:
Maioli A, Gianoglio S, Moglia A, Acquadro A, Valentino D, Milani AM, Prohens J, Orzaez D, Granell A, Lanteri S and Comino C (2020) Simultaneous CRISPR/Cas9 Editing of Three PPO Genes Reduces Fruit Flesh Browning in Solanum melongena L. Front. Plant Sci. 11:607161. doi: 10.3389/fpls.2020.607161

Polyphenol oxidases (PPOs) catalyze the oxidization of polyphenols, which in turn causes the browning of the eggplant berry flesh after cutting. This has a negative impact on fruit quality for both industrial transformation and fresh consumption. Ten *PPO* genes (named *SmelPPO1-10*) were identified in eggplant thanks to the recent availability of a high-quality genome sequence. A CRISPR/Cas9-based mutagenesis approach was applied to knock-out three target *PPO* genes (*SmelPPO4*, *SmelPPO5,* and *SmelPPO6),* which showed high transcript levels in the fruit after cutting. An optimized transformation protocol for eggplant cotyledons was used to obtain plants in which Cas9 is directed to a conserved region shared by the three *PPO* genes. The successful editing of the *SmelPPO4*, *SmelPPO5,* and *SmelPPO6* loci of *in vitro* regenerated plantlets was confirmed by Illumina deep sequencing of amplicons of the target sites. Besides, deep sequencing of amplicons of the potential off-target loci identified *in silico* proved the absence of detectable non-specific mutations. The induced mutations were stably inherited in the T_1 and T_2 progeny and were associated with a reduced PPO activity and browning of the berry flesh after cutting. Our results provide the first example of the use of the CRISPR/Cas9 system in eggplant for biotechnological applications and open the way to the development of eggplant genotypes with low flesh browning which maintain a high polyphenol content in the berries.

Keywords: gene editing, CRISPR/Cas 9, eggplant, polyphenol oxydase, knock-out

INTRODUCTION

The polyphenol oxidases (PPOs) are a group of enzymes catalyzing the oxidation of phenolic compounds into highly reactive quinones (Prohens et al., 2007; Mishra et al., 2013; Plazas et al., 2013; García-Fortea et al., 2020). The physiological role of PPOs in plants has not been fully clarified yet, but a defense role against pathogens and pests has been postulated because of their increased localized activity in response to cutting and wounding. The relationship between PPO expression or activation and pathogen infections was proved in tomato by either silencing (Thipyapong et al., 2004) or over-expressing PPO genes (Li and Steffens, 2002). PPOs oxidize polyphenols to toxic

quinones which bind to amino acids in the insect gut, exerting an anti-feeding role. Previous studies have associated PPO activity with resistance to various types of insects (Mahanil et al., 2008).

In recent years, PPOs have been largely investigated for their involvement in the browning process, a color reaction caused by the oxidation of phenolic compounds during postharvest processing and storage. Enzymatic browning is a two-step reaction, consisting of the oxidation of a monophenol to a o-diphenol (cresolase/monophenolase activity), which is further oxidized to yield a o-quinone (catecholase/diphenolase activity). O-quinones can then undergo condensation or polymerization reactions, producing the dark pigments melanins. Fruit cutting causes cellular disruption and damages membrane integrity, allowing the PPOs sequestered in the plastid to come into contact with the hydroxycinnamic acid derivatives, which are their substrates. Extensive browning of cut fruit and vegetable surface compromises food quality and usually impairs the properties of the product, representing a major economic problem both for the food industry (e.g., the industrial manipulation and preservation of these products) and for consumers (in the case of fresh and ready-to-eat fresh cut fruit and vegetables). Since PPO activity is influenced by factors such as pH, temperature and oxygen, the browning process is limited in the food industry through the use of chemical and/or physical agents, with a negative impact on nutritional and organoleptic properties. Browning negatively affects the commercial value of many key agricultural productions, including potato, lettuce, cereals, banana, cucumber, grape and eggplant (Taranto et al., 2017).

Eggplant (*Solanum melongena* L.) berries are characterized by a remarkable content in phenolic compounds, represented mainly by chlorogenic acid (5-O-caffeoylquinic acid). Chlorogenic acid plays important therapeutic roles due to its antioxidant, antibacterial, hepatoprotective, cardioprotective, anti-inflammatory and anti-microbial properties (Naveed et al., 2018). In eggplant, a correlation between the concentration of phenolics (mainly chlorogenic acid) and browning has been detected in the fruit flesh, although additional morphological and physiological factors may be involved in browning phenomena (Kaushik et al., 2017). Furthermore, in commercial varieties, the selection for berries with a reduced degree of browning in the flesh has resulted in the indirect selection of accessions with lower concentrations of phenolics (Prohens et al., 2007).

Shetty et al. (2011) identified six genes encoding PPOs in eggplant and, on the basis of both protein sequence similarity and organ-specific patterns of expression, they proposed the distinction of eggplant PPOs in two clades: A and B, with clade A encompassing genes expressed mostly in roots, while clade B genes are involved in defense mechanisms. This categorization was further extended to the rest of Solanaceae PPOs (Taranto et al., 2017).

The development of new technologies to disable genes coding for PPOs represents the most promising strategy to avoid undesired browning in plant-derived products, as it would allow to positively select genotypes enriched in beneficial phenolic compounds, while reducing the need for physical and chemical treatments in the food industry. The positive impact on the storability of these foods, in addition, would help reduce waste.

Several examples are available on the adoption of RNA silencing strategies to down-regulate PPO genes in order to reduce the enzymatic browning in potato tubers (Bachem et al., 1994; Coetzer et al., 2001; Rommens et al., 2006; Llorente et al., 2011; Chi et al., 2014). By using artificial micro-RNAs (amiRNAs) all *StuPPO* genes have been silenced individually or in combination, identifying $StuPPO_2$ as the main contributor to PPO activity (Chi et al., 2014). A few notable examples exist of commercially available genetically modified plants in which PPOs have been silenced, such as the Arctic Apple® and the Innate® potato. The emergent CRISPR/Cas9 technology has proved extremely efficient in gene editing and is expected to play a key role in crop breeding. This technology makes it possible to induce point mutations in one or multiple target sequences simultaneously, as well as to introduce new genetic variants through homology directed recombination (HDR), or to modulate transcription and chromatin structure at selected target loci (Doudna and Charpentier, 2014). While this technique has been successfully applied to some Solanaceae species, such as tomato and potato, including the knock out of the *StuPPO2* gene in the potato tetraploid cultivar Desiree (González et al., 2020), no examples of genome editing in eggplant have been reported in literature so far (Van Eck, 2018).

In this study, thanks to the recent availability of a high quality, annotated and anchored eggplant genome sequence (https://solgenomics.net/organism/Solanum_melongena/genome; Barchi et al., 2019), we report the homology-based characterization, functional domain identification and phylogenetic analysis, of 10 PPO (*SmelPPO1-PPO10*) genes in eggplant. On the basis of their expression in the fruit after cutting, *SmelPPO4*, *SmelPPO5,* and *SmelPPO6* were selected for the generation of knock-out mutants using the CRISPR/Cas9 technology. Regenerated T_0, T_1, and T_2 lines were screened for induced mutations in the target genes as well as in potential off-target loci. In addition, PPO activity and the degree of browning in the flesh of eggplant berries were analyzed in our knock-out T_1 and T_2 edited lines.

MATERIALS AND METHODS

Mining of PPO in the Eggplant Genome and Phylogenetic Analysis

The six eggplant PPO aminoacidic sequences previously reported (Shetty et al., 2011) were used for a BlastP search of the eggplant proteome (https://solgenomics.net/organism/Solanum_melongena/genome) with an E-value threshold of 1 e^{-5}. The polypeptide sequences of eggplant PPOs, together with those of six tomato and nine potato PPOs (**Data Sheet 1**), were used for a multiple alignment (Clustal Omega; https://www.ebi.ac.uk/Tools/msa/clustalo/). A phylogenetic analysis was performed with the MEGA X software. An unrooted phylogenetic tree was generated, applying the Neighbor-Joining (NJ) algorithm. The statistical significance of individual nodes was assessed by bootstrap analysis with 1,000 replicates, and the evolutionary distances were calculated using the p-distance method with default parameters.

qPCR Analysis

To identify *PPO* genes involved in the browning phenotype their corresponding mRNA levels were analyzed in the flesh of fruits of the "Black Beauty" variety harvested at the commercial ripening stage (Mennella et al., 2012) after cutting them transversally with a sharp knife. One gram of frozen fruit flesh was ground in liquid nitrogen to a fine powder and RNA was extracted using the "Spectrum plant total RNA kit" (Sigma-Aldrich, St. Louis, USA). RNA was extracted in three biological replicates from commercial grade ripe fruit 1 cm-wide slices exposed to air for 0 min (t_0) and 30 min (t_{30}).

cDNA was synthesized from 1 μg of RNA using a High Capacity RNA-to-cDNA kit (Applied Biosystems, Foster City, USA) as directed by the manufacturer. Using the Primer 3 software (http://bioinfo.ut.ee/primer3), primers targeting the ten identified eggplant *PPO* genes were designed (**Supplementary Table 1**). PCR reactions were carried out in three biological replicates using the StepOnePlus Real-Time PCR System (Applied Biosystems). The following PCR program was used: 95°C/10 min, followed by 40 cycles of 95°C/15 s and 60°C/1 min. Data were quantified using the $2^{-\Delta\Delta Ct}$ method based on Ct values of actin and elongation factor as housekeeping genes. Values are expressed as relative mRNA abundance at 30 min after cutting compared to time 0 (just after cutting).

Target Identification, DNA Construct Cloning, and Off-Target Search

Sequences of the wound-induced *SmelPPO4, SmelPPO5,* and *SmelPPO6* genes were aligned to find conserved regions, and BlastX and Prosite were used to annotate functional domains. A gRNA (ATGAATGGAAAGCAATCGGA) was designed to target a conserved region of these three genes and assembled into a CRISPR/Cas9 construct carrying the h*Cas9* and the *nptII* gene for kanamycin resistance, using the GoldenBraid (GB) assembly system and following GB software-directed procedures (https://gbcloning.upv.es/). An additional guanine was added at the 5'end in order to improve expression under the U6-26 RNA PolIII promoter (Cong and Zhang, 2015). The h*Cas9* expression is driven by the CaMV 35S promoter, while the gRNA is placed under the control of the *At*U6-26 RNA PolIII promoter. Putative off-target sites were identified with the CasOT software (http://casot.cbi.pku.edu.cn/), using the eggplant genome as reference. Four off-targets (OT1-OT4) were selected based on the number and position of mismatches (**Supplementary Table 2**); the corresponding loci (a 1 kb region around the putative off-target site) were inspected, to determine whether they corresponded to functional genes, and considered for sequencing analyses.

Genetic Transformation of Plants

The final pCambia vector *Tnos:nptII:Pnos-U6-26:gRNA:scaffold-P35S:*h*Cas9:Tnos* was transformed into LBA4404 *Agrobacterium tumefaciens* strain. A pre-culture was set up in a modified MGL liquid medium (tryptone 5 g l^{-1}, yeast extract 2.5 g l^{-1}, NaCl 0.1 g l^{-1}, mannitol 5 g l^{-1}, glutamic acid 1.15 g l^{-1}, KH_2PO_4 0.25 g l^{-1}, $MgSO_4.7H_2O$ 100 g l^{-1}, biotin 1 mg l^{-1}, pH 7) supplemented with 50 mg l^{-1} rifampicin and 50 mg l^{-1} kanamycin, and incubated overnight at 28°C. From this, a second culture was set up in TY liquid medium (tryptone 5 g l^{-1}, yeast extract 3 g l^{-1}, $MgSO_4.7H_2O$ 0.5 g l^{-1}, pH 5.8) supplemented with 200 μM acetosyringone and incubated overnight in the dark at 28°C. Before transformation, the optical density of the culture at 600 nm (OD_{600}) was measured and the bacterial culture was diluted to a final OD_{600} of 0.10–0.15 in TY medium supplemented with 200 μM acetosyringone. Explants of about 5 mm in length were cut from the cotyledons of *in vitro* germinated 'Black Beauty' seeds, dipped in the bacterial culture for a minimum of 10 min, blotted dry on filter paper and transferred for 48 h on a co-culture medium (MS basal salt mixture 4.5 g l^{-1}, MES 0.5 g l^{-1}, sucrose 30 g l^{-1}, phytoagar 10 g l^{-1}, Gamborg vitamin mixture 1 ml l^{-1}, trans-zeatin 2 mg l^{-1}, IAA 0.1 mg l^{-1}, acetosyringone 200 μM, pH 5.8), in the dark. For organogenesis and shoot induction, a common basal induction medium was used, as previously described (Muktadir et al., 2016) (MS basal salt mixture 4.5 g l^{-1}, MES 0.5 g l^{-1}, sucrose 30 g l^{-1}, phytoagar 10 g l^{-1}, Gamborg vitamin mixture 1 ml l^{-1}, trans-zeatin 2 mg l^{-1}, IAA 0.1 mg l^{-1}, kanamycin 30 mg l^{-1}, carbenicillin 400 mg l^{-1}, pH 5.8), with three different conditions: without further additives, with supplementation of ascorbic acid 5 mg l^{-1} and citric acid 5 mg l^{-1}, and with supplementation of polyvinylpyrrolidone (PVP40) 200 mg l^{-1}. Furthermore, for each medium composition, two conditions were tested during the first 3 days of induction: no incubation, or 3 days of incubation in the dark, after which explants were grown in the same conditions as the untreated group (16:8 light:dark cycle, 24°C). Elongation and rooting were performed on the same media for all conditions and explants were moved to a fresh medium every 2–3 weeks. Both media were previously described (Muktadir et al., 2016) and were not supplemented with antioxidants, as no oxidative damage was observed from this stage onwards. The elongation medium was supplemented with kanamycin 30 mg l^{-1} and carbenicillin 400 mg l^{-1}, but did not contain any hormone. Kanamycin was removed from the rooting medium to avoid inhibitory effects on root development, and 0.2 mg l^{-1} indolebutyric acid were added. Fully developed plantlets were then moved to soil and gradually acclimated to *ex vitro* conditions.

Target and Off-Target Sequencing

Genomic DNA was extracted using a CTAB protocol (Doyle and Doyle, 1987) from leaves sampled when plantlets were transferred from *in vitro* growth conditions to soil. The presence of the transgene was assessed by amplifying the h*Cas9* (**Supplementary Table 3**) gene by using qPCR (in three technical replicates) according to the protocol described in the previous paragraph. DNA was also extracted from T_1 and T_2 progeny plants (**Data Sheet 3**).

Mutation frequencies at the target and off-target sites were evaluated according to an adapted version of the 16S Metagenomic Sequencing Library preparation protocol provided by Illumina (16S Sample Preparation Guide). Amplifications were carried out using the KAPA HiFi HotStart ReadyMix PCR Kit (Kapa Biosystems, Boston, MA). Dual indexing was done using the Nextera XT system (Illumina, San Diego, CA) using

16 i5 indexes (S502-S522) and 24 i7 indexes (N701-N729), enabling the multiplexing of 333 individual libraries. Due to their high sequence identity, a differential amplification of *SmelPPO4* and *SmelPPO6* was obtained with a first specific PCR, using primers designed on flanking non conserved regions, while a second amplification was performed with non-specific primers carrying Illumina adapter sequences (**Supplementary Table 3**). Amplifications of *SmelPPO5*, OT1, OT2, OT3, OT4 were done directly using primers modified with Illumina adapter sequences (**Supplementary Table 3**). Products were diluted 1:50 and used as templates to add dual Nextera XT indexes (**Data Sheet 2**). Finally, indexed amplicons were purified using AmpureBeads (0,7X) and quantified using Qubit 2.0 (Life Technologies, Carlsbad, CA, USA), based on the Qubit dsDNA HS Assay (Life Technologies, Carlsbad, CA, USA). All samples were diluted to 4 nM and pooled in a single tube. Sequencing was performed with an Illumina MiSeq sequencer (Illumina Inc., San Diego, CA) and 150 bp paired-end reads were generated. From reads generated by WGS sequencing, adapters were removed and reads that were <50 nucleotides long were discarded using Trimmomatic v0.39 (Bolger et al., 2014). Processed reads were analyzed for CRISPR/Cas9 editing events with CRISPResso2 [http://crispresso2.pinellolab.org (Clement et al., 2019)] (**Supplementary Table 4**). Sequences can be can be downloaded at https://www.crispr-plants.unito.it/eggplant.

PPO Activity Assay

Fruits of the wild type and edited lines (T_1 and T_2) were collected in eight biological replicates at the commercial ripening stage (Mennella et al., 2012). Flesh slices about 1 cm thick, cut at the midpoint between the blossom and stem ends, were exposed to air for 30 min (t_{30}) before pictures were taken. After the exposition, all fresh tissues were immediately frozen in liquid nitrogen and stored at −80°C for PPO activity measurement of the eight biological replicates. PPO activity analysis was performed according to previously described protocols (Bellés et al., 2006; Plazas et al., 2013) with minor modifications: 1 g of fresh frozen peel tissue was taken and ground in a mortar with liquid nitrogen and 50 mg of polyvinylpolypyrrolidone before being resuspended in 4 ml 0.1 M sodium phosphate buffer pH 6. Samples were sonicated in a water bath for 10′ at 20°C, centrifuged at 12,000 rpm for 15′ at 4°C and the supernatant was collected. Protein concentration was evaluated using Bradford's dye (Sigma Aldrich) binding assay using bovine serum albumin (Sigma Aldrich) as a standard (Bradford, 1976). PPO activity was measured colorimetrically at room temperature using a spectrophotometer (Beckman Coulter, Brea, CA, USA) to follow the emerging enzymatic reaction. For sample analysis, 145 µl sodium phosphate buffer (0.1 M, pH 6, RT), 15 µl chlorogenic acid (Sigma Aldrich, 35.5 mg ml^{-1}), and 40 µl of protein extract were mixed and absorbance (415 nm) measured every 10 s for 25 min. A negative control without protein extract was even analyzed. One unit of enzyme activity was defined as the increase in 0.1 absorbance unit per minute per milligram of fresh weight (Kaushik et al., 2017).

RESULTS AND DISCUSSION

SmelPPO Identification and Phylogenetic Analysis

In addition to the six sequences previously reported (Shetty et al., 2011), four new loci in the eggplant genome were found to encode polyphenol oxidases and named *SmelPPO7-10* (**Table 1**). Coding sequences retain extensive structural similarities both within *S. melongena* and with homologs in tomato and potato. The CDS of *PPO*s range in size from 1,686 to 2,466 bp; all genes except *SmelPPO3* and *SmelPPO4* are on the negative strand and, like the *PPO* genes of tomato and potato, eggplant *PPO*s do not possess introns. In all the three *Solanum* species, *PPO* genes cluster on chromosome 8 (**Figure 1A**), with the exception of one orthologous gene (*SmelPPO10* in eggplant, *StuPPO9* in potato, and *SlPPOG* in tomato), mapping on chromosome 2. This suggests that *PPO* genes evolved from tandem duplications and further supports the notion that the structure of this gene family, and possibly its functional specializations, are conserved across Solanaceae species.

The *PPO* encoded proteins range in size from 562 to 822 aa (**Table 1**). All polypeptides possess the same functional domains, namely the central tyrosinase and PPO1_DWL domains, and a C-terminal domain of unknown function (DUF_B2219), characterized by the KFDV conserved motif. In accordance with previous reports (Taranto et al., 2017), we confirmed that in the Solanaceae family two main clusters can be distinguished among PPO proteins (**Figure 1B**), which correspond to a functional separation between PPOs that are preferentially expressed in roots (tomato *Sl*PPO A-D, potato *Stu*PPO2 and *Stu*PPO4 and eggplant class A proteins, i.e., *Smel*PPO1-3) and PPOs whose expression is associated to defense responses (tomato *Sl*PPO E and F, potato *Stu*PPO1 and eggplant class B proteins, i.e. *Smel*PPO4-6). Among the newly identified proteins, *Smel*PPO7 clusters with class A proteins, *Smel*PPO8 with *Stu*PPO5 and *Smel*PPO9 with *Stu*PPO8. Finally, *Smel*PPO10 clusters with *Stu*PPO9 and *Sl*PPOG.

Transcriptional Profiling in Response to Wounding

Oxidative browning in eggplant is influenced by multiple factors, including total phenolic content, *PPO* expression and also the way in which the plant integrates environmental stimuli to elicit defense responses (Mishra et al., 2013; Plazas et al., 2013; Docimo et al., 2016). The differential spatial and temporal expression patterns of PPOs *in planta* reflect the functional diversity among the *PPO* gene members. In eggplant, the expression of *SmelPPO1-6* genes was higher in young tissues and declined during plant development in mature and reproductive organs (Shetty et al., 2011). In fruits, *PPO* expression was mainly concentrated in the exocarp and in the areas surrounding the seeds in the mesocarp (Shetty et al., 2011). *PPO* expression is mainly induced by herbivores or by mechanical damage, such as cutting.

The promoters of group B genes (Shetty et al., 2011) are characterized by the presence of several responsive elements for wounding stress and defense response (Thipyapong et al., 1997). The structural similarity of eggplant class B *PPO*

TABLE 1 | Characteristics of PPO encoding genes and of PPO proteins.

Locus	Gene name	Chr	Chromosome location	ORF length (bp)	Strand	Size (aa)	Protein domains	Pfam domains
SMEL_008g312510.1.01	*Smel_PPO1*	8	97,412,508: 97,414,307	1,800	-	600	PPO1_DWL–DUF_B2219–Tyrosinase	Pfam 12142–Pfam 1243-Pfam 00264
SMEL_008g312500.1.01	*Smel_PPO2*	8	97,401,279: 97,403,066	1,788	-	596	PPO1_DWL–DUF_B2219–Tyrosinase	Pfam 12142–Pfam 1243-Pfam 00264
SMEL_008g312430.1.01	*Smel_PPO3*	8	97,284,426: 97,286,198	1,773	+	591	PPO1_DWL–DUF_B2219–Tyrosinase	Pfam 12142–Pfam 1243-Pfam 00264
SMEL_008g312420.1.01	*Smel_PPO4*	8	97,238,764: 97,239,741	1,734	+	578	PPO1_DWL–DUF_B2219–Tyrosinase	Pfam 12142–Pfam 1243-Pfam 00264
SMEL_008g311990.1.01	*Smel_PPO5*	8	96,314,480: 96,316,243	1,764	-	588	PPO1_DWL–DUF_B2219–Tyrosinase	Pfam 12142–Pfam 1243-Pfam 00264
SMEL_008g312010.1.01	*Smel_PPO6*	8	96,395,550: 96,397,448	1,899	-	633	PPO1_DWL–DUF_B2219–Tyrosinase	Pfam 12142–Pfam 1243-Pfam 00264
SMEL_008g312490.1.01	*Smel_PPO7*	8	97,397,374: 97,399,167	1,794	-	598	PPO1_DWL–DUF_B2219–Tyrosinase	Pfam 12142–Pfam 1243-Pfam 00264
SMEL_008g312460.1.01	*Smel_PPO8*	8	97,349,335: 97,351,020	1,686	-	562	PPO1_DWL–DUF_B2219–Tyrosinase	Pfam 12142–Pfam 1243-Pfam 00264
SMEL_008g312520.1.01	*Smel_PPO9*	8	97,429,811: 97,432,277	2,466	-	822	PPO1_DWL–DUF_B2219–Tyrosinase	Pfam 12142–Pfam 1243-Pfam 00264
SMEL_000g064350.1.01	*Smel_PPO10*	2	982,270: 984,463	2,193	-	731	PPO1_DWL–DUF_B2219–Tyrosinase	Pfam 12142–Pfam 1243-Pfam 00264

SmelPPO1-9 cluster on chromosome 8, while PPO10, which was initially located on an unanchored scaffold, is probably located on chromosome 2. All PPOs share the same functional domains (PPO1_DWL and Tyrosinase, and a conserved domain of unknown function, DUF_B2219).

genes (*SmelPPO4-5-6*) to wound-induced tomato *SlPPOF* might suggest an analogous pattern of gene regulation (Thipyapong et al., 1997).

In our study we analyzed the transcript levels of *PPO* genes in the flesh of full-ripe eggplant berries of the "Black Beauty" variety 30 min after cutting (**Figure 2**). A strong increase in gene transcription in the flesh was observed for all *PPO*s, and especially for *SmelPPO1* (7.45X), *SmelPPO4* (3.03X), *SmelPPO6* (4.00X), *SmelPPO8* (3.59X), and *SmelPPO10* (4.01X). The simultaneous activation of both A and B classes of *PPO* genes was already observed in the eggplant cultivars AM086 (Docimo et al., 2016) and Arka Shirish (Shetty et al., 2011). Based on this transcriptional profile, we hypothesized that the design of an appropriate editing strategy directed at reducing detrimental oxidative browning in fruit tissues might require simultaneous suppression of several members of this multigene family. In our experiments we targeted class B *PPO* genes (*SmelPPO4, SmelPPO5,* and *SmelPPO6*) through a CRISPR/Cas9 editing strategy. Due to their extremely high level of similarity, it was possible to design a unique gRNA against the tyrosinase domain of all class B genes.

Plant Regeneration

The development of new genome editing technologies in plant breeding has fostered a growing interest for *in vitro* culture and regeneration protocols, which represent a major bottleneck in the application of these techniques in many plant species of agricultural and industrial interest. Due to the difficulties often encountered in eggplant regeneration, with available protocols being mostly inefficient or highly dependent on the genotype, no examples of genome editing in this species has been reported in literature so far. After the first report of the *Agrobacterium*-mediated transformation of eggplant (Guri and Sink, 1988), several examples of genetic transformation have been proposed using seedling explants like the hypocotyl, epicotyl, and node segments and cotyledon segments, leaf disks or roots (Rotino et al., 2014; Saini and Kaushik, 2019; García-Fortea et al., 2020).

In many plant species, the browning of tissues, which leads to toxicity and necrosis, is one of the major causes of unsuccessful *in vitro* organogenesis and regeneration from explants. Browning is associated with the oxidation of phenolics, whose release is caused by cutting and manipulating explants and calli. This problem is particularly relevant in eggplant, whose tissues are rich in phenolic compounds. Among strategies to avoid browning, the most common include the supplementation of culture media with antioxidant or adsorbent compounds (Abdelwahd et al., 2008; Menin et al., 2013).

We tested different strategies to reduce browning during eggplant tissue culture, including the addition of citric and ascorbic acid and PVP supplementation, and we found out that PVP supplementation exerts a positive effect on shoot regeneration. Among a total of 15 rooted shoots, 10 derived from the PVP-supplemented medium, four from not supplemented medium, and only 1 from the medium supplemented with ascorbic and citric acids. No differences were found in the phenotype of regenerants from different culture conditions. However, in spite of their notably higher number, the emergence of shoots on the PVP-supplemented medium was slower.

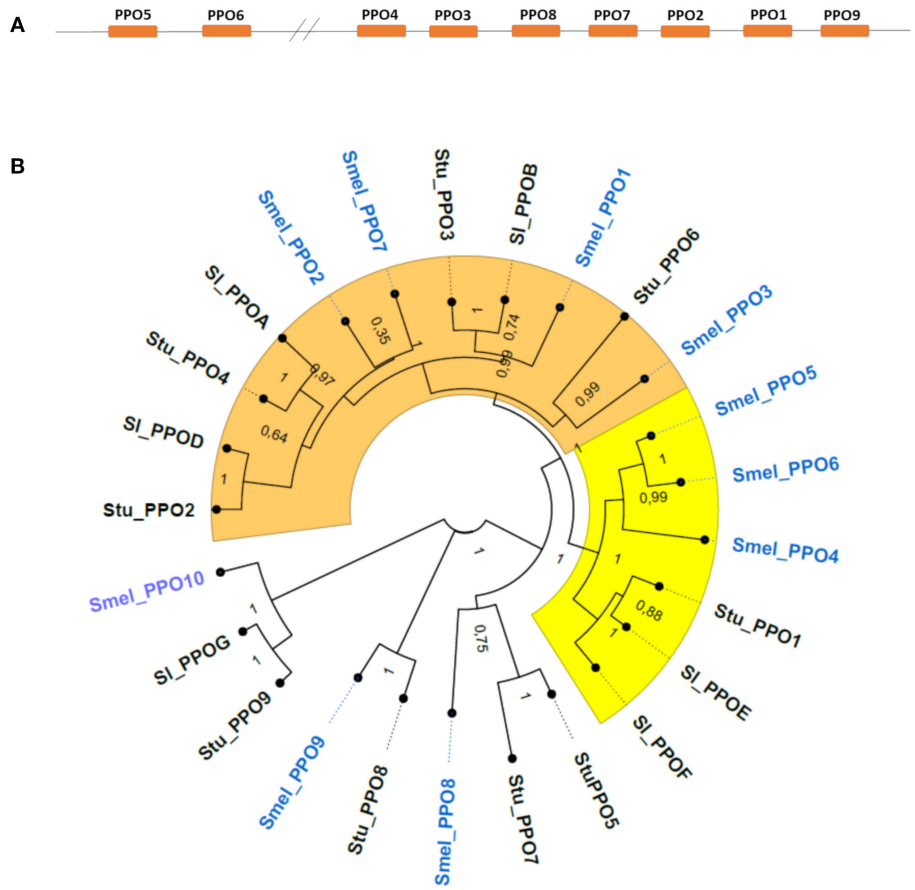

FIGURE 1 | (A) Relative position and organization of *PPO1-9* genes on chromosome 8 of *Solanum melongena.* All eggplant *PPO*s except *SmelPPO10* are located on chromosome 8. **(B)** Phylogenetic analysis of PPO proteins. The neighbor-joining trees was constructed by aligning the PPO protein sequences contained in **Data Sheet 1**. Clade A (orange) and B (yellow) proteins. The number at each node represents the bootstrap percentage value from 1,000 replicates. Smel, Solanum melongena; Sl, Solanum lycopersicum; Stu, Solanum tuberosum.

Dark treatments are known to increase adventitious shoot formation in cotyledon, leaf and hypocotyl explants in a number of species, including eggplant (Muktadir et al., 2016). However, we did not observe differences between shoots which underwent the 3-days dark treatment and those which did not. For all regenerating conditions, shoots apt for rooting were recovered in as short as 6 weeks (**Supplementary Figure 1**).

Screening for Mutations in the T_0 Generation

CRISPR/Cas9 induced mutagenesis can be employed to induce the simultaneous knockout of multiple targets within a gene family (Karunarathna et al., 2020; Sashidhar et al., 2020). Targeting a conserved gene family poses some challenges regarding the design of the gRNAs as well as the screening of edited genotypes and off-target effects. This can be particularly problematic for *PPO*s, since different members of this gene family, including the ones implicated in defense response, possess distinct activation patterns and specialized metabolic functions. By identifying a conserved region of *SmelPPO4* and *SmelPPO5*, corresponding to the tyrosinase domain, we designed a gRNA targeting both *SmelPPO4* and *SmelPPO5*, as well as *SmelPPO6* (**Figure 3A**).

After transformation of the CRISPR/Cas9 constructs in eggplant cotyledons and regeneration, 12 eggplant T_0 individuals (T_0_1-T_0_12) were analyzed (**Data Sheet 3**). The qPCR analysis using *Cas9* gene-specific primers revealed genomic integration of the construct in nine T_0 plants, while T_0_1, T_0_6 and T_0_10 did not possess the transgene. In order to detect mutations in *SmelPPO4-5-6*, we employed targeted deep sequencing of genomic DNA, which allowed us to comprehensively assess the editing efficiency and the types of mutations (**Data Sheet 3**). Among the nine transformed plants, the Illumina amplicon sequencing revealed that simultaneous editing of *SmelPPO4, SmelPPO5, and SmelPPO6* genes occurred in 2 lines (T_0_3 and T_0_4) (**Figure 3B**). For the remaining lines, T_0_5 and T_0_12 showed editing only at the *SmelPPO5* locus, while T_0_10 at the *SmelPPO4* locus (**Data Sheet 3**). In most transformants, *SmelPPO5* appears edited to a higher extent than *SmelPPO4* and *SmelPPO6*, with the exceptions of T_0_3, T_0_4 and T_0_10. Notably, in T_0_5 *SmelPPO5* reached an editing efficiency of 50% while the other two loci displayed negligible levels of mutation.

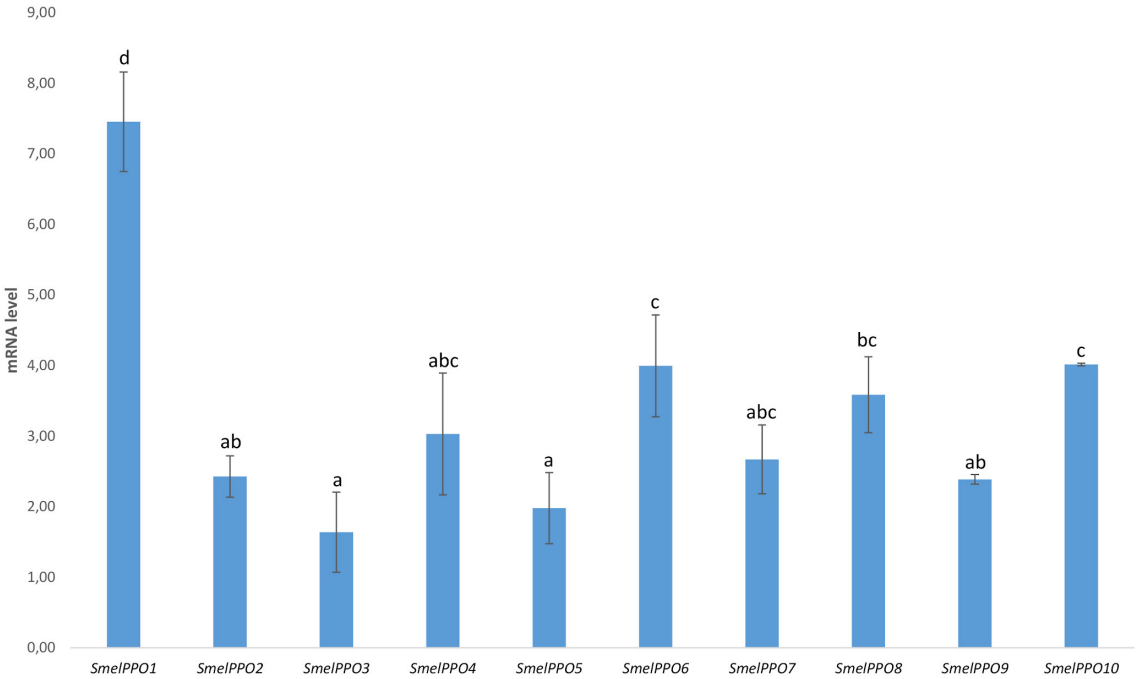

FIGURE 2 | Transcriptional levels of 10 PPO-encoding genes in the Black Beauty variety 30 min after fruit cutting. The values are expressed as relative mRNA abundance at 30 min after cutting compared to time 0 (just after cutting). Eggplant actin and elongation factor genes were used as the reference genes. Data are means of three biological replicates ± SE. Different letters associated with the set of means indicate a significant difference based on Tukey b test ($P \leq 0.05$).

Preferential editing of one member of a family sharing the same gRNA recognition sequence might depend on the transcriptional status of the target sequences. Although after wounding the expression of *SmelPPO5* is induced at lower levels than the ones of *SmelPPO4* and *SmelPPO6*, its transcript abundance seems to be generally higher, as suggested by its Ct values. The transcriptional accessibility of this locus might also reflect on its availability for the Cas9 endonuclease. It is interesting to point out that, in T_0_10, *SmelPPO4* was edited with an efficiency of over 70% although the transgene was not integrated, which highlights that it is possible to retrieve non-transgenic plants derived from edited cells in which the editing machinery presumably acted in a "transient" fashion.

T_0_3 showed the greatest editing efficiency for all three loci, i.e., 76% for *SmelPPO4*, 74% for *SmelPPO5* and 60% for *SmelPPO6*. In T_0_4, a high editing efficiency was also detected, i.e., 76% for *SmelPPO4*, 20% for *SmelPPO5* and 21% for *SmelPPO6* (**Data Sheet 3** and **Figure 3B**), although these values are lower than those of T_0_3. The number of plants edited at all loci was low (22%) and editing efficiencies were also significantly below the ones observed in tomato and potato, presumably as a consequence of low levels of expression of Cas9 and gRNAs (Pan et al., 2016). T_0_3 and T_0_4 had chimeric mutations (with at least 3 different alleles) in all targeted loci and retained a proportion of the wild type allele. The wild type copy of the target gene in chimeric plants could thus continue to mutate either in T_0 or in the following generations if the Cas9 transgene does not segregate. The predominance of this chimeric status in the T_0 resembles the pattern described in tomato (Pan et al., 2016; Nonaka et al., 2017). Chimerism suggests that gene editing occurred after the emergence of differentiated tissues, leading to a heterogeneous mutation pattern within the same plant. Transgene expression might be influenced by the chromatin status at its insertion locus and, of course, by the choice of promoters. In Arabidopsis, where mutants are obtained through floral dipping and where the expression of Cas9 in the germline is crucial to fix edited alleles, the use of egg cell-specific promoters for Cas9 expression allowed to efficiently obtain non-mosaic T_1 mutants for multiple target genes (Wang et al., 2015). In plants regenerated through somatic organogenesis, the use of egg-cell and embryo-specific promoters might also help retrieving T_1 generations with higher levels of homozygous or biallelic mutations (Zheng et al., 2020). Since no previous reports of gene editing dynamics existed for eggplant, and because we predicted the regeneration process to be the limiting factor (both in terms of efficiency and time consumption), we prioritized the use of standard gene editing constructs to maximize Cas9 expression and establish a baseline protocol. Based on this, other variants (e.g., tissue- or species-specific promoters) can be successively factored in to fine-tune the editing outcome.

Previous observations showed that small indels are the predominant mutations introduced in plants by gene editing and that the breakpoint introduced by Cas9 is placed at 3 nucleotides upstream of the PAM (Bortesi et al., 2016; Pan et al., 2016; Andersson et al., 2017). In plants, insertion of one nucleotide or deletion of 1–10 nucleotides are the most common mutations (Pan et al., 2016). The most common

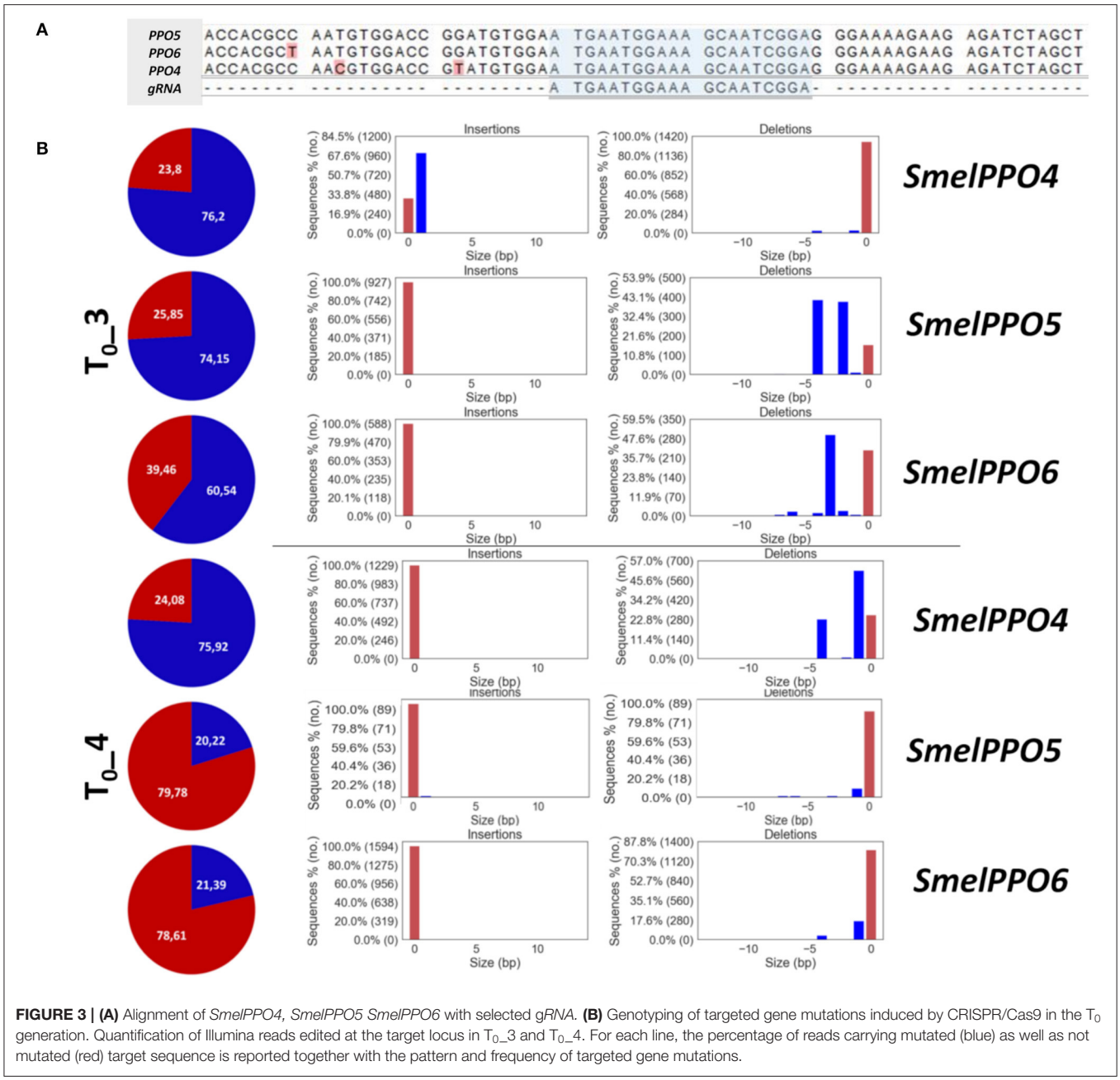

FIGURE 3 | (A) Alignment of *SmelPPO4, SmelPPO5 SmelPPO6* with selected g*RNA*. **(B)** Genotyping of targeted gene mutations induced by CRISPR/Cas9 in the T_0 generation. Quantification of Illumina reads edited at the target locus in T_0_3 and T_0_4. For each line, the percentage of reads carrying mutated (blue) as well as not mutated (red) target sequence is reported together with the pattern and frequency of targeted gene mutations.

mutations in our T_0 eggplant plantlets were represented by a single nucleotide insertion (+G; T_0_3-*SmelPPO4*) and by a deletion of one (T_0_4-*SmelPPO4/6*; T_0_5-*SmelPPO5*), two (T_0_3-*SmelPPO5*), three (T_0_3-*SmelPPO6*), or four (T_0_4-*SmelPPO5*; T_0_10-*SmelPPO4;* T_0_12-*SmelPPO5*) nucleotides (**Data Sheet 3**).

Analysis of Off-Target Mutations

Only few occurrences of low-frequency off-target mutations induced by CRISPR/Cas9 have been reported in plant species so far (Feng et al., 2013; Peterson et al., 2016; Wolt et al., 2016; Hahn and Nekrasov, 2019) contrary to what observed in human cells (Fu et al., 2013). The risk of off-target effects has been reported as comparable to that of somaclonal variation deriving from plant tissue culture itself (Ma et al., 2015). In order to reduce off-target effects, a strategy based on Cas9/sgRNA ribonucleoprotein complexes has been proposed (Hahn and Nekrasov, 2019). Indeed, only through a whole genome resequencing of the edited lines is it possible to exhaustively evaluate the presence of off-target mutations induced by the selected sgRNAs. However, other screening methods make it possible to rule out the occurrence of undesired mutations at selected loci, which is reliable particularly if they correspond to transcriptionally active sequences.

TABLE 2 | Quantification of Illumina reads edited at putative off-target *loci* in T_0 generation.

Sample	Target	Reads	Number of mutated reads	% of mutated reads
WT	OT1	17,926	549	3.06
	OT2	17,855	1,354	7.58
	OT3	27,671	10,758	38.88
	OT4	26,977	803	2.98
T_0_3	OT1	24,196	747	3.09
	OT2	21,205	922	4.35
	OT3	30,086	3,203	10.65
	OT4	34,541	822	2.38
T_0_4	OT1	20,621	591	2.87
	OT2	13,231	476	3.60
	OT3	20,282	1,648	8.13
	OT4	274	8	2.92

For each individual and for each locus the total number of reads is reported, together with the percentage of reads carrying the mutated off-target sequence. The percentage of mutated sequences is reported.

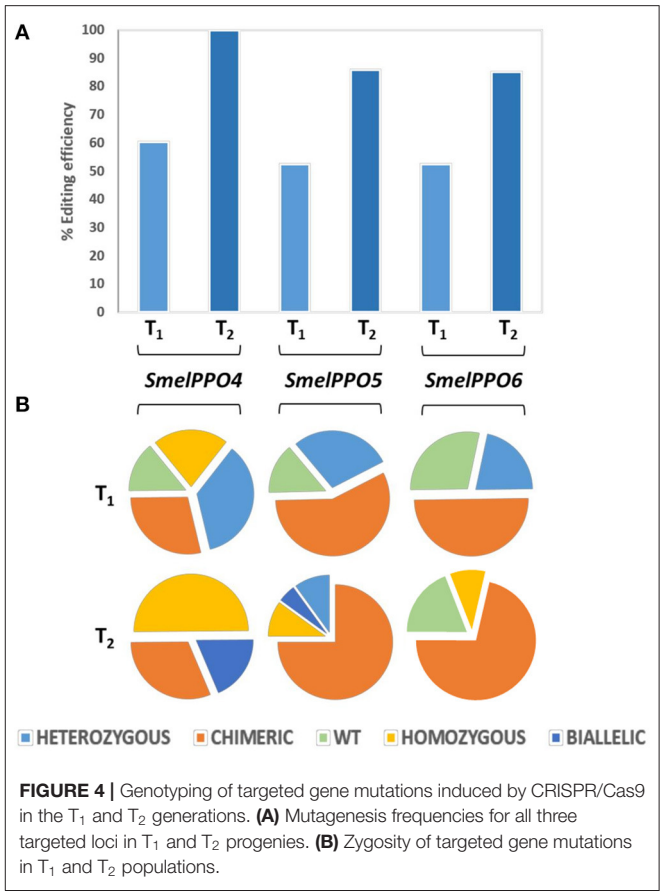

FIGURE 4 | Genotyping of targeted gene mutations induced by CRISPR/Cas9 in the T_1 and T_2 generations. **(A)** Mutagenesis frequencies for all three targeted loci in T_1 and T_2 progenies. **(B)** Zygosity of targeted gene mutations in T_1 and T_2 populations.

One of the major risks related to targeting conserved regions in a gene family is that putative off-targets are most likely other members of the same family which, in the case of PPOs, are also located in close proximity on the genome. This makes it much more difficult to eliminate potentially undesired off-targets by breeding, than it is for non-linked loci. With respect to our gRNA, four putative off-target sequences were identified: one was an intergenic sequence, while three corresponded to other members of the *PPO* family (*SmelPPO2, SmelPPO3,* and *SmelPPO7*) (**Supplementary Table 2**).

In order to confirm that our selected T_0 edited lines (T_0_3 and T_0_4) displayed mutations only in the *SmelPPO4-5-6* loci, we sequenced the candidate off-target loci by applying the same Illumina Amplicon Sequencing Protocol we used for the sequencing of target loci, and which allowed us to get a deep insight into possible non-specific editing activity. The total variation at putative off-target sites was compared between edited and wild type plants (**Table 2**). We seldom observed only base substitutions consistent with SNPs or sequencing errors and, even considering those, no increase in total variation was observed between wild type and mutants. Our analyses thus demonstrated the lack of off-target effects, confirming the specificity of Cas9-mediated *PPO* gene editing in eggplant. The presence of mismatches in the seed region between our selected sgRNA and the off-target *SmelPPO*s supports the specificity of our results (Hahn and Nekrasov, 2019), since this 3′ terminal region of the target sequence is known to strongly affect recognition by the Cas9 endonuclease.

Segregation of the Transgene and of Mutated Alleles in the T_1 and T_2 Progeny

Due to the early finding that in Arabidopsis many somatic mutations were not efficiently inherited, concerns about the heritability of CRISPR/Cas-induced mutations were initially raised (Feng et al., 2013). However, in all other edited monocot and dicot species, T_1 generations with high mutation efficiencies have been obtained, demonstrating the heritability of edited alleles (Miao et al., 2013; Gao et al., 2015; Li et al., 2015; Svitashev et al., 2015; Pan et al., 2016). In our case, 14 T_1 plants of the T_0_4 progeny were examined to investigate the transmission pattern of CRISPR/Cas9-induced mutations. Out of 14 analyzed individuals, 4 presented no detectable amplification of *hCas9* and therefore it is reasonable to deduce that the transgene was segregated (**Data Sheet 3**).

In order to detect the mutation efficiency and patterns at different sites in *SmelPPO4-5-6* genes, we employed targeted deep sequencing. The average editing efficiency was 60% for *SmelPPO4,* 52% for *SmelPPO5,* and 52% for *SmelPPO6* (**Figure 4A**). Focusing on the *SmelPPO4* locus, five were heterozygous mutants, four chimeric, three homozygous and two WT. At the *SmelPPO5* locus, four were homozygous mutants, eight chimeric and two WT. At the *SmelPPO6* locus, three were homozygous mutants, seven chimeric and four WT (**Figure 4B**; **Data Sheet 3**).

The most common mutation at the *SmelPPO4* locus was a single nucleotide deletion, followed by a 4 nucleotide deletion. At the *SmelPPO5* locus different mutations were present:−2/-1/-4/-3. The segregation pattern at the *SmelPPO6* locus (which

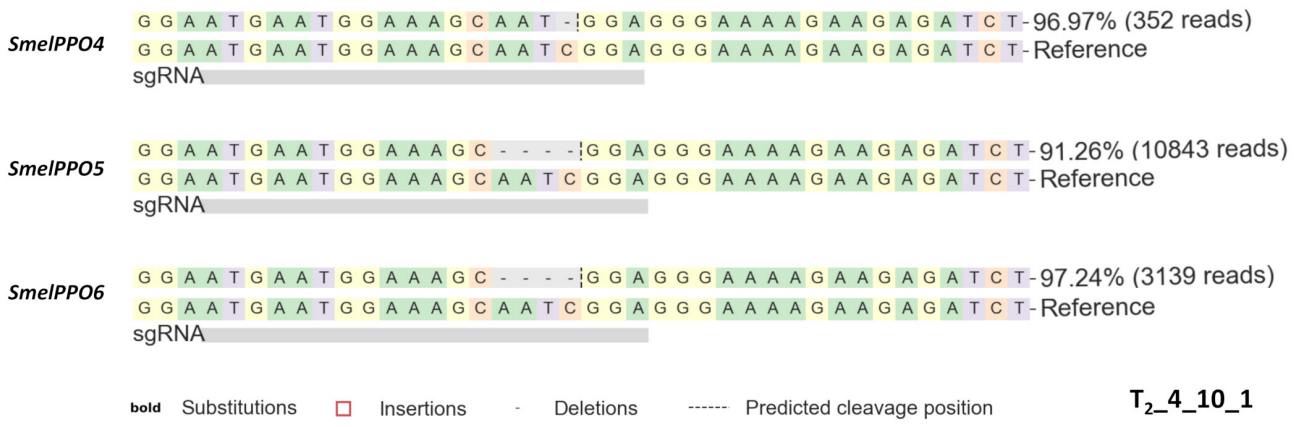

FIGURE 5 | Genotyping of targeted gene mutations induced by CRISPR/Cas9 in the T_2_4_10_1 plant. The dashed lines represent nucleotide deletions. The reported number represents the frequency and the number of reads carrying mutated (edited) target sequence.

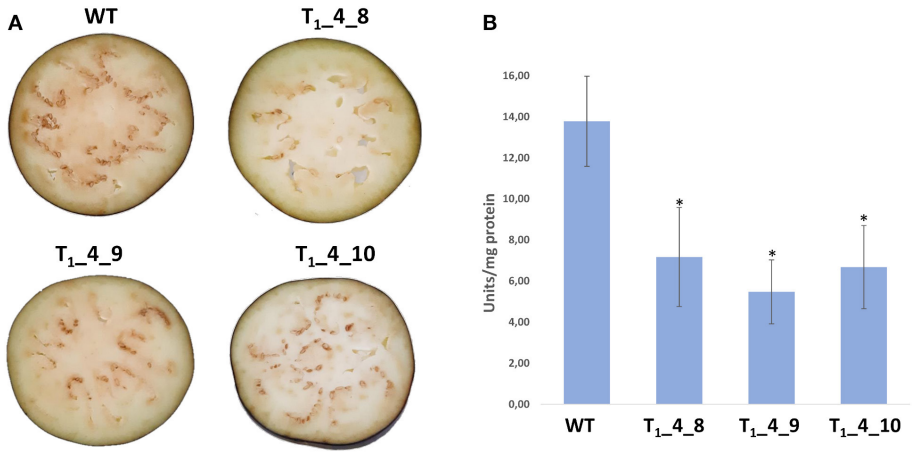

FIGURE 6 | Phenotypical and biochemical changes associated with postcut browning. **(A)** Cut fruits of Wild Type, T_1_4_8, T_1_4_9 and T_1_4_10 showing post-cut browning 30 min after cutting. **(B)** Polyphenoloxidase (PPO) activity in fruits of Wild Type, T_1_4_8, T_1_4_9 and T_1_4_10. Data are means of eight biological replicates ± SD. Asterisks indicate a significant difference based on Tukey's HSD test ($P \leq 0.05$).

was less mutated in T_0) was less predictable and a number of new mutations (-2/-3/-7) were found in the T_1 lines. The highest editing efficiency was highlighted for T_1_4_10: 85% for *SmelPPO4*, 90% for *SmelPPO5* and 90.7% for *SmelPPO6* (**Data Sheet 3**).

To further investigate the genetic stability of the targeted mutations we screened the T_2 plants derived from selfing T_1_4_8, T_1_4_9 and T_1_4_10 (**Data Sheet 3**). The presence of a transgene in most of the analyzed T_2 plants (19/21) suggested that more than one copy of the transgene was inserted in those T_0 regenerants, which explains that Cas9 can still be active in all T_2 plants.

Compared to the T_1 generation, the mutagenesis frequency (99% for *SmelPPO4,* 85% for *SmelPPO5* and 85% for *SmelPPO6*) as well as the overall proportion of homozygous, biallelic and chimeric assets increased (**Figure 4**). As expected, all 7 T2 progeny of T_1_4_11 were homozygous at the *SmelPPO4* locus, indicating that the mutations in the homozygotes were stably passed to the next generation in a Mendelian fashion. As previously observed in other species (Pan et al., 2016), the segregation patterns of the T_1 chimera lines were less predictable and a number of new mutants were obtained due to the probable continued Cas9 activity. Interestingly, T_2_4_10_1 showed homozygous mutations for *SmelPPO4* (-1/-1), *SmelPPO5* (-4/-4) and *SmelPPO6* (-4/-4) (**Figure 5**).

It has been previously demonstrated how off-target effects can be further exacerbated in the T_2 progeny as compared to T_0 and T_1 (Zhang et al., 2018). Targeted deep sequencing at putative off-target loci once again demonstrated the lack of significant mutated off-targets in our T_2 progeny, confirming the specificity of Cas9-mediated *PPO* gene editing in eggplant (**Data Sheet 3**). We observed only base substitutions consistent with SNPs or sequencing errors, with similar frequencies to those observed in the T_0, which did not represent an increase in total variation between wild type and mutant lines.

Enzymatic Browning and PPO Activity Analysis in Eggplant Berries

We hypothesized that the CRISPR/Cas-mediated knock out of *PPO*s would result in a lowered enzymatic browning, due to the reduced PPO activity. Selected T_1 lines (T_1_4_8, T_1_4_9 and T_1_4_10) carrying mutations in *SmelPPO4-5-6* genes were subjected to phenotypic analysis of enzymatic browning and PPO activity in berries. The lines were grown in a greenhouse and no growth alteration or changes in berry size/weight were observed during plant development when compared to wild type, as previously observed in potato (Llorente et al., 2011). The berries were cut and exposed to air for browning induction. After 30 min, the typical brown discoloration due to phenolic oxidation was detected and it was clearly more evident in wild type plants in comparison to edited lines (**Figure 6A**). The average PPO activity of T_1_4_8, T_1_4_9 and T_1_4_10 lines was also found to be reduced by 48, 61, and 52%, respectively, compared to the wild type (**Figure 6B**). By comparing the T_2 edited lines with wild type a reduction of PPO activity as well as of browning discoloration upon cutting was highlighted (**Supplementary Figure 2**).

Several studies applied RNA silencing technologies to down-regulate the expression of *PPO* genes in potato tubers (Bachem et al., 1994; Rommens et al., 2006; Llorente et al., 2011; Chi et al., 2014). In this species, by using the amiRNA technology (Chi et al., 2014), a reduction in PPO activity of 15–95% was obtained and it was more marked when *StuPPO1* to *4* were simultaneously suppressed. Furthermore, in a more recent study in potato, CRISPR/Cas mutants for the four alleles of the *StuPPO2* gene (which is considered the major contributor to the PPO protein content) displayed a reduction up to 69 and 73% in the PPO activity and enzymatic browning, respectively (González et al., 2020)

We can hypothesize that the partial reduction of PPO activity in eggplant, comparable to the one observed in potato mutants, might be enhanced through the knockout not only of class B PPOs (*SmelPPO4-5-6*), but even of class A PPOs (*SmelPPO1* and *SmelPPO3*). However, this approach could provoke downside effects, due to the involvement of the *PPO* multigene family in important cell functions (Jukanti and Bhatt, 2015).

CONCLUSIONS

We have established a successful protocol for gene editing in eggplant, adding to the list of Solanaceae species for which CRISPR/Cas9 represents an alluring option for the introduction of specific traits through a biotechnological approach. Our system, based on the use of one guide RNA directed simultaneously at three members of the *PPO* gene family, demonstrated to be specific for the target genes, without detectable off-target effects on other members of the same gene family.

Upon cutting, edited T_1 and T_2 eggplant fruits showed a reduction of the typical brown coloration due to phenolic oxidation. Through our approach it will be possible to develop eggplant varieties that maintain their antioxidant and nutritional properties during harvest and post-harvest procedures, without reducing the content in phenolics, which are beneficial for human health.

Phenolics provide a substrate to oxidative reactions catalyzed by PPOs that, consuming oxygen and producing fungitoxic quinones, play a role in making the medium unfavorable to the further development of pathogens (Taranto et al., 2017); however, contrasting results are reported in literature, as *PPO* silenced lines of potato were found to acquire higher resistance to *P. infestans* (Llorente et al., 2014). Our future studies will be thus focused in assessing the relationship between PPO knock-out and pathogen response in our mutant eggplant lines.

DATA AVAILABILITY STATEMENT

The original contributions presented in the study are included in the article/**Supplementary Materials**, further inquiries can be directed to the corresponding author/s.

AUTHOR CONTRIBUTIONS

AMo, SG, and CC: conceptualization. AMa, SG, AMo, and AA: data curation. AMa, SG, AMo, AA, DV, and AMM: investigation. AMo and CC: supervision. AMa, SG, and AMo: writing—original draft preparation. SG, AMo, JP, DO, AG, SL, and CC: writing—review and editing preparation. All authors contributed to the article and approved the submitted version.

FUNDING

Research was financially supported by the project CRISPR/Cas9–mediated gene knock-out in eggplant financed by Compagnia San Paolo.

ACKNOWLEDGMENTS

We thank Prof. Luigi Bertolotti (University of Turin) for his technical assistance.

SUPPLEMENTARY MATERIAL

The Supplementary Material for this article can be found online at: https://www.frontiersin.org/articles/10.3389/fpls.2020.607161/full#supplementary-material

REFERENCES

Abdelwahd, R., Hakam, N., Labhilili, M., and Udupa, S. M. (2008). Use of an adsorbent and antioxidants to reduce the effects of leached phenolics in *in vitro* plantlet regeneration of faba bean. *African J. Biotechnol.* 7, 997–1002.

Andersson, M., Turesson, H., Nicolia, A., Fält, A. S., Samuelsson, M., and Hofvander, P. (2017). Efficient targeted multiallelic mutagenesis in

tetraploid potato (Solanum tuberosum) by transient CRISPR-Cas9 expression in protoplasts. *Plant Cell Rep*. 36, 117–128. doi: 10.1007/s00299-016-2062-3

Bachem, C. W. B., Speckmann, G. J., Van der Linde Piet, C. G., Verheggen, F. T. M., Hunt, M. D., Steffens, J. C., et al. (1994). Antisense expression of polyphenol oxidase genes inhibits enzymatic browning in potato tubers. *Bio/Technology*. 12, 1101–1105. doi: 10.1038/nbt1194-1101

Barchi, L., Pietrella, M., Venturini, L., Minio, A., Toppino, L., Acquadro, A., et al. (2019). A chromosome-anchored eggplant genome sequence reveals key events in Solanaceae evolution. *Sci. Rep*. 9:11769. doi: 10.1038/s41598-019-47985-w

Bellés, J. M., Garro, R., Pallás, V., Fayos, J., Rodrigo, I., and Conejero, V. (2006). Accumulation of gentisic acid as associated with systemic infections but not with the hypersensitive response in plant-pathogen interactions. *Planta*. 223, 500–511. doi: 10.1007/s00425-005-0109-8

Bolger, A. M., Lohse, M., and Usadel, B. (2014). Trimmomatic: a flexible trimmer for Illumina sequence data. *Bioinformatics* 30, 2114–2120. doi: 10.1093/bioinformatics/btu170

Bortesi, L., Zhu, C., Zischewski, J., Perez, L., Bassié, L., Nadi, R., et al. (2016). Patterns of CRISPR/Cas9 activity in plants, animals and microbes. *Plant Biotechnol. J*. 14, 2203–2216. doi: 10.1111/pbi.12634

Bradford, M. M. (1976). A rapid and sensitive method for the quantitation of microgram quantities of protein utilizing the principle of protein-dye binding. *Anal. Biochem*. 72, 248–254. doi: 10.1016/0003-2697(76)90527-3

Chi, M., Bhagwat, B., Lane, W. D., Tang, G., Su, Y., Sun, R., et al. (2014). Reduced polyphenol oxidase gene expression and enzymatic browning in potato (Solanum tuberosum L.) with artificial microRNAs. *BMC Plant Biol*. 14:62. doi: 10.1186/1471-2229-14-62

Clement, K., Rees, H., Canver, M. C., Gehrke, J. M., Farouni, R., Hsu, J. Y., et al. (2019). CRISPResso2 provides accurate and rapid genome editing sequence analysis. *Nat. Biotechnol*. 37, 224–226. doi: 10.1038/s41587-019-0032-3

Coetzer, C., Corsini, D., Love, S., Pavek, J., and Turner, N. (2001). Control of enzymatic browning in potato (solanum tuberosum L.) by sense and antisense RNA from tomato polyphenol oxidase. *J. Agric. Food Chem*. 49, 652–657. doi: 10.1021/jf001217f

Cong, L., and Zhang, F. (2015). Genome engineering using CRISPR-Cas9 system. *Methods Mol. Biol*. 1239: 197–217. doi: 10.1007/978-1-4939-1862-1_10

Docimo, T., Francese, G., De Palma, M., Mennella, D., Toppino, L., Lo Scalzo, R., et al. (2016). Insights in the fruit flesh browning mechanisms in Solanum melongena genetic lines with opposite postcut behavior. *J. Agric. Food Chem*. 64, 4675–4685. doi: 10.1021/acs.jafc.6b00662

Doudna, J. A., and Charpentier, E. (2014). The new frontier of genome engineering with CRISPR-Cas9. *Science* 346:1258096. doi: 10.1126/science.1258096

Doyle, J., and Doyle, J. (1987). A rapid isolation procedure for small amounts of leaf tissue. *Phytochem. Bull*. 19, 11–15.

Feng, Z., Zhang, B., Ding, W., Liu, X., Yang, D. L., Wei, P., et al. (2013). Efficient genome editing in plants using a CRISPR/Cas system. *Cell Res*. 23, 1229–1232. doi: 10.1038/cr.2013.114

Fu, Y., Foden, J. A., Khayter, C., Maeder, M. L., Reyon, D., Joung, J. K., et al. (2013). High-frequency off-target mutagenesis induced by CRISPR-Cas nucleases in human cells. *Nat. Biotechnol*. 31, 822–826. doi: 10.1038/nbt.2623

Gao, J., Wang, G., Ma, S., Xie, X., Wu, X., Zhang, X., et al. (2015). CRISPR/Cas9-mediated targeted mutagenesis in Nicotiana tabacum. *Plant Mol. Biol*. 87, 99–110. doi: 10.1007/s11103-014-0263-0

García-Fortea, E., Lluch-Ruiz, A., Pineda-Chaza, B. J., García-Pérez, A., Bracho-Gil, J. P., Plazas, M., et al. (2020). A highly efficient organogenesis protocol based on zeatin riboside for in vitro regeneration of eggplant. *BMC Plant Biol*. 20:6. doi: 10.1186/s12870-019-2215-y

González, M. N., Massa, G. A., Andersson, M., Turesson, H., Olsson, N., Fält, A. S., et al. (2020). Reduced enzymatic browning in potato tubers by specific editing of a polyphenol oxidase gene via ribonucleoprotein complexes delivery of the CRISPR/Cas9 system. *Front. Plant Sci*. 10:1649. doi: 10.3389/fpls.2019.01649

Guri, A., and Sink, K. C. (1988). Agrobacterium transformation of eggplant. *J. Plant Physiol*. 133, 52–55. doi: 10.1016/S0176-1617(88)80083-X

Hahn, F., and Nekrasov, V. (2019). CRISPR/Cas precision: do we need to worry about off-targeting in plants? *Plant Cell Rep*. 38, 437–441. doi: 10.1007/s00299-018-2355-9

Jukanti, A. K., and Bhatt, R. (2015). Eggplant (Solanum melongena L.) polyphenol oxidase multi-gene family: a phylogenetic evaluation. *3 Biotech*. 5, 93–99. doi: 10.1007/s13205-014-0195-z

Karunarathna, N. L., Wang, H., Harloff, H. J., Jiang, L., and Jung, C. (2020). Elevating seed oil content in a polyploid crop by induced mutations in SEED FATTY ACID REDUCER genes. *Plant Biotechnol. J*. 18, 2251–2266. doi: 10.1111/pbi.13381

Kaushik, P., Gramazio, P., Vilanova, S., Raigón, M. D., Prohens, J., and Plazas, M. (2017). Phenolics content, fruit flesh colour and browning in cultivated eggplant, wild relatives and interspecific hybrids and implications for fruit quality breeding. *Food Res. Int*. 102, 392–401. doi: 10.1016/j.foodres.2017.09.028

Li, L., and Steffens, J. C. (2002). Overexpression of polyphenol oxidase in transgenic tomato plants results in enhanced bacterial disease resistance. *Planta* 215, 239–247. doi: 10.1007/s00425-002-0750-4

Li, Z., Liu, Z., Bin, X.ing, A., Moon, B. P., and Koellhoffer, J. P., Huang, L., et al. (2015). Cas9-guide RNA directed genome editing in soybean. *Plant Physiol*. 169, 960–970. doi: 10.1104/pp.15.00783

Llorente, B., Alonso, G. D., Bravo-Almonacid, F., Rodríguez, V., López, M. G., Carrari, F., et al. (2011). Safety assessment of nonbrowning potatoes: opening the discussion about the relevance of substantial equivalence on next generation biotech crops. *Plant Biotechnol. J*. 9, 136–150. doi: 10.1111/j.1467-7652.2010.00534.x

Llorente, B., López, M. G., Carrari, F., Asís, R., Di Paola Naranjo, R. D., Flawi,á, M. M., et al. (2014). Downregulation of polyphenol oxidase in potato tubers redirects phenylpropanoid metabolism enhancing chlorogenate content and late blight resistance. *Mol. Breed*. 34, 2049–2063. doi: 10.1007/s11032-014-0162-8

Ma, X., Zhang, Q., Zhu, Q., Liu, W., Chen, Y., Qiu, R., et al. (2015). A Robust CRISPR/Cas9 system for convenient, high-efficiency multiplex genome editing in monocot and dicot plants. *Mol. Plant*. 8, 1274–1284. doi: 10.1016/j.molp.2015.04.007

Mahanil, S., Attajarusit, J., Stout, M. J., and Thipyapong, P. (2008). Overexpression of tomato polyphenol oxidase increases resistance to common cutworm. *Plant Sci. Volume* 174, 456–466. doi: 10.1016/j.plantsci.2008.01.006

Menin, B., Moglia, A., Comino, C., Hakkert, J. C., Lanteri, S., and Beekwilder, J. (2013). In vitro callus-induction in globe artichoke (Cynara cardunculus L. var. scolymus) as a system for the production of caffeoylquinic acids. *J. Hortic. Sci. Biotechnol*. 88, 537–542. doi: 10.1080/14620316.2013.11513003

Mennella, G., Lo Scalzo, R., Fibiani, M., DAlessandro, A., Francese, G., Toppino, L., et al. (2012). Chemical and bioactive quality traits during fruit ripening in eggplant (S. melongena L.) and allied species. *J. Agric. Food Chem*. 60:11821–11831. doi: 10.1021/jf3037424

Miao, J., Guo, D., Zhang, J., Huang, Q., Qin, G., Zhang, X., et al. (2013). Targeted mutagenesis in rice using CRISPR-Cas system. *Cell Res*. 23, 1233–1236. doi: 10.1038/cr.2013.123

Mishra, B. B., Gautam, S., and Sharma, A. (2013). Free phenolics and polyphenol oxidase (PPO): The factors affecting post-cut browning in eggplant (Solanum melongena). *Food Chem*. 139, 105–114. doi: 10.1016/j.foodchem.2013.01.074

Muktadir, M. A., Habib, M. A., Khaleque Mian, M. A., and Yousuf Akhond, M. A. (2016). Regeneration efficiency based on genotype, culture condition and growth regulators of eggplant (*Solanum melongena* L.). *Agric. Nat. Resour*. 50, 38–42. doi: 10.1016/j.anres.2014.10.001

Naveed, M., Hejazi, V., Abbas, M., Kamboh, A. A., Khan, G. J., Shumzaid, M., et al. (2018). Chlorogenic acid (CGA): a pharmacological review and call for further research. *Biomed. Pharmacother*. 97, 67–74. doi: 10.1016/j.biopha.2017.10.064

Nonaka, S., Arai, C., Takayama, M., Matsukura, C., and Ezura, H. (2017). Efficient increase of Γ-aminobutyric acid (GABA) content in tomato fruits by targeted mutagenesis. *Sci. Rep*. 7:7057. doi: 10.1038/s41598-017-06400-y

Pan, C., Ye, L., Qin, L., Liu, X., He, Y., Wang, J., et al. (2016). CRISPR/Cas9-mediated efficient and heritable targeted mutagenesis in tomato plants in the first and later generations. *Sci. Rep*. 6:24765. doi: 10.1038/srep24765

Peterson, B. A., Haak, D. C., Nishimura, M. T., Teixeira, P. J. P. L., James, S. R., Dangl, J. L., et al. (2016). Genome-wide assessment of efficiency and specificity in crispr/cas9 mediated multiple site targeting in arabidopsis. *PLoS ONE*. 13:e0162169. doi: 10.1371/journal.pone.0162169

Plazas, M., López-Gresa, M. P., Vilanova, S., Torres, C., Hurtado, M., Gramazio, P., et al. (2013). Diversity and relationships in key traits for functional and

apparent quality in a collection of eggplant: fruit phenolics content, antioxidant activity, polyphenol oxidase activity, and browning. *J. Agric. Food Chem*. 61, 8871–8879. doi: 10.1021/jf402429k

Prohens, J., Rodríguez-Burruezo, A., Raigón, M. D., and Nuez, F. (2007). Total phenolic concentration and browning susceptibility in a collection of different varietal types and hybrids of eggplant: implications for breeding for higher nutritional quality and reduced browning. *J. Am. Soc. Hortic. Sci*. 132, 638–646. doi: 10.21273/JASHS.132.5.638

Rommens, C. M., Ye, J., Richael, C., and Swords, K. (2006). Improving potato storage and processing characteristics through all-native DNA transformation. *J. Agric. Food Chem*. 54, 9882–9887. doi: 10.1021/jf062477l

Rotino, G. L., Sala, T., and Toppino, L. (2014). "Eggplant," in Alien Gene Transfer in Crop. *Plants* 2, 381–409. doi: 10.1007/978-1-4614-9572-7_16

Saini, D. K., and Kaushik, P. (2019). Visiting eggplant from a biotechnological perspective: a review. *Sci. Hortic. (Amsterdam)*. 253, 327–340. doi: 10.1016/j.scienta.2019.04.042

Sashidhar, N., Harloff, H. J., Potgieter, L., and Jung, C. (2020). Gene editing of three BnITPK genes in tetraploid oilseed rape leads to significant reduction of phytic acid in seeds. *Plant Biotechnol. J*. 18, 2241–2250. doi: 10.1111/pbi.13380

Shetty, S. M., Chandrashekar, A., and Venkatesh, Y. P. (2011). Eggplant polyphenol oxidase multigene family: cloning, phylogeny, expression analyses and immunolocalization in response to wounding. *Phytochemistry* 72, 2275–2287. doi: 10.1016/j.phytochem.2011.08.028

Svitashev, S., Young, J. K., Schwartz, C., Gao, H., Falco, S. C., and Cigan, A. M. (2015). Targeted mutagenesis, precise gene editing, and site-specific gene insertion in maize using Cas9 and guide RNA. *Plant Physiol*. 169, 931–945. doi: 10.1104/pp.15.00793

Taranto, F., Pasqualone, A., Mangini, G., Tripodi, P., Miazzi, M. M., Pavan, S., et al. (2017). Polyphenol oxidases in crops: biochemical, physiological and genetic aspects. *Int. J. Mol. Sci*. 18:377. doi: 10.3390/ijms18020377

Thipyapong, P., Hunt, M. D., and Steffens, J. C. (2004). Antisense downregulation of polyphenol oxidase results in enhanced disease susceptibility. *Planta* 220, 105–117. doi: 10.1007/s00425-004-1330-6

Thipyapong, P., Joel, D. M., and Steffens, J. C. (1997). Differential expression and turnover of the tomato polyphenol oxidase gene family during vegetative and reproductive development. *Plant Physiol*. 13, 707–718. doi: 10.1104/pp.113.3.707

Van Eck, J. (2018). Genome editing and plant transformation of solanaceous food crops. *Curr. Opin. Biotechnol*. 49, 35–41. doi: 10.1016/j.copbio.2017.07.012

Wang, Z. P., Xing, H. L., Dong, L., Zhang, H. Y., Han, C. Y., Wang, X. C., et al. (2015). Egg cell-specific promoter-controlled CRISPR/Cas9 efficiently generates homozygous mutants for multiple target genes in Arabidopsis in a single generation. *Genome Biol*. 16:144. doi: 10.1186/s13059-015-0715-0

Wolt, J. D., Wang, K., and Yang, B. (2016). The Regulatory Status of Genome-edited Crops. *Plant Biotechnol. J*. 14, 510–518. doi: 10.1111/pbi.12444

Zhang, Q., Xing, H. L., Wang, Z. P., Zhang, H. Y., Yang, F., Wang, X. C., et al. (2018). Potential high-frequency off-target mutagenesis induced by CRISPR/Cas9 in Arabidopsis and its prevention. *Plant Mol. Biol*. 96, 445–456. doi: 10.1007/s11103-018-0709-x

Zheng, N., Li, T., Dittman, J. D., Su, J., Li, R., Gassmann, W., et al. (2020). CRISPR/Cas9-Based Gene Editing Using Egg Cell-Specific Promoters in Arabidopsis and Soybean. *Front. Plant Sci*. 11:800. doi: 10.3389/fpls.2020.00800

Conflict of Interest: The authors declare that the research was conducted in the absence of any commercial or financial relationships that could be construed as a potential conflict of interest.

frontiers in Plant Science

ORIGINAL RESEARCH
published: 12 January 2021
doi: 10.3389/fpls.2020.614534

Future-Proofing Potato for Drought and Heat Tolerance by Overexpression of Hexokinase and SP6A

*Günter G. Lehretz[1], Sophia Sonnewald[1], Nitsan Lugassi[2], David Granot[2] and Uwe Sonnewald[1]**

[1] Division of Biochemistry, Department of Biology, Friedrich-Alexander-University Erlangen-Nuremberg, Erlangen, Germany,
[2] The Volcani Center, Institute of Plant Sciences, Agricultural Research Organization, Rishon Le-Zion, Israel

Crop yield is largely affected by global climate change. Especially periods of heat and drought limit crop productivity worldwide. According to current models of future climate scenarios, heatwaves and periods of drought are likely to increase. Potato, as an important food crop of temperate latitudes, is very sensitive to heat and drought which impact tuber yield and quality. To improve abiotic stress resilience of potato plants, we aimed at co-expressing hexokinase 1 from *Arabidopsis thaliana* (*AtHXK1*) in guard cells and SELF-PRUNING 6A (*SP6A*) using the leaf/stem-specific StLS1 promoter in order to increase water use efficiency as well as tuberization under drought and heat stress. Guard cell-specific expression of *AtHXK1* decreased stomatal conductance and improved water use efficiency of transgenic potato plants as has been shown for other crop plants. Additionally, co-expression with the FT-homolog *SP6A* stimulated tuberization and improved assimilate allocation to developing tubers under control as well as under single and combined drought and heat stress conditions. Thus, co-expression of both proteins provides a novel strategy to improve abiotic stress tolerance of potato plants.

Keywords: potato, climate change, heat, drought, SP6A, Hexokinase, tuberization, combined stress

OPEN ACCESS

Edited by:
Glenn Bryan,
The James Hutton Institute,
United Kingdom

Reviewed by:
Helen H. Tai,
Agriculture and Agri-Food Canada (AAFC), Canada
Jiyi G. E. Zhang,
BASF, United States

****Correspondence:***
Uwe Sonnewald
uwe.sonnewald@fau.de

Specialty section:
This article was submitted to Plant Biotechnology, a section of the journal Frontiers in Plant Science

Received: *06 October 2020*
Accepted: *07 December 2020*
Published: *12 January 2021*

Citation:
Lehretz GG, Sonnewald S, Lugassi N, Granot D and Sonnewald U (2021) Future-Proofing Potato for Drought and Heat Tolerance by Overexpression of Hexokinase and SP6A. Front. Plant Sci. 11:614534. doi: 10.3389/fpls.2020.614534

INTRODUCTION

Global climate change has become a huge threat for food security worldwide (Birch et al., 2012; Mittler et al., 2012; Fahad et al., 2017; George et al., 2017; Lamaoui et al., 2018; Dahal et al., 2019). In particular rising temperatures and reduced water availability are challenging agriculture worldwide, especially in the northern hemisphere where most cultivated plants are not adapted to such conditions (Lafta and Lorenzen, 1995; Monneveux et al., 2013; George et al., 2017). One of them is the important and widely used crop potato (*Solanum tuberosum* L.). Potato plants are very sensitive to elevated temperatures (Lafta and Lorenzen, 1995; Levy and Veilleux, 2007; Hastilestari et al., 2018; Trapero-Mozos et al., 2018), but also drought susceptible (Deblonde and Ledent, 2001). They originate from relatively cool regions in the Andes of South America and produce starchy storage organs, the tubers, which form from underground stems, the stolons. Formation of tubers naturally occurs at the end of summer under SD conditions. This process has been described previously (Hannapel et al., 2017), and is amongst various other regulators mainly

controlled by a FLOWERING LOCUS T homolog (Navarro et al., 2011). In potato, this is referred to as SELF-PRUNING 6A (SP6A) and its expression correlates with tuber formation (Abelenda et al., 2011, 2014; Navarro et al., 2011, 2015; Teo et al., 2017; Lehretz et al., 2019). Besides the day length-dependent accumulation of *SP6A*, its expression is also under temperature control. Elevated temperatures result in down-regulation of *SP6A* expression, which correlates with decreased tuber yield (Hancock et al., 2014; Hastilestari et al., 2018). Recently a small RNA induced under heat and targeting *SP6A* was discovered as the underlying molecular mechanism (Lehretz et al., 2019).

Moreover, drought is an abiotic stress predicted to rise in the near future and thus harming yields (Monneveux et al., 2013). In potato, drought negatively affects plant growth, tuber number, tuber size and tuber bulking (Deblonde and Ledent, 2001; Schafleitner et al., 2007). Drought is often accompanied by heat and both together strongly decrease tuber yield (Schafleitner et al., 2007). However, even under ambient conditions lower transpiration and thus lower water consumption would be desirable to save water expenses. Previous work showed that guard cell specific overexpression of hexokinase 1 from *Arabidopsis thaliana* (*AtHXK1*) using the KST1 promoter from potato efficiently reduces transpiration and increases water use efficiency (WUE) in several crop plants including tomato and citrus (Kelly et al., 2013, 2017; Lugassi et al., 2015).

However, up to now only few reports show an improved tuber yield under heat or drought stress in potato. For example repression of TOC1 or overexpression of Hsc70 increased heat tolerance (Trapero-Mozos et al., 2018; Morris et al., 2019), whereas overexpression of a MYB or a bZIP transcription factor ameliorated drought tolerance (Shin et al., 2011; Moon et al., 2015). Improved yield under combined drought and heat stress has not been reported so far. Here, we aimed to enhance tuberization and to reduce water loss concurrently by creating transgenic potato plants overexpressing both *SP6A* and *AtHXK1*. Thereby, we achieved significant yield improvements under single as well as combined stress conditions. These transgenic plants exhibited reduced transpiration and enhanced tuberization under control conditions, but most importantly, yield reduction was much lower or not present under heat and drought stress. Moreover, the starch content of the tubers was hardly affected by stress treatments. Together, we provide a novel strategy to adopt potato plants to withstand expected climate changes and help to secure future carbohydrate food production while saving water resources at the same time.

RESULTS

Simultaneous Expression of Hexokinase and SP6A in Transgenic Potato Plants Reduces Transpiration and Enhances Tuberization

In previous studies it has been shown that guard cell-specific expression of *AtHXK1* improves WUE of several plant species (Kelly et al., 2013, 2017; Lugassi et al., 2015). To verify that guard cell-specific expression of *AtHXK1* in potato leads to reduced stomatal conductance and transpiration rates, transgenic potato lines overexpressing *AtHXK1* under the guard cell-specific KST1 promoter (GCHXK) were created. Transgene expression was verified by qPCR in two independent lines (**Supplementary Figure S1A**). Next, gas exchange parameters were measured in these transgenic lines which confirmed reduced stomatal conductance (**Supplementary Figure S1B**) and transpiration rates (**Supplementary Figure S1C**). Concurrently, no clear negative effect on CO_2 assimilation (**Supplementary Figure S1D**) was detected in these lines resulting in an enhanced WUE (**Supplementary Figure S1E**). Additionally, tuber yield of the highest expressing line was increased which can be attributed to a higher tuber weight rather than an increased tuber number (**Supplementary Figures S1H,G**).

Next, we attempted to co-express both, *AtHXK1* and *SP6A*, in transgenic potato plants. Therefore both constructs were assembled into one expression vector using the Golden Gate cloning system (Weber et al., 2011; **Figure 1A**). *AtHXK1* was expressed under the KST1 promoter (Müller-Röber et al., 1995), whereas *SP6A* was expressed under the StLS1 promoter (Stockhaus et al., 1987). Four transgenic lines were selected expressing both genes at high levels in source leaves (**Figures 1B,C**). Compared to untransformed control plants all transgenic plants showed a bushy habitus with reduced plant height (**Supplementary Figure S2A**). To investigate this further, several morphological parameters were measured (**Supplementary Figures S2B–D**), which indicate that the lower shoot length was accompanied by a higher number of leaves. Even though the individual leaves were smaller, the total leaf area per plant was slightly, but significantly, increased in all transgenic lines.

Following the molecular and morphological characterization, we investigated physiological changes in AtHXK1+SP6A plants. As shown in **Figure 1D**, transpiration rate of the double transgenic lines was reduced compared to the wild type. The lower transpiration was most likely caused by less opened stomata due to *AtHXK1* expression which was confirmed by measuring the stomata width and length (**Supplementary Figure S3A**). The ratio between both parameters was significantly reduced in the transgenic lines, while the number of stomata per leaf area was similar to the wild type (**Supplementary Figure S3B**). Thus, the less opened stomata led to an about 30% lower transpiration, but at the same time the CO_2 assimilation was only slightly negatively influenced (reduction by 10%) (**Figure 1E**) leading to an approximately 30% increased WUE in the transgenic lines (**Figure 1F**).

Transgenic AtHXK1+SP6A Potato Plants Show High Yield Stability Under Heat and Drought Stress

In further studies we investigated whether these transgenic plants are more resilient to abiotic stress factors and examined physiological and biochemical responses to heat and drought stress and a combination thereof. We designed an experimental setup (**Figure 2A**) in which all plants were first grown for 4 weeks

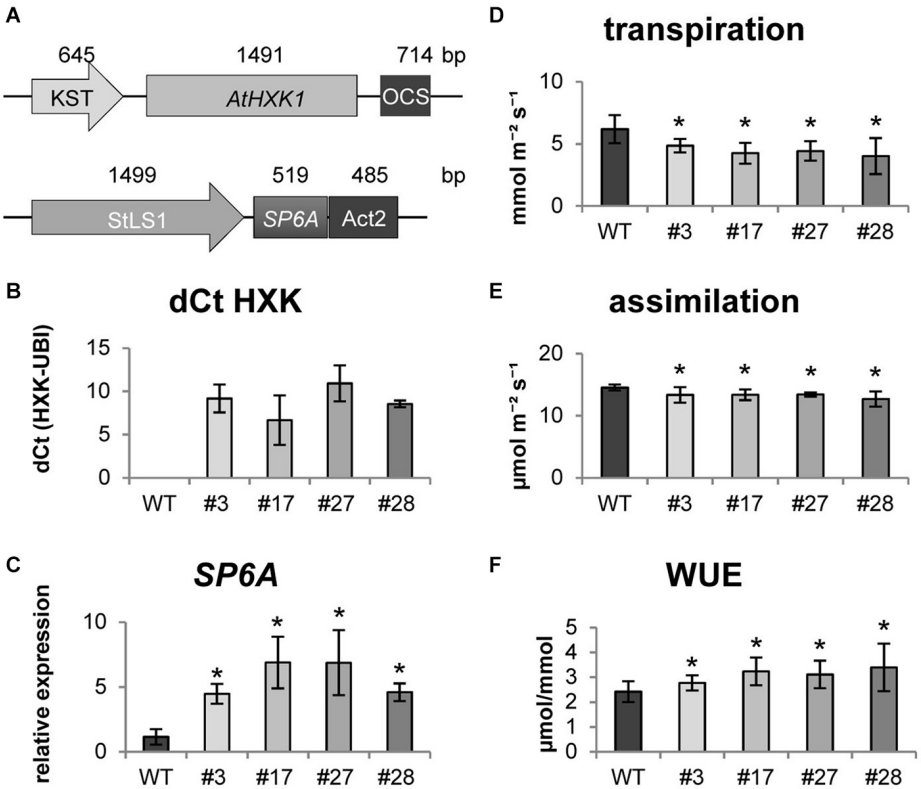

FIGURE 1 | Characterisation of HXK+SP6A potato plants under ambient conditions **(A)** schematic depiction of gene constructs **(B)** expression of AtHXK1 in source leaves, **(C)** expression of *SP6A* in source leaves, **(D)** transpiration **(E)** assimilation, **(F)** water use efficiency (WUE) at 28 days; values are the mean of four biological replicates ± SD, $^*p \leq 0.05$.

under well-watered control conditions (approx. 65% relative water content (RWC) in the soil). Then, half of the population was adapted to drought conditions (approx. 35% RWC) for 1 week. Soil humidity was adjusted by daily watering. Thereafter, one half of each group was shifted to elevated temperatures in order to investigate heat effects. All plants were grown for two more weeks under these conditions until harvest (**Figure 2A**).

The transpiration rate of the plants was determined under each condition. Similar to the first experiments, the transpiration rates were reduced in all AtHXK1+SP6A lines as compared to wild-type plants grown under control conditions (WC = water control) (**Figure 2B**). The transpiration rates of both wild type and AtHXK1+SP6A lines decreased in response to drought (DC = drought control), but total evaporation was lower in the transgenic plants (**Figure 2B**) consistent with the reduced stomatal aperture. Under elevated temperatures (WH = water heat), wild-type plants increased transpiration. A similar response was seen in AtHXK1+SP6A lines, but the absolute values were about 35% less than in wild-type plants (**Figure 2B**). Under combined stress conditions, i.e., drought and heat (DH), again the transpiration rate of transgenic lines was lower compared to wild-type plants.

CO_2 assimilation was, if at all, only mildly reduced in AtHXK1+SP6A lines under all growth conditions as compared to wild-type plants (**Figure 2C**). Consequently, WUE was improved by about 30–50% in the AtHXK1+SP6A lines under well-watered control (WC), drought (DC), heat (WH) as well as double stress (DH) conditions (**Figure 2D**). This effect was mainly driven by the lower transpiration rate caused by expression of AtHXK1.

As the focus of our research was a biotechnological improvement of the tuber crop potato, we were especially interested in tuber yield which was determined together with other growth parameters at the end of the experiments. As observed before, all transgenic plants exhibited a reduced shoot growth compared to wild-type plants under control conditions that persisted also under all stress treatments (**Figure 3A**). Under drought conditions, plant height as well as green biomass (e.g., leaves and stem) decreased in the wild type, while both parameters were less affected in the transgenic lines (**Figures 3A,B**). The increase in plant height under heat (WH), known as shade avoidance phenotype, was observed in all genotypes, but it was less pronounced in the transgenics. The heat-mediated shoot elongation was abolished by simultaneous drought and heat stress (DH) in wild-type plants. Under combined stress the transgenic lines were slightly smaller than their respective controls (**Figure 3A**). The green biomass accumulation seemed less impaired by drought stress in the transgenics compared to wild type. Most importantly, despite a lower green biomass, tuber yield of all transgenic lines was 30–70% higher under control conditions. Tuber yield of transgenic

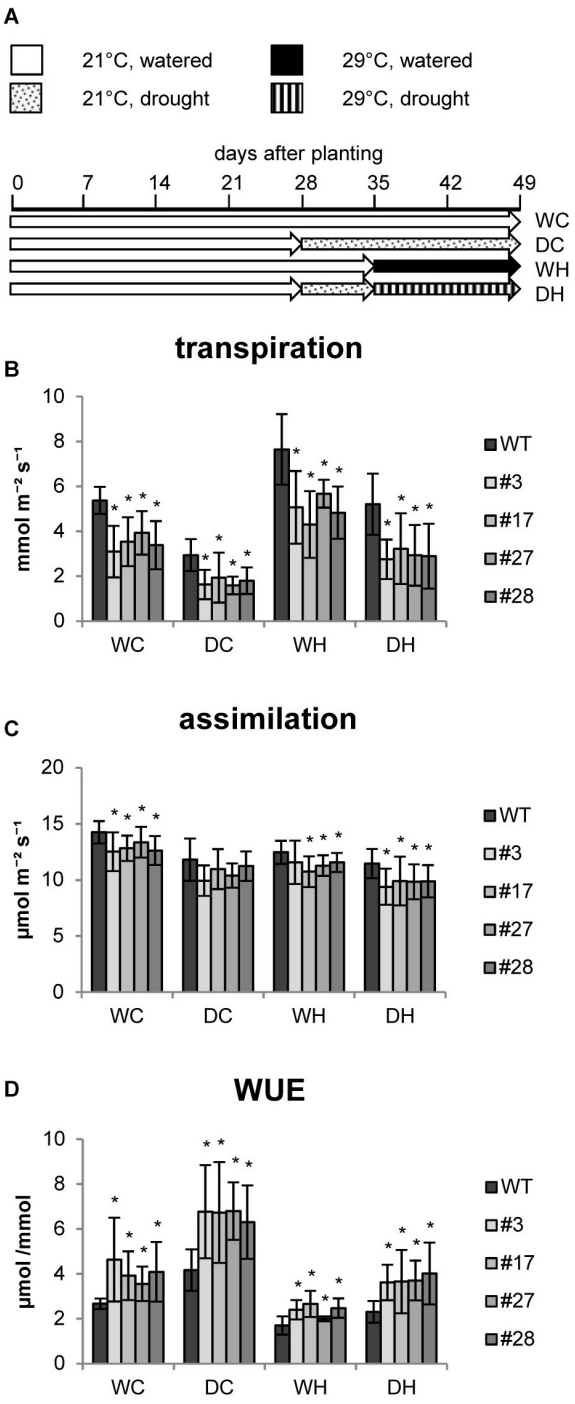

FIGURE 2 | Photosynthesis of HXK+SP6A potato plants under different stress treatments at the age of 5–6 weeks. **(A)** Experimental setup, **(B)** transpiration, **(C)** assimliation, **(D)** WUE, values are the mean of 8–12 biological replicates ± SD, $^*p \leq 0.05$ compared to respective WT.

plants was hardly affected by stress applications, indicating that they maintain high tuber yields even under stress conditions (**Figure 3C** and **Supplementary Figure S4**). In contrast, double stress application (DH) led to a severe yield reduction of roughly 70% in wild-type plants (**Figure 3C**). Under these conditions, the overall tuber yield of the transgenic plants was 4–5 times higher as compared to wild-type plants (**Figure 3C**). Even though tubers of transgenic plants were smaller (**Figure 3D**), a massive increase in tuber number more than compensated for this (**Figure 3E**) and contributed to higher yields. Finally, the harvest index of the transgenic plants was 2–8 times higher under all conditions (**Figure 3F**). The positive effects of AtHXK1 and SP6A co-expression especially on tuber yield were observed in three independent experiments using four plants per treatment and independent transgenic lines underlining the high reproducibility (**Figure 3** and **Supplementary Figures S5, S6**).

As a most likely reason for the yield reduction in the wild type, we reasoned a decreased *SP6A* expression in leaves and performed a quantitative RT-PCR. In fact, *SP6A* expression decreased upon both drought and heat in the wild type (**Supplementary Figure S7A**). However, the strongest downregulation of *SP6A* was detected under combined stress conditions. Overall, the pattern of yield reduction fitted well with *SP6A* expression level (Pearson correlation 0.91). In contrast, higher *SP6A* mRNA levels were measured in all transgenic lines under all conditions (**Supplementary Figure S7A**). In addition, expression levels of the small RNA (*SES*) described previously to repress *SP6A* under heat (Lehretz et al., 2019), was measured in wild type. The results confirmed its heat-mediated induction in wild type, while drought stress resulted in a down-regulation of *SES* (**Supplementary Figure S7B**).

Since more tubers per plant would have no agricultural value with reduced dry matter, we measured the tuber starch content. Under control conditions, no clear changes between tubers from wild type or transgenic plants were detected. Upon drought stress, no significant reduction in the starch content was seen in wild-type tubers. However, starch levels clearly decreased in wild type in response to heat and even further by combined heat and drought stress (**Figure 4**). Remarkably, starch contents were not significantly altered by stress treatments in most of the transgenic tubers and higher amounts of starch than in the corresponding wild-type tubers were observed under stress conditions (**Figure 4**).

DISCUSSION

Since global average temperatures are expected to rise further in the near future designing crop plants which can withstand heat stress is of utmost importance to secure food production (Birch et al., 2012; George et al., 2017; Lamaoui et al., 2018). Additionally, heat is often accompanied by drought, especially in tepid climate. Therefore, reduction of transpiration is a very desirable trait as it stabilizes yield and unleashes resources, allowing to be used elsewhere. With this goal in mind, transgenic potato plants were created that co-express two target genes, *AtHXK1* and *SP6A*, and were tested for improved stress tolerance toward heat, drought and combined stress conditions.

The water consumption of crop plants is an important topic. Even though potato is rather efficient in water usage compared to other crops it is still vulnerable to drought conditions.

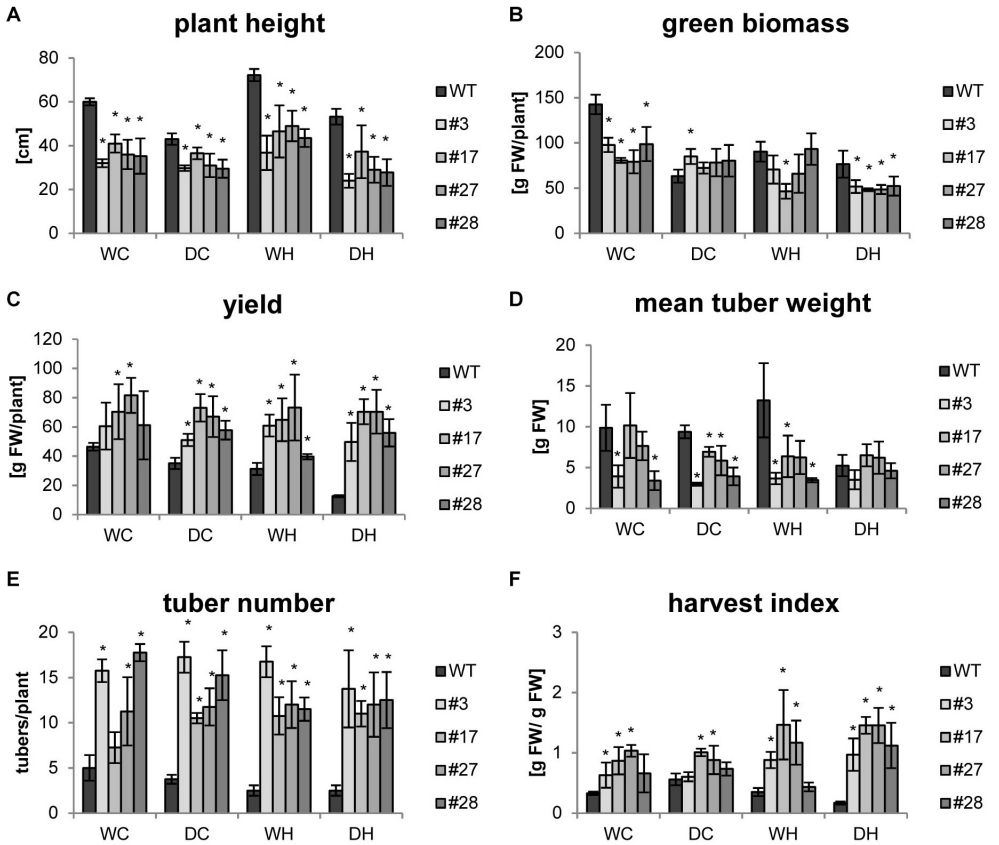

FIGURE 3 | Yields data for HXK+SP6A potato plants harvested at 49 days. **(A)** Plant height, **(B)** green biomass, **(C)** yield, **(D)** mean tuber weight, **(E)** tuber number, **(F)** harvest index; plants were harvested at the age of 7 weeks; values are the mean of 4 plants ± SD, $^*p \leq 0.05$ compared to respective WT.

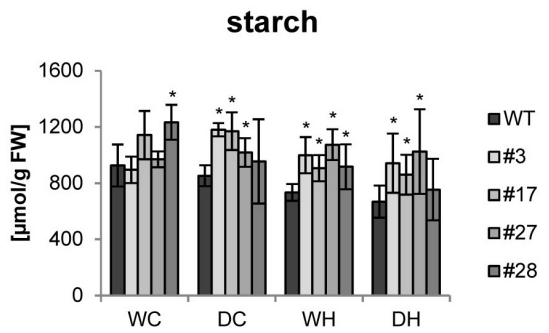

FIGURE 4 | Starch content of tubers of HXK+SP6A potato plants under different stress treatments. Bars show mean of four biological replicates ± SD, $^*p \leq 0.05$ compared to respective WT.

Decreased transpiration rates might solve this agricultural problem. AtHXK1 was shown to reduce transpiration when expressed in guard cells of *A. thaliana*, citrus and tomato without a negative effect on plant growth and CO_2 assimilation (Kelly et al., 2013, 2019; Lugassi et al., 2015). Although the molecular mechanism is not completely understood, it is assumed that AtHXK1 controls stomatal aperture to coordinate photosynthesis with transpiration through sugar signaling pathways (Kottapalli et al., 2018; Granot and Kelly, 2019) as it has been described as a sugar sensor before (Moore et al., 2003). According to a current model, it is supposed that a surplus of sucrose that is not transported by the phloem during high photosynthetic activity is carried with the transpiration stream toward the guard cells where it serves as a signal to close the stomata and thereby prevents unnecessary water loss (Kelly et al., 2013; Lugassi et al., 2015; Kottapalli et al., 2018).

We expressed the KST::AtHXK1 construct alone and together with *SP6A* in potato and provided clear evidence that the desired effect of *AtHXK1* expression (e.g., reduced transpiration) is also present in this crop plant under control conditions as shown for Arabidopsis (Kelly et al., 2013), citrus (Lugassi et al., 2015) and tomato (Kelly et al., 2019). Concurrently, stomata-specific expression of *AtHXK1* slightly affected photosynthetic CO_2 assimilation in potato. In concert, both effects led to a significantly increased water use efficiency. Although CO_2 assimilation per leaf area was negatively affected in the HXK+SP6A plants, the bushy growth phenotype, caused by *SP6A* overexpression, with more (smaller) leaves might counteract for this.

One common response to drought is stomatal closure (Liu et al., 2006). Therefore, we reasoned that plants with

already lower stomatal conductance may have an advantage under limited water availability. Accordingly, transpiration decreased under drought stress in wild-type plants as well as in AtHXK1+SP6A lines with the transgenic lines exhibiting a lower transpiration rate as compared to wild-type plants. The same effect was seen in heat and drought combination, while heat alone resulted overall in increased transpiration rates as described before (Hancock et al., 2014; Hastilestari et al., 2018). Thus, we conclude that reduced stomatal conductance helps to safe water under drought stress, but a lower transpiration is also advantageous under mild heat stress and combined heat and drought stress.

In order to stimulate tuberization the *FLOWERING LOCUS T* homologue *SP6A* was selected for overexpression. This gene was identified as a positive key regulator of tuberization that is controlled by the photoperiod pathway (Navarro et al., 2011). Hence, overexpression of *SP6A* in potato promoted tuberization in the short day-dependent *S. andigena* in a day length independent manner (Navarro et al., 2011) and also in modern day-length insensitive cultivars (Teo et al., 2017). We recently showed that overexpression of a codon optimized *SP6A* version in the tetraploid variety Solara was accompanied by a severely altered source-sink balance (Lehretz et al., 2019).

Furthermore, the downregulation in *SP6A* expression is seen as a cause for the heat-mediated inhibition of tuber formation (Hancock et al., 2014; Hastilestari et al., 2018). This occurs via transcriptional and post-transcriptional regulation. A small RNA was identified which targets the *SP6A* transcript for post-transcriptional degradation. Importantly, the expression of this small RNA was strongly induced under elevated temperatures and using a target mimicry approach the functional relevance of the small RNA for the regulation of *SP6A* under heat was demonstrated (Lehretz et al., 2019).

Our approach described here led to elevated *SP6A* levels and stimulated tuber formation under control conditions. By using the StLS1 promoter *SP6A* levels were only moderately increased (five to sevenfold) in chloroplast-containing cells and consequently the development of the shoot was not as strongly affected as compared to our previous approach using a codon-optimized *SP6A* transcript driven by the constitutive CaMV 35S promoter. Nevertheless, AtHXK1+SP6A overexpressing plants were smaller and accumulated less aboveground biomass than wild-type plants, but tuber number and yield increased significantly.

Under elevated temperatures as well as under drought stress tuber number and yield of wild-type potato plants were significantly decreased as reported in previous studies (Dahal et al., 2019). The heat-mediated decline in tuber yield is associated with a strong decrease in *SP6A* expression. For drought, this correlation has not been shown yet. In our study, we found that *SP6A* expression is inhibited by drought and most significantly by a combination of drought and heat stress. The strong correlation between *SP6A* expression and yield further supports the idea that *SP6A* is an important target for ensuring stable yields under changing environmental conditions.

Under heat conditions, the small RNA *SES* inhibits *SP6A* expression and is responsible for the observed yield decrease. Under drought conditions, we did not find increased *SES* expression levels. Therefore, we conclude that *SES* is not responsible for downregulation of *SP6A* under drought stress conditions. Instead, other mechanisms, such as posttranslational repression of members in the *CDF/CO* pathway or other miRNAs will be responsible for the observed *SP6A* regulation. Further studies are needed to unravel the molecular mechanisms responsible for the observed drought-mediated downregulation of *SP6A* expression. Taken together, high *SP6A* expression levels under conditions of water scarcity and elevated temperatures will be crucial to maintain high tuber yield under conditions of expected climate change.

Tuber fresh weight and tuber number of the transgenic HXK+SP6A lines were only slightly affected by the applied stress conditions. Even though *SP6A* transcript levels decreased in some transgenic lines under stress conditions, the remaining transcript level was three to fourfold higher compared to wild type under control conditions and therefore most likely sufficient to maintain tuberization and to further support assimilate translocation into growing tubers. SP6A was recently shown to interact with the sucrose efflux carrier SWEET11 and thereby prevents leakage of sucrose into the apoplast. It is assumed that this enhances assimilate allocation and promotes symplasmic unloading of sucrose into developing tubers (Abelenda et al., 2019). During tuber development the mode of sucrose unloading switches from apoplasmic to symplasmic (Viola et al., 2007). Thus, the interaction of SP6A with SWEET11 provides a functional link between photoperiodic control and assimilate unloading into developing tubers.

Consistent with this hypothesis, the starch content of the transgenic tubers was largely unaffected, under single and double stress, while it decreased with the severity of stress in the wild type. Together these results further support the assumption that SP6A plays a major role in development of potato tubers and maintenance of their sink strength.

Together, AtHXK1+SP6A co-expression combines a sustainable use of limited water resources with a high tuberization capacity under greenhouse conditions and thereby helps to maintain tuber formation and growth under heat, drought and combined stress conditions. Whether this positive effect is maintained under open field conditions and whether improved abiotic stress tolerance might negatively interfere with biotic stress responses needs to be validated in further studies.

MATERIALS AND METHODS

Plant Material and Growth Conditions

Potato (*Solanum tuberosum* L. cv. Désirée) was used for the experiments with the GCHXK lines. These plants were grown in a mixture of peat, quartz, and coconut fibers (Green 90, Even Ari, Israel) in a temperature-controlled greenhouse under natural conditions.

For all other experiments, *S. tuberosum L.* cv. Solara plants were grown under greenhouse conditions in 3.5 l pots (20 cm diameter) with 16 h supplemental lights (250 μE). Plants were maintained and amplified in tissue culture on Murashige and

Skoog medium (Murashige and Skoog, 1962) containing 2% sucrose. Walk-in growth chambers were used for controlled ambient and elevated temperature treatments (22 or 29°C during light period and 20 or 27°C during dark period, respectively) with supplemental light (350 μE). Drought stress was applied by stopping watering for 2–3 days and subsequent adjusting the relative water content (RWC) in the soil to 35%, while in control condition RWC was 65%. This was achieved through measurement of soil conductivity using the EM50 soil moisture sensor (Decagon, United States) and calibration of pot weight. Leaf area was measured using a LI-3100 area meter (LI-COR, United States). Plant height was measured from soil surface to apical meristem. Harvest index was calculated as ratio of tuber fresh weight per plant over green fresh weight per plant.

Plasmid Construction and Generation of Transgenic Plants

The GCHXK lines were generated by transforming the KST*pro*::AtHXK1 constructs described previously (Kelly et al., 2013) in potato plants (cv. Désirée) using the *Agrobacterium tumefaciens* strain EHA105. Following the screening on Kanamycin selection media, PCR with KST specific primers was used to distinguish between transgenic and non-transgenic plants. Twenty positive plants were identified. Positive plants were then checked for their gas exchange parameters, and two lines with significant reduction in transpiration, GCHXK3 and GCHXK12 were selected for further analysis.

The stacked construct was generated using the GoldenGate cloning system (Engler et al., 2008, 2009; Weber et al., 2011). Synthetic or PCR amplified gene sequences (Thermo Fisher Scientific GeneArt GmbH) and modules available from MoClo plant part kits[1] (Werner et al., 2012) were assembled into level 0 and subsequently level 1 vectors to generate the plasmids St-LS1::*StSP6A* and *KST1*::*AtHXK1*. Both plasmids were combined with a kanamycin-resistance cassette (pICSL70004) into a level 2 vector (pAGM4237, Addgene) which was transformed into potato cv. Solara by *Agrobacterium*-mediated gene transfer to generate the AtHXK1+SP6A lines (Rocha-Sosa et al., 1989). An overview of modules used to generate the plasmid is provided in **Supplementary Table S2**. Thirty-four transgenic lines were obtained and screened for the presence of both genes by qPCR. Four lines (# 3, 17, 27, 28) were selected for further studies that express both targets.

RNA Isolation, cDNA Synthesis, and Quantitative RT-PCR Analysis

Samples of source leaves were taken during the first half of the light period, 4 h after dawn. Total RNA was isolated from ca. 100 mg of frozen leaf material by grinding on 8M guanidiumchloride and 0.7% β-ME (Logemann et al., 1987). RNA quantity was measured with ND-1000 Spectrophotometer (NanoDrop Technologies). Complementary DNA synthesis and quantitative real time PCR (qPCR) analyses were conducted as described previously (Ferreira and Sonnewald, 2012). Quantitative Real-Time PCR (qPCR) was conducted on AriaMx (Agilent Technologies) and analyzed as described by Livak and Schmittgen (2001). Alternatively, RNA extraction, cDNA preparation, and quantitative real-time PCR analysis were performed as described before (Lugassi et al., 2015). Data were normalized using NAC (XM_006339185) or Ubi 3 (L22576) as reference genes. The primers used for amplification are listed in **Supplementary Table S1**.

Sugar Measurements

Starch was extracted using ca. 50 mg of tuber FW grinded in 80% Ethanol, incubated with 0.2 M KOH overnight, heated at 95°C for 90 min and neutralized with 1 N acidic acid. After amyloglucosidase digestion glucose contents were determined using a coupled optical assay as described previously (Hastilestari et al., 2018).

Photosynthesis Measurements

Photosynthesis, transpiration rates and stomatal conductance were measured on fully developed source leaves on the upper middle stem (5th–8th from top) under greenhouse conditions using a LI-COR 6800 or LI-COR 6400 device. All measurements were conducted between 3 and 6 h after dawn (09:00–12:00 a.m.) under the respective greenhouse conditions (400–600 $\mu mol\ m^{-2}\ s^{-2}$ light, 400–500 $\mu mol\ mol^{-1}$ CO_2, 50% relative humidity). WUE was calculated as assimilation/transpiration. Temperature was also adjusted according to the treatment in the greenhouse (22 and 29°C, respectively).

Microscopic Analysis of Stomata

In order to measure the length to width ratio of stomata source leaves were coated with transparent quick dry nail polish by brushing the abaxial side of fully developed source leaves 4 h after dawn. The coatings were immediately removed after drying and photographed with a Leica DMR Microscope. Lengths were measured using the FIJI software.

Statistical Analysis

Statistical analyses were done by Student's *t*-test. Specific details of the statistical test used, number of biological and technical replicates, and the description of error bars are included in the figure legends.

DATA AVAILABILITY STATEMENT

The original contributions presented in the study are included in the article/**Supplementary Material**, further inquiries can be directed to the corresponding author/s.

AUTHOR CONTRIBUTIONS

NL and DG designed and tested GCHXK lines. GL designed and performed all other experiments. GL and SS analyzed data. SS and US were responsible for project planning. GL, SS, and US wrote the manuscript with input from all other authors. All authors contributed to the article and approved the submitted version.

[1] http://www.addgene.org

FUNDING

The work received funding from the European Union's Horizon 2020 research and innovation program under grant agreement No. 862127 (PHOTOBOOST).

ACKNOWLEDGMENTS

We wish to acknowledge the great help of Stephen Reid and Ingrid Schießl in the lab. Many thanks also to the tissue culture team Eva Düll, Anja Saalbach, and Christiane Börnke for maintenance and propagation of the plant material and to the student's helpers Fee Breunig, Selina Beck, and Anna Henning.

SUPPLEMENTARY MATERIAL

The Supplementary Material for this article can be found online at: https://www.frontiersin.org/articles/10.3389/fpls.2020.614534/full#supplementary-material

Supplementary Table 1 | Primer sequences.

Supplementary Table 2 | AtHXK1+SP6A construct assembly.

REFERENCES

Abelenda, J. A., Bergonzi, S., Oortwijn, M., Sonnewald, S., Du, M., Visser, R., et al. (2019). 'Source-sink regulation is mediated by interaction of an FT- homolog with a SWEET protein in potato'. *Curr. Biol.* 29, 1178–1186. doi: 10.1016/j.cub.2019.02.018

Abelenda, J. A., Navarro, C., and Prat, S. (2011). 'From the model to the crop: Genes controlling tuber formation in potato'. *Curr. Opin. Biotechnol.* 22, 287–292. doi: 10.1016/j.copbio.2010.11.013

Abelenda, J. A., Navarro, C., and Prat, S. (2014). 'Flowering and tuberization: A tale of two nightshades'. *Trends Plant Sci.* 19, 115–122. doi: 10.1016/j.tplants.2013.09.010

Birch, P. R. J., Bryan, G., Fenton, B., Gilroay, E. M., Hein, I., Jones, J. T., et al. (2012). Crops that feed the world 8: Potato: Are the trends of increased global production sustainable? *Food Secur.* 4, 477–508. doi: 10.1007/s12571-012-0220-1

Dahal, K., Li, X. Q., Tai, H., Creelman, A., and Bizimungu, B. (2019). 'Improving potato stress tolerance and tuber yield under a climate change scenario – a current overview'. *Front. Plant Sci.* 10, 1–16. doi: 10.3389/fpls.2019.00563

Deblonde, P. M. K., and Ledent, J. F. (2001). 'Effects of moderate drought conditions on green leaf number, stem height, leaf length and tuber yield of potato cultivars'. *Eur. J. Agron.* 14, 31–41. doi: 10.1016/s1161-0301(00)00081-2

Engler, C., Gruetzner, R., Kandzia, R., and Marillonnet, S. (2009). 'Golden gate shuffling: A one-pot DNA shuffling method based on type ils restriction enzymes'. *PLoS One* 4:e5553. doi: 10.1371/journal.pone.0005553

Engler, C., Kandzia, R., and Marillonnet, S. (2008). A one pot, one step, precision cloning method with high throughput capability'. *PLoS One* 3:e3647. doi: 10.1371/journal.pone.0003647

Fahad, S., Bajwa, A. A., Nazir, U., Anjum, S. A., Farooq, A., Zohaib, A., et al. (2017). Crop Production under Drought and Heat Stress: Plant Responses and Management Options. *Front. Plant Sci.* 8:1147. doi: 10.3389/fpls.2017.01147

Ferreira, S. J., and Sonnewald, U. (2012). 'The mode of sucrose degradation in potato tubers determines the fate of assimilate utilization'. *Front. Plant Sci.* 3:23. doi: 10.3389/fpls.2012.00023

George, T. S., Taylor, M. A., Dodd, I. C., and White, P. J. (2017). (2017) 'Climate Change and Consequences for Potato Production: a Review of Tolerance to Emerging Abiotic Stress'. *Potato Res.* 60, 239–268. doi: 10.1007/s11540-018-9366-3

Granot, D., and Kelly, G. (2019). 'Evolution of Guard-Cell Theories: The Story of Sugars'. *Trends Plant Sci.* 24, 507–518. doi: 10.1016/j.tplants.2019.02.009

Hancock, R. D., Morris, W. L., Ducreux, L. J. M., Morris, J. A., Usman, M., Verrall, S. R., et al. (2014). 'Physiological, biochemical and molecular responses of the potato (Solanum tuberosumL.) plant to moderately elevated temperature'. *Plant Cell Environ.* 37, 439–450. doi: 10.1111/pce.12168

Hannapel, D. J., Sharma, P., Lin, T., and Banerjee, A. K. (2017). 'The Multiple Signals That Control Tuber Formation'. *Plant Physiol.* 174, 845–856. doi: 10.1104/pp.17.00272

Hastilestari, B. R., Lorenz, J., Reid, S., Hofmann, J., Pscheidt, D., Sonnewald, S., et al. (2018). 'Deciphering source and sink responses of potato plants (Solanum tuberosum L.) to elevated temperatures'. *Plant Cell Environ.* 41, 2600–2616. doi: 10.1111/pce.13366

Kelly, G., Egbaria, A., Khamaisi, B., Lugassi, N., Attia, Z., Moshelion, M., et al. (2019). 'Guard-Cell Hexokinase Increases Water-Use Efficiency Under Normal and Drought Conditions'. *Front. Plant Sci.* 10:1499. doi: 10.3389/fpls.2019.01499

Kelly, G., Lugassi, B. E., Wolf, D., Khamaisi, B., and Brandsma, D. (2017). The Solanum tuberosum KST1 partial promoter as a tool for guard cell expression in multiple plant species'. *J. Exp. Bot.* 68, 2885–2897. doi: 10.1093/jxb/erx159

Kelly, G., Moshelion, M., David-Schwartz, R., Halperin, O., Wallach, R., Attia, Z., et al. (2013). 'Hexokinase mediates stomatal closure'. *Plant J.* 75, 977–988. doi: 10.1111/tpj.12258

Kottapalli, J., David-Schwartz, R., Khamaisi, B., Brandsma, D., Lugassi, N., Egbaria, A., et al. (2018). 'Sucrose-induced stomatal closure is conserved across evolution'. *PLoS One* 13:e020535. doi: 10.1371/journal.pone.0205359

Lafta, A. M., and Lorenzen, J. H. (1995). 'Effect of High Temperature on Plant Grwoth and Carbohydrate Metabolism in Potato Plants'. *J. Plant Physiol.* 109, 637–643. doi: 10.1104/pp.109.2.637

Lamaoui, M., Jemo, M., Datla, R., and Bekkaoui, F. (2018). 'Heat and drought stresses in crops and approaches for their mitigation'. *Front. Chem.* 6:26. doi: 10.3389/fchem.2018.00026

Lehretz, G. G., Sonnewald, S., Hornyik, C., Corral, J. M., and Sonnewald, U. (2019). 'Post-transcriptional Regulation of FLOWERING LOCUS T Modulates Heat-Dependent Source-Sink Development in Potato'. *Curr. Biol.* 29, 1614–1624. doi: 10.1016/j.cub.2019.04.027

Levy, D., and Veilleux, R. E. (2007). 'Adaptation of potato to high temperatures and salinity - A review'. *Am. J. Potato Res.* 84, 487–506. doi: 10.1007/bf02987885

Liu, F., Shahnazari, A., Andersen, M., Jacobsen, S. E., and Jensen, C. R. (2006). 'Physiological responses of potato (Solanum tuberosum L.) to partial root-zone drying: ABA signalling, leaf gas exchange, and water use efficiency'. *J. Exp. Bot.* 57, 3727–3735. doi: 10.1093/jxb/erl131

Livak, K. J., and Schmittgen, T. D. (2001). 'Analysis of relative gene expression data using real-time quantitative PCR and the 2-ΔΔCT method'. *Methods* 25, 402–408. doi: 10.1006/meth.2001.1262

Logemann, J., Schell, J., and Willmitzer, L. (1987). 'Improved Method for the Isolation of RNA from Plant Tissues'. *Analyt. Biochem.* 163, 16–20. doi: 10.1016/0003-2697(87)90086-8

Lugassi, N., Kelly, G., Fidel, L., Yaniv, Y., Attia, Z., Levi, A., et al. (2015). 'Expression of Arabidopsis Hexokinase in Citrus Guard Cells Controls Stomatal Aperture and Reduces Transpiration'. *Front. Plant Sci.* 6:1114. doi: 10.3389/fpls.2015.01114

Mittler, R., Finka, A., and Goloubinoff, P. (2012). 'How do plants feel the heat?'. *Trends Biochem. Sci.* 37, 118–125. doi: 10.1016/j.tibs.2011.11.007

Monneveux, P., Ramírez, D. A., and Pinob, M.-T. (2013). 'Drought tolerance in potato (S. tuberosum L.): Can we learn from drought tolerance research in cereals?'. *Plant Sci.* 205, 76–86. doi: 10.1016/j.plantsci.2013.01.011

Moon, J., Han, S., Kim, D., Yoon, I., Shin, D., Byun, M., et al. (2015). 'Ectopic expression of a hot pepper bZIP - like transcription factor in potato enhances drought tolerance without decreasing tuber yield'. *Plant Mole. Biol.* 89, 421–431. doi: 10.1007/s11103-015-0378-y

Moore, B., Zhou, L., Rolland, F., Hall, Q., Cheng, W., Liu, Y., et al. (2003). 'Role of the Arabidopsis glucose sensor HXK1 in nutrient, light, and hormonal signaling'. *Science* 300, 332–336. doi: 10.1126/science.1080585

Morris, W. L., Ducreux, L. J. M., Morris, J., Campbell, R., Usman, M., Hedley, P. E., et al. (2019). Identification of TIMING of CAB EXPRESSION 1 as a temperature-sensitive negative regulator of tuberization in potato'. *J. Exp. Bot.* 70, 5703–5714. doi: 10.1093/jxb/erz336

Müller-Röber, B., Ellenberg, J., Provart, N., Willmitzer, L., Busch, H., Becker, D., et al. (1995). 'Cloning and electrophysiological analysis of KST1'. *EMBO J.* 14, 2409–2416. doi: 10.1002/j.1460-2075.1995.tb07238.x

Murashige, T., and Skoog, S. (1962). A revised medium for rapid growth and bio assays with tobacco tissue cultures. *Physiologia Plantarum* 15, 473–497. doi: 10.1111/j.1399-3054.1962.tb08052.x

Navarro, C., Abelenda, J. A., Cruz-Oró, E., Cuéllar, C. A., Tamaki, S., Silva, J., et al. (2011). Control of flowering and storage organ formation in potato by FLOWERING LOCUS T'. *Nature* 478, 119–122. doi: 10.1038/nature 10431

Navarro, C., Cruz-Oró, E., and Prat, S. (2015). 'Conserved function of FLOWERING LOCUS T (FT) homologues as signals for storage organ differentiation'. *Curr. Opin. Plant Biol.* 23, 45–53. doi: 10.1016/j.pbi.2014.10. 008

Rocha-Sosa, M., Sonnewald, U., Frommer, W., Stratmann, M., Schell, J., and Willmitzer, L. (1989). 'Both developmental and metabolic signals activate the promoter of a class I patatin gene'. *EMBO J.* 8, 23–29. doi: 10.1002/j.1460-2075. 1989.tb03344.x

Schafleitner, R., Gutierrez-Rosales, R. O., Gaudin, A., Alvarado Aliaga, A. A., Nomberto Martinez, G., Tincopa Marca, L. R., et al. (2007). Capturing candidate drought tolerance traits in two native Andean potato clones by transcription profiling of field grown plants under water stress'. *Plant Physiol. Biochem.* 45, 673–690. doi: 10.1016/j.plaphy.2007.06.003

Shin, D., Moon, S., Han, S., Kim, B., Park, S. R., Lee, S., et al. (2011). 'Expression of StMYB1R-1, a novel potato single MYB-like domain transcription factor, increases drought tolerance'. *Plant Physiol.* 155, 421–432. doi: 10.1104/pp.110. 163634

Stockhaus, J., Eckes, P., Rocha-Sosa, M., Schell, J., and Willmitzer, L. (1987). 'Analysis of cis-active sequences involved in the leaf-specific expression of a potato gene in transgenic plants'. *Proc. Natl. Acad. Sci.* 84, 7943–7947. doi: 10.1073/pnas.84.22.7943

Teo, C. J., Takahashi, K., Shimizu, K., Shimamoto, K., Taoka, K. I., et al. (2017). 'Potato tuber induction is regulated by interactions between components of a tuberigen complex'. *Plant Cell Physiol.* 58, 365–374.

Trapero-Mozos, A., Ducreux, L. J. M., Bita, C. E., Morris, W., Wise, C., Morris, J. A., et al. (2018). 'A reversible light - and genotype - dependent acquired thermotolerance response protects the potato plant from damage due to excessive temperature'. *Planta* 247, 1377–1392. doi: 10.1007/s00425-018-2874-1

Trapero-Mozos, A., Morris, W. L., Ducreux, L. J. M., McLean, K., Stephens, J., Torrance, L., et al. (2018). 'Engineering heat tolerance in potato by temperature-dependent expression of a specific allele of HEAT-SHOCK COGNATE 70'. *Plant Biotechnol. J.* 16, 197–207. doi: 10.1111/pbi.12760

Viola, R., Pelloux, J., van der Ploeg, A., Gillespie, T., Marquis, N., Roberts, A. R., et al. (2007). 'Symplastic connection is required for bud outgrowth following dormancy in potato (Solanum tuberosum L.) tubers'. *Plant Cell Environ.* 30, 973–983. doi: 10.1111/j.1365-3040.2007.01692.x

Weber, E., Engler, C., Gruetzner, R., Werner, S., Marillonnet, S., et al. (2011). 'A modular cloning system for standardized assembly of multigene constructs'. *PLoS One* 6:e16765. doi: 10.1371/journal.pone.0016765

Werner, S., Engler, C., Weber, E., Gruetzner, R., and Marillonnet, S. (2012). 'Fast track assembly of multigene constructs using golden gate cloning and the MoClo system'. *Bioengin. Bugs* 3, 38–43. doi: 10.4161/bbug.3.1.18223

Conflict of Interest: The authors declare that the research was conducted in the absence of any commercial or financial relationships that could be construed as a potential conflict of interest.

frontiers in Plant Science

ORIGINAL RESEARCH
published: 07 April 2021
doi: 10.3389/fpls.2021.633957

Variation for Composition and Quality in a Collection of the Resilient Mediterranean 'de penjar' Long Shelf-Life Tomato Under High and Low N Fertilization Levels

Elena Rosa-Martínez[1], Ana M. Adalid[1], Luis E. Alvarado[1], Resurrección Burguet[1], María D. García-Martínez[1], Leandro Pereira-Dias[1], Cristina Casanova[1], Elena Soler[1], María R. Figàs[1], Mariola Plazas[2], Jaime Prohens[1] and Salvador Soler[1]*

[1] *Instituto de Conservación y Mejora de la Agrodiversidad Valenciana, Universitat Politècnica de València, Valencia, Spain,* [2] *Meridiem Seeds S.L., Torre-Pacheco, Spain*

OPEN ACCESS

Edited by:
Amalia Barone,
University of Naples Federico II, Italy

Reviewed by:
Miquel À. Conesa,
University of the Balearic Islands, Spain
Fernando Carrari,
Consejo Nacional de Investigaciones Científicas y Técnicas (CONICET), Argentina

***Correspondence:**
Elena Rosa-Martínez
elromar@etsia.upv.es

Specialty section:
This article was submitted to Plant Metabolism and Chemodiversity, a section of the journal Frontiers in Plant Science

Received: *26 November 2020*
Accepted: *25 February 2021*
Published: *07 April 2021*

Citation:
Rosa-Martínez E, Adalid AM, Alvarado LE, Burguet R, García-Martínez MD, Pereira-Dias L, Casanova C, Soler E, Figàs MR, Plazas M, Prohens J and Soler S (2021) Variation for Composition and Quality in a Collection of the Resilient Mediterranean 'de penjar' Long Shelf-Life Tomato Under High and Low N Fertilization Levels. Front. Plant Sci. 12:633957. doi: 10.3389/fpls.2021.633957

The 'de penjar' tomato (*Solanum lycopersicum* L.) is a group of local varieties from the Spanish Mediterranean region carrying the *alc* mutation, which provides long shelf-life. Their evolution under low-input management practices has led to the selection of resilient genotypes to adverse conditions. Here we present the first evaluation on nutritional fruit composition of a collection of 44 varieties of 'de penjar' tomato under two N fertilization levels, provided by doses of manure equivalent to 162 kg N ha^{-1} in the high N treatment and 49 kg N ha^{-1} in the low N treatment. Twenty-seven fruit composition and quality traits, as well as plant yield and SPAD value, were evaluated. A large variation was observed, with lycopene being the composition trait with the highest relative range of variation (over 4-fold) under both N treatments, and significant differences among varieties were detected for all traits. While yield and most quality traits were not affected by the reduction in N fertilization, fruits from the low N treatment had, on average, higher values for hue (5.9%) and lower for fructose (−11.5%), glucose (−15.8%), and total sweetness index (−12.9%). In addition, lycopene and β-carotene presented a strongly significant genotype × N input interaction. Local varieties had higher values than commercial varieties for traits related to the ratio of sweetness to acidity and for vitamin C, which reinforces the appreciation for their organoleptic and nutritional quality. Highest-yielding varieties under both conditions displayed wide variation in the composition and quality profiles, which may allow the selection of specific ideotypes with high quality under low N conditions. These results revealed the potential of 'de penjar' varieties as a genetic resource in breeding for low N inputs and improving the organoleptic and nutritional tomato fruit quality.

Keywords: *Solanum lycopersicum*, plant breeding, local varieties, metabolites, taste, nutritional quality, abiotic stress

INTRODUCTION

Use of nitrogen (N)-enriched fertilizers has sharply escalated since the Green Revolution and has allowed dramatic increases in crop yields. However, severe impacts of overfertilization on the environment forced governments to implement sustainable agriculture policies (Zhang et al., 2015). The current environmental situation has prompted research studies to understand the effects of decreasing N inputs on different crops and the development of new varieties with improved N use efficiency. In general terms, N shortage is associated with a limitation of plant growth, photosynthetic rate, and synthesis and accumulation of bioactive compounds in fruits.

Tomato (*Solanum lycopersicum* L.) is the second vegetable in acreage after onions (FAOSTAT, 2020). Official recommendation of N inputs for intensive tomato cultivation varies between 200 and 240 kg N ha^{-1} in open field and between 380 and 410 kg N ha^{-1} in greenhouse (Ramos and Pomares, 2010). However, in the last decades, growers have been supplying nitrogen fertilizers well above those requirements (Thompson et al., 2007). Studies about the N supply effects on tomato showed that yield increased with N fertilization until a certain level, above which N had no longer a positive effect on yield, and even decreased it (Elia and Conversa, 2012; Djidonou et al., 2013). On the other hand, controversial responses to low N inputs are reported regarding tomato fruit quality (De Pascale et al., 2016; Truffault et al., 2019; Hernández et al., 2020).

Within the broad array of diversity of tomato types, there is a group of varieties (known as 'de penjar') which could potentially constitute a genetic resource in breeding for low N inputs. The 'de penjar' tomato is distinctively characterized by the presence of the *alc* mutation, which is associated with long shelf-life (LSL) of fruits, up to 6–12 months after harvest (Casals et al., 2012). The 'de penjar' (literally meaning "for hanging") type of tomato is mainly composed of local varieties preserved by generations of small farmers. Plants of 'de penjar' tomato generally produce round to flat, medium-sized fruits (30–90 g) with higher acidity and soluble solid content than standard tomato; however, the 'de penjar' varieties display a great variability in morphoagronomic and fruit quality characteristics, according to their traditional area of cultivation and to their uses (Cebolla-Cornejo et al., 2013; Casals et al., 2015; Figàs et al., 2015). Historically, 'de penjar' tomatoes have been cultivated in open field and under rain-fed, low-input conditions (Conesa et al., 2020). This has led to the selection for resilient varieties. The drought tolerance of LSL varieties is well documented and has been studied in recent years (Fullana-Pericàs et al., 2019). However, to our knowledge, scarce information is available on nitrogen fertilization for 'de penjar' or other LSL tomato cultivation. Some conducted trials indicate that N needs of 'de penjar' tomato are around 170–180 kg ha^{-1} (Seda and Muñoz, 2011), far below the N fertilization levels required for intensive standard tomato cultivation. Considering that 'de penjar' tomato has evolved under low input management practices and its already reported drought tolerance, we hypothesize that it could also show resilience against other abiotic stresses, such as low nitrogen supply.

In the present work, we evaluated a collection of 39 local varieties and 5 commercial varieties of 'de penjar' tomato, grown under two N levels, for agronomic and nutritional fruit composition traits. The aim was to provide information on the existing variability and behavior of these materials under different N supply conditions and to draw conclusions on the effect of the reduction of N inputs on their fruit quality and composition.

MATERIALS AND METHODS

Plant Material and Cultivation Conditions

A collection of 44 varieties of 'de penjar' tomato from different origins throughout the Valencian Region, located on the Spanish eastern coast, were evaluated under two N fertilization conditions. The collection was composed of 39 local varieties and 5 commercial varieties. Passport data on each of the accessions used is included as **Supplementary Table 1**.

Plants were grown during the spring–summer season of 2019 in two neighboring open-field plots located in Alcossebre (Castelló, Valencian Region; GPS coordinates of the field plots: 40°13′21′ N 0°15′51′ E). Both field plots were certified for organic farming and had followed the same agricultural practices for the last 5 years. Similar crop management practices and fertilization were applied to both field plots, except for the N fertilization level. One field plot was submitted to a N fertilization dose of 162 kg N ha^{-1}, equivalent to the levels commonly provided in the cultivation of 'de penjar' tomato (Seda and Muñoz, 2011). This dose has been considered in the present work as high N fertilization treatment (HN). For the other field plot, a dose of 49 kg of N ha^{-1} (i.e., 30.2% of the HN) was applied. This dose has been considered in the present work as low N fertilization treatment (LN). According to the organic farming practices that have been followed in the experiment, certified organic fertilizers were used. An organic basal dressing consisting of sheep manure (Organia, Fertinagro, Teruel, Spain) was applied in both field plots, shortly before cultivation, to provide the desired levels of N fertilization. Besides, the LN was supplemented with P (Fosfoser ECO GR, Mapryser, Barcelona, Spain) and K (Summum Líquido Quality 0-0-15, Fertinagro, Teruel, Spain), to equal the quantities of P and K present in the manure of the HN treatment (60 kg P_2O_5 ha^{-1} and 174 kg K_2O ha^{-1}). Both P and K fertilizers in the LN were supplied with the irrigation system. Since fertilization in the form of manure is characterized by a slow release of nutrients, the total P and K fertigation was distributed on a fortnight basis. Plantlets were transplanted at the five true-leaf stage on May 8th 2019. Plants in both field plots were irrigated throughout the entire cultivation period using an exudation irrigation system (16 mm; Poritex, Barcelona, Spain), for a total volume of 127 L $plant^{-1}$, so that the water would not be limiting in the evaluation, as confirmed by the lack of phenotypic symptoms of water stress and by the calculation of crop evapotranspiration (ETc) for 'de penjar' tomato. Immediately after the transplant, a watering of 5 L $plant^{-1}$ was applied. Subsequently, 4 L $plant^{-1}$ was applied weekly during the next 3 weeks, distributed in 2 days per week; from weeks 4 to 12, 6 L $plant^{-1}$ was applied weekly, distributed

in 3 days per week; from weeks 13 to 16, 8 L plant^{-1} was applied weekly, distributed in 4 days per week; finally, from weeks 17 to 20, plants were irrigated with 6 L plant^{-1} on a 2 days per week basis.

A total of six replicates per accession (i.e., three replicates per accession and N fertilization treatment, with two plants per replicate) were distributed in a completely randomized block design. Standard local practices for the 'de penjar' tomato were used during the experiment. Plants were staked with canes that were inclined so that a triangular structure was formed enabling a double-row distribution, with 3.00 and 0.80 m between wide and narrow rows, respectively. Plants were spaced at 0.35-m intervals within rows. Crop management included no pruning and manual weeding.

Climate conditions on the entire cultivation period are included as **Supplementary Figure 1**. Average temperature during the cultivation period varied between 15.6 and 28.1 °C. The month with the highest mean radiation was June, with 24.8 MJ m^{-2}, and this parameter declined during the following months, to an average of 16.6 MJ m^{-2} in September. Pluviometry was mostly concentrated on May 24th (12.1 mm), June 5th (14.3 mm), and at the end of the cultivation period, on August 20th (23.7 mm) and September 11th (21.3 mm), 13th (14.2 mm), and 21st (36.2 mm).

Soil Analysis

A soil physicochemical and composition analysis was performed in both field plots before the transplant and before applying the fertilization. Five samples consisting of five randomly selected spots per each of the two field plots were considered for soil analysis ($n = 5 \times 2 = 10$). For each sample, five fractions of soil surrounding the selected spot, between 10 and 30 cm deep, were extracted, homogenized, and left to dry at room temperature. A portion of 500 g of each dried homogenate was used for the analysis. Physical and chemical parameters were evaluated following the procedures described in Reeuwijk (2002): particle size analysis, pH in water and pH in potassium chloride, electrical conductivity, contents in total nitrogen, carbonates, and organic matter, carbon:nitrogen ratio, and mineral contents of available phosphorus, potassium, calcium, magnesium, iron, zinc, and copper. Soil texture for both fields was clay loam, with a composition of 41% sand, 36% clay, and 23% silt (Soil Science Division Staff, 2017). There were no significant differences between the two field plots for any of the soil physicochemical and composition parameters analyzed. According to the Spanish interpretation scales for each of the different elements evaluated (Yáñez Jiménez, 1989), the soil was slightly saline and had normal contents of total nitrogen and carbonates, high presence of organic matter, and moderately high carbon:nitrogen ratio. Data of soil characteristics is included as **Supplementary Table 2**.

Vegetative and Plant Trait Evaluation

A chlorophyll meter (SPAD-502, Minolta Camera Co., Osaka, Japan) was used to take SPAD values from upper fully expanded leaves. Four readings per replicate were taken. Readings were done according to manufacturer's instructions. Total number of fruits (fn) produced per replicate was counted during the harvest period (July 15th–September 30th). Fruits at the red stage of ripeness in both N fertilization treatments were harvested once a week during this period, so that the same number of harvests was made in the two treatments. Yield was calculated from the previous data and the average fruit weight (frw) per replicate as fn × frw. In addition, a resilience index, for each accession of the 44 evaluated and trait, was calculated as the ratio between the mean value under the low N treatment and the mean value under the high N treatment (LN/HN).

Fruit Trait Analysis

Five to ten fruits per replicate were brought to the laboratory to be processed for chemical composition analysis. The fruits were collected from the second to fifth truss at the red stage of ripeness. Before processing, five representative fruits per replicate were weighed in a digital scale in order to calculate the average fruit weight (frw). Units in which vegetative and fruit traits are expressed are included in **Table 1**.

Sample Preparation

Fruits were longitudinally cut in half, and seeds were eliminated. One half of cut tomatoes were bulked and squeezed with a domestic juice extractor for subsequent analysis of pH, titratable acidity, contents in soluble solids, reducing sugars (glucose, fructose), organic acids (citric, malic), and amino acids (glutamic, aspartic). For vitamin C analysis, 3% metaphosphoric acid (MPA) was added to the tomato liquid extract (1:1), in order to lower the pH for preventing degradation of ascorbic acid (Chebrolu et al., 2012). The other tomato halves were homogenized in liquid nitrogen using a domestic grinder, for subsequent freeze-drying. Homogenized tomato powder was used for analysis of contents in lycopene, β-carotene, total carotenoids, total nitrogen, and total carbon.

Soluble Solid Content, pH, and Titratable Acidity

Soluble solid content was measured using 0.5 mL of liquid extract with a HI 96801 digital refractometer (HANNA instruments, Padua, Italy). Titratable acidity and pH were measured with a PH-Matic 23 analyzer (Crison Instruments, Barcelona, Spain), from 10% (w/v) aqueous tomato extract, using NaOH 0.1 M as titrating reagent. From values of soluble solid content and titratable acidity, the ratio between those was calculated.

Sugars, Organic Acids, Vitamin C, and Amino Acids

Contents in reducing sugars, organic acids, vitamin C, and amino acids were measured by high-performance liquid chromatography (HPLC) using a 1220 Infinity LC System (Agilent Technologies, CA, United States) equipped with a binary pump, an automatic injector, and a UV detector. One aliquot of liquid extract per replicate was centrifuged for 5 min at 10,000 rpm, diluted with Milli-Q® water (1:1), and filtered through 0.22 μm PVDF MILLEX-GV filters (Merck Millipore, MA, United States). The same sample was used to perform the analysis of sugars and organic acids, following the method indicated in Fernández-Ruiz et al. (2004), with slight modifications. Glucose and fructose separations were performed

TABLE 1 | Vegetative and fruit traits evaluated in the 'de penjar' tomato collection, abbreviations used in tables and figures, and units in which they are expressed in the present work.

Trait	Abbreviation	Units
Vegetative and plant traits		
SPAD value	spad	–
Yield	y	kg plant^{-1}
Fruit traits		
Fruit mean weight	frw	g
Lightness (color coordinates)	L	–
Chroma (color coordinates)	chroma	–
Hue (color coordinates)	hue	°
Fruit nitrogen content	Nf	g kg^{-1} dm[1]
Fruit carbon content	Cf	g kg^{-1} dm
pH	pH	–
Soluble solid content	ssc	%
Titratable acidity	ta	%
Citric acid content	cit	g kg^{-1} fw[2]
Malic acid content	mal	g kg^{-1} fw
Total acid (citric + malic) content	tacid	g kg^{-1} fw
Citric:malic acid ratio	citmalr	–
Fructose content	fru	g kg^{-1} fw
Glucose content	glu	g kg^{-1} fw
Total sugar (fructose + glucose) content	tsug	g kg^{-1} fw
Fructose:glucose ratio	fruglur	–
Total sweetness index	tsi	–
Soluble solid content:titratable acidity ratio	ssctar	–
Total sugar:total acid ratio	tsugtacidr	–
Total sweetness index:titratable acidity ratio	tsitar	–
Vitamin C (ascorbic + dehydroascorbic) content	vitc	g kg^{-1} fw
Lycopene content	lyc	mg kg^{-1} fw
β-Carotene content	bcar	mg kg^{-1} fw
Total carotenoid content	tcar	mg kg^{-1} fw
Glutamic acid content	gluta	g kg^{-1} fw
Aspartic acid content	aspa	g kg^{-1} fw

[1] *dm: dry matter.*
[2] *fw: fresh weight.*

using a Luna® Omega SUGAR column (3 μm; 150 × 4.6 mm; Phenomenex, CA, United States) and a refractive index detector (350 RI detector, Varian, CA, United States) coupled to the HPLC system. The mobile phase consisted of solvent A (ACN 100%) and solvent B (water). The gradient was isocratic 75% A: 25% B, and the flow rate was 1 mL min^{-1}. Citric and malic acids were separated using a Rezex ROA-Organic Acid H+ (8%) column (150 × 7.8 mm; Phenomenex) and detected by HPLC-UV at 210 nm. The mobile phase consisted of an isocratic gradient of 100% 1 mM H_2SO_4, and the flow rate was 0.5 mL min^{-1}.

From the values of contents in fructose, glucose, citric and malic acids, total sugar content and total acid content were calculated as fructose + glucose and citric acid + malic acid, respectively. In addition, the ratios fructose:glucose, citric:malic, and total sugars:total acids were determined. Total sweetness index was also calculated as (Beckles, 2012) (0.76 × [glucose]) + (1.50 × [fructose]) and used for also determining the ratio between total sweetness index and titratable acidity.

For extraction of vitamin C, one aliquot of liquid tomato extract in 3% MPA per replicate was cold centrifuged and filtered through 0.22 μm PVDF filters. In order to quantify vitamin C as the sum of ascorbic (AA) and dehydroascorbic (DHA) acids, the DHA present in each sample was reduced to AA adding 5 mM tris(2-carboxyethyl)phosphine hydrochloride (TCEP) in 1:1 proportion. The AA peak was subsequently detected and quantified by HPLC-UV at 254 nm using a Brisa "LC^2" C18 column (3 μm; 150 × 4.6 mm; Teknokroma, Barcelona, Spain), following the method described in Chebrolu et al. (2012).

Determination of glutamic and aspartic acid contents was carried out using liquid tomato homogenate. After a previous derivatization with 30 mM 2,4-dinitro-1-fluorobenzene (DNFB) reagent at moderate basic pH and 60 °C, peak detection and analysis by reversed-phase HPLC-UV at 363 nm were performed as described by Agius et al. (2018).

Carotenoids

Lycopene, β-carotene, and total carotenoids were extracted using 30 mg of freeze-dried powdered material per replicate, which was incubated with ethanol:hexane 4:3 (v/v) in the darkness and shaken at 200 rpm for 1 h. Subsequently, carotenoids were quantified from UV/V spectrophotometric absorbance values at 452, 485, and 510 nm of the previously separated hexane phase, using the following equations (Zscheile and Porter, 1947):

$$\text{lycopene} = \frac{\text{Abs}_{510} \times 537 \times 2.7}{\text{weight} \times 172} \times 100$$

$$\beta\text{-carotene} = \frac{[\text{Abs}_{452} - (\text{Abs}_{510} \times 0.9285)] \times 533.85 \times 2.7}{\text{weight} \times 139} \times 100$$

$$\text{total carotenoids} = \frac{\text{Abs}_{485} \times 2.7}{\text{weight} \times 181} \times 100$$

Total Nitrogen and Carbon

A sample of 0.5 g of freeze-dried and powdered material per replicate was used for N and C determination in fruit. The analysis was based on a complete combustion of the sample at 950 °C in the presence of oxygen, using a TruSpec CN elemental analyzer (Leco, MI, United States) (Gazulla et al., 2012).

Data Analysis

A bifactorial (genotype and N treatment) analysis of variance was performed for every trait studied for the evaluation of differences among the accessions (genotypes, G), between N treatments (N), and for the occurrence of G × N interactions (Gomez and Gomez, 1984). In the ANOVA, two levels were established for the N treatment factor, corresponding to HN and LN, whereas levels of the genotype factor were the 44 accessions of the collection. Data from the six replicates per accession were used, making a total number of cases, n = 264. The block effect due to the experimental design was removed to evaluate the effect of the two factors and the interaction (Gomez and Gomez, 1984). Mean values and range for all traits were calculated from accession means for both LN (n = 44) and HN (n = 44). Comparisons of average differences between the sets of local (n = 39) and

commercial ($n = 5$) varieties were assessed with a *t*-student test at $p < 0.05$ using R statistical software v4.0.2 (R Core Team, 2013). Only traits with significant differences between both groups in the two environments were considered as displaying a stable significant difference.

A principal component analysis (PCA) was performed using pairwise Euclidean distances among accession means for each N treatment and for all the traits. PCA loading and score plots were drawn using R package *ggplot2* (Wickham, 2016). Prediction ellipses for LN and HN with a 95% level of confidence were added to the PCA score plot. Phenotypic and environmental correlations among traits were calculated from accession means and residuals, respectively, using the R packages *psych* (Revelle, 2018) and *corrplot* (Wei et al., 2017). Pearson linear coefficients of correlation (r) were calculated between pairs of traits, and significance of correlations was evaluated with the Bonferroni test at $p < 0.05$ (Hochberg, 1988).

Genetic Parameters

The genotypic (σ^2_G) and phenotypic variances ($\sigma^2_P = \sigma^2_G + \sigma^2_N + \sigma^2_{G \times N}$) of each trait were obtained from the mean squares (MS) of the genotype, G × N interaction, and residuals of the ANOVA performed, in order to estimate broad-sense heritability (H^2) using the formula $H^2 = \sigma_G{}^2/\sigma_P{}^2$ (Wricke and Weber, 2010). Standard errors (SE) of the heritabilities were calculated by the Delta method, using the following formulas (Nyquist, 1991):

$$SE\left(H^2\right) = H^2 \times \sqrt{\frac{\sigma_a^2}{A^2} + \frac{\sigma_b^2}{B^2} - 2 \times \frac{\mathrm{cov}\,(A, B)}{A \times B}}$$

$$A = \frac{M_1 - M_2}{\delta \times r}$$

$$B = \frac{M_1 - M_2}{\delta \times r} + \frac{M_2 - M_3}{r} + M_3$$

$$\sigma_a^2 = \left(\frac{1}{\delta \times r}\right)^2 \times \left[\frac{2 \times M_1^2}{df_{M1} + 2} + \frac{2 \times M_2^2}{df_{M2} + 2}\right]$$

$$\sigma_b^2 = \left(\frac{1}{\delta \times r}\right)^2 \times \frac{2 \times M_1^2}{df_{M1} + 2} + \left(\frac{\delta - 1}{\delta \times r}\right) \times \frac{2 \times M_2^2}{df_{M2} + 2} + \left(1 - \frac{1}{r}\right)^2 \times \frac{2 \times M_3^2}{df_{M3} + 2}$$

where M_1, M_2, and M_3 are the MS for genotype, G × N interaction, and residuals, respectively; df_{M1}, df_{M2}, and df_{M3} are the degrees of freedom on which M_1, M_2, and M_3 were calculated, respectively, δ is the number of treatments, and r is the number of replications.

The coefficients of genetic (CV_G) and phenotypic (CV_P) variation were estimated from the corresponding variance components (σ^2_G and σ^2_P) and the mean value of the trait (μ) as (Wricke and Weber, 2010)

$$CV = \frac{\sqrt{\sigma^2}}{\mu} \times 100$$

and their SE were calculated as

$$SE\,(CV) = \frac{CV \times \sqrt{1 + 2 \times (CV/100)^2}}{\sqrt{2 \times N}}$$

where N is the total number of individuals used in the CV estimation.

RESULTS

Analysis of Variance

Analysis of variance (ANOVA) revealed a significant effect of the genotype for all traits. For N treatment, no significant effect was observed, except for hue; contents of fructose, glucose, and

TABLE 2 | F-ratio values for genotype (G), nitrogen treatment (N; low or high), and genotype per nitrogen treatment interaction (G × N) of each trait evaluated in the present study, obtained from the bifactorial ANOVA, which considered the 44 'de penjar' accessions of the collection with three replicates per N treatment ($n = 44 \times 2 \times 3 = 264$).

Traits	Genotype (G)	N treatment (N)	G × N interaction
Vegetative and plant traits			
spad	4.15***	0.15	1.23
y	3.64***	0.66	0.83
Fruit traits			
frw	19.04***	2.13	0.82
L	4.16***	1.04	1.64*
chroma	5.80***	0.00	1.17
hue	4.70***	16.86*	1.11
Nf	3.25***	3.77	0.94
Cf	3.32***	4.87	1.54*
pH	2.27***	0.42	1.32
ssc	4.68***	0.90	0.91
ta	5.04***	0.02	0.91
cit	5.37***	0.54	1.28
mal	10.44***	0.96	1.33
tacid	4.51***	0.45	1.33
citmalr	11.31***	1.40	1.10
fru	3.83***	53.25**	1.25
glu	4.40***	10.90*	1.35
tsug	4.19***	23.70**	1.27
fruglur	3.93***	1.39	2.19***
tsi	4.09***	32.16**	1.25
ssctar	4.64***	0.01	0.93
tsugtacidr	3.78***	2.40	0.88
tsitar	4.83***	1.19	0.96
vitc	2.39***	0.91	0.91
lyc	1.80**	0.40	2.23***
bcar	2.69***	2.40	2.04***
tcar	1.92**	0.71	2.25***
gluta	2.29***	0.23	1.22
aspa	2.66***	0.78	1.03

The full name of each trait abbreviation in the first column can be found in ***Table 1****. Significant differences are indicated with * ($p < 0.05$), ** ($p < 0.01$), or *** ($p < 0.001$).*

total sugars; and total sweetness index (**Table 2**). For these five traits, F-ratio values were much greater than those of the genotype factor. However, no significant effect of the interaction G × N was detected for any of those traits. On the other hand, a significant G × N interaction was observed for lightness of color, fructose:glucose ratio, contents in lycopene and β-carotene, total carotenoids, and total carbon (**Table 2**). Except for lycopene and total carotenoid content, F-ratio values of the G × N interaction were lower than those of the genotype effect. In the cases of traits with a significant interaction G × N, it is worth mentioning the particular accessions that showed a significant difference between HN and LN and how the latter affected those traits. Therefore, for lightness of color, only three out of 44 accessions showed a significantly increased mean value under LN (MO1, MO2, TE1), among which MO2 had the largest increase (20%). For the fructose:glucose ratio, the same effect under LN was observed on three accessions (MO2, SN2, TO1), while AC1 and FA2 showed a significantly lower average fructose:glucose ratio. SN2 was the accession with the greatest difference between N treatments for the fructose:glucose ratio, which showed an increased mean value by 36% under LN. In the case of lycopene content, as well as for total carotenoids, LN significantly increased the mean values of three accessions (BL1, MT1, TO1), while it had the opposite effect on six accessions (AY1, LA2, LL2, TA1, VH2, VI1). For both lycopene and total carotenoid content, the largest difference between N treatments was found for BL1 (63% and 60% of increase under LN, respectively). Likewise, AC1, BL1, MT1, and TO1 showed a higher average β-carotene content under LN, and FI1, LA2, and VI1 had lower mean values of this trait under the same treatment. TO1 had the greatest percentage of increase for average β-carotene content under LN (45%), while VI1 had the highest percentage of decrease under the same conditions (47%). Finally, total carbon content was, in average, significantly higher under LN in four out of the 44 accessions evaluated (C4, C5, CO1, TO1). In this case, the commercial variety C5 had the highest percentage of increase (5%). Data of average values per accession and N treatment for each trait analyzed are included as **Supplementary Table 3**. For none of the traits where the G × N interaction was significant, a significant effect of N treatment was observed (**Table 2**).

Mean values with their standard difference and range, as well as the paired difference between mean values in high N and low N treatment, of the whole 'de penjar' tomato collection (n = 44) under each N treatment, are shown in **Table 3**. Average yield and fruit weight were, respectively, 2.20 kg plant^{-1} and 72.7 g (LN) and 1.98 kg plant^{-1} and 70.4 g (HN), while for total N and C, mean values were 21.1 g kg^{-1} of dry matter (dm) and 408.0 g kg^{-1} dm (LN), and 19.9 g kg^{-1} dm and 405.8 g kg^{-1} dm (HN), respectively (**Table 3**). Average soluble solid content was 5.52% (LN) and 5.69% (HN), while pH and titratable acidity mean values were 4.13 and 0.57% (LN) and 4.11 and 0.58% (HN), respectively. Average values for total organic acids and reducing sugars were, respectively, 8.03 g kg^{-1} of fresh weight (fw) and 34.30 g kg^{-1} fw (LN) and 7.62 g kg^{-1} fw and 39.65 g kg^{-1} fw (HN). Mean values of the fructose:glucose ratio were slightly above 1.0 under both treatments (1.26 for LN and 1.19 for HN), while the citric:malic acid ratio was over 5.0. Regarding ratios between sugar and acid parameters (soluble solids content:titratable acidity, total sugars:total acids, and total sweetness index:titratable acidity), mean values were a great deal above 1.0 in both treatments with values of 10.54, 4.64, and 7.68, respectively, for LN and 10.63, 5.57, and 8.63, respectively, for HN (**Table 3**).

When comparing significantly different average values between the N treatments, taking high N conditions as a reference, hue was significantly higher (5.6%) under low N conditions, while it was significantly lower for contents in fructose (−11.5%), glucose (−15.8%), total sugars (−13.5%), and total sweetness index (−12.9%).

Considerable variation was found among the 44 varieties under both conditions for the traits evaluated. Representative fruits of the 'de penjar' collection studied are pictured in **Figure 1**. In this way, the traits with a larger value for the relative range of variation (maximum/minimum values) for LN conditions were fruit weight (4.57-fold), lycopene content (4.36-fold), and glutamic acid content (4.05-fold). Under HN, fruit weight (4.59-fold) and lycopene content (4.34-fold) were also the traits with the highest relative range of variation, followed by total carotenoid content (3.83-fold). On the other side, the traits with the lowest values for the relative range of variation were total C content (1.04-fold for LN and 1.07-fold for HN), pH (1.21-fold for LN and 1.18-fold for HN), and lightness of color (1.35-fold for LN and 1.29-fold for HN). For all traits, the ranges of variation between both N conditions based on the accession means overlapped to a large extent (**Table 3**).

Differences Between Varietal Types

The groups of local varieties (n = 39) on one side and commercial varieties (n = 5) on the other did not display significant differences ($p < 0.05$) between them under both LN and HN conditions for most of the traits analyzed (**Table 4**). However, significant differences were found for ratios of both soluble solid content and total sweetness index with titratable acidity, and vitamin C content. For each of these traits, local varieties presented higher means than commercial varieties in both conditions. Thus, the average ratio between soluble solid content and titratable acidity for local varieties was 18.4% higher under LN and 30.0% under HN. The same occurred for the average ratio between total sweetness index and titratable acidity, with values being 22.0% (LN) and 28.8% (HN) higher in local varieties over commercial ones, as well as for vitamin C content, with the former displaying higher mean values by 25.0% (LN) and 17.2% (HN) (**Table 4**).

Genetic Parameters

Heritability in a broad sense (H^2), genetic and phenotypic coefficients of variation (CV_G and CV_P) for the traits studied are presented in **Table 5**. Considering both treatments and their interaction, fruit weight had the greatest H^2 with 0.76. Apart from that, only malic acid and citric:malic ratio showed a broad-sense heritability higher than 0.50. On the other hand, lycopene, β-carotene, and total carotenoid content had the lowest H^2. As expected, the coefficient of phenotypic variance was higher than the coefficient of genetic variance for all traits studied. The

TABLE 3 | Mean ± standard deviation (SD) and range, based on the accession averages, for the traits measured in the 'de penjar' tomato collection used in the present study in low- (LN) and high-nitrogen (HN) treatment ($n = 44 \times 2 = 88$), and mean of the paired difference HN – LN, based on the accession averages ($n = 44$).

	Low nitrogen ($n = 44$)		High nitrogen ($n = 44$)		Paired HN – LN ($n = 44$)
Traits	**Mean ± SD**	**Range**	**Mean ± SD**	**Range**	**Mean**
Vegetative and plant traits					
spad	49.64 ± 3.54	40.67–56.25	48.98 ± 5.41	36.38–60.90	−0.67
y (kg plant^{-1})	2.20 ± 0.47	0.96–3.18	1.98 ± 0.46	1.23–3.90	−0.22
Fruit traits					
frw (g)	72.7 ± 19.9	29.0–132.5	70.4 ± 20.3	29.3–134.6	−2.3
L	36.57 ± 2.95	32.01–43.29	35.50 ± 2.09	31.23–40.42	−1.07
chroma	21.50 ± 3.45	14.69–32.28	21.58 ± 3.28	15.30–33.23	0.08
hue (°)	40.00 ± 5.91	30.53–51.32	37.78 ± 4.19	29.27–46.11	−2.22*
Nf (g kg^{-1} dm)	21.1 ± 1.9	17.2–25.4	19.9 ± 2.2	14.6–26.6	−1.2
Cf (g kg^{-1} dm)	408.0 ± 3.1	402.3–416.3	405.8 ± 4.6	390.5–416.7	−2.26
pH	4.13 ± 0.17	3.83–4.63	4.11 ± 0.18	3.83–4.50	−0.02
ssc (%)	5.52 ± 0.57	4.28–6.58	5.69 ± 0.70	4.02–6.87	0.16
ta (%)	0.57 ± 0.13	0.34–0.96	0.58 ± 0.12	0.37–0.85	0.01
cit (g kg^{-1} fw)	6.73 ± 1.77	4.22–12.28	6.30 ± 1.62	4.31–12.66	−0.43
mal (g kg^{-1} fw)	1.30 ± 0.36	0.73–2.00	1.33 ± 0.33	0.83–2.36	0.03
tacid (g kg^{-1} fw)	8.03 ± 1.78	5.22–13.60	7.62 ± 1.60	5.55–13.98	−0.41
citmalr	5.71 ± 2.25	2.69–10.02	5.14 ± 1.99	2.75–9.44	−0.57
fru (g kg^{-1} fw)	18.83 ± 2.41	13.69–22.77	21.28 ± 2.46	16.31–27.50	2.45**
glu (g kg^{-1} fw)	15.47 ± 3.02	9.57–21.52	18.37 ± 3.06	10.99–24.93	2.90*
tsug (g kg^{-1} fw)	34.30 ± 5.17	24.27–42.87	39.65 ± 5.29	28.96–52.07	5.35**
fruglur	1.26 ± 0.18	1.01–1.88	1.19 ± 0.15	1.02–1.93	−0.06
tsi	4.00 ± 0.56	2.86–4.94	4.59 ± 0.58	3.43–5.97	0.59**
ssctar	10.54 ± 2.65	5.74–19.27	10.63 ± 2.38	6.84–16.41	0.09
tsugtacidr	4.64 ± 1.21	2.29–7.79	5.57 ± 1.15	3.11–8.70	0.92
tsitar	7.68 ± 2.14	4.14–14.40	8.63 ± 2.10	5.21–13.65	0.95
vitc (g kg^{-1} fw)	0.27 ± 0.04	0.15–0.39	0.29 ± 0.04	0.21–0.38	0.02
lyc (mg kg^{-1} fw)	7.99 ± 2.22	3.64–15.87	7.64 ± 2.84	3.34–14.50	−0.34
bcar (mg kg^{-1} fw)	3.45 ± 0.84	2.00–5.72	3.17 ± 0.80	1.96–5.15	−0.28
tcar (mg kg^{-1} fw)	15.41 ± 4.15	7.51–29.71	14.58 ± 5.04	6.79–26.01	−0.83
gluta (g kg^{-1} fw)	3.42 ± 1.08	1.73–7.01	3.83 ± 0.78	2.34–5.61	0.41
aspa (g kg^{-1} fw)	0.76 ± 0.21	0.33–1.33	0.90 ± 0.19	0.51–1.40	0.14

*The full name of each trait abbreviation in the first column is found in **Table 1**. Significant differences between LN and HN treatments are based on the results of the ANOVA (n = 264) and indicated with * ($p < 0.05$) and ** ($p < 0.01$).*

lowest percentages of CV_G were obtained for lycopene and total carotenoids, which, at the same time, had the highest values of CV_P, together with citric:malic acid ratio. The greatest values of CV_G were found for citric:malic acid ratio, fruit weight, and malic acid content. Finally, carbon content in fruit, pH, and lightness of color had the lowest values of CV_P.

Correlation Among Traits

Few significant ($p < 0.05$) phenotypic correlations were detected (**Figure 2**). In addition, the analysis did not reveal any significant correlation between SPAD, yield, or fruit weight on one side and fruit composition traits on the other. As for phenotypic correlations, fructose and glucose contents were positively and significantly correlated with each other ($r = 0.84$) and with total sugar content ($r = 0.95$ and 0.97, respectively), with total sweetness index ($r = 0.98$ and 0.94, respectively), and, with lower correlation coefficient values, with soluble solid content ($r = 0.73$ and 0.82, respectively). The same pattern was observed for correlations between citric acid content and citric:malic ratio ($r = 0.77$), total acid content ($r = 0.98$), or titratable acidity ($r = 0.80$). Citric acid content was also negatively correlated with total sugars:total acids ratio ($r = -0.75$). On the contrary, malic acid content was not significantly correlated with any of these traits. Different carotenoid contents were positively correlated with each other, with $r = 0.76$. Lycopene displayed higher correlation coefficient values than β-carotene to total carotenoids ($r = 0.99$ and 0.84, respectively) (**Figure 2**).

In the case of environmental correlations, the number of significant ones was higher than for phenotypic correlations (**Figure 2**). The same strong correlations found among traits in the phenotypic analysis were detected. Fruit weight and yield were environmentally correlated with $r = 0.61$. In the same way, a significant but slightly lower correlation was detected between vitamin C and traits related to sugar content,

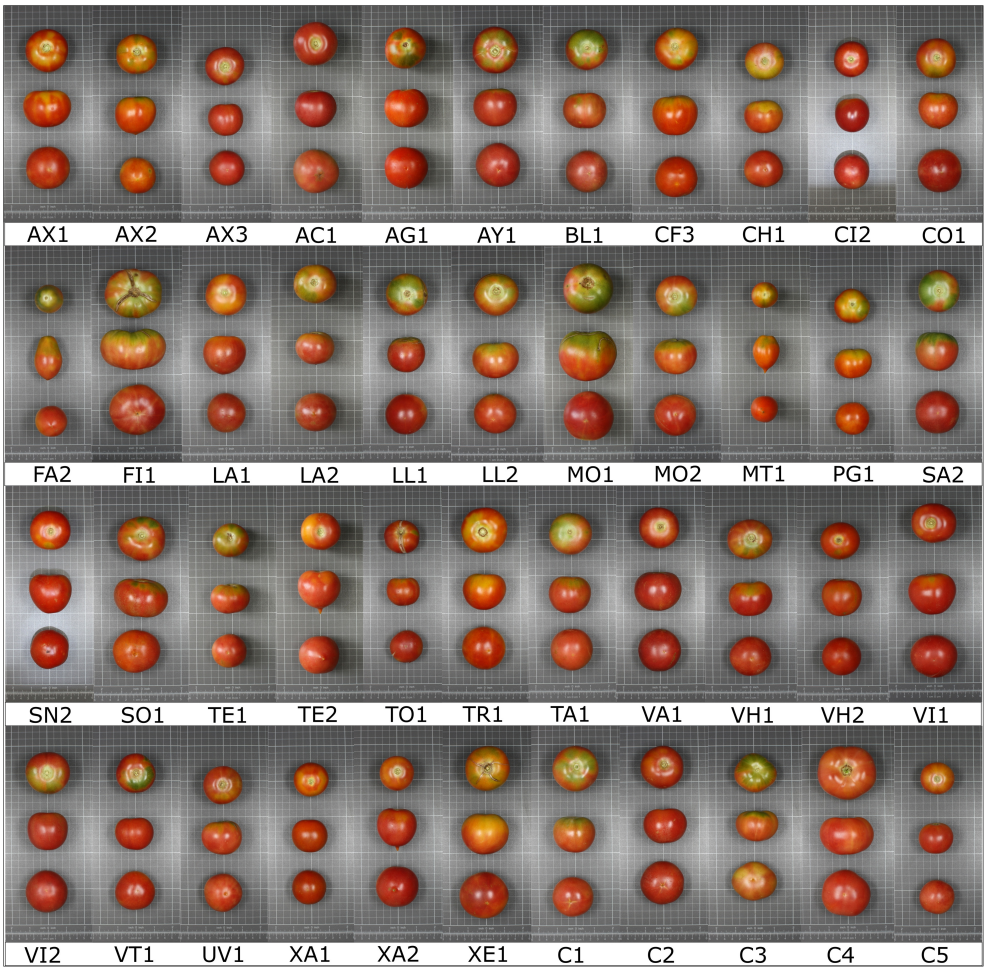

FIGURE 1 | Representative fruits of the 39 'de penjar' tomato local varieties and the five commercial varieties (accession name for each code is found in **Supplementary Table 1**) used for agronomic and composition characterization under two levels of nitrogen inputs. The grid cells in the pictures measure 1 × 1 cm.

with r values between 0.26 and 0.32. Vitamin C also had a significant and positive environmental correlation to aspartic and glutamic acid contents (r = 0.29 and 0.37, respectively). With respect to these amino acids, they were environmentally intercorrelated, with r = 0.79. Aspartic acid also presented a negative significant correlation to color parameters chroma (r = 0.26) and hue (r = −0.35), and positive, to vitamin C content (r = 0.29). Glutamic acid displayed significant positive environmental correlations to acidity and related traits, with r between 0.25 and 0.44, to vitamin C (r = 0.37) and lycopene contents (r = 0.24), but negative significant correlations to sugar:acid ratio-related traits (r = −0.28 to −0.40). Glucose content and total sugar:total acid ratio also showed negative environmental correlations to lycopene (r = −0.25 and −0.35, respectively) and total carotenoid content (r = −0.25 and −0.34, respectively) (**Figure 2**).

Principal Component Analysis

The first two principal components (PCs) of the PCA explained 40.5% of the total variation observed, with PC1 and PC2 accounting for 25.7% and 14.8% of the total variation, respectively. Total sugar:total acid ratio, total sweetness index:titratable acidity ratio, and glucose content were the traits displaying the highest positive correlation with PC1, while fructose:glucose ratio, citric acid, and total acid contents were the ones with the highest absolute negative values with PC1. On the other hand, titratable acidity and citric acid and total acid contents also displayed high positive correlations with PC2, whereas pH, soluble solid content:titratable acidity ratio, and yield were highly negatively correlated with PC2 (**Figure 3**).

The principal component analysis did not clearly separate the HN and LN treatments, although for the same variety, compared to the control, the projection corresponding to the LN treatment tended to display lower values for PC1 and PC2, which is associated with higher content of carotenoids, fructose:glucose ratio, hue, and slightly higher fruit carbon and nitrogen contents and yield, and associated with lower contents of sugars and slightly lower vitamin C (**Figure 3**).

It is noteworthy that a group of accessions under HN conditions (CH1, UV1, XA2, TE2, AX2, CO1, VI2, C1) plotted

TABLE 4 | Mean ± standard error (SE) and *t* value of the traits that showed a significant difference between local (L; *n* = 39) and commercial (C; *n* = 5) varieties used in the present study, for both nitrogen treatments.

	Low nitrogen			High nitrogen		
	Mean ± SE		*t* value	Mean ± SE		*t* value
Traits	**L (*n* = 39)**	**C (*n* = 5)**		**L (*n* = 39)**	**C (*n* = 5)**	
ssctar	10.76 ± 0.44	8.78 ± 0.25	3.96***	11.00 ± 0.36	7.70 ± 0.26	7.37***
tsitar	7.87 ± 0.35	6.14 ± 0.48	2.92*	8.92 ± 0.33	6.35 ± 0.24	6.36***
vitc (g kg^{-1} fw)	0.28 ± 0.01	0.21 ± 0.02	2.78*	0.29 ± 0.01	0.24 ± 0.02	3.06*

The full name of each trait abbreviation in the first column is found in ***Table 1****. Significant differences between varietal type are indicated with * ($p < 0.05$), ** ($p < 0.01$), *** ($p < 0.001$).*

TABLE 5 | Broad sense heritability estimates (H^2), genotypic and phenotypic variance coefficient (CV_G and CV_P, respectively), and their standard errors of the traits analyzed in our 'de penjar' tomato collection taking into account the two nitrogen conditions.

Traits	H^2 ± SE	CV_G (%) ± SE	CV_P (%) ± SE
Vegetative and plant traits			
spad	0.31 ± 0.08	6.82 ± 0.73	12.23 ± 1.32
y	0.33 ± 0.07	17.70 ± 1.95	30.77 ± 3.58
Fruit traits			
frw	0.76 ± 0.04	26.90 ± 3.07	30.78 ± 3.58
L	0.26 ± 0.08	4.68 ± 0.50	9.23 ± 0.99
chroma	0.42 ± 0.07	12.74 ± 1.38	19.60 ± 2.17
hue	0.37 ± 0.07	10.36 ± 1.12	17.12 ± 1.88
Nf	0.30 ± 0.07	7.51 ± 0.80	14.14 ± 1.54
Cf	0.40 ± 0.15	0.58 ± 0.06	1.29 ± 0.14
pH	0.12 ± 0.07	2.22 ± 0.24	6.28 ± 0.67
ssc	0.39 ± 0.07	9.36 ± 1.01	14.94 ± 1.63
ta	0.41 ± 0.07	18.21 ± 2.00	28.27 ± 3.25
cit	0.38 ± 0.08	20.44 ± 2.27	32.99 ± 3.88
mal	0.58 ± 0.07	23.19 ± 2.60	30.52 ± 3.54
tacid	0.32 ± 0.08	15.96 ± 1.74	28.08 ± 3.22
citmalr	0.62 ± 0.06	35.53 ± 4.24	45.05 ± 5.69
fru	0.28 ± 0.07	8.60 ± 0.92	16.13 ± 1.76
glu	0.31 ± 0.08	13.09 ± 1.42	23.39 ± 2.63
tsug	0.31 ± 0.08	10.36 ± 1.12	18.64 ± 2.05
fruglur	0.17 ± 0.09	7.24 ± 0.78	17.46 ± 1.92
tsi	0.28 ± 0.07	9.69 ± 1.04	17.59 ± 1.93
ssctar	0.39 ± 0.07	19.43 ± 2.15	31.20 ± 3.64
tsugtacidr	0.33 ± 0.07	18.24 ± 2.01	31.54 ± 3.68
tsitar	0.20 ± 0.04	21.29 ± 2.37	33.85 ± 4.00
vitc	0.20 ± 0.06	9.48 ± 1.02	21.10 ± 2.35
lyc	0.00 ± 0.07	0.00 ± 0.00	46.20 ± 5.88
bcar	0.07 ± 0.08	9.05 ± 0.97	33.22 ± 3.91
tcar	0.00 ± 0.08	0.00 ± 0.00	43.08 ± 5.38
gluta	0.14 ± 0.07	14.34 ± 1.56	37.97 ± 4.59
aspa	0.21 ± 0.07	16.26 ± 1.78	35.31 ± 4.21

The full name of each trait abbreviation in the first column is found in ***Table 1****.*

in the second quadrant of the PCA (positive values for PC1 and PC2), being associated with higher total sweetness index, total and individual contents of sugars, soluble solids and their ratios with total acids and titratable acidity, and vitamin C and glutamic and aspartic acid contents. Another group to highlight is that of the accessions AX1, FI1, TR1, C4, MO2, and CF3 under LN conditions, which plotted in the third quadrant (negative values of PC1 and PC2), which are associated with brighter fruits with external color tending to orange, higher fructose:glucose ratio, and β-carotene content, in addition to high yield. Besides that, there are some accessions that appear outside the 95% confidence ellipses. In this respect, UV1, TE1, and TO1 under LN conditions and VI1 under HN produced the most acidic tomatoes. XE1 under LN conditions also remained outside the ellipse, presenting high sugar contents, resulting in greater ratios of total sugars:total acids, soluble solid content:titratable acidity, and total sweetness index:titratable acidity. Finally, some accessions (AX3, AC1, TR1, XA1, XA2, XE1, and C3) seemed to perform similarly under LN and HN conditions as they appeared very close to each other according to PC1 and PC2 (**Figure 3**).

Characteristics of Highest-Yielding Varieties

Table 6 shows the ranking of the 10 best 'de penjar' tomato accessions evaluated in the present work for yield, with their performance and ranking position within the entire collection for the most important composition traits, under both treatments separately. The ranking of the top 10 'de penjar' tomato accessions of the collection for resilience in yield, with their resilience index and ranking position within the entire collection for the most important composition traits, is displayed in **Table 7**.

Several local varieties showed comparable or even better performance in yield and other composition traits than commercial varieties, both in LN and HN. As far as commercial varieties are concerned, in LN conditions, C2, C1, and C3 ranked fifth (2.89 kg $plant^{-1}$), sixth (2.65 kg $plant^{-1}$), and ninth (2.59 kg $plant^{-1}$) in yield, while only C3 and C4 were among the 10 best-yielding varieties in HN with 2.50 kg $plant^{-1}$ (5th place) and 2.24 kg $plant^{-1}$ (8th place) (**Table 6**). It is worth noting that, in addition, C2 and C1 ranked second (1.55) and fourth (1.44), respectively, in terms of yield resilience (**Table 7**). Regarding local varieties, TR1, MT1, and FI1 stood out as the three best-yielding varieties in LN (3.18, 3.13, and 3.06 kg $plant^{-1}$, respectively), while FI1, MO1, and AX1 were the highest yielding in HN (3.90, 2.89, and 2.77 kg $plant^{-1}$, respectively) (**Table 6**). None of these accessions were among the top 10 in resilience, although MO2 and CO1, which appeared among the 10 best accessions for yield

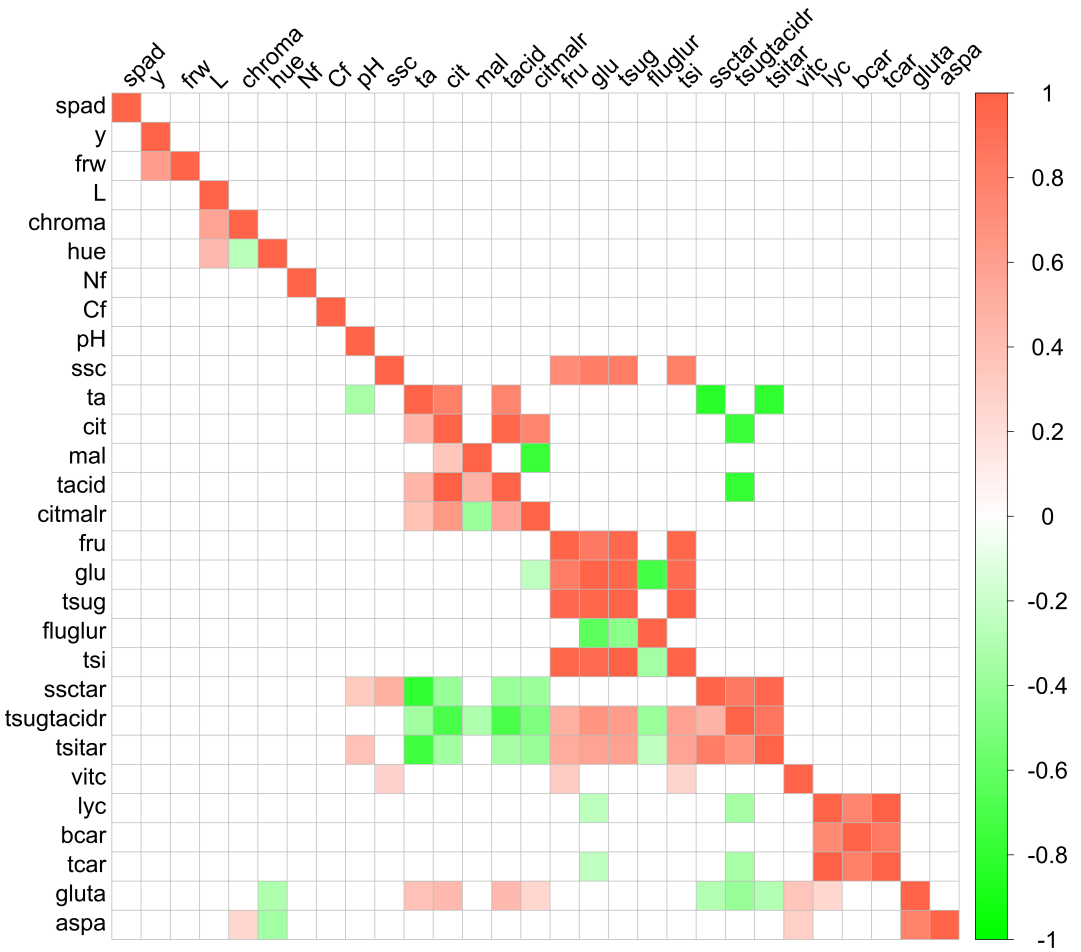

FIGURE 2 | Correlogram among traits evaluated in the 'de penjar' tomato collection. Phenotypic correlations are shown above the diagonal; environmental correlations below the diagonal. Only significant correlations at $p < 0.05$ according to the Bonferroni test are displayed. Green and red colors correspond to negative and positive correlations, respectively. The full name of each trait abbreviation is found in **Table 1**.

in LN, ranked third (1.45) and tenth (1.29), respectively, for yield resilience (**Table 7**). When considering the rest of traits, there is a wide variation among the two sets of 10 highest-yielding accessions. Among them, FI1 ranked first in both yield and fruit weight (134.6 g) in HN. Contrarily, MT1, with the lowest fruit mean weight in the whole collection (29.0 g in LN and 29.3 g in HN), appeared as the second and sixth best-yielding variety in LN (3.13 kg plant^{-1}) and HN (2.48 kg plant^{-1}), respectively (**Table 6**). Taking into account the average content of N in fruit, the local variety AX1 ranked third under both LN (23.9 g kg^{-1} dm) and HN (22.5 g kg^{-1} dm) (**Table 6**). Regarding sweetness, it is worth mentioning the local variety XE1, which presented an outstanding average in total sugar content (52.07 g kg^{-1} fw), ranking first, under HN. Furthermore, it also showed the highest average total sugar:total acid ratio under the same conditions (8.70). On the other hand, MO2, FI1, and C3 were among the top 10 varieties in fructose:glucose ratio under LN with mean values of 1.61, 1.50, and 1.38, respectively, while AC1 and again FI1 and C3 had the highest mean values in HN (1.50, 1.33, and 1.31, respectively) (**Table 6**). In general, the 10 best-yielding varieties, under LN and HN, ranked in intermediate or low positions for both average total acid content and citric:malic ratio (**Table 6**). Regarding main antioxidants evaluated, MO1 was the accession with the greatest average content of vitamin C (0.38 g kg^{-1} fw) under HN, followed by XE1 (5th place; 0.33 g kg^{-1} fw). MT1 stood out for accumulating, in average, the highest concentrations of β-carotene (5.72 mg kg^{-1} fw) and the second highest of total carotenoids (25.39 mg kg^{-1} fw) in their fruits, under LN, while under HN, FI1 ranked first in β-carotene content (5.15 mg kg^{-1} fw) (**Table 6**). As for glutamic and aspartic acid contents, any of the local varieties in both sets of best-yielding varieties ranked above commercial varieties C1 under LN and C4 under HN. However, MT1 was placed within the top 10 positions for glutamic acid under HN (6th; 4.71 g kg^{-1} fw). Regarding aspartic acid, the same happened for AX1 (10th; 0.89 g kg^{-1} fw) and AC1 (6th; 1.10 g kg^{-1} fw) under LN and HN, respectively (**Table 6**).

When considering the average resilience indexes of the other traits for the top 10 accessions in yield resilience, it is worth mentioning some accessions of both local and

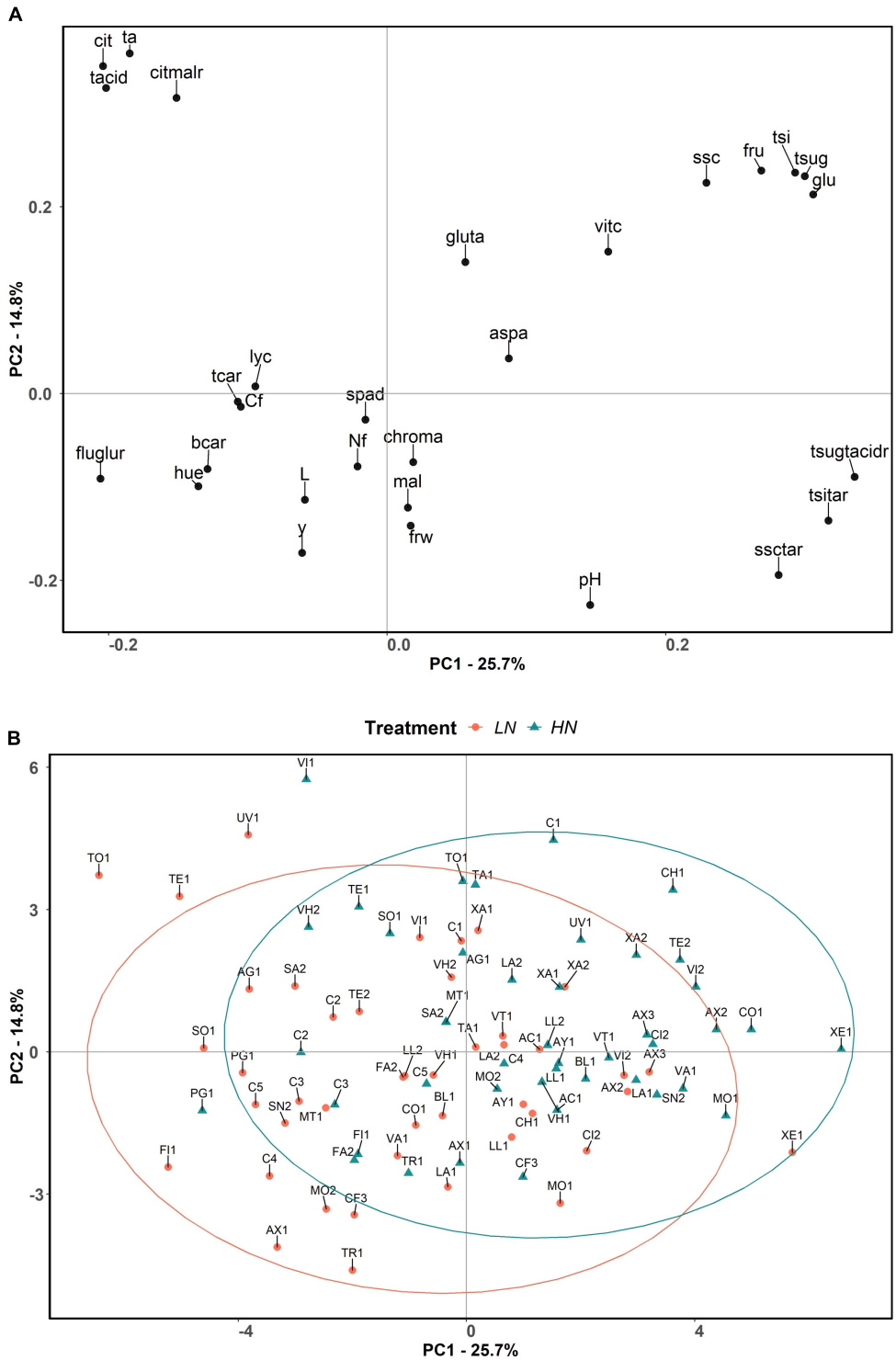

FIGURE 3 | Principal component analysis loading plot **(A)** and score plot **(B)** evaluated in the present study, based on the two first principal components of PCA. The first and second components account for 25.7 and 14.8% of the total variation, respectively. The accessions are represented by different symbols and color according to the treatment in which they were grown: orange colored circle for low nitrogen, and blue colored triangle for high nitrogen. Ellipses grouped the accessions for each treatment with a 95% confidence level. The full name of each trait abbreviation is found in **Table 1**. Accession name for each code can be found in **Supplementary Table 1**.

TABLE 6 | Ranking of the 10 best 'de penjar' tomato accessions evaluated in the present work for yield, with their performance and ranking position (in parentheses) within the entire collection for the most important composition traits, in both treatments separately.

	y (kg plant^{-1})	frw (g)	Nf (g kg^{-1} dm)	tsug (g kg^{-1} fw)	fruglur	tacid (g kg^{-1} fw)	citmalr	tsugtacidr	vitc (g kg^{-1} fw)	tcar (mg kg^{-1} fw)	bcar (mg kg^{-1} fw)	gluta (g kg^{-1} fw)	aspa (g kg^{-1} fw)
Low nitrogen													
TR1	3.18 (1)	84.5 (10)	20.4 (31)	29.32 (36)	1.24 (22)	6.09 (40)	3.58 (37)	5.05 (17)	0.24 (38)	16.88 (14)	4.59 (4)	2.08 (41)	0.56 (36)
MT1	3.13 (2)	29.0 (44)	19.8 (33)	37.09 (15)	1.25 (20)	7.38 (30)	3.30 (40)	5.14 (14)	0.25 (29)	25.39 (2)	5.72 (1)	2.95 (28)	0.58 (34)
FI1	3.06 (3)	132.5 (1)	20.7 (28)	25.66 (41)	1.50 (4)	10.32 (4)	4.24 (27)	2.49 (43)	0.29 (16)	14.36 (28)	3.33 (27)	2.54 (36)	0.33 (44)
MO2	2.90 (4)	86.5 (7)	18.2 (42)	31.35 (33)	1.61 (3)	7.41 (28)	3.17 (41)	4.31 (28)	0.27 (18)	17.96 (10)	3.82 (14)	3.24 (22)	0.71 (26)
C2	2.89 (5)	83.7 (12)	19.4 (35)	34.22 (24)	1.19 (26)	8.85 (11)	7.36 (13)	3.97 (32)	0.24 (32)	14.37 (27)	3.41 (24)	2.33 (38)	0.64 (30)
C1	2.65 (6)	85.1 (8)	20.4 (30)	42.68 (3)	1.14 (32)	8.49 (15)	7.53 (12)	5.07 (15)	0.24 (36)	15.52 (18)	3.56 (19)	3.98 (12)	0.89 (9)
MO1	2.62 (7)	117.8 (2)	22.9 (8)	35.47 (17)	1.01 (44)	5.73 (42)	6.07 (20)	6.20 (6)	0.25 (30)	12.58 (34)	3.44 (23)	3.53 (15)	0.75 (23)
CO1	2.62 (8)	76.7 (20)	21.1 (23)	33.79 (25)	1.10 (38)	6.87 (34)	6.14 (19)	5.03 (18)	0.24 (39)	12.64 (33)	2.62 (36)	2.87 (30)	0.85 (15)
C3	2.59 (9)	64.8 (29)	18.2 (41)	32.49 (30)	1.38 (7)	10.26 (5)	4.67 (22)	3.32 (37)	0.26 (28)	14.08 (32)	4.08 (8)	2.32 (39)	0.50 (40)
AX1	2.58 (10)	83.2 (13)	23.9 (3)	24.27 (44)	1.31 (12)	6.47 (36)	4.14 (32)	4.06 (31)	0.23 (40)	17.42 (12)	3.90 (13)	3.50 (16)	0.89 (10)
High nitrogen													
FI1	3.90 (1)	134.6 (1)	18.6 (33)	33.91 (37)	1.33 (5)	8.41 (12)	4.66 (20)	4.41 (37)	0.29 (24)	19.54 (8)	5.15 (1)	3.81 (19)	0.78 (33)
MO1	2.89 (2)	126.9 (2)	20.0 (21)	42.80 (12)	1.13 (29)	7.37 (20)	4.11 (25)	6.25 (12)	0.38 (1)	15.94 (17)	3.59 (16)	3.73 (25)	0.81 (30)
AX1	2.77 (3)	102.2 (3)	22.5 (3)	33.23 (38)	1.21 (18)	5.95 (40)	3.84 (27)	5.73 (21)	0.29 (22)	12.77 (28)	2.86 (28)	3.80 (20)	1.00 (12)
TR1	2.69 (4)	79.0 (12)	19.8 (23)	32.02 (40)	1.23 (13)	5.55 (44)	3.48 (34)	5.84 (18)	0.27 (32)	15.72 (18)	3.69 (14)	2.40 (43)	0.60 (41)
C3	2.50 (5)	59.1 (34)	14.6 (44)	31.99 (41)	1.31 (6)	7.94 (14)	4.18 (23)	4.29 (39)	0.21 (43)	11.29 (31)	2.97 (24)	2.43 (42)	0.58 (42)
MT1	2.48 (6)	29.3 (44)	16.6 (42)	38.86 (25)	1.18 (19)	7.03 (26)	4.34 (22)	5.57 (22)	0.21 (44)	12.48 (29)	3.24 (18)	4.71 (6)	0.93 (20)
XE1	2.35 (7)	97.7 (5)	21.2 (11)	52.07 (1)	1.08 (35)	5.93 (41)	3.66 (31)	8.70 (1)	0.33 (5)	17.56 (12)	3.88 (11)	3.74 (24)	0.84 (24)
C4	2.24 (8)	100.0 (4)	26.6 (1)	37.97 (27)	1.14 (26)	6.69 (31)	3.99 (26)	5.90 (17)	0.25 (38)	11.76 (30)	2.87 (27)	5.16 (3)	1.30 (2)
CF3	2.21 (9)	84.8 (8)	19.7 (24)	36.49 (35)	1.21 (16)	5.86 (42)	3.34 (37)	6.30 (11)	0.27 (34)	19.60 (7)	4.05 (6)	3.43 (29)	0.75 (36)
AC1	2.19 (10)	80.2 (11)	19.3 (29)	36.92 (32)	1.50 (2)	6.09 (39)	5.08 (19)	6.08 (14)	0.27 (33)	17.14 (13)	3.10 (21)	3.93 (18)	1.10 (6)

*The full name of each trait abbreviation in the first row is found in **Table 1**.*

TABLE 7 | Ranking of the 10 best 'de penjar' tomato accessions evaluated in the present work for resilience in yield, calculated as the ratio between mean value under low N treatment and mean value under high N treatment. Resilience and ranking position (in parentheses) within the entire collection of these 10 varieties for the most important composition traits are also shown.

	y	frw	Nf	tsug	fruglur	tacid	citmalr	tsugtacidr	vitc	tcar	bcar	gluta	aspa
Resilience index													
XA1	1.79 (1)	1.02 (24)	1.17 (7)	1.00 (8)	1.01 (31)	1.34 (3)	1.54 (2)	0.72 (31)	0.91 (26)	0.71 (37)	0.75 (37)	1.25 (7)	1.13 (7)
C2	1.55 (2)	1.19 (5)	0.93 (42)	1.12 (2)	1.02 (28)	1.13 (16)	1.02 (30)	0.95 (15)	1.12 (4)	1.82 (7)	1.40 (10)	0.89 (22)	0.75 (31)
MO2	1.45 (3)	1.23 (3)	0.96 (37)	0.83 (25)	1.29 (3)	1.05 (25)	1.02 (31)	0.80 (26)	0.97 (20)	1.16 (22)	0.96 (29)	0.78 (31)	0.86 (21)
C1	1.44 (4)	1.27 (2)	1.16 (12)	0.94 (12)	1.09 (16)	0.94 (34)	1.09 (23)	0.98 (12)	0.81 (35)	1.82 (8)	1.53 (7)	0.92 (20)	0.90 (19)
PG1	1.36 (5)	0.88 (41)	0.95 (40)	1.09 (3)	1.01 (30)	0.98 (33)	0.98 (33)	1.06 (5)	1.07 (10)	0.77 (35)	0.95 (31)	0.81 (29)	0.81 (27)
SO1	1.32 (6)	1.17 (6)	0.94 (41)	0.72 (41)	1.14 (9)	0.99 (31)	1.12 (17)	0.76 (30)	0.92 (25)	1.70 (9)	1.13 (23)	0.88 (24)	0.95 (13)
VI2	1.32 (7)	1.10 (13)	1.06 (23)	0.92 (15)	1.09 (17)	1.00 (30)	1.29 (7)	0.86 (22)	0.82 (34)	1.07 (25)	1.16 (22)	0.50 (43)	0.44 (43)
FA2	1.29 (8)	1.03 (23)	1.00 (30)	1.20 (1)	0.65 (44)	1.17 (15)	1.03 (28)	1.11 (3)	1.12 (5)	1.05 (26)	0.94 (33)	0.59 (40)	0.65 (38)
VT1	1.29 (9)	1.11 (11)	1.12 (16)	1.03 (5)	0.95 (38)	1.25 (8)	0.79 (41)	0.81 (23)	0.87 (32)	1.19 (20)	1.33 (17)	1.06 (11)	0.81 (25)
CO1	1.29 (10)	1.19 (4)	1.04 (24)	0.74 (39)	0.95 (39)	1.06 (22)	1.07 (27)	0.71 (34)	0.77 (38)	1.56 (11)	1.20 (20)	0.85 (26)	0.80 (28)

*The full name of each trait abbreviation in the first row is found in **Table 1**.*

commercial varieties. As for local varieties, MO2 ranked third for fructose:glucose resilience (1.29); FA2 stood out for having the highest resilience in total sugar content (1.20) and ranked third for total sugar:total acid resilience (1.11); XA1, which ranked first for yield resilience (1.79), had a remarkable resilience in glutamic and aspartic acid (1.25 and 1.13, respectively), ranking seventh for both of them (**Table 7**). With respect to commercial varieties, C2 stood out for its resilience in vitamin C (1.12) and total carotenoid content (1.82), ranking fourth and seventh, respectively, while C1 was highlighted for its resilience in β-carotene content (1.53), ranking seventh in the collection (**Table 7**).

DISCUSSION

The present work constitutes the first study of 'de penjar' tomato involving different doses of N fertilization. A diverse array of 39 local varieties together with five commercial varieties were characterized in open field under two nitrogen fertilization levels, one corresponding to similar values of their traditional cultivation (162 kg ha^{-1}; high N) (Seda and Muñoz, 2011) and the other to less than one third of the first dosage (49 kg ha^{-1}; low N). The large variability existing among the 'de penjar' collection for morphological, agronomic, and quality traits observed in this study paves the way for selection and breeding of this overlooked type of tomato. In terms of yield, average production in our collection (around 2 kg $plant^{-1}$) stands on intermediate values reported for other LSL varieties from the eastern Spain ('de penjar') and Balearic Islands ('de ramellet') (Casals et al., 2012; Cebolla-Cornejo et al., 2013; Figàs et al., 2015, 2018b; Fullana-Pericàs et al., 2019). Our data about fruit mean weight are in agreement with Conesa et al. (2020). Regarding fruit quality, soluble solid content in the collection studied ranged around 4–7%, with an average of 5.5%, similar to values found in Fullana-Pericàs et al. (2019) but slightly lower to the values found in Figàs et al. (2015, 2018b). Similarly, when looking at individual concentrations of reducing sugars, mean values of fructose and glucose under both low and high N treatment fitted within the range of values obtained in Casals et al. (2015), which evaluated the sugar and acid profile of 25 accessions of 'de penjar' tomato. However, the ranges obtained by Casals et al. (2015) were wider and showed higher maximum average values by 1.26- and 1.19-fold, respectively, than the collection of the present study. The average titratable acidity in the present collection was also similar to those found for other 'de penjar' and 'de ramellet' tomato varieties (Cebolla-Cornejo et al., 2013; Figàs et al., 2015, 2018b). However, none of the varieties showed means of titratable acidity higher than 1.0%, while this commonly happens in 'de ramellet' tomato (Fullana-Pericàs et al., 2019). This might be due to genetic differences or to differences in the ripening stage at the time of harvesting. In any case, our work supports previous information indicating that LSL varieties from Spain generally are slightly more acidic than the varieties from Italy, while the latter accumulate more soluble solids (Conesa et al., 2020). On the other side, as opposed to fructose and glucose contents, the 'de penjar' tomato collection of the present work showed mean values of individual citric and malic acid content slightly higher than in the collection evaluated in Casals et al. (2015), with larger ranges of variation among accessions. In addition, the maximum average values found in the present collection for contents in citric and malic acid were 12.66 g kg^{-1} fw and 2.36 g kg^{-1} fw, respectively, while the maximum values in Casals et al. (2015) were 1.78- and 1.50-fold lower, respectively. Ranges for content in glutamic acid in the 'de penjar' collection of this study showed wider variation than in other works (Casals et al., 2015), although both glutamic and aspartic acids are compounds still barely studied in 'de penjar' tomatoes.

Compared with USDA standard nutritional references of cultivated tomato (Haytowitz et al., 2011), the 'de penjar' collection studied contained in average around 1.5-fold more glucose and fructose and 2-fold more vitamin C. However, lycopene and β-carotene contents were 3.3- and 1.4-fold, respectively, lower in 'de penjar' fruits, probably due to the pleiotropic effect of the *alc* mutation (Kumar et al., 2018). The same trend was observed for glutamic and aspartic acids, with mean contents of 1.2- and 1.6-fold lower in our collection compared to the USDA standard nutritional references

(Haytowitz et al., 2011). This confirms that 'de penjar' LSL varieties are very different in composition terms to standard tomato varieties (Cebolla-Cornejo et al., 2013; Figàs et al., 2015).

Importance of Soil Conditions and Cultivation Practices

Some recent studies have addressed the impact of organic farming alone and together with low N inputs on agronomic and quality traits of tomato. De Pascale et al. (2016) suggested that organic cultivation practices might be a better approach than conventional methods for improving yield and nutritional quality of tomato under limiting N and water conditions, although it depends on cultivar and soil type. In this study, 'de penjar' tomato was cultivated following organic farming practices. In this respect, 'de penjar' tomato have been traditionally cultivated in open field under rain-fed, low-input conditions, which makes this tomato crop ideal for adaptation to organic farming.

The relationship between soil characteristics and fertilization is often overlooked, and there are interactions between different elements of its composition that heavily affect the efficiency of nutrient absorption by the roots (Jones, 2012). In this respect, the imbalanced N–P–K fertilization in the low N treatment was taken into account before setting the fertilization program by evaluating the possible impaired plant availability of other macronutrients. However, only synergistic or zero interactions have been identified in literature between nitrogen and phosphorus or potassium. Antagonistic effects are mostly found between divalent cations (Rietra et al., 2017). In addition, the soil texture influences the development of the roots and their degree of absorption (De Pascale et al., 2016). A clay-loam soil, as in the present work, would enhance root efficiency in exploring the soil for nutrients as it represents a well-balanced soil with intermediate compaction degree, which avoids rapid loss of nutrients and water and allows proper aeration (Tracy et al., 2013). Our experiment was carried out in an officially recognized area for 'de penjar' tomato cultivation. In this work, soil analysis showed slight salinity, which is optimal for 'de penjar'-type cultivation (Conesa et al., 2020), and high organic matter concentration, which is known to have a positive impact on nutrient availability and reducing soil compaction (Metzger and Yaron, 1987). No nutrient deficiencies were found in the soil of study. Contrarily, concentrations of K, Ca^{2+}, and Mg^{2+} were excessive, which could result in salt formation causing antagonism between ions (e.g., Na^+ vs. K^+, Cl^- vs. NO_3^-) and mineral imbalance with negative impact on plant growth (Jones, 2012). In addition, very high P concentrations were found in soil, which will eventually be washed out through the soil, contributing to pollution and eutrophication of waters. These data prove that there is scope for reducing, at a large extent, the supply of these nutrients in fertilization of 'de penjar' tomato.

Variation Observed

Considerable phenotypic variation was observed in our collection for most of the traits evaluated, which is in agreement with the large genetic diversity described for 'de penjar' tomato in other works (Casals et al., 2012; Cebolla-Cornejo et al., 2013; Esposito et al., 2020). Genotyping data of our collection would have been relevant to confirm at the genetic level the high diversity we have found. However, since we mostly evaluated quantitative traits with polygenic control, a larger number of accessions would have been needed for a robust "Genome Wide Association Study" (GWAS) (Korte and Farlow, 2013). The specific effect of the *alc* mutation on the traits investigated could be studied by means of crosses between parents carrying the *alc* mutation and its corresponding wild allele. The PCA confirmed the wide variation observed, visually represented with the different accessions studied scattered all over the score plot. This supports the definition of 'de penjar' tomato by Conesa et al. (2020) as a "population of landraces," in which the *alc* mutation is introgressed into different genetic backgrounds (Casals et al., 2012), maintaining high heterogeneity within the 'de penjar' type.

The higher value of phenotypic than genotypic variation for every trait analyzed shows an important environmental effect, especially for fruit bioactive and quality compounds. This is in agreement with previous studies that reported tomato quality traits being highly polygenic, strongly influenced by environmental conditions and showing low heritability (Causse et al., 2003). Fruit mean weight showed the highest broad-sense heritability estimate (H^2), followed by malic acid content and citric:malic acid ratio, which was in line with them showing the highest genotypic variation coefficient (CV_G). In these terms, similar results were reported in other works. Morphology traits in tomato, such as fruit weight and skin color, are known to have higher values of heritability than fruit quality traits or yield (Figàs et al., 2018a). Panthee et al. (2012) also observed that acid traits showed higher heritability than sugar and soluble solid content. Contrarily, lycopene, total carotenoid, and β-carotene contents had the lowest H^2 and the highest phenotypic variation coefficient (CV_P) in the collection of the present study. Both H^2 and CV_P estimates for lycopene and total carotenoid content showed values of 0. We attribute this phenomenon not to the absence of genetic variation in our collection but to a strong interaction G × N, meaning that different trends in the response to increasing or decreasing N inputs were observed among genotypes. Panthee et al. (2012) also found a similar interaction genotype × environment effect resulting in low heritability for lycopene in tomato. Both heritability and a strong interaction G × N constitute relevant information for breeding and selection (Panthee et al., 2012; Figàs et al., 2018b). While high heritability estimates would make more efficient the selection of genotypes expecting the same performance under different N supply conditions, having a strong interaction G × N would allow breeders to select varieties with the best response under certain conditions, in our case, low N.

Effects of Low Nitrogen Inputs on Traits Evaluated

Yield is one of the most valuable traits for growers, and it is directly correlated with N availability for plants (Zhang et al., 2015). In the present work, no significant differences were found between the two N treatments regarding average yields for any of the varieties evaluated. Our results suggested that, although

N supplied in the high N treatment could not be considered excessive in a detrimental way to yield, the N availability in the low N treatment was suitable for an optimal plant growth and for obtaining similar yields. More plant growth parameters would have been needed for better support of our statement. Most of the studies testing tomato cultivars in soil with different rates of N fertilization found that yield increased linearly with N input but reached a plateau where it became insensitive to more N fertilization levels (Elia and Conversa, 2012; Djidonou et al., 2013). However, among those studies, the minimum N fertilization level maximizing tomato yield was at least 168 kg ha^{-1} in open field (Djidonou et al., 2013), while for the 'de penjar' collection studied, we found that even with only 49 kg ha^{-1} of N fertilization, no differences were obtained compared to the standard fertilization. In addition, data of SPAD were similar to those of the plant yield. More data about plant morphological changes would be appropriate to robustly evaluate the effect of the LN treatment on plants, like plant biomass, plant height, leaf size, or root morphology (Hermans et al., 2006; Freschet et al., 2018). In particular, it would have been of interest to have plant biomass data to evaluate nitrogen use efficiency parameters. However, SPAD values have been widely used for evaluating plant N status in crop management, as leaf chlorophyll content is closely related to leaf N content, and a reduction in these values have been already reported for tomato under N fertilization stress (Ling et al., 2011; Padilla et al., 2015; Dunn et al., 2018). Thus, we decided to use this parameter to estimate plant N status for being a simple, nondestructive, and relatively quick measure to take. Fruit mean weight was also not influenced by the N rate in the present study. In fact, Elia and Conversa (2012) and Hernández et al. (2020) suggested that the effects of N inputs on tomato yield were due to changes in fruit load more than fruit mean weight. The external color of fruit was evaluated through lightness, chroma, and hue values, but only the collection average for hue was significantly affected by the N treatment, increasing when low N was applied. According to the HCL color space, this would represent a slight change of color toward orange under low N inputs, possibly due to a slightly higher content of β-carotene under these conditions.

Taste and flavor of 'de penjar' tomato is one of the attributes most appreciated by the local consumer, and it is associated with its traditional use (Conesa et al., 2020). Therefore, we considered important to evaluate the effects of lowering the dose of N fertilization on those characteristics. Our results showed that high N rate did not affect significantly either the N or the C content in fruit, probably due to a N redistribution between leaves and fruits in response to an exceeded N supply. In fact, Elia and Conversa (2012) found that increasing N inputs of tomato from 200 to 300 kg ha^{-1} increased leaf N, while N storage in fruits decreased. This was explained by a plant tendency to grow vegetatively rather than reproductively when N availability increases over the demand.

Citric, malic, and total acid contents and titratable acidity in fruits showed no significant differences between N treatments. Our results differed to the ones reported in recent studies for tomato, both under hydroponic and soil cultivation (De Pascale et al., 2016; Truffault et al., 2019), in which higher acidity was found related to an increasing N rate. In addition, our results suggest that citric acid is likely the highest contributor to the fruit acidity in 'de penjar' collection, as its content in fruits exceeds by 2.7- to 10.0-fold on average that of malic acid. This is in agreement with the results obtained in the collection evaluated by Casals et al. (2015), which showed nearly the same range of citric:malic ratio (2.4 to 9.3).

Fruit contents in fructose, glucose, total sugar, and total sweetness index were the only composition traits evaluated in this study that showed a significant effect of the N treatment. All of them suffered an average reduction of 10–20% in response to low N inputs. Although the ANOVA did not show significant differences for these traits between N treatments for each accession separately, the existence of a significant effect of the N treatment indicates a tendency toward the reduction of sugar content under low N in the 'de penjar' tomato. Results about the N effect on carbohydrates and total soluble solids in fruits are the most controversial among other works in tomato crop. Our results are in agreement with some of them (De Pascale et al., 2016). Others reported the opposite effect (Hernández et al., 2020), while others even found no significant effect of N rate on sugar content (Truffault et al., 2019). According to Hermans et al. (2006), N deficiency in plants may cause an accumulation of starch and sugars in leaves, consequently decreasing their content in fruits and regulating photosynthesis by negative feedback. This could explain our results. Level of sweetness is also related to different proportions of main sugars, with fructose being the sweetest, followed by sucrose and finally glucose. Fructose and glucose are also known to be usually in the same proportion (1:1) in tomato pericarp (Beckles, 2012). However, our results showed mean values of fructose:glucose ratio over 1.0 for every accession and it was not affected significantly by N inputs. Furthermore, a highly significant interaction G × N was observed, which gives scope to select accessions with higher fructose:glucose ratio under low N inputs for breeding purposes.

Since the end of the 20th century, flavor was increasingly understood as a complex parameter not only due to main sugars and organic acids but also due to their ratio, texture, and volatile compounds. Although studies including the different elements of flavor are emerging, it is still a difficult parameter to estimate objectively and not amenable for exhaustive assays for being time-consuming and expensive. Therefore, the horticultural industry has been using indexes highly correlated with flavor and consumer acceptability for selecting and breeding (Beckles, 2012). In tomato, Baldwin et al. (1998) reported that total sweetness index or its ratio to titratable acidity were closer than soluble solid content or its ratio to titratable acidity to their acceptability based on sweetness we perceive ($r \geq 0.80$). In the present study, while total sweetness index significantly decreased with LN treatment, soluble solid content was not affected. Despite the high correlation between sugar and soluble solid content and that the latter is easier and faster to measure, soluble solid content includes other compounds that do not contribute to sweetness. Thus, it could be interesting to quantify individual sugars (Fernández-Ruiz et al., 2004). On the other hand, as acidity level influences the perception of sweetness, parameters related to sweetness–acidity balance are more likely to correlate with taste

preferences than sugar and acid contents alone (Baldwin et al., 1998; Beckles, 2012). In this experiment, a significant decrease in average sugars associated with low N inputs was reflected as a slight reduction of their average ratios with organic acids and acidity-related traits. Remarkably, this reduction was not significant; thus, low N inputs may not change a great deal the taste of 'de penjar' tomatoes. On the other hand, taking into consideration the traditional conservation and consumption of the 'de penjar' tomato, up to a minimum of 2 months after harvest, having lower sugar content under low N treatment could be detrimental to its taste during postharvest life, since a decrease, first sharply and then more gradual, of sugar content in this type of tomato has been reported at 2 to 4 months postharvest, while organic acids decreased to a lesser degree in the same period (Casals et al., 2015). However, further studies are needed to draw an accurate conclusion, using experienced sensory panels and investigating the postharvest performance of the accessions evaluated, as diversity for these traits has been observed among 'de penjar' accessions (Casals et al., 2015).

One possible mitigation of the reduction of sugars under low N conditions would be the use of foliar sprays as a nutritional complement. The main advantage of fertilizing by foliar treatments is its efficiency with a minimal contribution to environment pollution. Recently, applications of 1 mg L^{-1} sodium selenate or 500 mg L^{-1} abscisic acid have been reported to improve fructose, glucose, and vitamin C, in tomato fruits (Barickman et al., 2017; Zhu et al., 2018). On the other hand, the best approach might be an optimized fertilization and irrigation management. As reported by Fullana-Pericàs et al. (2019), 'de penjar' tomato local varieties withstand low irrigation conditions with minimum yield losses, and even with enhanced sugar content in fruits. In any case, these are possible paths for further studies about the cultivation of 'de penjar' tomato using less N fertilization.

Aspartic and glutamic acids are major amino acids in tomato fruits. Tomato accumulate several-fold higher content of glutamic acid in their fruits than other vegetables such as pepper, onion, or carrot (Haytowitz et al., 2011). On the one hand, aspartic and glutamic acids function as other amino acid precursors in plants, e.g., glutamic acid constitutes the first element of the GABA (γ aminobutyric acid) synthesis, a bioactive molecule of recent interest for its health-promoting potential (Gramazio et al., 2020). On the other hand, those are the only amino acids that are related to taste, especially glutamic acid. In their ionized forms and in the presence of sodium salt, they give the fifth basic taste, umami, known as savory and taste-enhancing (Lioe et al., 2010). Due to its molecular N basis, the amount of amino acid in the plant will depend on the N content of the plant. In the case of aspartic and glutamic acids, no significant differences were found in our 'de penjar' collection by reducing nitrogen fertilization to one third of the usual supply.

Regarding bioactive compounds, tomatoes owe their antioxidant power mainly to their vitamin C and carotenoid content (Adalid et al., 2010). Although the effects of lowering N fertilization on these compounds are still not clear (Truffault et al., 2019; Hernández et al., 2020), in our experiment they were not significantly affected by N dosage. Interestingly, vitamin C showed a significant positive environmental correlation to sweetness (soluble solids content, fructose, total sweetness index). A positive correlation between fruit content in sugars and vitamin C has been already reported in other works (Causse et al., 2003) and could be explained by the role of sugars as precursors for vitamin C biosynthesis. On the other hand, sugars also function as signaling molecules in source–sink regulation and as regulators of gene expression, which could also be involved in this correlation (Eveland and Jackson, 2012). These positive correlations could help breeders to identify trends in several compounds measuring just a few easier ones.

Selection Based on Ideotype and Comparison of Local vs. Commercial Materials

Considering all the traits analyzed in the present work, there are prospects for selecting the best 'de penjar' varieties based on an ideotype under low N inputs with the aim to include them in breeding programs or directly cultivate them under those conditions. The desirable attributes pursued in our study would be high yield in the first place; high nitrogen content, due to its direct relationship with protein content; great sweetness, given by high content in sugars (mainly fructose), but moderate content in organic acids resulting in high sweetness:acidity ratio; high glutamic and aspartic acid contents, which would potentiate taste; and great content in antioxidant compounds (vitamin C, carotenoids) due to their reported bioactive role in the human body. In this regard, among the best ten yielding varieties under low N treatment, both MT1 and MO1 seemed to present the best ideotype. In addition, they showed opposite average fruit weight, which could be an advantage in breeding for different markets and maintaining the morphological variability within the 'de penjar' type. On the other hand, MO2 showed very good resilience in yield ranking third, besides being the fourth best-yielding variety under low N treatment. Among the 19 out of 44 accessions that showed significant differences between the two N treatments for some of the traits evaluated (lightness of color, fructose:glucose ratio, contents in lycopene, β-carotene, total carotenoids, and carbon), the already mentioned MT1 was very interesting for showing increased average contents of lycopene, β-carotene, and total carotenoids by 43–52% under low N treatment. In addition, TO1 stood out for showing increased mean values under the low N treatment compared to the high N for all the mentioned traits, except for lightness of color. Although TO1 did not rank in the top 10 positions for yield in any of the N treatments, nor for yield resilience, the cultivation and conservation of this local variety could be interesting for future breeding programs aimed at improving fruit quality under low N inputs.

Commercial tomato varieties are the result of the last 50 years of breeding toward high yield, pest resistance, and fruit uniform appearance (Casañas et al., 2017). However, in the last decade, with consumers demanding more tasteful and healthful fruits and agriculture facing the challenge of producing more with fewer resources and with less impact on the environment, local tomato varieties are being "rediscovered" as an important source

of variability. Several studies have been carried out in order to properly characterize the 'de penjar' tomato (Casals et al., 2012, 2015; Cebolla-Cornejo et al., 2013; Figàs et al., 2015). However, there is a lack of comparison of local vs. commercial varieties for this varietal type. Herein, we have found significant differences for three (soluble solid content:titratable acidity, total sweetness index:titratable acidity, and vitamin C) out of the 29 traits analyzed. For all three traits and both N treatments, local varieties showed a higher average value, which reinforces their appreciation for their organoleptic and nutritional quality.

CONCLUSION

The present work provided the first comprehensive characterization of the variability of 'de penjar' tomato varieties under contrasting levels of N fertilization. A wide diversity in our collection for agronomical, morphological, and fruit organoleptic and nutritional quality traits was revealed. Our data support the evidence of a current over-fertilization in 'de penjar' tomato cultivation. Under the experimental conditions tested, reducing to one third the usual nitrogen supply did not show any significant effect on yield and most of the traits evaluated related to fruit nutritional and organoleptic quality, except for a decrease in soluble sugars. Several varieties showed excellent results under low N supply conditions, being within the best ten yielding varieties with good fruit quality parameters. In addition, the present work highlights the value of local varieties for selection and breeding of 'de penjar' tomatoes and enhances their potential as a very useful gene pool for future tomato breeding programs for resilience under restrictive environmental conditions. Further studies on association of genetic and phenotypic data and on postharvest performance under low N fertilization conditions, as well as developing segregating generations for the *alc* mutation, will provide relevant information for the enhancement of the 'de penjar' tomato for selection and breeding for resilience.

DATA AVAILABILITY STATEMENT

The raw data supporting the conclusions of this article will be made available by the authors upon request, without undue reservation.

AUTHOR CONTRIBUTIONS

JP, SS, and MP planned the study and supervised the research. ER-M, LA, and RB performed the morphological and chemical composition characterization. AA and ER-M performed the chemical analyses by HPLC. LP-D, CC, ES, MF, RB, LA, and ER-M performed the agronomic characterization. MG-M performed the soil analysis. LP-D, CC, ES, MF, and SS supervised the crops. ER-M and RB curated the data. LP-D and ER-M performed the statistical analyses. ER-M, JP, SS, and MP drafted the manuscript. All authors contributed to the article and approved the submitted version.

FUNDING

This work has been funded by the European Union's Horizon 2020 Research and Innovation Programme under grant agreement no. 774244 (Breeding for resilient, efficient and sustainable organic vegetable production; BRESOV), by the Spanish Agencia Estatal de Investigación under grant agreement no. PCI2019-103375 (project SOLNUE in the framework of the H2020 call SusCrop-ERA-Net; ID#47), and by Generalitat Valenciana (Conselleria d'Innovació, Universitats, Ciència I Societat Digital) under grant agreement no. AICO/2020/042. ER-M is grateful to the Spanish Ministerio de Economía, Industria y Competitividad for a pre-doctoral grant (BES-2016-077482).

SUPPLEMENTARY MATERIAL

The Supplementary Material for this article can be found online at: https://www.frontiersin.org/articles/10.3389/fpls.2021.633957/full#supplementary-material

Supplementary Figure 1 | Daily maximum (purple line), average (red line) and minimum (green line) temperatures **(A)**, and radiation (orange area) and pluviometry (blue columns) **(B)** since the transplant, on May 8th 2019, until the end of cultivation, on September 30th 2019.

Supplementary Table 1 | Accession name, code used in the present work and geographical origin within Spain or breeding company or institution of the 'de penjar' tomato local and commercial varieties used for their evaluation under low and high nitrogen fertilization treatments.

Supplementary Table 2 | Mean values and standard error of the soil chemical composition for each soil of both low and high nitrogen fertilization field plots ($n = 5 \times 2 = 10$).

Supplementary Table 3 | Mean values of the three replicates per accession and treatment ($n = 3 \times 2 = 6$) for all the traits evaluated. Acronyms LN and HN refer to low nitrogen and high nitrogen treatment, respectively.

REFERENCES

Adalid, A. M., Roselló, S., and Nuez, F. (2010). Evaluation and selection of tomato accessions (*Solanum* section *Lycopersicon*) for content of lycopene, β-carotene and ascorbic acid. *J. Food Compos. Anal.* 23, 613–618. doi: 10.1016/j.jfca.2010.03.001

Agius, C., von Tucher, S., Poppenberger, B., and Rozhon, W. (2018). Quantification of glutamate and aspartate by ultra-high performance liquid chromatography. *Molecules* 23, 1–15. doi: 10.3390/molecules23061389

Baldwin, E. A., Scott, J. W., Einstein, M. A., Malundo, T. M. M., Carr, B. T., Shewfelt, R. L., et al. (1998). Relationship between sensory and instrumental analysis for tomato flavor. *J. Am. Soc. Hortic. Sci.* 123, 906–915. doi: 10.21273/jashs.123.5.906

Barickman, T. C., Kopsell, D. A., and Sams, C. E. (2017). Abscisic acid improves tomato fruit quality by increasing soluble sugar concentrations. *J. Plant Nutr.* 40, 964–973. doi: 10.1080/01904167.2016.1231812

Beckles, D. M. (2012). Factors affecting the postharvest soluble solids and sugar content of tomato *(Solanum lycopersicum* L.) fruit.

Postharvest Biol. Technol. 63, 129–140. doi: 10.1016/j.postharvbio.2011.05.016

Casals, J., Marti, R., Casañas, F., and Cebolla-Cornejo, J. (2015). Sugar-and-acid profile of penjar tomatoes and its evolution during storage. *Sci. Agric.* 72, 314–321. doi: 10.1590/0103-9016-2014-0311

Casals, J., Pascual, L., Cañizares, J., Cebolla-Cornejo, J., Casañas, F., and Nuez, F. (2012). Genetic basis of long shelf life and variability into Penjar tomato. *Genet. Resour. Crop Evol.* 59, 219–229. doi: 10.1007/s10722-011-9677-6

Casañas, F., Simó, J., Casals, J., and Prohens, J. (2017). Toward an evolved concept of landrace. *Front. Plant Sci.* 8:145. doi: 10.3389/fpls.2017.00145

Causse, M., Buret, M., Robini, K., and Verschave, P. (2003). Inheritance of nutritional and sensory quality traits in fresh market tomato and relation to consumer preferences. *J. Food Sci.* 68, 2342–2350. doi: 10.1111/j.1365-2621.2003.tb05770.x

Cebolla-Cornejo, J., Roselló, S., and Nuez, F. (2013). Phenotypic and genetic diversity of Spanish tomato landraces. *Sci. Hortic. (Amsterdam)* 162, 150–164. doi: 10.1016/j.scienta.2013.07.044

Chebrolu, K. K., Jayaprakasha, G. K., Yoo, K. S., Jifon, J. L., and Patil, B. S. (2012). An improved sample preparation method for quantification of ascorbic acid and dehydroascorbic acid by HPLC. *LWT Food Sci. Technol.* 47, 443–449. doi: 10.1016/j.lwt.2012.02.004

Conesa, M., Fullana-Pericàs, M., Granell, A., and Galmés, J. (2020). Mediterranean long shelf-life landraces: an untapped genetic resource for tomato improvement. *Front. Plant Sci.* 10:1651. doi: 10.3389/fpls.2019.01651

De Pascale, S., Maggio, A., Orsini, F., and Barbieri, G. (2016). Cultivar, soil type, nitrogen source and irrigation regime as quality determinants of organically grown tomatoes. *Sci. Hortic. (Amsterdam)* 199, 88–94. doi: 10.1016/j.scienta.2015.12.037

Djidonou, D., Zhao, X., Simonne, E. H., Koch, K. E., and Erickson, J. E. (2013). Yield, water-, and nitrogen-use efficiency in field-grown, grafted tomatoes. *HortScience* 48, 485–492. doi: 10.21273/hortsci.48.4.485

Dunn, B. L., Singh, H., and Goad, C. (2018). Relationship between chlorophyll meter readings and nitrogen in poinsettia leaves. *J. Plant Nutr.* 41, 1566–1575. doi: 10.1080/01904167.2018.1459697

Elia, A., and Conversa, G. (2012). Agronomic and physiological responses of a tomato crop to nitrogen input. *Eur. J. Agron.* 40, 64–74. doi: 10.1016/j.eja.2012.02.001

Esposito, S., Cardi, T., Campanelli, G., Sestili, S., Díez, M. J., Soler, S., et al. (2020). ddRAD sequencing-based genotyping for population structure analysis in cultivated tomato provides new insights into the genomic diversity of Mediterranean 'da serbo' type long shelf-life germplasm. *Hortic. Res.* 7:134. doi: 10.1038/s41438-020-00353-6

Eveland, A. L., and Jackson, D. P. (2012). Sugars, signalling, and plant development. *J. Exp. Bot.* 63, 3367–3377. doi: 10.1093/jxb/err379

FAOSTAT (2020). *FAOSTAT*. Available online at: http://www.fao.org/faostat/en/ (accessed September 18, 2020).

Fernández-Ruiz, V., Sánchez-Mata, M. C., Cámara, M., Torija, M. E., Chaya, C., Galiana-Balaguer, L., et al. (2004). Internal quality characterization of fresh tomato fruits. *HortScience* 39, 339–345. doi: 10.21273/hortsci.39.2.339

Figàs, M. R., Prohens, J., Casanova, C., Fernández-de-Córdova, P., and Soler, S. (2018a). Variation of morphological descriptors for the evaluation of tomato germplasm and their stability across different growing conditions. *Sci. Hortic. (Amsterdam)* 238, 107–115. doi: 10.1016/j.scienta.2018.04.039

Figàs, M. R., Prohens, J., Raigón, M. D., Fita, A., García-Martínez, M. D., Casanova, C., et al. (2015). Characterization of composition traits related to organoleptic and functional quality for the differentiation, selection and enhancement of local varieties of tomato from different cultivar groups. *Food Chem.* 187, 517–524. doi: 10.1016/j.foodchem.2015.04.083

Figàs, M. R., Prohens, J., Raigón, M. D., Pereira-Dias, L., Casanova, C., García-Martínez, M. D., et al. (2018b). Insights into the adaptation to greenhouse cultivation of the traditional Mediterranean long shelf-life tomato carrying the *alc* mutation: a multi-trait comparison of landraces, selections, and hybrids in open field and greenhouse. *Front. Plant Sci.* 9:1774. doi: 10.3389/fpls.2018.01774

Freschet, G. T., Violle, C., Bourget, M. Y., Scherer-Lorenzen, M., and Fort, F. (2018). Allocation, morphology, physiology, architecture: the multiple facets of plant above- and below-ground responses to resource stress. *New Phytol.* 219, 1338–1352. doi: 10.1111/nph.15225

Fullana-Pericàs, M., Conesa, M., Douthe, C., El Aou-ouad, H., Ribas-Carbó, M., and Galmés, J. (2019). Tomato landraces as a source to minimize yield losses and improve fruit quality under water deficit conditions. *Agric. Water Manag.* 223:105722. doi: 10.1016/j.agwat.2019.105722

Gazulla, M. F., Rodrigo, M., Orduña, M., and Gómez, C. M. (2012). Determination of carbon, hydrogen, nitrogen and sulfur in geological materials using elemental analysers. *Geostand. Geoanalytical Res.* 36, 201–217. doi: 10.1111/j.1751-908X.2011.00140.x

Gomez, K. A., and Gomez, A. A. (1984). *Statistical Procedures for Agricultural Research*. New York, NY: John Wiley & Sons, Inc.

Gramazio, P., Takayama, M., and Ezura, H. (2020). Challenges and prospects of new plant breeding techniques for GABA improvement in crops: tomato as an example. *Front. Plant Sci.* 11:577980. doi: 10.3389/fpls.2020.577980

Haytowitz, D. B., Lemar, L. E., Pehrsson, P. R., Exler, J., Patterson, K. K., Thomas, R. G., et al. (2011). USDA national nutrient database for standard reference, release 24. *USDA Natl. Nutr. Database Stand. Ref.* Available online at: http://www.ars.usda.gov/Services/docs.h (accessed September 18, 2020).

Hermans, C., Hammond, J. P., White, P. J., and Verbruggen, N. (2006). How do plants respond to nutrient shortage by biomass allocation? *Trends Plant Sci.* 11, 610–617. doi: 10.1016/j.tplants.2006.10.007

Hernández, V., Hellín, P., Fenoll, J., and Flores, P. (2020). Impact of nitrogen supply limitation on tomato fruit composition. *Sci. Hortic. (Amsterdam)* 264:109173. doi: 10.1016/j.scienta.2020.109173

Hochberg, Y. (1988). A sharper Bonferroni procedure for multiple tests of significance. *Biometrika* 75:800. doi: 10.2307/2336325

Jones, J. B. J. (2012). *Plant Nutrition and soil Fertility Manual*, 2 Edn. Boca Raton, FL: Taylor & Francis Group.

Korte, A., and Farlow, A. (2013). The advantages and limitations of trait analysis with GWAS: a review. *Plant Methods* 9, 1–9. doi: 10.1186/1746-4811-9-29

Kumar, R., Tamboli, V., Sharma, R., and Sreelakshmi, Y. (2018). NAC-NOR mutations in tomato Penjar accessions attenuate multiple metabolic processes and prolong the fruit shelf life. *Food Chem.* 259, 234–244. doi: 10.1016/j.foodchem.2018.03.135

Ling, Q., Huang, W., and Jarvis, P. (2011). Use of a SPAD-502 meter to measure leaf chlorophyll concentration in *Arabidopsis thaliana*. *Photosynth. Res.* 107, 209–214. doi: 10.1007/s11120-010-9606-0

Lioe, H. N., Selamat, J., and Yasuda, M. (2010). Soy sauce and its umami taste: a link from the past to current situation. *J. Food Sci.* 75, 71–76. doi: 10.1111/j.1750-3841.2010.01529.x

Metzger, L., and Yaron, B. (1987). "Influence of sludge organic matter on soil physical properties," in *Advances in Soil Science*, Vol. 7, ed. B. A. Stewart (New York, NY: Springer), 141–163.

Nyquist, W. E. (1991). Estimation of heritability and prediction of selection response in plant populations. *CRC. Crit. Rev. Plant Sci.* 10, 235–322. doi: 10.1080/07352689109382313

Padilla, F. M., Peña-Fleitas, M. T., Gallardo, M., and Thompson, R. B. (2015). Threshold values of canopy reflectance indices and chlorophyll meter readings for optimal nitrogen nutrition of tomato. *Ann. Appl. Biol.* 166, 271–285. doi: 10.1111/aab.12181

Panthee, D. R., Cao, C., Debenport, S. J., Rodríguez, G. R., Labate, J. A., Robertson, L. D., et al. (2012). Magnitude of genotype × environment interactions affecting tomato fruit quality. *HortScience* 47, 721–726. doi: 10.21273/hortsci.47.6.721

R Core Team (2013). *R: A Language and Environment for Statistical Computing*. Vienna: R Core Team.

Ramos, C., and Pomares, F. (2010). *Abonado de los Cultivos Hortícolas. Guía Práctica de la Fertilización Racional de los Cultivos en España. Parte II: Ministerio de Medio Ambiente y Medio Rural y Marino*. Madrid: Centro de Publicaciones, 181–192.

Reeuwijk, L. (2002). *Procedures for Soil Analysis*, 6th Edn. Wageningen: International Soil Reference and Information Centre.

Revelle, M. W. (2018). *Package Version 2.0.12 "psych."* October, 1–250.

Rietra, R. P. J. J., Heinen, M., Dimkpa, C. O., and Bindraban, P. S. (2017). Effects of nutrient antagonism and synergism on yield and fertilizer use efficiency. *Commun. Soil Sci. Plant Anal.* 48, 1895–1920. doi: 10.1080/00103624.2017.1407429

Seda, M., and Muñoz, P. (2011). *Fertilització del Tomàquet de Penjar en Producció Ecològica: Fitxes Tecniques PAE*. Barcelona: PAE. 1–3.

Soil Science Division Staff (2017). "Soil survey manual," in *USDA Agriculture Handbook No. 18*, eds C. Ditzler, K. Scheffe, and H. C. Monger (Washington, D.C: Government Printing Office).

Thompson, R. B., Martínez-Gaitan, C., Gallardo, M., Giménez, C., and Fernández, M. D. (2007). Identification of irrigation and N management practices that contribute to nitrate leaching loss from an intensive vegetable production system by use of a comprehensive survey. *Agric. Water Manag.* 89, 261–274. doi: 10.1016/j.agwat.2007.01.013

Tracy, S. R., Black, C. R., Roberts, J. A., and Mooney, S. J. (2013). Exploring the interacting effect of soil texture and bulk density on root system development in tomato (*Solanum lycopersicum* L.). *Environ. Exp. Bot.* 91, 38–47. doi: 10.1016/j.envexpbot.2013.03.003

Truffault, V., Marlene, R., Brajeul, E., Vercambre, G., and Gautier, H. (2019). To stop nitrogen overdose in soilless tomato crop: a way to promote fruit quality without affecting fruit yield. *Agronomy* 9:80. doi: 10.3390/agronomy9020080

Wei, T., Simko, V., Levy, M., Xie, Y., Jin, Y., and Zemla, J. (2017). Visualization of a correlation matrix. *Statistician* 56, 316–324.

Wickham, H. (2016). *ggplot2: Elegant Graphics for Data Analysis*. Basel: Springer International Publishing.

Wricke, G., and Weber, E. (2010). *Quantitative Genetics and Selection in Plant Breeding*. Berlin: Walter de Gruyter & Co.

Yáñez Jiménez, J. (1989). Análisis de suelos y su interpretación. Recomendaciones agronómicas. *Horticultura* 49, 75–89.

Zhang, X., Davidson, E. A., Mauzerall, D. L., Searchinger, T. D., Dumas, P., and Shen, Y. (2015). Managing nitrogen for sustainable development. *Nature* 528, 51–59. doi: 10.1038/nature15743

Zhu, Z., Zhang, Y., Liu, J., Chen, Y., and Zhang, X. (2018). Exploring the effects of selenium treatment on the nutritional quality of tomato fruit. *Food Chem.* 252, 9–15. doi: 10.1016/j.foodchem.2018.01.064

Zscheile, F. P., and Porter, J. W. (1947). Analytical methods for carotenes of Lycopersicon species and strains. *Anal. Chem.* 19, 47–51. doi: 10.1021/ac60001a013

Conflict of Interest: MP was employed by company Meridiem Seeds S.L.

The remaining authors declare that the research was conducted in the absence of any commercial or financial relationships that could be construed as a potential conflict of interest.

frontiers in Plant Science

ORIGINAL RESEARCH
published: 17 May 2021
doi: 10.3389/fpls.2021.638195

An Eggplant Recombinant Inbred Population Allows the Discovery of Metabolic QTLs Controlling Fruit Nutritional Quality

Maria Sulli[1†], Lorenzo Barchi[2†], Laura Toppino[3], Gianfranco Diretto[1], Tea Sala[3], Sergio Lanteri[2], Giuseppe Leonardo Rotino[3] and Giovanni Giuliano[1]*

[1] Italian National Agency for New Technologies, Energy and Sustainable Economic Development (ENEA), Casaccia Research Centre, Rome, Italy, [2] Department of Agricultural, Forest and Food Sciences (DISAFA), Plant Genetics and Breeding, University of Turin, Grugliasco, Italy, [3] CREA, Council for Agricultural and Economics Research, Research Centre for Genomics and Bioinformatics, Montanaso Lombardo, Italy

OPEN ACCESS

Edited by:
Amalia Barone, University of Naples Federico II, Italy

Reviewed by:
José Juan Ordaz-Ortiz, Instituto Politécnico Nacional de México (CINVESTAV), Mexico
Yoshihito Shinozaki, Tokyo University of Agriculture and Technology, Japan
Valentino Ruggieri, Sequentia Biotech, Spain

***Correspondence:**
Giovanni Giuliano
giovanni.giuliano@enea.it

† These authors have contributed equally to this work

Specialty section:
This article was submitted to Plant Metabolism and Chemodiversity, a section of the journal Frontiers in Plant Science

Received: *05 December 2020*
Accepted: *22 March 2021*
Published: *17 May 2021*

Citation:
Sulli M, Barchi L, Toppino L, Diretto G, Sala T, Lanteri S, Rotino GL and Giuliano G (2021) An Eggplant Recombinant Inbred Population Allows the Discovery of Metabolic QTLs Controlling Fruit Nutritional Quality. Front. Plant Sci. 12:638195. doi: 10.3389/fpls.2021.638195

Eggplant (*Solanum melongena* L.) represents the third most important crop of the Solanaceae family and is an important component of our daily diet. A population of 164 F6 recombinant inbred lines (RILs), derived from two eggplant lines differing with respect to several key agronomic traits, "305E40" and "67/3," was grown to the commercial maturation stage, and fruits were harvested, separated into peel and flesh, and subjected to liquid chromatography Liquid Chromatography/Mass Spectrometry (LC/MS) analysis. Through a combination of untargeted and targeted metabolomics approaches, a number of metabolites belonging to the glycoalkaloid, anthocyanin, and polyamine classes and showing a differential accumulation in the two parental lines and F1 hybrid were identified. Through metabolic profiling of the RILs, we identified several metabolomic quantitative trait loci (mQTLs) associated with the accumulation of those metabolites. Each of the metabolic traits proved to be controlled by one or more quantitative trait loci (QTLs); for most of the traits, one major mQTL (phenotypic variation explained [PVE] $\geq$ 10%) was identified. Data on mQTL mapping and dominance–recessivity relationships of measured compounds in the parental lines and F1 hybrid, as well as an analysis of the candidate genes underlying the QTLs and of their sequence differences in the two parental lines, suggested a series of candidate genes underlying the traits under study.

Keywords: *Solanum melongena* (L.), metabolic profiling, glycoalkaloids, anthocyanins, polyamine conjugates

INTRODUCTION

Eggplant (*Solanum melongena L.*) is a diploid species ($2n = 2x = 24$) belonging to the Solanaceae family, genus *Solanum* and subgenus *Leptostemonum*. It has originated in Africa and was probably domesticated in Asia (Weese and Bohs, 2010), where it has been cultivated for over 1,500 years. Cultivated eggplant represents the third most important crop of the Solanaceae family after potato and tomato; it is cultivated worldwide, with a global production of 54 Mt in 2018 (FAOSTAT[1]) China, India, Iran, and Indonesia are the leading producing countries, while Egypt, Turkey, and Italy are the main producers in the Mediterranean region. Two other *Solanum* species, native from

[1] Available online at: http://faostat.fao.org

Africa, are commonly cultivated: the scarlet eggplant (*Solanum aethiopicum* L.) and the gboma eggplant (*Solanum macrocarpon* L.), with which eggplant is fully cross-compatible.

Eggplant fruits differ strongly in size, shape, and skin color. Most of their nutritional properties are related to their content in phenolics, especially chlorogenic and hydroxycinnamic acids and their conjugates, as well as in the skin of pigmented genotypes, anthocyanins, and other phenylpropanoids (Whitaker and Stommel, 2003; Mennella et al., 2012).

Eggplant genetic maps have been constructed from both interspecific (Doganlar et al., 2002a,b; Frary et al., 2003; Wu et al., 2009) and intraspecific crosses (Barchi et al., 2010, 2012; Fukuoka et al., 2012). These have been used to map quantitative trait loci (QTLs) controlling morphological and domestication traits, including fruit weight, shape, and color (Portis et al., 2014), disease resistances (Barchi et al., 2018), and some biochemical features (Toppino et al., 2016). Finally, an association panel of 191 accessions, genotyped with the restriction site associated DNA (RAD) markers developed by Barchi et al. (2011) and mapped by Barchi et al. (2012), was recently employed for a genome-wide association (GWA) approach for identifying genomic regions involved in anthocyanin and many other traits of agronomic interest (Cericola et al., 2014; Portis et al., 2015). To this date, however, few systematic efforts have been conducted to map QTLs controlling fruit metabolic composition (Gramazio et al., 2014; Toppino et al., 2016).

A chromosome-anchored eggplant genome sequence has been recently published (Barchi et al., 2019). This sequence, in combination with the technical advances in metabolic profiling (Fiehn et al., 2000; Schauer et al., 2006), creates new opportunities to study the genetic basis of eggplant fruit nutritional quality.

We undertook the metabolic characterization of fruits of an eggplant recombinant inbred line (RIL) population (Toppino et al., 2020). The population consists of 164 F6 RILs, obtained by crossing the breeding line "305E40," a doubled haploid derivative of an interspecific somatic hybrid between *S. aethiopicum* and *S. melongena*, and the breeding line "67/3," an F6 selection from an intraspecific *S. melongena* cross. The female parent "305E40" produces long, highly pigmented dark purple fruit, while the male parent "67/3" produces round lilac fruits (**Figure 1**). The "67/3" genotype has been used for the generation of a high-quality genome sequence, and the "305E40" line has been re-sequenced (Barchi et al., 2019). First, metabolites that differentially accumulated in the two parental lines and the F1 hybrid were identified through an untargeted approach and a combination of accurate mass, isotopic patterns, MS^2 profiles, and comparison with authentic standards. Then, additional metabolites belonging to the same metabolic pathways were identified through targeted approaches. Both untargeted and targeted metabolites were quantified in the RILs, leading to the discovery of metabolic QTLs controlling their levels.

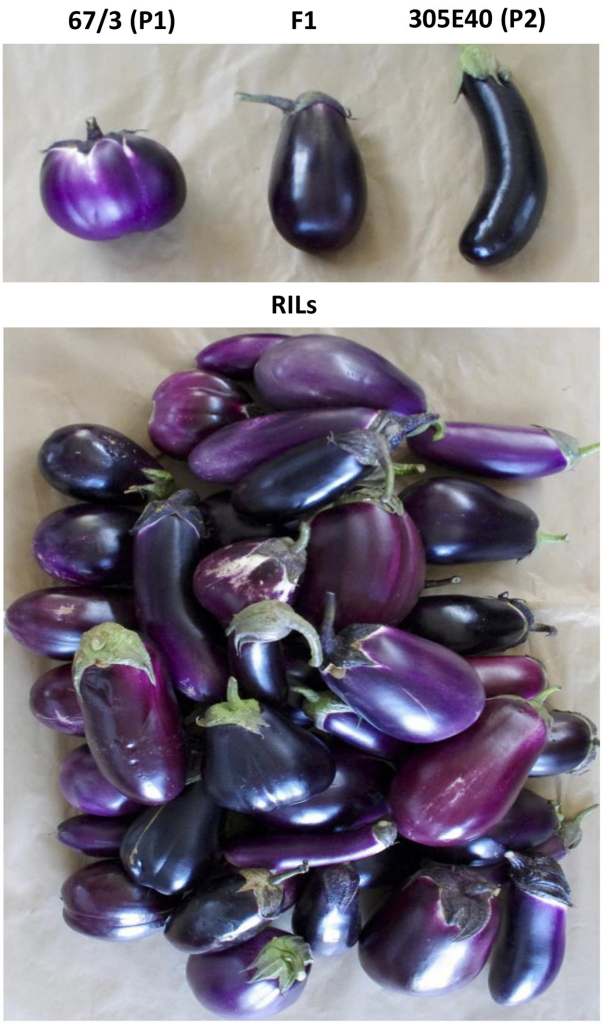

FIGURE 1 | Phenotypes of fruits at commercial maturation. Top: the two parents "67/3" (P1, male) and "305E40" (P2, female) of the RIL population, and the F1 hybrid. Bottom: the F6 RILs.

MATERIALS AND METHODS

Plant Material

An F6 RIL population, bred from a cross between lines "305E40" and "67/3," was field grown, along with both parents and the F1 hybrid, in the field at Montanaso Lombardo (45°20′N, 9°26′E). Each individual RIL progeny was sown in the greenhouse, and plantlets were transplanted in an open field at the four- to five-leaf stage. One leaflet per RIL was stored at −80°C for DNA extraction. The material was arranged as a set of two randomized complete blocks with four plants per entry per block. For fruit sampling, at least four different fruits were collected from four different plants for each biological replicate at the commercial ripening stage B (∼30 days after flowering [DAF]) as described by Mennella et al. (2012). A 2-mm-deep layer comprising the peel was carefully harvested using a sharp knife peel, taking slices of about 4 cm^2 from opposite sides of the fruits to pool pieces of peel tissues that were exposed to different sunlight intensities. Pulp was reduced to square slices 1 cm thick, removing the seeds. Tissues were frozen in liquid nitrogen and stored at −80°C.

Polar Extraction and LC/ESI/MS Analysis

Frozen tissues were freeze-dried and ground in 2 ml Eppendorf tubes with a tungsten bead using a TissueLyser (Qiagen) at 30 Hz for 30 s. Five milligrams of powder from either flesh or peel were extracted with 1.5 ml of 75% methanol/0.05% v/v trifluoroacetic acid, spiked with 3 μg/L formononetin (Sigma-Aldrich) as an internal standard. After vortexing for 30 s and centrifugation (15 min at 20,000 g, 15°C), 0.6 ml of the supernatant was removed and transferred into filter (PTFE) vials for LC/MS analysis (Waters). Ten microliters of filtered extract were injected. LC analysis was performed using a C18 Luna column (Phenomenex, Macclesfield, UK), 2.0 × 150 mm, 2.5 μm particle size. Total run time was 32 min using an elution system running at 0.250 ml/min and consisting of (A) water (0.1% formic acid and 10 pg/ml caffeine) and (B) acetonitrile:H_2O 90:10 (0.1% formic acid and 10 pg/ml caffeine as an internal mass reference, to improve mass accuracy). Gradient was 0 to 0.5 min 95% A/5% B, 24 min 25% A/75% B, and 26 min 95% A/5%. The MS analysis was performed using an LTQ Orbitrap Discovery mass spectrometer using an ESI, with an FTMS m/z range of 110–1,800 and source operating in positive ion mode (resolution 30,000), which was the one found, in preliminary trials, to give the highest number of differentially abundant (DA) metabolites.

Parameters were capillary temperature 270°C; sheath and auxiliary gas set at, respectively, 50 and 5 units; spray voltage 4.5 kV, capillary voltage set at 10 V, and tube lens at 80 V. All the chemicals and solvents used during the entire procedure were of LC/MS grade (Chromasolv).

Untargeted and Targeted Analysis of Polar Metabolites

Untargeted analysis of DA metabolites was carried out using the SIEVE software (v1.2, Thermo Fisher Scientific), which performs chromatogram alignment, peak picking, and public database (e.g., ChemSpider, KEGG, PubChem, and PlantCyc databases) querying based on accurate masses (m/z). LC/MS data were processed, applying a "control compare trend" type of experiment for "small molecules," using an already-described method (Coppola et al., 2019). With this automated analysis, MS intensities from raw LC/MS data were processed, grouping MS chromatograms as replicates assigned to each sample and generating a list of "frames" for each group of peaks found in the samples, within a specified m/z value and retention time. Frames showing intensity value differences of more than 2-fold, with a $p \leq 0.05$, between the two parental lines or between the F1 hybrid and either of the parental line were selected. Compounds were tentatively identified based on accurate mass (m/z) in full-scan MS (M+H+ or M+) and isotopic ratios (level C); MS^2 spectra generated by data-dependent MS/MS, compared to public (KEGG, Metlin, and PubChem), in-house, or *in silico* generated MS^2 spectra (Ruttkies et al., 2016) (level B); and co-migration with authentic standards (level A), using the Xcalibur software 4.4.16 Qual browser (Thermo Fisher Scientific, USA). Authentic standards were purchased from Sigma-Aldrich. The identification levels of each metabolite are described in **Supplementary Table 1**, and examples of MS^2 identification are given in the **Supplementary Text and Figures**. For pathway walking, metabolites metabolically related to the ones initially identified through untargeted analysis were identified based on accurate mass (m/z), isotopic ratios, and, when available, MS^2 data (**Supplementary Table 1**). Relative levels of accumulation of investigated metabolites were calculated as fold average and the standard deviation of integrated areas under the m/z peak of the adduct of each metabolite and the internal standard peak area (Fold/ISTD), using the TraceFinder 4.1 software (Thermo Fisher Scientific, USA), using two biological replicates (Coppola et al., 2019).

Statistical Analyses and mQTL Detection

Statistical analyses were performed using the R software (R Team, 2013). A conventional analysis of variance was applied to estimate genotype and environment effects based on the linear model $Y_{ij} = \mu + g_i + b_j + e_{ij}$, where μ, g, b, and e represent, respectively, the overall mean, the genotypic effect, the replicate effect, and the error. Broad-sense heritability values were given by $\sigma^2 G/([\sigma^2 G + \sigma^2 E]/n)$, where $\sigma^2 G$ represented the genetic variance, $\sigma^2 E$ the residual variance, and n the number of replicates. Correlations between traits were estimated using the Spearman coefficient, and kurtosis and skewness were calculated. Segregation was considered as transgressive when at least one individual RIL recorded a trait value higher or lower by at least two standard deviations than the higher or lower scoring parental line. A recently developed single-nucleotide polymorphism (SNP)-based map (Toppino et al., 2020) was used for QTL detection. Briefly, library construction was carried out using the *Hin*dIII–*Mse*I enzyme combination followed by a biotin/streptavidin-coated beads-based purification step. DNA libraries were pooled and sequenced on an Illumina HiSeq 2500 platform (Illumina Inc., San Diego, CA, USA), using 150 PE chemistry and following the manufacturer protocol at Biodiversa srl (Rovereto, TN, Italy). Overall, the map includes 7,249 SNP markers and spans 2,169 cM.

A multiple QTL mapping (MQM) method (Jansen, 1993, 1994), as implemented in the MapQTL v4 software (Van Ooijen, 2004) was used for QTL analysis. QTLs were initially identified using interval mapping; afterwards, one linked marker per putative QTL was treated as a cofactor in the approximate multiple QTL model. Cofactor selection and MQM analysis were repeated until no new QTL could be identified. LOD thresholds for declaring a QTL to be significant at the 5% genome-wide probability level were established empirically by applying 1,000 permutations per trait (Churchill and Doerge, 1994). Additive genetic effect and the percentage of the phenotypic variation explained (PVE) by each QTL were obtained from the final multiple QTL model. Individual QTLs were prefixed by a trait abbreviation, followed by the relevant chromosome designation. The confidence interval of the QTL was calculated as the $LODmax^{-1}$ interval or at least by considering 0.3 Mb upstream and downstream (if not differently reported in the text) of the marker identified at the QTL.

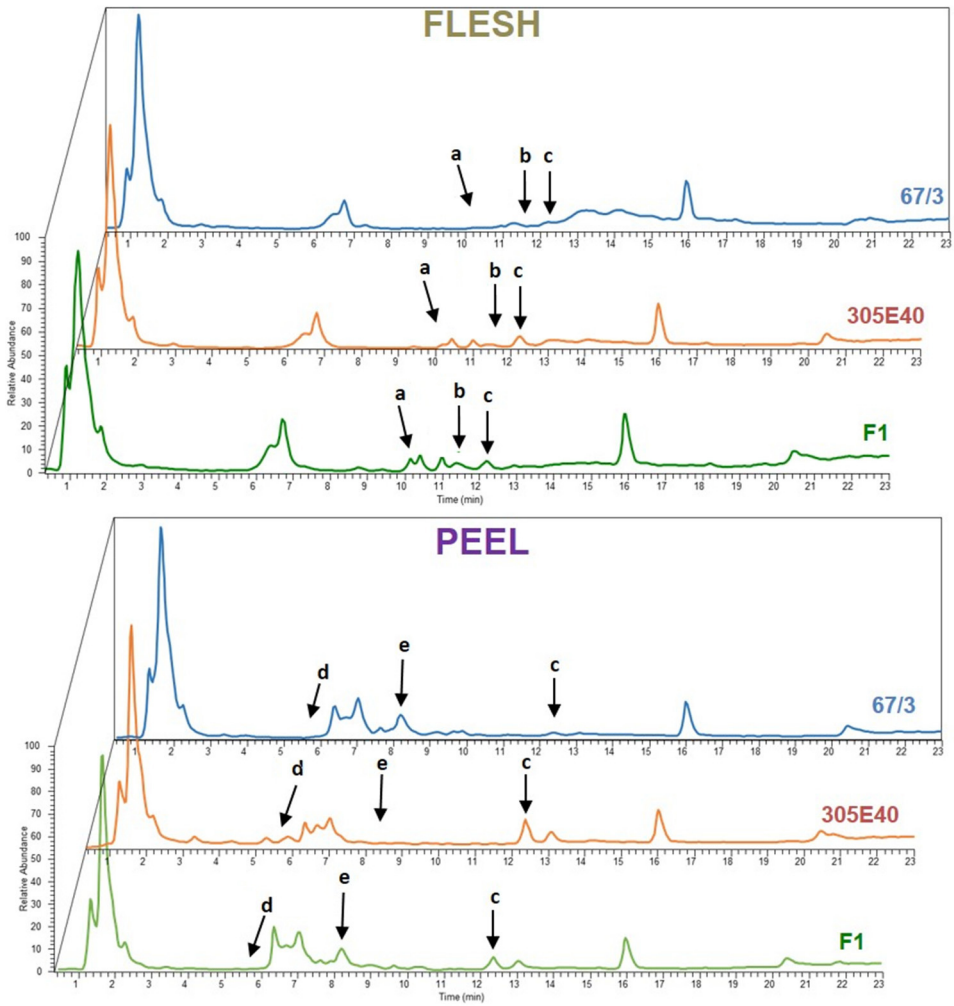

FIGURE 2 | Representative Total Ion Current (TIC) chromatograms of flesh and peel samples from parental lines "67/3" (blue), "305E40" (orange), and F1 hybrid (green). Arrows indicate differentially expressed peaks: a, solamargine; b, malonylsolamargine; c, pseudoprotodioscin; d, delphinidin-3-rutinoside; e, nasunin.

Based on the annotation v3.0, the confidence intervals of QTLs were analyzed with the SnpEff v4.3 program (Cingolani et al., 2012) to infer any potential deleterious effect on candidate genes for the metabolites in study. Briefly, resequencing data of the parental line "305E40" (Barchi et al., 2019) were aligned against the reference "67/3" eggplant genome, using the Burrows-Wheeler Aligner (BWA) (Li, 2013) (i.e., mem command) with default parameters and avoiding multiple-mapping reads. BAM files were processed and used for SNP calling using bcftools mpileup/call/norm utilities (Li, 2011) with default parameters, except for the use of the multiallelic calling model (–m option), minimum mapping quality ($Q = 20$), and the filtering out of multimapping events ($-q > 1$).

The effect of each SNP/indel was classified into four classes of effects: (1) modifier effect, as variants located outside genes (non-transcribed regions or introns); (2) low effect, as synonymous variants in coding regions; (3) moderate effect, as variants altering the aminoacidic sequence; and (4) high effect, as variants changing frameshift, thereby introducing/eliminating stop codons or modifying splice sites. For variant annotation, the CMplot[2] was used for drawing QTL results.

RESULTS

Untargeted Metabolic Profiling of Fruits From the Parental Lines and the F1 Hybrid

The RIL population composed of 164 F6 RILs (Toppino et al., 2020), as well as the two parental lines "305E40" (P1, female parent) and "67/3" (male parent) and the F1 hybrid (HF1), were grown in an experimental field at Montanaso Lombardo (45°20′N, 9°26′E) in two independent, randomized blocks, each constituting a biological replicate. Fruits were harvested from each of the two blocks at the commercial ripe (B) stage (∼30 DAF) (Mennella et al., 2012), separated into peel and flesh

[2]Available online at: https://github.com/YinLiLin/CMplot

fractions, and freeze-dried. Polar metabolites from flesh and peel were extracted from parental lines and the HF1 hybrid as previously described and analyzed by LC/ESI/MS analysis (see Materials and Methods). MS spectra collected were analyzed by performing an untargeted search for DA metabolites between "305E40" and "67/3" parents and the F1 hybrid. To this end, the MS data from the three genotypes were analyzed in all possible pairwise comparisons using the SIEVE software v1.2 (Thermo Fisher Scientific). An example of the chromatograms is shown in **Figure 2**. Peaks showing more than a 2-fold change between the two parental lines or between the F1 hybrid and either of the parental line with a $p \leq 0.05$ were classified as DA and are shown in the "untargeted" section of **Table 1**.

In the flesh, two main classes of DA metabolites were identified: (a) steroidal glycoalkaloids (SGAs)/saponins (SGAs: pseudoprotodioscin, solamargine, and malonyl solamargine) and (b) polyamine conjugates. Most metabolites showed higher relative levels in the "305E40" parent, especially pseudoprotodioscin, while both isomers of *n*, *n′*-dicaffeoylspermidine were not detectable in the "67/3" parent.

A higher number of DA metabolites were identified in peels: (a) glycosylated flavonols and anthocyanins (rutin, delphinidin-3-rutinoside, and nasunin); (b) one SGA (pseudoprotodioscin); (c) polyamine conjugates (*n*, *n′*-dicaffeoylspermidine, *n*-caffeoylputrescine, *n*-dihydrocaffeoyl-*n′*-caffeoylspermidine, and *p*-coumaroylputrescine); (d) amino acid glutamine; and (e) acetylcholine and trigonelline. Again, all compounds, except nasunin, trigonelline, and acetylcholine, showed higher relative levels in the "305E40" parent.

Depending on the compound, identification was based on accurate mass, isotopic patterns, MS^2 fragmentation patterns based on data from literature or *in silico* prediction, or comparison with authentic standards (**Supplementary Table 1** and **Supplementary Text and Figures**). Metabolites were defined as overdominant, dominant, semidominant, recessive, or under-recessive, according to the metabolite levels found in the F1 hybrid compared to those found in the two parental lines (**Table 1**).

Pathway Walking

In order to better understand the possible nature of the mutations underlying the differences between the two parental lines, we decided to identify and measure, in the MS data, metabolites that are located on the same biosynthetic pathways with respect to the ones initially identified by the untargeted analysis. We call this approach "pathway walking." Through this approach, we identified two additional DA SGAs in the flesh and three DA flavonoids (one anthocyanin and two glycosylated flavonols) in the peel (shown in the "targeted" section of **Table 1**).

A schematic biosynthetic pathway of eggplant SGAs is shown in **Figure 3**. Solamargine was the first compound identified as DA and showed higher relative levels in the flesh of the "305E40" parent, while the F1 hybrid showed intermediate levels, thus suggesting semidominant inheritance. Solasonine, a compound also synthesized from the same precursor of solasodine, showed comparable levels in the two parental lines and largely increased levels in the F1 hybrid, suggesting overdominance. Downstream of solamargine, we identified malonyl-solamargine (Wu et al., 2009; Lelario et al., 2019), which showed higher levels of accumulation in the F1 hybrid compared to both parental lines, again suggesting overdominance. On the other hand, pseudoprotodioscin, a steroidal saponin synthesized from the first precursor of SGAs (Cardenas et al., 2015), was detected in both the flesh and peel, was 3.6- to 8.6-fold higher in the "305E40" parent, and was shown to be recessive or semidominant in the F1 hybrid.

Glycosylated flavonols and anthocyanins were investigated in peel extracts, starting from the DA metabolites described above, and their biosynthesis is depicted in **Figure 4**. Rutin was 30-fold more abundant in the "305E40" parent and was recessive in the F1 hybrid. A similar trend was shown by a second compound carrying a rutinoside moiety, delphinidin-3-rutinoside (D3R). The direct precursors of these two compounds, i.e., quercetin 3-glucoside and delphinidin-3-glucoside, showed very similar relative levels in the two parental lines and in the hybrid. However, two coumaroylated derivatives of delphinidin, i.e., delphinidin 3-*O*-D-glucoside-5-(6-coumaroyl-D-glucoside) and nasunin (delphinidin-3-coumaroyl-rutinoside-5-glucoside), showed the opposite trend with respect to rutin and D3R, being more abundant in the "67/3" parent and semidominant or dominant in the F1 hybrid. This is suggestive of a clear biochemical mechanism underlying the mQTL controlling fruit pigmentation (see **Discussion**).

Polyamine conjugates are derived from the polyamines spermidine and putrescine (**Figure 5**). Unfortunately, our LC/MS settings did not allow the measurement of these precursors. All the polyamine conjugates we identified were strongly upregulated in the "305E40" parent and recessive or semidominant in HF1, again suggesting a possible biochemical mechanism underlying this metabolic trait (see **Discussion**).

Targeted Metabolic Profiling of the RIL Population

The flesh and peel fractions of the RILs were analyzed for the presence of all metabolites shown in **Table 1**. Two heatmaps summarizing the results are shown in **Figure 6**, and the detailed results are shown in **Supplementary Tables 2, 3**. As can be seen, related metabolites often clustered together in the heatmap, indicating a strong co-segregation in the RIL population. This can be observed, for instance, for solasonine/solamargine/malonyl-solamargine in the flesh and for kaempferol 3-*O*-glucoside/kaempferol 3-*O*-beta-D-sophoroside/rutin and delphinidin-3-rutinoside/nasunin in the peel.

Metabolic Variation and Inter-trait Correlations

A summary of the metabolic performance for each trait in the two parental lines, the F1, and the RILs, together with broad-sense heritability (h^2_{BS}) and other parameters such as skewness,

TABLE 1 | Differentially abundant metabolites in flesh and peel extracts of the parental lines, the F1 hybrid and the RIL populations.

	Metabolite	Code	67/3 (P1)	305E40 (P2)	F1	cv	FC P2/P1	FC F1/P1	FC HF1/P2	Inh	RILs
FLESH											
Untargeted	Pseudoprotodioscin	*F-PPROT*	0.05 ± 0.01	0.18 ± 0.04	0.07 ± 0.01	0.57	3.6**	1.4**	0.38**	R	0.12 ± 0.06
	Solamargine	*F-SOLM*	0.04 ± 0.005	0.09 ± 0.02	0.07 ± 0.02	1.83	2.25**	1.75**	0.78	D	0.18 ± 0.33
	Malonyl-solamargine	*F-MSOLM*	0.05 ± 0.02	0.08 ± 0.03	0.13 ± 0.03	1.55	1.6	2.6**	1.62*	O	0.13 ± 0.21
	n,n'-dicaffeoylspermidine	*F-DCASP*	ND	0.24 ± 0.02	0.06 ± 0.01	0.98	**	**	0.25**	S	0.13 ± 0.13
	n,n'-dicaffeoylspermidine iso	*F-DCASP2*	ND	0.11 ± 0.01	0.03 ± 0.01	0.96	**	**	0.27**	S	0.07 ± 0.06
Targeted	Demissine	*F-DEM*	0.01 ± 0.001	ND	0.003 ± 0.001	1.46	**	0.3*	**	D	0.00
	Solasonine	*F-SOLA*	0.03 ± 0.01	0.04 ± 0.01	0.08 ± 0.03	1.80	1.3	2.6**	2**	O	0.09 ± 0.16
PEEL											
Untargeted	Delphinidin-3-rutinoside	*P-D3R*	0.02 ± 0.002	0.29 ± 0.09	0.02 ± 0.001	1.16	14.5**	1	0.07**	R	0.25 ± 0.29
	Nasunin	*P-NAN*	0.57 ± 0.10	ND	0.56 ± 0.07	0.78	**	0.98	**	D	0.36 ± 0.28
	Rutin	*P-RUT*	0.01 ± 0.001	0.30 ± 0.04	0.02 ± 0.002	0.56	30**	2*	0.07**	R	0.02 ± 0.01
	Pseudoprotodioscin	*P-PPROT*	0.05 ± 0.01	0.43 ± 0.09	0.15 ± 0.04	0.55	8.6**	3**	0.35**	S	0.18 ± 0.10
	n,n'-dicaffeoylspermidine	*P-DCASP*	0.01 ± 0.002	0.13 ± 0.04	0.04 ± 0.01	0.90	13**	4**	0.31**	S	0.07 ± 0.06
	n-caffeoylputrescine	*P-CAPTR*	0.17 ± 0.05	0.65 ± 0.11	0.17 ± 0.04	0.50	3.82**	1	0.26**	R	0.17 ± 0.09
	n-dihydrocaffeoyl-n'-caffeoylspermidine	*P-DHCNCS*	0.13 ± 0.03	0.64 ± 0.18	0.31 ± 0.08	0.72	4.92**	2.38**	0.48**	S	0.69 ± 0.50
	n-coumaroylputrescine	*P-COPTR*	0.01 ± 0.002	0.12 ± 0.03	0.01 ± 0.003	0.91	12**	1*	0.08**	R	0.06 ± 0.06
	Glutamine	*P-GLUT*	0.08 ± 0.03	0.17 ± 0.05	0.05 ± 0.01	0.97	2.1*	0.6	0.29**	U	0.08 ± 0.08
	Unknown	*P-UNKN*	0.07 ± 0.01	0.15 ± 0.04	0.08 ± 0.02	0.66	2.14**	1.14	0.53**	R	0.56 ± 0.37
	Trigonelline	*P-TRIG*	0.17 ± 0.03	0.08 ± 0.02	0.06 ± 0.01	0.54	0.4**	0.35**	0.75	R	0.05 ± 0.03
	Acetylcholine	*P-ACH*	0.48 ± 0.05	0.08 ± 0.02	0.22 ± 0.02	0.58	0.16**	0.46**	2.75**	S	0.26 ± 0.15
Targeted	delphinidin 3-O-D-glucoside-5-(6-coumaroyl-D-glucoside)	*P-D3G5CG*	0.04 ± 0.01	ND	0.03 ± 0.004	0.59	**	0.75**	**	S	0.05 ± 0.03
	Kaempferol 3-O-beta-D-sophoroside	*P-KSOPH*	ND	0.03 ± 0.003	0.01 ± 0.002	0.73	**	**	0.33**	R	0.03 ± 0.02
	kaempferol-3-O-D-glucoside	*P-K3G*	0.003 ± 0.001	0.02 ± 0.01	0.006 ± 0.002	0.90	6.7**	2*	0.30**	S	0.03 ± 0.03

*Metabolite codes, averages, standard deviations (SD), coefficients of variation (cv), fold changes (FC; *significant at p-value <0.05, **significant at p-value < 0.01), and the inheritance (Inh.) in the F1 hybrid (D, Dominant; S, Semidominant; R, Recessive; O, overdominant; U, under-recessive) are shown. ND, not detectable.*

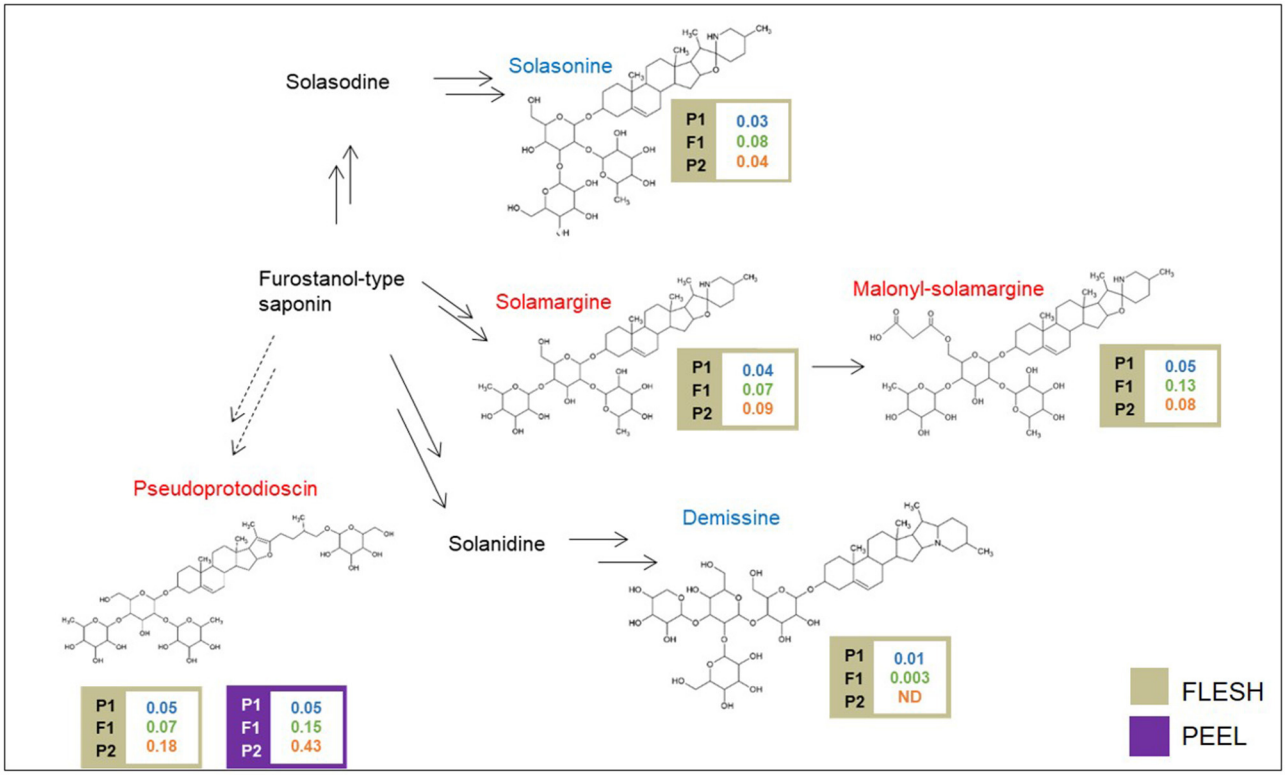

FIGURE 3 | Biosynthetic pathway of steroidal glycoalkaloids. Levels of detectable metabolites are expressed as fold/ISTD (Internal Standard: formononetin) in parental lines male P1 "(67/3)", female P2 ("305E40"), and the F1 progeny. Metabolites marked in red have been identified by the untargeted analysis, in blue by the targeted one.

kurtosis, and presence of transgressive genotypes, is listed in **Table 1** and **Supplementary Table S4**.

Transgressive genotypes among the RILs were identified for several metabolites in the study, generally accumulating higher relative levels than the higher accumulating parent "305E40," with the exclusion of some compounds, such as *n*-caffeoylputrescine (P-CAPTR), for which the transgressive RILs were characterized by a reduced accumulation. Heritability was overall high, ranging from 0.48 (P-TRIG) to 0.95 (P-D3R and P-NAN).

Significant positive and negative inter-trait correlations were detected (**Supplementary Figure 15**). As an example, delphinidin-3-rutinoside (P-D3R) was negatively ($p < 0.01$) correlated in the peel with nasunin (P-NAN), the alternative anthocyanin form synthesized in the same tissue, and glutamine (P-GLUT), and, in the flesh, with demissine (F-DEM), malonyl-solamargine (F-MSOLM), and solasonine (F-SOLA). Conversely, delphinidin-3-rutinoside (P-D3R) was positively correlated in the peel with biochemically related metabolites such as rutin (P-RUT) and kaempferol-3-*O*-D-glucoside (P-K3G) and, moreover, with pseudoprotodioscin (P-PPROT), *n*, *n*′-dicaffeoylspermidine (P-DCASP), *n*-caffeoylputrescine (P-CAPTR), *n*-dihydrocaffeoyl-*n*′-caffeoylspermidine (P-DHCNCS), and *n*-*p*-coumaroylputrescine (P-COPTR), while in the flesh level it was positively correlated with both isomers of *n*, *n*′-dicaffeoylspermidine (F-DCASP and F-DCASP2). Conversely, nasunin (P-NAN) was negatively correlated with pseudoprotodioscin (P-PPROT), *n*, *n*′-dicaffeoylspermidine (P-DCASP), *n*-caffeoylputrescine (P-CAPTR), *n*-dihydrocaffeoyl-*n*′-caffeoylspermidine (P-DHCNCS), and *n*-*p*-coumaroylputrescine (P-COPTR).

Mapping of mQTLs

QTL analyses were performed using a recently developed map (Toppino et al., 2020), constituting 7,249 SNP markers, and yielded a total of 16 major QTLs (PVE > 10%) and eight minor QTLs (**Table 2** and **Figure 7**). The largest single QTL effect was associated with P-D3R, with a PVE of 57.3%. The additive effects of all QTLs were significant at $p < 0.05$.

Twenty-four QTLs were discovered, distributed over seven chromosomes, namely, chrs. 03, 04, 05, 06, 07, 08, and 10, comprising eight isolated QTLs and five QTL clusters (**Figure 7**), whose position, closest marker, LOD, and confidence interval are detailed in **Table 2**. The isolated QTLs controlled the levels of ACH (chr. 03, 146.8 cM, and chr. 08, 113.1 cM), and UNKN (04, 8.2 cM, and 05, 88.2 cM) in the peel; DEM in the flesh (chr. 05, 5.8 cM); and COPTR (chr. 05, 61.5 cM, the only major QTL), PPROT (chr. 05, 75.5 cM, and chr. 10, 237.0 cM), and KSOPH (chr. 07, 86.4 cM, and chr. 10, 231.4 cM) in the peel.

Of the QTL clusters, one maps around 66.4 cM on chr. 05 and contains three overlapping major QTLs for delphinidin-3-rutinoside (P-D3R), nasunin (P-NAN), and *n*-caffeoylputrescine

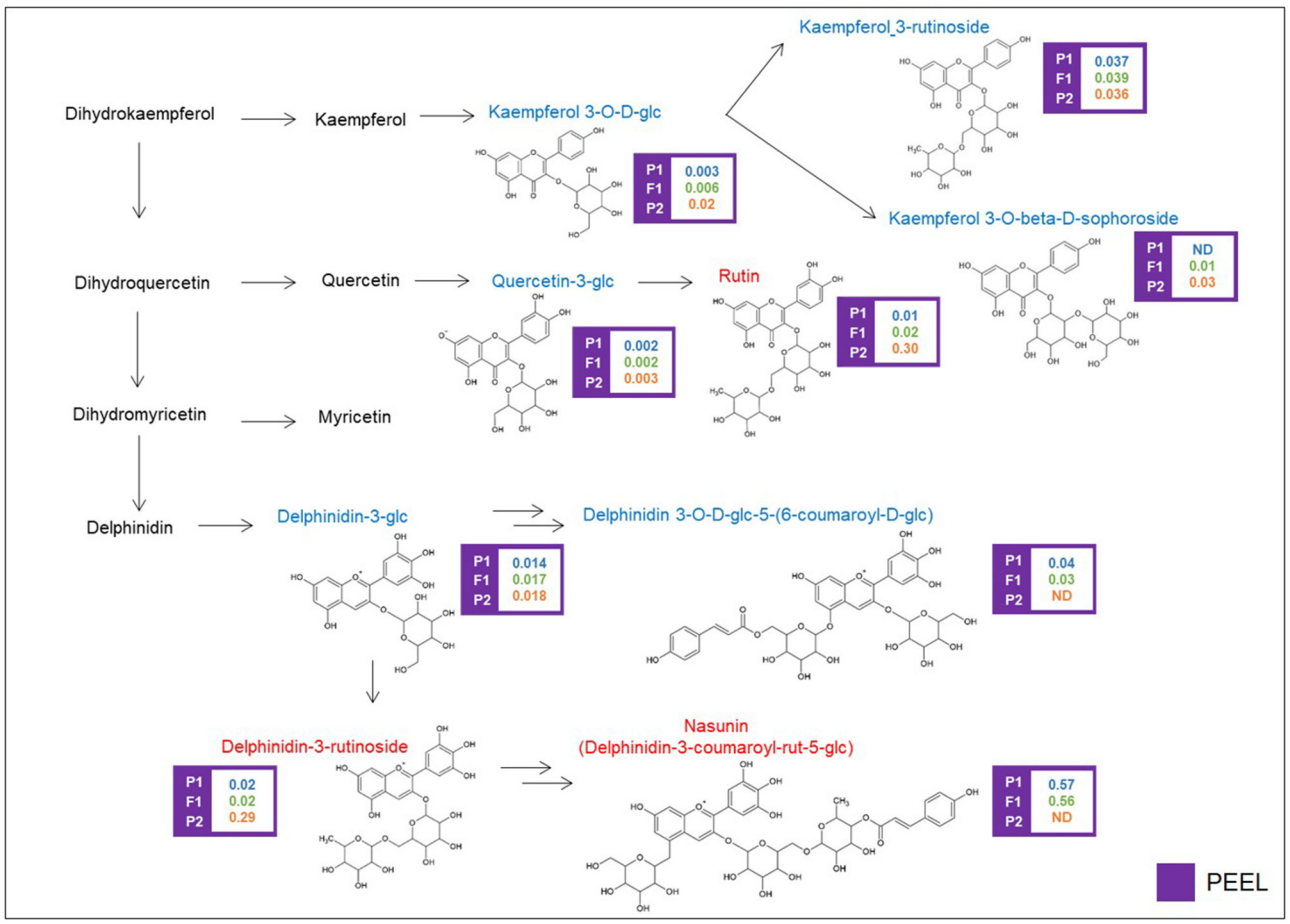

FIGURE 4 | Biosynthetic pathway of flavonoids. Levels of detectable metabolites are expressed as fold/ISTD (Internal Standard: formononetin) in parental lines "67/3" (male) and "305E40" (female) and the F1 progeny. ND, not detectable. Metabolites marked in red have been identified by the untargeted analysis, in blue by the targeted one.

(P-CAPTR); a second QTL cluster maps around 116.4 cM on chr. 05 and includes two major QTLs for *n*, *n*′-dicaffeoylspermidine (F-DCASP_05) and its isomer (F-DCASP2_05), plus two major QTLs for *n*, *n*′-dicaffeoylspermidine (P-DCASP_05) and *n*-dihydrocaffeoyl-*n*′-caffeoylspermidine (P-DHCNCS_05); the third one maps between 122.0 and 123.1 cM on chr. 06 and includes two major QTLs for solamargine and malonyl-solamargine (F-SOLM.6.1 and F-MSOLM.6.1) and minor QTLs for demissine (F-DEM) and solasonine (F-SOLA); a fourth one maps between 54.6 and 75.8 cM on chr. 08 and contains overlapping minor QTLs for an unknown (P-UNKN.8.1) and *n*-caffeoylputrescine (P-CAPTR.8.1); and, finally, a cluster mapping on chr. 10 between 230.2 and 237.0 cM contained major QTLs for kaempferol 3-*O*-beta-D-sophoroside (P-KSOPH.10.1) and pseudoprotodioscin (P-PPROT.10.1) and a minor QTL for rutin (P-RUT.10.1).

Candidate Genes Underlying the mQTLs

The candidate genes putatively involved in the genetic control of the metabolites in this study were identified among those underlying the confidence intervals of the identified QTLs and QTL clusters (shown in **Supplementary Table 5**). The possible impact of SNPs and/or indels (if any) identified in the "305E40" with respect to the "67/3" reference sequence was predicted using the SnpEff program (Cingolani et al., 2012). For each QTL or cluster of QTLs, the list of selected candidate genes is reported in **Table 3**, along with the annotation, the SnpEff-predicted effect on the function of the encoded protein in the "305E40" allele variant (**Supplementary Table 5**), and the expression in "67/3" fruits at 2–4 cm (stage 1), at commercial ripening (stage 2), and at physiological ripening (stage 3).

DISCUSSION

mQTLs Mapping

Genome-wide metabolic profiling is a powerful tool to identify components of fruit metabolic composition and isolate the underlying genes. Metabolic profiling of RIL and/or introgression line (IL) populations was used to map metabolic QTLs controlling biomass production content in *Arabidopsis* (Lisec

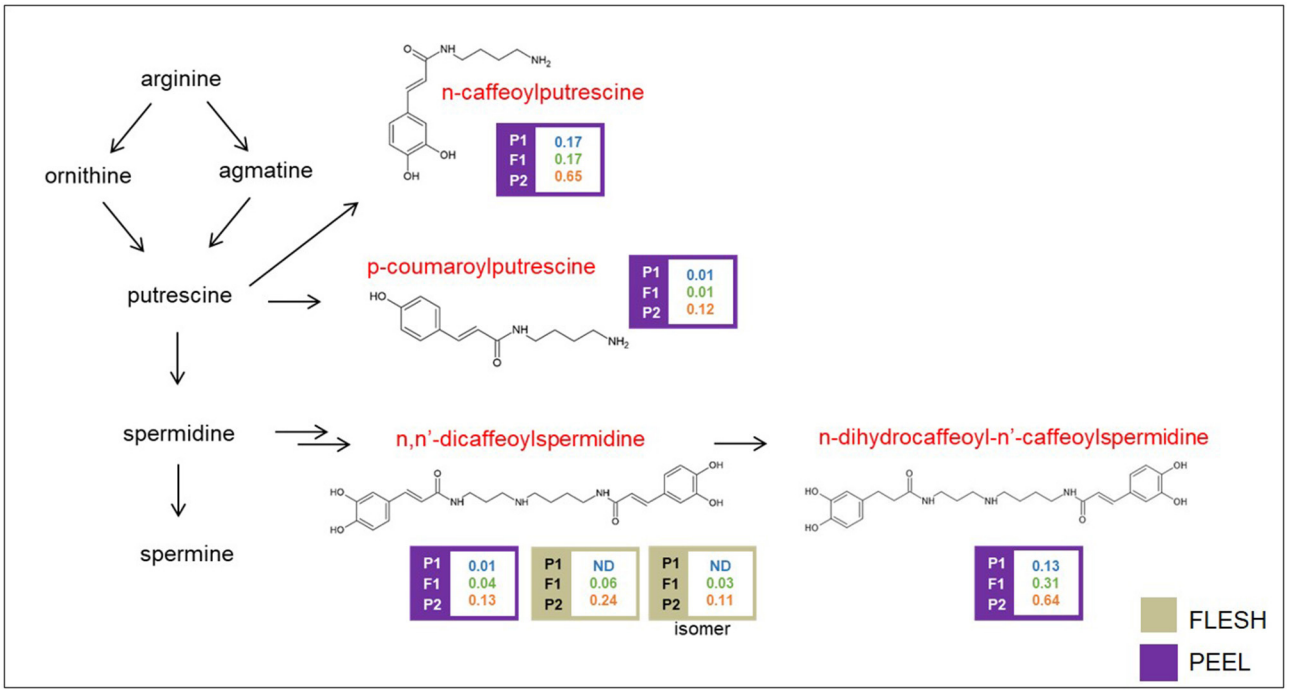

FIGURE 5 | Biosynthetic pathway of polyamine conjugates. Levels of detectable metabolites are expressed as fold/ISTD (Internal Standard: formononetin) in parental lines "67/3" (male) and "305E40" (female) and the F1 progeny. Metabolites marked in red were identified by the untargeted analysis.

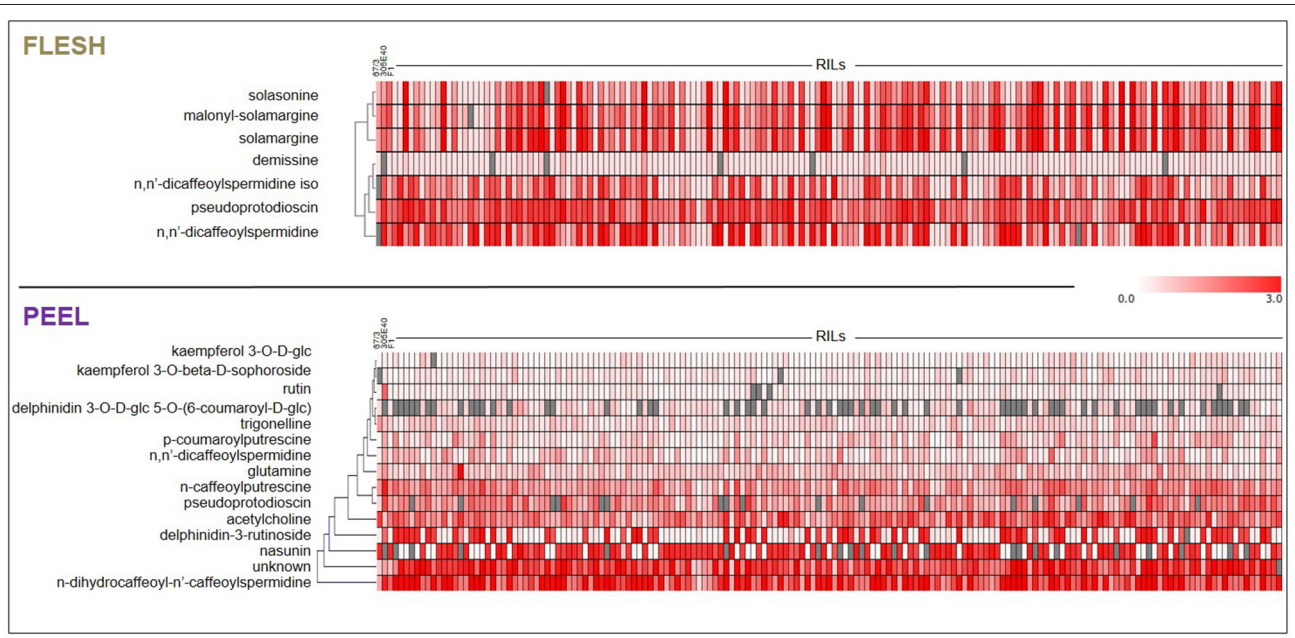

FIGURE 6 | Heat-maps representing levels of accumulation of differentially metabolites in flesh and peel extracts. Metabolites were subjected to Hierarchical Clustering Analysis (HCA). Color coding represents the average signal intensity (fold/ISTD) in individual lines.

et al., 2008) or influencing nutritional quality in tomato fruits (Schauer et al., 2006) and potato tubers (Carreno-Quintero et al., 2012). With respect to other Solanaceae, eggplant genome-wide metabolic profiling has lagged behind, mainly due to the lack, until recently, of a high-quality reference sequence and of reliable metabolic profiling methods.

TABLE 2 | mQTLs and mQTL clusters detected in the mapping population.

Cluster	QTL	GW	Chr.	cM	Marker	LOD	CI	% PVE	A
	P-ACH.3.1	3.3	03	146.8	CH03_76097038	4.29	146.8	10.7	−0.0506
	P-UNKN.4.1	3.1	04	8.2	CH04_3119177	3.13	8.2	6.9	−0.1002
	F-DEM.5.1	3.2	05	5.8	CH05_7953029	5.42	4.0–5.9	14.0	−0.0028
	P-COPTR.5.1	3	05	61.5	CH05_34699887	12.01	61.5–63.5	29.5	0.0332
P-FLAVO/POLY 5	*P-D3R.5.1*	3.4	05	66.4	CH05_36124744	28.91	64.0–66.0	57.3	0.2324
	P-NAN.5.1	3.3	05	66.4	CH05_36124744	23.69	64.3–66.4	54.0	−0.2202
	P-CAPTR.5.1	3.3	05	66.4	CH05_36124744	11.53	64.3–66.4	26.2	0.0457
	P-PPROT.5.1	3.2	05	75.5	CH05_37533757	3.52	75.5	9.1	0.0321
	P-UNKN.5.1		05	88.2	CH05_38677476	5.03	86.1–92.2	11.4	0.1325
F/P-POLY 5	*F-DCASP.5.1*	3.1	05	116.4	CH05_39954700	6.54	116.1–120.3	17.3	0.0529
	F-DCASP2.5.1	3.3	05	116.4	CH05_39954700	6.12	116.1–120.3	16.3	0.0261
	P-DCASP.5.1	3.2	05	116.4	CH05_39954700	18.67	116.4	42.4	0.0388
	P-DHCNCS.5.1	3.2	05	116.4	CH05_39954700	22.45	116.1–120.3	48.5	0.3492
F-GLYKO 6	*F-MSOLM.6.1*	2.7	06	122.0	CH06_98079686	4.20	122.0	11.5	−0.0696
	F-SOLM.6.1	2.6	06	122.0	CH06_98079686	3.69	121.3–123.1	10.1	−0.1071
	F-SOLA.6.1	2.7	06	122.0	CH06_98079686	3.32	121.3–123.1	9.2	−0.0497
	F-DEM.6.1		06	123.1	CH06_96696408	3.15	123.1	7.8	−0.0020
	P-KSOPH.7.1	3.2	07	86.4	CH07_131303988	5.18	86.4	11.8	0.0088
P-POLY/UNKN 8	*P-UNKN.8.1*		08	54.6	CH08_73641123	3.61	54.6–55.6	8.0	0.1079
	P-CAPTR.8.1		08	75.7	CH08_73925400	3.89	75.8	7.7	0.0245
	P-ACH.8.1		08	113.1	CH08_69973401	3.68	113.0	9.1	0.0506
P-FLAVO/GLYKO 10	*P-RUT.10.1*	3.1	10	230.2	CH10_94979390	3.34	228.2–230.2	9.4	−0.0042
	P-KSOPH.10.1		10	231.5	CH10_94779014	6.62	231.5	15.5	0.0099
	P-PPROT.10.1		10	236.0	CH10_94997738	4.32	236.9	11.3	0.0350

For each metabolite, the chromosome, the closest marker, and the LOD value are indicated, along with the confidence interval (CI), the percentage of variation explained (%PVE), and the genome-wide thresholds (GW) at p = 0.05 (as determined from 1,000 permutations). Values in A indicate the directionality of the QTL (i.e., for positive values, the "305E40" parent contributes higher relative levels of the metabolite; for negative values, the opposite is true).

A chromosome-anchored eggplant genome sequence has been recently developed (Barchi et al., 2019) and, in combination with the metabolic profiling methods described here, paves the way for the discovery of genes controlling major metabolic traits. Here, we describe a method for comprehensive metabolic profiling of polar metabolite eggplant fruits, based on LC/HRMS. An untargeted approach was applied to identify metabolites showing contrasting regulations in the two parental lines and the F1 hybrid. The DA metabolites, as well as additional ones biosynthetically related to those initially identified, were then quantified in an F6 population composed of 164 RILs, and the data were used to infer and map mQTLs influencing fruit nutritional quality.

Based on metabolite relative levels of the F1 hybrid and the two parental genotypes, we were able to identify overdominant, dominant, semidominant, recessive, or under-recessive traits. This was in good agreement with the transgressive genotypes identified in the RIL population, in which some individuals showed higher relative levels of metabolites with respect to the highest scoring parent "305E40" and the F1 for the dominant/overdominant metabolites malonyl-solamargine and *n*, *n*′-dicaffeoylspermidine and lower relative levels of the recessive metabolites delphinidin-3-rutinoside and rutin.

Major mQTLs were identified influencing the content of several classes of metabolites: SGAs (flesh and peel), anthocyanins and glycosylated flavonols (peel), polyamine conjugates (flesh and peel), and acetylcholine (peel). Analyses using a high-density genetic linkage map (Toppino et al., 2020) revealed that eight isolated QTLs and five QTL clusters control the accumulation of metabolites in this study.

Steroidal Glycoalkaloids (SGAs)

SGAs are triterpene-derived, toxic defense compounds synthesized by many Solanaceae and Liliaceae (Cardenas et al., 2015). The main eggplant SGAs are alpha-solasonine and alpha-solamargine (Sanchez-Mata et al., 2010; Mennella et al., 2012) (**Figure 3**). Depending on the dosage, SGAs, including eggplant SGAs, have a variety of harmful (toxic) and beneficial (anticarcinogenic) effects in both animals and humans (Friedman, 2006, 2015). Previous studies showed that chrs. 07 and 12 of tomato, potato, and eggplant harbor clusters of genes

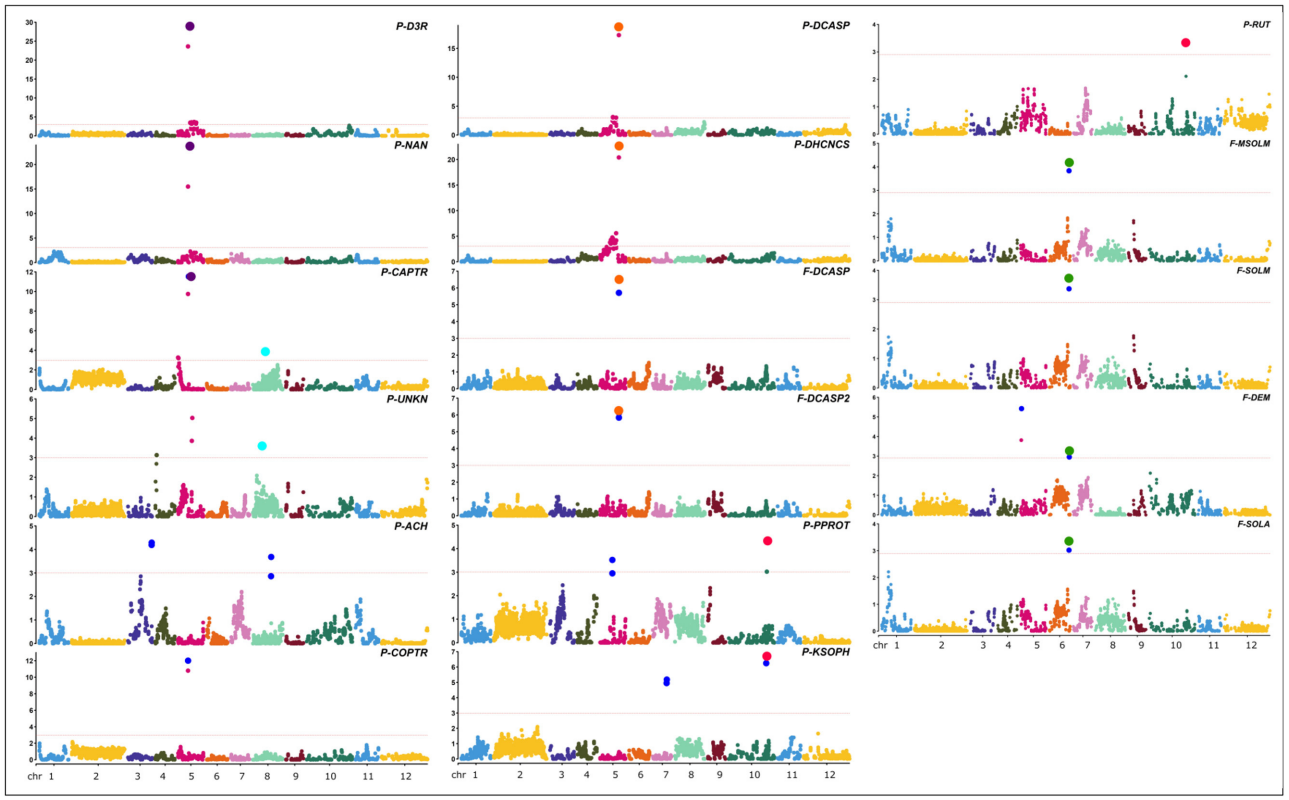

FIGURE 7 | Positions of QTLs identified for the metabolites in study. Red lines in the Manhattan plots indicate LOD significance threshold. Blue dots represent significant markers within the confidence interval of the QTL (LODmax-1 interval), with LOD values plotted against genome locations. Cluster of QTLs are indicated as purple (P - FLAVO/POLY 5), orange (F/P - POLY 5), green (F-GLYKO 6), light blue (P-POLY/ ACTPH 8), and red (P-FLAVO/GLYKO 10) dots.

involved in SGA biosynthesis (Itkin et al., 2013; Barchi et al., 2019).

With the untargeted approach, the SGAs solamargine and its derivative malonyl-solamargine, as well as a steroidal saponin, pseudoprotodioscin, were detected as DAs, with higher relative levels in the "305E40" parent, which carries introgressions from *S. aethiopicum* (Barchi et al., 2010), an edible species known to contain high levels of solamargine (Sanchez-Mata et al., 2010). Two additional SGAs, solasonine and demissine, were detected by pathway walking. One QTL cluster controlling the levels of solasonine, solamargine, malonyl-solamargine, and demissine maps on chr. 06 and co-localizes with the SGA QTL mapped by Toppino et al. (2016). Candidate genes underlying this cluster include two multidrug and toxin efflux (MATE) transporters, possibly involved in vacuolar sequestration of SGAs; a cytochrome P450 contributing to SGA biosynthesis in potato (Manrique-Carpintero et al., 2014); and a cluster of genes encoding possible beta-amyrin 28-monooxygenases, involved in a competing branch of triterpenoid biosynthesis (Daniel et al., 2017). A QTL for demissine in the flesh (F-DEM.5.1) contains a gene encoding a UGT94 enzyme (a tomato GAME18 homolog) (Cárdenas et al., 2019). Within the confidence interval of the major QTL on chr. 10 for pseudoprotodioscin in the peel, the gene SMEL_010g352880, coding for an abscisic acid receptor PYL4 involved in the regulation of tobacco alkaloid biosynthesis (Lackman et al., 2011), was detected. None of the SGA QTLs maps on chr. 07 or 12, which have been previously shown to harbor clusters of genes involved in SGA biosynthesis in tomato, potato, and eggplant (Itkin et al., 2013; Barchi et al., 2019), suggesting that SGA accumulation in the present population is controlled by different genomic regions. The results presented here increase our understanding of SGA inheritance and accumulation in eggplant, generating useful knowledge for the marker-assisted breeding of these bioactive compounds.

Flavonoids

Anthocyanins and glycosylated flavonols are phenylpropanoid pigments, important both for fruit antioxidant properties and for their health-promoting effects (He and Giusti, 2010). In particular, nasunin has been described for its antioxidant and cholesterol-lowering properties (Kayamori and Igarashi, 1994; Noda et al., 2000; Casati et al., 2016). In eggplant, they are synthesized in leaves and in the peel of ripe fruits, which show large variation with regard to pigmentation (Cericola et al., 2013) (**Figure 4**). The genetic control of anthocyanin formation, distribution, and accumulation has been widely studied in Solanaceae species including eggplant (van Eck et al., 1993;

TABLE 3 | Candidate genes underlying the mQTLs and mQTL clusters.

Cluster/QTL	Genes within CI	Candidate Gene	Annotation	SnpEff impact	FPKM stage 1	FPKM stage 2	FPKM stage 3
P-ACH.3.1	27	SMEL_003g182830.1	Similar to ND4: NADH-ubiquinone oxidoreductase chain 4	Mod	0.26	0.90	4.59
F-DEM.5.1	55	SMEL_005g229780.1	Protein of unknown function	Mod	0.00	0.48	0.00
		SMEL_005g229640.1	Similar to ycf2-A	Mod	0.00	0.00	0.00
		SMEL_005g230040.1	Similar to UGT94E5: Beta-d-glucosyl crocetin beta-1%2C6-glucosyltransferase	No	13.40	112.15	29.69
P-COPTR.5.1	45	SMEL_005g235160.1	Similar to At4g09670: Uncharacterized oxidoreductase At4g09670	Mod	20.59	22.49	56.48
		SMEL_005g235240.1	Similar to WRKY51: Probable WRKY transcription factor 51	Mod	0.00	0.09	0.00
		SMEL_005g235090.1	Similar to KTI2: Kunitz trypsin inhibitor 2	Mod	57.38	9.35	0.00
P-FLAVO/POLY 5	73	SMEL_005g235650.1	Similar to CRY1: Cryptochrome-1	No	9.53	7.77	8.58
		SMEL_005g235690.1	Similar to UGT85A24: 7-deoxyloganetin glucosyltransferase	High	0.00	0.09	0.00
		SMEL_005g235810.1	Similar to AGL70: Agamous-like MADS-box protein AGL70	High	17.46	16.39	25.61
		SMEL_005g235830.1	Protein of unknown function	High	0.00	5.05	19.96
		SMEL_005g236240.1	Similar to BEAT: Acetyl-CoA-benzyl alcohol acetyltransferase	High	34.71	50.28	0.24
P-PPROT.5.1	5	SMEL_005g236880.1	Protein of unknown function	Mod	6.00	19.95	10.13
		SMEL_005g236890.1	Similar to Polcalcin Cup a 4	Mod	0.00	0.46	0.00
		SMEL_005g236900.1	Similar to SYRV3: Polcalcin Syr v 3	Mod	0.00	0.00	0.00
F/P-POLY 5	134	SMEL_005g240620.1	Similar to At5g48380: Probably inactive leucine-rich repeat receptor-like protein kinase	High	2.73	5.28	0.63
		SMEL_005g237380.1	Protein of unknown function	High	0.00	0.00	0.00
		SMEL_005g240050.1	Similar to N: TMV resistance protein N	High	0.00	0.01	0.12
		SMEL_005g240370.1	Similar to SALAT: Salutaridinol 7-*O*-acetyltransferase	Mod	35.78	32.00	0.28
		SMEL_005g240400.1		Mod	1.89	2.93	2.88
		SMEL_005g240350.1	Similar to BEAT: Acetyl-CoA-benzyl alcohol acetyltransferase	Mod	1.40	0.20	0.00
		SMEL_005g240550.1		Mod	100.36	69.23	0.07
F-GLYKO 6	159	SMEL_006g259360.1	Similar to N: TMV resistance protein N	Mod	2.45	2.56	2.03
		SMEL_006g258510.1	Similar to ndhH: NAD(P)H-quinone oxidoreductase subunit H%2C chloroplastic	Mod	0.00	0.00	0.00
		SMEL_006g258660.1	Similar to DTX54: Protein DETOXIFICATION 54	Mod	0.00	0.00	0.00
		SMEL_006g258670.1		Mod	0.00	0.00	0.00
		SMEL_006g259540.1	Similar to CYP71D7: Cytochrome P450 71D7	No	0.00	0.00	0.00

(Continued)

TABLE 3 | Continued

Cluster/QTL	Genes within CI	Candidate Gene	Annotation	SnpEff impact	FPKM stage 1	FPKM stage 2	FPKM stage 3
		SMEL_006g259050.1	Similar to CYP716A15: Beta-amyrin 28-monooxygenase	No	0.00	0.00	0.00
		SMEL_006g259060.1		No	0.48	0.42	0.00
P-KSOPH.7.1	34	SMEL_007g288740.1	Similar to CYCU1-1: Cyclin-U1-1	Mod	0.70	0.17	0.00
		SMEL_007g288700.1	Protein of unknown function	Mod	19.47	9.53	9.66
		SMEL_007g288720.1	Similar to PCMP-A3: Pentatricopeptide repeat-containing protein At1g71460%2C	Mod	2.00	1.73	2.81
		SMEL_007g288660.1	Similar to PER3: Peroxidase 3 (*Arabidopsis thaliana* OX%3D3702)	Mod	62.19	23.87	17.71
		SMEL_007g288690.1		Mod	0.00	0.00	0.08
		SMEL_007g288730.1	Similar to PEX22: Peroxisome biogenesis protein 22	Mod	21.72	23.65	41.05
		SMEL_007g288920.1	Similar to BHLH117: Transcription factor bHLH117	No	0.00	0.00	0.00
P-POLY/UNKN 8	26	SMEL_008g307770.1	Similar to PCMP-E22: Pentatricopeptide repeat-containing protein At2g02750	High	0.00	0.00	0.00
		SMEL_008g307900.1	Similar to ycf2-A: Protein Ycf2	High	0.00	0.00	0.00
		SMEL_008g307850.1	Protein of unknown function	High	0.00	0.00	0.00
		SMEL_008g307910.1	Similar to PAB7: Polyadenylate-binding protein 7	High	0.00	0.00	0.00
		SMEL_008g307740.1	Similar to CBL10: Calcineurin B-like protein 10	High	12.01	9.91	4.77
		SMEL_008g307920.1	Similar to Acyl-lipid (9-3)-desaturase	Mod	22.21	14.70	22.65
P-ACH.8.1	10	SMEL_008g307500.1	Protein of unknown function	Mod	0.00	0.00	0.00
		SMEL_008g307450.1	Similar to vacuolar-processing enzyme	Mod	1.32	2.30	0.09
		SMEL_008g307530.1	Similar to At4g32950: Probable protein phosphatase 2C 61	Mod	0.00	0.06	0.15
		SMEL_008g307440.1	Similar to vacuolar-processing enzyme	Mod	107.04	89.38	428.99
		SMEL_008g307520.1	Similar to At4g32950: Probable protein phosphatase 2C 61	Mod	0.00	0.00	0.07
P-FLAVO/GLYKO 10	40	SMEL_010g353210.1	Protein of unknown function	High	0.00	0.00	0.00
		SMEL_010g352840.1	Similar to WAK2: Wall-associated receptor kinase 2	Mod	0.00	0.00	0.00
		SMEL_010g352880.1	Similar to PYL4: Abscisic acid receptor PYL4	No	0.16	0.08	0.00
		SMEL_010g352930.1	Similar to DREB2C: Dehydration-responsive element-binding protein 2C	No	0.00	0.00	0.00
		SMEL_010g353090.1	Similar to RAPTOR1: Regulatory-associated protein of TOR 1	No	7.28	4.16	7.11
		SMEL_010g353110.1		No	0.32	1.43	1.33
		SMEL_010g353170.1	Similar to peroxidases and cationic peroxidases	No	0.00	0.00	0.00
		SMEL_010g353190.1		No	0.00	0.11	0.15

For each mQTL/mQTL cluster, the total number of genes within the confidence interval, the candidate genes, and the impact of the mutations (high, moderate, or no effect) is indicated. SnpEff output for the below candidate genes is reported in ***Supplementary Table 5****. Expression values (FPKM, from Barchi et al., 2019) for candidate genes in fruits at 2–4 cm (stage 1), at commercial ripening (stage 2), and at physiological ripening (stage 3) of the line "67/3" are reported.*

Chaim et al., 2003; Borovsky et al., 2004; Bovy et al., 2007; Gonzali et al., 2009; Stommel and Dumm, 2015).

An F2 population derived from the same cross ("305E40" × "67/3") was employed for the development of a RAD-tag-based linkage map and for the identification of QTL associated with phenotypic and biochemical traits, as well as for the identification of chromosome regions involved in anthocyanin distribution in eggplant tissues and organs, highlighting their synteny with tomato (Barchi et al., 2012; Ge et al., 2013; Cericola et al., 2014; Toppino et al., 2016). More recently, the RIL population employed in this study was used to elucidate the genetic basis of seven traits related to anthocyanin content in different organs (Toppino et al., 2020). Both studies revealed the presence of two main QTL clusters on chrs. 05 and 10, with the cluster on chr. 10 being mainly involved in anthocyanin intensity in leaves, stems, and corollas, while the cluster on chr. 05 is more associated with the type of anthocyanin accumulated (Barchi et al., 2012; Toppino et al., 2020). We show here that the cluster identified on chr. 10 controls the levels of the glycosylated flavonols rutin (P-RUT) and kaempferol 3-*O*-beta-D-sophoroside (P-KSOPH) in the peel. This cluster contains several candidate genes, including a PYL4 abscisic acid receptor (SMEL_010g352880), which was also identified as a candidate for P-PPROT. Indeed, abscisic acid not only seems to regulate alkaloid accumulation (see the paragraph on steroidal glycoalkaloids) but is also known to positively regulate flavonoid/anthocyanin biosynthesis in several plant species (Hattori et al., 1992; Ban et al., 2003; Diretto et al., 2020).

We identified a dehydration-responsive element-binding protein 2C and a PPC6-1—protein phosphatase 2C—lying within the cluster. Several peroxidase-encoding genes have been also identified, which may be involved in the degradation of anthocyanin, leading to pigment concentration reduction and color fading (Luo et al., 2019).

Three peroxidases have also been identified in the confidence interval of the QTL for P-KSOPH on chr. 07, together with a BHLH transcription factor, similar to one putatively involved in anthocyanin biosynthesis in peony (Zhang et al., 2015), which carries a moderate effect according to SnpEff analysis.

The cluster on chr. 05 around 66.5 cM presents different characteristics: it controls, in an opposite way, the levels of nasunin and delphinidin-3-rutinoside (D3R), the two alternative anthocyanin forms in the parental lines of the RIL population. This cluster was already described as a genomic region involved in the control of several anthocyanin-related traits, such as stem anthocyanin, corolla color, and peel fruit color (Barchi et al., 2012; Toppino et al., 2016, 2020).

Nasunin is a coumaroylated form of D3R (**Figure 4**), and the two compounds show opposite trends, with nasunin being higher in the "67/3" parent and dominant, while D3R is higher in the "305E40" parent and recessive. This suggests that the QTL affects the function of an acyl transferase, which is active in the "67/3" parent and totally or partially inactive in the "305E40" one. Indeed, the candidate genes underlying the QTL cluster contain the presence of a gene (SMEL_005g240420.1) with high similarity to the *Clarkia breweri* acetyl-CoA benzyl alcohol acetyltransferase (BEAT), an enzyme involved in the generation of floral scent (Dudareva et al., 1998). It is conceivable that in eggplant, this gene acts on anthocyanins instead rather than on benzyl alcohol and accepts different acyl group donors, such as coumaroyl-CoA. Analysis of additional compounds in the same pathway supports this hypothesis: delphinidin 3-glucoside-5-coumaroyl-glucoside shows distribution and dominance relationships similar to those of nasunin. The SnpEff analysis performed on the two parental lines revealed a SNP which could determine a severe effect of loss-of-function mutation in the SMEL_005g240420.1 CDS sequence of the "305E40" parent, in agreement with the biochemical data. For these reasons, a more detailed functional study of this gene was started (Toppino et al., unpublished). Other interesting genes lying within the confidence interval of the cluster are SMEL_005g235650.1, a cryptochrome 1 blue light photoreceptor, controlling photomorphogenesis and anthocyanin accumulation in tomato (Ninu et al., 1999).

Polyamine Conjugates

Polyamines play different key functions in the regulation of many physiological processes involving floral and fruit development and leaf senescence, as well as abiotic and biotic plant stress responses (Alcázar et al., 2010; Tiburcio et al., 2014). Their schematic biosynthesis is shown in **Figure 5**. They are found often as conjugates with acyl (coumaroyl, caffeoyl, and sinapoyl) groups, which play a role in the defense against herbivores (Kaur et al., 2010).

We found several major mQTLs and QTL clusters for polyamine conjugates. A major cluster maps on chr. 05 around 116.4 cM, with the "305E40" parent contributing higher relative levels of these metabolites. Underlying genes comprise genes for pathogen resistance (LRR, N) and a cluster of seven acyltransferases showing similarity to BEAT as well as to salutaridinol 7-*O*-acetyltransferase (SALAT), an enzyme involved in alkaloid biosynthesis in *Papaver somniferum* (Grothe et al., 2001). All these genes show lesions with high or moderate impact in their coding sequence in one of the two parental lines.

A second cluster for polyamine conjugates maps on chr. 05 around 66.4 cM. It controls the levels of *n*, *n*′-dicaffeoylspermidine in the flesh and peel and (only in the peel) of *n*-dihydrocaffeoyl-*n*′-caffeoylspermidine and *n*-caffeoylputrescine. This cluster overlaps with the one controlling nasunin/D3R. However, the relative levels and dominance characteristics of polyamine conjugates are antiparallel with respect to those of nasunin. Therefore, it is difficult to assume the two overlapping QTLs are due to a single acyltransferase with broad substrate specificity, acting on both classes of compounds. Since a second acyltransferase is not found within the confidence interval of this QTL cluster, it is possible that the polyamine QTL is mediated by the action of regulatory proteins, many of which are found in this interval. Within the confidence interval of the mQTL cluster on chr. 08, which contains overlapping QTLs for P-COPTR and UNKN, five genes having a severe SnpEff impact were detected, including an acyl-lipid (9-3)-desaturase, reported to play a role in polyamine biosynthesis (Christopher and Holtum, 2000) (**Supplementary Table 5**).

CONCLUSIONS

The plant metabolome represents a bridge between the genome and the phenome of plants, and thanks to the available high-throughput metabolic profiling and genotyping technologies, it is now possible to shed light on the genetic bases of metabolism in crop plants.

We previously developed a high-density linkage map by genotyping a RIL mapping population obtained from the cross of two parental lines differing for many traits, including the shape, dimension, and pigmentation of their fruits.

Our metabolomic strategy led to the identification of DA metabolites in the fruit flesh and peel, most of which belong to the glycoalkaloid, anthocyanin, and polyamine conjugate classes. The metabolic profiling of the F1 hybrid and each RIL progeny made it possible to detect for the first time mQTLs and QTL clusters influencing the regulation of these compounds and influencing the fruit nutritional quality in eggplant.

Genome annotation in combination with sequence differences in the two parental lines supplied a key tool to gather valuable information for QTL fine mapping, candidate gene identification, and the identification of molecular markers suitable for identifying favorable alleles, thus increasing the precision and efficiency of selection in breeding. Our data also demonstrate the benefits of the methods described here for broad metabolomics studies in fruit-bearing crop species.

DATA AVAILABILITY STATEMENT

For genotypic data refer to Toppino et al. (2020): https://doi.org/10.3390/genes11070745. The metabolite levels are provided in the **Supplementary Tables S2, S3**. The raw metabolomic data are available upon request.

AUTHOR CONTRIBUTIONS

MS and LB produced and analyzed the data and wrote the manuscript. LT provided the materials, analyzed the data, and wrote the manuscript. GD helped in producing the data. TS provided the materials. SL revised the manuscript. GLR conceived the study and reviewed the paper. GG conceived and coordinated the study, analyzed the data, and wrote the manuscript. All authors read and approved the final manuscript.

FUNDING

This work was supported by the EC-funded project G2P-SOL (contract no. 677379).

ACKNOWLEDGMENTS

We thank Gianluca Francese and Giuseppe Mennella (CREA, Research Centre for Vegetable and Ornamental Crops) for their help with the metabolic profiling.

SUPPLEMENTARY MATERIAL

The Supplementary Material for this article can be found online at: https://www.frontiersin.org/articles/10.3389/fpls.2021.638195/full#supplementary-material

REFERENCES

Alcázar, R., Altabella, T., Marco, F., Bortolotti, C., Reymond, M., Koncz, C., et al. (2010). Polyamines: molecules with regulatory functions in plant abiotic stress tolerance. *Planta* 231, 1237–1249. doi: 10.1007/s00425-010-1130-0

Ban, T., Ishimaru, M., Kobayashi, S., Goto-Yamamoto, N., and Horiuchi, S. (2003). Abscisic acid and 2, 4-dichlorophenoxyacetic acid affect the expression of anthocyanin biosynthetic pathway genes in 'Kyoho'grape berries. *J. Hortic. Sci. Biotechnol.* 78, 586–589. doi: 10.1080/14620316.2003.11511668

Barchi, L., Lanteri, S., Portis, E., Acquadro, A., Vale, G., Toppino, L., et al. (2011). Identification of SNP and SSR markers in eggplant using RAD tag sequencing. *BMC Genomics* 12:304. doi: 10.1186/1471-2164-12-304

Barchi, L., Lanteri, S., Portis, E., Stagel, A., Vale, G., Toppino, L., et al. (2010). Segregation distortion and linkage analysis in eggplant (*Solanum melongena* L.). *Genome* 53, 805–815. doi: 10.1139/G10-073

Barchi, L., Lanteri, S., Portis, E., Vale, G., Volante, A., Pulcini, L., et al. (2012). A RAD tag derived marker based eggplant linkage map and the location of QTLs determining anthocyanin pigmentation. *PLoS ONE* 7:e43740. doi: 10.1371/journal.pone.0043740

Barchi, L., Pietrella, M., Venturini, L., Minio, A., Toppino, L., Acquadro, A., et al. (2019). A chromosome-anchored eggplant genome sequence reveals key events in Solanaceae evolution. *Sci. Rep.* 9, 1–13. doi: 10.1038/s41598-019-47985-w

Barchi, L., Toppino, L., Valentino, D., Bassolino, L., Portis, E., Lanteri, S., et al. (2018). QTL analysis reveals new eggplant loci involved in resistance to fungal wilts. *Euphytica* 214:20. doi: 10.1007/s10681-017-2102-2

Borovsky, Y., Oren-Shamir, M., Ovadia, R., De Jong, W., and Paran, I. (2004). The A locus that controls anthocyanin accumulation in pepper encodes a MYB transcription factor homologous to Anthocyanin2 of Petunia. *Theoret. Appl. Genet.* 109, 23–29. doi: 10.1007/s00122-004-1625-9

Bovy, A., Schijlen, E., and Hall, R. D. (2007). Metabolic engineering of flavonoids in tomato (*Solanum lycopersicum*): the potential for metabolomics. *Metabolomics* 3:399. doi: 10.1007/s11306-007-0074-2

Cárdenas, P. D., Almeida, A., and Bak, S. (2019). Evolution of structural diversity of triterpenoids. *Front. Plant Sci.* 10:1523. doi: 10.3389/fpls.2019.01523

Cardenas, P. D., Sonawane, P. D., Heinig, U., Bocobza, S. E., Burdman, S., and Aharoni, A. (2015). The bitter side of the nightshades: genomics drives discovery in Solanaceae steroidal alkaloid metabolism. *Phytochemistry* 113, 24–32. doi: 10.1016/j.phytochem.2014.12.010

Carreno-Quintero, N., Acharjee, A., Maliepaard, C., Bachem, C. W., Mumm, R., Bouwmeester, H., et al. (2012). Untargeted metabolic quantitative trait loci analyses reveal a relationship between primary metabolism and potato tuber quality. *Plant Physiol.* 158, 1306–1318. doi: 10.1104/pp.111.188441

Casati, L., Pagani, F., Braga, P. C., Scalzo, R. L., and Sibilia, V. (2016). Nasunin, a new player in the field of osteoblast protection against oxidative stress. *J. Funct. Foods* 23, 474–484. doi: 10.1016/j.jff.2016.03.007

Cericola, F., Portis, E., Lanteri, S., Toppino, L., Barchi, L., Acciarri, N., et al. (2014). Linkage disequilibrium and genome-wide association analysis for anthocyanin pigmentation and fruit color in eggplant. *BMC Genomics* 15:896. doi: 10.1186/1471-2164-15-896

Cericola, F., Portis, E., Toppino, L., Barchi, L., Acciarri, N., Ciriaci, T., et al. (2013). The population structure and diversity of eggplant from Asia and the Mediterranean Basin. *PLoS ONE* 8:e73702. doi: 10.1371/journal.pone.0073702

Chaim, A., Borovsky, Y., De Jong, W., and Paran, I. (2003). Linkage of the A locus for the presence of anthocyanin and fs10. 1, a major fruit-shape

QTL in pepper. *Theoret. Appl. Genet.* 106, 889–894. doi: 10.1007/s00122-002-1132-9

Christopher, J. T., and Holtum, J. A. (2000). Dicotyledons lacking the multisubunit form of the herbicide-target enzyme acetyl coenzyme A carboxylase may be restricted to the family Geraniaceae. *Funct. Plant Biol.* 27, 845–850. doi: 10.1071/PP99160

Churchill, G. A., and Doerge, R. W. (1994). Empirical threshold values for quantitative trait mapping. *Genetics* 138, 963–971. doi: 10.1093/genetics/138.3.963

Cingolani, P., Platts, A., Wang, L. L., Coon, M., Nguyen, T., Wang, L., et al. (2012). A program for annotating and predicting the effects of single nucleotide polymorphisms, SnpEff: SNPs in the genome of *Drosophila* melanogaster strain w1118; iso-2; iso-3. *Fly* 6, 80–92. doi: 10.4161/fly.19695

Coppola, M., Diretto, G., Digilio, M. C., Woo, S. L., Giuliano, G., Molisso, D., et al. (2019). Transcriptome and metabolome reprogramming in tomato plants by Trichoderma harzianum strain T22 primes and enhances defence responses against aphids. *Front. Physiol.* 10:745. doi: 10.3389/fphys.2019.00745

Daniel, B., Konrad, B., Toplak, M., Lahham, M., Messenlehner, J., Winkler, A., et al. (2017). The family of berberine bridge enzyme-like enzymes: a treasure-trove of oxidative reactions. *Arch. Biochem. Biophys.* 632, 88–103. doi: 10.1016/j.abb.2017.06.023

Diretto, G., Frusciante, S., Fabbri, C., Schauer, N., Busta, L., Wang, Z., et al. (2020). Manipulation of β-carotene levels in tomato fruits results in increased ABA content and extended shelf life. *Plant Biotechnol. J.* 18:1185. doi: 10.1111/pbi.13283

Doganlar, S., Frary, A., Daunay, M. C., Lester, R. N., and Tanksley, S. D. (2002a). A comparative genetic linkage map of eggplant (*Solanum melongena*) and its implications for genome evolution in the solanaceae. *Genetics* 161, 1697–1711.

Doganlar, S., Frary, A., Daunay, M. C., Lester, R. N., and Tanksley, S. D. (2002b). Conservation of gene function in the solanaceae as revealed by comparative mapping of domestication traits in eggplant. *Genetics* 161, 1713–1726.

Dudareva, N., D'auria, J. C., Nam, K. H., Raguso, R. A., and Pichersky, E. (1998). Acetyl-CoA: benzylalcohol acetyltransferase–an enzyme involved in floral scent production in *Clarkia breweri*. *Plant J.* 14, 297–304. doi: 10.1046/j.1365-313X.1998.00121.x

Fiehn, O., Kopka, J., Dormann, P., Altmann, T., Trethewey, R. N., and Willmitzer, L. (2000). Metabolite profiling for plant functional genomics. *Nat. Biotechnol.* 18, 1157–1161. doi: 10.1038/81137

Frary, A., Doganlar, S., Daunay, M. C., and Tanksley, S. D. (2003). QTL analysis of morphological traits in eggplant and implications for conservation of gene function during evolution of solanaceous species. *Theor. Appl. Genet.* 107, 359–370. doi: 10.1007/s00122-003-1257-5

Friedman, M. (2006). Potato glycoalkaloids and metabolites: roles in the plant and in the diet. *J. Agric. Food Chem.* 54, 8655–8681. doi: 10.1021/jf061471t

Friedman, M. (2015). Chemistry and anticarcinogenic mechanisms of glycoalkaloids produced by eggplants, potatoes, and tomatoes. *J. Agric. Food Chem.* 63, 3323–3337. doi: 10.1021/acs.jafc.5b00818

Fukuoka, H., Miyatake, K., Nunome, T., Negoro, S., Shirasawa, K., Isobe, S., et al. (2012). Development of gene-based markers and construction of an integrated linkage map in eggplant by using Solanum orthologous (SOL) gene sets. *Theor. Appl. Genet.* 125, 47–56. doi: 10.1007/s00122-012-1815-9

Ge, H., Liu, Y., Jiang, M., Zhang, J., Han, H., and Chen, H. (2013). Analysis of genetic diversity and structure of eggplant populations (*Solanum melongena* L.) in China using simple sequence repeat markers. *Sci. Hortic.* 162, 71–75. doi: 10.1016/j.scienta.2013.08.004

Gonzali, S., Mazzucato, A., and Perata, P. (2009). Purple as a tomato: towards high anthocyanin tomatoes. *Trends Plant Sci.* 14, 237–241. doi: 10.1016/j.tplants.2009.02.001

Gramazio, P., Prohens, J., Plazas, M., Andújar, I., Herraiz, F. J., Castillo, E., et al. (2014). Location of chlorogenic acid biosynthesis pathway and polyphenol oxidase genes in a new interspecific anchored linkage map of eggplant. *BMC Plant Biol.* 14:350. doi: 10.1186/s12870-014-0350-z

Grothe, T., Lenz, R., and Kutchan, T. M. (2001). Molecular characterization of the salutaridinol 7-O-acetyltransferase involved in morphine biosynthesis in opium poppy *Papaver somniferum*. *J. Biol. Chem.* 276, 30717–30723. doi: 10.1074/jbc.M102688200

Hattori, T., Vasil, V., Rosenkrans, L., Hannah, L. C., McCarty, D. R., and Vasil, I. K. (1992). The Viviparous-1 gene and abscisic acid activate the C1 regulatory gene for anthocyanin biosynthesis during seed maturation in maize. *Genes Dev.* 6, 609–618. doi: 10.1101/gad.6.4.609

He, J., and Giusti, M. M. (2010). Anthocyanins: natural colorants with health-promoting properties. *Annu. Rev. Food Sci. Technol.* 1, 163–187. doi: 10.1146/annurev.food.080708.100754

Itkin, M., Heinig, U., Tzfadia, O., Bhide, A. J., Shinde, B., Cardenas, P. D., et al. (2013). Biosynthesis of antinutritional alkaloids in solanaceous crops is mediated by clustered genes. *Science* 341, 175–179. doi: 10.1126/science.1240230

Jansen, R. C. (1993). Interval mapping of multiple quantitative trait loci. *Genetics* 135, 205–211. doi: 10.1093/genetics/135.1.205

Jansen, R. C. (1994). Controlling the type I and type II errors in mapping quantitative trait loci. *Genetics* 138, 871–881. doi: 10.1093/genetics/138.3.871

Kaur, H., Heinzel, N., Schöttner, M., Baldwin, I. T., and Gális, I. (2010). R2R3-NaMYB8 regulates the accumulation of phenylpropanoid-polyamine conjugates, which are essential for local and systemic defense against insect herbivores in *Nicotiana attenuata*. *Plant Physiol.* 152, 1731–1747. doi: 10.1104/pp.109.151738

Kayamori, F., and Igarashi, K. (1994). Effects of dietary nasunin on the serum cholesterol level in rats. *Biosci. Biotechnol. Biochem.* 58, 570–571. doi: 10.1271/bbb.58.570

Lackman, P., González-Guzmán, M., Tilleman, S., Carqueijeiro, I., Pérez, A. C., Moses, T., et al. (2011). Jasmonate signaling involves the abscisic acid receptor PYL4 to regulate metabolic reprogramming in Arabidopsis and tobacco. *Proc. Natl. Acad. Sci. U.S.A.* 108, 5891–5896. doi: 10.1073/pnas.1103010108

Lelario, F., De Maria, S., Rivelli, A. R., Russo, D., Milella, L., Bufo, S. A., et al. (2019). A complete survey of glycoalkaloids using LC-FTICR-MS and IRMPD in a commercial variety and a local landrace of eggplant (*Solanum melongena* L.) and their anticholinesterase and antioxidant activities. *Toxins* 11:230. doi: 10.3390/toxins11040230

Li, H. (2011). A statistical framework for SNP calling, mutation discovery, association mapping and population genetical parameter estimation from sequencing data. *Bioinformatics* 27, 2987–2993. doi: 10.1093/bioinformatics/btr509

Li, H. (2013). Aligning sequence reads, clone sequences and assembly contigs with BWA-MEM. *arXiv preprint arXiv:*1303.3997.

Lisec, J., Meyer, R. C., Steinfath, M., Redestig, H., Becher, M., Witucka-Wall, H., et al. (2008). Identification of metabolic and biomass QTL in *Arabidopsis thaliana* in a parallel analysis of RIL and IL populations. *Plant J.* 53, 960–972. doi: 10.1111/j.1365-313X.2007.03383.x

Luo, H., Li, W., Zhang, X., Deng, S., Xu, Q., Hou, T., et al. (2019). In planta high levels of hydrolysable tannins inhibit peroxidase mediated anthocyanin degradation and maintain abaxially red leaves of *Excoecaria cochinchinensis*. *BMC Plant Biol.* 19:315. doi: 10.1186/s12870-019-1903-y

Manrique-Carpintero, N. C., Tokuhisa, J. G., Ginzberg, I., and Veilleux, R. E. (2014). Allelic variation in genes contributing to glycoalkaloid biosynthesis in a diploid interspecific population of potato. *Theoret. Appl. Genet.* 127, 391–405. doi: 10.1007/s00122-013-2226-2

Mennella, G., Lo Scalzo, R., Fibiani, M., D'Alessandro, A., Francese, G., Toppino, L., et al. (2012). Chemical and bioactive quality traits during fruit ripening in eggplant (*S. melongena L.)* and allied species. *J. Agric. Food Chem.* 60, 11821–11831. doi: 10.1021/jf3037424

Ninu, L., Ahmad, M., Miarelli, C., Cashmore, A. R., and Giuliano, G. (1999). Cryptochrome 1 controls tomato development in response to blue light. *Plant J.* 18, 551–556. doi: 10.1046/j.1365-313X.1999.00466.x

Noda, Y., Kneyuki, T., Igarashi, K., Mori, A., and Packer, L. (2000). Antioxidant activity of nasunin, an anthocyanin in eggplant peels. *Toxicology* 148, 119–123. doi: 10.1016/S0300-483X(00)00202-X

Portis, E., Barchi, L., Toppino, L., Lanteri, S., Acciarri, N., Felicioni, N., et al. (2014). QTL mapping in eggplant reveals clusters of yield-related loci and orthology with the tomato genome. *PLoS ONE* 9:e89499. doi: 10.1371/journal.pone.0089499

Portis, E., Cericola, F., Barchi, L., Toppino, L., Acciarri, N., Pulcini, L., et al. (2015). Association mapping for fruit, plant and leaf morphology traits in eggplant. *PLoS ONE* 10:e0135200. doi: 10.1371/journal.pone.0135200

Ruttkies, C., Schymanski, E. L., Wolf, S., Hollender, J., and Neumann, S. (2016). MetFrag relaunched: incorporating strategies beyond *in silico* fragmentation. *J. Cheminform.* 8, 1–16. doi: 10.1186/s13321-016-0115-9

Sanchez-Mata, M. C., Yokoyama, W. E., Hong, Y. J., and Prohens, J. (2010). Alpha-solasonine and alpha-solamargine contents of gboma (*Solanum macrocarpon* L.) and scarlet (*Solanum aethiopicum* L.) eggplants. *J. Agric. Food Chem.* 58, 5502–5508. doi: 10.1021/jf100709g

Schauer, N., Semel, Y., Roessner, U., Gur, A., Balbo, I., Carrari, F., et al. (2006). Comprehensive metabolic profiling and phenotyping of interspecific introgression lines for tomato improvement. *Nat. Biotechnol.* 24, 447–454. doi: 10.1038/nbt1192

Stommel, J. R., and Dumm, J. M. (2015). Coordinated regulation of biosynthetic and regulatory genes coincides with anthocyanin accumulation in developing eggplant fruit. *J. Am. Soc. Horticult. Sci.* 140, 129–135. doi: 10.21273/JASHS.140.2.129

Team, R. C. (2013). *"R: A Language and Environment for Statistical Computing"*. Vienna.

Tiburcio, A. F., Altabella, T., Bitrián, M., and Alcázar, R. (2014). The roles of polyamines during the lifespan of plants: from development to stress. *Planta* 240, 1–18. doi: 10.1007/s00425-014-2055-9

Toppino, L., Barchi, L., Lo Scalzo, R., Palazzolo, E., Francese, G., Fibiani, M., et al. (2016). Mapping quantitative trait loci affecting biochemical and morphological fruit properties in eggplant (*Solanum melongena* L.). *Front. Plant Sci.* 7:256. doi: 10.3389/fpls.2016.00256

Toppino, L., Barchi, L., Mercati, F., Acciarri, N., Perrone, D., Martina, M., et al. (2020). A new intra-specific and high-resolution genetic map of eggplant based on a RIL population, and location of QTLs related to plant anthocyanin pigmentation and seed vigour. *Genes* 11:745. doi: 10.3390/genes 11070745

van Eck, H. J., Jacobs, J. M., van Dijk, J., Stiekema, W. J., and Jacobsen, E. (1993). Identification and mapping of three flower colour loci of potato (*S. tuberosum* L.) by RFLP analysis. *Theoret. Appl. Genet.* 86, 295–300. doi: 10.1007/BF00222091

Van Ooijen, J. W. (2004). *MapQTL® 5. Software for the Mapping of Quantitative Trait Loci in Experimental Populations*. Wageningen: Kyazma BV.

Weese, T. L., and Bohs, L. (2010). Eggplant origins: out of Africa, into the Orient. *Taxon* 59, 49–56. doi: 10.1002/tax.591006

Whitaker, B. D., and Stommel, J. R. (2003). Distribution of hydroxycinnamic acid conjugates in fruit of commercial eggplant (*Solanum melongena* L.) cultivars. *J. Agric. Food Chem.* 51, 3448–3454. doi: 10.1021/jf026250b

Wu, F., Eannetta, N. T., Xu, Y., and Tanksley, S. D. (2009). A detailed synteny map of the eggplant genome based on conserved ortholog set II (COSII) markers. *Theor. Appl. Genet.* 118, 927–935. doi: 10.1007/s00122-008-0950-9

Zhang, Y., Cheng, Y., Ya, H., Xu, S., and Han, J. (2015). Transcriptome sequencing of purple petal spot region in tree peony reveals differentially expressed anthocyanin structural genes. *Front. Plant Sci.* 6:964. doi: 10.3389/fpls.2015.00964

Conflict of Interest: The authors declare that the research was conducted in the absence of any commercial or financial relationships that could be construed as a potential conflict of interest.

frontiers in Plant Science

ORIGINAL RESEARCH
published: 04 June 2021
doi: 10.3389/fpls.2021.642828

Natural Genetic Diversity in Tomato Flavor Genes

*Lara Pereira[1], Manoj Sapkota[2], Michael Alonge[3], Yi Zheng[4], Youjun Zhang[5,6], Hamid Razifard[7], Nathan K. Taitano[2], Michael C. Schatz[3], Alisdair R. Fernie[5,6], Ying Wang[7], Zhangjun Fei[4,8], Ana L. Caicedo[9], Denise M. Tieman[10] and Esther van der Knaap[1,2,11]**

[1] Center for Applied Genetic Technologies, University of Georgia, Athens, GA, United States, [2] Institute for Plant Breeding, Genetics and Genomics, University of Georgia, Athens, GA, United States, [3] Department of Computer Science, Johns Hopkins University, Baltimore, MD, United States, [4] Boyce Thompson Institute, Ithaca, NY, United States, [5] Max-Planck-Institut für Molekulare Pflanzenphysiologie, Potsdam, Germany, [6] Center of Plant Systems Biology and Biotechnology, Plovdiv, Bulgaria, [7] Department of Biological Sciences, Mississippi State University, Starkville, MS, United States, [8] U.S. Department of Agriculture, Agricultural Research Service, Robert W. Holley Center for Agriculture and Health, Ithaca, NY, United States, [9] Biology Department, University of Massachusetts Amherst, Amherst, MA, United States, [10] Horticultural Sciences, University of Florida, Gainesville, FL, United States, [11] Department of Horticulture, University of Georgia, Athens, GA, United States

OPEN ACCESS

Edited by:
Amalia Barone, University of Naples Federico II, Italy

Reviewed by:
Christopher Sauvage, Syngenta SAS France, France
Gianfranco Diretto, Italian National Agency for New Technologies, Energy and Sustainable Economic Development (ENEA), Italy

***Correspondence:**
Esther van der Knaap
vanderkn@uga.edu

Specialty section:
This article was submitted to Plant Metabolism and Chemodiversity, a section of the journal Frontiers in Plant Science

Received: *16 December 2020*
Accepted: *23 April 2021*
Published: *04 June 2021*

Citation:
Pereira L, Sapkota M, Alonge M, Zheng Y, Zhang Y, Razifard H, Taitano NK, Schatz MC, Fernie AR, Wang Y, Fei Z, Caicedo AL, Tieman DM and van der Knaap E (2021) Natural Genetic Diversity in Tomato Flavor Genes. Front. Plant Sci. 12:642828. doi: 10.3389/fpls.2021.642828

Fruit flavor is defined as the perception of the food by the olfactory and gustatory systems, and is one of the main determinants of fruit quality. Tomato flavor is largely determined by the balance of sugars, acids and volatile compounds. Several genes controlling the levels of these metabolites in tomato fruit have been cloned, including *LIN5*, *ALMT9*, *AAT1*, *CXE1*, and *LoxC*. The aim of this study was to identify any association of these genes with trait variation and to describe the genetic diversity at these loci in the red-fruited tomato clade comprised of the wild ancestor *Solanum pimpinellifolium*, the semi-domesticated species *Solanum lycopersicum cerasiforme* and early domesticated *Solanum lycopersicum*. High genetic diversity was observed at these five loci, including novel haplotypes that could be incorporated into breeding programs to improve fruit quality of modern tomatoes. Using newly available high-quality genome assemblies, we assayed each gene for potential functional causative polymorphisms and resolved a duplication at the *LoxC* locus found in several wild and semi-domesticated accessions which caused lower accumulation of lipid derived volatiles. In addition, we explored gene expression of the five genes in nine phylogenetically diverse tomato accessions. In general, the expression patterns of these genes increased during fruit ripening but diverged between accessions without clear relationship between expression and metabolite levels.

Keywords: flavor, tomato, genetic, diversity, metabolomics, breeding

INTRODUCTION

Flavor is defined as the perception of food by multiple senses, including taste and olfaction (Baldwin et al., 2000; Small and Prescott, 2005). Flavor is one of the main determinants of produce quality, especially when consumed as non-processed food. Consumers preferred tomato (*Solanum lycopersicum* var. *lycopersicum*) flavor is determined by the right balance of sugars and organic acids,

as well as a range of volatile organic compounds, the latter detected primarily by olfaction (Baldwin et al., 2000; Tandon et al., 2003; Tieman et al., 2012).

Despite the relevance to consumer appeal, produce flavor has been overlooked in breeding programs for decades (Tieman et al., 2017; Klee and Tieman, 2018). Instead, recent crop improvement has focused on agronomic traits, such as yield and disease resistance, which are important to growers and producers. This selection process has led to less flavorful modern cultivars in a range of crops, and in particular to a high level of consumer dissatisfaction of tomato (Tieman et al., 2017). An appropriate balance of sugars and organic acids as well as a rich and diverse volatile profile must be achieved to improve modern varieties that are considered less flavorful than heirlooms. Unlike sugars and acids, most volatiles are active at picomolar to nanomolar concentrations, which would permit flavor improvement without compromising yield. However, metabolite quantification can be technically challenging, labor-intensive and expensive, especially for breeding programs. Thus genetic improvement using molecular selection for alleles of known genes that enhance fruit flavor is one of the major goals in current breeding programs (Rambla et al., 2014; Tieman et al., 2017).

More than 400 volatiles have been detected in tomato (Buttery et al., 1989). Empirical studies, including extensive biochemical characterization and trained consumer panels, have shown that only 20 to 30 volatiles are correlated to consumer liking (Tandon et al., 2003; Tieman et al., 2012). Different volatiles contribute to several aspects of flavor. For example, lipid-derived volatiles, such as *Z*-3-hexen-1-ol and hexyl alcohol, are associated with tomato flavor intensity (Li et al., 2020). Acetate esters such as isobutyl acetate and 2-methylbutyl acetate confer a floral-like or fruity aroma and are negatively associated with good tomato flavor (Goulet et al., 2012).

The major biochemical pathways involved in metabolite production and accumulation in tomato have been partially elucidated in recent years (Klee and Tieman, 2018; Martina et al., 2021). The key underlying genes in these pathways were often identified using introgression lines, relying on interspecific variation between cultivated tomato and the distantly related green-fruited *Solanum pennellii* (Fridman et al., 2004; Goulet et al., 2012, 2015). The high rate of divergence between the parents facilitated the identification of the genes by functional or positional cloning approaches. However, the likely nucleotide polymorphisms leading to trait evolution resulting from domestication remains unknown for most known flavor genes.

Genetic variation within cultivated tomato and the closely related red-fruited wild relatives has been explored through genome-wide association studies (GWAS). These studies have identified hundreds of loci involved in the production of multiple compounds, which paved the way for a targeted molecular breeding approach to recover the flavor in modern tomatoes (Tieman et al., 2017; Zhu et al., 2018; Zhao et al., 2019; Razifard et al., 2020). Several significant GWAS loci colocalize with known genes, demonstrating that in many cases these same genes that were identified among distantly related species underlie the accumulation of metabolites in the red-fruited tomato clade as well. For example, using new long-read sequencing technology, the natural diversity at the *Non-Smoky Glycosyl Transferase* gene, known to control the emission of guaiacol and methylsalicylate via sugar conjugation, showed multiple haplotypes that were associated with the levels of these volatiles (Tikunov et al., 2013; Alonge et al., 2020). Specifically, structural variants (SVs) consisting of deletions, insertions, duplications, inversions and translocations of a certain size, usually above 50-100 bp (Torkamaneh et al., 2018) have often been found to underlie phenotypic variation in tomato (Xiao et al., 2008; Mu et al., 2017; Soyk et al., 2017; Wu et al., 2018; Alonge et al., 2020).

Flavor is a key trait in the domestication syndrome of fruit crops (Meyer and Purugganan, 2013). The flavor palette of tomato changed dramatically during the domestication and diversification of the species (Schauer et al., 2006; Rambla et al., 2017; Zhu et al., 2018). The fully wild, red-fruited species *Solanum pimpinellifolium* (SP) gave rise to *Solanum lycopersicum* var. *cerasiforme* (SLC) in South America from which cultivated tomato *Solanum lycopersicum* var. *lycopersicum* (SLL) eventually arose in Mexico (Razifard et al., 2020). As an intermediate between SLL and SP, SLC accessions have been shown to have high genetic and phenotypic diversity. The goal of this study was to investigate the genetic diversity and gene expression in a set of five genes associated with fruit flavor and to identify beneficial haplotypes that could be incorporated into breeding germplasm. To accomplish this aim, we used a genetically well characterized collection of SP, SLC and SLL from South and Central America (collectively called the Varitome collection) and a combination of whole-genome and RNA sequences, as well as their metabolic profiles.

MATERIALS AND METHODS

Plant Material

The Varitome collection consists of 166 accessions from South and Central America (Mata-Nicolás et al., 2020). Using whole genome sequencing and passport information, the accessions are classified into SP, SLC, and SLL (Razifard et al., 2020). Each phylogenetic group was divided in several subpopulations: three SP subpopulations with well-defined geographical origin (South Ecuador, SP-SECU; Northern Ecuador, SP-NECU; and Peru, SP-PER); five SLC subpopulations, three from South America (Ecuador, SLC-ECU; Peru, SLC-PER; and the San Martin region of Peru, SLC-SM), one with wide geographical distribution in Central, Northern South and Southern North America (collectively called SLC-CA) and one from Mexico (SLC-MEX). The SLL represented one subpopulation of early domesticated landraces from Mexico (Razifard et al., 2020). Eight accessions were excluded from the haplotype analysis because they were classified as SLC admixtures or lacked the metabolic profiles. The plants were grown in the fields at the University of Florida, North Florida Research and Education Center–Suwannee Valley in the spring of 2016 using standard commercial production practices. The plants used for transcriptomic analysis were grown in the greenhouse at the Ohio State University, Columbus, OH, United States at 20°C night and 30°C day temperature, and

a 16/8 hr light/dark cycle. Seedlings were transplanted in 1.6-gallon pots in Sungrow Metro soil mix supplemented with three tablespoons of a 5:1 blend of Florikan Nutricote Total 18-6-8 270day and Florikan Meg-Iron V Micronutrient Mix. The plants were hand watered when the pots were dry but before wilting.

Variant Calling

Raw ILLUMINA read files of the Varitome accessions were downloaded from NCBI ([1]SRA: SRP150040, BioProject: PRJNA454805). The read quality of raw sequencing data was evaluated using FastQC[2]. Low quality reads (read length less than 20) and adapter sequences were trimmed with the tool Trimmomatic (Bolger et al., 2014a). The reads were then aligned to SL4.0 build of tomato reference genome[3] using "speedseq align" component of SpeedSeq framework (Chiang et al., 2015).

SNP and small INDEL variant calling was performed using GATK v3.8 following GATK best practices workflow (Van der Auwera et al., 2013). HaplotypeCaller was used to produce individual gVCF files, which were later combined in a multi-sample VCF file with GenotypeGVCFs. SNPs and INDELs were extracted using SelectVariants. Raw SNPs were then filtered based on the following quality parameters: MQ > 40, QD > 2, FS < 60, MQRankSum > -12.5 and ReadPosRankSum > -8. Similarly, raw INDELs were filtered using QD > 2, FS > 200, ReadPosRankSum < -20. Variants with missing data in more than 10% of the accessions were filtered out.

SVs (> 100 bp) were detected using aligned BAM files and its corresponding splitter and discordant files using "lumpyexpress" function of LUMPY (Layer et al., 2014). The resulting SVs were filtered based on following criteria: minimum number of pair end (PE) 1, minimum number of split read (SR) 1, SR less than or equal to PE, and total number of supporting reads greater than or equal to half of average read depth and less than or equal to three times of average read depth. Then, filtered SVs were merged to generate a single multi-sample VCF file using SURVIVOR (Jeffares et al., 2017). SVs within a maximum allowed distance of 500 bp were merged.

The same pipeline was employed to analyze a subset of cultivated accessions representative of the genetic diversity within heirloom and modern varieties, previously sequenced (Tieman et al., 2017). The sequencing data were downloaded from NCBI (SRA: SRP045767, SRP094624, PRJNA353161), and only accessions with a coverage larger than 5x were used. All the filtering parameters were identical except the missing data cutoff. In this case, variants with missing data in more than 50% of the accessions were filtered out as a result of the lower sequencing coverage in the Tieman et al. (2017) data compared to the Varitome data.

Association Mapping

First, we compiled a list of known genes affecting fruit flavor (**Table 1**). To our knowledge, the list included all the known genes affecting sugars, acids, acetate esters, lipid-derived volatiles, phenylalanine-derived volatiles, guaiacol, methylsalicylate and carotenoids. Variant data (SNPs, INDELs and SVs) of the loci described in **Table 1** as well as 1 Mb upstream and 1 Mb downstream of the transcription start and termination were extracted from the multi-sample VCF files using bedtools (Quinlan and Hall, 2010), and used for the local association analysis. The ITAG4.1 version of the annotation was used to delimit gene coordinates. Phenotypes deviating from normality (p-Value from Shapiro test < 0.01) were normalized using quantile normalization. Genome-wide kinship matrix was calculated based on SNPs using the Centered IBS method, to generate the Hapmap files in TASSEL 5.2.44 (Bradbury et al., 2007). Associations between the genotype and phenotype were estimated using BLINK (Huang et al., 2019) model in GAPIT (version 3) (Tang et al., 2016). Minor allele frequency was set to 2% for the analysis. This was set lower than the usual 5% threshold to account for rare alleles in the collection which we did not want to exclude as they could have an impact on protein function. The significance thresholds for the association were set to a –logP of >6.59 and 4.11 representing p-Values of 0.01 and 0.05 respectively, after multiple testing correction by the Benjamini and Hochberg FDR estimation. The phenotypic variation explained (PVE) by a SNP was approximated subtracting the likelihood ratio-based R^2 of the model with the SNP and the likelihood ratio-based R^2 of the model without the SNP (Xu et al., 2016).

Linkage disequilibrium (LD) heatmaps were generated using LDBlockShow 1.33 (Dong et al., 2020) using mean r^2 values. SNPs 1 Mb upstream and downstream of the gene locus were used for LD analyses. Because of high computational demand of the analysis, we used a reduced input data file with one SNP per kb. The reduced data file was generated using "–thin 1000" parameter in VCFtools (Danecek et al., 2011). The results are representative since recombination within the 1-kb window in tomato is insignificant.

Haplotype Analysis

SNPs and small INDELs within the gene sequence as well as 3 kb upstream of the start site and 1 kb downstream of the termination site were extracted using VCFtools (Danecek et al., 2011). This region was much shorter than the region used for the association mapping because of the unwieldy number of polymorphisms in a larger region as well as the chance of recombination that could result in a large number of haplotypes. SVs detected by Lumpy were not included in the haplotype analysis because of low incidence. Relevant SVs are mentioned in the results section. Additional filter parameters were –mac 4 –max-missing 0.9 –minQ 100. Multiallelic variants were split into multiple rows and left-aligned using BCFTools norm (Li, 2011). Variants were annotated using SnpEff (Cingolani et al., 2012) using a local built database for the SL4.0 tomato reference genome. Since *CXE1* was absent in the ITAG4.1 gene model[4], we used the FGENESH (Salamov and Solovyev, 2000) tool to predict the gene model and analyzed the locus manually.

[1]https://www.ncbi.nlm.nih.gov/

[2]https://www.bioinformatics.babraham.ac.uk/projects/fastqc/

[3]https://solgenomics.net/organism/Solanum_lycopersicum/genome

[4]https://solgenomics.net

TABLE 1 | Compilation of known flavor-related genes in tomato.

Metabolites	Gene	Gene ID	Genomic position	References
Sugars	*LIN5*	*Solyc09g010080*	SL4.0ch09:3508156-3512282	Fridman et al., 2004
Organic acids (malate)	*ALMT9*	*Solyc06g072920*	SL4.0ch06:42612816-42619107	Ye et al., 2017
Acetate esters	*AAT1*	*Solyc08g005770*	SL4.0ch08:617070-619717	Goulet et al., 2015
	CXE1	*Solyc01g108585*	SL4.0ch01:88169038-88170233	Goulet et al., 2012
Lipid-derived volatiles	*LoxC*	*Solyc01g006540*	SL4.0ch01:1119976-1130114	Shen et al., 2014
	HPL	*Solyc07g049690*	SL4.0ch07:59963576-59970053	Shen et al., 2014
	ADH2	*Solyc06g059740*	SL4.0ch06:35287450..35289927	Speirs et al., 1998
	LIP1	*Solyc12g055730*	SL4.0ch12:61316763..61320764	Garbowicz et al., 2018
	LIP8	*Solyc09g091050*	SL4.0ch09:66484639-66495126	Li et al., 2020
Phenylalanine-derived volatiles	*PAR1*	*Solyc01g008530*	SL4.0ch01:2578092..2584487	Tieman et al., 2007
	PAR2	*Solyc01g008550*	SL4.0ch01:2593768..2597462	
	AADC2	*Solyc08g006740*	SL4.0ch08:1306822..1309453	Tieman et al., 2006b
	AADC2	*Solyc08g006750*	SL4.0ch08:1332553..1336469	
	AADC1C	*Solyc08g068600*	SL4.0ch08:55827604..55829855	
	AADC1B	*Solyc08g068610*	SL4.0ch08:55836822..55838978	
	AADC1D	*Solyc08g068630*	SL4.0ch08:55860361..55862523	
	AADC1A	*Solyc08g068680*	SL4.0ch08:55909433..55911654	
	PPEAT	*Solyc02g079490*	SL4.0ch02:42004857-42007233	Domínguez et al., 2020
	FLORAL4	*Solyc04g063350*	SL4.0ch04:54805156-54812314	Tikunov et al., 2020
Guaiacol and methylsalicylate	*SAMT*	*Solyc09g091550*	SL4.0ch09:66901227..66903818	Tieman et al., 2010
	COMT	*Solyc10g005060*	SL4.0ch10:64725323..64728276	Mageroy et al., 2012
Carotenoids and apocarotenoid volatiles	*PSY1*	*Solyc03g031860*	SL4.0ch03:4234654-4238638	Fray and Grierson, 1993
	CrtISO	*Solyc10g081650*	SL4.0ch10:61789271..61794607	Isaacson et al., 2002
	CYCB	*Solyc06g074240*	SL4.0ch06:43562526-43564022	Ronen et al., 2000
	CrtL-e	*Solyc12g008980*	SL4.0ch12:2334383..2339689	Ronen et al., 1999
	SlCCD1A	*Solyc01g087250*	SL4.0ch01:74432005-74442676	Simkin et al., 2004
	SlCCD1B	*Solyc01g087260*	SL4.0ch01:74444645-74454599	

The haplotype heatmap was generated using the R package "pheatmap" (Kolde, 2019). The function pheatmap was implemented using the clustering method "ward.D" for accessions (rows) and no clustering method for variants (columns). The number of clusters was set to 6 after testing multiple values, as this value produced the optimal interpretable haplotype clusters at all the analyzed genes. The phylogeny of the accession was extracted from previous whole genome analysis of the same dataset (Razifard et al., 2020). The metabolite content of each accession was classified as low, medium or high depending on the decile position from low: 1st to 5th decile; medium: 6th to 8th decile; high 9th to 10th decile. The variants were classified by their location and functional annotation; variants predicted to affect splicing sites were considered frameshift mutations.

The multiple mean comparison to test significant differences between clusters was conducted in R using a linear model. We used the functions lsmeans from package "emmeans" (Lenth, 2020) to calculate the *p*-Value of pairwise comparisons among clusters and cld from package "multcompView" (Graves et al., 2015) to display the Tukey test, fixing the significance threshold at 0.05.

To generate the haplotype networks, we only used the coding sequence of each gene. A FASTA sequence for each accession and gene was generated by substituting the alternate allele of SNPs and INDELs in the reference sequence using FastaAlternateReferenceMaker from GATK (McKenna et al., 2010). Only the homozygous alternate genotypes were substituted, while the heterozygous genotypes were kept as reference. These were aligned using MAFFT algorithm (Katoh and Standley, 2013) to select the coding sequences according to the ITAG4.1 annotation for each gene. The haplotype networks were constructed using PopART (Leigh and Bryant, 2015) and the minimum spanning tree method (Epsilon = 0) (Bandelt et al., 1999). Sequence from one accession of *S. pennelli* (Bolger et al., 2014b) was included to provide a root for the network.

Diversity Analysis

Nucleotide diversity (π) was estimated per subpopulation using exclusively SNPs within each gene and flanking sequences (3 kb upstream and 1 kb downstream). The quality thresholds were the same as described before (see "Variant calling"). We classified the SNPs as non-synonymous (resulting in protein changes), synonymous (silent mutations in coding sequence), and non-coding (within introns, UTRs and flanking sequence) by following SnpEff annotation (Cingolani et al., 2012). Then we calculated π estimates per subpopulation using VCFTools (Danecek et al., 2011) using –window-pi function (window of 1000 bp) for non-synonymous, synonymous, non-coding and all SNPs.

Identification and Genotyping of *LoxC* Duplication

To evaluate whether *LoxC* was duplicated in SP accessions, we used the new high-quality assembly of PAS014479, a SP-PER accession from the Varitome collection that carries the two paralogs (Alonge et al., 2020). The trimmed reads from the Varitome accessions as well as Heinz (SRA: SRP010718) and LA2093 (SRA: SRP267721) were then mapped to the PAS014479_MAS1.0[5] using the same workflow as described above for the other genes using the SL4.0 reference genome. We aligned *LoxC* and the flanking regions (±50 kb) of PAS014479 to itself and generated a dot-plot to identify identical sequence matches using MUMmer (Kurtz et al., 2004). To check whether the duplication was predicted to be a functional protein, we estimated the gene model using FGENESH web tool and aligned the protein sequences. In addition, we analyzed the alignment files using PAS014479_MAS1.0 as reference genome at *LoxC* locus for a subset of representative accessions using the package "Gviz" (Hahne and Ivanek, 2016). The coordinates of the gene model of the second copy of *LoxC*, denominated *LoxC-SP*, were plotted along with *LoxC* ITAG4.1 gene model.

To genotype the duplication across the Varitome collection *in silico*, we used three approaches: normalized coverage, heterozygosity when aligning to Heinz SL4.0 reference genome, and presence of a deletion when aligning to PAS014479_MAS1.0. At least two out of these three criteria must be met to consider a certain accession to carry *LoxC-SP* featuring both paralogs.

Metabolic Phenotyping

Fresh fruit volatiles were collected and quantitated as described previously (Tieman et al., 2006a). Sugars and acids were quantitated as described in Vogel et al. (2010).

Total RNA Isolation, Library Construction, and Sequencing

The tomato maturation timeline for nine accessions was determined prior to collecting the fruit development samples. Five developmental stages per accession were sampled: flower at anthesis, young fruit, mature green fruit, fruit at breaker stage and red ripe fruit and each sample included three biological replicates. Total RNA was isolated using the RNAzol^{RT} reagent (Sigma-Aldrich, St. Louis, MO, United States). Strand-specific RNA-Seq libraries were constructed using an established protocol (Zhong et al., 2011). All libraries were quality checked using the Bioanalyzer and sequenced on an Illumina HiSeq 2500 system at Weill Cornell Medicine, NY, United States.

RNA-Seq Read Processing, Transcript Assembly, and Quantification of Expression

Single-end RNA-Seq reads were processed to remove adapters as well as low-quality bases using Trimmomatic (Bolger et al., 2014a), and trimmed reads shorter than 80 bp were discarded. The remaining reads were subjected to rRNA sequence removal by aligning to an rRNA database (Quast et al., 2013) using Bowtie (Langmead et al., 2009) allowing up to three mismatches. The resulting reads were aligned to the tomato reference genomes (Build SL4.0 see text footnote 3) using STAR (Dobin et al., 2013) allowing up to two mismatches. The gene expression was measured by counting the number of reads mapped to gene regions. Then the gene expression was normalized to the number of reads per kilobase of exon per million mapped reads (RPKM) based on all mapped reads. A principal component analysis was performed for each developmental stage using DESeq2 (Love et al., 2014). Thirteen biological replicates that deviated in the principal component analysis were excluded from the analysis. After this quality filtering, out of the total 45 samples, 36 samples included three biological replicates, seven samples included two biological replicates and two samples were completely excluded. Given the presence of two variables (i.e., genotypes and developmental stages), we used linear modeling differential expression analysis via the Likelihood Ratio Test function in DESeq2 (Clevenger et al., 2017). *P*-value was calculated based on the Benjamini and Hochberg correction with a false discovery rate of 5%. We used P-value < 0.05 as a cutoff for defining differentially expressed genes.

Protein Modeling and Activity

The online software Phyre2 (Kelley et al., 2015) normal mode setting was used to predict the secondary and tertiary structures of the five studied proteins. The location of the active site and the mutational sensitivity were explored using the tool PhyreInvestigator (Yates et al., 2014).

For LIN5, we studied the protein activity *in vitro*. The reference and alternate invertase coding sequences, resulting in the Asn366Asp amino acid substitution, were optimized for tomato expression and synthetic coding regions were obtained from Invitrogen (Tieman et al., 2017). The coding sequences were then cloned into p112A1 yeast expression vector. Protein expression and enzyme activity assays were performed as previously described (Fridman et al., 2004).

RESULTS

Local Association Mapping Lead to Several Known Flavor Genes

We compiled a list of known genes that affect tomato flavor (**Table 1**). For each gene, we determined whether the proposed candidate locus was significantly associated with trait variation in the Varitome collection by analyzing the coding region as well as 1 Mb upstream and 1 Mb downstream of each gene (**Figure 1** and **Supplementary Figure 1**). The association analyses showed that variants within and near *LIN5*, *ALMT9*, *AAT1*, *CXE1*, and *LoxC* were associated with trait variation in the Varitome collection. These genes function in sugar and acid metabolism affecting taste (*LIN5* and *ALMT9*) or in volatile production affecting smell (*AAT1*, *CXE1*, and *LoxC*) (**Supplementary Figure 2**). The other genes listed in **Table 1** did not show association with biochemical levels (**Supplementary Figure 1**). In addition to the metabolites displayed in **Supplementary Figure 1**, other metabolites from the

[5]https://solgenomics.net/projects/tomato13

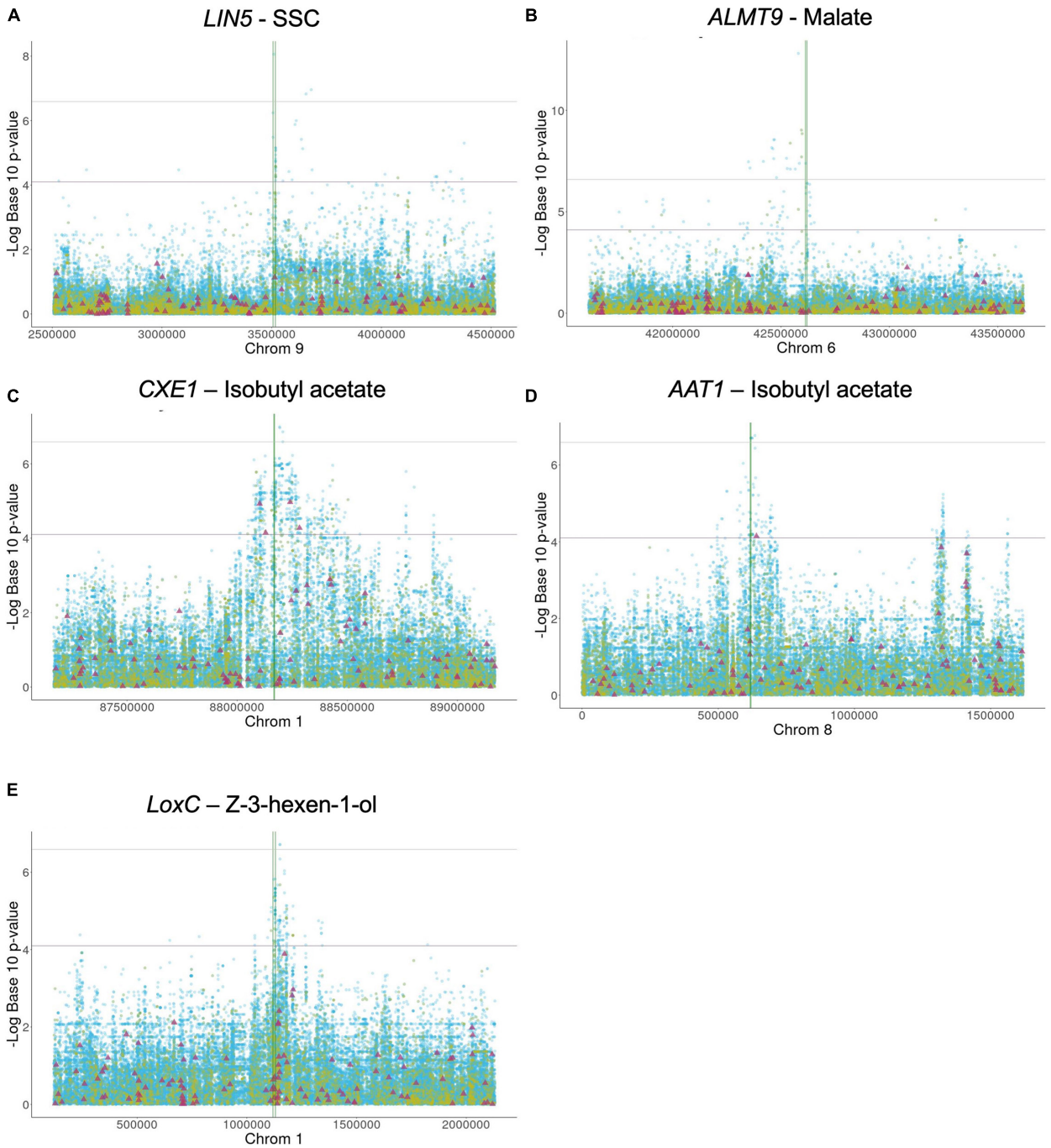

FIGURE 1 | (A-E) Local association mapping for flavor genes and their corresponding metabolites. SNPs are plotted as blue dots, INDELs as yellow dots and SVs as purple triangles. Horizontal lines represent 0.05 and 0.01 significance thresholds. Vertical lines mark the genic region.

same pathway were tested for association as well but did not show association either (data not shown).

LIN5- The simple sugars, glucose and fructose, are among the most important metabolites in tomato as higher levels contribute to high consumer liking (Jones and Scott, 1983; Tandon et al., 2003; Causse et al., 2010; Tieman et al., 2012). Sugars are typically evaluated by measuring the soluble solid content (SSC) which is expressed in Brix degrees. *LIN5* encodes a cell-wall invertase that hydrolyzes sucrose, and higher enzyme activity leads to increased glucose and fructose levels (Fridman et al., 2004; Zanor et al., 2009). One critical amino acid mutation between *S. pennellii* and cultivated tomato at position 348 underlies the sugar level variation between these two distantly related species. In the Varitome collection, 44 variants within or

around *LIN5* were significantly associated with SSC: two SNPs in the promoter (∼2 kb upstream), one SNP in the coding region resulting in a missense mutation from asparagine to aspartate at position 366 (SL4.0ch09:3510682) and 20 variants that mapped 4 to 7 kb downstream (**Figure 1A**). The PVE of the most significant SNP was 14.5%. In addition, 21 significant SNPs were located further away from the gene, most of them between positions SL4.0ch09:3551616 – SL4.0ch09:4376974 (**Supplementary Table 1A**). Many SVs were found within and near the gene but none appeared to be associated with sugar levels (**Figure 1A**). The critical amino acid change between *S. pennellii* and cultivated tomato was not found in the Varitome collection.

ALMT9- An appropriate balance between sugars and acids is also essential for desirable tomato flavor. One major contributor to malate content is the transporter *ALMT9* that is proposed to control the accumulation of this metabolite in the vacuole (Sauvage et al., 2014; Ye et al., 2017). Higher expression of *ALMT9* leads to higher malate content in ripe fruits. Previous studies using a population of SP, SLC, and SLL implied that a 3-bp deletion in the promoter of *ALMT9* is the causative variant affecting its expression (Ye et al., 2017). In the Varitome collection, the local association mapping identified multiple highly associated variants within or around the gene (**Figure 1B**). A total of 66 significant variants were confined to an interval of ∼100 kb upstream of *ALMT9*. In the genic region, we found four significant SNPs, one resulting in a synonymous mutation in the second exon (SL4.0ch06:42613870) and three in the second intron (**Supplementary Table 1B**). The PVE of the most significant SNP was 32.7%. The 3-bp deletion in the promoter was found in 9 accessions but was not associated with malate levels in the Varitome collection.

CXE1 and *AAT1*- Tomato flavor is highly influenced by the fruit aroma, characterized by volatile content. Acetate esters confer fruity or floral scent and are liked in high quantities in fruits such as banana, apple and melon. In tomato however, acetate esters are undesirable volatiles (Goulet et al., 2012). Acetate ester levels are controlled by a feedback loop comprised of a carboxylesterase, CXE1, and an alcohol acyltransferase, AAT1 (Goulet et al., 2012, 2015). AAT1 synthesizes acetate esters using an alcohol as precursor, whereas CXE1 catalyzes the reverse reaction (**Supplementary Figure 2**). The cloning of the genes revealed two different transposable elements that had integrated in the promoter of *CXE1* in SP and SLL. The transposon insertions appeared to lead to higher expression of *CXE1* in cultivated tomato compared to *S. pennellii*, thereby reducing acetate ester content (Goulet et al., 2012). For *AAT1*, on the other hand, the polymorphisms described in a previous study were several SNPs resulting in missense mutations leading to a less active protein in SLL compared to *S. pennellii* (Goulet et al., 2015). Lower AAT1 enzyme activity leads to lower levels of acetate esters in the fruit. In the Varitome collection, we selected isobutyl acetate as a proxy for all acetate esters to determine how genetic variation affected volatile levels.

At the *CXE1* locus, the local association mapping in the Varitome collection identified an interval of ∼500 kb (**Figure 1C**) with 650 variants that were significantly associated with isobutyl acetate levels. They included 597 SNPs, 49 INDELs and four SVs (**Supplementary Table 1C**). The PVE of the most significant SNP was 14.9%. Three SNPs were in the *CXE1* coding region (SL4.0ch01:88169422, SL4.0ch01:88169774 and SL4.0ch01:88169988), two resulted in missense mutations from serine to glycine at amino acid position 94 and from valine to glycine at position 211, respectively. The SVs were three deletions of 445 bp, 3.3 and 4.8 kb and one duplication of 7.0 kb (**Supplementary Table 2**). In nearly all cases, these four SVs were completely linked. The closest significantly associated SV was 40 kb upstream of the start site of transcription that could act as an open chromatin region affecting gene expression. Alternatively, the associated amino acid changes might alter the activity of the protein. All accessions in the Varitome collection carried the transposons in the *CXE1* promoter.

At the *AAT1* locus, an interval of 200 kb around the gene was highly associated with the phenotype in the Varitome collection (**Figure 1D**). The variants included 148 SNPs, three INDELs and one SV (**Supplementary Table 1D**). The PVE of the most significant SNP was 14.4%. Fourteen SNPs were located within the gene, including eight in the UTRs, two in introns and four resulting in missense mutations. The amino acid changes were from serine to proline at position 24, from phenylalanine to valine at position 161, and from threonine to isoleucine at positions 354 and 398. These four amino acid changes were also found between *S. pennellii* and cultivated tomato (Goulet et al., 2015). A significant 401-bp deletion was found ∼20 kb downstream the gene, which could affect gene expression. In addition, 54 SNPs were located nearly 1 Mb downstream of the gene, but their association was likely due to LD (average R^2 value of 0.28, ranging from 0.12 to 0.55).

LoxC- Lipid-derived volatiles are also significantly associated with consumer liking as they contribute to flavor intensity (Tieman et al., 2012). Several enzymes in the biosynthetic pathway have been identified (Speirs et al., 1998; Shen et al., 2014; Li et al., 2020). LoxC catalyzes the peroxidation of linoleic and linolenic acids, producing C5 and C6 volatiles (Chen et al., 2004; Shen et al., 2014). In the Varitome collection, *LoxC* was associated with *Z*-3-hexen-1-ol, a C6 alcohol. A total of 13 INDELs and 144 SNPs were significantly associated with the volatile (**Figure 1E** and **Supplementary Table 1E**). The region that showed higher association with the phenotype was found at the 3′ end of the gene, specifically in the two last exons and the last intron. Of the 53 variants within the gene, 44 were located in introns and nine in exons. The PVE of the most significant SNP was 14.6%. Three amino acid changes were found: from valine to isoleucine at position 580, from glycine to alanine at position 598 and from threonine to leucine at position 607. In addition, a large interval of about 200 Kb downstream of the gene was associated with volatile levels, including a deletion of ∼8 Kb.

Genetic Diversity for Flavor Genes in the Varitome Collection

LIN5

The evolution of the *LIN5* locus may provide insights into how selection for flavor or lack thereof were part of the tomato domestication syndrome. To determine the evolution of this

locus, we identified the haplotypes from the regions flanking (3 kb upstream and 1 kb downstream) and covering the *LIN5* gene. A total of 228 variants were identified at the locus (**Supplementary Table 3A**), of which 76 were INDELs (ranging from 1 to 97 bp), 152 were SNPs and none were SVs comprised of 100 bp or more. Most variants (60.5%) were found in the regulatory regions, defined as sequences that are upstream and downstream of the transcription start and termination site of the gene, and in the UTRs (**Figure 2A**). Within the gene, we identified 18 non-synonymous mutations, including 15 that resulted in amino acid changes, one in-frame deletion of five amino acids, one affecting a splicing site and one frameshift mutation leading to a presumptive null. Clustering of haplotypes into six groups revealed some association with population origins (**Figure 2A**). All SP were found in Clusters I and II, and both included six SLC. Cluster I mainly consisted of Ecuadorian accessions, while Cluster II consisted of Peruvian accessions. Cluster III grouped 11 SLC-ECU that shared many of the non-reference alleles found in SP. Although multiple haplotypes were observed, many of the variants were in LD with each other (**Supplementary Figure 3**). The remaining three clusters were similar to the Heinz 1706 reference haplotype. Cluster IV represented SLC with diverse geographical origin with three or less variants compared to the reference genome. Cluster V included SLL and a subset of SLC, primarily from Ecuador and San Martin, Peru. And lastly, Cluster VI consisted of SLC from Central America. This cluster showed the non-reference allele at three positions in nearly all accessions: a SNP at 2.7 kb upstream the transcription start site, a non-synonymous replacement in the second exon and a SNP in the 3′-UTR. The latter was also identified as a non-reference SNP in all Cluster IV accessions.

Average SSC values for each of the 6 haplotype clusters showed that Cluster IV and V displayed the lowest SSC values whereas Cluster VI and to a lesser extent Cluster II displayed the highest SSC values and Clusters I and III presented intermediate SSC values (**Figure 2B**). Surprisingly, only a few polymorphisms were found between Clusters IV through VI, yet Cluster VI showed the highest SSC values. Two of the significantly associated SNPs

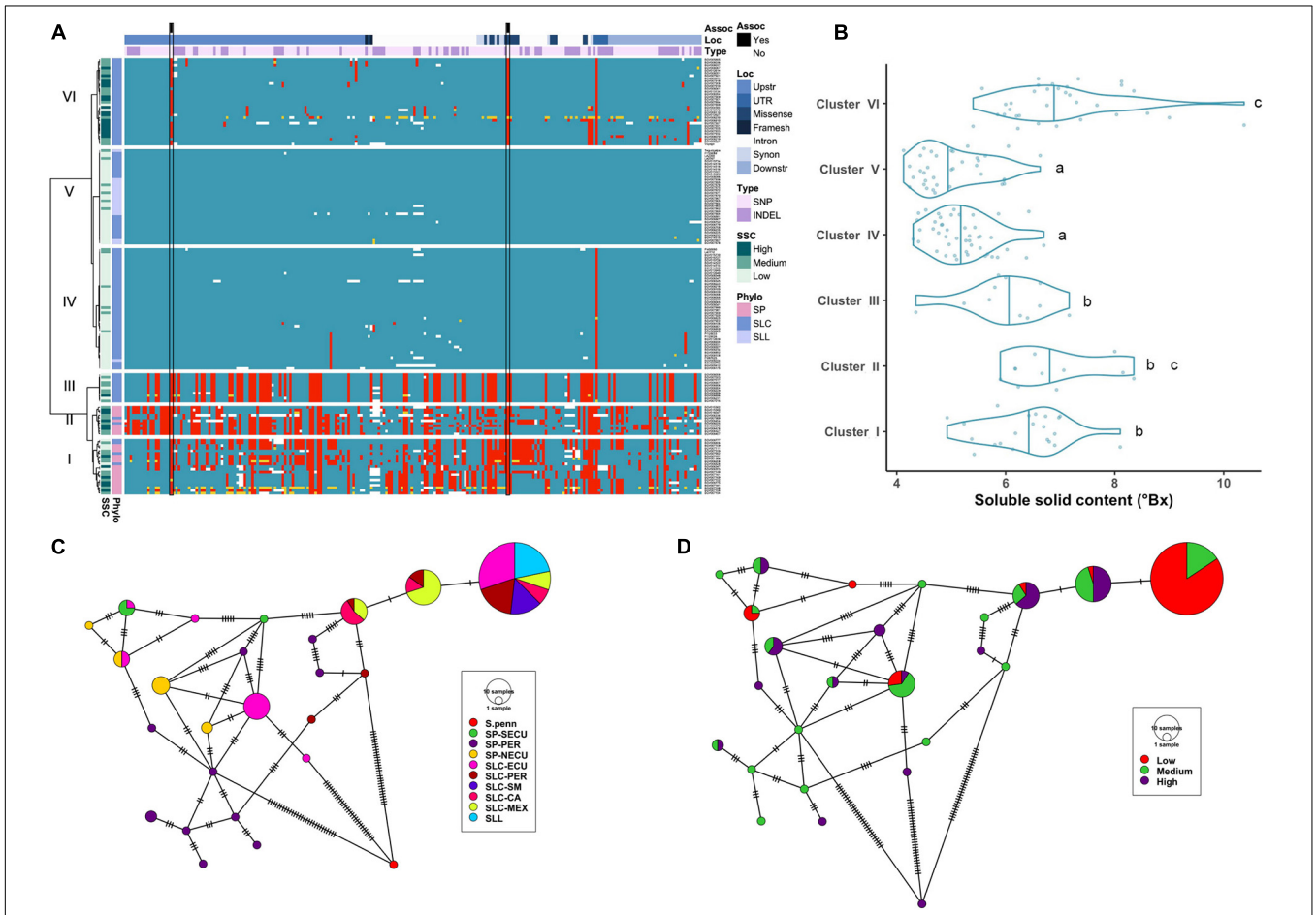

FIGURE 2 | Haplotype analysis of *LIN5* locus. **(A)** Heatmap representing the genotypes of accessions (rows) for the polymorphisms identified (columns). Reference genotype are represented in blue, alternate in red, heterozygous in yellow and missing data in white. **(B)** Violin plots of the SSC content in the Varitome collection, classified by haplotype cluster. **(C)** Haplotype network classified by the phylogenetic classification of the accession. Each circle represents a haplotype, its size is proportional to the number of accessions carrying that haplotype, and lines across the edges represent mutational steps **(D)** Haplotype network classified by the SSC content.

(SL4.0ch09:3505480 and SL4.0ch09:3519565) were fixed for the alternate allele in Clusters I, II, III and VI and for the reference allele at Clusters IV and V, the latter resulting in the amino acid change at position 366 (**Supplementary Table 1A**). An in-frame deletion resulting in a loss of five amino acids (positions 343-347) was found in 21 SP accessions belonging to Clusters I and II. This deletion could have an impact on protein activity, since an amino acid change in the adjacent position 348 was shown to be relevant in *S. pennellii* introgression line (Fridman et al., 2004). In the Varitome collection, we detected a novel frameshift mutation, which caused a loss of the start codon. This allele was found in only two accessions in Cluster VI that showed average SSC levels. Glucose and fructose levels showed the same trend as SSC, with both sugars being highest in Clusters II and VI and lowest in Clusters IV and V (data not shown).

We constructed haplotype networks using the coding sequence of *LIN5* and determined their association with the phylogenetic groups previously determined in the Varitome collection (Razifard et al., 2020; **Figure 2C**). Using *S. pennellii* as an outgroup, we identified 24 haplotypes demonstrating a high level of genetic diversity. The most common haplotype was identical to the reference genome, and was found in all SLL and diverse SLC populations. Only one to two mutations differentiated this haplotype from the second and third most common haplotype that were represented by SLC MEX, SLC-CA and SLC-PER. Another common haplotype was found in SLC-ECU and was closely related to the SP-NECU haplotypes. The Peruvian SP haplotypes were unique with one accession being the most ancestral haplotype. We plotted the same haplotype network to the sugar levels from high to medium to low (**Figure 2D**). Many ancestral SLC-MEX and SLC-CA haplotypes were associated with higher SSC values. Low SSC levels were predominant in accessions carrying the most common and reference genome haplotype, differing by only one nucleotide variant in the coding region.

ALMT9

For the *ALMT9* gene, 112 SNPs and 31 INDELs (ranging from 1 to 28 bp) were identified (**Supplementary Table 3B**). The variants were distributed predominantly in regulatory regions and UTRs (71.3%) and introns (14.0%). Of those that were in the coding region, 12 were non-synonymous, including a SNP that was predicted to affect splicing. The haplotype clustering analysis showed that all SP and some SLC-ECU were found in Clusters I and II (**Figure 3A**). Cluster I contained multiple haplotypes, indicating high genetic diversity among these accessions. A deletion of ∼2.7 kb was found in the second intron corresponding to a CopiaSL_37 retrotransposon (Ye et al., 2017) that was present in the reference genome. Most SP in Cluster I lacked the transposon insertion (**Supplementary Table 2**). Many SP-NECU were found in Cluster II exhibiting high genetic similarity to the SLC-ECU found in Clusters III and VI. Cluster V represented most SLL as well as SLC of diverse origin whereas Cluster VI contained SLC from diverse subpopulations.

The malate content in ripe fruits ranged from ∼0.1 to 1.7 mg/g (**Figure 3B**). The highest content was observed in the accessions belonging to Cluster V, although the levels were highly variable within this cluster. The median malate content was below 0.5 mg/g in all Clusters. The only two Clusters that were significantly different from one another were Cluster VI and Cluster V.

The haplotype network with the coding sequence of *ALMT9* showed 22 haplotypes (**Figure 3C**). The most ancestral haplotype was found in an SP-PER accession. Two common haplotypes were identified in SLC-ECU, and both differed from SP haplotypes with one unique variant. Interestingly, one haplotype appeared to have originated from SP-NECU whereas the other from SP-SECU. In the center of the network, one haplotype was shared by SP from all three geographical origins, as well as SLC-ECU and SLC-MEX. Further mutations gave rise to three additional haplotypes in SLC-CA and SLL. The most common haplotype for *ALMT9* was found in a group comprised of SLC-PER, SLC-SM, SLC-MEX and SLL. The presence of the same haplotype in multiple subpopulations indicates gene flow or lineage sorting. Seven rare SP *ALMT9* haplotypes as well as two common SLL haplotypes showed high levels of malate (**Figure 3D**). Most of the SLC haplotypes presented low to medium malate content, especially within the SLC-ECU.

CXE1 and *AAT1*

The significant association of the *CXE1* and *AAT1* loci with acetate ester content indicated that causative alleles segregated in the Varitome collection (**Figure 1**). *CXE1* is an intronless gene of ∼1.1 kb. Most variants were SNPs (96, 92.3%) and the remaining eight were INDELs (ranging from 1 to 14 bp) (**Supplementary Table 3C**). Eight missense and three synonymous mutations were found in the coding region. Of the missense mutations, five were non-conservative changes. None of the variants were predicted to lead to a significant knock down of the gene, suggesting that *CXE1* might have a critical function in adaptation. In the clustering of the gene, the upstream and downstream regions showed that the SP clustered in three groups (**Figure 4A**). Clusters I and II contained a mixture of SP and SLC from Ecuador and Peru respectively. Cluster III featured fewer polymorphisms with respect to the reference and included SP from all subpopulations. Cluster V contained mainly SLC-CA and seven SLL. Two variants were conserved in Cluster V, whereas 13 SNPs showed low allelic frequency in the population. Cluster VI was the largest group (78 accessions) and, compared to the reference genome, carried only one conserved SNP located ∼2 kb upstream of the gene.

Even though the normalized data showed association to isobutyl acetate levels at the *CXE1* locus, the distribution of actual levels was skewed toward 0, with ∼50% of the accessions showing less than 1 ng/g of the volatile (**Figure 4B**). However, a few accessions produced as high as 18 ng/g of the volatile. Accessions producing the highest content of isobutyl acetate were found in Clusters I and II, although the range within each cluster was large. Clusters III, V and VI showed low content of isobutyl acetate, with a few outliers reaching ∼5 ng/g.

The coding region haplotype network showed 10 classes. The most common haplotype (124 accessions) was found in all SLL, SLC-MEX, and SLC-SM as well as subsets from

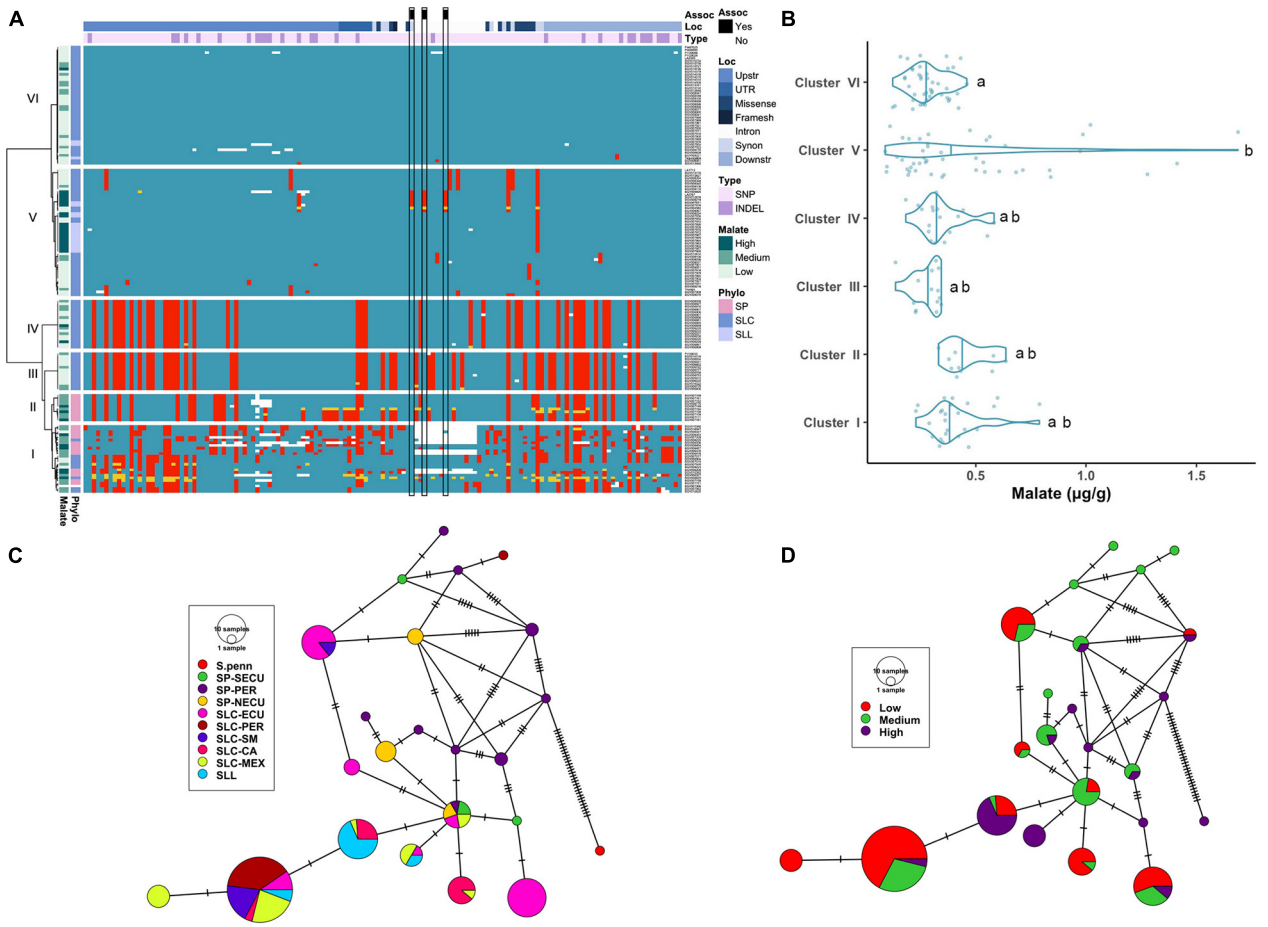

FIGURE 3 | Haplotype analysis of *ALMT9* locus. **(A)** Heatmap representing the genotypes of accessions (rows) for the polymorphisms identified (columns). Reference genotype are represented in blue, alternate in red, heterozygous in yellow and missing data in white. **(B)** Violin plots of the malate content in the Varitome collection, classified by haplotype cluster. **(C)** Haplotype network classified by the phylogenetic classification of the accession. Each circle represents a haplotype, its size is proportional to the number of accessions carrying that haplotype, and lines across the edges represent mutational steps **(D)**. Haplotype network classified by the malate content.

the other subpopulations (**Figure 4C**). Only one mutation differentiated the most common haplotype from SP-NECU and other unique SP haplotypes. Four haplotypes were associated with high isobutyl acetate content and they were represented predominantly by SP-NECU and SLC-ECU (**Figure 4D**). The most common haplotype included accessions that produced low (53%) as well as medium to high (47%) isobutyl acetate levels.

The cluster analysis of the *AAT1* locus encompassed 167 variants including 128 SNPs, 37 INDELs (ranging from 1 to 59 bp) and two SVs (**Supplementary Tables 2, 3D**). A relatively high proportion of these variants affected the protein sequence, resulting in missense (all SNPs) and four frameshift mutations (two SNPs, one INDEL and one SV) (**Figure 5A**). Four clusters each carried few accessions whereas Cluster VI was very large and identical to the reference genome except for one SNP that was located ∼2.8 kb upstream of the coding region (**Figure 5A**). Cluster I was genetically diverse, featuring many non-conserved polymorphisms, and was composed of SP-SECU and SP-PER. Cluster II was composed of SP from all subpopulations and a few SLC-ECU. Cluster III carried six SLC-CA where the upstream region was more similar to the reference genome than the gene and the downstream region. Cluster IV was represented by SP-NECU with high genetic similarity among the accessions. Cluster V contained SLC from Central America and Ecuador which had a similar haplotype compared to the reference, with only seven non-conserved polymorphisms. Cluster VI included all SLL and SLC from all subpopulations. Curiously, BGV006775, an SP-NECU, was found in this cluster, indicating most likely gene flow between SLC and SP accessions.

Although no significant differences in isobutyl acetate content were observed among the *AAT1* gene clusters (**Figure 5B**), interesting correlations between specific haplotypes and metabolite levels were noted. For example, all accessions in Cluster III carried a duplication of 13 nucleotides in the second exon that resulted in a frameshift at position 327 affecting ∼25% of the protein (**Supplementary Table 3D**); the average content of isobutyl acetate for accessions in Cluster III was very low, likely

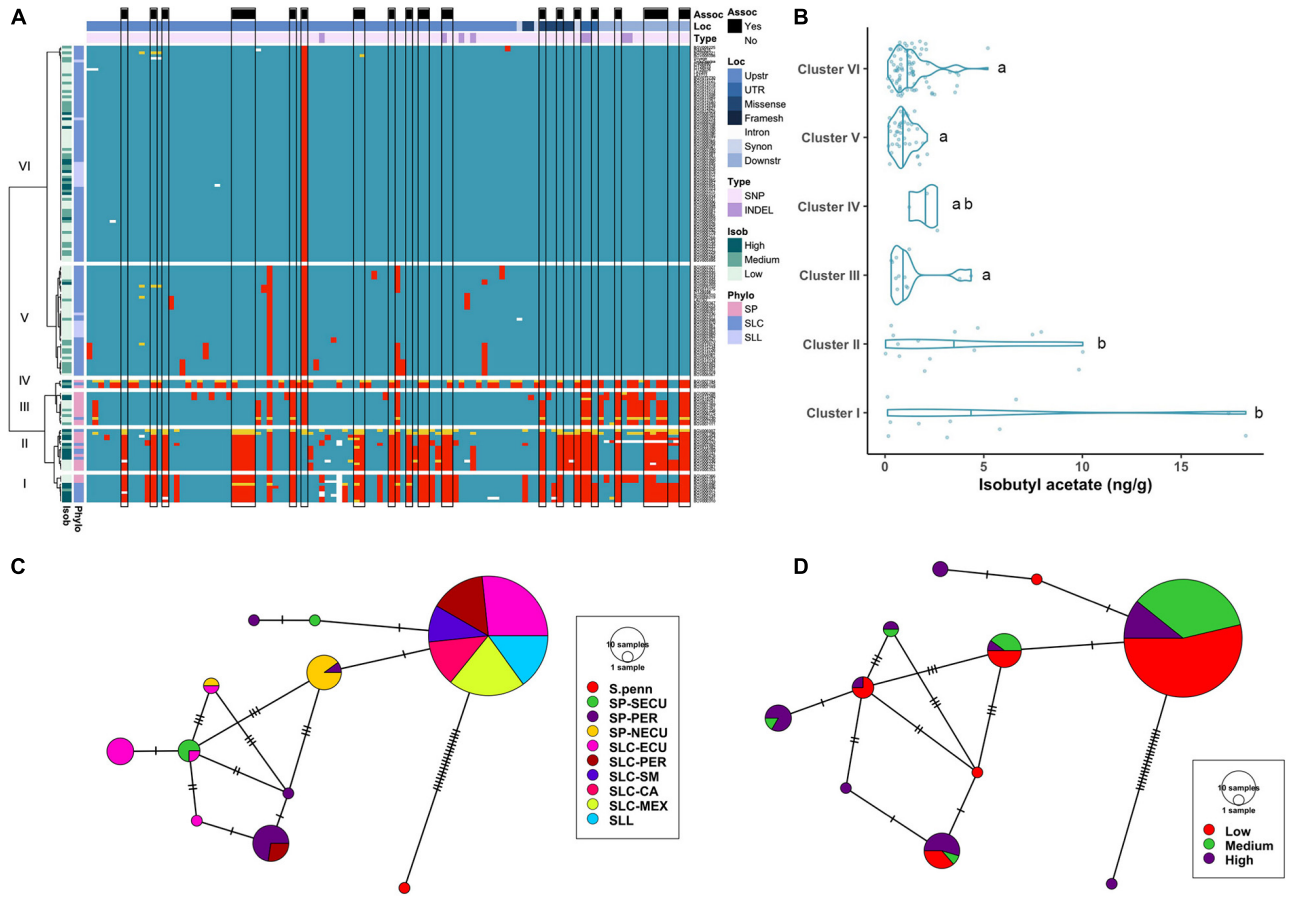

FIGURE 4 | Haplotype analysis of *CXE1* locus. **(A)** Heatmap representing the genotypes of accessions (rows) for the polymorphisms identified (columns). Reference genotype are represented in blue, alternate in red, heterozygous in yellow and missing data in white. **(B)** Violin plots of the isobutyl acetate content in the Varitome collection, classified by haplotype cluster. Each circle represents a haplotype, its size is proportional to the number of accessions carrying that haplotype, and lines across the edges represent mutational steps **(C)**. Haplotype network classified by the phylogenetic classification of the accession. **(D)** Haplotype network classified by the isobutyl acetate content.

due to abolished activity of the enzyme (**Figure 5B**). Similarly, two SP_NECU from Cluster IV, which also showed low content of isobutyl acetate, carried a deletion of ∼850 kb within the gene resulting in the knock-out of the gene.

The haplotype network using the coding sequence identified 21 haplotypes, 12 of which were unique (**Figure 5C**). On the left side of the network, we found 10 rare haplotypes represented by SP-PER accessions and some SP-SECU. Surprisingly, a rare haplotype was found in one SLC-PER that was quite distinct from all other SLC and closer to SP-PER by six mutations. All SLL and most SLC carried the most common haplotype and differed by one mutation from a subset of SP-NECU and SLC-ECU. Isobutyl acetate levels did not show a clear pattern of distribution in the haplotype network (**Figure 5D**). About half of the rare haplotypes were associated with low isobutyl acetate levels. Similarly, the most common haplotype showed a mixture of high, medium and low values for isobutyl acetate.

Since AAT1 and CXE1 act in a feedback loop to control acetate ester levels, different haplotypes in one of the genes could explain the variation in clusters in the other gene. Therefore, we analyzed the haplotype distribution of each locus in the background of the most common haplotype at the other locus (Cluster VI). When selecting the accessions from Cluster VI for *AAT1*, the variation of *CXE1* explained the high content of isobutyl acetate in seven accessions from Clusters V and VI (**Supplementary Figures 4A,B**). These accessions shared two non-synonymous SNPs (Ser94Gly and Val211Gly), two INDELs and one SNP in the 3′-UTR and several SNPs in regulatory regions. Conversely, when the most common *CXE1* haplotype is fixed, the *AAT1* locus contributed to very low levels of isobutyl acetate, as observed in five accessions from Clusters III-VI (**Supplementary Figures 4C,D**).

LoxC

For *LoxC*, read mapping indicated an unusual high level of apparent heterozygosity in SP accessions and we sought to explore that first (**Supplementary Figure 5A** and **Supplementary Table 3E**). Because such extensive heterozygosity is rare in tomato, we hypothesized that this signal actually indicated a duplication with respect to the reference genome. In this

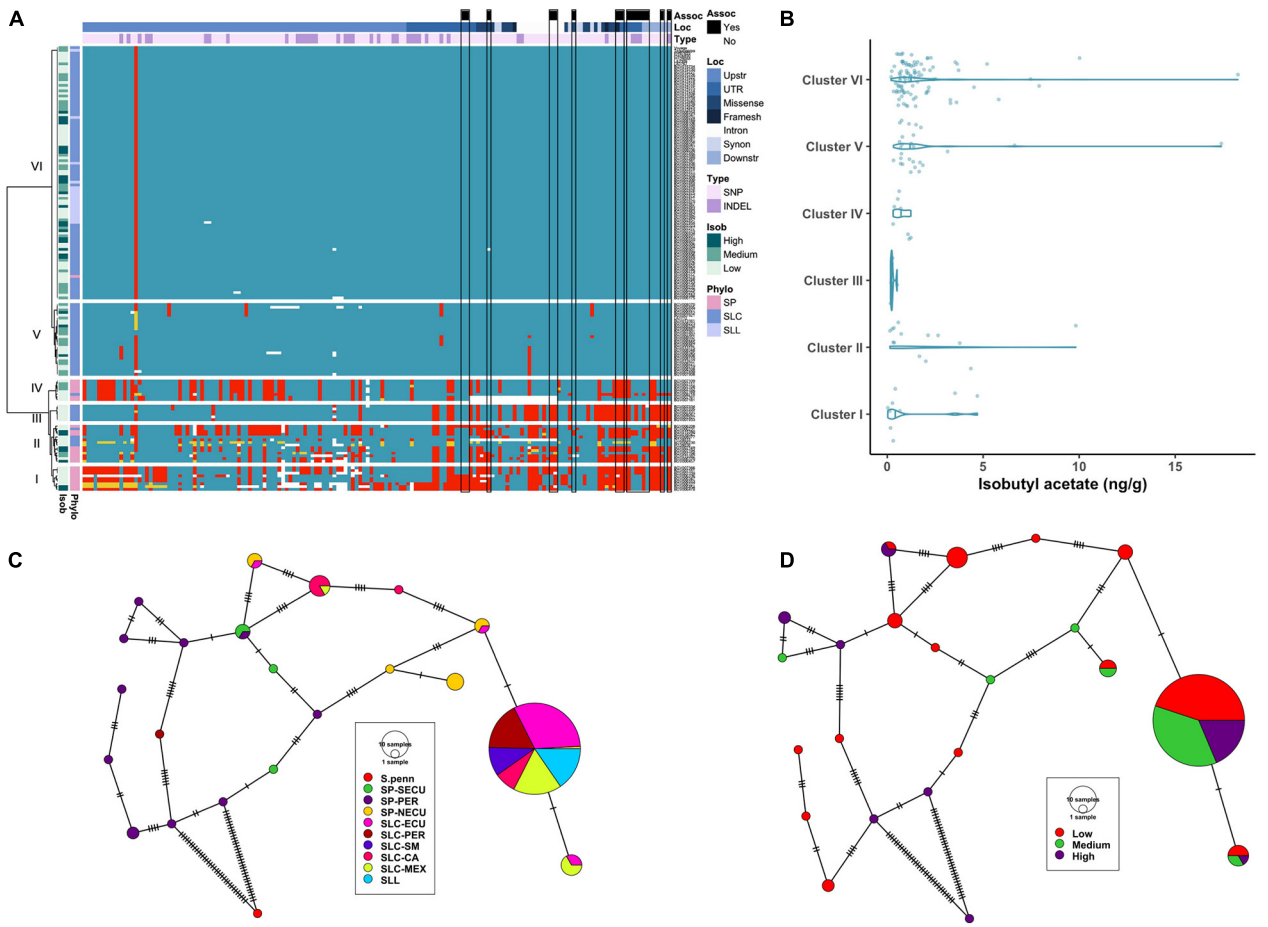

FIGURE 5 | Haplotype analysis of *AAT1* locus. **(A)** Heatmap representing the genotypes of accessions (rows) for the polymorphisms identified (columns). Reference genotype are represented in blue, alternate in red, heterozygous in yellow and missing data in white. **(B)** Violin plots of the isobutyl acetate content in the Varitome collection, classified by haplotype cluster. **(C)** Haplotype network classified by the phylogenetic classification of the accession. Each circle represents a haplotype, its size is proportional to the number of accessions carrying that haplotype, and lines across the edges represent mutational steps **(D)**. Haplotype network classified by the isobutyl acetate content.

scenario, duplication heterogeneity appears as heterozygosity when paralogous reads are mismapped to the single-copy reference locus. Using the previously established long-read assembly of PAS014479 accession, an SP-PER (Alonge et al., 2020), we identified a duplication of ∼15 kb, covering the entire *LoxC* gene (**Figure 6A**). A third partial copy in the reverse strand, which appeared to have arisen from an inversion, was found downstream *LoxC*. This sequence was also found in the Heinz reference genome (data not shown) and did not appear to encode another paralog of *LoxC* since no gene model was predicted. To check whether this duplication was correlated with heterozygosity signal, we analyzed the alignments of a subset of representative accessions using PAS014479 as the reference. The reference genome and accessions with a similar haplotype at this locus, e.g., BGV007990, carried a deletion of ∼15 kb immediately upstream *LoxC* in accordance with the duplication coordinates, while the apparent heterozygous accessions, e.g., BGV006370, lacked the deletion (**Figure 6B**). In addition, alternative structural variants were found in certain SLC-ECU accessions, e.g., BGV006906, and this was shared with another sequenced accession, LA2093 (Wang et al., 2020). Altogether, we propose that *LoxC* experienced an ancestral tandem duplication in SP, which later diverged generating two copies of the gene with 91% protein identity. The non-reference copy of *LoxC*, *LoxC-SP*, was deleted in most SLC and SLL, and another deletion partially affecting both *LoxC* and *LoxC-SP* appeared in a small group of SLC-ECU.

LoxC-SP was found in 28 accessions (**Supplementary Table 4**), including SP from both Peru and Ecuador and several SLC-ECU. The average *Z*-3-hexen-1-ol content in accessions containing both *LoxC* and *LoxC-SP* was 16.4 ng/g, whereas the accession carrying exclusively *LoxC* showed 25.6 ng/g of the volatile (**Supplementary Figure 5B**). Although this difference is significant (*p*-Value = 0.021), *Z*-3-hexen-1-ol content varied within each group, with a range from 0.01 to 70.61 and 0.14-98.77 ng/g when the duplication was present and absent, respectively. Therefore, additional genetic variation at the locus was likely responsible for the

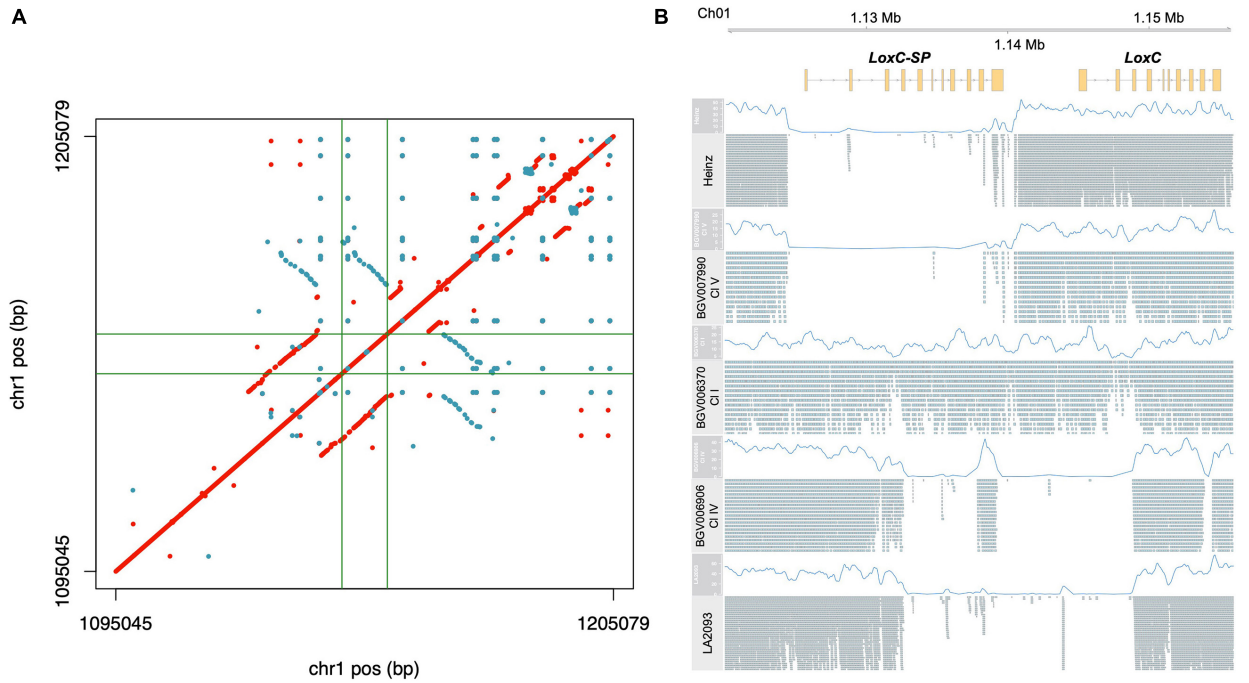

FIGURE 6 | Characterization of the duplication in LoxC locus. **(A)** Dotplot resulting the pairwise comparison of *LoxC* ± 50 kb in the assembly PAS014479_MAS1.0. Each dot corresponds to an identical match of 50 bp, red in the positive strand and blue in the reverse strand. The gene coordinates are delimited by green lines. **(B)** Alignment of five representative accessions against the PAS014479_MAS1.0 assembly at *LoxC* locus, including the coverage data (blue line) and the Illumina reads.

phenotypic variation found within the groups. We performed the association mapping at the locus using the subset of accessions containing exclusively *LoxC* and obtained seven significant SNPs (**Supplementary Figure 5C** and **Supplementary Table 1F**). All significant SNPs were still significant when analyzing the entire Varitome collection. Three of the significant SNPs were located upstream the gene, one in the first intron and other three downstream the gene.

When excluding the accessions carrying *LoxC-SP*, we identified 426 variants, of which 332 were SNPs, 92 were INDELs and 2 were SVs (**Supplementary Table 3F**). Among them, two mutations were predicted to affect splicing, and 15 SNPs were missense mutations. The SVs were two deletions of 291 bp and 795 bp in the first intron, present in two and three accessions respectively.

The haplotype analysis produced three clusters containing few, divergent accessions and three large clusters similar to the reference (**Figure 7A**). Cluster I was composed of SP accessions, and Clusters II and III of SLC-ECU. Of these three clusters, Cluster III was the most divergent with respect to the reference genome. Clusters I and II shared most of the variants, except those located at the 3′ end of the gene. Cluster III presented a putative deletion in the promoter, ∼500 bp upstream of the start site, which may impact *LoxC* expression. Clusters II and III featured low *Z*-3-hexen-1-ol content, suggesting that the polymorphisms at the 3′ end of the gene could have an impact on the phenotype (**Figure 7B**). Cluster IV was the largest group, containing 7 SLL and 56 SLC from all subpopulations, whereas most SLL were grouped in Cluster V. Both clusters showed several polymorphisms compared to the reference genome, although none of them impacted protein sequence. Lastly, Cluster VI was the most similar to the reference genome and was comprised of SLC from all subpopulations. Clusters IV and VI presented on average higher volatile content than Cluster V.

The haplotype network using the coding sequence generated one common haplotype shared by SLL and many diverse SLC (**Figure 7C**). Only two polymorphisms differentiated this haplotype from the SP-PER haplotype, identified as the most ancestral haplotype. Another four divergent haplotypes were found exclusively in SLC-ECU. The latter were carried exclusively by accessions with low *Z*-3-hexen-1-ol content, indicating that those mutations could have a role in protein activity (**Figure 7D**). In contrast, the most common haplotype contained similar proportions of low, medium and high volatile producers, suggesting that the difference between these accessions was likely regulatory in nature.

Distribution of Genetic Variation in Flavor Genes

To estimate the genetic diversity of these five flavor-related genes among subpopulations, we estimated the nucleotide diversity (**Supplementary Figure 6**). When considering overall genetic diversity, SP-PER is the most diverse group, followed by other SP and SLC-ECU, which showed similar values. In general, genetic diversity was reduced in other SLC

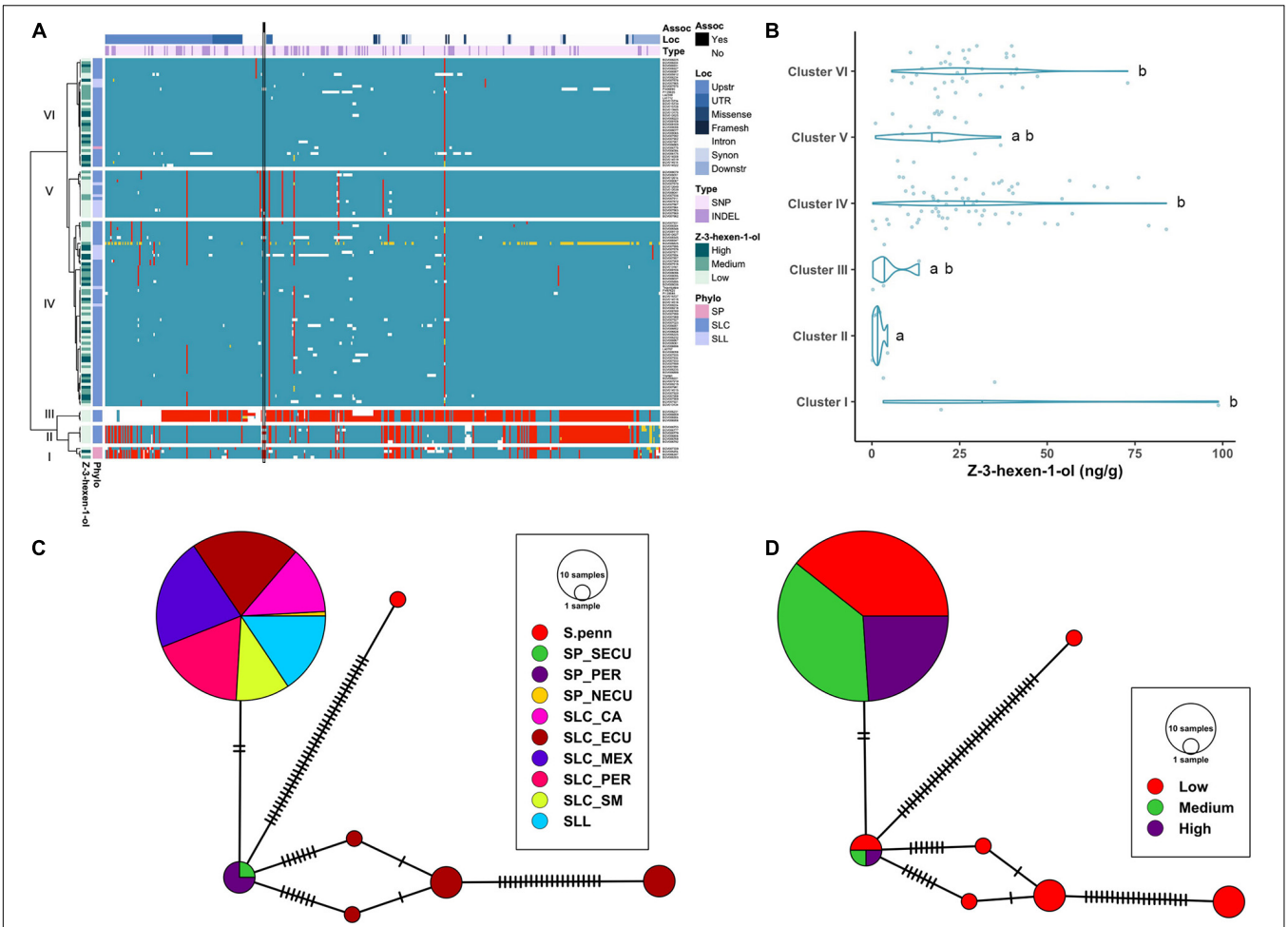

FIGURE 7 | Haplotype analysis of *LoxC* locus for accessions without duplication. **(A)** Heatmap representing the genotypes of accessions (rows) for the polymorphisms identified (columns). Reference genotype are represented in blue, alternate in red, heterozygous in yellow and missing data in white. **(B)** Violin plots of the Z-3-hexen-1-ol content in the Varitome collection, classified by haplotype cluster. **(C)** Haplotype network classified by the phylogenetic classification of the accession. Each circle represents a haplotype, its size is proportional to the number of accessions carrying that haplotype, and lines across the edges represent mutational steps **(D)**. Haplotype network classified by the Z-3-hexen-1-ol content.

subpopulations, and further reduced in SLL, in agreement with whole-genome genetic diversity (Razifard et al., 2020). However, specific subpopulations showed higher levels of diversity in some genes, e.g., SLC-SM for *ALMT9* and SLC-CA for *AAT1*, likely due to gene flow between these groups and SP.

For all five genes, non-coding regions carried the highest proportion of genetic diversity, as expected (**Supplementary Figure 6**). Synonymous and non-synonymous π estimates were similar overall, yet in some cases non-synonymous genetic diversity was predominant (e.g., *ALMT9* in SLC-MEX, *AAT1* in SP-SECU and SP-PER and *CXE1* in SLC-ECU, SLC-PER and SLC-CA), which may suggest positive selection on non-synonymous mutations with beneficial impact.

We hypothesized that some potentially valuable haplotypes may have been left behind during domestication and improvement of tomato. To test whether novel haplotypes conferring superior flavor found in the Varitome collection were absent in cultivated tomato, we selected a representative subset of cultivated accessions for which sufficiently high-quality sequencing data were publicly available. As expected, for all genes except *LoxC*, the number of polymorphisms found in cultivated tomato was lower than in the Varitome collection (**Supplementary Table 5**). Furthermore, most of the accessions carried none or few alternate alleles (<5 variants). Around one to four accessions showed a divergent haplotype with most variants homozygous for alternate allele, probably resulting from introgressions of genomic regions from related wild species. The most common haplotype of the known flavor genes did not appear to be the optimal haplotype. For *LIN5*, the best haplotype (Cluster VI) was not found in cultivated tomato. Five accessions carried the alternate allele of the two associated variants from this cluster, but in combination with other polymorphisms. For *ALMT9*, the desirable haplotype associated with lowest malate content (Cluster VI) was present in both the Varitome collection

and cultivated tomato. For *CXE1*, the best haplotype was difficult to discern. One of the likely beneficial haplotypes in *CXE1* (Cluster VI) was found in cultivated tomato. For *AAT1*, the best haplotypes (Clusters III and VI) were absent from cultivated tomato; only one accession from Tunisia carried a likely beneficial haplotype. For *LoxC*, three haplotypes were associated with higher levels of *Z*-3-hexen-1-ol (Clusters I, IV, and VI) and only Cluster VI haplotype was present in cultivated tomato.

Haplotype analyses showed that SLL had no unique haplotypes. Hence, the haplotypes of flavor genes that characterize cultivated tomato appeared to have come from standing genetic variation present in ancestral populations. Novel mutations in flavor genes rarely appeared during domestication according to the results at these five genes. Since only certain haplotypes were selected and those were now nearly fixed in cultivated tomato, SLC accessions from South and Central America continues to be a good source of improved haplotypes at these loci.

Gene Expression of Flavor Genes

For each known gene in a metabolic pathway, its protein activity (Fridman et al., 2004; Goulet et al., 2015) and gene expression (Goulet et al., 2015) collectively contribute to the accumulation of the metabolite. To evaluate whether expression of the studied genes was associated with the accumulation of metabolites, we performed a transcriptome analysis of nine diverse accessions from different phylogenetic groups presenting a range of metabolite content (**Table 2**). Five developmental stages of fruit development were selected, from flower at anthesis to ripe red fruit, for insights into gene expression dynamics. Since there are two variables (genotype and developmental stage), we used linear modeling instead of pairwise comparison to identify differentially expressed genes. In brief, the Likelihood Ratio Test is used to provide a *P*-value for each gene for identifying differential expression based on a cut-off value of 0.05 (Clevenger et al., 2017). Although the five studied genes were all involved in fruit flavor, the expression patterns observed were different among the accessions that were used in the study (**Figure 8**). The raw mapping data were listed in **Supplementary Table 6**.

For *LIN5*, the expression dynamics varied substantially between accessions (**Figure 8A**) which was confirmed by the calculated *P*-value of 7.21 - 10^{-13}. The flower stage showed the highest expression level in most accessions. BGV006370, an SP-PER accession in haplotype Cluster II, featured high SSC and showed the highest expression of *LIN5* in mature green fruit. The same pattern was observed but to a lesser extent in BGV007151, an SP-SECU accession. In accessions that accumulated lower SSC, *LIN5* expression peaked at the flower stage. BGV008219 showed a different expression pattern that peaked at the ripening stage, albeit that the replicates were variable. These data suggested that the timing of expression may be relevant for fruit sugar content which could have changed during domestication.

For *ALMT9*, the expression pattern was similar in all accessions (**Figure 8B**) with a calculated *P*-value of 1, with low expression that peaked at the flower stage. Of the nine accessions in the expression analysis, only one (BGV008219) carried the 3-bp INDEL in the promoter described before as likely causative (Ye et al., 2017). However, BGV008219 *ALMT9* expression levels did not differ dramatically from any of the other accessions. Moreover, malate content did not correlate to expression levels among these nine accessions. For example, of the four accessions in Cluster VI, two accessions showed higher expression, but the malate content was still low. The lack of correlation between gene expression and malate content could be due to the limited number of samples analyzed and/or genetic background effects. The expression of *ALMT9* could also be restricted to a very specific tissue or stage of development, which would impede to reach conclusions from the current experiment. In addition, any of the missense mutations could alter protein activity and cause the observed phenotype.

For *AAT1* and *CXE1*, we observed a similar pattern of expression in most accessions, showing low expression in flower and the first stages of fruit development. Expression started to increase at breaker and peaking in ripe fruits (**Figures 8C,D**). However, the levels of expression in red ripe fruit varied greatly among accessions, therefore both of *AAT1* (*P*-value of 3.01 - 10^{-10}) and *CXE1* (*P*-value of 2.77 - 10^{-12}) were categorized as differentially expressed genes in linear modeling analysis. In most cases, the expression of *AAT1* and *CXE1* was equally high; for example, BGV008189 showed the highest expression for *AAT1* and also one of the highest for *CXE1*. However, in the SP accessions BGV007151 and BGV006370, expression of *AAT1* was low, limiting the synthesis of isobutyl acetate, whereas expression of *CXE1* was high, further enhancing the degradation of the limited amount of the volatile. The two accessions that

TABLE 2 | Accessions used for transcriptomic analysis and corresponding metabolite levels.

Accession	Subpopulation	SSC (°Bx)	Malate (μg/g)	Isobutyl acetate (ng/g)	Z-3-hexen-1-ol (ng/g)
BGV006370	SP_PER	8.15	0.45	0.73	53.44
BGV007151	SP_SECU	6.90	0.35	0.13	23.59
PI129026	SLC_ECU	5.33	0.29	0.36	26.01
BGV007023	SLC_ECU	6.40	0.42	5.21	37.07
BGV007990	SLC_PER	6.43	0.21	1.36	20.11
BGV008189	SLC_PER	5.37	0.25	4.52	1.02
BGV008219	SLC_MEX	6.25	0.84	0.71	11.60
BGV005895	SLC_MEX	6.60	1.28	0.75	32.00
BGV007863	SLL	5.47	1.02	0.92	1.04

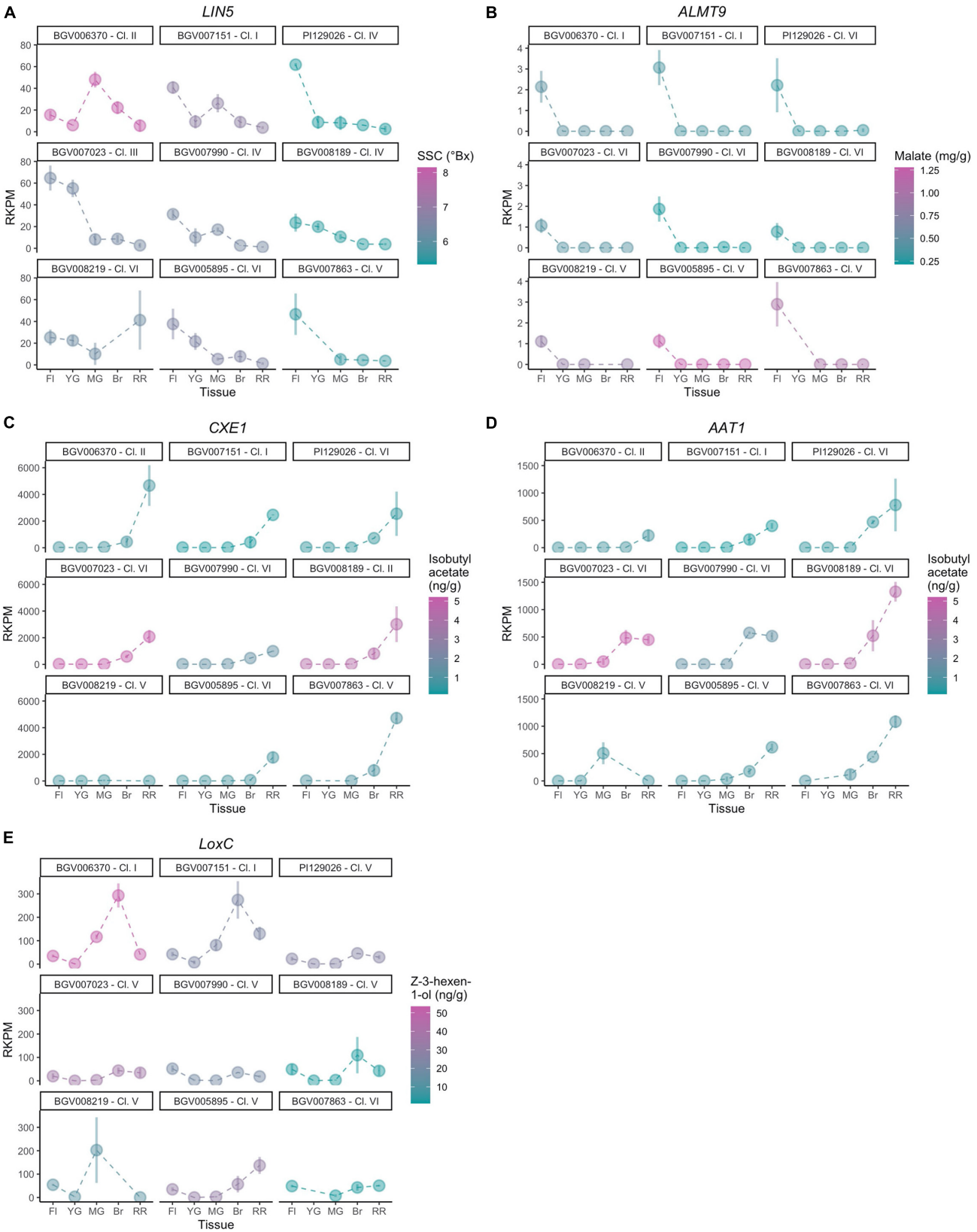

FIGURE 8 | (A–E) Gene expression of nine representative accessions for flavor-related genes.

showed high *CXE1* expression in ripe fruit showed medium to low isobutyl acetate content, which fits the hypothesis of these esters to be catalyzed at a high rate. Four SLC contained in Cluster VI showed lower *CXE1* expression on average, yet the metabolite content was variable within the group. *AAT1* expression was lower (<500 RKPM) in the two SP accessions, from Clusters I and II, than in accessions from Cluster VI, the most common haplotype (∼1000 RKPM).

The expression levels of *LoxC* were variable across accessions as indicated by a *P*-value of 1.22 - 10^{-18}, although the dynamics were similar. In most of them, the expression was low at flower and young fruit, increased gradually until it peaked at breaker and then slightly reduced in ripe red fruits (**Figure 8E**). *LoxC* expression at breaker stage was nearly tripled in the two SP accessions carrying the duplication, suggesting a gene dosage effect. No general relationship among gene expression and *Z*-3-hexen-1-ol content was observed. However, BGV006370 presented the highest expression level at breaker as well as the highest *Z*-3-hexen-1-ol content and the SLL accession BGV007863 showed low levels of both expression and metabolite level.

Effects on Protein Structure

Several variants that alter protein sequences were identified in the five known flavor genes. To estimate how these variants could alter the protein structure and function, we predicted the 3D model for each protein and the effect of missense mutations.

The best model template for LIN5 was a cell-wall invertase from *Arabidopsis thaliana* (**Supplementary Figure 7** and **Supplementary Table 7**). The prediction was of high quality, and the identified domains were members of the glycosyl hydrolases family 32. One transmembrane domain was predicted between positions 524-539. Of the 15 missense mutations, only one was predicted to have a high impact on protein structure, a change from Phenylalanine to Leucine in position 318 in the active site (**Table 3**). The in-frame deletion of five amino acids from 343 to 347 positions affected two amino acids predicted to be part of the active site; however, their mutational sensitivity was considered low. Therefore, it was unclear whether this INDEL could have a measurable impact on protein structure and activity. The change from Asparagine to Aspartate at position 366 was the most highly associated SNP in our analyses as well as former studies (Fridman et al., 2004; Tieman et al., 2017), yet it was predicted to have minimum effect on protein structure. These two variants of the LIN5 protein when overexpressed in tomato revealed that plants overexpressing the alternate version of the protein had higher sugar levels than those expressing the reference version of the protein (Tieman et al., 2017). To determine the biochemical basis for this phenotype, we expressed the two variants of the LIN5 protein in yeast. The alternate version of the protein containing Asp at position 366 exhibited higher activity with respect to sucrose substrate than the reference version of LIN5 (**Supplementary Table 8**).

For ALMT9, the model presented low quality, reaching only 56.1% of confidence, on the contrary to the other models (**Supplementary Figure 7** and **Supplementary Table 6**). The model contained seven transmembrane domains, which would

TABLE 3 | Amino acid changes and predicted impact in protein structure.

Protein	Mutation	Impact severity in the protein structure	Pocket	Associated with phenotype
LIN5	Phe21Tyr	1		
	Ile208Val	1		
	Tyr265His	2		
	Met290Val	1		
	Phe318Leu	7	*	
	Asn366Asp	1		*
	Leu373Val	1		
	Lys385Arg	1		
	Leu390Trp	2		
	Lys393Asn	1		
	Leu422Phe	2		
	Val440Leu	1		
	Val458Leu	1		
	Ser494Thr	1		
	Asn498Asp	1		
ALTM9	Lys47Asn	2		
	Val86Ile	1		
	Val152Phe	3		
	Gly215Ser	1		
	Pro277Leu	3		
	His307Arg	1		
	Tyr406Asn	3		
	Glu412Ala	2		
	Leu458Ser	2		
	Arg504His	2		
	Ala554Val	2		
CXE1	Gln66Leu	2		
	Gly77Ser	5		
	Ser94Gly	5		*
	Phe154Ile	5		
	Gly200Asp	2	*	
	Val211Gly	2		*
	Leu214His	2		
	Ser266Tyr	3		
AAT1	Ile4Thr	2		
	Ser24Pro	1		*
	Leu41Phe	1	*	
	Leu60Pro	2		
	Lys88Arg	1	*	
	Tyr123Cys	2		
	His129Arg	3		
	Ile145Val	1		
	Phe161Val	5		*
	Asn176Lys	2		
	Cys209Phe	2		
	Val245Phe	1		
	Arg270Cys	6		
	Leu284Phe	3		
	Thr354Ile	1		*
	Thr398Ile	1		*
LoxC	Leu43Ile	2		
	Ile52Thr	1		
	Glu57Gln	1		
	Val72Leu	1		
	Pro178Ser	1		
	Leu190Ile	2		
	Ser191Pro	1		
	Asn264Lys	1	*	
	Gln294Lys	1		
	His337Gln	2		
	Asn366Asp	1		
	Val580Ile	1		*
	Gly598Ala	2		*
	Thr607Leu	3		*

**Indicates the amino acid changes affecting the pocket of the enzyme (column 4) and/or significantly associated with the phenotype (column 5).*

be consistent with the subcellular localization of the protein in the tonoplast (Ye et al., 2017). None of the 11 missense mutations was predicted to cause a meaningful effect on protein structure (**Table 3**).

The best model template for CXE1 was an alpha-beta hydrolase from *Catharanthus roseus*, which covered 98% of the protein sequence (**Supplementary Figure 7** and **Supplementary Table 6**). Three out of the eight missense mutations were predicted to produce a moderate effect on protein structure (**Table 3**). In addition, one of these amino acid changes, from Serine to Glycine in position 94, was significantly associated with isobutyl acetate levels, suggesting that it might alter the activity of the enzyme.

For AAT1, the best model template was a hydroxycinnamoyl-coA transferase from *Coffea canephora*, which carried a domain from a transferase family as well as one transmembrane domain between positions 257-272 (**Supplementary Figure 6** and **Supplementary Table 5**). Two amino acid changes were predicted to cause a moderate effect on protein structure, from Phenylalanine to Valine at position 161 and Arginine to Cysteine at position 270 (**Table 3**). The position 161 amino acid change-causing SNP was significantly associated with isobutyl acetate levels in the local association mapping result (**Figures 1**, **4**) and was one of the amino acid changes identified between *S. pennellii* and cultivated tomato (Goulet et al., 2015).

The best model template for LoxC was a lipoxygenase from plants. The model contained the two known domains, PLAT and lipoxygenase, that are found in these enzymes (**Supplementary Figure 6** and **Supplementary Table 5**). Most amino acid changes were predicted to have a low impact on protein structure. However, the change from Threonine to Leucine at position 607 showed the highest likelihood of changing protein structure and the underlying SNP was highly associated with *Z*-3-hexen-1-ol (**Table 3**).

DISCUSSION

Fruit flavor is a complex trait that is genetically controlled by several independently regulated pathways (Tieman et al., 2012, 2017). For good tomato flavor, the balance of sugars and acids is complemented by the production of a specific bouquet of volatile organic compounds. Flavor is also affected by the environment and levels of certain metabolites can range from ∼20 to 80% (Bauchet et al., 2017). Some metabolic traits also show a significant interaction between genetic and environmental effects (Diouf et al., 2018). Despite environmental effects, five previously cloned genes representing four flavor pathways, were significantly associated with trait variation in the Varitome collection. This suggested that these five genes were major contributors to flavor change during the evolution of the vegetable. The domestication of tomato started with the origin of semi-domesticated SLC in South America, the northward spread of SLC and the further domestication into SLL in Mexico. Of the candidate genes examined, only *LIN5* showed evidence of having been subjected to positive selection during the final steps of domestication (Razifard et al., 2020). *AAT1* was also associated with sweeps in the transition from SP to SLC-ECU and in the sweep in the northward migrations of SLC. The lack of evidence on the positive selection on three of the five flavor genes during domestication is consistent with our view and that of others (Blanca et al., 2012, 2015; Sauvage et al., 2017), that some potentially valuable haplotypes may have been left behind during the evolution from a fully wild to a cultivated type. The selected haplotypes for *LIN5* and *AAT1* seemed to have contributed negatively to flavor, meaning they could have hitchhiked due to linkage drag with another trait in the region. Alternatively, the flavor deterioration could have been a tradeoff for improved agricultural performance, e.g., sugar content and fruit size are often inversely correlated (Georgelis et al., 2004; Prudent et al., 2009). In this case, positive selection for larger fruits would lead to fixation of haplotypes conferring lower SSC.

To determine whether the diversity in the Varitome collection is useful toward improving modern tomato flavor, we sought to find the optimal allele for each gene. For *LIN5*, an enzymatic assay from a previous study showed that the change at position 348 from Aspartate in *S. pennellii* to Glutamate in *S. lycopersicum* played a role in protein activity (Fridman et al., 2004). In the red-fruited Varitome collection, a different change from Asparagine to Aspartate at position 366, was significantly associated with sugar content (**Figure 1A**), consistent with findings from other GWAS (Tieman et al., 2017; Razifard et al., 2020). Protein expression studies showed that this amino acid replacement altered protein activity (**Supplementary Table 8**) and overexpression of the Asp^{366} *LIN5* allele in tomato increased sugar content (Tieman et al., 2017). The less desirable Asn^{366} allele is present at high frequency in SLL, and in 94.6% of the selected heirloom and modern varieties (**Supplementary Table 5**). Thus, the optimal allele of *LIN5* appeared to be rare in modern tomato.

For *ALMT9*, a 3-bp INDEL in the promoter was proposed to be causative to trait variation (Ye et al., 2017). This small INDEL would impact a W-box binding motif thereby affecting gene expression. In the Varitome collection, the most significant variants were three SNPs located in the second exon (synonymous) and the second intron (**Figure 3**). The 3-bp INDEL was not associated with the trait, possibly due to low allele frequency in the Varitome collection, which could reduce the statistical power to detect significant associations. In the subset of heirloom and modern tomatoes, this INDEL and the three SNPs were in complete LD, suggesting that the effect on the phenotype was by a combination of these variants. This haplotype found in some SLL and SLC, is thought to contribute to increased malate content in fruits, which is associated with negative flavor. Therefore, this haplotype may not be desirable in breeding programs aimed at improving flavor. In addition to its role in fruit flavor, ALMT9 contributes to Al tolerance in roots (Ye et al., 2017). None of the haplotypes found in the Varitome collection and the heirloom and modern accessions were predicted to be a gene knock-out, suggesting that a functional *ALMT9* may be essential. These

findings suggest that it may be relevant for plant performance and adaptation to novel environments. However, the effect of the less tasty *ALMT9* allele on plant performance in this collection is unknown. In the Varitome collection, two novel haplotypes (Clusters III and IV) were also associated with low malate content and could be used in breeding programs for improved flavor.

The transposable elements in the promoter of *CXE1* are proposed to increase expression in red fruited tomato compared to the green fruited *S. pennellii* (Goulet et al., 2012). These transposable elements were fixed in the Varitome collection, yet differences in gene expression were still observed. For example, two accessions from Cluster II showed a 2-fold increase in expression of *CXE1* compared to accessions in Cluster VI at the ripe fruit stage (**Figure 8**). Several SNPs and INDELs in regulatory regions differed between these two groups, which could lead to differences in gene expression. In addition, eight missense SNPs were identified in the Varitome collection, of which only one was found in the heirloom and modern accessions (**Supplementary Table 5**). Haplotypes found in Clusters I and II were associated with higher acetate esters content. Since acetate esters are negatively correlated with consumer liking (Tieman et al., 2012), the Cluster I and II haplotypes were undesirable. The most common and most desirable haplotype in SLL were found in Clusters V and VI and were identical or nearly identical to the reference genome (**Figure 4**). In addition, a novel SP haplotype from Cluster III contributes to low acetate content and may also be used in breeding programs to enhance fruit flavor.

The *S. pennellii* AAT1 enzyme is proposed to be more active than cultivated AAT1 (Goulet et al., 2015). The specific polymorphism(s) causing the variation in acetate ester levels is not known, however. Several polymorphic SNPs leading to amino acid changes between *S. pennellii* and cultivated tomato were also segregating in the Varitome collection, three of which were significantly associated with acetate ester levels (**Table 3**). Interestingly, some of the polymorphisms found in *S. pennellii* were shared by SP. However, SP showed low acetate ester levels whereas *S. pennellii* showed high levels implying that these polymorphisms are inconsequential. In addition, two haplotypes that were predicted to result in a knock-out or knock-down of the gene were found. One haplotype carried a deletion of ∼850 bp affecting the coding sequence and another carried a 13-bp duplication resulting in a coding region frame shift. Both haplotypes were associated with low content of acetate esters, which is positively correlated to consumer liking. The latter polymorphisms were largely absent in the heirloom and modern varieties. Therefore, these *AAT1* knock-down haplotypes leading to reduced production of acetate esters could be easily introduced into breeding programs to contribute to flavor improvement.

The availability of improved long-read genome assemblies allowed us to resolve several SVs affecting the *LoxC* locus. A heterozygous promoter allele is reported to be associated with higher gene expression in a previous study (Gao et al., 2019). However, we found a gene duplication causing a misleading level of heterozygosity. The duplication was mainly found in SP and, on average, contributed to lower levels of *Z*-3-hexen-1-ol. The expression of *LoxC* in SP was higher, as previously reported, but this did not appear to result in higher *Z*-3-hexen-1-ol accumulation. The encoded LoxC and LoxC-SP showed only a 91% amino acid identity (data not shown), implying that these paralogs arose millions of years ago. In addition, a QTL mapping study using a RIL population derived from a cross with NC EBR-1 (only reference *LoxC* copy) and LA2093 (incomplete *LoxC* and *LoxC-SP* copies) found increases in multiple lipid-derived volatiles and apocarotenoids controlled by the NC EBR-1 haplotype (Gao et al., 2019; Wang et al., 2020). According to our findings, LA2093 suffered a deletion of ∼16 kb which fused the first three exons of *LoxC-SP* to the last eight exons of *LoxC*, with the third exon being duplicated (**Figure 6B**). Since the LA2093 haplotype was associated with low content of volatiles, it was conceivable that the encoding enzyme was not functional. When excluding the accessions carrying both copies of *LoxC*, the Cluster III haplotype (**Figure 7**) differed in most variants, suggesting that these accessions could only carry the *LoxC-SP* paralog and/or the deletion found in LA2093. Among the other reference *LoxC* haplotypes, we could not find a likely causative variant. The reference haplotype (Cluster VI) seems to be adequate for high lipid-derived volatile content (**Figure 7**). In addition, the haplotype found in Cluster IV might also be beneficial for flavor improvement.

Regulatory mutations are often causative of trait variation (Muños et al., 2011; Goulet et al., 2012; Ye et al., 2017). Surprisingly, we did not find a clear correlation between gene expression and metabolite levels for none of the five studied genes. This lack of correlation may be due to several biological and technical factors. On one hand, the causative variants may affect the coding region and/or UTRs instead of being regulatory, as shown for *LIN5*. On the other hand, we limited the transcriptomic analyses to nine representative accessions, which we thought to be representative of the Varitome collection, yet may not reflect completely all haplotypes. For example for *ALMT9,* only clusters I, V and VI were represented in the expression analysis (**Figure 8**).

To envision the use of the findings from these studies in tomato breeding programs, the beneficial haplotypes at these five loci could be introgressed through conventional breeding into cultivated germplasm and evaluated for their performance. Moreover, we showed that SLC maintained levels of genetic diversity comparable to SP at the five flavor loci even though SP is evolutionary quite distinct from SLC and instead SLC is much closer to SLL (**Supplementary Figure 6**). Therefore, an added benefit of using SLC accessions as donors for beneficial alleles is the reduced linkage drag of deleterious alleles that often accompanies the introgression of targeted loci from more distant wild relatives. The detailed analyses of the fruit metabolite loci permitted us to propose the likely relevant variant(s), which can be used to identify the best donor accession as well as the development of molecular markers to monitor the introgression.

Once incorporated into modern accessions, the effect of these haplotypes could be directly tested and validated.

The genetic variation for each locus in the Varitome collection was large. Moreover, even within genetic clusters, we observed wide phenotypic variation, suggesting that additional genetic factors are segregating in the population for these pathways. These other genes could be previously cloned genes (albeit that they did not show association in the Varitome collection) or representing novel genes. Our collection would be an excellent material to discover new flavor genes through genetic mapping approaches.

DATA AVAILABILITY STATEMENT

The datasets analyzed for this study can be found in NCBI, accession numbers SRA: SRP150040, SRA: SRP045767, and SRA: SRP094624.

AUTHOR CONTRIBUTIONS

LP and EvdK conceived the study. LP, MS, MA, NT, YiZ, YoZ, and HR performed the experiments and data analyses. DT generated the metabolic data. YW generated the RNA-seq data. AF, AC, ZF, and MCS provided advice and resources. LP and EvdK drafted the original manuscript. All authors reviewed and agreed to the published version of the manuscript.

FUNDING

This research was funded by grants from the National Science Foundation IOS 1564366 and IOS 1732253.

ACKNOWLEDGMENTS

We acknowledge Zachary Lippman for the long-read sequencing assemblies.

SUPPLEMENTARY MATERIAL

The Supplementary Material for this article can be found online at: https://www.frontiersin.org/articles/10.3389/fpls.2021.642828/full#supplementary-material

Supplementary Figure 1 | Local association mapping for flavor-related genes and their corresponding metabolites. SNPs are plotted as blue dots, INDELs as yellow dots and SVs as purple triangles. Horizontal lines represent 0.05 and 0.01 significance thresholds.

Supplementary Figure 2 | Function of the known genes used in this study, as detailed previously in the literature.

Supplementary Figure 3 | Linkage disequilibrium of SNPs in the gene regions.

Supplementary Figure 4 | Haplotype analysis of AAT1 and CXE1 A. Heatmap of AAT1 including only accessions which belong to Cluster VI in CXE1 clustering B. Violin plots of the isobutyl acetate content classified by haplotype cluster. C. Heatmap of CXE1 including only accessions which belong to Cluster VI in AAT1 clustering D. Violin plots of the isobutyl acetate content classified by haplotype cluster.

Supplementary Figure 5 | Haplotype analysis of *LoxC* locus for the complete set of accessions. **(A)** Heatmap representing the genotypes of accessions (rows) for the polymorphisms identified (columns). Reference genotype are represented in blue, alternate in red, heterozygous in yellow and missing data in white. **(B)** Violin plots of the Z-3-hexen-1-ol content for accessions carrying the duplication (*LoxC-SP* present) and without the duplication (*LoxC-SP* absent).

Supplementary Figure 6 | Nucleotide diversity in the gene regions, including flanking sequences 3 kb upstream and 1 kb downstream, within each subpopulation.

Supplementary Figure 7 | Protein modeling predictions of the five proteins using amino acid sequences. The predicted pocket of the enzyme is displayed in red.

Supplementary Table 1 | Association mapping results. The variant ID includes a first code letter: S for SNP, I for indel and V for SV. The significant *p*-Values are highlighted in pink color.

Supplementary Table 2 | Genotyping of SVs detected using Lumpy **(A)**. For all five genes and the complete Varitome collection. **(B)** For LoxC when excluding the accessions carrying LoxC-SP.

Supplementary Table 3 | Genotyping table. Each column corresponds with a variant and the coordinate, reference and alternate alleles and variant annotation from SnpEff are included. Each row corresponds to an accession and the ID of the accession, Cluster at which belongs according to the haplotype clustering and subpopulation according to Razifard et al. (2020) are included.

Supplementary Table 4 | Genotyping of the duplication at the *LoxC* locus using three different criteria: normalized coverage and heterozygosity when aligning against Heinz SL4.0 reference genome and detection of a deletion when aligning to the PAS014479_MAS1.0 assembly. 0 means only *LoxC* copy, 1 means both *LoxC-SP* and *LoxC* copies.

Supplementary Table 5 | Genotyping results of the selected cultivated varieties at the five loci. Information about the origin and whether the variety is modern or heirloom was extracted from Tieman et al. (2017).

Supplementary Table 6 | RPKM values for each biological replicate used in the expression analysis.

Supplementary Table 7 | Quality parameters of the protein modeling predictions.

Supplementary Table 8 | Enzymatic activity of reference and alternate LIN5 alleles.

REFERENCES

Alonge, M., Wang, X., Benoit, M., Soyk, S., Pereira, L., Zhang, L., et al. (2020). Major impacts of widespread structural variation on gene expression and crop improvement in tomato. *Cell* 182, 145–161.e23.

Baldwin, E. A., Scott, J. W., Shewmaker, C. K., and Schuch, W. (2000). Flavor trivia and tomato aroma: biochemistry and possible mechanisms for control of important aroma components. *HortScience* 35, 1013–1022. doi: 10.21273/hortsci.35.6.1013

Bandelt, H. J., Forster, P., and Röhl, A. (1999). Median-joining networks for inferring intraspecific phylogenies. *Mol. Biol. Evol.* 16, 37–48. doi: 10.1093/oxfordjournals.molbev.a026036

Bauchet, G., Grenier, S., Samson, N., Segura, V., Kende, A., Beekwilder, J., et al. (2017). Identification of major loci and genomic regions controlling acid and volatile content in tomato fruit: implications for flavor improvement. *New Phytol.* 215, 624–641. doi: 10.1111/nph.14615

Blanca, J., Cañizares, J., Cordero, L., Pascual, L., Diez, M. J., and Nuez, F. (2012). Variation revealed by SNP genotyping and

morphology provides insight into the origin of the tomato. *PLoS One* 7:e0048198.

Blanca, J., Montero-Pau, J., Sauvage, C., Bauchet, G., Illa, E., Díez, M. J., et al. (2015). Genomic variation in tomato, from wild ancestors to contemporary breeding accessions. *BMC Genomics* 16:257.

Bolger, A. M., Lohse, M., and Usadel, B. (2014a). Trimmomatic: a flexible trimmer for Illumina sequence data. *Bioinformatics* 30, 2114–2120. doi: 10.1093/bioinformatics/btu170

Bolger, A., Scossa, F., Bolger, M. E., Lanz, C., Maumus, F., Tohge, T., et al. (2014b). The genome of the stress-tolerant wild tomato species *Solanum pennellii*. *Nat. Genet.* 46, 1034–1038. doi: 10.1038/ng.3046

Bradbury, P. J., Zhang, Z., Kroon, D. E., Casstevens, T. M., Ramdoss, Y., and Buckler, E. S. (2007). TASSEL: software for association mapping of complex traits in diverse samples. *Bioinformatics* 23, 2633–2635. doi: 10.1093/bioinformatics/btm308

Buttery, R. G., Teranishi, R., Flath, R. A., and Ling, L. C. (1989). "Fresh tomato volatiles," in *Flavor Chemistry ACS Symposium Series*, eds R. Teranishi and R. G. Buttery (Washington, DC: American Chemical Society), 17–213.

Causse, M., Friguet, C., Coiret, C., Lepicier, M., Navez, B., Lee, M., et al. (2010). Consumer preferences for fresh tomato at the european scale: a common segmentation on taste and firmness. *J. Food Sci.* 75, S531–S541.

Chen, G., Hackett, R., Walker, D., Taylor, A., Lin, Z., and Grierson, D. (2004). Identification of a specific isoform of tomato lipoxygenase (TomloxC) involved in the generation of fatty acid-derived flavor compounds. *Plant Physiol.* 136, 2641–2651. doi: 10.1104/pp.104.041608

Chiang, C., Layer, R. M., Faust, G. G., Lindberg, M. R., Rose, D. B., Garrison, E. P., et al. (2015). SpeedSeq: ultra-fast personal genome analysis and interpretation. *Nat. Methods* 12, 966–968. doi: 10.1038/nmeth.3505

Cingolani, P., Platts, A., Wang, L. L., Coon, M., Nguyen, T., Wang, L., et al. (2012). A program for annotating and predicting the effects of single nucleotide polymorphisms, SnpEff: SNPs in the genome of Drosophila melanogaster strain w1118; iso-2; iso-3. *Fly* 6, 80–92. doi: 10.4161/fly.19695

Clevenger, J., Chu, Y., Arrais Guimaraes, L., Maia, T., Bertioli, D., Leal-Bertioli, S., et al. (2017). Gene expression profiling describes the genetic regulation of *Meloidogyne arenaria* resistance in Arachis hypogaea and reveals a candidate gene for resistance. *Sci. Rep.* 7:1317.

Danecek, P., Auton, A., Abecasis, G., Albers, C. A., Banks, E., DePristo, M. A., et al. (2011). The variant call format and VCFtools. *Bioinformatics* 27, 2156–2158. doi: 10.1093/bioinformatics/btr330

Diouf, I. A., Derivot, L., Bitton, F., Pascual, L., and Causse, M. (2018). Water deficit and salinity stress reveal many specific QTL for plant growth and fruit quality traits in tomato. *Front. Plant Sci.* 9:279.

Dobin, A., Davis, C. A., Schlesinger, F., Drenkow, J., Zaleski, C., Jha, S., et al. (2013). STAR: ultrafast universal RNA-seq aligner. *Bioinformatics* 29, 15–21. doi: 10.1093/bioinformatics/bts635

Domínguez, M., Dugas, E., Benchouaia, M., Leduque, B., Jimenez-Gomez, J., Colot, V., et al. (2020). The impact of transposable elements on tomato diversity. *bioRxiv [Preprint]* doi: 10.1016/j.solener.2019.02.027

Dong, S.-S., He, W.-M., Ji, J.-J., Zhang, C., Guo, Y., and Yang, T.-L. (2020). LDBlockShow: a fast and convenient tool for visualizing linkage disequilibrium and haplotype blocks based on variant call format files. *bioRxiv [Preprint]* doi: 10.1101/2020.06.14.151332

Fray, R. G., and Grierson, D. (1993). Identification and genetic analysis of normal and mutant phytoene synthase genes of tomato by sequencing, complementation and co-suppression. *Plant Mol. Biol.* 22, 589–602. doi: 10.1007/bf00047400

Fridman, E., Carrari, F., Liu, Y. S., Fernie, A. R., and Zamir, D. (2004). Zooming in on a quantitative trait for tomato yield using interspecific introgressions. *Science* 305, 1786–1789. doi: 10.1126/science.1101666

Gao, L., Gonda, I., Sun, H., Ma, Q., Bao, K., Tieman, D. M., et al. (2019). The tomato pan-genome uncovers new genes and a rare allele regulating fruit flavor. *Nat. Genet.* 51, 1044–1051. doi: 10.1038/s41588-019-0410-2

Garbowicz, K., Liu, Z., Alseekh, S., Tieman, D., Taylor, M., Kuhalskaya, A., et al. (2018). Quantitative trait loci analysis identifies a prominent gene involved in the production of fatty acid-derived flavor volatiles in tomato. *Mol. Plant* 11, 1147–1165. doi: 10.1016/j.molp.2018.06.003

Georgelis, N., Scott, J. W., and Baldwin, E. A. (2004). Relationship of tomato fruit sugar concentration RAPD markers. *J. Am. Soc. Hortic. Sci.* 129, 839–845. doi: 10.21273/jashs.129.6.0839

Goulet, C., Kamiyoshihara, Y., Lam, N. B., Richard, T., Taylor, M. G., Tieman, D. M., et al. (2015). Divergence in the enzymatic activities of a tomato and solanum pennellii alcohol acyltransferase impacts fruit volatile ester composition. *Mol. Plant* 8, 153–162. doi: 10.1016/j.molp.2014.11.007

Goulet, C., Mageroy, M. H., Lam, N. B., Floystad, A., Tieman, D. M., and Klee, H. J. (2012). Role of an esterase in flavor volatile variation within the tomato clade. *Proc. Natl. Acad. Sci. U. S. A.* 109, 19009–19014. doi: 10.1073/pnas.1216515109

Graves, S., Piepho, H.-P., Selzer, L., and Dorai-Raj, S. (2015). *multcompView: Visualizations of Paired Comparisons. R Packag. version 0.1–7*.

Hahne, F., and Ivanek, R. (2016). "Visualizing genomic data using gviz and bioconductor BT," in *Statistical Genomics: Methods and Protocols*, eds E. Mathé and S. Davis (New York, NY: Springer), 335–351. doi: 10.1007/978-1-4939-3578-9_16

Huang, M., Liu, X., Zhou, Y., Summers, R. M., and Zhang, Z. (2019). BLINK: a package for the next level of genome-wide association studies with both individuals and markers in the millions. *Gigascience* 8:giy154.

Isaacson, T., Ronen, G., Zamir, D., and Hirschberg, J. (2002). Cloning of tangerine from tomato reveals a carotenoid isomerase essential for the production of beta-carotene and xanthophylls in plants. *Plant Cell* 14, 333–342. doi: 10.1105/tpc.010303

Jeffares, D. C., Jolly, C., Hoti, M., Speed, D., Shaw, L., Rallis, C., et al. (2017). Transient structural variations have strong effects on quantitative traits and reproductive isolation in fission yeast. *Nat. Commun.* 8:14061.

Jones, R. A., and Scott, S. J. (1983). Improvement of tomato flavor by genetically increasing sugar and acid contents. *Euphytica* 32, 845–855. doi: 10.1007/bf00042166

Katoh, K., and Standley, D. M. (2013). MAFFT multiple sequence alignment software version 7: improvements in performance and usability. *Mol. Biol. Evol.* 30, 772–780. doi: 10.1093/molbev/mst010

Kelley, L. A., Mezulis, S., Yates, C. M., Wass, M. N., and Sternberg, M. J. E. (2015). The Phyre2 web portal for protein modeling, prediction and analysis. *Nat. Protoc.* 10, 845–858. doi: 10.1038/nprot.2015.053

Klee, H. J., and Tieman, D. M. (2018). The genetics of fruit flavour preferences. *Nat. Rev. Genet.* 19, 347–356. doi: 10.1038/s41576-018-0002-5

Kolde, R. (2019). *pheatmap: Pretty Heatmaps. R Packag. version 1.0.12*.

Kurtz, S., Phillippy, A., Delcher, A. L., Smoot, M., Shumway, M., Antonescu, C., et al. (2004). Versatile and open software for comparing large genomes. *Genome Biol.* 5:R12.

Langmead, B., Trapnell, C., Pop, M., and Salzberg, S. L. (2009). Ultrafast and memory-efficient alignment of short DNA sequences to the human genome. *Genome Biol.* 10:R25.

Layer, R. M., Chiang, C., Quinlan, A. R., and Hall, I. M. (2014). LUMPY: a probabilistic framework for structural variant discovery. *Genome Biol.* 15:R84. doi: 10.1007/978-3-642-85092-9_22

Leigh, J. W., and Bryant, D. (2015). popart: full-feature software for haplotype network construction. *Methods Ecol. Evol.* 6, 1110–1116. doi: 10.1111/2041-210x.12410

Lenth, R. (2020). *emmeans: Estimated Marginal Means, aka Least-Squares Means. R Packag. version 1.5.0*.

Li, H. (2011). A statistical framework for SNP calling, mutation discovery, association mapping and population genetical parameter estimation from sequencing data. *Bioinformatics* 27, 2987–2993. doi: 10.1093/bioinformatics/btr509

Li, X., Tieman, D., Liu, Z., Chen, K., and Klee, H. J. (2020). Identification of a lipase gene with a role in tomato fruit short-chain fatty acid-derived flavor volatiles by genome-wide association. *Plant J.* 104, 631–644. doi: 10.1111/tpj.14951

Love, M. I., Huber, W., and Anders, S. (2014). Moderated estimation of fold change and dispersion for RNA-seq data with DESeq2. *Genome Biol.* 15:550.

Mageroy, M. H., Tieman, D. M., Floystad, A., Taylor, M. G., and Klee, H. J. (2012). A *Solanum lycopersicum* catechol-O-methyltransferase involved in synthesis of the flavor molecule guaiacol. *Plant J.* 69, 1043–1051. doi: 10.1111/j.1365-313x.2011.04854.x

Martina, M., Tikunov, Y., and Portis, E. (2021). The genetic basis of tomato aroma. *Genes* 12:226. doi: 10.3390/genes12020226

Mata-Nicolás, E., Montero-Pau, J., Gimeno-Paez, E., Garcia-Carpintero, V., Ziarsolo, P., Menda, N., et al. (2020). Exploiting the diversity of tomato: the development of a phenotypically and genetically detailed germplasm collection. *Hortic. Res.* 7:66.

McKenna, A., Hanna, M., Banks, E., Sivachenko, A., Cibulskis, K., Kernytsky, A., et al. (2010). The genome analysis toolkit: a MapReduce framework for analyzing next-generation DNA sequencing data. *Genome Res.* 20, 1297–1303. doi: 10.1101/gr.107524.110

Meyer, R. S., and Purugganan, M. D. (2013). Evolution of crop species: genetics of domestication and diversification. *Nat. Rev. Genet.* 14, 840–852. doi: 10.1038/nrg3605

Mu, Q., Huang, Z., Chakrabarti, M., Illa-Berenguer, E., Liu, X., Wang, Y., et al. (2017). Fruit weight is controlled by cell size regulator encoding a novel protein that is expressed in maturing tomato fruits. *PLoS Genet.* 13:e1006930. doi: 10.1371/journal.pgen.1006930

Muños, S., Ranc, N., Botton, E., Bérard, A., Rolland, S., Duffé, P., et al. (2011). Increase in tomato locule number is controlled by two single-nucleotide polymorphisms located near WUSCHEL. *Plant Physiol.* 156, 2244–2254. doi: 10.1104/pp.111.173997

Prudent, M., Causse, M., Génard, M., Tripodi, P., Grandillo, S., and Bertin, N. (2009). Genetic and physiological analysis of tomato fruit weight and composition: influence of carbon availability on QTL detection. *J. Exp. Bot.* 60, 923–937. doi: 10.1093/jxb/ern338

Quast, C., Pruesse, E., Yilmaz, P., Gerken, J., Schweer, T., Yarza, P., et al. (2013). The SILVA ribosomal RNA gene database project: improved data processing and web-based tools. *Nucleic Acids Res.* 41, D590–D596.

Quinlan, A. R., and Hall, I. M. (2010). BEDTools: a flexible suite of utilities for comparing genomic features. *Bioinformatics* 26, 841–842. doi: 10.1093/bioinformatics/btq033

Rambla, J. L., Medina, A., Fernández-Del-Carmen, A., Barrantes, W., Grandillo, S., Cammareri, M., et al. (2017). Identification, introgression, and validation of fruit volatile QTLs from a red-fruited wild tomato species. *J. Exp. Bot.* 68, 429–442.

Rambla, J. L., Tikunov, Y. M., Monforte, A. J., Bovy, A. G., and Granell, A. (2014). The expanded tomato fruit volatile landscape. *J. Exp. Bot.* 65, 4613–4623. doi: 10.1093/jxb/eru128

Razifard, H., Ramos, A., Della Valle, A. L., Bodary, C., Goetz, E., Manser, E. J., et al. (2020). Genomic evidence for complex domestication history of the cultivated tomato in Latin America. *Mol. Biol. Evol.* 37, 1118–1132. doi: 10.1093/molbev/msz297

Ronen, G., Carmel-Goren, L., Zamir, D., and Hirschberg, J. (2000). An alternative pathway to β-carotene formation in plant chromoplasts discovered by map-based cloning of Beta and old-gold color mutations in tomato. *Proc. Natl. Acad. Sci. U. S. A.* 97, 11102–11107. doi: 10.1073/pnas.190177497

Ronen, G., Cohen, M., Zamir, D., and Hirschberg, J. (1999). Regulation of carotenoid biosynthesis during tomato fruit development: expression of the gene for lycopene epsilon-cyclase is down-regulated during ripening and is elevated in the mutant Delta. *Plant J.* 17, 341–351. doi: 10.1046/j.1365-313x.1999.00381.x

Salamov, A. A., and Solovyev, V. V. (2000). Ab initio gene finding in Drosophila genomic DNA. *Genome Res.* 10, 516–522. doi: 10.1101/gr.10.4.516

Sauvage, C., Rau, A., Aichholz, C., Chadoeuf, J., Sarah, G., Ruiz, M., et al. (2017). Domestication rewired gene expression and nucleotide diversity patterns in tomato. *Plant J.* 91, 631–645. doi: 10.1111/tpj.13592

Sauvage, C., Segura, V., Bauchet, G., Stevens, R., Do, P. T., Nikoloski, Z., et al. (2014). Genome-wide association in tomato reveals 44 Candidate loci for fruit metabolic traits. *Plant Physiol.* 165, 1120–1132. doi: 10.1104/pp.114.241521

Schauer, N., Semel, Y., Roessner, U., Gur, A., Balbo, I., Carrari, F., et al. (2006). Comprehensive metabolic profiling and phenotyping of interspecific introgression lines for tomato improvement. *Nat. Biotechnol.* 24, 447–454. doi: 10.1038/nbt1192

Shen, J., Tieman, D., Jones, J. B., Taylor, M. G., Schmelz, E., Huffaker, A., et al. (2014). A 13-lipoxygenase, TomloxC, is essential for synthesis of C5 flavour volatiles in tomato. *J. Exp. Bot.* 65, 419–428. doi: 10.1093/jxb/ert382

Simkin, A. J., Schwartz, S. H., Auldridge, M., Taylor, M. G., Klee, H. J., Sciences, H., et al. (2004). The tomato carotenoid cleavage dioxygenase 1 genes contribute to the formation of the flavor volatiles beta -ionone, pseudoionone, and geranylacetone. *Plant J.* 40, 882–892. doi: 10.1111/j.1365-313x.2004.02263.x

Small, D. M., and Prescott, J. (2005). Odor/taste integration and the perception of flavor. *Exp. Brain Res.* 166, 345–357. doi: 10.1007/s00221-005-2376-9

Soyk, S., Lemmon, Z. H., Oved, M., Fisher, J., Liberatore, K. L., Park, S. J., et al. (2017). Bypassing negative epistasis on yield in tomato imposed by a domestication gene. *Cell* 169, 1142–1155.e12.

Speirs, J., Lee, E., Holt, K., Yong-Duk, K., Scott, N. S., Loveys, B., et al. (1998). Genetic manipulation of alcohol dehydrogenase levels in ripening tomato fruit affects the balance of some flavor aldehydes and alcohols. *Plant Physiol.* 117, 1047–1058. doi: 10.1104/pp.117.3.1047

Tandon, K., Baldwin, E., Scott, J., and Shewfelt, R. (2003). Linking sensory descriptors to volatile and nonvolatile components of fresh tomato flavor. *J. Food Sci.* 68, 2366–2371. doi: 10.1111/j.1365-2621.2003.tb05774.x

Tang, Y., Liu, X., Wang, J., Li, M., Wang, Q., Tian, F., et al. (2016). GAPIT Version 2: an enhanced integrated tool for genomic association and prediction. *Plant Genome* 9:0120. doi: 10.3835/plantgenome2015.11.0120

Tieman, D., Bliss, P., McIntyre, L. M., Blandon-Ubeda, A., Bies, D., Odabasi, A. Z., et al. (2012). The chemical interactions underlying tomato flavor preferences. *Curr. Biol.* 22, 1035–1039. doi: 10.1016/j.cub.2012.04.016

Tieman, D., Taylor, M., Schauer, N., Fernie, A. R., Hanson, A. D., and Klee, H. J. (2006b). Tomato aromatic amino acid decarboxylases participate in synthesis of the flavor volatiles 2-phenylethanol and 2-phenylacetaldehyde. *Proc. Natl. Acad. Sci. U. S. A.* 103, 8287–8292. doi: 10.1073/pnas.0602469103

Tieman, D., Zeigler, M., Schmelz, E., Taylor, M. G., Rushing, S., Jones, J. B., et al. (2010). Functional analysis of a tomato salicylic acid methyl transferase and its role in synthesis of the flavor volatile methyl salicylate. *Plant J.* 62, 113–123. doi: 10.1111/j.1365-313x.2010.04128.x

Tieman, D., Zhu, G., Resende, M. F. R., Lin, T., Nguyen, C., Bies, D., et al. (2017). A chemical genetic roadmap to improved tomato flavor. *Science* 355, 391–394. doi: 10.1126/science.aal1556

Tieman, D. M., Loucas, H. M., Kim, J. Y., Clark, D. G., and Klee, H. J. (2007). Tomato phenylacetaldehyde reductases catalyze the last step in the synthesis of the aroma volatile 2-phenylethanol. *Phytochemistry* 68, 2660–2669. doi: 10.1016/j.phytochem.2007.06.005

Tieman, D. M., Zeigler, M., Schmelz, E. A., Taylor, M. G., Bliss, P., Kirst, M., et al. (2006a). Identification of loci affecting flavour volatile emissions in tomato fruits. *J. Exp. Bot.* 57, 887–896. doi: 10.1093/jxb/erj074

Tikunov, Y. M., Molthoff, J., de Vos, R. C. H., Beekwilder, J., van Houwelingen, A., van der Hooft, J. J. J., et al. (2013). Non-smoky GLYCOSYLTRANSFERASE1 prevents the release of smoky aroma from tomato fruit. *Plant Cell* 25, 3067–3078. doi: 10.1105/tpc.113.114231

Tikunov, Y. M., Roohanitaziani, R., Meijer-Dekens, F., Molthoff, J., Paulo, J., Finkers, R., et al. (2020). The genetic and functional analysis of flavor in commercial tomato: the FLORAL4 gene underlies a QTL for floral aroma volatiles in tomato fruit. *Plant J.* 103, 1189–1204. doi: 10.1111/tpj.14795

Torkamaneh, D., Boyle, B., and Belzile, F. (2018). Efficient genome-wide genotyping strategies and data integration in crop plants. *Theor. Appl. Genet.* 131, 499–511. doi: 10.1007/s00122-018-3056-z

Van der Auwera, G. A., Carneiro, M. O., Hartl, C., Poplin, R., Del Angel, G., Levy-Moonshine, A., et al. (2013). From FastQ data to high confidence variant calls: the genome analysis toolkit best practices pipeline. *Curr. Protoc. Bioinforma.* 43, 11.10.1–11.10.33.

Vogel, J. T., Tieman, D. M., Sims, C. A., Odabasi, A. Z., Clark, D. G., and Klee, H. J. (2010). Carotenoid content impacts flavor acceptability in tomato (*Solanum lycopersicum*). *J. Sci. Food Agric.* 90, 2233–2240.

Wang, X., Gao, L., Jiao, C., Stravoravdis, S., Hosmani, P. S., Saha, S., et al. (2020). Genome of Solanum pimpinellifolium provides insights into structural variants during tomato breeding. *Nat. Commun.* 11:5817.

Wu, S., Zhang, B., Keyhaninejad, N., Rodríguez, G. R., Kim, H. J., Chakrabarti, M., et al. (2018). A common genetic mechanism underlies morphological diversity in fruits and other plant organs. *Nat. Commun.* 9:4734.

Xiao, H., Jiang, N., Schaffner, E., Stockinger, E. J., and van Der Knaap, E. (2008). A retrotransposon-mediated gene duplication underlies morphological variation of tomato fruit. *Science* 319, 1527–1530.

Xu, F., Bao, J., He, Q., and Park, Y. (2016). Genome-wide association study of eating and cooking qualities in different subpopulations of rice (*Oryza sativa* L.). *BMC Genomics* 17:663.

Yates, C. M., Filippis, I., Kelley, L. A., and Sternberg, M. J. E. (2014). SuSPect: enhanced prediction of single amino acid variant (SAV) phenotype using network features. *J. Mol. Biol.* 426, 2692–2701.

Ye, J., Wang, X., Hu, T., Zhang, F., Wang, B., Li, C., et al. (2017). An InDel in the promoter of AI-ACTIVATED MALATE TRANSPORTER9 selected during tomato domestication determines fruit malate contents and aluminum tolerance. *Plant Cell* 29, 2249–2268.

Zanor, M. I., Osorio, S., Nunes-Nesi, A., Carrari, F., Lohse, M., Usadel, B., et al. (2009). RNA interference of LIN5 in tomato confirms its role in controlling brix content, uncovers the influence of sugars on the levels of fruit hormones, and demonstrates the importance of sucrose cleavage for normal fruit development and fertility. *Plant Physiol.* 150, 1204–1218.

Zhao, J., Sauvage, C., Zhao, J., Bitton, F., Bauchet, G., Liu, D., et al. (2019). Meta-analysis of genome-wide association studies provides insights into genetic control of tomato flavor. *Nat. Commun.* 10:1534.

Zhong, S., Joung, J. G., Zheng, Y., Chen, Y. R., Liu, B., Shao, Y., et al. (2011). High-throughput illumina strand-specific RNA sequencing library preparation. *Cold Spring Harb. Protoc.* 6, 940–949.

Zhu, G., Wang, S., Huang, Z., Zhang, S., Liao, Q., and Zhang, C. (2018). Rewiring of the fruit metabolome in tomato breeding. *Cell* 172, 249–261.e12.

Conflict of Interest: The authors declare that the research was conducted in the absence of any commercial or financial relationships that could be construed as a potential conflict of interest.

The reviewer GD declared a past co-authorship with one of the authors AF and the reviewer CS declared a past co-authorship with several of the authors AF and DT to the handling editor.

frontiers in Plant Science

ORIGINAL RESEARCH
published: 22 July 2021
doi: 10.3389/fpls.2021.648193

Screening and Interaction Analysis Identify Genes Related to Anther Dehiscence in *Solanum melongena* L.

Zhimin Wang[1,2†], *Chao Yuan*[1,2†], *Shaowei Zhang*[1,2†], *Shibing Tian*[3], *Qinglin Tang*[1,2], *Dayong Wei*[1,2] *and Yi Niu*[1,2*]

[1] College of Horticulture and Landscape Architecture, Southwest University, Chongqing, China, [2] Key Laboratory of Horticulture Science for Southern Mountains Regions, Ministry of Education, Chongqing, China, [3] The Institute of Vegetables and Flowers, Chongqing Academy of Agricultural Sciences, Chongqing, China

Anther indehiscence is an important form of functional male sterility that can facilitate the production of hybrid seeds. However, the molecular mechanisms of anther indehiscence-based male sterility in eggplant (*Solanum melongena* L.) have not been thoroughly explored. We performed transcriptome sequencing and real-time quantitative reverse transcription-PCR (qRT-PCR) assays to compare the fertile line (F142) and male sterile line (S12) eggplant. We identified 2,670 differentially expressed genes (DEGs) between lines. Gene ontology (GO) and Kyoto Encyclopedia of Genes and Genomes (KEGG) pathway analyses identified 31 DEGs related to hormone biosynthesis. We, therefore, measured phytohormone contents, such as jasmonic acid (JA), auxin (IAA), gibberellin (GA), and abscisic acid (ABA) in S12 and F142. There were differences in IAA, GA_3, and ABA levels between S12 and F142, while JA levels were significantly lower in S12 than in F142. Five key genes in the JA signaling pathway were differentially expressed in S12 vs. F142. Of these, *SmJAZ1* and *SmJAR1* were significantly upregulated and *SmDAD1*, *SmLOX,* and *SmCOI1* were downregulated in S12 vs. F142. Protein–protein interaction studies identified a direct interaction between SmDAD1 and SmLOX, while SmDAD1 failed to interact with SmJAR1, SmCOI1, and SmJAZ1. The data represent a valuable resource for further exploration of regulatory mechanisms underlying anther dehiscence in eggplant.

Keywords: eggplant (*Solanum melongena* L.), transcriptome, phytohormone, gene expression, interaction

OPEN ACCESS

Edited by:
Amalia Barone,
University of Naples Federico II, Italy

Reviewed by:
Ezio Portis,
University of Turin, Italy
Laura Toppino,
Council for Research in Agriculture and the Analysis of Agrarian Economy (CREA), Italy

***Correspondence:**
Yi Niu
niuy2001134@163.com

[†]These authors have contributed equally to this work and share first authorship

Specialty section:
This article was submitted to Plant Biotechnology, a section of the journal Frontiers in Plant Science

Received: *31 December 2020*
Accepted: *08 June 2021*
Published: *22 July 2021*

Citation:
Wang Z, Yuan C, Zhang S, Tian S, Tang Q, Wei D and Niu Y (2021) Screening and Interaction Analysis Identify Genes Related to Anther Dehiscence in Solanum melongena L. Front. Plant Sci. 12:648193. doi: 10.3389/fpls.2021.648193

INTRODUCTION

Eggplant (*Solanum melongena* L.), a popular vegetable crop that is thought to have originated in Africa, is widely cultivated in Africa, Asia, Europe, and the Near East (Bohs, 2010). The major characteristic of eggplant exhibits obvious heterosis, and the early use of hybrid vigor in the breeding of eggplant cultivars has been described (Kakizaki, 1931; Rodríguez et al., 2008). The use of reliable male-sterile systems could simplify the process and reduce the labor, cost, and time involved in producing hybrid eggplant seeds (Mennella et al., 2010). Functional genic male sterility (GMS) was reported in eggplant in 1954 and 1963 (Jasmin, 1954; Nuttall, 1963). The first functional male sterile eggplant mutant UGA 1-MS (Phatak and Jaworski, 1989) was discovered in 1989 and further characterized in 1991 (Phatak et al., 1991), and this kind of

sterility was also further explored in 2009 as the result of crossing eggplant with wild relatives (Khan and Isshiki, 2009, 2010). The GMS line showed anther indehiscence in which the anthers did not open to release pollen, thereby disabling pollination (Wang et al., 2021). Anther dehiscence is a vital process in which mature pollen grains are released from the locules of the anther, thus enabling pollination (Sanders et al., 1999, 2005). Although morphological changes in anthers during dehiscence have been thoroughly described (Beals, 1997; Sanders et al., 2005), the molecular mechanisms controlling anther dehiscence remain relatively unknown.

Jasmonic acid (JA) is a lipid-derived hormone that functions as an important regulator of plant responses to various stresses as well as development (Scott et al., 2004). Analyses show that JA affects wheat development, including germination, growth, flowering time, senescence, and alters tolerance to environmental stresses (Wasternack and Strnad, 2018). Wheat plants with high JA levels are characterized by delayed germination, slower growth, late flowering, and senescence, and improves tolerance to short-term freezing (Nausica et al., 2007). The application of exogenous jasmonate significantly stimulates root hair elongation (Bohs, 2010). JA also plays an important role in regulating anther dehiscence (Ishiguro et al., 2001; Xiao et al., 2014).

Jasmonic acid signal transduction pathways have been investigated in *Arabidopsis thaliana* (Schaller and Stintzi, 2009; Wasternack and Strnad, 2018). JA biosynthesis originates from fatty acids in chloroplasts, and then its metabolic compounds are produced from 12 different pathways in peroxisomes and cytosol, respectively (Wasternack and Strnad, 2018). Gene mutations involved in JA biosynthesis cause failure or delay of anther dehiscence and may lead to male sterility. Several of these genes have been identified, such as anther dehiscence defect 1 (*DAD1*) (Ishiguro et al., 2001), *AOS* (Bae et al., 2010), *LOX* (Caldelari et al., 2011), *COI1* (Xie et al., 1998), *DEHISCENCE 1* (*DDE1*), /*OPR3* (Schaller et al., 2000; Stintzi and Browse, 2000), and the triple mutation (*fad3*, *fad7*, and *fad8*) (Mcconn and Browse, 1996). In addition, *JAR1* (a JA-amino acid synthetase) has a biological function in regulating flower opening and closure, and anther dehiscence in rice (Xiao et al., 2014). Some studies have found possible mechanisms that JA was a significant regulator of anther dehiscence. The JA pathway genes *SmJAZ1* and *SmOPR3* are downregulated in the male sterility S16 (Zhang et al., 2020). Moreover, SmOPR3 could interact with the transcript accumulation of the eggplant CORONATINE INSENSITIVE1 (SmCOI1) to form a protein complex, and COI1 interacts with JAZ1 in the presence of JA-Ile (Zhang et al., 2020). Through activating *DAD1* in *Arabidopsis*, a RING-type E3 ligase controls anther dehiscence (Peng et al., 2013). However, the exact mechanisms of JA activity regulating anther dehiscence in eggplant remain to be elucidated.

In this study, we performed transcriptome analysis to identify differentially expressed genes (DEGs) in eggplant S12 (indehiscent anthers) and F142 (dehiscent anthers) in order to uncover differences in the anther dehiscence network. Enrichment analysis of the DEGs and endogenous hormone measurements highlighted the effect of JA signal transduction pathways in anther dehiscence. Finally, we analyzed the relationships between five genes in the JA pathway by yeast two-hybrid (Y2H) analyses. The results lay the foundation for further uncovering the molecular mechanisms and biological function of anther dehiscence in eggplant.

MATERIALS AND METHODS

Plant Materials and Growth Conditions

The functional male sterile line S12 and fertile line F142 were provided and grown at the Institute of Vegetables and Flowers, Chongqing Academy of Agricultural Sciences (Chongqing, China) from 2017 to 2019. The male fertile line was an advanced-generation inbred line. The functional male sterile line was obtained from the continuous backcross of male sterile plant in progenies F2 of interspecific hybrid (Tian et al., 2001). The eggplant seeds were sterilized and sown in trays. Then, the seedlings were transferred and grown under normal conditions. Selected anthers in flower buds with open petals about 10 am were immediately frozen in liquid nitrogen and stored at −80°C until they were used for further analysis. Three biological replicates per sample were used for sequencing.

RNA Extraction, Library Construction, and RNA-Seq

The total RNA of each sample was extracted from the anther on the day of flowering of eggplant according to the instruction manual of the TRlzol Reagent (Life Technologies, Carlsbad, CA, United States). Each anther sample was taken from five eggplant flowers. RNA integrity and concentration were examined using Agilent 2100 Bioanalyzer (Agilent Technologies, Inc., Santa Clara, CA, United States). The mRNA was isolated by NEBNext Poly (A) mRNA Magnetic Isolation Module (NEB, E7490). The cDNA library was constructed following the instructions of the manufacturer of NEBNext Ultra RNA Library Prep Kit for Illumina (NEB, E7530) and NEBNext Multiplex Oligos for Illumina (NEB, E7500). In brief, the enriched mRNA was fragmented into ∼200 nt RNA inserts, which were used to synthesize the first-strand cDNA and the second cDNA. End-repair/dA-tail and adaptor ligation was performed on the double-stranded DNA. Suitable fragments were isolated by Agencourt AMPure XP beads (Beckman Coulter, Inc., Brea, CA, United States) and enriched by PCR amplification. Finally, constructed cDNA libraries of the eggplant were sequenced on a flow cell using an Illumina HiSeq^{TM} (Illumina, San Diego, CA, United States) sequencing platform. The RNA-seq reads have been deposited in the NCBI Short Read Archive and are accessible under PRJNA746400.

Transcriptome Analysis Using Reference Genome-Based Reads Mapping

Low-quality reads, such as only adaptor and unknown nucleotides >5%, or Q20 <20% (percentage of sequences with sequencing error rates <1%), were removed by Perl script. The clean reads that were filtered from the raw reads were mapped to the eggplant genome (SME_r2.5.1) (Hideki et al., 2014) using Tophat2 software2 (version2.1.0) (Kim et al., 2013).

The aligned records from the aligners in BAM/SAM format were further examined to remove potential duplicate molecules. Gene expression levels were estimated using FPKM values (fragments per kilobase of exon per million fragments mapped) by the Cufflinks software.

Sequence Annotation

Genes were compared against various protein databases by BLASTX, such as the National Center for Biotechnology Information (NCBI) non-redundant protein (Nr) database, and the Swiss-Prot database, with a cut-off E-value of 10^{-5}. Furthermore, genes were searched against the NCBI non-redundant nucleotide sequence (Nt) database using BLASTn with a cut-off E-value of 10^{-5}. Genes were retrieved based on the best BLAST hit (highest score) along with their protein functional annotation.

To annotate the gene with GO terms, the Nr BLAST results were imported into the Blast2 GO program. GO annotations for the genes were obtained by Blast2GO. This analysis mapped all of the annotated genes to GO terms in the database and counted the number of genes associated with each term. Perl script was then used to plot GO functional classification for the unigenes with a GO term hit to view the distribution of gene functions. The obtained annotation was enriched and refined using TopGo (R package). The gene sequences were also aligned to the Clusters of Orthologous Group (COG) database to predict and classify functions. KEGG pathways were assigned to the assembled sequences by the Perl script.

Identification of Differential Gene Expression

DESeq2 and Q-value were employed and used to evaluate differential gene expression between F142 and S12. After that, gene abundance differences between those samples were calculated based on the ratio of the 2 FPKM values. In order to compute the significance of the differences, the false discovery rate (FDR) control method was used to identify the threshold of the *P*-value in multiple tests. Here, only genes with an absolute value of log2 ratio $\geq$2 and an FDR significance score of $<$0.01 were used for subsequent analysis.

Gene Ontology and Kyoto Encyclopedia of Genes and Genome Enrichment Analysis of DEGs

Gene ontology enrichment analysis of DEGs was implemented by the GOseq R package. GO terms with corrected *P*-values $<$0.05 were considered to be significantly enriched by differentially expressed genes (Young et al., 2010). The KOBAS software (Mao et al., 2005) was used to test the statistical enrichment of DEGs in KEGG pathways.

Hormone Extraction and Determination

High-performance liquid chromatography was performed using Shimadzu LC-60A (Shimadzu, Kyoto, Japan. The chromatographic conditions were as follows: mobile phase was methanol 0.8% glacial acetic acid solution = 55/45, column temperature was 30°C, flow rate was 0.8 mL/min, detection wavelength was 254 nm, and injection volume was 10 μL. Each sample was tested three times and averaged. All data were analyzed by ANOVA, and the differences were compared by Duncan's multiple range test.

Gene Cloning and Real-Time Quantitative Reverse Transcription-PCR

The full length of *SmDAD1* (Smechr0500450), *SmLOX* (Smechr0800437), *SmJAR1* (Smechr0101378), *SmCOI1* (Smechr0500307), and *SmJAZ1* (Smechr1200204) was cloned using homologous cloning technology. Tomato and potato sequences closely related to eggplant were obtained from the NCBI database. After the two Blast, the software Primer 5.0 was used to design gene-specific primers (GSPs). RNA was extracted from eggplant anthers and reverse transcribed into cDNA. Then, RT-PCR was performed using the extracted RNA as a template to obtain ORFs of *SmDAD1*, *SmLOX*, *SmJAR1*, *SmCOI1*, and *SmJAZ1* genes.

Quantitative reverse transcription-PCR was performed as previously described. The primers used to test the transcript levels of all the genes were shown in **Supplementary Table 1**, using *GAPDH* as the internal reference. The qRT-PCR mixtures contained 2 μL primers, 2 μL cDNA, 10 μL SsoFast™EvaGreen®Supermix (Bio-Rad, Hercules, CA, United States) and distilled water to a final volume of 20 μL. The reaction conditions were as follows: 95°C for 30 s, 95°C for 5 s, 59°C for 30 s, and 65°C for 5 s (39 cycles). The fold changes were calculated using the $2^{-\Delta\Delta Ct}$ method. Each sample was repeated three times for qRT-PCR detection. And the fold changes were calculated using the $2^{-\Delta\Delta Ct}$ method.

FIGURE 1 | Morphological analysis of *Solanum melongena* L. F142 and S12 flowers and anthers on the day of flowering. **(A,B)** The flower of F142 and S12. Bars = 5 mm. **(C,D)** The anther of F142 and S12. Bars = 100 μm.

Transactivation Test in Yeast

SmDAD1, *SmLOX*, *SmJAR1*, *SmCOI1*, and *SmJAZ1* were separately sub-cloned into the activation domain of pGADT7 and pGBKT7 using the *Bam*HI and *Xho*I sites and then ligated into pGADT7 or pGBKT7 to construct recombinant plasmids. First, gene-pGBKT7 recombinant plasmids were transformed into Y2H (Clontech) using the PEG/LiAC method. The transformed strains were screened on synthetic dropout (SD medium) lacking tryptophan (Trp; SD/-Trp) for selection of positive clones. Subsequently, positive clones were transferred to SD medium supplemented with X-α-gal(SD/-Trp/X-α-gal). The trans-acting activity was assessed based on the blue colonies that grew on the SD/-Trp/X-α-gal medium.

Yeast Two-Hybrid Assay

Yeast two-hybrid assays were performed based on the instructions of the manufacturer (Clontech, Palo Alto, CA, United States). The gene-pGADT7 and gene-pGBKT7 recombinant plasmids were co-transformed into yeast strainY2HGold cells as described above, which were then added to SD medium lacking leucine (Leu) and tryptophan (Trp) (DDO; SD/-Leu/-Trp). The potential physical interactions between proteins were evaluated by screening the yeast transformants on QDO/X-α-gal/AbA medium [SD medium lacking Leu, Trp, adenine (Ade), and histidine (His) but supplemented with X-a-gal and aureobasidin A (AbA)].

Pull-Down Assay

SmDAD1 was sub-cloned into the pET32a(+) vector, while *SmLOX*, *SmJAR1*, *SmCOI1*, and *SmJAZ1* were cloned into the pGEX-4T-1 vector. Then, the plasmids were transformed into *Escherichia coli* Rosetta (DE3) competent cells, and 1 mM isopropyl β-D-thiogalactoside was added before incubation at 37°C for 3.5 h. The SmDAD1-HIS protein was purified using BeaverBeads IDA-Nickel Kit-10 (Beaver, Beijing, China). The SmLOX-GST, SmJAR1-GST, SmCOI1-GST, and SmJAZ1-GST

TABLE 1 | Statistical analysis of RNA-seq reads mapped to the ancestor genome.

Samples	Total reads	Mapped reads	Uniq mapped reads	Multiple map reads	Clean reads	GC content	%≥Q30
F142	42,791,674.67	39,368,088	38,019,098	1,348,989	21,395,837	42.68%	94.41%
S12	43,133,323.33	39,694,750	38,266,857	1,427,894	21,566,662	42.93%	94.70%

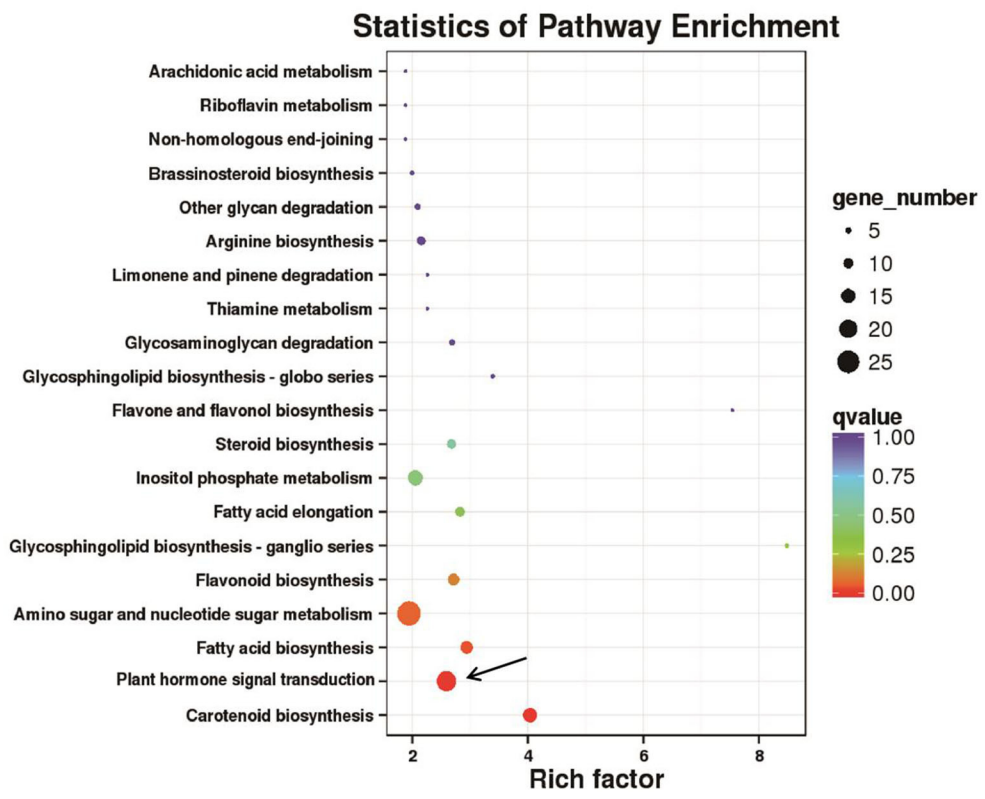

FIGURE 2 | Kyoto Encyclopedia of Genes and Genomes (KEGG) pathway enrichment analysis of 2,670 differentially expressed genes (DEGs). The pathway of plant hormone signal transduction was mainly enriched (black arrows).

proteins were purified by BeaverBeads GSH (Beaver). Protein–protein interactions were detected by sodium dodecyl sulfate-polyacrylamide gel electrophoresis (SDS-PAGE).

RESULTS

Morphological Comparison of F142 and S12

Male sterility is an important tool for leveraging eggplant heterosis. Anther indehiscence is the main form of functional male sterility. By morphological analysis, we observed that anthers were indehiscent in S12 relative to F142 (**Figure 1**). On the day of flowering, in F142, the anthers presented small holes to release pollens, whereas in S12 the anthers were tightly closed without dehiscence and pollen releasing.

Transcriptome Assembly

To detect potential molecular differences between eggplant accessions S12 and F142, we performed transcriptome sequencing on anther tissue on the day of flowering. The genome-directed stratagem Trinity was used to assemble transcriptome sequences and align single RNA-seq library data with the *S. melongena* genome (SME_r2.5.1). As a result, the mean of clean reads from three biological repeats per sample was more than 20 million, the mean of mapped reads and uniquely mapped reads were far great than 10 million, and the highest localization ration of each library was roughly 50% in the *S. melongena* genome (**Table 1**; **Supplementary Table 2**). After being assembled, the average length of the contig was 1,204 bp, while for the contig of N50 the average length was 1,538 bp. We found that the average GC content in the libraries reached 40–50% (**Supplementary Tables 2, 3**). When redundant and short reads were removed, we obtained about 257,800 transcript assembly contigs (TAC) >100 bp (**Supplementary Table 2**). Overall, the abundant transcriptome data were enough for further analysis.

Functional Classification of the DEGs by GO and KEGG Pathway Analysis

We identified 2,670 DEGs in S12 vs. F142 (**Supplementary Table 4**; **Supplementary Figure 2**), including 1,928 upregulated and 742 downregulated DEGs (**Supplementary Figure 2**). We constructed a heat map representing the differential expression of the 2,670 DEGs (**Supplementary Figure 5**) in S12 vs. F142. We detected dynamic changes in the transcriptomes during anther development in S12 (anther indehiscence). In the heat map, the original gene expression data were transformed into log2 fold change values (**Supplementary Table 4**). Further cluster analysis revealed significant differences in gene expression between S12 and F142.

To characterize the DEGs in detail, we performed GO analysis to uncover their putative functions. We constructed histograms

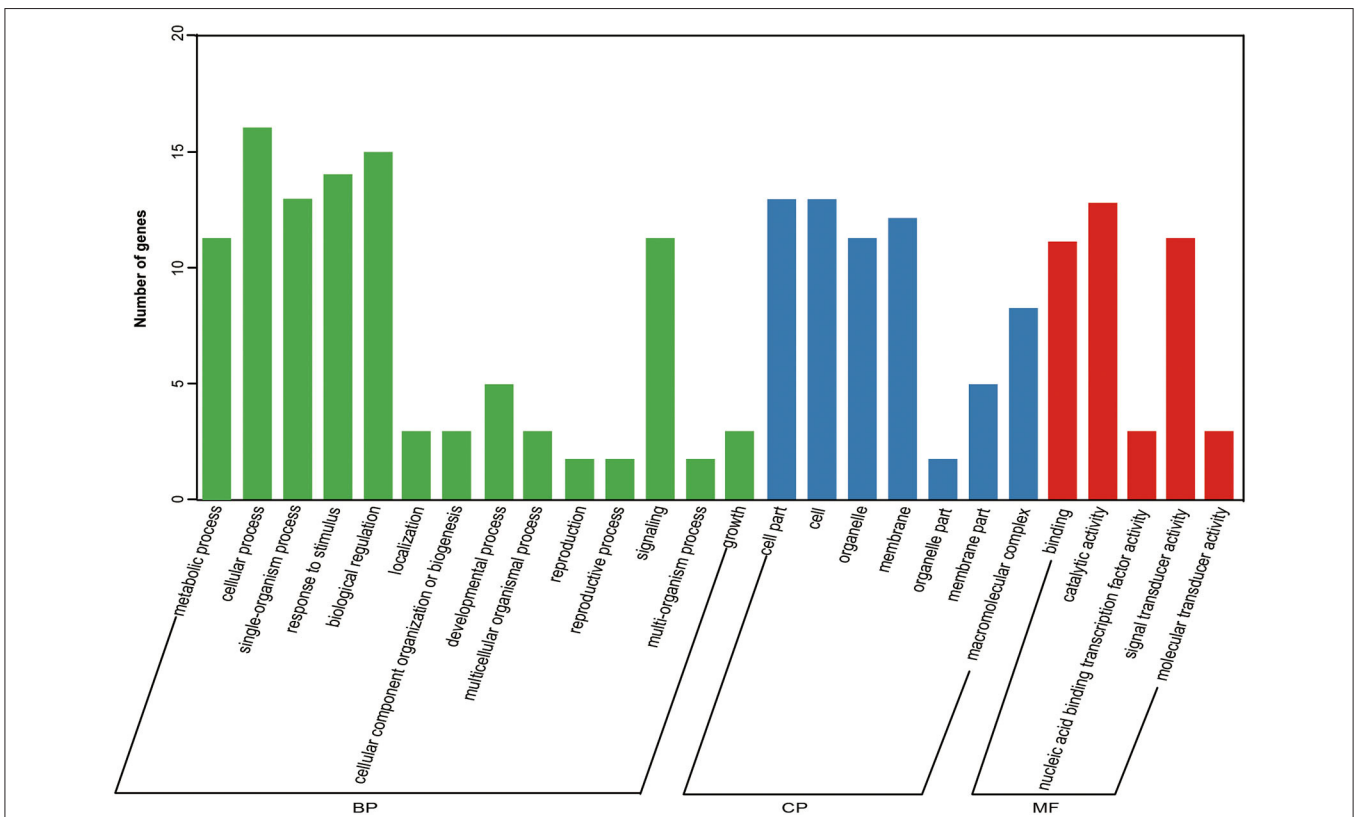

FIGURE 3 | Gene ontology (GO) enrichment analysis of 31 hormone DEGs. BP, biological processes; CP, cellular compartments; MF, molecular functions.

based on the categories of DEGs in anther indehiscent eggplant (S12), such as biological processes, molecular functions, and cellular compartments (**Supplementary Figure 3**). Metabolic process was the major group in the biological processes category, namely, GO terms cellular, single-organism, response to stimulus, and biological regulation. The molecular functions category contained at least 882 DEGs involved in nucleic acid binding transcription factor activity and more than 888 DEGs involved in signal transducer activity, transcription factor activity, and protein binding. Most of the DEGs were present in the top three groups, such as the cell, organelle, and membrane (**Supplementary Figure 4**). We performed KEGG pathway analysis to categorize all annotated genes. Most of the 2,670 DEGs were categorized into six pathways (**Supplementary Figure 4**). The most highly enriched biological processes in the anther indehiscent eggplant were plant hormone signal transduction, protein processing in endoplasmic reticulum, amino sugar and

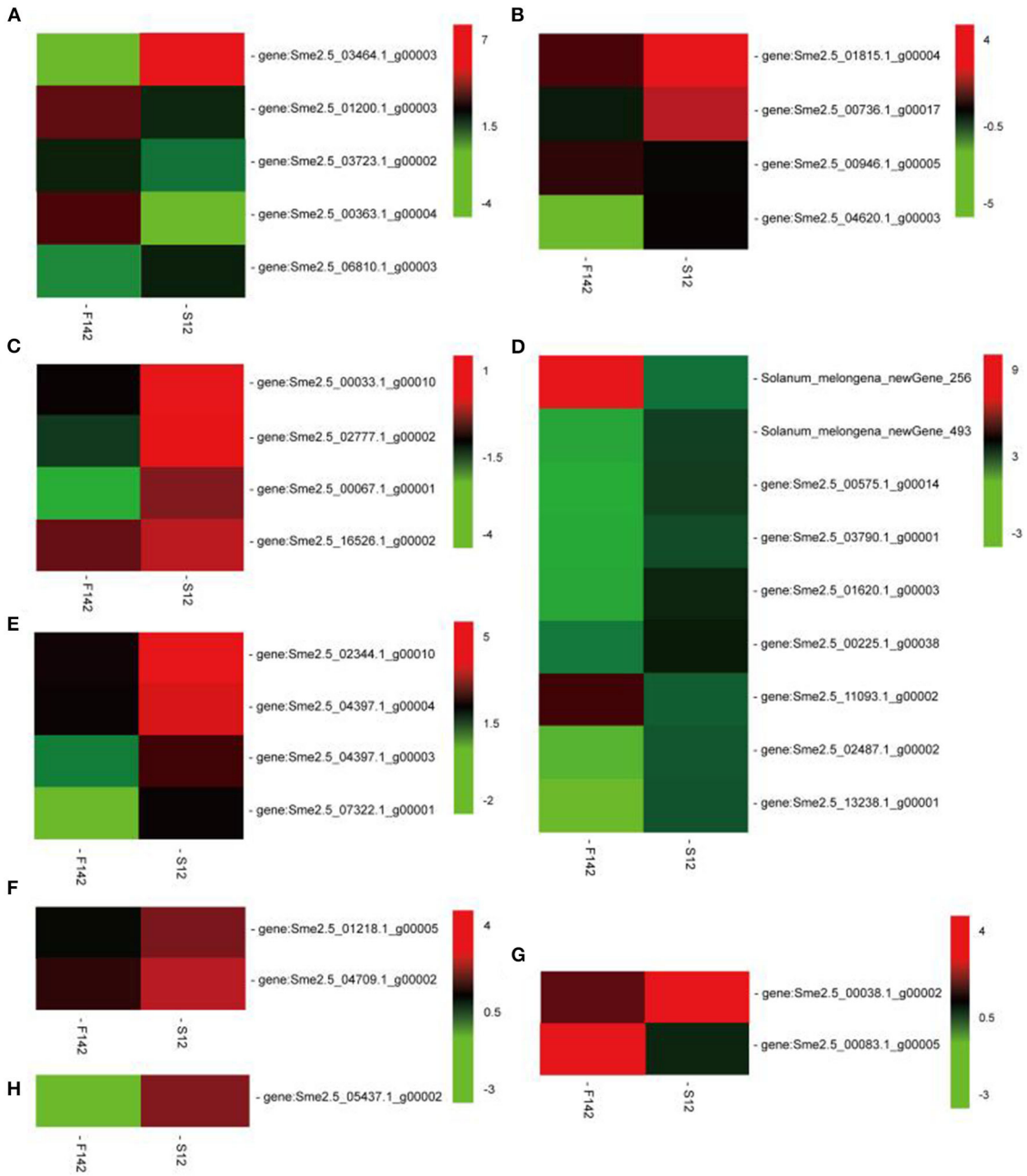

FIGURE 4 | Expression changes in the genes involved in the **(A)** jasmonic acid, **(B)** ethylene, **(C)** auxin, **(D)** other hormones, **(E)** crassinolide, **(F)** cytokinin, **(G)** gibberellin, and **(H)** abscisic acid signaling pathways in F142 and S12.

TABLE 2 | Differentially expressed genes (DEGs) involved in hormone signaling pathways.

Gene_Id	Function description	Up_Down
Jasmonate acid		
Sme2.5_03464.1_g00003	Jasmonate ZIM-domain protein 1	Up
Sme2.5_01200.1_g00003	Defective in anther dehiscence1	Down
Sme2.5_03723.1_g00002	Coronatine-insensitive 1	Down
Sme2.5_00363.1_g00004	Lipoxygenase	Down
Sme2.5_06810.1_g00003	Jasmonic acid-amido synthetase JAR1	Up
Auxin		
Sme2.5_01815.1_g00004	Auxin influx carrier (LAX family), LAX1	Up
Sme2.5_00736.1_g00017	Auxin responsive GH3 gene family, indole-3-acetic acid-amido synthetase GH3.1	Up
Sme2.5_00946.1_g00005	Auxin-responsive protein IAA26-like	Down
Sme2.5_04620.1_g00003	Auxin responsive GH3 gene family, indole-3-acetic acid-amido synthetase GH3.6	Up
Brassinosteroid		
Sme2.5_00033.1_g00010	Brassinosteroid resistant 1-like	Up
Sme2.5_02777.1_g00002	Brassinosteroid insensitive 2, shaggy-related protein kinase eta-like	Up
Sme2.5_00067.1_g00001	Brassinosteroid insensitive 1, BRI1	Up
Sme2.5_16526.1_g00002	Brassinosteroid resistant 1, BES1/BZR1 homolog protein 2-like	Up
Ethylene		
Sme2.5_02344.1_g00010	Ethylene receptor 2-like	Up
Sme2.5_04397.1_g00003	Ethylene-insensitive protein 3, EIN3	Up
Sme2.5_04397.1_g00004	Ethylene-insensitive protein 3, EIN3-like	Up
Sme2.5_07322.1_g00001	Ethylene receptor 1, ETR1	Up
Cytokinin		
Sme2.5_05437.1_g00002	Histidine kinase 2-like isoform X1 (cytokinin receptor)	Up
Abscisic Acid		
Sme2.5_01218.1_g00005	Abscisic acid-insensitive responsive element binding factor, ABA 5-like protein 7	Up
Sme2.5_04709.1_g00002	ABA responsive element binding factor, G-box-binding factor 4	Up
Gibberellin		
Sme2.5_00083.1_g00005	Gibberellin receptor GID1B-like	Down
Sme2.5_00038.1_g00002	F-box protein GID2	Up
Other hormone		
Sme_newGene_256	SAUR family protein, uncharacterized LOC107006819	Down
Sme_newGene_493	Myb-like DNA-binding domain, two-component response regulator ARR14	Up
Sme2.5_00575.1_g00014	Protein phosphatase 2C 6-like	Up
Sme2.5_03790.1_g00001	Myb-like DNA-binding domain, Two-component response regulator ARR18-like	Up
Sme2.5_01620.1_g00003	Serine/threonine-protein kinase SRK2	Up
Sme2.5_00225.1_g00038	Somatic embryogenesis receptor kinase 3B precursor, SERK3B	Up
Sme2.5_11093.1_g00002	SAUR family protein, uncharacterized protein LOC104880086	Down
Sme2.5_02487.1_g00002	Serine/threonine-protein kinase, SAPK3	Up
Sme2.5_13238.1_g00001	Two-component response regulator ARR17-like	Up

nucleotide sugar metabolism, biosynthesis of amino acids, carbon metabolism, and plant–pathogen interactions (**Figure 2**; **Supplementary Figure 4**).

Enrichment Analysis of DEGs in Hormone Signal Transduction Pathways

We performed KEGG pathway analysis to investigate the major regulatory pathways of the DEGs. The DEGs in S12 vs. F142 were mainly enriched in the pathways inositol phosphate metabolism (16 DEGs), plant hormone signal transduction (31 DEGs), flavonoid biosynthesis (12 DEGs), amino sugar and nucleotide sugar metabolism (39 DEGs), and fatty acid biosynthesis (25 DEGs) (**Figures 2**, **3**). To investigate the hormonal control of anther indehiscence in more detail, we analyzed the expression levels of key DEGs in the JA, IAA, GA, ABA, cytokinin (CTK), ethylene (ETH), and brassinosteroid (BR) signaling pathways (**Figure 4**; **Table 2**). Five key genes were identified in the JA signaling pathway, namely, *SmDAD1*, *SmLOX*, *SmCOI1*, *SmJAZ1*, and *SmJAR*-like, of which two genes were significantly upregulated and three genes were downregulated in S12 vs. F142. One key gene in the CTK signaling pathway and two genes in the

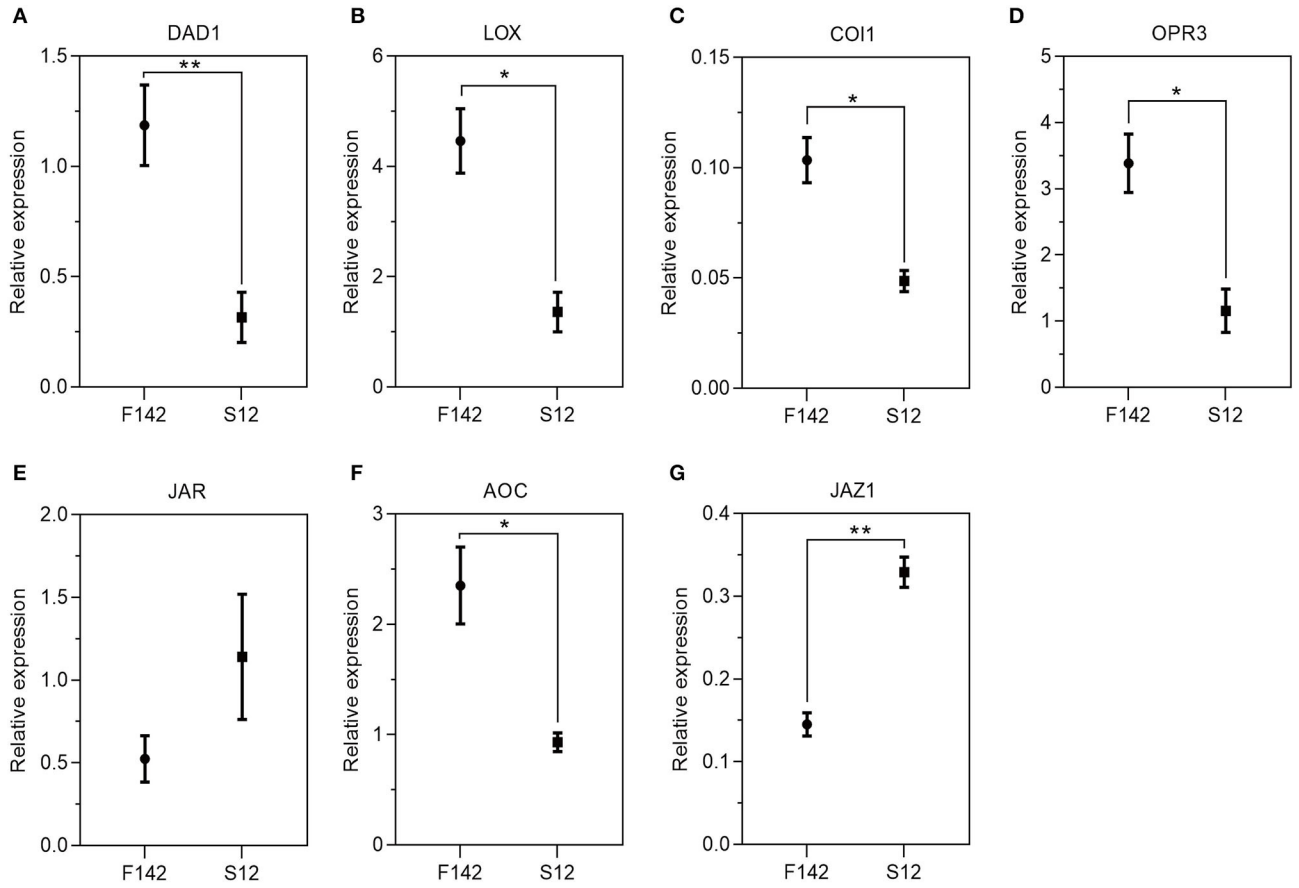

FIGURE 5 | The transcript accumulation of **(A)** *SmDAD1*, **(B)** *SmLOX*, **(C)** *SmCOI1*, **(D)** *SmOPR3*, **(E)** *SmJAR1*, **(F)** *SmAOC*, and **(G)** *SmJAZ1*. Total RNA was extracted in anthers and used for RT-q PCR analyses. Three biological replicates (each including three technical repeats) were assessed. Paired *t*-tests, $^{*}p < 0.05$, $^{**}p < 0.01$.

ABA signaling pathway were differentially expressed. One gene in the GA signaling pathway was significantly upregulated, and the other was significantly downregulated. Four key genes in the IAA signaling pathway were differentially expressed. Four key genes in the ETH signaling pathway were also differentially expressed, which were all significantly upregulated. Four genes in the BR pathway were significantly upregulated as well. Finally, nine genes in other hormone signaling pathways were differentially expressed, including two that were significantly downregulated in indehiscent accession (**Figure 4**).

Endogenous Hormone Measurements and Validation of the Expression Patterns of Several Key Genes

We collected independent anther samples from the plants and performed qRT-PCR analysis to validate the expression levels of several key JA-related genes. In total, we measured the expression levels of seven JA-related unigenes via qRT-PCR. *SmJAZ1* and *SmJAR1* were significantly upregulated and *SmDAD1*, *SmLOX*, *SmOPR3*, *SmAOC,* and *SmCOI1* were significantly downregulated in S12. The expression patterns of these genes corresponded well with the FPKM values obtained by RNA-seq (**Figure 5**), suggesting that the expression patterns of most unigenes were consistent between the two methods. Finally, we measured JA, IAA, GA_3, and ABA levels in S12 and F142 (**Figure 6**). Compared with F142, the levels of IAA, GA_3 and ABA in S12 were significantly increased, while JA level was significantly decreased. These findings suggested that plant hormones play an important role in anther dehiscence, and the decrease of JA may cause anther indehiscence in eggplant.

Interaction of SmDAD1 With SmLOX, SmJAR1, SmCOI1, and SmJAZ1

We first analyzed the trans-acting activity of SmDAD1, SmLOX, SmJAR1, SmCOI1, and SmJAZ1 in a yeast system. The yeast cells containing gene-pGBKT7 recombinant plasmids grew well and appeared white when screened on the selective medium (SD/-Trp) supplemented with X-α-gal (**Supplementary Figure 6**). These results reflected the *trans*-acting activity of SmDAD1-BD, SmLOX-BD, SmJAR1-BD, SmCOI1-BD, and SmJAZ1-BD that was similar to that of BD.

Subsequently, we performed yeast two-hybrid assays to detect the interactions of SmDAD1 protein with SmLOX, SmJAR1, SmCOI1, and SmJAZ1 (**Figure 7A**). SmDAD1 directly interacted with SmLOX but not with SmJAR1, SmCOI1, or SmJAZ1 (**Figure 7A**). We also performed pull-down assays to determine whether SmDAD1 interacts with SmJAR1, SmCOI1, and SmJAZ1 (**Figure 7B**). SmLOX-GST was pulled down by SmDAD1-HIS but SmJAR1-GST, SmCOI1-GST, and SmJAZ1-GST were not. Therefore, our yeast two-hybrid results were replicated in the pull-down assays (**Figure 7**).

DISCUSSION

Transcriptome analysis facilitates the comprehensive investigation of altered gene expression patterns in genetic variants and provides insights into the molecular basis of specific biological processes (Liu et al., 2019). Transcriptome sequencing provides a systematic approach for studying gene expression patterns and network interactions underlying various processes in plants. In this study, to explore the molecular mechanism underlying anther dehiscence in eggplant, we generated a high-quality transcriptome dataset from dehiscence (F142) and indehiscence (S12) anthers. The most highly enriched biological processes among the DEGs in the indehiscent anthers were plant hormone signal transduction, protein processing in endoplasmic reticulum, amino sugar and nucleotide sugar metabolism, biosynthesis of amino acids, carbon, metabolism, and plant–pathogen interaction. In addition, by comparing the transcripts of F142 and two male-sterile lines (S12 and S13), the differentially expressed genes in the sterile line were mainly enriched in "metabolic process," "catalytic activity," "biosynthesis of amino acids," and "carbon metabolism" (Yuan et al., 2020).

Thirty-one DEGs were identified (**Table 2**) involved in hormone signal transduction pathways, such as JA, IAA, GA, ABA, CTK, ETH, and BR. Phytohormones play essential roles in regulating plant growth and development as well as plant fertility. The accumulation or deficiency of auxin in plants is related to the occurrence of male sterility. The IAA content in a cytoplasmic male sterile rapeseed line was consistent with that of normal plants under low-temperature conditions. However, the IAA content of the sterile line increased with increasing temperature, whereas no change in IAA levels was detected in fertile plants (Singh et al., 1992). This phenomenon was also observed in tomato mutants (Amit and Sawhney, 1993). Horner suggested that auxin accumulation caused male sterility in crops, as high IAA levels in pepper induced the production of ETH, which induced male sterility (Horner, 1977). In addition, during pollen abortion, IAA levels were lower in two types of sterile wheat than in fertile anthers (Li et al., 1976). This phenomenon was also observed in rice (Xu et al., 1990), citrus (Tian et al., 1998), and mustard (Kojima, 1997).

Moreover, CTK levels were lower in cytoplasmic male sterile barley lines than in their maintainer lines (Chen et al., 1995). The excess ABA in the leaves and anthers of cytoplasmic male sterile cabbage lines might be related to the occurrence of microspore abortion (Shi and Hou, 2004). Liu found that in male sterile wheat lines (induced by GENESIS), after induction, ETH levels were significantly higher in sterile lines than in fertile lines during the mononuclear, dinuclear, and trinuclear stages of anther development (Liu et al., 2003). The rate of infertility increased with increasing induction, and the rate of infertility and the ETH release rate also increased. Finally, wild-type *Arabidopsis* plants treated with GA and double mutants in the GA signaling repressors RGA and GAI exhibited loss of fertility (Dill and Sun, 2001).

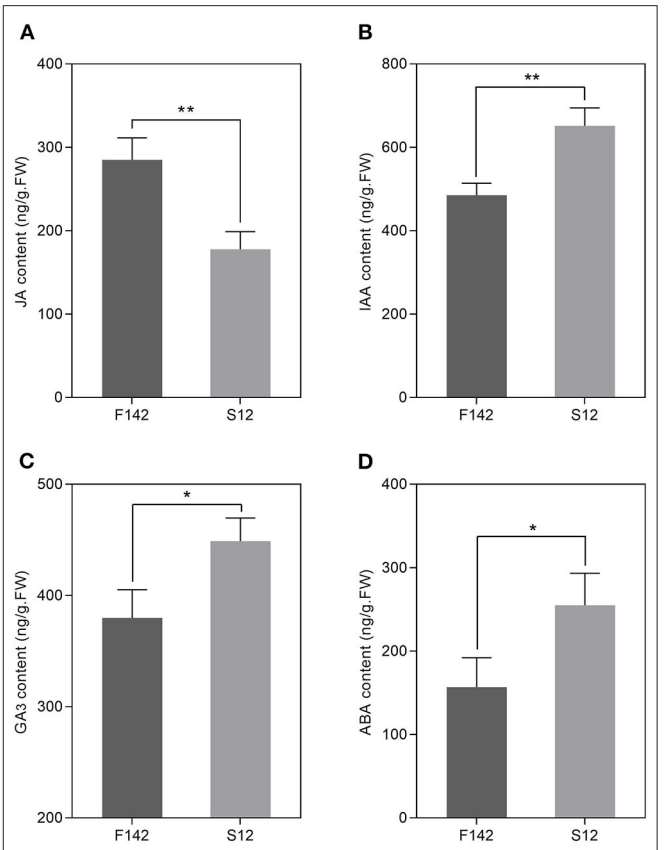

FIGURE 6 | Changes in JA, IAA, GA_3, and ABA concentrations in F142 and S12. **(A)** JA concentration. **(B)** IAA concentration. **(C)** GA_3 concentration. **(D)** ABA concentration. Three independent biological replicates were used. Three biological replicates were assessed. Paired *t*-tests, $^{*}p < 0.05$, $^{**}p < 0.01$.

Plant development and responses to environmental signals are coordinated by complex multicomponent signaling networks. JA, a phytohormone derived from fatty acids, is an important component of this regulatory system. It participates in all stages of plant growth and development and also regulates anther dehiscence (Ching-Fang et al., 2014; Xiao et al., 2014). In this study, the transcript levels of JA biosynthesis genes were lower in anther indehiscent plants than in plants with normal anther development. The JA content was also significantly lower in these plants than in fertile eggplant. This observation, which is consistent with the results of transcriptome sequencing, confirms the notion that JA is an essential factor affecting anther dehiscence. This finding validates the results of previous studies

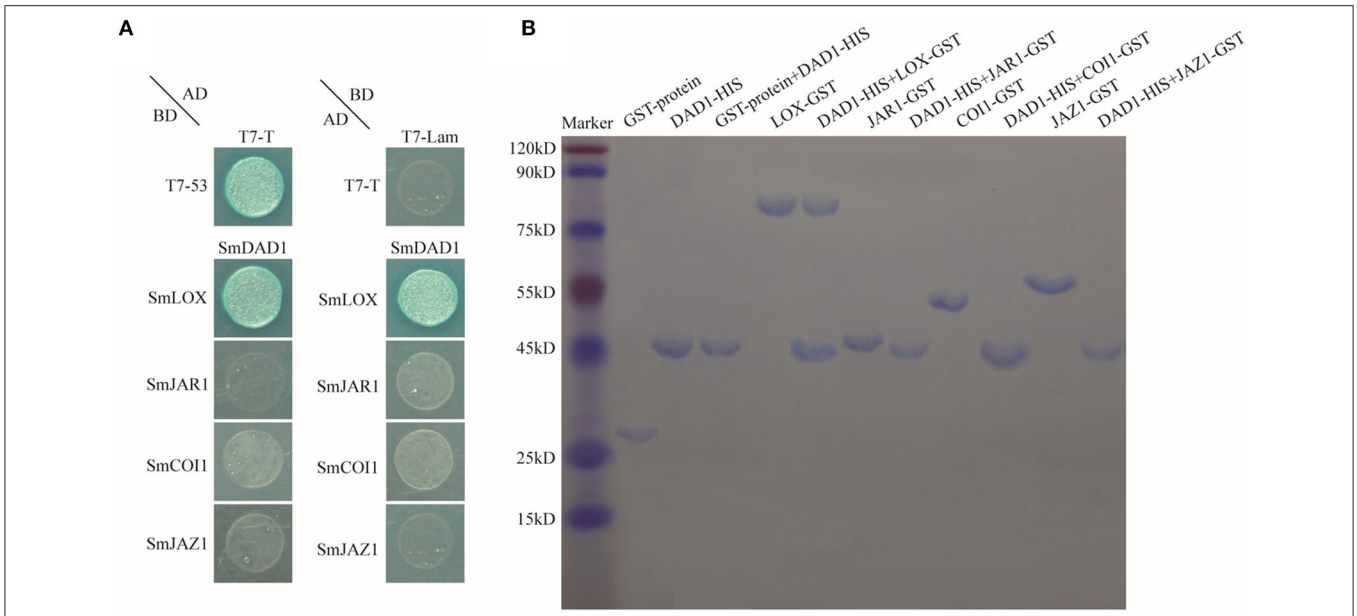

FIGURE 7 | Protein interactions of SmDAD1 with SmLOX, SmJAR1, SmCOI1, and SmJAZ1. **(A)** Detecting interactions of SmDADA1 with SmLOX, SmJAR1, SmCOI1, and SmJAZ1 by yeast two-hybrid assay. Transformed yeast cells were plated on SD/-Ade/-His/-Leu/-Trp/X-a-Gal medium to grow at 30°C for 3–5 days. pGBKT7-T53 (T7-T53) combined with pGADT7-T (T7-T) was used as positive controls, and pGBKT7-lam (T7-lam) combined with pGADT7-T (T7-T) was used as negative controls. **(B)** Examining the interactions of SmDAD1 with the other proteins by Pull-down. The HIS-tagged SmDAD1 protein was generated by cloning into the pET32a (+) vector (19 kDa). The GST-tagged proteins of SmLOX, SmJAR1, SmCOI1, and SmJAZ1 were generated by cloning into the pGEX-4T-1 vector (26 kDa). Bound proteins were eluted and stained with Coomassie Brilliant Blue 250 and then separated by 12.5% SDS-PAGE.

(Sanders, 2000; Stintzi and Browse, 2000; Malek et al., 2002). For example, mutations in genes involved in JA biosynthesis typically caused delayed or failed anther dehiscence, such as *DAD1* (Ishiguro et al., 2001; Qin et al., 2011) and *OPR3* (Stintzi and Browse, 2000; Chini et al., 2018).

Based on the current transcriptome data for genes in the JA biosynthesis pathway, we propose that feedback regulation of JA signaling in anther-indehiscent eggplant alters the expression patterns of genes at the mRNA level during anther development (Sanders, 2000; Zhao and Ma, 2000; Hong, 2005). In this study, we identified five genes in the JA pathway (*SmDAD1*, *SmLOX*, *SmCOI1*, *SmJAZ1*, and *SmJAR1*) that were differentially expressed in the S12 vs. F142 eggplant. *SmDAD1*, *SmLOX*, and *SmCOI1* were clearly downregulated in S12, whereas *SmJAZ1* and *SmJAR1* were upregulated in S12 vs. F142. *SmDAD1* is crucial for JA biosynthesis. *Arabidopsis DAD1* (*At2g44810*) encodes the first chloroplastic lipase identified. This enzyme is involved in supplying α-linolenic acid for the JA-biosynthetic pathway (Ishiguro et al., 2001). Mutations in *DAD1* reduced JA levels in flower buds, causing a delay in their development, failed anther dehiscence during flower opening, and lack of pollen grain maturation (Ishiguro et al., 2001). In the *Arabidopsis coi1*, *opr3*, and *dad1* mutants, the anthers failed to crack and the filaments were short; however, these phenotypes were significantly altered by the external application of JA (Stintzi and Browse, 2000; An et al., 2018).

The JA pathway involves a series of gene-encoded hormone-related factors involved in anther dehiscence (Grunewald et al., 2009; Xiao et al., 2014; Chini et al., 2018). Previous gene expression analysis has demonstrated that overexpressing *AtOPR3* selectively affected the expression of various genes of the endogenous jasmonate system, while the expression of other genes remained unaltered. Transgenic wheat plants with high *AtOPR3* expression levels exhibited notably altered plant growth and development, including delayed germination, slower growth, and anther indehiscence (Pigolev et al., 2018). These findings indicate that these plant phenotypes are regulated by direct or indirect interactions of these genes.

Melotto et al. (2008) demonstrated that the physical interaction between COI1 and JAZ proteins could be effectively promoted by treatment with biologically active jasmonates (JA-Ile) (Singh et al., 1992; Melotto et al., 2008). In addition, AtMYC2 interacts with JAZs (Wasternack, 2017; Chini et al., 2018). Here, we demonstrated that SmDAD1 interacts with SmLOX1 both *in vitro* and *in vivo*. However, how these proteins regulate anther dehiscence remains unclear and should be addressed in future studies.

CONCLUSIONS

The outcomes of this study revealed that 31 DEGs related to hormone biosynthesis were identified by transcriptome between the anther-dehiscent eggplant (F142) and the anther-indehiscent eggplant (S12). Among them, the JA level of S12 was significantly lower than that of F142. The study on protein–protein interaction confirmed the direct interaction between SmDAD1 and SmLOX. Therefore, JA was confirmed to play an important role in anther dehiscence of eggplant.

DATA AVAILABILITY STATEMENT

The RNA-seq reads presented in the study are publicly available. This data can be found at the NCBI Short Read Archive (PRJNA746400).

AUTHOR CONTRIBUTIONS

ZW and YN designed the research. CY and SZ performed the molecular biology experiments. QT, DW, and ST carried out the bioinformatics analysis. ZW, CY, and SZ analyzed the data and wrote the study manuscript. All the authors approved the final version of the manuscript.

FUNDING

This study was supported by grants from the National Natural Science Foundation of China (Grant No: 31501756), the Chongqing Special Key Project of Technology Innovation and Application Development (Grant No: cstc2019jscx-gksbX0149), and the Chongqing Foundation Research and Frontier Exploration Project (Grant No: cstc2019jcyj-msxmX0448).

ACKNOWLEDGMENTS

We thank the reviewers and editors for the careful reading of the manuscript and constructive comments. We appreciate the assistance of the scientific instrument platform of the Key Laboratory of Horticulture Science for Southern Mountains Regions, Ministry of Education in this study. We sincerely thank the Institute of Vegetables and Flowers, Chongqing Academy of Agricultural Sciences for providing the eggplant materials.

SUPPLEMENTARY MATERIAL

The Supplementary Material for this article can be found online at: https://www.frontiersin.org/articles/10.3389/fpls.2021.648193/full#supplementary-material

REFERENCES

Amit, S., and Sawhney, V. K. (1993). Metabolism of dihydrozeatin in floral buds of wild-type and a genic male sterile line of rapeseed (*Brassica napus* L.). *J. Exp. Bot.* 44, 1497–1505. doi: 10.1093/jxb/44.9.1497

An, L., Ahmad, R. M., Ren, H., Qin, J., and Yan, Y. (2018). Jasmonate signal receptor gene family *Zmcois* restore male fertility and defense response of *Arabidopsis* mutant *coi1-1*. *J. Plant Growth Regul.* 38, 479–493. doi: 10.1007/s00344-018-9863-2

Bae, H. K., Kang, H. G., Kim, G. J., Eu, H. J., Oh, S. A., and Song, J. T. (2010). Transgenic rice plants carrying RNA interference constructs of AOS (allene oxide synthase) genes show severe male sterility. *Plant Breed* 129, 647–651. doi: 10.1111/j.1439-0523.2010.01784.x

Beals, T. P. (1997). A novel cell ablation strategy blocks tobacco anther dehiscence. *Plant Cell* 9, 1527–1545. doi: 10.1105/tpc.9.9.1527

Bohs, W. L. (2010). Eggplant origins: out of africa, into the orient. *Taxon* 59, 49–56. doi: 10.1002/tax.591006

Caldelari, D., Wang, G., Farmer, E., E., and Dong, X. (2011). *Arabidopsislox3 lox4*double mutants are male sterile and defective in global proliferative arrest. *Plant Mol Biol.* 75, 25–33. doi: 10.1007/s11103-010-9701-9

Chen, Z., J., Zhang, M., F., Wang, B., L., et al.(1995). A study on fertility and agronomic characters of CMS lines for tuber mustard. *ActaHorticulturae Sinica*22, 40–46.

Ching-Fang, S., Wei-Han, H., Yan-Jhu, P., and Chang-Hsien, Y. (2014). The NAC-like gene anther indehiscence factor acts as a repressor that controls anther dehiscence by regulating genes in the jasmonate biosynthesis pathway in *Arabidopsis*. *J. Exp. Bot.* 65, 621–639. doi: 10.1093/jxb/ert412

Chini, A., Monte, I., Zamarreño, A. M., Hamberg, M., Lassueur, S., Reymond, P., et al. (2018). An OPR3-independent pathway uses 4,5-didehydrojasmonate for jasmonate synthesis. *Nat. Chem. Biol.* 14, 171–178. doi: 10.1038/nchembio.2540

Dill, A., and Sun, T. (2001). Synergistic derepression of gibberellin signaling by removing RGA and GAI function in *Arabidopsis thaliana*. *Genetics* 159:777. doi: 10.1093/genetics/159.2.777

Grunewald, W., Vanholme, B., and Pauwels, L. (2009). Expression of the *Arabidopsis* jasmonate signalling repressor *JAZ1/TIFY10A* is stimulated by auxin. *EMBO Rep.* 10, 923–928. doi: 10.1038/embor.2009.103

Hideki, H., Kenta, S., Koji, M., Tsukasa, N., Satomi, N., Akio, O., et al. (2014). Draft genome sequence of eggplant (*Solanum melongena* L.): the representative solanum species indigenous to the old world. *DNA Res.* 21, 649–660. doi: 10.1093/dnares/dsu027

Hong, M. (2005). Molecular genetic analyses of microsporogenesis and microgametogenesis in flowering plants. *Annu. Rev. Plant Biol.* 56, 393–434. doi: 10.1146/annurev.arplant.55.031903.141717

Horner, H. T. (1977). A comparative light- and electron-microscopic study of microsporogenesis in male-fertile and cytoplasmic male-sterile sunflower (*Helianthus annuus*). *Am. J. Bot.* 64, 745–759. doi: 10.1002/j.1537-2197.1977.tb11916.x

Ishiguro, S., Kawai-Oda, A., Ueda, J., Nishida, I., and Okada, K. (2001). The *DEFECTIVE IN ANTHER DEHISCENCE1* gene encodes a novel phospholipase A1 catalyzing the initial step of jasmonic acid biosynthesis, which synchronizes pollen maturation, anther dehiscence, and flower opening in *Arabidopsis*. *Plant Cell* 13, 2191–2209. doi: 10.1105/tpc.010192

Jasmin, J. J. (1954). Male sterility in *Solanum melongena* L. preliminary report on a functional type of male sterility in eggplants. *Proc. Am. Soc. Hort. Sci.* 63, 443–443.

Kakizaki, Y. (1931). Hybrid Vigor in Egg-Plants and Its Practical Utilization. *Genetics* 16, 1–25. doi: 10.1093/genetics/16.1.1

Khan, M. R., and Isshiki, S. (2009). Functional male-sterility expressed in eggplant (*Solanum melongena* L.) containing the cytoplasm of S. kurzii Brace and Prain. *J. Pomol. Hortic. Sci.* 84, 92–96. doi: 10.1080/14620316.2009.11512486

Khan, M. R., and Isshiki, S. (2010). Development of the male-sterile line of eggplant utilizing the cytoplasm of solanum aethiopicum L. Aculeatum Group. *J. Jpn. Soc. Hortic. Sci.* 79, 348–353. doi: 10.2503/jjshs1.79.348

Kim, D., Pertea, G., Trapnell, C., Pimentel, H., Kelley, R., and Salzberg, S. L.(2013). TopHat2: accurate alignment of transcriptomes in the presence of insertions, deletions, and gene fusions. *Genome Biol.* 4:R36. doi: 10.1186/gb-2013-14-4-r36

Kojima, K. (1997). Changes of ABA, IAA, and GAs levels in reproductive organs of citrus. *Jarq. Jpn. Agric. Res. Q.* 31, 271–280.

Li, Y. X., Zhang, A. M., and Huang, T. C. (1976). Relationship between wheat cytoplasmic male sterilityand the content of endogenous hormones in the anther. *J. Agric. Biotechnol.* 4, 307–313.

Liu, H., Gu, J., Lu, Q., Li, H., Hong, Y., Chen, X., et al. (2019). Transcriptomic analysis reveals the high-oleic acid feedback regulating the homologous gene expression of Stearoyl-ACP Desaturase 2 (SAD2) in peanuts. *Int. J. Mol. Sci.* 20:3091. doi: 10.3390/ijms20123091

Liu, H. W., Zhang, G. S., Wang, J. W., Wang, X. L., and Fang, Z. W. (2003). Relation between ethylene of young spike andmale sterility induced by GENESIS in wheat. *J. Northwest Sci. Tech. Univ. Agric. For.* 31, 39–42. doi: 10.13207/j.cnki.jnwafu.2003.03.009

Malek, B. V., Graaff, E., Schneitz, K., and Keller, B. (2002). The Arabidopsis male-sterile mutant dde2-2 is defective in the ALLENE OXIDE SYNTHASE gene encoding one of the key enzymes of the jasmonic acid biosynthesis pathway. *Planta* 216, 187–192. doi: 10.1007/s00425-002-0906-2

Mao, X., Tao, C., Olyarchuk, J. G., and Wei, L. (2005). Automated genome annotation and pathwayidentification using the KEGG Orthology (KO) as a controlled vocabulary. *Bioinformatics* 21, 3787–3793. doi: 10.1093/bioinformatics/bti430

Mcconn, M., and Browse, J. (1996). The critical requirement for linolenic acid is pollen development, not photosynthesis, in an*Arabidopsis* mutant. *Plant Cell* 8, 403–416. doi: 10.1105/tpc.8.3.403

Melotto, M., Mecey, C., Niu, Y. J., Chung, H. S., Katsir, L., Yao J., et al. (2008). A critical role of two positively charged amino acids in the Jas motif of Arabidopsis JAZ proteins in mediating coronatine-and jasmonoyl isoleucine-dependent interactions with the COI1 F-box protein. *Plant J.* 55, 979–988. doi: 10.1111/j.1365-313X.2008.03566.x

Mennella, G., Rotino, G. L., Fibiani, M., D' Alessandro, A., Francese, G., Toppino, L., et al. (2010). Characterization of health-related compounds in eggplant (Solanum melongena L.) lines derived from introgression of allied species. *J. Agric. Food Chem*. 58: 7597–7603. doi: 10.1021/jf101004z

Nausica, L., Gianni, V., Otto, M., Guy, S., Claus, W., and Willy, J. P. (2007). The jasmonate-induced expression of the *Nicotiana tabacum* leaf lectin. *Plant Cell Physiol*. 48, 1207–1218. doi: 10.1093/pcp/pcm090

Nuttall, V. W. (1963). The inheritance and possible usefulness of functional male sterility in *Solanum melongena* L. *Can. J. Genet. Cytol.* 5, 197–199. doi: 10.1139/g63-029

Peng, Y. J., Shih, C. F., Yang, J. Y., Tan, C. M., Hsu, W. H., Huang, Y. P., et al. (2013). A RING-type E3 ligase controls anther dehiscence by activating the jasmonate biosynthetic pathway gene*DEFECTIVEINANTHERDEHISCENCE 1* in *Arabidopsis*. *Plant J*. 74, 310–327. doi: 10.1111/tpj.12122

Phatak, S. C., and Jaworski, C. A. (1989). UGA 1-MS male-sterile eggplant germplasm. *Hortscience* 24:1050.

Phatak, S. C., Liu, J., Jaworski, C. A., and Sultanbawa, A. F. (1991). Functional male-sterility in eggplant - inheritance and linkage to the purple fruit color gene. *J. Hered.* 1, 81–83. doi: 10.1093/jhered/82.1.81

Pigolev, A., Miroshnichenko, D., Pushin, A., Terentyev, V., Boutanayev, A., Dolgov, S., et al. (2018). Overexpression of *Arabidopsis* in hexaploid wheat (*Triticum aestivum* L.) alters plant development and freezing tolerance. *Int. J. Mol. Sci.* 19:3989. doi: 10.3390/ijms19123989

Qin, Y., Lei, J., Cao, B., Chen, G., Zhai, Y., and Yang, C. (2011). Cloning and sequence analysis of the, defective in anther dehiscence1, (dad1) gene fragment of Chinese kale. *Afr. J. Biotechnol.* 10, 11829–11831. doi: 10.1186/1471-2164-12-467

Rodríguez, B., Prohens, J., and Nuez, F. (2008). Performance of hybrids between local varieties of eggplant (*solanum melongena*) and its relation to the mean of parents and to morphological and genetic distances among parents. *Eur. J. Hortic. Sci.* 73, 76–83.

Sanders, P. M. (2000). The *Arabidopsis* delayed dehiscence1 gene encodes an enzyme in the jasmonic acid synthesis pathway. *Plant Cell* 12, 1041–1062. doi: 10.1105/tpc.12.7.1041

Sanders, P. M., Bui, A. Q., Le, B. H., and Goldberg, R. B. (2005). Differentiation and degeneration of cells that play a major role in tobacco anther dehiscence. *Sex. Plant Reprod.* 17, 219–241. doi: 10.1007/s00497-004-0231-y

Sanders, P. M., Bui, A. Q., Weterings, K., Mcintire, K. N., and Goldberg, R. B. (1999). Anther developmental defects in *Arabidopsis thaliana* male-sterile mutants. *Sex. Plant Reprod.* 11, 297–322. doi: 10.1007/s004970050158

Schaller, A., and Stintzi, A. (2009). Enzymes in jasmonate biosynthesis–structure, function, regulation. *Phytochemistry* 70, 1532–1538. doi: 10.1016/j.phytochem.2009.07.032

Schaller, F., Biesgen, C., Mussig, C., Altmann, T., and Weiler, E. W. (2000). 12-oxophytodienoate reductase 3 (OPR3) is the isoenzyme involved in jasmonate biosynthesis. *Planta* 210, 979–984. doi: 10.1007/s004250050706

Scott, R. J., Spielman, M., and Dickinson, H. G. (2004). Stamen structure and function. *Plant Cell* 16, S46–S60. doi: 10.1105/tpc,.017012

Shi, G. J., and Hou, L. (2004). Changes of endogenous hormones and polyamines in cytoplasmic male sterile non-heading Chinese cabbage during anther development. *Hortscience* 24, 2109–2112. doi: 10.21273/HORTSCI.39.4.881D

Singh, S., Sawhney, V. K., and Pearce, D. W. (1992). Temperature effects on endogenous indole-3-acetic acid levels in leaves and stamens of the normal and male sterile 'stamenless-2tamenlessd levels in*lycopersicon esculentum* mill.). *Plant Cell Environ.* 15, 373–377. doi: 10.1111/j.1365-3040.1992.tb00986.x

Stintzi, A., and Browse, J. (2000). The *Arabidopsis* male-sterile mutant, *opr3*, lacks the 12-oxophytodienoic acid reductase required for jasmonate synthesis. *Proc. Natl. Acad. Sci. U.S.A.* 97, 10625–10630. doi: 10.1073/pnas.190264497

Tian, C. E., Duan, J., Liang, C. Y., Huang, Y. W., and Liu, H. C. (1998). Changes in phytohormones in cytoplasmic male sterile rice and its maintainer line during panicle development. *J. Trop. Subtrop. Bot.* 2, 137–143.

Tian, S. B., Huang, B., Luo, Z. Y., Pi, W., Chen, Y. K., Wang, Y. Q., et al. (2001). Combining ability analysis of functional male sterile lines and restorers in eggplant. *Southwest China J. Agric. Sci.* 14, 58–61. doi: 10.16213/j.cnki.scjas.2001.02.017

Wang Z. M., Yuan, C., Ding Z. Q., Hu, R. L., Niu, Y., Tang Q. L., et al. (2021). Analysis of differential genes and metabolic pathway related to functional male sterility in eggplant. *Chin. J. Biotechan.* 37, 253–265. doi: 10.13345/j.cjb.200393

Wasternack, C. (2017). The Trojan horse coronatine: the COI1-JAZ2-MYC2,3,4-ANAC019,055,072 module in stomata dynamics upon bacterial infection. *New Phytol.* 213, 972–975. doi: 10.1111/nph.14417

Wasternack, C., and Strnad, M. (2018). Jasmonates: news on occurrence, biosynthesis, metabolism and action of an ancient group of signaling compounds. *Int. J. Mol. Sci.* 19:2539. doi: 10.3390/ijms19092539

Xiao, Y. G., Chen, Y., Charnikhova, T., Mulder, P. J., Ouwerkerk, P., and Heijmans, J. (2014). *OsJAR1*is required for JA-regulated floret opening and anther dehiscence in rice. *Plant Mol. Biol.* 86, 19–33. doi: 10.1007/s11103-014-0212-y

Xie, D. X., Feys, B. F., James, S., Nieto-Rostro, M., and TurnerXie, J. G. (1998). *COI1*: an *Arabidopsis* gene required for jasmonate-regulated defense and fertility. *Science* 280, 1091–1094. doi: 10.1126/science.280.5366.1091

Xu, M. L., Liu, W. F., and Xiao, Y. H. (1990). The content change of IAA of HPGMR during its panicle development. *J. Huazhong Agric.* 9, 381–386.

Young, M. D., Wakefield, M. J., Smyth, G. K., and Oshlack, A. (2010). Gene ontology analysis forRNA-seq: accounting for selection bias. *Genome Biol.* 11:R14. doi: 10.1186/gb-2010-11-2-r14

Yuan, C., Zhang, S. W., Hu, R. L., Wei, D. Y., Tang, Q. L., and Tian, S. B. (2020). Comparative transcriptome analysis provides insight into the molecular mechanisms of anther dehiscence in eggplant (*Solanum melongena* L.). *Genomics* 113, 497–506. doi: 10.1016/j.ygeno.2020.12.032

Zhang, S. W., Yuan, C., An, L. Y., Niu, Y., Song M., Tang, Q. L., et al. (2020). *SmCOI1* affects anther dehiscence in a male-sterile *Solanum melongena* line. *Plant Biotechnol.* 37, 1–8. doi: 10.5511/plantbiotechnology.19.1107a

Zhao, D., and Ma, H. (2000). Male fertility: a case of enzyme identity. *Curr. Biol.* 10, R904–R907. doi: 10.1016/S0960-9822(00)00848-4

Conflict of Interest: The authors declare that the research was conducted in the absence of any commercial or financial relationships that could be construed as a potential conflict of interest.

frontiers in Plant Science

ORIGINAL RESEARCH
published: 16 August 2021
doi: 10.3389/fpls.2021.594400

Ascorbic Acid-Induced Photosynthetic Adaptability of Processing Tomatoes to Salt Stress Probed by Fast OJIP Fluorescence Rise

Xianjun Chen[1,2†], *Yan Zhou*[3†], *Yundan Cong*[1,2], *Pusheng Zhu*[1,2], *Jiayi Xing*[1,2], *Jinxia Cui*[1,2], *Wei Xu*[1,2], *Qinghua Shi*[4], *Ming Diao*[1,2*] *and Hui-ying Liu*[1,2*]

[1] Department of Horticulture, Agricultural College, Shihezi University, Shihezi, China, [2] Key Laboratory of Special Fruits and Vegetables Cultivation Physiology and Germplasm Resources Utilization of Xinjiang Production and Construction Corps, Shihezi, China, [3] Department of Biological Science, Life Science and Technology School, Lingnan Normal University, Zhanjiang, China, [4] Department of Vegetables, Science and Engineering, Shandong Agricultural University, Tai'an, China

OPEN ACCESS

Edited by:
Glenn Bryan,
The James Hutton Institute,
United Kingdom

Reviewed by:
Pedro Carrasco,
University of Valencia, Spain
Peter Mabbitt,
New Zealand Forest Research Institute Limited (Scion), New Zealand
Costas Delis,
University of Peloponnese, Greece

***Correspondence:**
Hui-ying Liu
hyliuok@aliyun.com
Ming Diao
diaoming@shzu.edu.cn

[†] These authors have contributed equally to this work

Specialty section:
This article was submitted to Plant Metabolism and Chemodiversity, a section of the journal Frontiers in Plant Science

Received: 26 October 2020
Accepted: 14 July 2021
Published: 16 August 2021

Citation:
Chen X, Zhou Y, Cong Y, Zhu P, Xing J, Cui J, Xu W, Shi Q, Diao M and Liu H-y (2021) Ascorbic Acid-Induced Photosynthetic Adaptability of Processing Tomatoes to Salt Stress Probed by Fast OJIP Fluorescence Rise. Front. Plant Sci. 12:594400. doi: 10.3389/fpls.2021.594400

In this study, the protective role of exogenous ascorbic acid (AsA) on salt-induced inhibition of photosynthesis in the seedlings of processing tomatoes under salt stress has been investigated. Plants under salt stress (NaCl, 100 mmol/L) were foliar-sprayed with AsA (0.5 mmol/L), lycorine (LYC, 0.25 mmol/L, an inhibitor of key AsA synthesis enzyme l-galactono-γ-lactone dehydrogenase activity), or AsA plus LYC. The effects of AsA on fast OJIP fluorescence rise curve and JIP parameters were then examined. Our results demonstrated that applying exogenous AsA significantly changed the composition of O-J-I-P fluorescence transients in plants subjected to salt stress both with and without LYC. An increase in basal fluorescence (F_o) and a decrease in maximum fluorescence (F_m) were observed. Lower K- and L-bands and higher I-band were detected on the OJIP transient curves compared, respectively, with salt-stressed plants with and without LYC. AsA application also significantly increased the values of normalized total complementary area (S_m), relative variable fluorescence intensity at the I-step (V_I), absorbed light energy (ABS/CS_m), excitation energy (TR_o/CS_m), and reduction energy entering the electron transfer chain beyond Q_A (ET_o/CS_m) per reaction centre (RC) and electron transport flux per active RC (ET_o/RC), while decreasing some others like the approximated initial slope of the fluorescence transient (M_o), relative variable fluorescence intensity at the K-step (V_K), average absorption (ABS/RC), trapping (TR_o/RC), heat dissipation (DI_o/RC) per active RC, and heat dissipation per active RC (DI_o/CS_m) in the presence or absence of LYC. These results suggested that exogenous AsA counteracted salt-induced photoinhibition mainly by modulating the endogenous AsA level and redox state in the chloroplast to promote chlorophyll synthesis and alleviate the damage of oxidative stress to photosynthetic apparatus. AsA can also raise the efficiency of light utilization as well as excitation energy dissipation within the photosystem II (PSII) antennae, thus increasing the stability of PSII and promoting the movement of electrons among PS1 and PSII in tomato seedling leaves subjected to salt stress.

Keywords: processing tomatoes, ascorbic acid, NaCl stress, fast OJIP fluorescence rise curve, photosynthesis

INTRODUCTION

Xinjiang Province is one of the main producing regions of processing tomatoes in China. However, because of excessive use of fertilizers, unreasonable methods of irrigation and drainage, and the special climatic conditions (such as dryness due to less rain and strong evaporation in Xinjiang), the area is threatened by soil salinization, and soil secondary salinization has exceeded more than half of the total cultivated land dedicated to processing tomatoes. In recent years, this salinization problem became more and more serious, as it results in declines in photosynthetic rates, environmental resistance, and yield and quality of processing tomatoes. Increasing levels of salt in soil have become a primary abiotic stress that limits the productivity of processing tomatoes in Xinjiang Province (Pang et al., 2005). High salinity inhibits crop growth by disrupting a range of physiological processes involved in cell metabolism, especially photosynthesis (Thagela et al., 2017; Yang et al., 2020). Photosynthesis is the primary metabolic mechanism in plants (Singh et al., 2014) and is particularly sensitive to salinity (Ashraf and Harris, 2013). Salinity causes stomatal closure, destruction of chlorophyll pigments, inhibition of photochemical efficiency of photosystem II (PSII), and CO_2 assimilation (Dietz and Pfannschmidt, 2011). The presence of salt increases the buildup of reactive oxygen species (ROS) (Oukarroum et al., 2015; Hossain et al., 2017). The accumulated ROS severely damage the ultrastructure of photosynthetic apparatus, disrupting the use of light energy and causing the photoinhibition of PSII, consequently leading to plant growth retardation, and even cell and plant death (Jiang et al., 2017). Therefore, it is very important for plants to increase their salt tolerance and maintain their economic yield to counteract the adverse effects of salt stress on photosynthesis.

Reduced ascorbic acid (AsA) is by far the most abundant low-molecular weight antioxidant in plants, and AsA plays a key role in protecting plants from ROS generated during normal metabolic processes and under stress conditions including wounding, pathogen attack, salt, heat, light, and ozone exposure (Conklin, 2010). As an efficient electron donor and important non-enzymatic antioxidant, AsA constitutes a redox buffer that keeps the intracellular environment reduced and maintains the cellular redox homeostasis by directly or indirectly scavenging ROS (including H_2O_2, O_2^-, $\cdot OH^-$, and $^1O_2$). AsA can act as a signaling agent participating in the interaction with the environment (Linster and Clarke, 2008). AsA is also associated with several biosynthetic pathways, such as the xanthophyll cycle, which guard against the negative effects of surplus energy from excitation. Furthermore, many authors have demonstrated in the past years that AsA still exerts other significant roles in a wide range of processes, such as plant growth control, α-tocopherol regeneration, cell division and expansion regulation, resistance to insect feeding (Foyer and Graham, 2011), carbon–nitrogen metabolism, fruit quality and seed germination, as well as the expression of genes related to hormone synthesis and signal transduction. The cellular AsA pool size in plants can be regulated by the coordinated action of many related enzymes, and an enhanced AsA level has been confirmed to increase the tolerance and adaptation of crops to abiotic stresses such as high light intensity, cold, drought, salinity, UV-B, and ozone stresses (Xie et al., 2009). Similarly, exogenous application of AsA to plants has been shown to confer tolerance to several abiotic stresses in many crop plants (Xie et al., 2009; Wang et al., 2014; Alhasnawi et al., 2016; Akram et al., 2017; Penella et al., 2017). Our previous research demonstrated that optimal concentrations of exogenous AsA could relieve the salt-induced inhibition on the seedling growth of processing tomatoes, increasing its adaptability to salt stress (**Supplementary Materials**). It also showed that tomato salt tolerance improvement induced by exogenous selenium, glutathione (GSH), and nitric oxide (NO) is accompanied by the increase of endogenous AsA content and AsA/dehydroascorbate (DHA) ratio (He et al., 2015; Wen et al., 2018; Zhou et al., 2018).

The mechanisms of salt tolerance are very complex. Recent studies aiming to understand the mechanisms of AsA effects on plant salt tolerance have shown that salt tolerance induced by endogenous AsA or application of exogenous AsA mainly ascribed to the improvement of antioxidant, ion balance, and osmotic balance regulation (Wang et al., 2019). Although the photosynthetic apparatus is the most sensitive component for evaluating the degree of salt stress damage, few studies concerning the protection mechanisms of exogenous AsA on its structure and function under salt stress were carried out and more detailed ones are needed. The fluorescence transient (OJIP) technique is a quick, precise, and non-invasive method for reliably detecting and analyzing the effects of abiotic and biotic stress on the composition and processes of PSII and photosystem I (PSI), such as the redox condition of both photosystems, alterations in the main photosynthetic processes, and the efficiency of the transfer of electrons via the cross-system bond to the electron acceptors on the PSI acceptor node (Brestic et al., 2014). The conditions observed in the JIP test as well as the composition of the OJIP transient are easily affected by various stressors and have also been successfully employed in assessing and screening the tolerance of plants to environmental stresses (Chen et al., 2016; Çiçek et al., 2017; Essemine et al., 2017; Banks, 2018; Maliba et al., 2019). As such, we created tomato plants with various levels of endogenous AsA by applying AsA, the leaves of tomato seedlings that have been exposed to salt. Hence, we constructed tomato plants with different endogenous AsA levels by spraying salt-stressed tomato seedling leaves with AsA, Lycorine (LYC, an inhibitor of key AsA synthesis enzyme l-galactono-γ-lactone dehydrogenase activity), or AsA and LYC. The purpose of this experiment was to use OJIP transient analyses to assess the processes by which AsA impacts the photosystem stability, the processes of the photosynthetic electron transport chain, and the relationship between energy use and expenditure in the photosynthetic system of processing tomatoes subjected to salt stress. Increasing the exogenous AsA to expand PSII stability and regulate the photosynthetic activity and efficiency of the distribution of energy significantly contributed to mitigating the negative effects of salt stress, namely, the inhibition of photosynthetic processes and plant growth.

MATERIALS AND METHODS

Plant Materials and Treatments

Processing tomatoes (*Lycopersicon esculentum* L. cv. Ligeer87-5) were utilized for the relevant experiments, which were conducted hydroponically in a solar-powered greenhouse in Shihezi University, Xinjiang Uygur Autonomous Region, China. We transplanted seedlings (each with two euphylla) to a 12 L plastic container containing 10 L of full-strength, oxygenated Hoagland nutrient mixture ($pH = 6.2$).

Five treatments were performed on the seedlings of processing tomatoes after allowing them to pre-culture for 7 days. The NaCl was added to the nutrient mixtures, and LYC and AsA were sprayed on the leaves. This was made for five different treatments: (1) no added NaCl, no sprayed AsA and LYC (Control); (2) 100 mmol/L NaCl (NaCl); (3) 100 mmol/L NaCl and 0.5 mmol/L AsA (NA); (4) 100 mmol/L NaCl and 0.25 mmol/L LYC (NL); and (5) 100 mmol/L NaCl, 0.25 mmol/L LYC, and 0.5 mmol/L AsA (NLA). AsA and LYC were purchased from Sigma (United States) and YuanYe (China), respectively.

The methods, volumes, and concentrations of LYC and AsA application were based on a prior experiment (**Supplementary Materials**). The containers were arranged in a randomized complete block with three replicates per treatment. Each container contains five plants. The seedlings were exposed to light for 14 h at temperatures of 24–30°C during daytime and 17–20°C during nighttime. The nutrient mixtures were replaced every third day. The samples of tomato seedling leaves were obtained on the 9th day of treatment.

Growth Measurements

The following growth indices, such as plant height, stem diameter, shoot dry weight, root dry weight, root fresh weight, and shoot fresh weight, were measured. In details, the length from the cotyledonary internode to the growth point was measured and considered as the plant height; the diameter of cotyledonary node was measured and considered as the stem diameter of the seedling. Then, the seedlings were washed with tap water and wiped with paper. The shoot and root of each seedling were separated and weighed, dried for 15 min in a 105°C oven, and then to a constant weight at 75°C. Then, the samples were weighed.

Determination of Photosynthetic Pigment

Fresh processing tomato leaves (0.1 g) were harvested from the different treatments and put into a 25 mL brown volumetric flask, mixed with a 10 mL acetone–ethanol mix (1:1), and placed in the dark at room temperature until turning white. The extracting reagent was used as a negative control. We measured the chlorophyll extract absorbance at 470, 646, and 663 nm and analyzed the concentration of photosynthetic pigments according to the following (Wellburn and Lichtenthaler, 1984): mass concentration of chlorophyll *a* (Chl*a*) (mg/g FW) = $(12.21A_{663} - 2.81A_{646}) \times 10/(1{,}000 \times 0.1)$; mass concentration of chlorophyll *b* (Chl*b*) (mg/g FW) = $(20.13A_{646} - 5.03A_{663}) \times 10/(1{,}000 \times 0.1)$; total mass concentration of chlorophyll (Chl$a$ + b) (mg/g FW) = Chl$a$ + Chl$b$; and mass concentration of carotenoids (Car) (mg/g FW) = $(1{,}000A_{470} - 3.27 \times$ Chl*a*-104 $\times$ Chl*b*$) \times 10/(1{,}000 \times 0.1)$.

Determination of Photosynthetic Parameters

Photosynthetic parameters measurements were performed using a portable photosynthetic system (Li6400, LI-COR, United States) at 9:00–11:00 h on the fully developed leaf of each plant, according to a method previously described by Diao et al. (2014). To measure the net photosynthetic rate (P_n), intracellular CO_2 concentration (C_i), transpiration rate (T_r), and stomatal conductance (G_s), the air temperature, relative humidity, CO_2 concentration, and PPFD were maintained at 28–32°C, 80%, 380–390 μmol/mol, and 1,500 μmol/m^2/s, respectively, by automatic control device of the Li6400 photosynthetic system.

Ascorbic Acid Contents

The total AsA and AsA content were determined following the procedure by Jiang and Zhang (2001) with slight modifications. Leaves (0.3 g) were homogenized in ice-cold 5% (w/v) trichloroacetic acid and centrifuged at 15,000 × *g* for 10 min. Half of each sample was assayed for total AsA, and the other half was assayed for AsA content only. The dehydroascorbate (DHA) content was calculated as the difference between the total AsA content and the AsA content.

Measurement of OJIP Transients and Analysis of Fast Fluorescence Induction Kinetics

The chlorophyll (Chl) fluorescence transient (OJIP) curves were measured on fully expanded leaves that were still attached. Prior to these measurements, a leaf clip to subject five leaves to darkness for 30 min each was used. Then, the kinetics of Chl fluorescence (prompt fluorescence, PF) was measured, and the reflection at 820 nm (I/I_o) with a plant efficiency analyzer (Handy PEA, Hansatech Instrument Ltd, Lynn, United Kingdom) at room temperature was modulated. When all of the PSII reaction centers (RCs) were open (O step), the minimum fluorescence intensity signal (F_o) was assessed at 20 μs, and when all of the PSII RCs were close (P step), the maximum intensity signal (F_m) was assessed at 200–500 ms (Strasser et al., 2004). The fluorescence intensities between these two outliers: 30 ms (I step), 3 ms (J step), 300 μs (K step), and 150 μs (L step) were designated as F_I, F_J, F_K, and F_L, respectively (Kalaji et al., 2017).

In order to perform a thorough assessment of the O–K and O–J periods, we normalized an original transient curve as a variable relative fluorescence according to the following: $W_{O-K} = (F_t - F_o)/(F_K - F_o)$ and $W_{O-J} = (F_t - F_o)/(F_J - F_o)$, respectively (Oukarroum et al., 2010; Ceppi et al., 2012). We analyzed the kinetic differences based on the variable relative fluorescence according to the following: $\Delta W_{O-K} = [W_{O-K}(\text{stress}) - W_{O-K}(\text{control})]$ and $\Delta W_{O-J} = [W_{O-J}(\text{stress}) - W_{O-J}(\text{control})]$, which determined the presence of the L- and K-bands, respectively (Dalberto et al., 2017).

TABLE 1 | Summary of parameters and formulae using data extracted from chlorophyll (Chl) *a* fluorescence (OJIP) transient.

Parameters	Explanation
Parameters using data extracted from OJIP transient	
$F_v/F_m = (F_t - F_o)/(F_m - F_o)$	The maximal photochemical efficiency of PSII
$V_J = (F_J - F_o)/(F_m - F_o)$	Relative variable fluorescence intensity at the J-step
$V_I = (F_I - F_o)/(F_m - F_m)$	Relative variable fluorescence intensity at the I-step
$V_K = (F_K - F_o)/(F_m - F_o)$	Relative variable fluorescence intensity at the K-step
$W_k = (F_K - F_o)/(F_J - F_o)$	Ratio of variable fluorescence F_K to the amplitude $F_J - F_o$
$W_L = (F_L - F_o)/(F_K - F_o)$	Ratio of variable fluorescence F_L to the amplitude $F_K - F_o$
$S_m = (\text{Area})/(F_m - F_o)$	Normalized total complementary area
$M_o = 4(F_{300\mu s} - F_o)/(F_m - F_o)$	Approximated initial slope of the fluorescence transient
Flux ratios of PSII	
$\Phi p_o = TR_o/ABS = [1-(F_o/F_m)]$	Maximum quantum yield of primary photochemistry
$\phi E_o = ET_o/ABS = [1-(F_o/F_m)]\psi_o$	Quantum yield for electron transport (at $t = F_o$)
$\phi D_o = 1-\phi_{Po} = (F_o/F_m)$	Quantum yield at $t = F_O$ for energy dissipation
$\psi_o = ET_o/TR_o = (1-V_J)$	Probability that a trapped exciton moves an electron into the electron transport chain beyond Q_{A^-} (at $t = F_o$)
Activities per reaction center (RC)	
$ABS/RC = M_o(1/V_J)(1/\phi_{Po})$	Absorption flux per RC
$TR_o/RC = M_o(1/V_J)$	Trapped energy flux per RC (at $t = F_o$)
$DI_o/RC = ABS/RC - TR_o/RC$	Dissipated energy flux per RC (at $t = F_o$)
$ET_o/RC = M_o(1/V_J)\ (1/V_J)$	Electron transport flux per RC (at $t = F_o$)
Phenomenological energy fluxes per excited cross section (CS_m, subscript *M* refer to time $t = F_m$):	
$ABS/CS_m \approx F_m$	Absorption flux per CS (at $t = Fm$)
$TR_o/CS_m = \Phi_{po}\ (ABS/CS_m)$	Trapped energy flux per CS (at $t = F_m$)
$DI_o/CS_m = (ABS/CS_m) - (TR_o/CS_m)$	Dissipated energy flux per CS (at $t = F_m$)
$ET_o/CS_m = \Phi_{Eo}\ (ABS/CS_m)$	Electron transport flux per CS (at t = F_m)
Flux ratios of PS I	
$\delta R_o = RE_o/ET_o = (1-V_I)/(1-V_J)$	Efficiency with which an electron from the intersystem electron carriers is transferred to reduce end electron acceptors at the PSI acceptor side
$\phi R_o = RE/ABS = TR_o/ABS\ (1-V_I)$	Quantum yield for reduction of end electron acceptors at the PSI acceptor side
$\Delta I/I_o = (I_{max} - I_{min})/I_o$	Maximal redox capacity of PSI
Vitality indexes	
$PI_{ABS} = RC/ABS\ [\phi P_o/(1-\phi P_o)]\ [\psi_o/(1-\psi_o)]$	Performance index on absorption basis

The OJIP transient parameters were calculated according to the JIP test (Strasser et al., 2010). The formulas and their description of JIP test parameters are listed in **Table 1**.

Statistical Analysis

All data are presented as means ± standard deviation (SD) of three replicates. Statistical analyses were performed by the analysis of variance (ANOVA) using SPSS version 19.0 (SPSS Inc., Chicago, IL, United States). The significant differences among treatments were analyzed by the Duncan's multiple range test at a 0.05 probability level. Differences at $P < 0.05$ were considered to be significant.

RESULTS

Plant Growth

In comparison with the control treatment, plant height, stem diameter, dry and fresh weights of root and shoot were decreased by 31.9%, 25.5%, 66.1%, 45.8%, 74.2%, and 73.8% ($P < 0.05$) in the leaves of tomato plants under salt stress, respectively.

Lycorine (LYC) spraying (NL treatment) significantly reduces those effects on plant height, stem diameter, and fresh weights of shoot, but not on dry weight of shoot and fresh weight of root. However, exogenous application of AsA can mitigate NaCl and LYC effects (NA and NLA treatments) (**Table 2**; **Figure 1**).

Endogenous Ascorbic Acid Content and Redox State

Both the total AsA and AsA contents and the AsA/dehydroascorbate (DHA) ratio are considerably lower compared with the control under NaCl stress, which the AsA spraying increases. On the contrary, the DHA content is increased compared with the control (**Figure 2**). Compared with NaCl treatment, the AsA application to NaCl-stressed plants increases the content of total AsA, AsA, and AsA/DHA ratio by

TABLE 2 | The plant height (cm), stem diameter (mm), shoot FW (g), and root FW (g), shoot DW (g), and root DW (g) in the leaves of salt-stressed tomato seedlings as affected by exogenous ascorbic acid (AsA) and lycorine (LYC).

Treatment	Plant height	Stem diameter	Shoot FW	Root FW	Shoot DW	Root DW
Control	21.43 ± 0.76a	8.58 ± 0.53a	57.65 ± 1.04a	24.97 ± 5.92a	5.24 ± 0.32a	1.71 ± 0.09a
NaCl	14.60 ± 0.26d	6.39 ± 0.16c	15.10 ± 0.49c	13.55 ± 0.28c	1.35 ± 0.15c	0.58 ± 0.07d
NA	16.97 ± 0.47b	7.69 ± 0.41b	41.84 ± 0.71b	19.14 ± 1.50b	2.14 ± 0.28b	0.94 ± 0.07b
NL	12.37 ± 0.42e	5.60 ± 0.19d	13.11 ± 0.48d	10.00 ± 0.36c	1.27 ± 0.07c	0.55 ± 0.03d
NLA	15.70 ± 0.72c	6.44 ± 0.40c	14.81 ± 0.43c	14.23 ± 0.64bc	1.59 ± 0.06bc	0.76 ± 0.04c

Different letters (a, b, c, d, and e) indicate significant difference at $P < 0.05$ among treatments. Note: Control, no added NaCl, no sprayed AsA and LYC; NaCl, added 100 mmol/L NaCl; NA, added 100 mmol/L NaCl and sprayed 0.5 mmol/L AsA; NL, added 100 mmol/L NaCl and sprayed 0.25 mmol/L LYC; NLA, added 100 mmol/L NaCl and sprayed 0.25 mmol/L LYC and 0.5 mmol/L AsA.

FIGURE 1 | Growth of salt-stressed tomato seedlings with or without exogenous ascorbic acid (AsA) and lycorine (LYC) spraying. Control, no added NaCl, no sprayed AsA and LYC; NaCl, added 100 mmol/L NaCl; NA, added 100 mmol/L NaCl and sprayed 0.5 mmol/L AsA; NL, added 100 mmol/L NaCl and sprayed 0.25 mmol/L LYC; NLA, added 100 mmol/L NaCl and sprayed 0.25 mmol/L LYC and 0.5 mmol/L AsA.

26.3%, 49.4%, and 56.1% ($P < 0.05$), respectively, and the DHA content is decreased by 13.3% ($P < 0.05$). The AsA application to NL-treated plants also significantly increases the contents of total AsA and AsA and the ratio of AsA/DHA, but has no influence on the DHA level (**Figure 2**).

Photosynthetic Pigments Content

Tomato plants submitted to salt stress show a considerable decline in the chlorophyll (Chl) content, carotenoids (Car) content, and Car/Chl$a$+b ratio, whereas the Chl$a$/b ratio increased compared with the control. The AsA application to NaCl-stressed plants increases the content of Chl$a$, Chl$b$, Chl$a$+b, and Car by 28.0%, 52.4%, 33.3%, and 69.41% (P<0.05), respectively, compared with the NaCl treatment. The LYC application to salt-stressed plants (NL-treatment) accentuates the negative effects of NaCl stress on photosynthetic pigments content, but AsA application (NLA-treatment) can attenuate them (**Table 3**).

Gas Exchange

In comparison with the control treatment, the net photosynthetic rate (P_n), stomatal conductance (G_s), and transpiration rate (T_r) are respectively and significantly decreased by 26.6%, 10.6%, and 11.9%, whereas the intercellular CO_2 concentration (C_i) is increased by 10.6% ($P < 0.05$) in the leaves of tomato plants under salt stress. The application of LYC further decreases P_n, G_s, and T_r under salt stress. However, the application of AsA significantly alleviates the reduction of leaf P_n, G_s, and T_r induced by NaCl and NL treatments. C_i values in tomatoes under NaCl treatment and NL treatment are decreased after AsA spraying (NA and NLA conditions) (**Figure 3**).

OJIP Transient Curves

The OJIP transient curves between O and P phases are presented in **Figure 4A**. As illustrated in the figure, the NaCl treatment markedly increases J phase, but decreases I and P phases, and the amplitude of I–P phase. The NA treatment reverses salt-induced changes in OJIP curve, with an even higher PF intensity during I and P phases and a greater amplitude of I–P phase than that in the control. In the NL-treated leaves, the PF intensity during O and J phases is higher than that in the NaCl-treated leaves, but the I and P phases are not affected. The NLA-treated plants show lower PF intensity during the J phase and a higher one during the I and P phases compared with the NL-treated seedlings.

We normalized the fluorescence data and displayed it as the kinetics of relative variable fluorescence at any time $W_{O-P} = (F_t - F_o)/(F_m - F_o)$ (**Figure 4B**) to assess the polyphasic processes of the OJIP curves for the processes observed in the O–J, J–I, and I–P phases. Assessing W_{O-P} helped identify the sites where various electron transport chains on the acceptor end of PSII were treated (Kalaji et al., 2017). **Figure 4B** shows that there are no variations of W_{O-P} in both J–I and I–P phases between all treatments. However, in the O–J phase, a strong increase of PF intensity under salt stress is observed in comparison with the control, enhanced by LYC application. However, the AsA spraying has the opposite effect of LYC on both NaCl- and NL-treated leaves with a decrease in PF intensity during the O–J phase (**Figure 4B**).

The K-band appearing at 300 s reflects, when positive, a degradation or inactivation of the oxygenation complex (OEC) and is the specific marker of photoinhibition on the PSII receptor side (Yusuf et al., 2010). In order to observe K-band, the relative fluorescence between the phases O and J was normalized (**Figure 5A**), and the ratios of variable fluorescence F_K to the amplitude $F_J - F_o$ (W_K) were calculated (**Figure 5B**). Under salt stress, K-band and W_K are significantly higher than that in

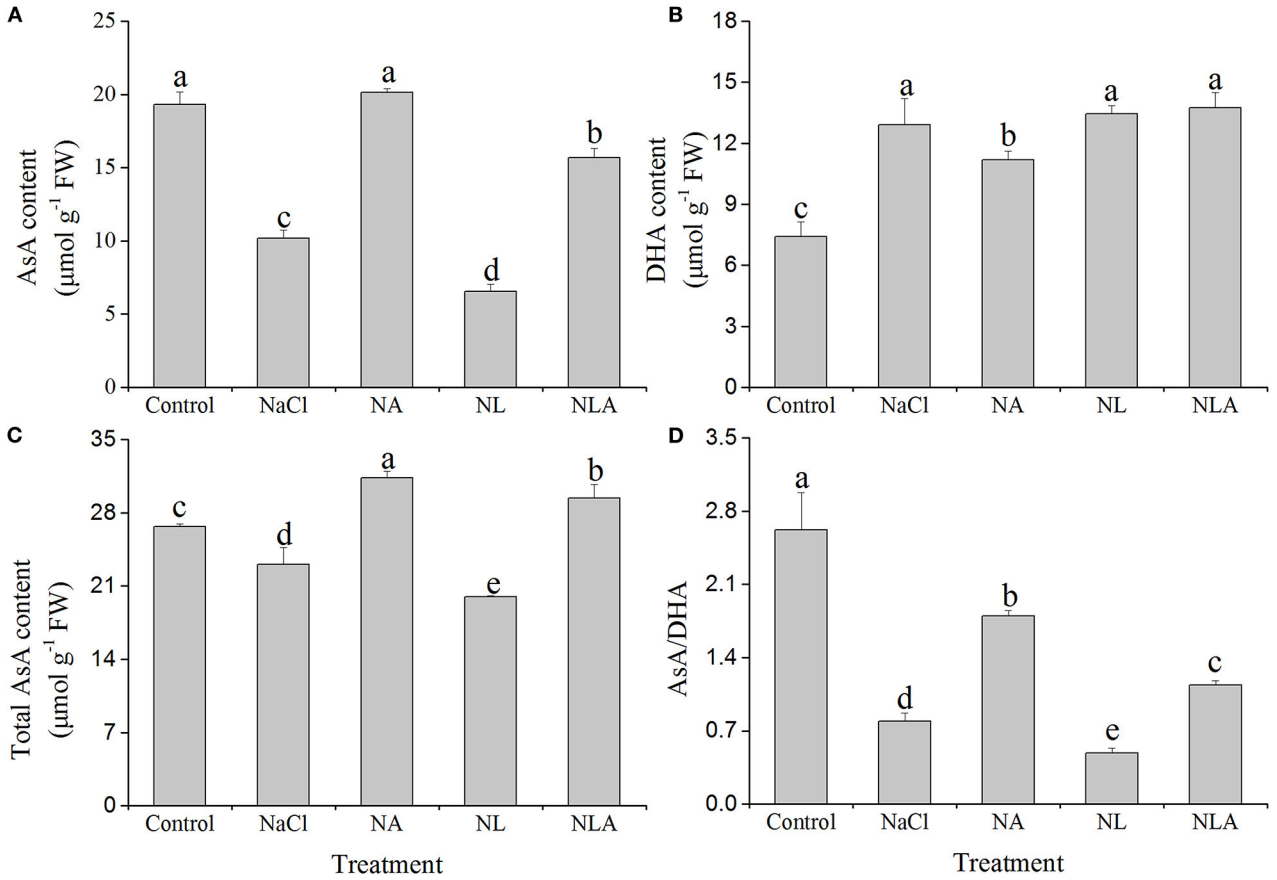

FIGURE 2 | Values of ascorbic acid (AsA) content **(A)**, dehydroascorbate (DHA) content **(B)**, total AsA content **(C)**, and AsA/DHA **(D)** in the leaves of salt-stressed tomato seedlings with or without exogenous AsA and lycorine (LYC) spraying. Values are means ± SD ($n = 3$). Different letters (a, b, c, d, and e) indicate significant difference at $P < 0.05$ among treatments. Control, no added NaCl, no sprayed AsA and LYC; NaCl, added 100 mmol/L NaCl; NA, added 100 mmol/L NaCl and sprayed 0.5 mmol/L AsA; NL, added 100 mmol/L NaCl and sprayed 0.25 mmol/L LYC; NLA, added 100 mmol/L NaCl and sprayed 0.25 mmol/L LYC and 0.5 mmol/L AsA.

TABLE 3 | The chlorophyll content (mg/g FW), Chl*a*/*b* ratio, carotenoids content (mg/g FW), and Car/Chl*a*+*b* ratio in the leaves of salt-stressed tomato seedlings as affected by exogenous acid (AsA) and lycorine (LYC).

Treatment	Chlorophyll (Chl) content			Chl*a*/*b*	Carotenoids (Car) content	Car/Chl*a*+*b*
	Chl*a*	Chl*b*	Chl*a* + Chl*b*			
Control	0.89 ± 0.02b	0.36 ± 0.01a	1.25 ± 0.02a	2.48 ± 0.13d	74.36 ± 0.26b	59.39 ± 1.33c
NaCl	0.75 ± 0.01d	0.21 ± 0.02c	0.96 ± 0.01c	3.60 ± 0.13ab	47.56 ± 1.35c	49.47 ± 1.74e
NA	0.96 ± 0.02a	0.32 ± 0.01b	1.28 ± 0.03a	3.04 ± 0.07c	80.57 ± 1.72a	63.01 ± 2.50b
NL	0.57 ± 0.04e	0.16 ± 0.01d	0.74 ± 0.05d	3.47 ± 0.03b	40.44 ± 3.08d	54.38 ± 0.32d
NLA	0.81 ± 0.01c	0.21 ± 0.05c	1.03 ± 0.07b	3.75 ± 0.15a	74.82 ± 2.05b	72.32 ± 2.21a

Values are means ± SD (n = 3). Different letters (a, b, c, d, and e) indicate significant difference at P < 0.05 among treatments. Note: Control, no added NaCl, no sprayed AsA and LYC; NaCl, added 100 mmol/L NaCl; NA, added 100 mmol/L NaCl and sprayed 0.5 mmol/L AsA; NL, added 100 mmol/L NaCl and sprayed 0.25 mmol/L LYC; NLA, added 100 mmol/L NaCl and sprayed 0.25 mmol/L LYC and 0.5 mmol/L AsA.

the control, with further increase by the application of LYC. Exogenous foliar spray of AsA in the NaCl treatment and the NL treatment alleviates this increase.

The L-band appears at 150 μs, and its rise is used as a specific marker for thylakoid dissociation. We normalized the relative fluorescence between the O and K phases (W_{O-K}) (**Figure 6A**, left), displaying them as the kinetic difference ΔW_{O-K} (**Figure 6A**, right). The kinetic difference ΔW_{O-K} makes the L-band visible. As shown in **Figures 6A,B**, exposure to salt stress leads to higher L-band and W_L in the leaves compared with the control plants. This increase is significantly higher after the LYC application. AsA-treated plants (both

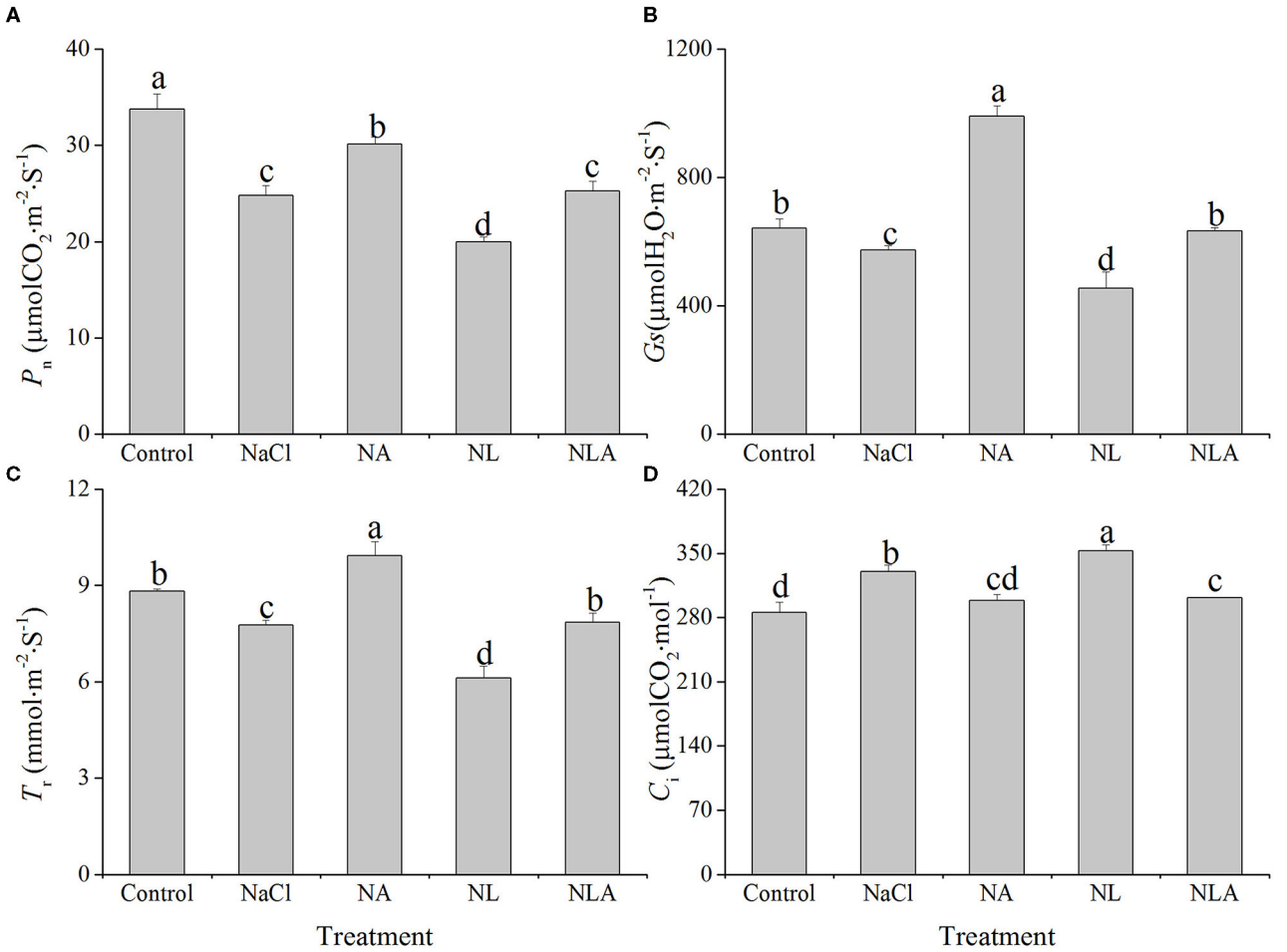

FIGURE 3 | Values of net photosynthetic rate (P_n) **(A)**, stomatal conductance (G_s) **(B)**, transpiration rate ($_{Tr}$) **(C)**, and intercellular CO_2 concentration (C_i) **(D)** in the leaves of salt-stressed tomato seedlings with or without exogenous ascorbic acid (AsA) and lycorine (LYC) spraying. Values are means ± SD ($n = 3$). Different letters (a, b, c, and d) indicate significant difference at $P < 0.05$ among treatments. Control, no added NaCl, no sprayed AsA and LYC; NaCl, added 100 mmol/L NaCl; NA, added 100 mmol/L NaCl and sprayed 0.5 mmol/L AsA; NL, added 100 mmol/L NaCl and sprayed 0.25 mmol/L LYC; NLA, added 100 mmol/L NaCl and sprayed 0.25 mmol/L LYC and 0.5 mmol/L AsA.

NA and NLA treatments) have significantly lower L-band and W_L ($P < 0.05$).

JIP Test Parameters

PSII

The values of the JIP test parameters (presented in **Table 1**) are shown as a spider plot in **Figure 7**. In the leaves of seedlings under NaCl treatment, the values of ψ_o, ϕE_o, S_m, F_m, and V_I are lower than that in the control, whereas the values of ϕD_o, M_o, F_o, V_K, and V_J are higher than that in the control. In the JIP parameters of NL-treated plants, the values of ψ_o, ϕE_o, S_m, F_m, and V_I are lower and the values of ϕD_o, M_o, F_o, V_K, and V_J are higher than that under NaCl treatment. Conversely, the AsA-treated plants with NaCl treatment have higher ψ_o, ϕE_o, S_m, F_m, and V_I and lower ϕD_o, M_o, F_o, V_K, and V_J than that under NaCl treatment. The AsA application to NL-treated plants also increased the values of ψ_o, ϕE_o, S_m, F_m, and V_I and decreased the values of ϕD_o, M_o, F_o, V_K, and V_J.

As shown in **Figure 8**, ABS/RC, TR_o/RC, and DI_o/RC (presented in **Table 1**) in the leaves of tomatoes under salt stress increased significantly compared with the control treatment, but ET_o/RC decreased markedly. Compared with the NaCl treatment, ABS/RC, TR_o/RC, and DI_o/RC under NL treatment also increased significantly but ET_o/RC decreased notably. However, the AsA spraying decreases ABS/RC, TR_o/RC, and DI_o/RC but increases ET_o/RC with or without LYC.

As presented in **Figure 9**, ABS/CS_m, TR_o/CS_m, and ET_o/CS_m decreased by 14.3%, 18.9%, and 14.1%, respectively, in tomato leaves under salt stress, and DI_o/CS_m increased significantly by 17.2% ($P < 0.05$), further decreasing with LYC application. However, the AsA application to NaCl- and NL-treated plants increases ABS/CS_m, TR_o/CS_m and ET_o/CS_m significantly and decreases DI_o/CS_m in both conditions.

In order to visualize and understand more deeply how exogenous AsA can alleviate the changes of photosynthetic apparatus caused by salt stress, based on the data in **Figures 8**, **9**

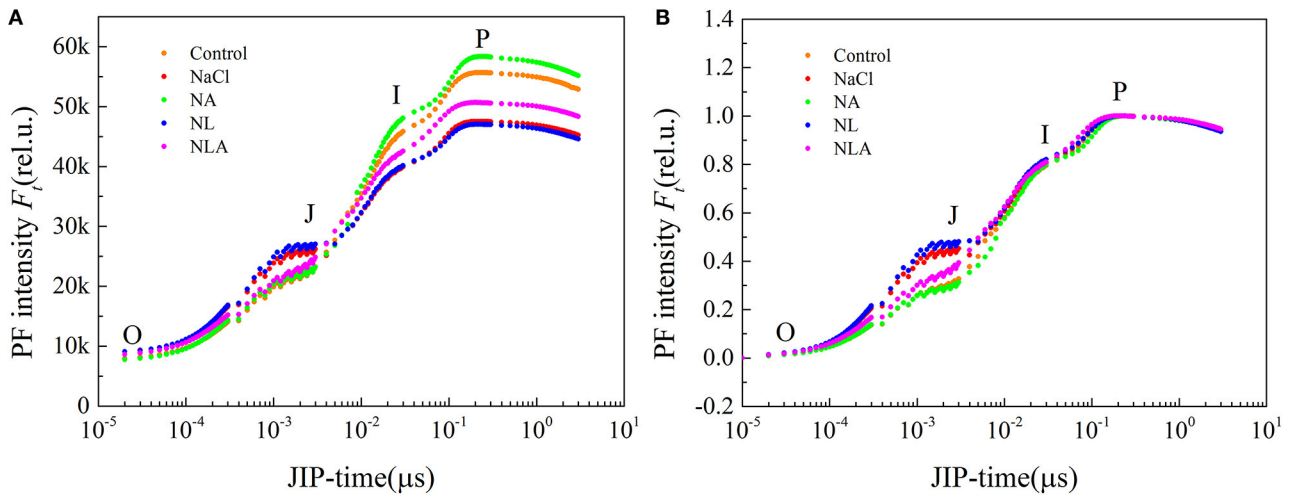

FIGURE 4 | Prompt fluorescence (PF) curves **(A)** and its normalized curves between O and P steps expressed as $W_{O-P} = [(F_t - F_o)/(F_m - F_o)]$ **(B)** in the leaves of salt-stressed tomato seedlings with or without exogenous ascorbic acid (AsA) and lycorine (LYC) spraying. Values are means ± SD ($n = 3$). Control, no added NaCl, no sprayed AsA and LYC; NaCl, added 100 mmol/L NaCl; NA, added 100 mmol/L NaCl and sprayed 0.5 mmol/L AsA; NL, added 100 mmol/L NaCl and sprayed 0.25 mmol/L LYC; NLA, added 100 mmol/L NaCl and sprayed 0.25 mmol/L LYC and 0.5 mmol/L AsA.

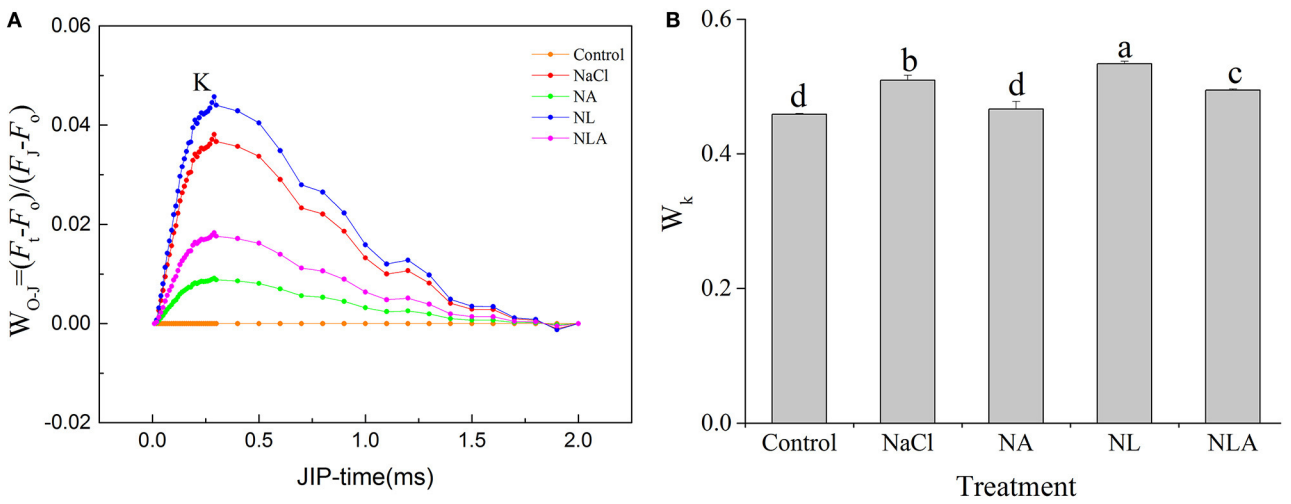

FIGURE 5 | Normalized prompt fluorescence (PF) curves between O and J steps expressed as $W_{O-J} = [(F_t - F_o)/(F_J - F_o)]$ **(A)** and ratio of variable fluorescence F_K to the amplitude $F_J - F_O$ expressed as $W_K = (F_K - F_o)/(F_J - F_o)$ **(B)** in the leaves of salt-stressed tomato seedlings with or without exogenous ascorbic acid (AsA) and lycorine (LYC) spraying. Values are means ± SD ($n = 3$). Different letters (a, b, c, and d) indicate significant difference at $P < 0.05$ among treatments. Control, no added NaCl, no sprayed AsA and LYC; NaCl, added 100 mmol/L NaCl; NA, added 100 mmol/L NaCl and sprayed 0.5 mmol/L AsA; NL, added 100 mmol/L NaCl and sprayed 0.25 mmol/L LYC; NLA, added 100 mmol/L NaCl and sprayed 0.25 mmol/L LYC and 0.5 mmol/L AsA.

(**Supplementary Materials**), the energy pipeline models of specific fluxes per RC and the phenomenological fluxes per excited cross-section (CS_m) in the membrane of the tomatoes (**Figure 10**, left) and the leaf (**Figure 10**, right) under different treatments were constructed, respectively. Compared with the control, F_v/F_m and PI_{ABS} values reduced significantly under salt stress (**Figure 11**). Applying the exogenous AsA significantly raises both the PI_{ABS} and F_v/F_m values found in seedling leaves subjected to salt stress ($P < 0.05$). On the contrary, applying the exogenous LYC significantly decreases F_v/F_m by 5.0% and PI_{ABS} by 10.6% in the salt-stressed leaves. NLA treatment significantly increased F_v/F_m and PI_{ABS} compared with the NL treatment.

Photosystem I

$\Delta I/I_o$, ϕR_o, and δR_o are significantly and respectively decreased by 26.3%, 23.6%, and 15.8% ($P < 0.05$) in NaCl-stressed plants, compared with the plants used as controls (**Figure 12**). Applying AsA significantly raises δR_o, $\Delta I/I_o$, and ϕR_o in the seedling leaves

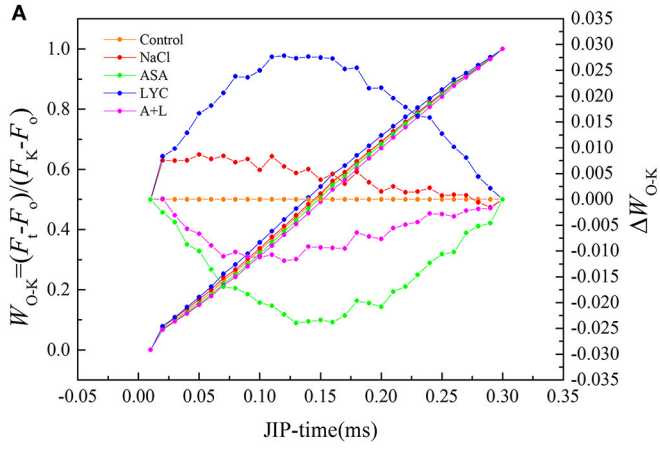

FIGURE 6 | Shape of the prompt fluorescence (PF) transient curves normalized between O and K steps expressed as $W_{O-K} = [(F_t-F_o)/(F_K-F_o)]$, $\Delta W_{O-K} = W_{O-K}$(stress)–W_{O-K} (control) **(A)**, $W_L = [(F_L-F_o)/(F_K-F_o)]$ **(B)** in leaves of salt-stressed tomato seedling with or without exogenous reduced ascorbic acid (AsA) and lycorine (LYC) spraying. Values are means ± SD ($n = 3$). Different letters (a, b, c, d, and e) indicate significant difference at $P < 0.05$ among treatments. Error bar is smaller than the line at the top of the graph. Control, no added NaCl, no sprayed AsA and LYC; NaCl, added 100 mmol/L NaCl; NA, added 100 mmol/L NaCl and sprayed 0.5 mmol/L AsA; NL, added 100 mmol/L NaCl and sprayed 0.25 mmol/L LYC; NLA, added 100 mmol/L NaCl and sprayed 0.25 mmol/L LYC and 0.5 mmol/L AsA.

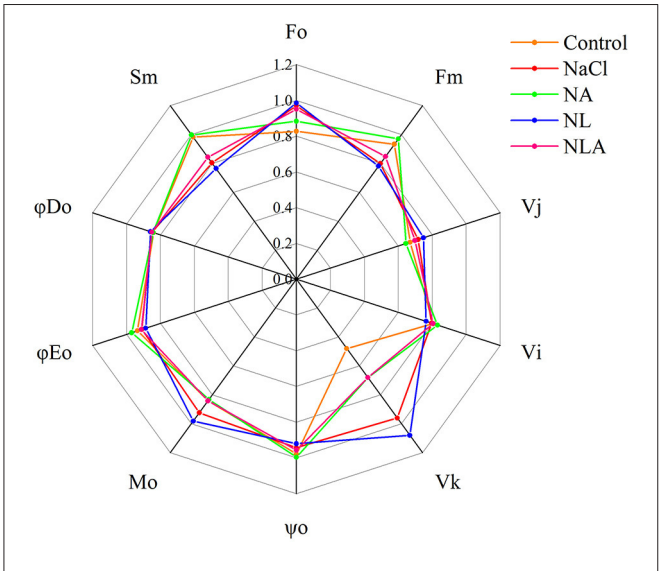

FIGURE 7 | Spider plots of the JIP parameters deduced from chlorophyll a fluorescence OJIP transient curves in leaves of salt-stressed tomato seedlings with or without exogenous ascorbic acid (AsA) and lycorine (LYC) spraying. Values are means ± SD ($n = 3$). Control, no added NaCl, no sprayed AsA and LYC; NaCl, added 100 mmol/L NaCl; NA, added 100 mmol/L NaCl and sprayed 0.5 mmol/L AsA; NL, added 100 mmol/L NaCl and sprayed 0.25 mmol/L LYC; NLA, added 100 mmol/L NaCl and sprayed 0.25 mmol/L LYC and 0.5 mmol/L AsA.

subjected to NaCl stress. In contrast, the application of LYC significantly decreases $\Delta I/I_o$, ϕR_o, and δR_o in the plant leaves stressed by NaCl. $\Delta I/I_o$, ϕR_o, and δR_o are significantly higher in the NLA treatment than that in the NL treatment.

DISCUSSION

Growth is the comprehensive embodiment of plant response to stress, and it is also a common index to determine stress tolerance (Liu et al., 2018). Salt stress is one of the primary abiotic factors affecting the quality and yield of crops (Landi et al., 2017). In this study, the results showed that AsA addition can alleviate the deleterious effects of salt stress (**Figure 1**; **Table 2**). This observation on the role of AsA in circumventing the adverse effects of salinity on plant biomass coincides with earlier reports (Wang et al., 2014; Terzi et al., 2015; Aliniaeifard et al., 2016). Meanwhile, we found that exogenous AsA application on salt-stress tomato seedlings is accompanied by an increase of endogenous AsA level and AsA/DHA ratio (**Figure 2**). Significant evidence demonstrates that the intracellular redox condition and the ROS scavenging capacity affect the resistance of abiotic stress in plants (Dietz, 2010). Keeping high redox pools and antioxidative level of GSH and AsA (or GSH/GSSG and AsA/DHA ratios) is necessary for plants to consume surplus ROS and maintain the sulfhydryl groups of membrane and soluble proteins in a lowered condition (Wang et al., 2020a). Our findings demonstrate that the exogenous application of AsA can induce tomato seedling growth under salt-stress conditions, and it was associated with increases in endogenous AsA levels. To further probe the role of AsA, we applied lycorine (LYC, an inhibitor of AsA synthesis key enzyme L-galactono-γ-lactone dehydrogenase activity) on the leaves of salt-stressed tomato seedlings prior or not to AsA treatment. LYC was used to reduce endogenous AsA content (Arrigoni et al., 1997). In this study, we observed that application of exogenous LYC under salt stress exacerbated growth inhibition and also significantly decreased the endogenous AsA level and the ratio of AsA/DHA (**Figure 1**; **Table 2**). However, the application of exogenous AsA can also

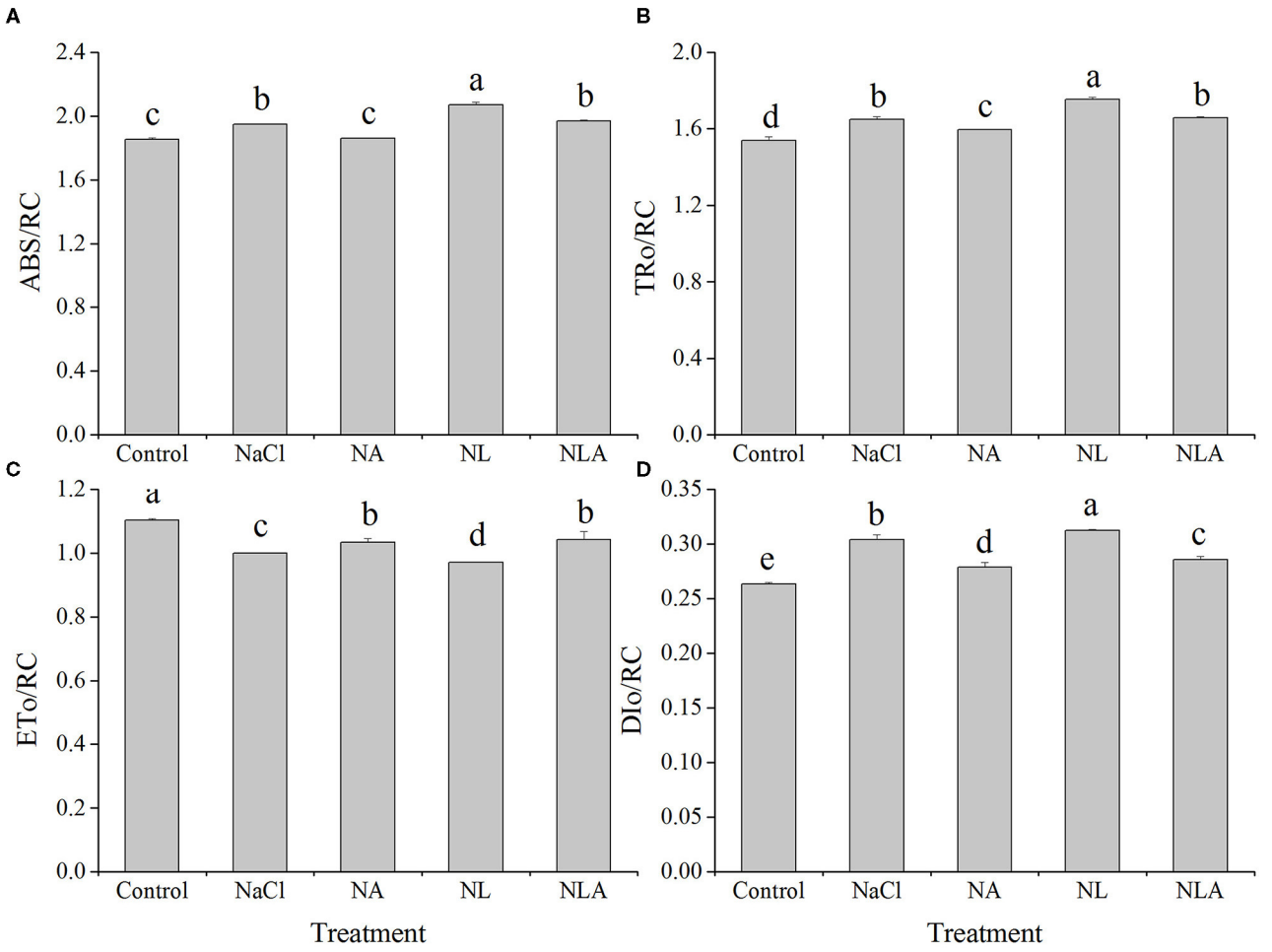

FIGURE 8 | Parameters of absorption flux per reaction center (RC) (ABS/RC) **(A)**, trapped energy flux per RC (at $t = F_o$) (TR_o/RC) **(B)**, electron transport flux per RC (at $t = F_o$) (ET_o/RC) **(C),** and dissipated energy flux per RC (at $t = F_o$) (DI_o/RC) **(D)** in leaves of salt-stressed tomato seedling with or without exogenous ascorbic acid (AsA) and lycorine (LYC) spraying. Values are means ± SD ($n = 3$). Different letters (a, b, c, d, and e) indicate significant difference at $P < 0.05$ among treatments. Error bar is smaller than the line at the top of the graph. Control, no added NaCl, no sprayed AsA and LYC; NaCl, added 100 mmol/L NaCl; NA, added 100 mmol/L NaCl and sprayed 0.5 mmol/L AsA; NL, added 100 mmol/L NaCl and sprayed 0.25 mmol/L LYC; NLA, added 100 mmol/L NaCl and sprayed 0.25 mmol/L LYC and 0.5 mmol/L AsA.

effectively reverse the effects of LYC on the growth of tomato seedlings and the redox state of endogenous AsA (**Figures 1**, **2**). These results give strong evidence that AsA can enhance the resistance of tomato seedlings to salt stress or salt stress with LYC application by mediating high reducing power and ROS scavenging capacity of endogenous AsA and redox state. This is consistent with the reports in barley by Agami (2014).

Under stressful environment, the decline in plant growth often relates to a decrease in photosynthetic capacity (Li et al., 2017; Zahoor et al., 2017). Reduced photosynthesis under salinity is not only attributed to stomatal closure factors but also attributed to non-stomatal limitation factors (Melesse and Caesar, 2010). Our findings demonstrate that a decrease in leaf P_n due to salt (**Figure 3A**) was mainly induced by non-stomatal factors, since salt-stress response elevated C_i (**Figure 3D**), even though G_s decreased (**Figure 3B**). In this experiment, exogenously applying AsA effectively combatted the negative effects of salt stress and NL treatment on C_i, G_s, and P_n in tomato seedling leaves (**Figure 3**). These results showed that AsA might help to relieve salt-induced photosynthetic inhibition mainly by the regulation of non-stomatal limitation factors, such as the decrease in photosynthetic pigments content, the chloroplast ultrastructure disorganization, the photochemical reaction activity decrease, or the decrease of enzyme activity involved in the process of carbon assimilation.

Chlorophyll molecules have high sensitivity to environmental stresses, and chlorophyll content, due to positive correlation with photosynthesis, is widely used as an index of abiotic tolerance in plants (An et al., 2018; Wang et al., 2020b). High salinity causes an increased ROS generation in chloroplasts, which can destroy chlorophyll. Also, reduction of chlorophyll content induced by salinity stress is due to the enhanced activity of chlorophyll

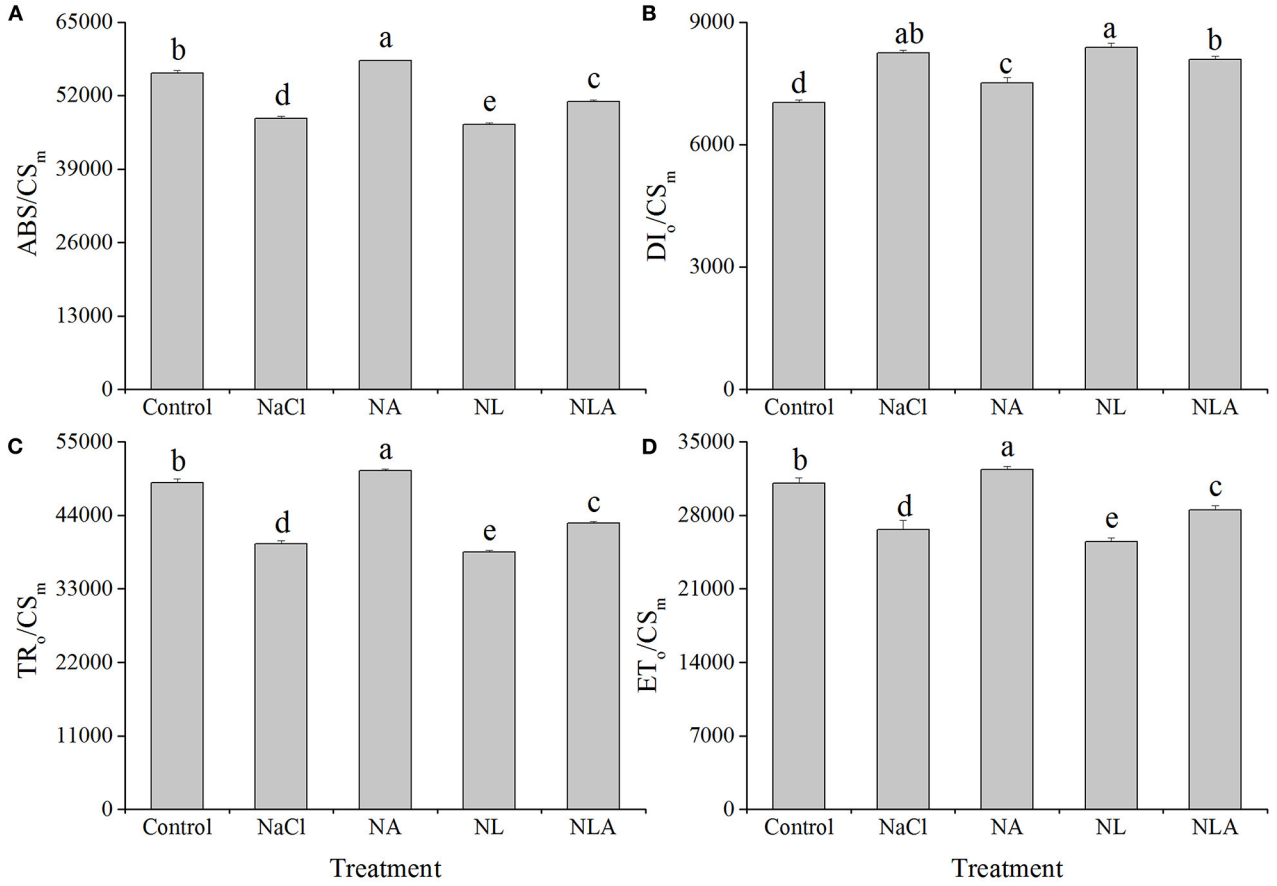

FIGURE 9 | Parameters of absorption flux per CS (at $t = F_m$) (ABS/CS_m) **(A)**, dissipated energy flux per CS (at $t = F_m$) (DI_o/CS_m) **(B)**, trapped energy flux per CS (at $t = F_m$) (TR_o/CS_m) **(C)**, and electron transport flux per CS (at $t = F_m$) (ET_o/CS_m) **(D)** in leaves of salt-stressed tomato seedlings with or without exogenous reduced ascorbic acid (AsA) and lycorine (LYC) spraying. Values are means ± SD ($n = 3$). Different letters (a, b, c, d, and e) indicate significant difference at $P < 0.05$ among treatments. Error bar is smaller than the line at the top of the graph. Control, no added NaCl, no sprayed AsA and LYC; NaCl, added 100 mmol/L NaCl; NA, added 100 mmol/L NaCl and sprayed 0.5 mmol/L AsA; NL, added 100 mmol/L NaCl and sprayed 0.25 mmol/L LYC; NLA, added 100 mmol/L NaCl and sprayed 0.25 mmol/L LYC and 0.5 mmol/L AsA.

enzymes and the instability of pigment–protein complex (Aghaleh et al., 2009; Hamid and Ashraf, 2010). In addition, salt stress reduces chlorophyll content by decreasing the uptake and accumulation of key nutrients such as Mg^{2+}, Fe^{2+}, and Cu^{2+}, which are involved in the biosynthesis of chlorophyll (Evelin et al., 2012). The activities of Mg-chelatase and ferrochelatase are regulated by the redox state in chloroplast. Under the oxidized state in chloroplast, the activity of Mg-chelatase is inhibited and the activity of ferrochelatase is improved, finally resulting in the inhibition of chlorophyll biosynthesis (Walker and Willows, 1997; Adhikari et al., 2011). In this study, the reduced chlorophyll contents in salt-stressed plant leaves might be due to chlorophyll degradation and chlorophyll biosynthesis inhibition (**Table 3**). This is in line with what has been reported earlier in *Phaseolus vulgaris* L. (Taïbi et al., 2016), *Gossypium* spp (Saleh, 2012), and *Brassica chinensis* L. (Muhammad and Shafiq, 2014). AsA levels in plants increase when subjected to stress and serve important roles when defending against oxidative stress (Xu et al., 2015). Exogenous application of AsA has been reported to increase the chlorophyll contents in diverse plants (Saeidi-Sar et al., 2012; Ahmad et al., 2013; Kostopoulou et al., 2014). In this study, the exogenous application of AsA counteracted the adverse effects on photosynthetic pigments of salt stress with or without LYC (**Figure 3**; **Table 3**), and the AsA application to NaCl-treated or NL-treated tomato seedlings caused a considerable increase in the endogenous AsA content and AsA/DHA ratio (**Figure 2**), thereby promoting the biosynthesis of chlorophyll and protecting the chloroplasts from oxidative damage. Furthermore, higher carotenoids contents were also observed in the NA-treated and NLA-treated plants compared with the NaCl-treated and NL-treated plants (**Table 3**). Carotenoids can protect the photosynthetic apparatus from photooxidative damage by quenching the triplet state of chlorophyll and helping dissipate the excessive energy of excitation, thereby preventing the formation of ROS (Derks et al., 2015). Above all, these results suggest that alleviating chloroplasts

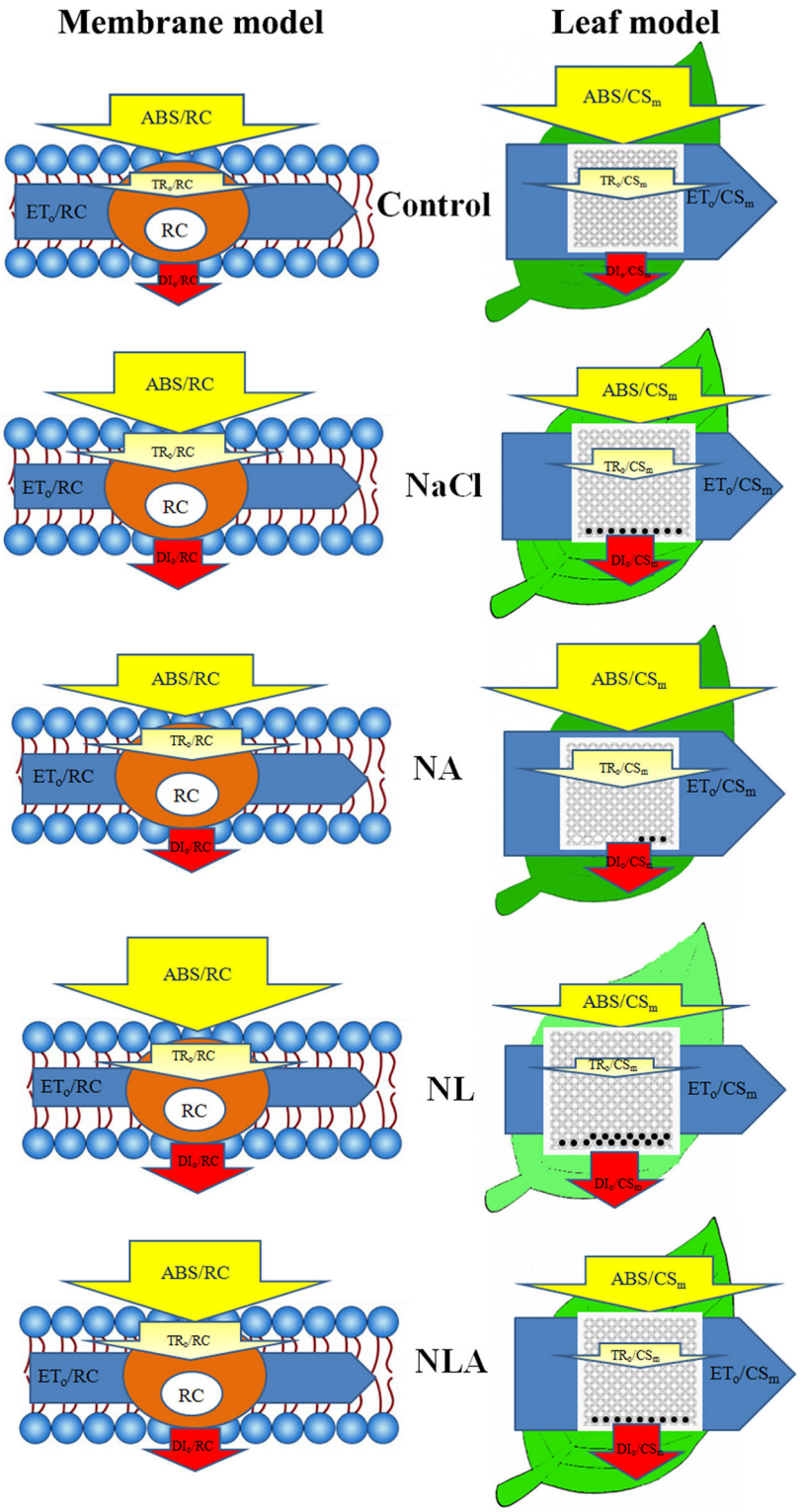

FIGURE 10 | Energy pipeline models of specific fluxes per reaction center (RC) and phenomenological fluxes per excited cross-section (CS_m) in the member (left) and the leaf (right) of salt-stressed tomato seedling with or without exogenous ascorbic acid (AsA) and lycorine (LYC) spraying. In the member and leaf models, ABS, TRo, ETo, and DIo indicate absorption, maximum trapping flux beyond Q_A, electron transport, and dissipation flux, respectively. In the leaf models (right), the leaf color represents the pigment concentration, and the active and inactive RCs are indicated by open circles and closed circles, respectively. The detailed calculation of each parameter is given in **Table 1**. Control, no added NaCl, no sprayed AsA and LYC; NaCl, added 100 mmol/L NaCl; NA, added 100 mmol/L NaCl and sprayed 0.5 mmol/L AsA; NL, added 100 mmol/L NaCl and sprayed 0.25 mmol/L LYC; NLA, added 100 mmol/L NaCl and sprayed 0.25 mmol/L LYC and 0.5 mmol/L AsA.

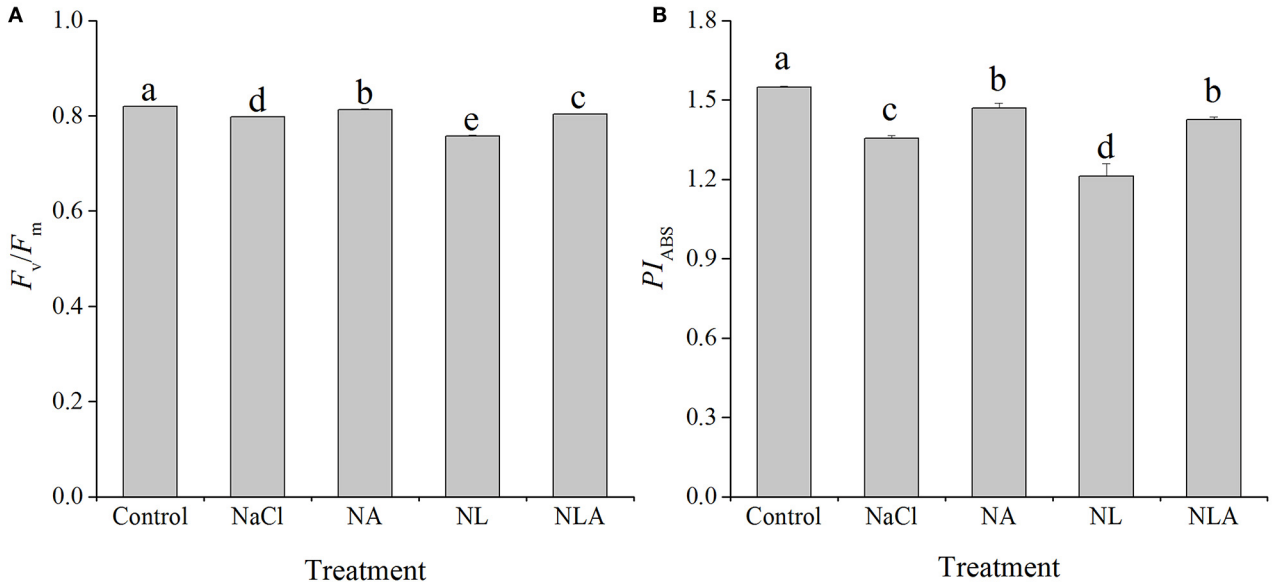

FIGURE 11 | Values of the maximal photochemical efficiency of PSII (F_v/F_m) **(A)** and performance index on absorption basis (*PI*ABS) **(B)** in the leaves of salt-stressed tomato seedlings with or without exogenous ascorbic acid (AsA) and lycorine (LYC) spraying. Values are means ± SD ($n = 3$). Different letters (a, b, c, d, and e) indicate significant difference at $P < 0.05$ among treatments. Error bar is smaller than the line at the top of the graph. Control, no added NaCl, no sprayed AsA and LYC; NaCl, added 100 mmol/L NaCl; NA, added 100 mmol/L NaCl and sprayed 0.5 mmol/L AsA; NL, added 100 mmol/L NaCl and sprayed 0.25 mmol/L LYC; NLA, added 100 mmol/L NaCl and sprayed 0.25 mmol/L LYC and 0.5 mmol/L AsA.

oxidative stress damage and promoting chlorophyll synthesis, by enhancing the antioxidant capacity and modulating redox state in chloroplast of tomato seedlings under salt stress, is one of the mechanisms by which exogenous AsA could increase the photosynthetic capacity of salt-stressed tomato seedlings.

In order to further decipher the mechanism of action of salt stress on the electron transport chain and the mechanism of how exogenous AsA improve the performance of photosynthetic organs in salt-stressed tomato seedlings, the effects of AsA application on the structure and functioning of the photochemical apparatus of tomato seedlings under salt stress with or without LYC were investigated by rapid chlorophyll fluorescence technique. Our findings indicate that OJIP curve shapes are sensitive to salt stress. The OJIP curve was flatter in salt-stressed leaves than that in the control, because of decreases in F_m (P-step) and increases in F_o (O-step) (**Figures 4A**, **7**). The normalized curve demonstrated relative J-step elevations, which can also be seen in the elevated V_J parameter, compared with that of control (**Figure 7**). These alterations in the values of F_o, F_m, and V_J suggest that the PSII donor end deteriorates as a result of salt stress and that the capacity of the PSII donor end to give electrons also decreases due to an increase in the closed PSII RCs (Strasser et al., 2010). The appearance of K- and L-bands in the OJIP transient curve of salt-treated leaves, as well as the increases in W_K and W_L values (**Figures 5** and **6**), also confirms the destruction of OEC and the integrity of the thylakoid membrane in the donor side of PSII, leading to the decrease in the electron donation capacity of the PSII donor side (Gomes et al., 2012; Li et al., 2014), as found for barley and passion fruit under drought stress (Oukarroum et al., 2007). The parameters, such as V_J, M_o, S_m, ϕE_o, and ψ_o, mainly reflect the changes of the acceptor side of PSII. According to the higher V_J in salt-treated leaves (**Figure 7**), we concluded that the acceptor side of PSII also suffered damage from salt stress. Photoinhibitory damage on the PSII acceptor end of leaves that have been treated with salt is confirmed by our observations that the stress of salt decreases S_m, ϕE_o and ψ_o and increases M_o (**Figure 7**) (Alaka Srivastava and Strasser, 2003; Oukarroum et al., 2004). Additionally, our results demonstrate that salt stress lowered the maximal redox threshold of PSI (I/I_o and $\Delta I/I_o$), the quantum yield necessary to reduce the end electron acceptors on the PSI acceptor end (ϕR_o), and how efficiently an electron is moved from the intersystem electron carriers to reduce the end electron accepted on the PSI acceptor end (δR_o) (**Figure 12**). These results indicate that salt stress reduced the capability of the photosynthetic electron transport from the PSII donor side and reduced the PSI end acceptors, reducing the photosynthetic capacity of the leaves. These findings suggest that both donor and acceptor sides of PSII and PSI are the target sites under salinity stress in tomato seedlings. Those results are consistent with the conclusions suggested by Shamshiri and Fattahi (2016) in pistachio (*Pistacia vera*). However, the application of AsA on the leaves of the tomato seedlings salt-stressed with or without LYC effectively reversed these changes on the donor side and acceptor side of photosystem (including PSII and PSI). These findings confirm that exogenously applying AsA serves an important role during the movement of electrons from the PSII donor end to the PSI acceptor ends. AsA can promote the electron transport activity

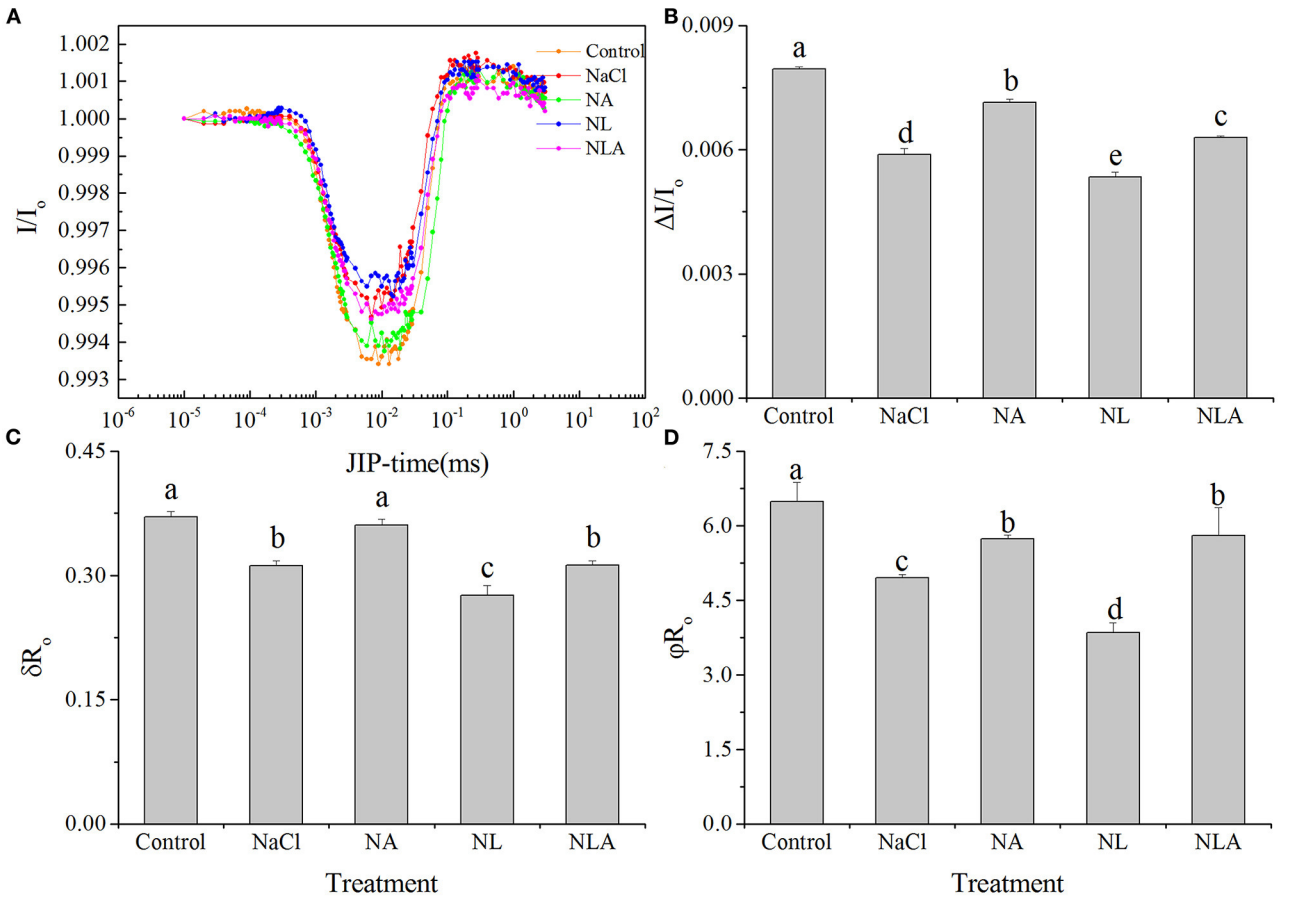

FIGURE 12 | Curves of light induced modulated 820 nm reflection (I/I_o) kinetics **(A)** and maximal redox capacity of PSI ($\Delta I/I_o$) **(B)**, efficiency with which an electron from the intersystem electron carriers is transferred to reduce end electron acceptors at the PSI acceptor side (δR_o) **(C)**, and quantum yield for reduction of end electron acceptors at the PSI acceptor side (ϕR_o) (D) in the leaves of salt-stressed tomato seedling with or without exogenous ascorbic acid (AsA) and lycorine (LYC) spraying. Values are means ± SD ($n = 3$). Different letters (a, b, c, d, and e) indicate significant difference at $P < 0.05$ among treatments. Error bar is smaller than the line at the top of the graph. Control, no added NaCl, no sprayed AsA and LYC; NaCl, added 100 mmol/L NaCl; NA, added 100 mmol/L NaCl and sprayed 0.5 mmol/L AsA; NL, added 100 mmol/L NaCl and sprayed 0.25 mmol/L LYC; NLA, added 100 mmol/L NaCl and sprayed 0.25 mmol/L LYC and 0.5 mmol/LAsA.

(ϕE_o and ψ_o), enhance the PQ pool size (S_m), and lower the rate of reduction of Q_A to Q_A^- (Mo) on the PSII acceptor end. As such, there are increases in both the electron transport flux per reaction center (ET_o/RC) and the primary photochemical efficiency (ψ_o), improving the efficiency of photochemical processes in tomato seedlings under salt stress.

Regulating the activity of PSII reaction centers and improving the ability of chloroplasts to absorb and dissipate energy is the key to improving plant salt tolerance. In this study, the increase of ABS/CS_m, TR/CS_m, and ET_o/CS_m in tomato seedlings under salt stress (**Figures 9**, **10**) may be a protective mechanism under salt stress (Sane et al., 2002). In contrast, the decreased ABS/RC and TR_o/RC under salt stress (**Figures 9**, **10**) means that the effective average absorption of the antenna and trapping per active RC are both higher because of certain RC inactivation (Yusuf et al., 2010). The increased DI_o/RC indicates that the proportion of total dissipation to active RCs increases due to high dissipation of the inactive RCs (Gerosa et al., 2003), which is consistent with previous results in cucumber under salt stress (Yuan et al., 2014). However, the negative effects of salt stress (in the presence of LYC or not) on active RC density and the use and expenditure of absorbed energy in PSII RCs were counteracted by exogenous application of AsA. The majority of plants dissipate excitation energy surpluses thermally, along with decreased regulation of PSII activity. This defends the photosynthetic apparatus abiotic environmental stressors, which can damage them. Xu (2017) reported that exogenous AsA can effectively promote xanthophyll loops in wheat under Cr^{6+} stress to dissipate excessive excitation light energy, thus avoiding the occurrence of photoinhition. So, our results suggest that AsA may act as a cofactor of violaxanthin de-epoxidase in the xanthophyll cycle (Muller-Moule et al., 2002) which helps protects tomatoes against the harmful effects of excess excitation energy induced by salt stress. Additionally, the role of AsA in regulating the photosynthetic capacity has been extensively studied by assessing patterns in the fluorescence parameters F_v/F_m as well as the performance index PI_{ABS}. We determined that lower F_v/F_m

levels in the leaves of tomatoes due to salt stress were associated with lower levels of PI_{ABS} (**Figure 11**), suggesting that salt-induced photoinhibition was due to damaged photosynthetic apparatus caused by excess light energy absorption compared with the level required for photosynthesis and limited component mechanism efficiency like the movement of electrons within a system and the trapping of energy (Song et al., 2003; Campos et al., 2014). The results in **Figure 11** show that AsA played a key role in regulating the use and expenditure of energy absorbed by PSII RCs in seedlings subjected to salt stress, both in the presence of LYC and without LYC. This is supported by the increased F_v/F_m and PI_{ABS} values (**Figure 11**). Therefore, these findings indicate that photosynthetic defense due to AsA was a result of increased capacity not only to protect photosynthetic processes from the negative effects of salt stress but also to inactivate the RCs of PSII replacement and regulation of the light striking PSII RCs, which is where absorbed energy is captured and energy from the dissipation of heat is transferred to a photochemical reaction. Additional energy from excitation was converted to transport electrons, a process that could provide additional transport capacity for electrons on the PSII donor end. As such AsA serves an important role in protecting the photosynthetic capacity during salt-stress conditions.

CONCLUSION

In conclusion, this study clearly demonstrated that salt stress lowered the capacity of several parts of the photosynthetic electron transport path. The OEC was damaged, PSII RCs were inactivated, the connections among independent PSII units were decreased, there was little electron transport beyond Q_A, and electron transporters on the PSI acceptor end in the leaves of tomato seedlings were damaged. However, exogenously applying AsA decreased the photoinhibition and lessened the negative effects on photosynthesis. Thus, under salt-stress conditions AsA can enhance salt-stress tolerance by promoting chlorophyll synthesis and alleviate the damage of oxidative stress to chloroplasts by modulating the redox state in chloroplast and dissipating excitation energy in the PSII antennae. AsA can also stabilize the molecular structure of photosynthetic reaction center, keeping the electron transport chain opened and enhancing the electron transfer efficiency, which is helpful to promote the improvement of photochemical activity and photosynthetic performance and the efficient distribution of energy. Moreover, the several beneficial effects of AsA during salt stress make AsA a good candidate for potential use as a chemical in agriculture.

DATA AVAILABILITY STATEMENT

The original contributions presented in the study are included in the article/**Supplementary Material**, further inquiries can be directed to the corresponding author/s.

AUTHOR CONTRIBUTIONS

The work presented here was carried out in collaboration between all authors. H-yL, MD, and XC defined the research theme. XC designed methods and experiments, carried out the laboratory experiments, analyzed the data, interpreted the results, and wrote the manuscript. YZ co-designed the experiments, carried out the laboratory experiments, and discussed the analyses and interpretation. YC, PZ, JC, WX, and QS co-worked on the analysis of fast fluorescence induction kinetics curve and JIP test parameters and discussed analyses and interpretation. H-yL and MD conceived and coordinated the study. All authors have contributed to, seen, and approved the final manuscript.

FUNDING

This work was supported by the National Natural Science Foundation of China (No. 31860550 and No. 31360478), Basic and Applied Basic Research Fund of Guangdong Province (No. 2019A1515110138), School-level Talents Project of Lingnan Normal University (No. ZL2032), and Project of 2020 Innovation and Entrepreneurship Training Program for Undergraduates (No.1076).

SUPPLEMENTARY MATERIAL

The Supplementary Material for this article can be found online at: https://www.frontiersin.org/articles/10.3389/fpls.2021.594400/full#supplementary-material

REFERENCES

Adhikari, N. D., Froehlich, J. E., Strand, D. D., Buck, S. M., Kramer, D. M., and Larkin, R. M. (2011). GUN4-porphyrin complexes bind the ChlH/GUN5 subunit of Mg-Chelatase and promote chlorophyll biosynthesis in *Arabidopsis*. *Plant Cell* 23, 1449–1467. doi: 10.1105/tpc.110.082503

Agami, R. A. (2014). Applications of ascorbic acid or proline increase resistance to salt stress in barley seedlings. *Biol. Plant.* 58, 341–347. doi: 10.1007/s10535-014-0392-y

Aghaleh, M., Niknam, V., Ebrahimzadeh, H., and Razavi, K. (2009). Salt stress effects on growth, pigments, proteins and lipid peroxidation in *Salicornia persica* and *S. europaea*. *Biol. Plant.* 53, 243–248. doi: 10.1007/s10535-009-0046-7

Ahmad, I., Basra, S. M. A., Afzal, I., Farooq, M., and Wahid, A. (2013). Growth improvement in spring maize through exogenous application of ascorbic acid, salicylic acid and hydrogen peroxide. *Int. J. Agric. Biol.* 15, 95–100. doi: 10.1684/agr.2012.0578

Akram, N. A., Shafiq, F., and Ashraf, M. (2017). Ascorbic acid-a potential oxidant scavenger and its role in plant development and abiotic stress tolerance. *Front. Plant Sci.* 8:613. doi: 10.3389/fpls.2017.00613

Alaka Srivastava, G., and Strasser, R. J. (2003). Characterization of the 820-nm transmission signal paralleling the chlorophyll a fluorescence rise (OJIP) in pea leaves. *Funct. Plant Biol.* 30, 785–796. doi: 10.1071/FP03032

Alhasnawi, A. N., Che, R. C. M. Z., Kadhimi, A. A., Isahak, A., Mohamad, A., Ashraf, M. F., et al. (2016). "Impact of exogenous ascorbic acid on biochemical activities of rice callus treated with salt stress," in *Ukm Fst Postgraduate Colloquium: Universiti Kebangsaan Malaysia, Faculty of Science & Technology Postgraduate Colloquium*, Vol. 1784 (AIP Publishing), 020005-1-020005-5. doi: 10.1063/1.4966715

Aliniaeifard, S., Hajilou, J., Tabatabaei, S. J., and Sifi-Kalhor, M. (2016). Effects of ascorbic acid and reduced glutathione on the alleviation of salinity stress in olive plants. *Int. J. Fruit Sci.* 16, 395–409. doi: 10.1080/15538362.2015.1137533

An, X. H., Tian, Y., Chen, Y. H., Li, E. M., Li, M., and Cheng, C. G. (2018). Functional identification of apple *MdGLK1* which regulates chlorophyll biosynthesis in *Arabidopsis*. *J. Plant Growth Regul.* 38, 778–787. doi: 10.1007/s00344-018-9889-5

Arrigoni, O., Gara, L. D., Paciolla, C., Evidente, A., Pinto, M. C. D., and Liso, R. (1997). Lycorine: a powerful inhibitor of L-galactono-γ-lactone dehydrogenase activity. *J. Plant Physiol.* 150, 362–364. doi: 10.1016/S0176-1617(97)80134-4

Ashraf, M., and Harris, P. J. C. (2013). Photosynthesis under stressful environments: an overview. *Photosynthetica* 51, 163–190. doi: 10.1007/s11099-013-0021-6

Banks, J. M. (2018). Chlorophyll fluorescence as a tool to identify drought stress in acer genotypes. *Environ. Exp. Bot.* 155, 118–127. doi: 10.1016/j.envexpbot.2018.06.022

Brestic, M., Zivcak, M., Olsovska, K., Kalaji, H. M., Shao, H., and Hakeem, K. R. (2014). "Heat signaling and stress responses in photosynthesis," in *Plant signaling: understanding the molecular crosstalk*, eds K. R. Hakeem, R. Rehman, and I. Tahir (Berlin: Springer Verlag). doi: 10.1007/978-81-322-1542-4_12

Campos, H., Trejo, C., Peña-Valdivia, C. B., García-Nava, R., Conde-Martínez, F. V., and Cruz-Ortega, M. R. (2014). Stomatal and non-stomatal limitations of bell pepper (*Capsicum annuum* L.) plants under water stress and re-watering: delayed restoration of photosynthesis during recovery. *Environ. Exp. Bot.* 98, 56–64. doi: 10.1016/j.envexpbot.2013.10.015

Ceppi, M. G., Oukarroum, A., N, Ç., Strasser, R. J., and Schansker, G. (2012). The IP amplitude of the fluorescence rise OJIP is sensitive to changes in the photosystem I content of leaves: a study on plants exposed to magnesium and sulfate deficiencies, drought stress and salt stress. *Physiol. Plantarum* 144, 277–288. doi: 10.1111/j.1399-3054.2011.01549.x

Chen, S., Yang, J., Zhang, M., Strasser, R. J., and Sheng, Q. (2016). Classification and characteristics of heat tolerance in *Ageratina adenophora* populations using fast chlorophyll a fluorescence rise O-J-I-P. *Environ. Exp. Bot.* 122, 126–140. doi: 10.1016/j.envexpbot.2015.09.011

Çiçek, N., Oukarroum, A., Strasser, R. J., and Schansker, G. (2017). Salt stress effects on the photosynthetic electron transport chain in two chickpea lines differing in their salt stress tolerance. *Photosyn. Res.* 136, 1–11. doi: 10.1007/s11120-017-0463-y

Conklin, P. L. (2010). Recent advances in the role and biosynthesis of ascorbic acid in plants[Review]. *Plant Cell Environ.* 24, 383–394. doi: 10.1046/j.1365-3040.2001.00686.x

Dalberto, D. S., Martinazzo, E. G., and Bacarin, M. A. (2017). Chlorophyll a fluorescence reveals adaptation strategies in drought stress in *Ricinus communis*. *Braz. J. Bot.* 40, 861–870. doi: 10.1007/s40415-017-0412-1

Derks, A., Schaven, K., and Bruce, D. (2015). Diverse mechanisms for photoprotection in photosynthesis. Dynamic regulation of photosystem II excitation in response to rapid environmental change. *Biochimica et Biophysica Acta* 1847, 468–485. doi: 10.1016/j.bbabio.2015.02.008

Diao, M., Ma, L., Wang, J., Cui, J., Fu, A., and Liu, H. Y. (2014). Selenium promotes the growth and photosynthesis of tomato seedlings under salt stress by enhancing chloroplast antioxidant defense system. *J. Plant Growth Regul.* 33, 671–682. doi: 10.1007/s00344-014-9416-2

Dietz, K. J. (2010). Redox-dependent regulation, redox control and oxidative damage in plant cells subjected to abiotic stress. *Methods Mol. Biol.* 639, 57–70. doi: 10.1007/978-1-60761-702-0_4

Dietz, K. J., and Pfannschmidt, T. (2011). Novel regulators in photosynthetic redox control of plant metabolism and gene expression. *Plant Physiol.* 155, 1477–1485. doi: 10.1104/pp.110.170043

Essemine, J., Xiao, Y., Qu, M., Mi, H., and Zhu, X. G. (2017). Cyclic electron flow may provide some protection against PSII photoinhibition in rice (*Oryza sativa* L.) leaves under heat stress. *J. Plant Physiol.* 211, 138–146. doi: 10.1016/j.jplph.2017.01.007

Evelin, H., Giri, B., and Kapoor, R. (2012). Contribution of Glomus intraradices inoculation to nutrient acquisition and mitigation of ionic imbalance in NaCl-stressed *Trigonella foenum-graecum*. *Mycorrhiza* 22, 203–217. doi: 10.1007/s00572-011-0392-0

Foyer, C. H., and Graham, N. (2011). Ascorbate and glutathione: the heart of the redox hub. *Plant Physiol.* 155, 2–18. doi: 10.1104/pp.110.167569

Gerosa, G., Marzuoli, R., Bussotti, F., Pancrazi, M., and Ballarin-Denti, A. (2003). Ozone sensitivity of *Fagus sylvatica* and *Fraxinus excelsior* young trees in relation to leaf structure and foliar ozone uptake. *Environ. Pollut.* 125, 0–98. doi: 10.1016/S0269-7491(03)00094-0

Gomes, M. T. G., Luz, A. C. D., Santos, M. R. D., Batitucci, M. D. C. P., Silva, D. M., and Falqueto, A. R. (2012). Drought tolerance of passion fruit plants assessed by the OJIP chlorophyll a fluorescence transient. *Sci. Hortic.* 142, 49–56. doi: 10.1016/j.scienta.2012.04.026

Hamid, M., and Ashraf, M. Y. (2010). Salicylic acid-induced growth and biochemical changes in salt-stressed wheat. *Commun. Soil Sci. Plant Anal.* 41, 373–389. doi: 10.1080/00103620903494343

He, X., Wang, S., Wang, P., Xin, B., Ma, Z., Diao, M., et al. (2015). Protective effects of exogenous selenium on oxidative damagein tomato seedling leaves under NaCl stress. *J. Shihezi Univ. Nat. Sci.* 33, 281–286 (in Chinese). doi: 10.13880/j.cnki.65-1174/n.2015.03.004

Hossain, M. S., Elsayed, A. I., Moore, M., and Dietz, K. J. (2017). Redox and reactive oxygen species network in acclimation for salinity tolerance in sugar beet. *J. Exp. Bot.* 68, 1283–1298. doi: 10.1093/jxb/erx019

Jiang, C., Zu, C., Lu, D., Zheng, Q., Shen, J., Wang, H., et al. (2017). Effect of exogenous selenium supply on photosynthesis, Na^+ accumulation and antioxidative capacity of maize (*Zea mays* L.) under salinity stress. *Sci. Rep.* 7:42039. doi: 10.1038/srep42039

Jiang, M., and Zhang, J. (2001). Effect of abscisic acid on active oxygen species, antioxidative defence system and oxidative damage in leaves of maize seedlings. *Plant Cell Physiol.* 42:1265. doi: 10.1093/pcp/pce162

Kalaji, H. M., Schansker, G., Brestic, M., Bussotti, F., Calatayud, A., Ferroni, L., et al. (2017). Frequently asked questions about chlorophyll fluorescence, the sequel. *Photosyn. Res.* 132, 13–66. doi: 10.1007/s11120-016-0318-y

Kostopoulou, Z., Therios, I., Roumeliotis, E., Kanellis, A. K., and Molassiotis, A. (2014). Melatonin combined with ascorbic acid provides salt adaptation in *Citrus aurantium* L. seedlings. *Plant Physiol. Biochem.* 86, 155–165. doi: 10.1016/j.plaphy.2014.11.021

Landi, S., Hausman, J.-F., Guerriero, G., and Esposito, S. (2017). Poaceae vs. abiotic stress: focus on drought and salt stress, recent insights and perspectives. *Front. Plant Sci.* 8:1214. doi: 10.3389/fpls.2017.01214

Li, X.-Q., Wang, F., Wang, C., Zou, T., Xu, N., and Sun, X. (2017). Comparative transcriptional profiling of *Gracilariopsis lemaneiformis* in response to salicylic acid- and methyl jasmonate-mediated heat resistance. *PLoS ONE* 12:e0176531. doi: 10.1371/journal.pone.0176531

Li, X. M., Chen, M. J., Li, J., Ma, L. J., Bu, N., Li, Y. Y., et al. (2014). Effect of endophyte infection on chlorophyllafluorescence in salinity stressed rice. *Biol. Plant.* 58, 589–594. doi: 10.1007/s10535-014-0428-3

Linster, C. L., and Clarke, S. G. (2008). Ascorbate biosynthesis in higher plants: the role of VTC2. *Trends Plant Sci.* 13, 567–573. doi: 10.1016/j.tplants.2008.08.005

Liu, Z., Zhu, J., Yang, X., Wu, H., Wei, Q., Wei, H., et al. (2018). Growth performance, organ-level ionic relations and organic osmoregulation of *Elaeagnus angustifolia* in response to salt stress. *PLoS ONE* 13:e0191552. doi: 10.1371/journal.pone.0191552

Maliba, B. G., Inbaraj, P. M., and Berner, J. M. (2019). The use of OJIP fluorescence transients to monitor the effect of elevated ozone on biomass of canola plants. *Water Air Soil Pollut.* 230:75. doi: 10.1007/s11270-019-4149-2

Melesse, T., and Caesar, K. (2010). Stomatal and non-stomatal effects of salinity on photosynthesis in faba beans (*Vicia faba* L.). *J. Agron. Crop Sci.* 168, 345–353. doi: 10.1111/j.1439-037X.1992.tb01018.x

Muhammad, J., and Shafiq, R. (2014). Response of growth, PSII photochemistry and chlorophyll content to salt stress in four *Brassica* species. *Life Sci. J.* 11, 139–145. doi: 10.7537/marslsj110314.19

Muller-Moule, P., Conklin, P. L., and Niyogi, K. K. (2002). Ascorbate deficiency can limit violaxanthin de-epoxidase activity *in vivo*. *Plant Physiol.* 128, 970–977. doi: 10.1104/pp.010924

Oukarroum, A., Bussotti, F., Goltsev, V., and Kalaji, H. M. (2015). Correlation between reactive oxygen species production and photochemistry of photosystems I and II in *Lemna gibba* L. plants under salt stress. *Environ. Exp. Bot.* 109, 80–88. doi: 10.1016/j.envexpbot.2014.08.005

Oukarroum, A., Madidi, S. E., Schansker, G., and Strasser, R. J. (2007). Probing the responses of barley cultivars (*Hordeum vulgare* L.) by chlorophyll a fluorescence

OLKJIP under drought stress and re-watering. *Environ. Exp. Bot.* 60, 438–446. doi: 10.1016/j.envexpbot.2007.01.002

Oukarroum, A., Schansker, G., and Strasser, R. J. (2010). Drought stress effects on photosystem I content and photosystem II thermotolerance analyzed using Chl a fluorescence kinetics in barley varieties differing in their drought tolerance. *Physiol. Plant.* 137, 188–199. doi: 10.1111/j.1399-3054.2009.01273.x

Oukarroum, A., Strasser, R. J., and Staden, J. V. (2004). Phenotyping of dark and light adapted barley plants by the fast chlorophylla fluorescence rise OJIP. *S. Afr. J. Bot.* 70, 277–283. doi: 10.1016/S0254-6299(15)30246-5

Pang, S., Wang, Z., and Zhang, R. (2005). Industry status and development prospect of Xinjiang processing tomato. *China Vegetables* 1, 39–41.

Penella, C., Calatayud, Á., and Melgar, J. C. (2017). Ascorbic acid alleviates water stress in young peach trees and improves their performance after rewatering. *Front. Plant Sci.* 8:1627. doi: 10.3389/fpls.2017.01627

Saeidi-Sar, S., Abbaspour, H., Afshari, H., and Yaghoobi, S. R. (2012). Effects of ascorbic acid and gibberellin AG3 on alleviation of salt stress in common bean (*Phaseolus vulgaris* L.) seedlings. *Acta Physiol. Plant.* 35, 667–677. doi: 10.1007/s11738-012-1107-7

Saleh, B. (2012). Effect of salt stress on growth and chlorophyll content of some cultivated cotton varieties grown in Syria. *Commun. Soil Sci. Plant Anal.* 43, 1976–1983. doi: 10.1080/00103624.2012.693229

Sane, P. V., Ivanov, A. G., Sveshnikov, D., Huner, N. P., and Oquist, G. (2002). A transient exchange of the photosystem II reaction center protein D1:1 with D1:2 during low temperature stress of Synechococcus sp. PCC 7942 in the light lowers the redox potential of QB. *J. Biol. Chem.* 277, 32739–32745. doi: 10.1074/jbc.M200444200

Shamshiri, M. H., and Fattahi, M. (2016). Effects of arbuscular mycorrhizal fungi on photosystem II activity of three pistachio rootstocks under salt stress as probed by the OJIP-test. *Russ. J. Plant Physiol.* 63, 101–110. doi: 10.1134/S1021443716010155

Singh, S. K., Reddy, V. R., Fleisher, D. H., and Timlin, D. J. (2014). Growth, nutrient dynamics, and efficiency responses to carbon dioxide and phosphorus nutrition in soybean. *J. Plant Interact.* 9, 838–849. doi: 10.1080/17429145.2014.959570

Song, L., Guo, Y., Kai, X. U., and Zhang, L. (2003). Protective mechanism in photoinhibition of photosynthesis in *Citrus unshiu* leaves. *Chin. J. Appl. Ecol.* 14, 47–50. doi: 10.1023/A:1022289509702

Strasser, R. J., Tsimilli-Michael, M., Qiang, S., and Goltsev, V. (2010). Simultaneous *in vivo* recording of prompt and delayed fluorescence and 820 nm reflection changes during drying and after rehydration of the resurrection plant *Haberlea rhodopensis*. *Biochim. Biophys. Acta* 1797, 1313–1326. doi: 10.1016/j.bbabio.2010.03.008

Strasser, R. J., Tsimillimichael, M., and Srivastava, A. (2004). "Analysis of the Chlorophyll a Fluorescence Transient," in *Chlorophyll a Fluorescence: A Signature of Photosynthesis*, eds G. C. Papageorgiou and Govindjee (New York, NY: Springer), 321–362. doi: 10.1007/978-1-4020-3218-9_12

Taïbi, K., Taïbi, F., Abderrahim, L. A., Ennajah, A., Belkhodja, M., and Mulet, J. M. (2016). Effect of salt stress on growth, chlorophyll content, lipid peroxidation and antioxidant defence systems in *Phaseolus vulgaris* L. *S. Afr. J. Bot.* 105, 306–312. doi: 10.1016/j.sajb.2016.03.011

Terzi, R., Kalaycioglu, E., Demiralay, M., Saglam, A., and Kadioglu, A. (2015). Exogenous ascorbic acid mitigates accumulation of abscisic acid, proline and polyamine under osmotic stress in maize leaves. *Acta Physiol. Plant.* 37, 43. doi: 10.1007/s11738-015-1792-0

Thagela, P., Yadav, R. K., Mishra, V., Dahuja, A., Ahmad, A., Singh, P. K., et al. (2017). Salinity-induced inhibition of growth in the aquatic pteridophyte Azolla microphylla primarily involves inhibition of photosynthetic components and signaling molecules as revealed by proteome analysis. *Protoplasma* 254, 303–313. doi: 10.1007/s00709-016-0946-2

Walker, C. J., and Willows, R. D. (1997). Mechanism and regulation of Mg-chelatase. *Biochem. J.* 327, 321–333. doi: 10.1042/bj3270321

Wang, M., Ding, F., and Zhang, S. (2020a). Mutation of SlSBPASE aggravates chilling-induced oxidative stress by impairing glutathione biosynthesis and suppressing ascorbate-glutathione recycling in tomato plants. *Front. Plant Sci.* 11:565701. doi: 10.3389/fpls.2020.565701

Wang, R., Liu, S., Zhou, F., and Ding, C. (2014). Exogenous ascorbic acid and glutathione alleviate oxidative stress induced by salt stress in the chloroplasts of *Oryza sativa* L. *Zeitschrift für Naturforschung C* 69, 226–236 doi: 10.5560/znc.2013-0117

Wang, Y., Diao, P., Kong, L., Yu, R., Zhang, M., Zuo, T., et al. (2020b). Ethylene enhances seed germination and seedling growth under salinity by reducing oxidative stress and promoting chlorophyll content via ETR2 pathway. *Front. Plant Sci.* 11:1066. doi: 10.3389/fpls.2020.01066

Wang, Y. H., Zhang, G., Chen, Y., Gao, J., and Chen, J. P.. (2019). Exogenous application of gibberellic acid and ascorbic acid improved tolerance of okra seedlings to nacl stress. *Acta Physiol. Plant.* 41:93. doi: 10.1007/s11738-019-2869-y

Wellburn, A. R., and Lichtenthaler, H. (1984). "Formulae and program to determine total carotenoids and chlorophylls A and B of leaf extracts in different solvents," in *Advances in Photosynthesis Research. Advances in Agricultural Biotechnology*, ed. C. Sybesma (Dordrecht: Springer Netherlands), 9–12. doi: 10.1007/978-94-017-6368-4_3

Wen, Z. L., Liu, H. Y., Zhou, Y., Chen, X. J., Feng, Y. L., Horticulture, D. O., et al. (2018). The involvement of nitric oxide in exogenous glutathione regulates antioxidant defense capacity against salt stress in tomato seedlings. *Plant Physiol. J.* 54, 607–617. doi: 10.13592/j.cnki.ppj.2017.0432

Xie, J. Q., Li, G. X., Wang, X. K., Zheng, Q. W., and Feng, Z. Z. (2009). Effect of exogenous ascorbic acid on photosynthesis and growth of rice under O_3 stress. *Chin. J. Eco-Agric.* 17, 1176–1181. doi: 10.3724/SP.J.1011.2009.01176

Xu, W. (2017). *Alleviative Effects and Mechanism of Exogenous Ascorbic Acid on Chromium (Cr6+) Toxicity in Wheat*. Nanjing: phd, Nanjing Agricultural University.

Xu, Y., Xu, Q., and Huang, B. (2015). Ascorbic acid mitigation of water stress-inhibition of root growth in association with oxidative defense in tall fescue (*Festuca arundinacea Schreb.*). *Front. Plant Sci.* 6:807. doi: 10.3389/fpls.2015.00807

Yang, W., Wang, F., Liu, L.-N., and Sui, N. (2020). Responses of membranes and the photosynthetic apparatus to salt stress in cyanobacteria. *Front. Plant Sci.* 11:713. doi: 10.3389/fpls.2020.00713

Yuan, Y., Shu, S., Li, S., He, L., Li, H., Du, N., et al. (2014). Effects of exogenous putrescine on chlorophyll fluorescence imaging and heat dissipation capacity in cucumber (*Cucumis sativus* L.) under salt stress. *J. Plant Growth Regul.* 33, 798–808. doi: 10.1007/s00344-014-9427-z

Yusuf, M. A., Kumar, D., Rajwanshi, R., Strasser, R. J., Tsimilli-Michael, M., Govindjee, and Sarin, N. B. (2010). Overexpression of γ-tocopherol methyl transferase gene in transgenic *Brassica juncea* plants alleviates abiotic stress: physiological and chlorophyll a fluorescence measurements. *Biochimica et Biophysica Acta* 1797, 1428–1438. doi: 10.1016/j.bbabio.2010.02.002

Zahoor, R., Dong, H., Abid, M., Zhao, W., Wang, Y., and Zhou, Z. (2017). Potassium fertilizer improves drought stress alleviation potential in cotton by enhancing photosynthesis and carbohydrate metabolism. *Environ. Exp. Bot.* 137, 73–83. doi: 10.1016/j.envexpbot.2017.02.002

Zhou, Y., Diao, M., Cui, J.-X., Chen, X.-J., Wen, Z.-L., Zhang, J.-W., et al. (2018). Exogenous GSH protects tomatoes against salt stress by modulating photosystem II efficiency, absorbed light allocation and H_2O_2-scavenging system in chloroplasts. *J. Integr. Agric.* 17, 2257–2272. doi: 10.1016/S2095-3119(18)62068-4

Conflict of Interest: The authors declare that the research was conducted in the absence of any commercial or financial relationships that could be construed as a potential conflict of interest.

Publisher's Note: All claims expressed in this article are solely those of the authors and do not necessarily represent those of their affiliated organizations, or those of the publisher, the editors and the reviewers. Any product that may be evaluated in this article, or claim that may be made by its manufacturer, is not guaranteed or endorsed by the publisher.

Advantages of publishing in Frontiers

OPEN ACCESS
Articles are free to read for greatest visibility and readership

FAST PUBLICATION
Around 90 days from submission to decision

HIGH QUALITY PEER-REVIEW
Rigorous, collaborative, and constructive peer-review

TRANSPARENT PEER-REVIEW
Editors and reviewers acknowledged by name on published articles

Frontiers
Avenue du Tribunal-Fédéral 34
1005 Lausanne | Switzerland

Visit us: www.frontiersin.org
Contact us: frontiersin.org/about/contact

REPRODUCIBILITY OF RESEARCH
Support open data and methods to enhance research reproducibility

DIGITAL PUBLISHING
Articles designed for optimal readership across devices

FOLLOW US
@frontiersin

IMPACT METRICS
Advanced article metrics track visibility across digital media

EXTENSIVE PROMOTION
Marketing and promotion of impactful research

LOOP RESEARCH NETWORK
Our network increases your article's readership